Targeting the Fanconi anaemia DNA damage repair pathway to establish effective combinatorial strategies in glioblastoma

Ola Rominiyi

BSc (Hons) MB ChB (Hons) MRCS

Academic Unit of Molecular Oncology

Department of Oncology and Metabolism

University of Sheffield

Primary Supervisor: Dr Spencer Collis

Thesis submitted to the University of Sheffield

for the degree of Doctor of Philosophy

June 2020

Kindly supported by…

Abstract

Introduction: Glioblastoma represent around half of newly diagnosed glial tumours and continue to portend poor survival (median 15.6 months) despite maximal safe surgical resection followed by DNA-damaging adjuvant therapies. Anomalies within the cellular DNA damage response (DDR) contribute to the treatment refractory nature of this devastating brain tumour with difficult-to-treat glioblastoma stem cell (GSC) subpopulations reported to exhibit heightened activity in various DDR processes. The Fanconi anaemia (FA) pathway represents a key DDR process which remains relatively inactive in normal brain, but is re-activated in glioblastoma, raising its value as a foundational target for cancer-specific treatment. However, similar to other difficult-to-treat diseases such as HIV and multi-drug resistant TB, novel drug combinations may be required to overcome the extensive genetic heterogeneity and resistance mechanisms observed in glioblastoma. This thesis therefore, considers whether combined targeting of the FA pathway and interconnected DDR processes could form a basis for new, effective multimodal therapies.

Methods: Established cell lines and more clinically-relevant 2D and 3D primary, patient-derived glioblastoma stem cell (GSC) models were used in conjunction with viability and clonogenic survival assays to assess therapeutic combinations targeting the DDR. Inhibitors of the FA pathway (FAPi), including novel specific FAPi under development (nFAPi), were validated and assessed alongside other key DDR targets including PARP1, ATR and ATM, and a range of techniques were used to assess FA pathway activity and the effects of combinatorial strategies on DNA damage and responses in GSCs.

Results: Elevated FA pathway gene expression in gliomas is associated with poor survival. Furthermore, patient-derived GSC populations, which drive therapeutic resistance, display high FA pathway expression relative to paired bulk tumour cell populations. We further show that inhibition of a single DDR process (FA pathway, PARP, ATR or ATM) increases the susceptibility of glioblastoma cell lines and patient-derived GSCs to current adjuvant therapy. Importantly, clinically approved PARP inhibitor (PARPi) monotherapy stimulates robust FANCD2 monoubiquitination, supporting a role of FA pathway activation in response to current DDR-targeted therapy. In clinically-relevant 3D GSC models, simultaneous inhibition of the FA pathway (FAPi) and PARP or ATR enhanced temozolomide sensitisation compared to a single DDR inhibitor (DDRi). Furthermore, combined PARPi + FAPi

consistently conferred radiosensitisation whilst combined ATRi + FAPi led to a profoundly radiosensitising effect. Furthermore, comparison of α/β ratio enhancement suggests dual-DDRi strategies fundamentally alter the response of GSCs, whilst single cell gel electrophoresis and immunofluorescence studies suggest FA pathway-based DDRi combinations substantially delay the resolution of IR-induced DNA strand breaks at 6 hours post-treatment, with increased persistent DNA double strand breaks at 24 hours. In contrast to PARPi + FAPi, treatment with the ATRi + FAPi combination portended marked generation of RNA:DNA hybrids, however the substantial efficacy of both combinations over single DDRi strategies appeared to be independent of their cell cycle modulatory effects.

Finally, during these studies a 'living biobank' of 24 clinically- and surgically-relevant GSC models has been established. These include novel resected and residual disease models based on careful macrodissection of rare *en-bloc* partial lobectomy specimens to liberate parallel GSC lines from the tumour core and adjacent infiltrated brain, which represent cells removed and those typically left behind after surgery. Relative to resected disease models generated from the same patient, biological characterisation reveals residual disease models display increased connecting tumour microtube formation, stem marker expression and early evidence of elevated DDR marker expression including BRCA2, ATM and ATR. These are all consistent with enhanced therapeutic resistance in disease normally left behind after surgery.

Conclusion: Simultaneously targeting the FA pathway and interconnected DDR processes represents an appealing therapeutic strategy. Novel preclinical models which recapitulate spatiofunctional intratumoural heterogeneity have been developed and will support future evaluation of combinatorial strategies against recalcitrant post-surgical disease. Additionally, constitutive lack of FA pathway function in some tumours, could serve as a novel predictive biomarker for patient response to PARPi and ATRi which are currently in clinical trials.

Declaration

I hereby declare that all work presented within this thesis has not been previously submitted for any academic award at this or any other institution. All work submitted is my own, unless otherwise stated, and has not been plagiarised.



Ola Rominiyi

Acknowledgements

I would like to acknowledge Dr Spencer J. Collis, my primary supervisor, for the expert advice, guidance, support and inspiration he has provided throughout my PhD studies. He has helped a daunting undertaking become a thoroughly enjoyable journey and for this I will be eternally grateful. I also thank my secondary supervisors Dr Helen Bryant, whose insightful comments led to course corrections on numerous occasions, and Mr Yahia Al-Tamimi, whose clinical acumen has been invaluable to realise the patient-facing aspects of these studies. I also thank Mr Thomas Carroll whose experience provided a large part of my inspiration to undertake this PhD, Mr David Jellinek whose confidence in me has been a huge encouragement, and Mr Saurabh Sinha along with the entire neurosurgical team at Sheffield Teaching Hospitals who were staunch supporters of my time spent in the laboratory, even when it made smooth operation of a busy surgical unit less straightforward.

I am also incredibly grateful to Dr Natividad Gomez Roman, Dr Ross Carruthers and the entire Chalmers team for their support and training during the coldest winter I have ever experienced whilst on secondment at the University of Glasgow.

A special thanks is needed for Dr Katie Myers and Dr Natasha Carmell who have both gone above and beyond during my PhD studies to ensure I was able to make progress, whether that required teaching me new practical skills, sharing protocols, answering my (many) questions, or just being there to support me when things didn't go as planned – for all these things and countless more, I will forever be grateful.

Thank you to everyone in the Collis, Bryant, Thompson and Chen laboratories, members past and present for all your help, friendship and support over the years (including, but absolutely not limited to, David, Thomas, Charlotte, Clair, Carlo, Emma, Fatma, Callum and Rachel – it has been a privilege to work with you all). I've also been privileged to co-supervise Aurelie, Dawoud, Nikita, Connor and Eva. I have enjoyed every moment of working with you and am excited by the bright futures you each hold in your hands.

Finally, I express my heartfelt gratitude to our phenomenal funders and to every patient who has contributed selflessly to these studies. You inspire me to keep going and work towards better treatment strategies to combat this devastating disease.

Dedication

This thesis is dedicated to Ibukun, Ariyo and Aralana Rominiyi – without your love and support, it would not have been possible.

Abbreviations

αKG	α-ketoglutarate
2-HG	R(-)-2-hydroxyglutarate
5-ALA	5-aminolevulinic acid
ACNU	Nimustine
ADP	Adenosine diphosphate
ALT	Alternative lengthening of telomeres
AML	Acute myeloid leukaemia
AML	Acute myeloid leukaemia
APEX1	Apurinic/apyrimidinic (AP) endonuclease
ATM	Ataxia telangiectasia mutated
ATMi	ATM inhibitor
ATP	Adenosine triphosphate
ATR	Ataxia telangiectasia and Rad3 related
ATRi	ATR inhibitor
ATRIP	ATR interacting protein
BBB	Blood-brain barrier
BCNU	Bis-chloroethylnitrosourea (carmustine)
BER	Base excision repair
BMF	Bone marrow failure
BOD1L	Biorientation of chromosomes in cell division protein 1-like
BRCA1	Breast cancer 1, early onset
BRCA2	Breast cancer 2, early onset
BSA	Bovine serum albumin
BTB	Blood-tumour barrier
CD4	Cluster of differentiation 4
CD8	Cluster of differentiation 8
CDC25	Cell cycle division 25
CDC45	Cell cycle division 45
CDK	Cyclin-dependent kinase
CDKN2A	Cyclin-dependent kinase inhibitor 2A (p16)
CDKN2B	Cyclin-dependent kinase inhibitor 2B (p15)
CETSA	Cellular thermal shift assay

CHK1	Checkpoint kinase 1
CHK2	Checkpoint kinase 2
CI	Combination index
CNS	Central nervous system
CpG	Cytosine-phosphate-guanine site
CRISPR	Clustered Regularly Interspaced Short Palindromic Repeats
CRUK	Cancer Research UK
CSC	Cancer stem cell
DAXX	Death domain associated protein
ddH_2O	Deionised water
DDR	DNA damage response
DDRi	DNA damage response inhibitor
DIPG	Diffuse intrinsic pontine glioma
DMEM	Dulbecco's modified Eagle's medium
DMF	Dose modifying factor
DMPK	Drug Metabolism and Pharmacokinetics
DMSO	Dimethyl sulfoxide
DNA	Deoxyribonucleic acid
DSB	Double-strand break
ECM	Extracellular matrix
EDTA	Ethylenediaminetetraacetic acid
EGF	Epidermal growth factor
EGFR	Epidermal growth factor receptor
EHS	Engelbreth–Holm–Swarm
EXO1	Exonuclease-1
FA	Fanconi anaemia
FACS	Fluorescence-activated cell sorting
FANC	Fanconi anaemia complementation group
FAP	FA pathway
FAPi	FA pathway inhibitor
FCS	Foetal calf serum
FFPE	Formalin-fixed paraffin-embedded
FGF	Fibroblast growth factor

FOXM1	Forkhead box protein M1
G-CIMP	CpG island methylator phenotype
GBM	Glioblastoma multiforme
GeCIP	Genomics England Clinical Interpretation Partnership
GEMM	Genetically engineered mouse model
GFR	Growth factor reduced
GLICO	Glioma cerebral organoid
GSC	Glioblastoma stem cell
HBOC	Hereditary breast and ovarian/fallopian tube cancer
HCl	Hydrochloric acid
HDAC	Histone deacetylase
HIF	Hypoxia-inducible factor
HPLC	High-performance liquid chromatography
HR	Homologous recombination
HRR	HR-mediated DNA repair
ICL	Interstrand crosslink
IDH	Isocitrate dehydrogenase
IHC	Immunohistochemistry
IL-1β	Interleukin 1 beta
IL-6	Interleukin 6
IMS	Industrial methylated spirit
LD	Lethal dose
MAPK	Mitogen-activated protein kinase
MDM2	Mouse double minute 2 homolog
MDS	Myelodysplastic syndrome
MDT	Multi-disciplinary team
MEM	Minimum Essential Medium
MFI	Mean fluorescence intensity
MGMT	O^6-methylguanine-DNA-methyltransferase
MMC	Mitomycin C
MMR	Mismatch repair
MPG	Methylpurine DNA glycosylase
MRE11A	Meiotic recombination 11 homologue A

MRI	Magnetic resonance imaging
MTIC	5-(3-methyltriazen-1-yl)imidazole-4-carboxamide
mTOR	Mechanistic target of rapamycin
MTT	3-(4,5dimethylthiazol-2-yl)-2,5-diphenyltetrazolium bromide
N^3-meA	N^3-methyladenine
N^7-meG	N^7-methylguanine
NBS1	Nijmegen breakage syndrome 1
NC3Rs	National Centre for the Replacement, Refinement & Reduction of Animals in Research
NER	Nucleotide excision repair
NF1	Neurofibromatosis 1
nFAPi	Novel FA pathway inhibitor
NFkβ	Nuclear factor kappa-light-chain-enhancer of activated B cells
NGS	Next-generation sequencing
NHEJ	Non-homologous end joining
NO	Nitric oxide
NOD-SCID	Non-obese diabetic - severe combined immunodeficiency
O^6-meG	O^6-methylguanine
OD	Optical density
PALB2	Partner and localizer of BRCA2
PARP-1	Poly ADP-ribose polymerase 1
PARP-2	Poly ADP-ribose polymerase 2
PARPi	PARP inhibitor
PBS	Phosphate buffered saline
PCNA	Proliferating cell nuclear antigen
PDGFRA	Platelet-derived growth factor receptor α
PDK1	Phosphoinositide-dependent protein kinase-1
PDX	Patient-derived xenograft
PE	Plating efficiency
PFA	Paraformaldehyde
PI3K	Phosphatidylinositol-3-kinase
Pol-β	DNA polymerase β
Pol-δ	DNA polymerase δ

PRC2	Polycomb repressive complex 2
PTEN	Phosphate and tensin homolog
Q.S.	*Quantum satis* (the amount which is enough)
QoL	Quality of life
Rb	Retinoblastoma
REC	NHS Research Ethics Committee
REIMS	Rapid evaporative ionization mass spectrometry
REMBRANDT	Repository of Molecular Brain Neoplasia Data
RFC	Replication Factor C
RHH	Royal Hallamshire Hospital
RNA	Ribonucleic acid
ROS	Reactive oxygen species
RPA	Replication protein A
RTK	Receptor tyrosine kinase
SAHA	Suberoylanilide hydroxamic acid
SCT	Stem cell transplant
SD	Standard deviation
SEM	Standard error of the mean
SER	Sensitiser enhancement ratio
SF	Surviving fraction
siRNA	Short interfering ribonucleic acid
SSB	Single-strand break
SSC	Saline sodium citrate
ssDNA	Single-strand DNA
SSL	Synthetic sensitivity or lethality
STH	Sheffield Teaching Hospitals NHS Foundation Trust
TCGA	The Cancer Genome Atlas
TERT	Telomerase reverse transcriptase
TET	Ten-eleven translocation
TLS	Translesion DNA synthesis
TMZ	Temozolomide
TNF-α	Tumour necrosis factor alpha
TP53	Tumour protein P53

TTFields	Tumour treating fields
US	Ultrasound
UV	Ultraviolet
VEGF	Vascular endothelial growth factor
WES	Whole exome sequencing
WGS	Whole genome sequencing
WHO	World Health Organisation
XRCC1	X-ray repair cross-complementing protein 1

Contents

ABSTRACT 2

DECLARATION 4

ACKNOWLEDGEMENTS 5

DEDICATION 6

ABBREVIATIONS 7

CONTENTS 13

LIST OF FIGURES 21

LIST OF SUPPLEMENTARY FIGURES 27

LIST OF TABLES 28

LIST OF EQUATIONS 29

LIST OF PUBLICATIONS & MANUSCRIPTS 29

LIST OF PUBLISHED ABSTRACTS 30

LIST OF PRESENTATIONS 31

AWARDS AND PRIZES DURING PHD 32

LIST OF RESEARCH FUNDING SECURED 33

1 CHAPTER 1 – INTRODUCTION 37

1.1 CENTRAL NERVOUS SYSTEM TUMOURS 39

1.1.1 Molecular classification of gliomas 40

1.2 CHARACTERISATION AND TREATMENT OF GLIOBLASTOMA 43

1.2.1 Glioblastoma: an unmet clinical need 43

1.2.2 Genomic aberrations in glioblastoma 44

1.2.3 Current multimodal therapy for glioblastoma 47

1.3 PRECLINICAL EXPERIMENTAL MODELS OF GLIOBLASTOMA 49

1.4 THE FANCONI ANAEMIA PATHWAY & RELATED CELLULAR RESPONSES TO DNA DAMAGE 53

1.4.1 Conceptual overview of the DNA damage response 53

1.4.2 DNA damage and responses to standard glioblastoma therapy 53

1.4.3 DNA damage signalling and checkpoint induction 54
1.4.4 The Fanconi anaemia DNA damage repair pathway 57
1.4.5 Fanconi anaemia 62
1.4.6 Solid tumours and Fanconi anaemia 64
1.4.7 Related DNA damage repair pathways 64
1.4.8 Synthetic lethality and sensitivity 70
1.4.9 Molecular interplay within the overall DDR 70
1.5 RATIONALE FOR COMBINATION TARGETING OF THE DDR IN GLIOBLASTOMA 73
1.5.1 Parallel targeting of the DDR 73
1.5.2 Integrative strategies based on the Fanconi anaemia pathway 74
1.6 STUDY AIMS 75
1.6.1 Aims of the study 75
1.6.2 Hypotheses 75
1.6.3 Objectives 75

2 CHAPTER 2 – MATERIALS & METHODS 78

2.1 GENERAL LABORATORY EQUIPMENT 78
2.1 CONSUMABLES 79
2.2 STERILISATION 81
2.3 PURIFIED WATER 81
2.4 REAGENTS 81
2.5 INHIBITORS AND CYTOTOXIC AGENTS 84
2.6 PROPRIETARY COMPOUNDS 84
2.7 PRIMARY ANTIBODIES 85
2.8 SECONDARY ANTIBODIES 87
2.9 TAQMAN™ GENE EXPRESSION PROBES FOR QUANTITATIVE PCR 87
2.10 STANDARD SOLUTIONS 88
2.11 ESTABLISHED HUMAN CELL LINE CULTURE 89
2.11.1 Procurement of established cell lines 89
2.11.2 Cell culture 89
2.11.3 Growth conditions 89
2.11.4 Serial passaging of established cell lines 89
2.11.5 Counting cells 90
2.11.6 Cryopreservation 90
2.11.7 Thawing cells 90

2.12 PRIMARY PATIENT-DERIVED CELL LINE CULTURE 90
2.12.1 Procurement of the 'Cambridge' patient-derived glioblastoma stem cell lines ..90
2.12.2 Derivation of 'Sheffield' patient-derived glioblastoma stem cell lines..... 91
2.12.3 Parallel 'Sheffield' patient-derived glioblastoma stem cell lines to model resected & residual disease 93
2.12.4 Parallel 'Sheffield' patient-derived glioblastoma stem cell lines to model random intra-tumoural heterogeneity 93
2.12.5 Propagation of patient-derived glioblastoma stem cell lines 94
2.12.6 Generation of paired tumour bulk populations 95
2.12.7 Growth conditions for patient-derived glioblastoma cells..... 95
2.12.8 Serial passaging of patient-derived glioblastoma cells..... 96
2.12.9 Counting patient-derived glioblastoma stem cells 96
2.12.10 Cryopreservation of patient-derived glioblastoma stem cell lines..... 96
2.12.11 Thawing cells..... 97
2.13 MTT CELL VIABILITY ASSAY 97
2.13.1 MTT cell viability assay in established cell lines..... 97
2.13.2 MTT heatmap meta-analysis 99
2.14 CLONOGENIC SURVIVAL ASSAY 99
2.14.1 Clonogenic set up and treatments..... 99
2.14.2 Clonogenic staining and counting 101
2.15 3D ALVETEX™ CLONOGENIC SURVIVAL ASSAY..... 101
2.15.1 Preparation of 3D Alvetex™ plates..... 102
2.15.2 3D clonogenic set up and treatments..... 103
2.15.3 3D clonogenic staining and counting 103
2.16 IMMUNOBLOTTING 104
2.16.1 Protein extraction and quantification 104
2.16.2 Protein extraction from 3D Alvetex™ scaffolds 106
2.16.3 SDS-PAGE & protein transfer..... 106
2.16.4 Immunodetection..... 106
2.16.5 Calculation of FANCD2 L:S ratios 107
2.17 IMMUNOFLUORESCENCE 108
2.17.1 2-dimensional immunofluorescence in established and primary patient-derived cell lines 108
2.17.2 Confocal immunofluorescence in customised 3D Alvetex™ scaffolds 109
2.17.3 R-loop (RNA:DNA hybrid) immunostaining and confocal immunofluorescence 110

2.17.4 RNA:DNA hybrid image analysis 111
2.18 TAQMAN™ RT-PCR 111
2.18.1 RNA extraction 111
2.18.2 Reverse transcription 112
2.18.3 Real time qPCR – relative mRNA expression 113
2.19 FLOW CYTOMETRY AND ANALYSIS OF CELL CYCLE DISTRIBUTION 113
2.19.1 Sample preparation and PI staining 113
2.19.2 FACSCalibur flow cytometric analysis 114
2.20 SINGLE CELL GEL ELECTROPHORESIS: ALKALINE COMET ASSAY 114
2.20.1 Alkaline comet assay procedure 115
2.20.2 Image acquisition and analysis 116
2.21 STATISTICAL ANALYSIS 116
2.21.1 Clonogenic survival curve fitting and analysis 116

3 CHAPTER 3 – EXPLOITING SINGLE DDR TARGETS IN GLIOBLASTOMA TO CONFER CHEMOSENSITISATION 120

3.1 INTRODUCTION 120
3.1.1 The Fanconi anaemia (FA) pathway in glioblastoma 120
3.1.2 PARP, ATR and ATM as chemosensitisation targets in glioblastoma 124
3.1.3 Development and clinical translation of pharmacological inhibitors of the FA pathway and interconnected DDR processes 127
RESULTS 135
3.2 INHIBITION OF KEY DDR TARGETS SENSITISES ESTABLISHED GLIOBLASTOMA CELL LINES TO DNA DAMAGING THERAPY 135
3.2.1 Inhibition of the DNA damage response following DNA damaging therapy 135
3.2.2 Inhibition of the FA pathway, PARP1 and ATR sensitise established glioblastoma cultures to temozolomide chemotherapy 136
3.2.3 Effects of Fanconi anaemia pathway inhibition with curcumin on temozolomide response 138
3.2.4 Effects of PARP inhibition on temozolomide response 139
3.2.5 Effects of ATR and ATM inhibition on temozolomide response 139
3.2.6 Inhibition of the FA pathway, PARP1 and ATR sensitise U87 glioblastoma cultures to DNA crosslinking chemotherapy 142
3.3 NOVEL, SPECIFIC COMPOUNDS TO INHIBIT THE FA PATHWAY (NFAPI) AS A THERAPEUTIC STRATEGY 143

3.3.1 The development of nFAPi *143*
3.3.2 Cell-free evaluation of nFAPi compound activity *144*
3.3.3 Curcumin and nFAPi reduce temozolomide-induced FANCD2 foci formation and FANCD2 monoubiquitination *146*
3.3.4 Evaluation of the effects of nFAPi on temozolomide sensitivity *148*
3.4 DEVELOPING DDR-BASED COMBINATORIAL APPROACHES TO TREAT GLIOBLASTOMA 153
3.4.1 Combined targeting of DDR processes in tandem (proof-of-concept using HeLa Silencix cells) *154*
3.4.2 Combined inhibition of the FA pathway and PARP1 in the absence of conventional DNA damaging therapy *155*
3.5 SUMMARY OF KEY FINDINGS 156
3.6 DISCUSSION 158
3.6.1 General Study limitations *158*
3.6.2 nFAPi require further development *161*
3.6.3 Targeting the DNA damage response represents an appealing therapeutic strategy in glioblastoma *164*
3.6.4 Recapitulating therapeutic resistance in vitro *168*
3.6.5 Assessing therapeutic strategies incorporating DDRi combinations and DNA damaging therapy *168*

4 CHAPTER 4 – DEVELOPMENT AND VALIDATION OF CLINICALLY-RELEVANT GLIOBLASTOMA STEM CELL MODELS 171

4.1 INTRODUCTION 171
4.1.1 Cancer stem cell theory *171*
4.1.2 Cancer stem cells in glioblastoma and other brain tumours *172*
4.1.3 3-dimensional glioblastoma stem cell models *176*
4.2 VALIDATION OF 2D AND 3D SCAFFOLD-BASED CAMBRIDGE PATIENT-DERIVED GLIOBLASTOMA STEM CELL MODELS 182
4.2.1 Propagation and validation of Cambridge-derived GSCs *182*
4.2.2 Putative stem cell marker expression in 2D and 3D GSC models *183*
4.2.3 Comparison of GSC colony formation and IR response in 2D and 3D culture systems 185
4.3 DEVELOPMENT OF CLINICALLY- AND SURGICALLY-RELEVANT SHEFFIELD PATIENT-DERIVED GLIOBLASTOMA STEM CELL MODELS 186
4.3.1 Derivation of Sheffield primary, patient-derived glioblastoma stem cell lines .. *186*

4.3.2 Parallel 'Sheffield' GSCs to model random intra-tumoural heterogeneity.....190
4.3.3 Parallel 'Sheffield' GSCs to model resected and post-surgical residual disease191
4.4 EARLY DEVELOPMENT OF A 3D *EX VIVO* SCAFFOLD-BASED SYSTEM TO ASSESS TUMOUR TREATING FIELDS AND REPLACE ANIMAL STUDIES.....199
4.4.1 Model development and TTFields delivery via Inovitro™.....199
4.5 SUMMARY OF KEY FINDINGS.....203
4.6 DISCUSSION.....205
4.6.1 General Study Limitations.....205
4.6.2 Differences in IR response between 2D and 3D GSCs.....210
4.6.3 Developing the Sheffield Living Biobank of clinically- and surgically-relevant glioblastoma models.....211
4.6.4 Ongoing preclinical TTFields 3D model development.....213

5 CHAPTER 5 – FA PATHWAY-BASED DDR TARGETED COMBINATIONS TO ENHANCE CHEMOTHERAPY AND RADIOTHERAPY RESPONSE IN GLIOBLASTOMA STEM CELLS.....216

5.1 INTRODUCTION.....216
5.1.1 A new foundation for DNA damage response targeted combinations.....216
5.2 CLINICAL RELEVANCE OF FA PATHWAY GENE EXPRESSION IN GLIOMAS.....217
5.2.1 FA pathway functional groups are highly expressed in gliomas and associated with poor survival.....217
5.2.2 Glioblastoma stem cells demonstrate elevated FA pathway gene expression relative to bulk populations.....222
5.2.3 Activation kinetics of the FA pathway and other key DDR processes in glioblastoma stem cells.....223
5.3 TARGETING THE FA PATHWAY TO OVERCOME INHERENT THERAPEUTIC RESISTANCE IN GLIOBLASTOMA STEM CELLS.....225
5.3.1 The 'heart failure' medication ouabain inhibits the FA pathway and potently radiosensitises glioblastoma cell cultures.....226
5.3.2 The effects of novel FA pathway inhibitor F76 on FA pathway activation and radiosensitivity in glioblastoma stem cells.....230
5.3.3 Inhibition of the FA pathway in glioblastoma stem cells using curcumin.....232
5.4 COMBINED FA PATHWAY AND PARP INHIBITION TO ENHANCE CHEMOTHERAPY AND RADIATION RESPONSE.....234
5.4.1 Radiosensitisation with combined FA pathway and PARP1 inhibition in 2D and 3D scaffold-based primary, patient-derived glioblastoma stem cell models.....234

5.4.2 Combined FA pathway and PARP1 inhibition augments radiation-induced DNA damage 239

5.4.3 Effects of combined FA pathway and PARP1 inhibition on temozolomide sensitivity in 3D scaffold-based primary, patient-derived glioblastoma stem cell models 242

5.5 COMBINED FA PATHWAY AND ATM OR ATR INHIBITION TO ENHANCE CHEMOTHERAPY AND RADIATION RESPONSE 243

5.5.1 Radiosensitisation with combined FA pathway and ATR or ATM inhibition in 3D scaffold-based primary, patient-derived glioblastoma stem cell models 243

5.5.2 The effects of combined FA pathway and ATR or ATM inhibition on temozolomide sensitivity in 3D scaffold-based primary, patient-derived glioblastoma stem cell models 248

5.6 THE EFFECTS OF FA PATHWAY-BASED DDRI COMBINATIONS ON DNA STRAND BREAKS, REPLICATION STRESS AND CELL CYCLE PROGRESSION 250

5.6.1 Combined FA pathway and PARP or ATR inhibition augments radiation-induced DNA damage and delays repair in glioblastoma stem cells 250

5.6.2 The effects of combined FA pathway and PARP or ATR inhibition on replication-transcription conflicts in glioblastoma stem cells 255

5.6.3 The effects of combined FA pathway and PARP or ATR inhibition on cell cycle progression in glioblastoma stem cells 262

5.7 SUMMARY OF KEY FINDINGS 266

5.8 DISCUSSION 268

5.8.1 General Study limitations 268

5.8.2 Emerging clinical relevance of the FA pathway in glioblastoma 273

5.8.3 FA pathway-based, DDR-targeting combinations as a novel therapeutic strategy for glioblastoma 277

5.9 SUPPLEMENTARY FIGURES 284

6 CHAPTER 6 – CONCLUSIONS AND FUTURE STUDIES 286

6.1 CONCLUSIONS 286

6.2 FUTURE STUDIES 290

6.2.1 Developing more effective FA pathway inhibitors to underpin single and combination DDRi strategies 291

6.2.2 Combining TTFields and inhibitors of the DNA damage response 292

6.2.3 Ex vivo 3D models of post-surgical residual disease to improve biological understanding and treatment 292

6.2.4 Ex vivo drug screening using human tissue to personalise cancer therapy and replace murine avatars 294

6.2.5 Understanding and predicting patient-specific responses to therapy for glioblastoma 295

7 REFERENCES 298

List of Figures

		PAGE
Figure 1.1	The categorisation and origins of common central nervous system tumours.	39
Figure 1.2	Integrated histological and molecular classification of diffuse gliomas.	41
Figure 1.3	Cancers of unmet need.	44
Figure 1.4	Histological and molecular subtyping in glioblastoma.	46
Figure 1.5	Summary of the mechanisms of action of TTFields.	48
Figure 1.6	The role of ATM and ATR in cell cycle regulation following DNA damage.	56
Figure 1.7	A schematic model for the FA pathway.	58
Figure 1.8	A schematic model for homologous recombination.	66
Figure 1.9	A schematic model for non-homologous end-joining.	67
Figure 1.10	A schematic model for DNA mismatch repair.	68
Figure 1.11	A summary of base excision repair.	69
Figure 1.12	Global and FA pathway-related interactions within the DNA damage response.	72
Figure 2.1	Schematic diagram of primary, patient-derived glioblastoma stem cell line generation.	93
Figure 2.2	Schematic representation of parallel patient-derived glioblastoma stem cell line derivation.	94
Figure 2.3	Example of cell number optimisation for the MTT cell viability assay using established glioblastoma cells.	98
Figure 2.4	3-dimensional Alvetex™ 12-well plate diagram.	102
Figure 2.5	Flowchart protocol for a typical 3-dimensional clonogenic experiment.	104
Figure 2.6	Inter-rater reliability of 3-dimensional clonogenic experiments.	104
Figure 2.7	BSA standard curve.	105
Figure 3.1	Inhibition of FANCD2 monoubiquitination and PARylation in established glioblastoma cell lines.	136
Figure 3.2	Optimisation of chemotherapeutic agent and DDR inhibitor dose using U87 glioblastoma cells.	138

Figure 3.3	Targeting the DNA damage response in established glioblastoma cultures to enhance temozolomide response.	141
Figure 3.4	Inhibition of the FA pathway, PARP1 and ATR sensitise established U87 glioblastoma cultures to crosslinking chemotherapy.	143
Figure 3.5	Novel compounds targeting FANCL reduce FANCD2 monoubiquitination in cell-free AlphaScreen assay.	146
Figure 3.6	Novel specific FA pathway inhibitors reduce temozolomide-induced FANCD2 foci formation and FANCD2 monoubiquitination in established glioblastoma cultures.	148
Figure 3.7	Assessing the putative therapeutic effects of novel specific FA pathway inhibitors as a strategy to sensitise established glioblastoma cultures to temozolomide chemotherapy.	150
Figure 3.8	Assessing the putative therapeutic effects of novel specific FA pathway inhibitors as a strategy to sensitise established glioblastoma cultures to temozolomide chemotherapy.	151
Figure 3.9	Assessing the putative therapeutic effects of novel specific FA pathway inhibitors as a strategy to sensitise established glioblastoma cultures to cisplatin chemotherapy.	152
Figure 3.10	Assessing the putative therapeutic effects of (second generation) novel specific FA pathway inhibitors as a strategy to sensitise established glioblastoma cultures to cisplatin chemotherapy.	153
Figure 3.11	*BRCA1*-deficient and *BRCA-2* deficient cells are sensitive to the FA pathway inhibitor curcumin.	154
Figure 3.12	Combined inhibition of the FA pathway and PARP as a treatment strategy in the absence of conventional DNA damaging therapy.	155
Figure 4.1	Cambridge primary, patient-derived glioblastoma stem cell lines.	183
Figure 4.2	Stem cell marker expression in Cambridge primary, patient-derived glioblastoma stem cell lines.	184

Figure 4.3	2- and 3-dimensional colony formation and response to ionizing radiation in Cambridge patient-derived glioblastoma stem cells.	185
Figure 4.4	Derivation of Sheffield patient-derived glioblastoma stem cell lines.	189
Figure 4.5	Comparison of stem cell marker expression in Sheffield primary GSCs, Cambridge primary cell lines and established commercial glioblastoma cell lines.	190
Figure 4.6	Derivation of Sheffield *ex vivo* random heterogeneity GSC models and representative pictures.	191
Figure 4.7	Derivation of Sheffield *ex vivo* resected and residual GSC models with representative pictures.	193
Figure 4.8	Differences in connecting tumour microtube formation between Sheffield *ex vivo* resected and residual GSC models.	195
Figure 4.9	2- and 3-dimensional colony formation with Sheffield *ex vivo* resected and residual GSC models.	196
Figure 4.10	Stem cell marker expression in Sheffield *ex vivo* resected and residual GSC models.	198
Figure 4.11	Expression of DDR and 'stemness' genes in Sheffield *ex vivo* resected and residual GSC models.	198
Figure 4.12	Inovitro™ preclinical TTFields delivery equipment and early efficacy.	199
Figure 4.13	Conceptual representation of an *ex vivo* 3D scaffold-based TTFields culture and delivery system to replace animal studies.	200
Figure 4.14	Feasibility of TTFields delivery to cells within a 3D culture system.	202
Figure 4.15	The Sheffield Living Biobank cohort survival.	210
Figure 5.1	mRNA expression of FA pathway genes increases with glioma grade.	218
Figure 5.2	Canonical association of mRNA expression levels for FA pathway functional complexes is apparent in gliomas.	219
Figure 5.3	High mRNA expression of FA pathway functional groups is associated with poor overall survival in glioma patients.	221

Figure 5.4	FA pathway mRNA expression is elevated in patient-derived glioblastoma stem cells.	223
Figure 5.5	The dynamics of FA pathway activation following temozolomide chemotherapy in 2D patient-derived glioblastoma stem cells.	224
Figure 5.6	The dynamics of related DNA damage response processes following temozolomide chemotherapy in 2D patient-derived glioblastoma stem cells.	225
Figure 5.7	Ouabain effect on cell viability in established glioblastoma cultures following 24 hour and 120 hour exposure.	227
Figure 5.8	Ouabain effect on clonogenic survival in primary, patient-derived glioblastoma stem cells following 24 hour and 120 hour exposure.	227
Figure 5.9	The 'heart failure' medication ouabain inhibits the FA pathway in 2D established and primary, patient-derived glioblastoma stem cells.	228
Figure 5.10	The cardiac glycoside ouabain sensitises 2D established and primary, patient-derived glioblastoma cultures to radiotherapy.	230
Figure 5.11	The 'heart failure' medication ouabain augments radiation-induced γH2AX foci formation in glioblastoma stem cells.	230
Figure 5.12	Maximal effect of the novel FA pathway inhibitor F76 and curcumin on clonogenic survival in 2D primary, patient- derived glioblastoma stem cells.	231
Figure 5.13	The novel FA pathway inhibitor F76 reduces FANCD2 monoubiquitination in 2D primary, patient-derived glioblastoma stem cells following DNA damage.	231
Figure 5.14	Effects of the novel FA pathway inhibitor F76 on radiosensitivity in 2D primary, patient-derived glioblastoma stem cells.	232
Figure 5.15	Curcumin inhibits the FA pathway in 2D primary, patient-derived glioblastoma stem cell cultures.	233
Figure 5.16	Optimising FA pathway inhibition using curcumin following DNA damage in 3D scaffold-based glioblastoma stem cell cultures.	234

Figure 5.17	Combined FA pathway and PARP inhibition enhances radiosensitisation in 2D primary, patient-derived glioblastoma stem cells.	236
Figure 5.18	Combined FA pathway and PARP inhibition enhances radiosensitisation in 3-dimensional Alvetex™ scaffold- based glioblastoma stem cell models.	237
Figure 5.19	Combined FA pathway and PARP inhibition modifies α/β ratios in 3-dimensional Alvetex™ scaffold-based glioblastoma stem cell models.	239
Figure 5.20	Combined FA pathway and PARP inhibition enhance radiation-induced γH2AX in 3-dimensional Alvetex™ scaffold-based glioblastoma stem cell models.	240
Figure 5.21	Combined FA pathway and PARP inhibition delays resolution of radiation-induced γH2AX foci in G7 3-dimensional Alvetex™ scaffold-based glioblastoma stem cell models.	241
Figure 5.22	Combined FA pathway and PARP inhibition enhances temozolomide sensitisation in 3-dimensional Alvetex™ scaffold-based glioblastoma stem cell models.	243
Figure 5.23	Inhibition of ATR and ATM in 2D primary, patient-derived glioblastoma stem cell cultures.	245
Figure 5.24	Combined FA pathway and ATR or ATM inhibition enhances radiosensitisation in G7 3-dimensional Alvetex™ scaffold-based glioblastoma stem cell models.	247
Figure 5.25	The effects of combined FA pathway and ATR or ATM inhibition on temozolomide sensitivity in G7 3-dimensional Alvetex™ scaffold-based glioblastoma stem cell models.	249
Figure 5.26	Combined FA pathway and PARP or ATR inhibition augment DNA damage and delay repair in 2D G7 primary, patient-derived glioblastoma stem cells.	252
Figure 5.27	Combined FA pathway and PARP or ATR inhibition augment DNA damage and delay repair in 2D G7 primary, patient-derived glioblastoma stem cells (comet tail moment).	254

Figure 5.28	Summary of the kinetics of DNA damage and repair in 2D G7 primary, patient-derived glioblastoma stem cells treated with FA pathway based DDRi combinations.	255
Figure 5.29	Specificity of S.9.6 staining for RNA:DNA hybrids and effects of replication stress-inducing positive controls.	259
Figure 5.30	Combined FA pathway and ATR inhibition generates additional RNA:DNA hybrids in 2D G7 primary, patient-derived glioblastoma stem cells.	260
Figure 5.31	The effects of FA pathway, PARP and ATR inhibition on cell cycle progression in 2D G7 primary, patient- derived glioblastoma stem cells.	264
Figure 5.32	The effects of FA pathway, PARP and ATR inhibition on cell cycle progression in 2D G1 and G7 primary, patient-derived glioblastoma stem cells (representative cell cycle profiles).	265
Figure 5.33	FA pathway molecular alterations in 603 glioblastoma samples (TCGA cohort).	276
Figure 5.34	Schematic summary of models developed and FA pathway-based DDRi combinations investigated.	283
Figure 6.1	Schematic for planned studies using resected and residual 3D GSC models to evaluate therapeutic combinations targeting the DNA damage response.	293
Figure 6.2	Schematic representation and feasibility of *ex vivo* single-cell drug response profiling for solid tumours.	295
Figure 6.3	Schematic representation of studies using comprehensive genetic profiling of the Sheffield Living Biobank to understand and predict patient-specific responses to novel therapies.	296

List of Supplementary Figures

		PAGE
Supplementary Figure 5.1	The 'heart failure' medication ouabain inhibits the FA pathway in G7 glioblastoma stem cells at 250nM but not at 100nM.	284
Supplementary Figure 5.2	Combined FA pathway and ATR inhibition provides similar radiosensitisation to combined inhibition of PARP and ATR, but with less toxicity in the absence of irradiation in G7 3-dimensional Alvetex™ scaffold- based glioblastoma stem cell models.	284

List of Tables

		PAGE
Table 1.1	Commonly used models in preclinical glioblastoma research.	51
Table 2.1	General laboratory equipment.	78
Table 2.2	Consumables.	79
Table 2.3	Reagents.	81
Table 2.4	Inhibitors and cytotoxic agents.	84
Table 2.5	Proprietary compounds.	84
Table 2.6	Primary antibodies.	85
Table 2.7	Secondary antibodies.	87
Table 2.8	TaqMan™ gene expression probes for quantitative PCR.	87
Table 2.9	Standard solutions.	88
Table 2.10	List of Neurosurgeons providing brain tumour specimens for research.	92
Table 2.11	Matrigel™ coating plasticware.	95
Table 2.12	MTT cell plating densities.	98
Table 2.13	Seeding densities for G1, G7 & E2 glioblastoma stem cell lines treated with radiotherapy.	100
Table 2.14	Seeding densities for G1, G7 & E2 glioblastoma stem cell lines treated with temozolomide chemotherapy.	100
Table 2.15	Lysis buffer.	105
Table 2.16	Reverse transcription reaction mix.	112
Table 2.17	Reverse transcription PCR programme for cDNA.	113
Table 3.1	PARP inhibitor trials in high-grade glioma.	131
Table 3.2	ATM inhibitor trials in high-grade glioma.	134
Table 3.3	Summary of previously established sensitisation activity during early SAR studies.	144
Table 4.1	Towards a living biobank of patient-derived glioblastoma stem cell models – clinicopathological features of the Sheffield lines.	187

List of Equations

		PAGE
Equation 2.1	Percentage of DNA in comet tail.	116
Equation 2.2	Comet tail moment.	116
Equation 2.3	The linear-quadratic (LQ) model.	117
Equation 2.4	Calculation of sensitiser enhancement ratios.	117
Equation 2.5	Non-linear regression for temozolomide clonogenic studies.	117

List of Publications & Manuscripts

Rominiyi O, Myers K, Lad N, Dar D, Vanderlinden A, Gomez-Roman N, Jellinek DA, Chalmers AJ, Carroll TA, Chen B, Al-Tamimi Y & Collis SJ. *FA pathway-based combinations targeting the DNA damage response to enhance chemotherapy and radiotherapy response in glioblastoma stem cells*. Details: *Manuscript in preparation.*

Rominiyi O, Al-Tamimi Y & Collis SJ. *Future therapeutic strategies targeting the DNA damage response in glioblastoma*. Details: *Manuscript (review article) in preparation.*

Rominiyi O, Dar D, Vanderlinden A, Bagga V, Myers K, Gomez- Roman N, Jellinek DA, Carroll TA, Chalmers AJ, Al-Tamimi Y & Collis SJ. *Ex vivo 3-dimensional models of post-surgical residual disease in human glioblastoma*. **Journal of Visualized Experiments (2020)**. Manuscript invited by the editor: submission scheduled September 2020. Details: Outlines our unique pragmatic methodology which uses surgical dissection of rare *en-bloc* tumour specimens to liberate cancerous cells from infiltrated brain adjacent to a brain tumour. These are used to model cancer cells normally left behind after surgery, and should help better understand why glioblastoma comes back despite best current treatment.

Rominiyi O*, Vanderlinden A*, Clenton S, Bridgewater B, Al-Tamimi Y & Collis S. *Tumour Treating Fields for the treatment of glioblastoma: new advances and future directions.* **British Journal of Cancer (2020)**. Online ahead of print (https://doi.org/10.1038/s41416-020-01136-5). *Denotes joint first authors. Details: Comprehensive review summarising recent clinical and preclinical developments in TTFields research with notable emphasis on the emerging DDR modulatory effects of TTFields.

Rominiyi O, Al-Tamimi Y & Collis S. *The 'Ins and Outs' of Early Preclinical Models for Brain Tumor Research: Are They Valuable and Have We Been Doing It Wrong?* **Cancers (2019)** 11(3):426-428. Details: Mini-review highlighting the value of clinically-relevant in-vitro 3D models for brain tumour research, and desirable advances for the field including models we are currently developing.

Hardman S, **Rominiyi O**, King D & Snelson E. *Is cranial computed tomography unnecessary in children with a head injury and isolated vomiting?* **BMJ (2019)** 365:l1875. Details: Estimates the risk of developing a brain tumour (or other malignancy) following CT head scan and provides evidence to support avoiding unnecessary scans in a specific group of children – includes a systematic review. Featured on **'Front Cover'** and as **'Editor's Choice'** (https://doi.org/10.1136/bmj.l2288).



Patil AA, Sellwood MA, **Rominiyi O**, Sayal P, Jellinek DA, Carroll TA, Chen B & Collis SJ. *A novel class of Fanconi Anaemia small molecule inhibitors potentiate temozolomide cytotoxicity in high-grade gliomas.* Details: Currently embargoed due to university IP protection and patenting processes.

List of Published Abstracts

Rominiyi O, Myers K, Gomez-Roman N, Lad N, Dar D, Jellinek DA, Chalmers AJ, Carroll TA, Chen B, Al-Tamimi Y & Collis SJ. *The Fanconi anaemia (FA) pathway and glioblastoma: a new foundation for DNA damage response targeted combinations.* **Neuro-Oncology (2019)** 21(supp_6):vi209. https://doi.org/10.1093/neuonc/noz175.871.

Rominiyi O, Myers K, Vanderlinden A, Dar D, Bagga V, Gomez-Roman N, Jellinek DA, Carroll TA, Chalmers AJ, Al-Tamimi Y & Collis SJ. *Ex-vivo 3-dimensional models of post-surgical residual disease in human glioblastoma.* **Neuro-Oncology (2019)** 21(supp_6):vi271. https://doi.org/10.1093/neuonc/noz175.1138.

Rominiyi O, Gomez-Roman N, Lad N, Al-Tamimi Y, Jellinek DA, Chalmers AJ, Carroll TA, Chen B & Collis SJ. *Preclinical evaluation of combinations targeting the DNA damage response in 2D and 3D models of glioblastoma stem cells.* **Neuro-Oncology (2018)** 20(supp_3):iii297. https://doi.org/10.1093/neuonc/noy139.308.

Rominiyi O, Gomez-Roman N, Lad N, Al-Tamimi Y, Jellinek DA, Chalmers AJ, Carroll TA, Chen B & Collis SJ. *FA-based combinations to target the DNA damage*

response in glioblastoma. **Neuro-Oncology (2018)** 20(supp_5):v358. https://doi.org/10.1093/neuonc/noy130.066 .

Rominiyi O, Gomez-Roman N, Lad N, Al-Tamimi Y, Jellinek DA, Chalmers AJ, Carroll TA, Chen B & Collis SJ. *Combinations targeting the DNA damage response to treat glioblastoma.* **British Journal of Neurosurgery (2018)** 32(2):228. https://doi.org/10.1080/02688697.2018.1463666.

List of Presentations

Society of Academic & Research Surgery (SARS) Annual Meeting, Dublin, Ireland.
Towards a living biobank of surgically-relevant 3-dimensional glioblastoma stem cell models to evaluate novel therapeutics and interrogate intratumoural heterogeneity. Date scheduled: 19-20th March 2020 – *meeting postponed due to COVID-19 pandemic*. Selected to present in RCS Fellows session (Oral).

Society for Neuro-Oncology (SNO) 24th Annual Meeting, Phoenix, Arizona, USA.
The Fanconi anaemia (FA) pathway and glioblastoma: a new foundation for DNA damage response targeted combinations (Oral) on 24th November 2019.
Ex-vivo 3-dimensional models of post-surgical residual disease in human glioblastoma (Poster) on 23rd November 2019.

British Neurosurgical Research Group Meeting (BNRG), Edinburgh, UK.
The Fanconi anaemia (FA) pathway and glioblastoma: a new foundation for DNA damage response targeted combinations (Oral) on 7th November 2019.
Ex-vivo 3-dimensional models of post-surgical residual disease in human glioblastoma (Oral) on 7th November 2019.

Inovitro™ Meeting, Haifa, Israel.
Developing a 3-dimensional scaffold-based system to assess Tumour Treating Fields (TTFields) using patient-derived cancer stem cells (Invited Oral) on 3rd July 2019.

York Medical Society, York, UK.
Malignant tumours invading the anterior skull base: a single-institutional review of clinical management over one decade and long-term outcomes (Selected Oral) on 5th April 2019.

AACR-Novocure Users Group Meeting, Atlanta, Georgia, USA.

Combinations targeting the DNA damage response to enhance Tumour Treating Fields in 2D and 3D models of glioblastoma (Oral) on 30th March 2019.

13th Meeting of the European Association of Neuro-Oncology, Stockholm, Sweden.
Preclinical evaluation of combinations targeting the DNA damage response in 2D and 3D models of glioblastoma stem cells (Poster) on 11-14th October 2018.

British Neuro-Oncology Society Annual Meeting, Winchester, UK.
FA-based combinations to target the DDR in glioblastoma (Poster) on 4-6th July 2018.

The University of Sheffield Medical School Research Meeting, Sheffield, UK.
Combinations targeting the DDR to treat glioblastoma (Oral & Poster) on 14-15th June 2018.

Genomics and Personalisation of Cancer Care Conference, Leeds, UK.
Post-operative consent pathway: a perspective from Neurosurgery (Invited Oral) on 18th May 2018.

British Neurosurgical Research Group Meeting 2018, Sheffield, UK.
Combinations targeting the DNA damage response to treat glioblastoma (Poster) on 8-9th March 2018.

Awards and Prizes during PhD

Learned Society Fund Conference Award: to attend and present at the Society for Neuro-Oncology Annual Meeting 2019, Phoenix, Arizona – awarded £750.

'Founders Prize' at York Medical Society. Awarded 5th April 2019. Awarded £50 prize.

Royal College of Surgeons Travel Fellowship: to present at the 13th Annual Meeting of the European Association of Neuro-Oncology 2018, Stockholm, Sweden – awarded £500.

NC3R's Poster Presentation Competition Winner: for implementation of customized 3D Alvetex™ patient-derived glioblastoma stem cell models at TUoS Medical School Research Meeting 2018 – awarded £50 voucher.

Oral Presentation 2nd Prize: 'Combinations targeting the DNA damage response to treat glioblastoma' at TUoS Medical School Research Meeting 2018 – awarded £150 prize.

Learned Society Fund Conference Award: to attend and present at the British Neurosurgical Research Group Meeting 2018, Sheffield – awarded £165.

Royal College of Surgeons Research Training Secondment: to fund research training in 3D models of glioblastoma during a 6-week secondment in Prof. Anthony Chalmers' Laboratory 2018, Wolfson Wohl Cancer Research Institute, The University of Glasgow – awarded £3,000.

Poster Prize: awarded at Health Education England – Yorkshire and the Humber Academic Trainee Conference 2017.

List of Research Funding Secured

Detecting a 'pink drink' in the blood as an early warning system for brain tumours. *Sheffield NIHR Biomedical Research Centre (BRC)* – co-funded with SHC/WPCC (see below). Awarded £11,852 (co-PI with Dr C Bridgewater and Dr S Collis) – 2020-2022.

DNA methylation-based classification and retrospective analysis of clinically aggressive meningiomas: a pilot study. *Neurocare*. Awarded £9,700 (co-I with Mr Yahia Al-Tamimi) – 2020-2021.

Detecting a 'pink drink' in the blood as an early warning system for brain tumours. *Sheffield Hospitals Charity & Weston Park Cancer Charity (SHC/WPCC) Research Fund* – co-funded with Sheffield NIHR BRC (see Above). Awarded £55,928 (co-PI with Dr C Bridgewater and Dr S Collis) – 2020-2022.

***Ex vivo* drug screening using human tissue to personalise cancer therapy and replace murine avatars.** *NC3Rs PhD Studentship*. Awarded £90,000 (co-I with Professor T Helleday, Dr J Rantala and Dr S Collis) – 2020-2023. Link: https://nc3rs.org.uk/ex-vivo-drug-screening-using-human-tissue-personalise-cancer-therapy-and-replace-murine-avatars.

A living biobank of post-surgical residual glioblastoma to replace animal studies. *NC3Rs PhD Studentship*. Awarded £90,000 (co-PI with Dr S Collis) – 2020-2023. Link: https://nc3rs.org.uk/living-biobank-post-surgical-residual-glioblastoma-replace-animal-studies.

***Ex vivo* 3-dimensional models of post-surgical residual disease in glioblastoma to improve biological understanding and treatment.** *The Brain Tumour Charity – Expanding Theories*. Awarded £119,935 (co-PI with Dr S Collis) – 2020-2022. Link: https://www.thebraintumourcharity.org/brain-tumour-diagnosis-treatment/types-of-brain-tumour-adult/glioblastoma/glioblastoma-research/new-3d-models-invading-glioblastoma/.

Combinations targeting the DNA damage response to enhance Tumour Treating Fields in 2D and 3D models of glioblastoma stem cells. *Novocure*. In-kind award of equipment and training – value ~ $50,000 (co-PI with Dr Spencer Collis) – 2019-2022.

Combining TTFields with therapeutic DDRi for the improved treatment of brain tumours. *Faculty PGT-PGR PhD Scholarship* – awarded to Miss Aurelie Vanderlinden. Value ~£60,000 (co-I with Dr Spencer Collis) – 2019-2022.

Combining TTFields with therapeutic DDRi for the improved treatment of brain tumours. *Sheffield NIHR Biomedical Research Centre Strategic funding award*. Awarded £15,000 (co-I with Dr Spencer Collis) – 2019-2022.

FA/BRCA-based combinations to target the DNA damage response in 3-dimensional glioblastoma stem cells. *Neurocare & Sheffield Hospitals Charity – Clinical Research Fellowship* (PhD Year 3). Awarded £76,474 (co-PI with Dr Spencer Collis) – 2018-2019.

Specialist equipment to test novel treatments in 3D models. *Weston Park Cancer Charity*. Awarded £2,162 (co-PI with Dr Spencer Collis) – 2018-2019.

Disrupting DNA repair in brain tumours: a two-pronged approach. *Sheffield Hospitals Charity* (PhD Year 2). Awarded £13,000 (co-PI with Dr Spencer Collis) – 2017-2018.

3-Dimensional glioma models to develop novel therapeutic combinations. *Royal College of Surgeons – One-Year Surgical Research Fellowship* (PhD Year 2). Awarded £63,035 (co-PI with Dr Spencer Collis) – 2017-2018. Link: https://www.rcseng.ac.uk/standards-and-research/research/fellowships-awards-grants/fellowships/current-and-past/one-year-fellowships-2017-2018/#mrolamiderominiyi.

Disrupting DNA repair in brain tumours: a two-pronged approach. *Neuroscience Research Fund (by Sheffield Hospitals Charity)* – co-funded with YBTC (PhD Year 1). Awarded £12,600 (co-PI with Dr Spencer Collis) – 2016-2017.

Disrupting DNA repair in brain tumours: a two-pronged approach. *Yorkshire's Brain Tumour Charity (YBTC; formerly Brain Tumour Research and Support across Yorkshire, BTRS)* – co-funded with SHC. Awarded £18,975 (co-PI with Dr Spencer Collis) – 2016-2019. Link: https://www.yorksbtc.org.uk/Loving-Research/Research/Previous-Research-Stories/OLa-Rominiyi.

Chapter 1 – Introduction

1 CHAPTER 1 – Introduction

Brain tumours kill 5,000 people each year in the UK alone, and are responsible for the greatest reduction in life expectancy of any cancer – around 20 years on average[5,6]. Glioblastoma multiforme (glioblastoma, grade IV glioma), the most frequently diagnosed primary brain tumour in adults, is associated with an exceptionally poor clinical course characterised by treatment resistance, disease recurrence and death[7-9]. Current multimodal therapy, for glioblastoma consists of maximal safe surgical resection followed by radiotherapy and chemotherapy with concomitant and adjuvant temozolomide[10,11]. In this context, median survival is 14.6 months with less than 10% of patients surviving more than 5 years[11].

In most cases, glioblastoma arise rapidly in the absence of histological or clinical evidence of a less malignant precursor. In a minority, signs of progression from a lower grade diffuse (WHO grade II) or anaplastic (WHO grade III) astrocytoma are evident. However, classification and representation of these tumours increasingly relies on the molecular characterisation of inherent genetic aberrations[12]. This bares colossal implications for future therapeutic strategies intended to supersede the present treatment paradigm, which has not changed substantially over the last decade.

Effective future therapies for glioblastoma will need to tackle the biological mechanisms that enable treatment resistance in these aggressive cancers. The remarkable degree of intratumoural heterogeneity glioblastoma exhibit provides an assemblage of spatiotemporally divergent subpopulations with varying profiles of vulnerability and resistance within a given tumour[13-15]. Consequently, it seems intuitive that intratumoural heterogeneity contributes to inevitable local disease recurrence and progression in glioblastoma. Increasing evidence alludes to minority subpopulations possessing an innate capacity for unlimited regeneration and self-renewal[16,17]. Often described as cancer stem cells (CSCs) or glioblastoma stem cells (GSCs), these cells are deemed responsible for resistance to conventional chemoradiotherapy through augmented DNA damage checkpoint activation and DNA repair[18,19].

Temozolomide, the most commonly used chemotherapy for glioblastoma, engenders DNA damage through methylating DNA bases at specific oxygen and nitrogen positions. These

lesions impede DNA replication and previous research has demonstrated that the Fanconi anaemia (FA) pathway of DNA damage repair promotes resistance to alkylating chemotherapy, including temozolomide[20],[21,22]. The FA pathway is the principle cellular mechanism for ICL repair and helps to avoid the failure of strand separation followed by deleterious DNA breakage and chromosomal rearrangements that would ensue in the context of unrepaired ICLs[23],[2]. However, FA pathway proteins also have broader functions in genome maintenance including the stabilization of replication forks and regulation of cytokinesis[2]. Indeed, even radiotherapy doses below 1 Gy elicit robust localization of FA pathway proteins to stalled replication forks and DNA double strand breaks (DSBs) during S-phase[24]. A finding consistent with the reported radiosensitivity, in addition to well described profound chemosensitivity, in tissues of patients with Fanconi anaemia[25-27]. Therefore, the prospect of manipulating cancer cells therapeutically to adopt a sensitivity profile similar to patients with FA is highly attractive.

High-grade gliomas appear to exhibit re-expression of an active FA pathway, in contrast to healthy brain tissue and benign schwannomas[22]. Furthermore, expression levels of FANCD2 (a quantifiable marker of FA pathway activity) are strongly correlated with tumour grade in adult gliomas[22]. Taken together, its role in genome maintenance and reactivation in more aggressive tumours make the FA pathway a particularly appealing therapeutic target specifically in glioblastoma. The objectives of manipulating FA pathway activity within a putative therapeutic strategy include enhancing sensitivity to conventional adjuvant therapy or potentially reducing the dose of chemotherapy or radiation required to achieve optimal clinical response. Additionally, since the FA pathway interacts with a range of other possible targets within the collective cellular DNA damage response (DDR), there is a conceivable theoretical basis for effective therapeutic strategies targeting a combination of DDR mediators to: overwhelm mechanisms of resistance; improve treatment responses; and/or potentially obviate the need for traditional chemoradiotherapy.

Here an overview of glioblastoma and the DDR is provided, however further discussion of potential therapeutics which target the DDR in glioblastoma is detailed in Chapter 3 (Section 3.1). In this Chapter, particular emphasis is given to the FA pathway, and its potential for manipulation towards therapeutic gain in glioblastoma is detailed. Firstly, the molecular and phenotypic characteristics of these aggressive tumours are described in the context of other glial neoplasms arising in the central nervous system (CNS). Present therapeutic strategies

for glioblastoma are detailed. Subsequently, a brief overview of key experimental models utilised in preclinical glioblastoma research is provided as a prelude to Chapter 4 (Section 4.1) in which the relative merits of various 2- and 3-dimensional (3D), clinically-relevant *in vitro* models of glioblastoma are reviewed further. Finally, cellular responses to DNA damage will be considered here with a focus on how these can be exploited to develop novel treatments for glioblastoma.

1.1 Central nervous system tumours

Tumours arising from the CNS have an annual age-adjusted incidence of 28.6 per 100,000[28]. Of clinical relevance, these neoplasms can be broadly categorised into two groups: those situated within the substance of the brain or spinal cord (often referred to as intrinsic or intra-axial) and those emerging from tissues that enclose or are adjacent to the neuro-axis (often described as extrinsic or extra-axial lesions). Although extrinsic tumours are diagnosed with greater frequency, most are benign lesions which portend good survival, including: tumours arising from the meningeal coverings of the brain (meningiomas); those arising from the pituitary gland; and nerve sheath tumours (schwannomas).

Intrinsic tumours arising from within the brain or spinal cord originate from either neurons or glial cells, most of which are astrocytes and oligodendrocytes. In contrast to neurons, which rarely divide in the mature CNS and retain only a small stem cell fraction, glial cells maintain the propensity to proliferate throughout life[29]. Consequently, it is perhaps unsurprising that the vast majority of primary brain tumours are of glial origin. Figure 1.1 illustrates the lineage of common tumours arising within the CNS.

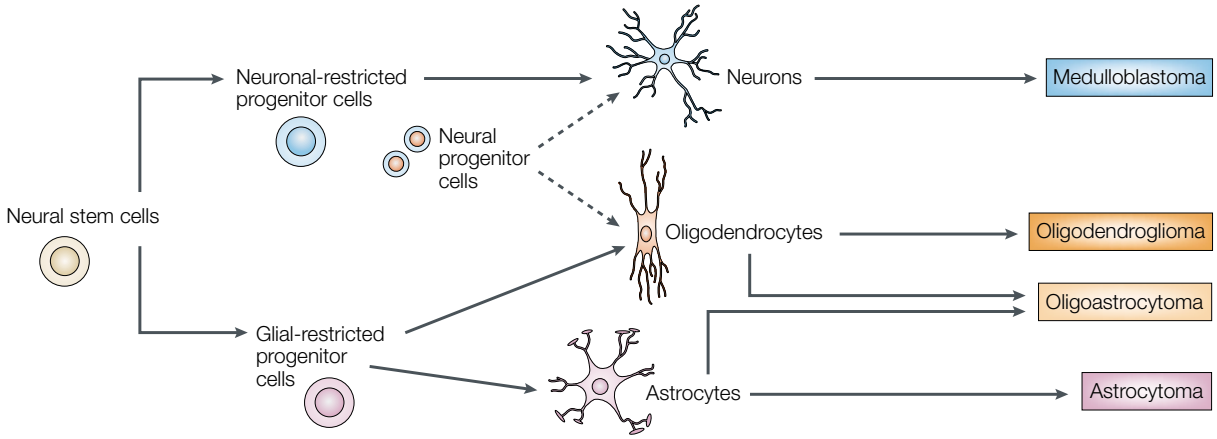


Figure 1.1: The categorization and origins of common central nervous system tumours – Glial tumors of the CNS are named on the basis of the mature cell of origin they arise from, namely astrocytes or oligodendrocytes. These are thought to share a distinct progenitor cell which arises from multipotent neural stem cells. True oligoastrocytomas, containing distinct astrocytic and oligodendroglial components exist, but are found to be less common than diagnosed in the past, since increased use and accuracy of molecular testing has enabled more tumours to be categorically defined as either

astrocytoma or oligodendroglioma[12]. Some brain tumours, such as medulloblastoma, arise from a neuronal lineage. These neoplasms tend to be most prevalent in children. *Adapted from Zhu et al. (2002)*[29].

Clarification is often required when using the term 'CNS tumour' as numerous sources, including the WHO, accommodate all intrinsic and extrinsic tumours within this umbrella term[12]. However, others use the term purely in reference to those (intrinsic) tumours arising from the substance of the brain or spinal cord[9]. Differences in categorisation likely contribute to the variability observed in published epidemiological data[28], but of greater concern, have the potential to cause confusion for patients and families faced with a brain tumour diagnosis. Here, to aid simplicity, the term 'brain tumour' (rather than CNS tumour) will be used to refer to tumours found in the brain. The term 'primary brain tumour' is used to describe those originating from within the substance of the brain, in contrast to 'secondary brain tumours' which occur as a result of metastasis from an extra-cranial malignancy. And finally, the term 'glioma' refers to primary brain (or spinal cord) tumours arising specifically from glial cells. Gliomas are reported to arise with an annual incidence of 6.6 per 100,000[28].

1.1.1 Molecular classification of gliomas

Prior to this decade, the classification of gliomas was based almost exclusively on histopathological features. Although this approach has served clinicians and scientists for many years, it is hampered by considerable inter-observer variability with the risk of under- or over-treatment of patients since treatment decisions were based on histological diagnosis and grading, which are susceptible to a degree of subjectivity[30]. The increasing sophistication and availability of molecular diagnostic techniques has enabled a fundamental shift in the way gliomas are classified. 'The 2016 World Health Organization Classification of Tumours of the Central Nervous System'[12] represents a landmark advance in glioma categorisation. Building on increasing understanding of the mutational landscape in various gliomas, garnered from comprehensive studies which utilised genome-wide molecular profiling[31-35], the updated WHO classification revolutionised diagnosis with the incorporation of clinically validated molecular information in a multi-layered approach. The final 'integrated diagnosis' provided by this approach represents a composite of: histological tumour type (Layer 1); histological tumour grade (Layer 2); and results of molecular testing for diagnostic biomarkers (Layer 3). Figure 1.2 provides an overview of the integrated molecular and histological classification of gliomas.

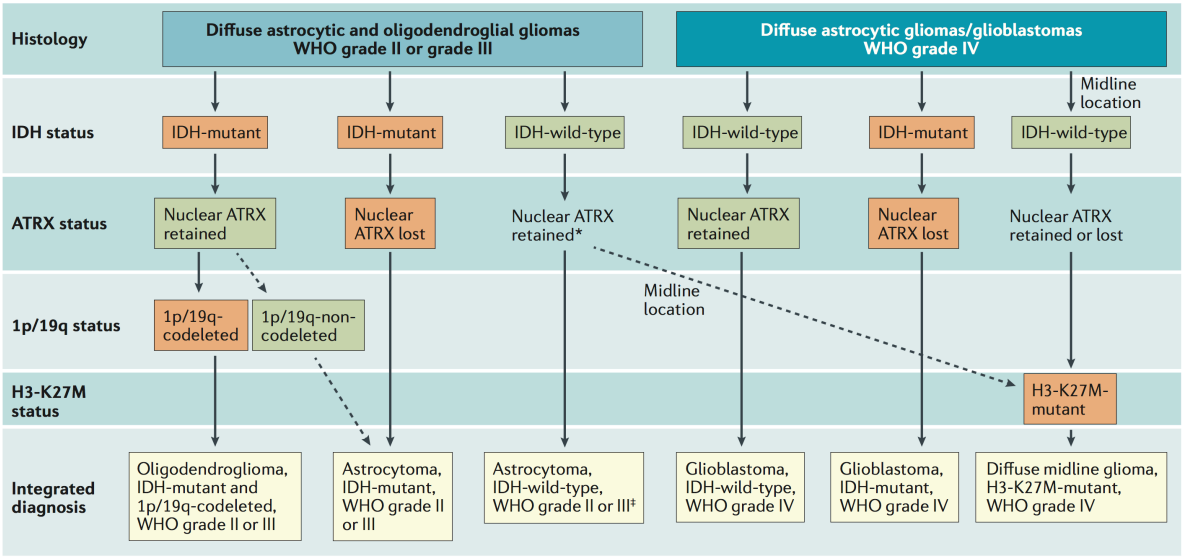


Figure 1.2: Integrated histological and molecular classification of diffuse gliomas based on the '2016 WHO Classification of Tumours of the Central Nervous System' – Histological tumour type, including 'astrocytic' or 'oligodendroglial', represents the first 'Layer' of formal WHO integrated diagnosis for CNS tumours. 'Layer 2' consists of histological tumour grade – tumours are graded on the basis of general histological features including: nuclear abnormalities, growth rate, state of differentiation, neovascularization and necrosis. Tumours are allocated a grade between I-IV, with WHO grade IV representing the most aggressive tumours. Conventionally, WHO grade III & IV gliomas are often described collectively as 'high-grade gliomas'. Finally, 'Layer 3' includes genetic aberrations of diagnostic significance. In some cases, these have become definitional of a tumour type – for example, a WHO grade II or III glioma confirmed to be IDH-mutant and chromosome 1p/19q-codeleted is now invariably described as oligodendroglioma. Key diagnostic mutations are discussed below. *Adapted from Reifenberger et al. (2017)*[36].

Since prevailing evidence suggests that molecular classification of gliomas is more predictive of clinical outcome than histological category[34,35,37], it is almost certain that this information will assume an ever-increasing significance in research and clinical management for these tumours.

Neomorphic mutation of the metabolic enzymes – isocitrate dehydrogenase (IDH) 1 and 2 are worthy of specific mention. IDH mutation occurs in the majority of WHO grade II-III gliomas[12] and a minority, but characteristically distinct, subset of glioblastoma (WHO grade IV). Positive mutational status provides IDH with an acquired ability to convert α-ketoglutarate (αKG) to R(-)-2-hydroxyglutarate (2-HG). Increasing evidence suggests that raised levels of 2-HG, of confirmed prevalence in gliomas[38], may function as an 'oncometabolite'. Specifically, 2-HG competitively inhibits αKG-dependent dioxygenases including ten-eleven translocation (TET) family 5-methylcytosine hydroxylases and the Jumonji-C-domain-containing histone-lysine demethylases[36,38,39]. This leads to abnormal levels of DNA and histone methylation culminating in widespread hypermethylation of CpG islands often referred to as the 'glioma CpG island methylator phenotype' (G-CIMP). *IDH1* mutations and G-CIMP portend improved patient outcome across all glioma grades, and with reference to glioblastoma, appear to belong to the proneural subgroup (discussed

below) exclusively[40]. Approximately 90% of IDH mutated gliomas harbour a common heterozygous missense mutation resulting in substitution of arginine to histidine (IDH1-R132H) [41]. Clinically, this mutation is most commonly detected via immunohistochemistry (IHC) from paraffin-embedded tumour sections. However, immunonegative tumours in patients below the age of 55 years usually require DNA sequencing to exclude alternative, less prevalent *IDH1* or *IDH2* mutations[12]. Interestingly, novel inhibitors of IDH1 (ivosidenib) and IDH2 (enasidenib) have been found to promote cancer cell differentiation and improve outcome in patients with treatment refractory AML[42,43], but these drugs appear to be much less effective in gliomas[44]. Indeed, paradoxically the effects of *IDH1/2* mutation in the context of glioma may be causally implicated in relatively enhanced survival since 2-HG inhibits homologous recombination (HR) DNA repair to promote a 'BRCAness' phenotype and therefore may underlie enhanced sensitivity to conventional chemoradiotherapy and DNA damage response inhibitors (DDRi) including PARP inhibitors (PARPi) and ATR inhibitors (ATRi)[44,45].

ATRX mutation results in a loss of the nuclear expression of this important chromatin remodelling factor, which can be detected using IHC. These mutations are more common in paediatric gliomas of astrocytic lineage, but can also occur in adult high-grade gliomas where they appear to be associated with *IDH1* and *TP53* mutations. Interestingly, gliomas with mutations in *ATRX* almost exclusively eschew the use of telomerase to avoid replicative senescence, and instead display evidence of telomere lengthening via an alternative HR-mediated mechanism – termed 'alternative lengthening of telomeres' (ALT)[46]. ALT is associated with high levels of genomic instability, however loss of *ATRX* in isolation is insufficient to drive ALT, and additional genetic or epigenetic modifications are thought to be required[47]. Mutations in the histone variant H3.3 (*H3F3A),* including the H3.3K27M mutant, appear to be related to *ATRX* mutations with the two often co-existing[46]. These allude to a role for overarching ATRX/DAXX/H3.3 histone deposition pathway dysfunction underling the pathology of a subset of gliomas. The development of ALT-positive cancer appears to require both H3.3 mutation and either ATRX or DAXX mutation (which are mutually exclusive)[48-50]. Interestingly, components of the FA pathway appear to be implicated in facilitating HR-mediated maintenance of telomeres during ALT, for example FANCD2 co-localises with TRF1 (a component of the shelterin complex which is inherently associated with telomeres) in a FANCA, FANCL and ATR-dependent manner[51,52]. Additionally, ribosylation-mediated displacement of TRF1 from telomeres (which is

indirectly influenced by FANCD2, via tankyrase 1[53]) permits FANCP/SLX4 to nucleolytically resolve T-loop structures[54], whilst FANCM appears to be critical for the maintenance of ALT-driven cancers[48]. These raise the possibility that therapeutic targeting of the FA pathway could be particularly effective in gliomas with loss of *ATRX*.

Although assessment of these genetic features is now integrated into clinical diagnostics, emerging molecular alternatives may hold the potential to further enhance diagnostic accuracy and fidelity. For example, the use of DNA methylation-based classification has recently been demonstrated to complement existing molecular diagnostics, enabling the refinement of diagnostic criteria for existing entities, more robust subclassification (with prognostic implications in the case of ependymomas), and discovery of putative new entities[55-57].

1.2 Characterisation and treatment of glioblastoma

1.2.1 Glioblastoma: an unmet clinical need

Diagnoses of glioblastoma arise with an incidence of 3.19 per 100,000 adults per year[58]. These tumours account for just over half of primary brain tumours[9] but influence poor survival disproportionately due to an inherently aggressive nature. Survival rates for primary brain tumours collectively over the last 40 years demonstrate a paucity of improvement. This contrasts markedly with the doubling of patient survival seen in other cancers such as breast cancer and melanoma over the same period, as illustrated in Figure 1.3. The disparity is likely contributed to by comparatively low investment in brain tumour research and has led to the designation of brain tumours as a 'cancer of unmet need' by numerous charities including Cancer Research UK (CRUK), Brain Tumour Research and The Brain Tumour Charity. Given the exceptionally poor survival (discussed below) of patients with glioblastoma, this disease in particular is likely to benefit from increasing prioritisation. However, advancements in our understanding of the fundamental biology of these difficult to treat tumours is likely to be the key precursor required for improved patient outcomes.

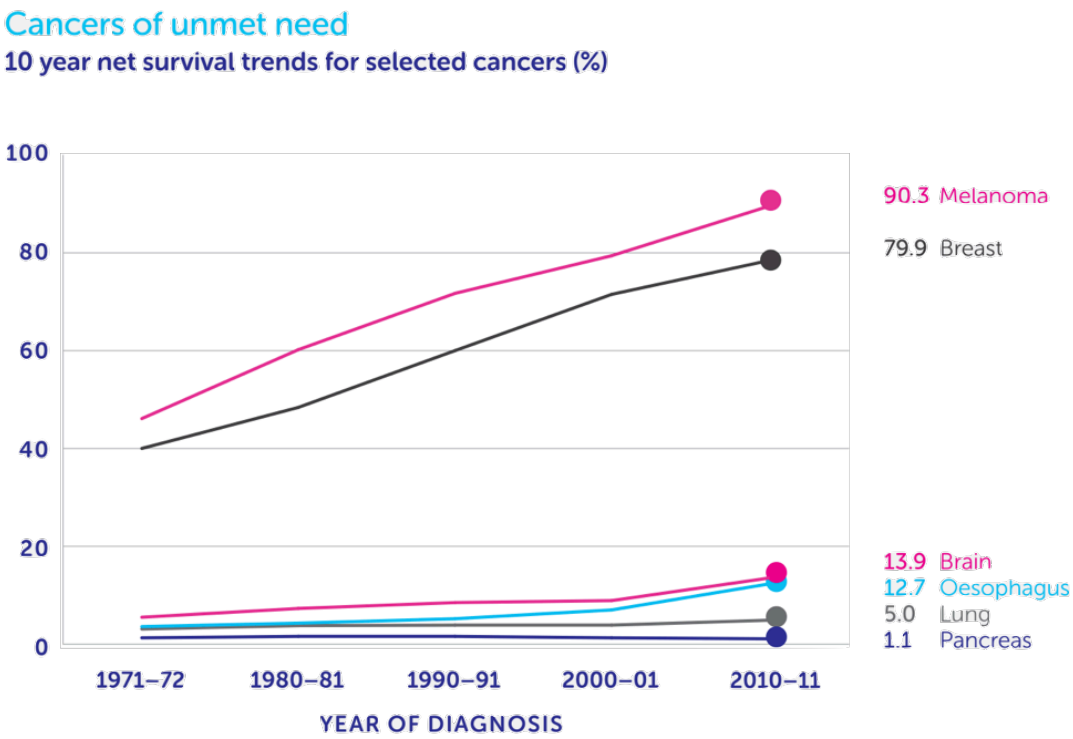


Figure 1.3: Cancers of unmet need – The 10-year net survival* trends for patients with various cancers including those designated 'cancers of unmet need' (brain, oesophagus, lung and pancreatic cancers) by a number of charities in view of poor prognosis with little progress seen over the last 40 years. Progress in survival rates and recent survival for patients with brain tumours (13.9%) should be contrasted with that for patients diagnosed with melanoma (90.3%) and breast cancer (79.9%). It is likely that increased research investment and greater focus on the complex biology and treatment resistance mechanisms brain tumours use will be required to promote substantial improvements in future survival. **Net survival refers to overall survival rates adjusted for mortalities due to unrelated causes. Adapted from Cancer Research UK*[59].

1.2.2 Genomic aberrations in glioblastoma

In a landmark study, The Cancer Genome Atlas (TCGA) Research Network provided comprehensive characterisation of genetic and epigenetic features for 206 glioblastoma tumours[60]. Further work, including expansion of the interim TCGA cohort (Brennan *et al.* 2013[32]) to include over 500 patients, has led to a detailed understanding of common genomic aberrations occurring in glioblastoma. These are detailed below.

The pattern of genetic and epigenetic abnormalities observed in glioblastoma support the assertion of two biologically divergent entities, and correlate with the clinical differences observed between those glioblastomas which arise *de novo* (primary glioblastoma) vs those resulting from progression of a lower grade glioma (secondary glioblastoma). Primary glioblastoma typically present with a brief clinical history (<3-4 months) in patients over 55 years of age who then rarely survive more than two years. These account for account for approximately 95% of glioblastoma. In contrast, the median age of diagnosis for patients with secondary glioblastoma is approximately 44 years of age, following an often much

longer clinical history. Median overall survival for these patients is estimated at 31 months[61]. The most recent WHO classification of CNS tumours highlights *IDH1* and *IDH2* gene mutations (discussed earlier) as key abnormalities in glioblastoma, such that *IDH* mutational status is definitional in providing a final 'integrated diagnosis' of either 'glioblastoma, *IDH* wild-type' or 'glioblastoma, *IDH* mutant'[12]. Here, *IDH* wild type and *IDH* mutant tumours are essentially synonymous with primary and secondary glioblastoma, respectively – in line with their clear clinical correlations.

The most common genomic aberrations observed in *IDH* wild-type glioblastoma appear to be[36,62]:

1) *PTEN* mutation or homozygous deletion;
2) *CDKN2A* and *CDKN2B* homozygous deletion;
3) *TERT*-promotor mutations;
4) Chromosomal rearrangements – most commonly gain of chromosome 7, and monosomy of chromosome 10;
5) Receptor Tyrosine Kinase (RTK) gene amplifications – with the *EGFR* gene most commonly involved.

With less common mutations involving *TP53, NF1, PIK3CA* and *PIK3R1*.

The spectrum of genomic aberrations seen in *IDH* mutant glioblastoma differs considerably. Intuitively, abnormalities also observed in gliomas of lower grade including the G-CIMP and mutations of *ATRX* and *TP53* are prevalent in these tumours[62], consistent with the notion of progression from a lower grade precursor. Abnormalities suspected to play a role in high-grade progression include chromosomal deletions involving *CDKN2A* and *CDKN2B* (chromosomes 9p21 and 19q, respectively), RTK/RAS/PI3K pathway up-regulation, activation of MYC, up-regulated FOXM1 expression, mutations affecting members of the retinoblastoma pathway, and epigenetic silencing of developmental transcription factor genes regulated by the polycomb repressive complex 2 (PRC2) [36,63].

Many of the genomic abnormalities observed in primary and secondary glioblastoma demonstrate convergence in dysregulation of three core biological pathways: RTK/RAS/PI3K signalling, Rb, and p53[32]. As well established mechanisms providing unrestricted cell division and growth when aberrant in the majority of human cancers,

dysfunction of these pathways is required to enable tumorigenesis and progression in glioblastoma.

Integrative analyses of the data provided by the TCGA network has also fuelled attempts to delineate glioblastoma into subtypes based on molecular characterisation, with some success in terms of providing groups that bare a semblance of predictive clinical utility [40,64]. These are described in Figure 1.4.

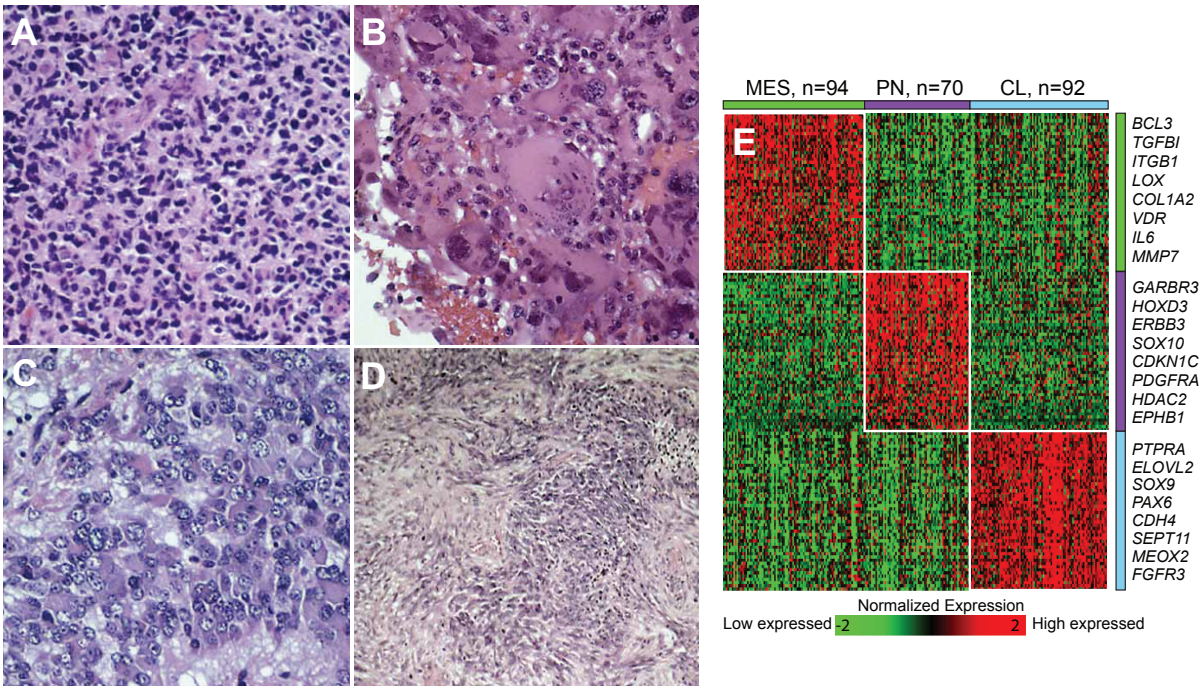


Figure 1.4: Histological and molecular subtyping in glioblastoma – A-D. Histological variants of glioblastoma. The **small cell variant** is characterised by discohesive proliferation of tightly packed small cells with scant cytoplasm, resembling small cell lung carcinoma (A). The **giant cell variant** of glioblastoma exhibits numerous large multinucleated astrocytic cells (B). Rounded cells with distinct cytoplastic borders and prominent nucleolation are observed in the **epithelioid variant** of glioblastoma (C); whilst **gliosarcoma** variants of glioblastoma contain an admixture of areas resembling sarcoma, likely representing some degree of mesenchymal differentiation from a common cell of origin (D). The prognostic utility of histological subtyping is limited. E. Subsequent attempts to categorize glioblastoma focused on the identification and clustering of genetic aberrations. Verhaak *et al.*[65] categorized gene expression data from a core set of 173 TCGA database glioblastoma samples into four distinct molecular subtypes (proneural, neural, classical and mesenchymal) before using this data to classify gene expression data from previously published data sets (validation samples) and glioblastoma xenograft samples. *TP53*, the most frequently mutated gene in glioblastoma, is not mutated in **classical** (CL) type glioblastoma tumours. This molecular subtype is characterised by mutations causing abnormally high levels of epidermal growth factor receptor (**EGFR**). **Proneural** (PN) glioblastoma have the most frequent mutations in the isocitrate dehydrogenase 1 (***IDH1***) gene, being indicative of glioblastoma that have transformed from a lower grade precursor (i.e. secondary glioblastoma) as opposed to primary (*de novo*) glioblastoma and is associated with improved patient survival. Proneural subtype glioblastoma were also the only subtype to harbor platelet-derived growth factor receptor alpha (***PDGFRA***) mutations causing abnormally high expression levels of this receptor tyrosine kinase. The **mesenchymal** (MES) subgroup contains the highest number of aberrations in the neurofibromatosis 1 (***NF1***) tumour suppressor gene, in addition to frequent mutations in the ***PTEN*** and ***TP53*** tumour suppressor genes. The fourth **'neural'** subgroup was initially reported as characterised by several gene expression signatures resembling normal neural tissue. However, this 'subtype' was later established to be artefactual, arising from normal cell contamination of cancer specimens[66,67]. Comparison of response to aggressive therapy revealed a differential between subtypes with classic glioblastoma demonstrating the most benefit, whilst patients with proneural glioblastoma derived little benefit. Other genetic and epigenetic aberrations of diagnostic and prognostic significance in gliomas include: hypermethylation (which promotes epigenetic silencing) of the dealkylating enzyme O^6-methylguanine-DNA methyltransferase (**MGMT**)

leading to increased sensitivity to alkylating chemotherapies such as temozolomide; and chromosome **1p-19q co-deletion** which has become definitional of the lower grade oligodendroglioma based on the revised World Health Organization 2016 classification of central nervous system tumours[12]. Research attempting to establish which of these genetic and epigenetic aberrations drive the genesis of glioblastoma vs which are merely 'passengers', and the influence of spatiotemporal factors on such molecular aberrations continues to evolve[68]. But a more complete understanding of gliomagenesis is needed to help prioritise candidate targeted therapies and accelerate advances in patient care. *Adapted from Prayson et al. (2006)[69] and Wang et al. (2017)[67].*

1.2.3 Current multimodal therapy for glioblastoma

Current management of glioblastoma consists of maximal surgical resection followed by radiotherapy with concomitant and adjuvant temozolomide[10,11]. In this context, median survival is 14.6 months with less than 10% of patients surviving more than 5 years[11]. More recently, a novel therapeutic modality utilizing locoregional delivery of alternating electrical fields via a treatment array has been approved for clinical usage in the context of recurrent and newly-diagnosed glioblastoma[70,71]. This therapy, called tumour-treating fields (TTFields), is postulated to disrupt mitotic spindle assembly leading to anti-mitotic effects in cancerous cells. However, emerging data support a range of anticancer effects exerted by this modality (as summarized in Figure 1.5) including via the modulation of DDR processes[72-74]. In a large phase III clinical trial treating patients with newly-diagnosed glioblastoma, TTFields was associated with a gain in overall median survival from 15.6 months (standard therapy control) to 20.5 months (standard therapy + TTFields)[75,76]. However, opportunities for patients to receive TTFields are not geographically equitable. For example, TTFields is widely used in the USA but NICE recently deemed the modality to not represent adequate cost-effectiveness to justify delivery for UK patients within the NHS[77]. Furthermore, although early concerns regarding the balance of modest survival benefit against potential quality of life (QoL) intrusion may be unfounded (TTFields requires electrodes fixed to the bare scalp to be worn >18 hours per day), since objective studies support stable or enhanced QoL[75,78] whilst using TTFields, some challenges remain unresolved. For example, the practicability of delivering this labour-intensive (but relatively safe) therapy to patients with a poor performance status to ensure greater equity of access.

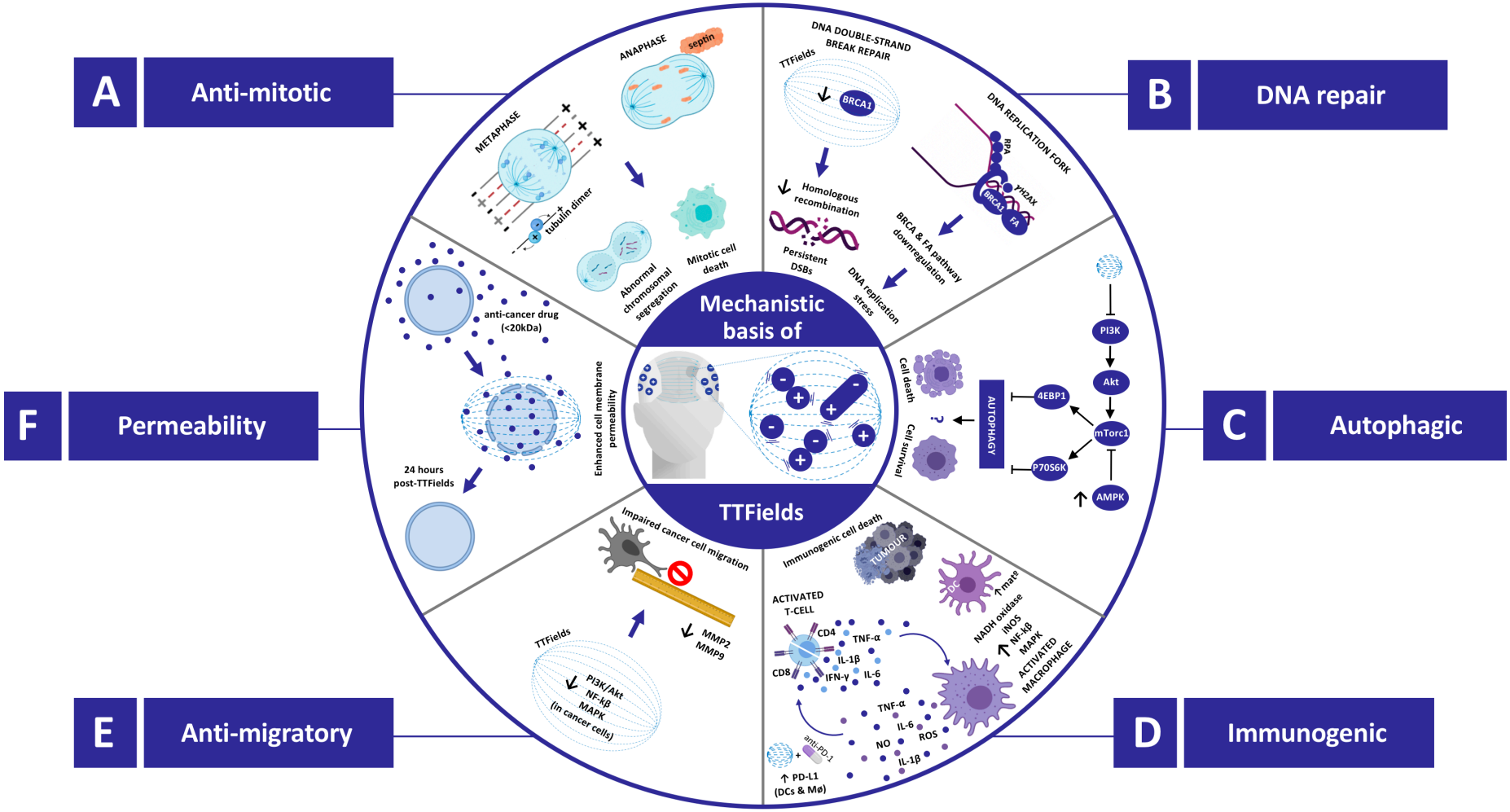


Figure 1.5: Summary of the mechanisms of action of TTFields. Low-intensity, intermediate-frequency alternating electrical fields exert biophysical forces on a variety of charged and polarizable molecules to elicit a spectrum of biological effects. A. **Anti-mitotic effects:** During metaphase, the electric fields are uniform, causing dipolar molecules, such as tubulin, to align with the field. TTFields therefore interferes with tubulin polymerisation and depolymerisation during metaphase. At anaphase, TTFields prevent localisation of septin proteins to the mitotic spindle and prevent assembly of the septin complex into a ring structure at the cleavage furrow. During cytokinesis, the electric fields are non-uniform, with the fields converging to the cleavage furrow, where the field intensity is highest. As a result, strong dielectric force is applied on polarizable objects pushing them towards the high intensity region. Taken together, these effects result in abnormal chromosome segregation and/or cell death. B. **DNA repair:** TTFields have been shown to downregulate BRCA and FA pathway genes. This has been associated with increased replication stress and increased DSB formation. Additionally, HRR is impaired by TTFields resulting in reduced efficiency of DSB repair. C. **Autophagy:** TTFields have been suggested to prevent the inhibitory effects of the mTorc1/PI3K/AKT signaling pathway on autophagy, resulting in increased activation of autophagy with TTFields. D. **Anti-tumour immunity.** TTFields stimulates macrophages (Mø) to secrete ROS, NO and pro-inflammatory cytokines, such as IL-1β, TNF-α, and IL-6. Additionally, TTFields promote immunogenic cell death via dendritic cell (DC) recruitment and maturation (mat°) ultimately leading to an increase in the accumulation of CD4+ and CD8+ T- cells at the tumour site. E. **Anti-migratory:** TTFields reduces the capacity of cancer cells for migration and invasion via NF-kβ, MAPK and PI3K/AKT-dependent mechanisms. F. **Cell membrane permeability:** TTFields increase cell membrane permeability by increasing the number and size of holes in the cell membrane. *Adapted from Rominiyi & Vanderlinden et al. (submitted 2020)*[79].

Building on the premise that resection of greater than 98% of glioblastoma tumour volume appears to represent an independent correlate of enhanced median survival[80], numerous surgical innovations have been directed towards optimising surgical resection rates. Multimodal neuronavigation, intraoperative MRI/US and fluorescence-guided surgery with 5-aminolevulinic acid (5-ALA) have demonstrated potential to augment surgical reduction of tumour burden[81-85]. However, the benefit of such innovations is not always as clear cut outside the context of clinical trials[86]. Future innovations including the application of iKnife, which utilizes rapid evaporative ionization mass spectrometry (REIMS) to differentiate between tumour and healthy tissue[87,88] or ramen spectroscopy used to achieve similar tumour-brain resolution in a non-destructive manner[89,90], may support further improvement in resection rates. Nevertheless, given the highly infiltrative nature of glioblastoma and limited ability to resect infiltrated regions of eloquent cortex without unacceptable morbidity, it is hard to envisage advances in surgical technology providing more than incremental gain in patient outcomes. There is, therefore, a clear and urgent need for therapies that effectively exploit the fundamental biology of glioblastoma.

1.3 Preclinical experimental models of glioblastoma

Over the last decade there has been a lack of success in translating promising novel agents from preclinical studies into clinical survival benefit for patients with glioblastoma[91]. To some degree, this failure represents the inability of commercialized clonal glioblastoma cell lines passaged and cultured *in vitro* to adequately recapitulate the complexities of treatment resistance observed in the clinic. The concept of heterogeneity is a vital consideration for the development of future therapies. Variation in the genetic aberrations, phenotypic characteristics and clinical progression of individual patient tumours presupposes the need for personalized therapeutic strategies informed by a range of molecular biomarkers[92]. The ability to delineate glioblastoma into specific molecular subclasses (proneural, mesenchymal and classical; IDHwt vs IDHmut; MGMT methylated vs unmethylated) of some validated prognostic value[10,64,67,93,94] supports the utility of personalized medicine.

Adding a new dimension of complexity, accumulating evidence describe a phylogenetic hierarchy of spatiotemporally divergent subclones within individual tumours, each possessing a distinct collection of putative driver mutations and characteristic transcriptome

[13-15,95,96]. Tackling such intratumoural heterogeneity represents a critical therapeutic challenge. Clearly, coarse categorization by glioblastoma subtype may be a detrimental oversimplification as illustrated by studies demonstrating the expression of numerous conflicting 'Verhaak' subtype classifiers within the same tumour[13,15].

Furthermore, a distinct subpopulation of cancer cells in glioblastoma, which assume the hierarchical apex, seem to possess an innate capacity for unlimited regeneration and self-renewal[16,17]. Often described as cancer stem cells (CSCs) or glioblastoma stem cells (GSCs), these heterogeneous subpopulations are deemed responsible for inherent resistance to conventional chemoradiotherapy and inevitable disease progression observed in glioblastoma through augmented checkpoint activation and repair of DNA damage[18,19]. It is therefore imperative that representative models utilized to investigate potential future therapies are able to appropriately recapitulate the staggering intratumoural heterogeneity and therapeutic recalcitrance that glioblastoma exhibits. Table 1.1 provides an overview of the various model systems used in preclinical glioblastoma research. Additionally, detailed discussion of the more clinically-relevant *in vitro* models is presented in Chapter 4 – Section 4.1.

Table 1.1: Commonly used models in preclinical glioblastoma research.

Summary of preclinical glioblastoma research models				
Model & description	**Affordability**	**Ease of use**	**Clinical relevance**	**Comments**
In vitro (2-dimensional)				
Established cell culture Historically derived cultures propagated and used over a long period of time (e.g. U87, T98G, U251, LN18).	★★★★★	★★★★★	★	• Traditionally the most widely used models in glioblastoma research. • May not accurately reflect molecular features of patient tumours and recently derived primary lines[97].
Primary, patient-derived cell culture Cultures recently derived from a patient specimen and propagated in standard, serum-containing media[98].	★★★★★	★★★★	★★	• Potential availability of more detailed clinical information to enable correlation.
Primary, patient-derived GSC culture Cultures recently derived from a patient specimen propagated exclusively in serum-free media supplemented with mitogens which maintain 'stemness'[99,100].	★★★★	★★★★	★★★	• Ease of clinical correlation as above. • Maintains therapeutically recalcitrant subpopulations[18,19].
3-dimensional in vitro glioblastoma stem cell models				
Neurosphere culture Typically primary GSCs cultured in non-adherent conditions to enable self-aggregation into spherical structures[99,101].	★★★★	★★★	★★★	• Some recapitulation of regional heterogeneity with potential for nutrient and oxygen gradients with central necrosis in larger neurospheres.
Tumouroid & organoid culture Larger aggregations of primary GSCs as a single cell type (tumouroid)[102] or with normal neural stem cells (organoid)[103-105].	★★★	★★	★★★★	• More robust recapitulation of hypoxic gradients and regional heterogeneity[102]. • Lengthy culture process and challenging to assess therapeutic response efficiently.
Alvetex™ scaffold-based culture Primary GSCs cultured within Matrigel™-coated 3D scaffolds[106-108].	★★★	★★★★	★★★★	• Maintains robust and consistent stem cell marker expression[108] (and see Chapter 4 – Figure 4.2). • Recapitulates key histological features of glioblastoma[106,108]. • Validated to reliably predict clinical efficacy[108].
Microfluidic glioblastoma-on-a-chip culture Typically primary GSCs (+/-) other cell types printed onto a 'chip' using bioinks to achieve a specific configuration[109,110].	★★★	★	★★★	• Requires bespoke set-up/equipment and engineering expertise. • Unrealistic therapeutic sensitivities have been reported[109,110].
In vivo (mouse) models				
Syngeneic mouse models Murine glioblastoma cells implanted (either heterotopically or orthotopically) within a murine host, which can therefore be immunologically compentant[111].	★★	★★	★★★	• Suitable for evaluation of therapies requiring an intact immune system such as immunotherapies. • Cannot be used to directly study therapeutic response of human glioblastoma cells.

Subcutaneous xenograft models Typically established or primary glioblastoma cell lines implanted into the flank of immunocompromised murine hosts[112].	★★	★★	★★★	• Tumour development can be followed visually and permits regular measurement of dimensions. • Lacks CNS microenvironment and influence of BBB.
Orthotopic patient-derived xenograft (PDX) models Primary glioblastoma cells implanted into the CNS of immunocompromised hosts[112,113].	★	★	★★★★	• Appropriate CNS microenvironment (with the exception of immunological function) and incorporates influence of the BBB[112]. • Implanted human cells can undergo mouse specific evolution[114].
Genetically engineered mouse models (GEMM) Use of transgenic models to perturb key genes implicated in gliomagenesis. For example, transgenic mice with GFAP-promoter-driven expression of the TVA retrovirus receptor to enable astrocyte specific expression of avian leukosis virus-derived RCAS vectors carrying relevant expression cassettes (e.g. EGFRvIII) following intracerebral injection of benign RCAS-vector producing cells[112,113,115].	★	★	★★★★	• Allows interrogation of molecular causality and the earliest stages of gliomagenesis. • Maintains an intact immune system an incorporates influence of the BBB. • High complexity, cost and tumours may take a long time to develop. • Lack the molecular diversity and intratumoural heterogeneity observed in human glioblastomas[112].
Abbreviations: BBB = blood-brain barrier; CNS = central nervous system; GEMM = genetically engineered mouse model; GSC = glioblastoma stem cell; PDX = patient-derived xenograft model. ★ (lowest) to ★★★★★ (highest) affordability / ease of use / clinical relevance (ratings indicative only).				

1.4 The Fanconi anaemia pathway & related cellular responses to DNA damage

1.4.1 Conceptual overview of the DNA damage response

The structural integrity of DNA is constantly threatened due to replication stress, telomere shortening, and a multitude of endogenous and exogenous DNA targeting exposures including, metabolic by-products such as reactive oxygen species (ROS), UV light, ionizing radiation and chemical toxins[116,117]. Failure to repair the damage these processes induce can lead to mutagenesis or cell death. It is therefore, perhaps unsurprising that an intricate network of signalling pathways and reparative mechanisms have evolved to deal with DNA lesions, preserving genomic architecture and stability. Constituents of this global reparative network are involved in: (1) initial detection of a DNA lesion and activation of signalling processes that promote cell cycle checkpoint induction (permitting the requisite time for lesion resolution); (2) repair of DNA lesions; (3) induction of programmed cell death pathways, in the event of catastrophic DNA damage. Collectively, this interwoven network of processes is often referred to as the DNA damage response (DDR).

The mechanisms repairing DNA respond to four categories of lesion, namely: (1) base modifications (including methylation damage) and mis-paired bases; (2) intrastrand or interstrand crosslinks; (3) single strand breaks (SSB) and; (4) double strand breaks (DSB)[118]. Distinct, but interconnected, pathways that permit efficient repair of each type of lesion are discussed later in this section. Additionally, although DSBs are often considered amongst the most toxic of DNA lesions, it is worth considering that each type of lesion is not an enduringly separate entity. For example, collision of a replication fork with a SSB or interstrand crosslink (ICL) can result in formation of a DSB[117]. Dynamic relationships between various DNA lesions and reparative processes underlie functional redundancy (which is likely to contribute treatment resistance), and the rationale of tackling multiple pathways of, or defects in, the overall DDR to help overcome treatment resistance.

1.4.2 DNA damage and responses to standard glioblastoma therapy

Abrogation of the mechanisms glioblastoma use to repair cellular DNA damaged by chemo- and radiotherapy may represent a key to effective multimodal treatment approaches. The most effective chemotherapeutic agent in current clinical usage for glioblastoma, temozolomide, engenders DNA damage through methylation of DNA bases. Of the notable

products, O^6-methlyguanine acts as a miscoding base during DNA replication leading to a corresponding C to T transversion in the complementary strand. Since O^6-methlyguanine is not successfully excised by mismatch repair (MMR), it endures as a perpetually miscoding base, instigating futile cycling of MMR with consequent stalling of DNA replication forks or double strand breakage[119]. The de-alkylating enzyme, MGMT, can sequester the methyl group from O^6-methlyguanine to restore the guanine residue to its original state, but leaving MGMT irreversibly inactivated and subject to ubiquitin-mediated proteasomal degradation[120]. Consequently, high *MGMT* expression contributes to temozolomide resistance. On the other hand, approximately 40% of *IDH*-wild type glioblastomas exhibit transcriptional repression of *MGMT* expression due to hypermethylation of an *MGMT*-associated 5' CpG island. These tumours are associated with greater benefit from temozolomide therapy and prolonged survival[94]. The more prevalent, but less toxic, temozolomide-induced DNA lesions: N^3-methyladenine and N^7-methylguanine, are removed via base excision repair (BER) leaving an intermediary abasic (or apurinic/apyrimidinic – AP) site. The nucleotide gap is recognized, filled and ligated – a process involving an AP endonuclease (APEX1), DNA polymerase β (pol-β), and DNA ligases respectively[119,121,122].

Radiotherapy exerts cellular damage by inducing single and double stranded DNA breaks. Poly (ADP-ribose) polymerase-1 (PARP1) plays a pivotal role in detection of single strand breaks with subsequent promotion of co-localisation of the single strand break repair (SSBR) polypeptide x-ray repair cross-complementing protein 1 (XRCC1)[123]. Reparative action for double stranded DNA breaks is predominantly the preserve of non-homologous end joining (NHEJ) and homologous recombination (HR), with HR being preferential in terms of fidelity, but only possible during S- and G2-phase due to the requirement for a sister chromatid. A brief discussion concerning intracellular responses to DNA damage and the various DNA damage repair pathways follows.

1.4.3 DNA damage signalling and checkpoint induction

Maintenance of genome integrity relies not only on accurate DNA repair, but also on the processes that detect DNA damage and co-ordinate cell cycle checkpoints, allowing time for DNA to be repaired. The regulation of cell cycle checkpoints has been reviewed in detail by Sherr and Bartek (2017)[124] and Lukas *et al.* (2004)[125], however two specific kinases are of particular relevance to this study and are therefore mentioned below.

The roles of ATM & ATR

ATM represents an apical, multifunctional kinase within the DDR and plays a key role in cellular responses to DNA DSBs where it helps co-ordinate all major cell cycle checkpoints via the ATM-CHK2 axis[126], as illustrated in Figure 1.6. ATR helps preserve DNA integrity in response to replication stress (the slowing or stalling of replication forks during duplication of DNA). Single-stranded DNA (ssDNA) is coated by replication protein A (RPA) which recruits ATR interacting protein (ATRIP), which exists constitutively as a heterodimer with ATR. Downstream actions of the ATR-CHK1 axis are illustrated in Figure 1.6 and a detailed review of the functions of ATR can be found in Marechal and Zou (2013)[127]. It is critical to emphasise that, in addition to the roles summarised above, both ATM and ATR assume a plethora of roles orchestrating signal transduction in response to cellular DNA damage and the overall DDR. However, whilst there is some functional overlap between their diverse roles, their functions are not considered to be redundant, highlighting the distinct potential of both ATM and ATR as specific targets for anti-cancer therapies. Furthermore, given the known interactions between constituents of the FA pathway and either ATM or ATR (see Figure 1.12), tentative therapeutic strategies targeting these DDR processes simultaneously could potentially provide highly effective therapies. The rationale of which might include maximising the failure of cancer cells to resolve DNA lesions (which may be exogenous caused by chemo- and radiotherapy, and/or endogenous as a result of the constitutively elevated levels of DNA damage neoplastic cells harbour) coupled with loss of checkpoint integrity, depriving cancerous cells of the time required for adequate DNA repair.

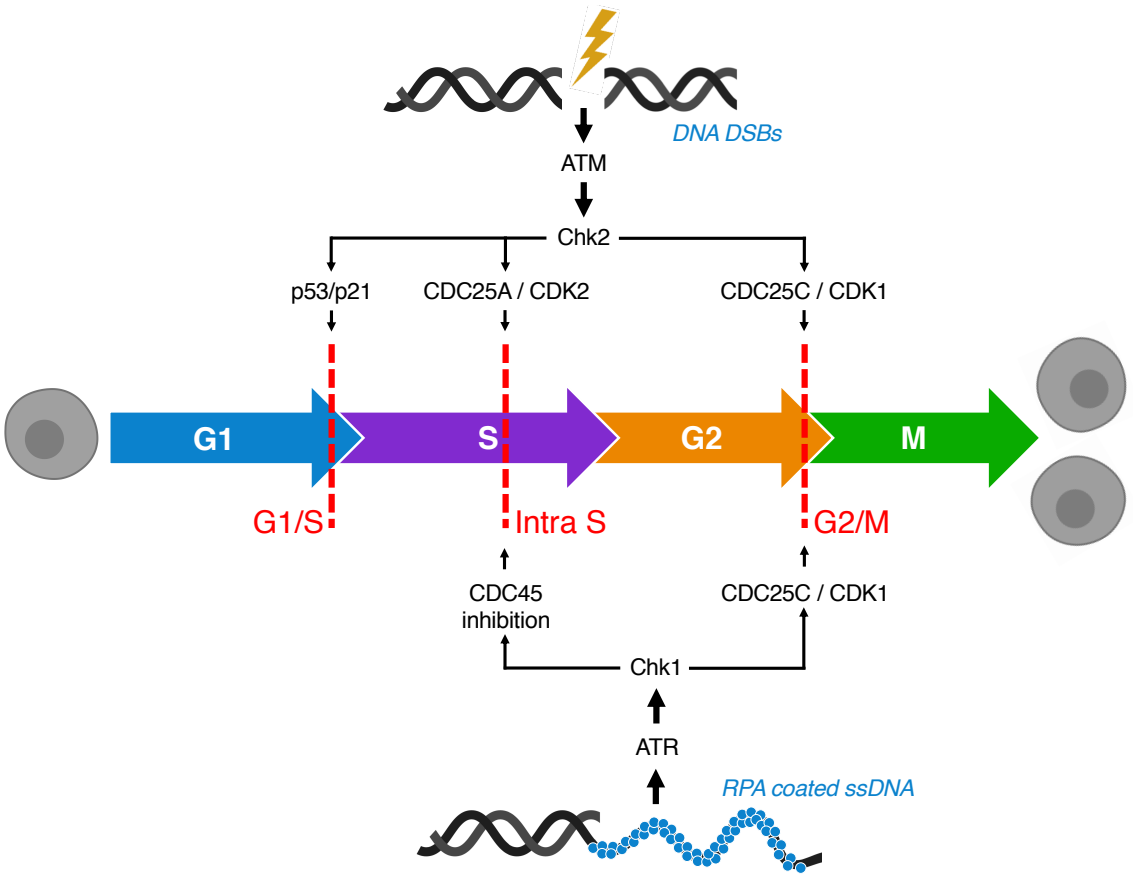
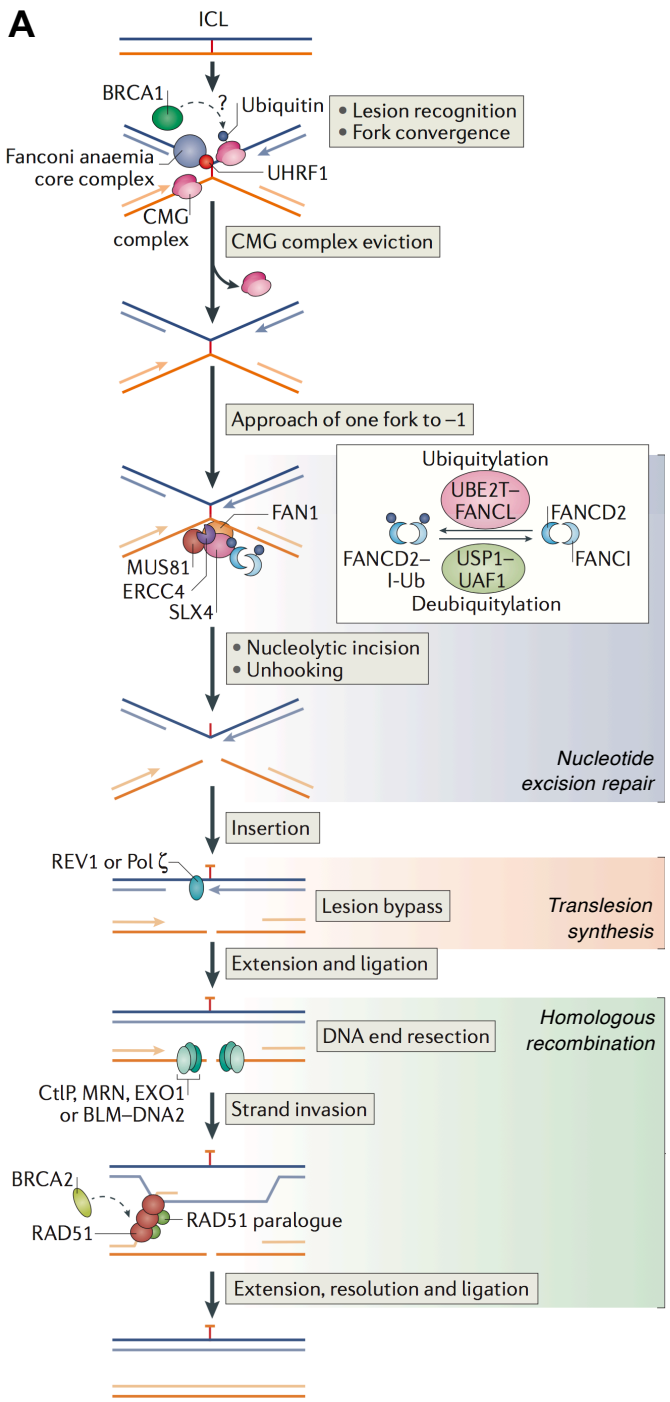


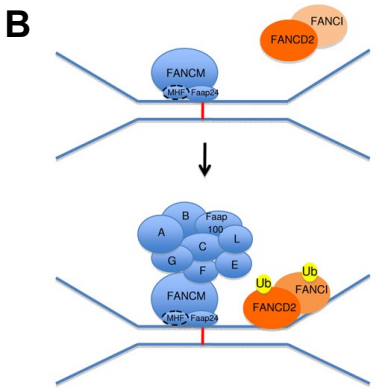
Figure 1.6: The role of ATM and ATR in cell cycle regulation following DNA damage. The processes of cell division (mitosis, M phase) and DNA synthesis (S phase) are separated by two important gap phases (G1 & G2). Progression of mitotic cells through the cell cycle is controlled by periodic accumulation and destruction of the aptly named cyclin dependent kinases (CDKs) and cyclins. Inappropriate progression through phases of the cell cycle is prevented by three main checkpoints (G1/S, Intra S & G2/M checkpoints; dashed red lines). Following DNA damage, checkpoint activation is critical to provide ample time and recruit the necessary machinery required to restore genomic integrity.
Checkpoint activation: DNA **DSBs** activate the apical DDR kinase ATM, which can influence all three major cell cycle checkpoints via the phosphorylation of CHK2 and subsequent downstream signaling. In contrast, ATR is activated by the presence of **RPA coated ssDNA** and contributes to maintenance of the intra S phase and G2/M checkpoints via phosphorylation of CHK1 and subsequent downstream signaling as indicated.
G1/S checkpoint: Phosphorylation of **p53** by **CHK2** and **ATM** directly (arrow not shown) results in a reduction in the binding of mouse double minute 2 homolog (MDM2) to p53 and p53 activation promoting its nuclear accumulation and stabilization. Subsequently, elevated p53 levels promote increased transcription of **p21** which inhibits CDK2-cyclin E activity resulting in prevention of progression to S phase.
Intra-S checkpoint: Within S phase, the activation of cell division cycle 25 (CDC25) phosphatases predominantly by prevention of CDC45 loading onto replication origins (preventing subsequent DNA replication) primarily via the **ATR-CHK1** axis, but also via ATM-CHK2 mediated phosphorylation of CDC25A, can instigate an intra S checkpoint in response to replication stress or other perturbations to optimal DNA synthesis, permitting a slowing of DNA replication.
G2/M checkpoint: Both **ATM** and **ATR** mediated phosphorylation of CHK2 and CHK1, respectively, leads to the phosphorylation of CDC25C phosphatases which influence the G2/M checkpoint via interaction with the cyclinB1/CDK1 complex[128].

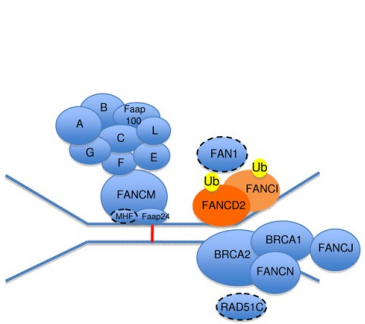
1.4.4 The Fanconi anaemia DNA damage repair pathway

The FA pathway is frequently activated in response to DNA strand breaks, replication arrest, and other cytotoxic secondary lesions induced by alkylating and cross-linking chemotherapeutic agents[20,129,130]. The pathway is named after the rare (Fanconi) anaemia in which mutations in this DNA damage repair pathway were uncovered. Importantly, patients who suffer from Fanconi anaemia are exquisitely sensitive to chemotherapeutic agents that induce DNA interstrand crosslinks[131]. This observation from a rare anaemia could be pivotal in helping to generate new cancer therapies.

The pathway consists of at least 22 proteins predominantly arranged into 3 protein complexes/groups[132],[130], see Figure 1.7; through sequential interaction, these complexes facilitate lesion repair via physical removal of the lesion followed by homologous recombination (HR) and/or promotion of lesion bypass[4]. FANCD2 is a key protein of the FA pathway and a marker of quantifiable pathway activity. Patil *et al*. demonstrated re-expression of an active FA pathway in primary glioblastoma tissue, in contrast to normal brain tissue and benign schwannomas[22]. Furthermore, expression levels of FANCD2 were strongly associated with tumour grade, leading to postulation that chemical inhibition of the FA pathway (FAPi) could preferentially target glioblastoma cells and increase susceptibility to DNA damaging treatments. Further investigation confirmed inhibition of the FA pathway sensitised glioblastoma cells to the effects of temozolomide and BCNU, irrespective of status for the established prognostic biomarker MGMT. This work opens up the possibility of developing FAPi for the clinical management of glioblastoma.







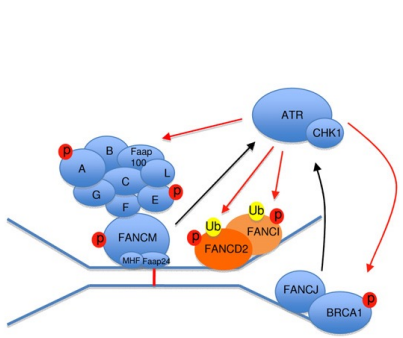


Figure 1.7: A schematic model for the FA pathway – A-D. Activation of the FA pathway. The primary function of the FA pathway appears to be removal of DNA interstrand crosslinks (ICLs) which would otherwise impede DNA replication (A). ICLs are recognized by the FANCM-FAAP24-MHF protein complex. This recruits the FA core complex by direct interaction between FANCM and FANCF (B). FANCM promotes ATR mediated phosphorylation of multiple core complex proteins. The activated FA core complex subsequently monoubiquitinates two key substrates, FANCD2 and FANCI, via a PHD E3 ubiquitin ligase domain in its FANCL subunit and its partner ubiquitin-conjugating enzyme FANCT/UBE2T[2].

Monoubiquitination of FANCD2-FANCI activates this (ID) complex, which then recruits the nuclease FAN1 or interacts with a series of DNA repair proteins (including FANCS/BRCA1, FANCN/PALB2, FANCD1/BRCA2, and FANCJ/BACH/BRIP1) at the site of DNA damage, and facilitates the co-ordinated interplay of downstream repair pathways (A & C).

Nucleotide excision repair: FANCS/BRCA1 evicts the replicative helicase CMG complex allowing the approach of one replication fork to within one nucleotide of the ICL. Ubiquitinated ID complex at the ICL region then serves as a landing pad for several factors including SLX4 and FAN1 to co-ordinate nucleolytic incisions (likely mediated by ERCC4) to 'unhook' the DNA leaving the crosslinked nucleotide tethered to the complementary strand.

Translesion synthesis: the defect is bypassed by translesion synthesis polymerases REV1 or DNA polymerase ζ (REV3-REV7 – NB: REV7 = FANCV) then ligated to restore an intact DNA duplex.

Homologous recombination: the intact DNA duplex is used as a template to facilitate HR-mediated repair of the DSB.

The FA pathway cross-talks with ATR–CHK1 checkpoint proteins (D). ATR and its effector kinase, CHK1, are required for damage-inducible activation of the FA pathway. ATR–CHK1 phosphorylates (red arrows) multiple FA and FA-associated proteins, including FANCA, FANCE, FANCD2, FANCI, and BRCA1. FANCM is also phosphorylated upon DNA damage by an unknown kinase. In turn, the stability and activity of ATR–CHK1 are promoted (black arrows) by the FANCM–FAAP24 heterodimer and FANCJ by independent mechanisms. FANCM also mediates the formation of the BRAFT complex, which contains the FA core complex members and the BLM complex containing Topo IIIa and RMI1/2 (not shown). *Adapted from Kee, Y & D'Andrea AD (2010)[4] and Ceccaldi et al. (2016)[2]*

Proteins within the FA pathway can be ascribed to functional groups namely, those within the core complex (FANCA, FANCB, FANCC, FANCE, FANCF, FANCG/XRCC9, FANCL, FANCM, FANCT/UBE2T), those that comprise the ID complex (FANCD2, FANCI), and additional proteins which typically function downstream in the pathway (FANCP/SLX4, FANCD1/BRCA2, FANCJ/BRIP, FANCN/PALB2, FANCO/RAD51C, FANCR/RAD51, FANCS/BRCA1, FANCU/XRCC2, FANCV/REV7/MAD2L2, FANCW/RFWD3, FANCQ/ERCC4/XPF[27]. Collectively, proteins of the FA pathway act as a master regulator of genomic integrity in detecting replication impeding DNA lesions such as ICLs then orchestrating interconnected DNA repair processes to facilitate lesion resolution.

The FA core complex

The DNA translocase FANCM, in complex with FAAP24, MHF1 and MHF2 (FANCM-FAAP24-MHF complex) plays a key role in identifying stalled replication forks at the site of ICLs then directing recruitment of the multi-subunit FA core complex to the site of damage[133]. FANCM promotes ATR-mediated phosphorylation of multiple core complex proteins to activate the complex[2]. Recent structural studies confirm with high resolution the composition of the core complex with a central scaffold of two heterotrimers, each consisting of FANCB, FA-associated protein of 100kDa (FAAP100) and FANCL. The central scaffold assembles the remaining subunits (FANCA, FANCG, FANCC, FANCE, FANCF) generating an extended asymmetrical complex where a FANCL subunit at the 'base' of the molecule is relatively constrained spatially, whereas FANCL at the 'top' of molecule is afforded greater mobility as a product of conformational flexibility within the molecule, thus potentially alluding to differential activity of these FANCL subunits[134]. Combined structures of the FANCC-FANCE-FANCF subcomplex towards the base of the molecule are proposed to form a substrate recognition module whilst towards the top of the molecule, FANCA and FANCG provide chromatin targeting properties[134-138]. Recruitment of FA core complex proteins to coalesce as foci at sites of DNA damage occurs during S and G2 phases of the cell cycle and relies on the intact function of FANCM-FAAP24, ATR and FANCS/BRCA1[139]. The activated FA core complex then serves as a large ubiquitin ligase for FANCD2 and FANCI (see below) via a PHD E3 ubiquitin ligase domain in its FANCL subunit and its partner E2 ubiquitin-conjugating enzyme FANCT/UBE2T[2,140-143].

FANCD2 and FANCI

FANCD2 and FANCI form a heterodimer of asymmetrical saxophone-shaped molecules which present an open-'C' configuration in cross-section. The monoubiquitination of FANCD2 and FANCI (at K561 and K523, respectively , in humans) represents a key signal of activity within the FA pathway[144]. Recent structural studies confirm that binding of the ID complex to DNA at stalled replication forks promotes a conformational change in the heterodimer with hinge-like rotation of FANCD2 and FANCI causing transition from the open-'C' configuration to an 'O'-like configuration which completely encircles dsDNA. The target site of FANCD2 monoubiquitination lies at the back of this molecular hinge and therefore may only be accessible in the 'O' configuration. The addition of a ubiquitin molecule to FANCD2 then locks the FANCD2-FANCI DNA clamp into this closed conformation[145]. Therefore, although recent studies suggest monoubiquitination may not specifically increase the binding affinity of FANCD2-FANCI to downstream interacting DDR proteins (relative to the non-ubiquitinated heterodimer), monoubiquitination does appear to stabilise the ID complex on dsDNA, which would bring the complex into closer proximity with known binding partners and therefore dramatically increase the frequency of interactions[146]. Interestingly, FANCI monoubiquitination is not required to facilitate closed conformation of the FANCD2-FANCI DNA clamp around dsDNA[145], however FANCI monoubiquitination may enhance the efficiency of ID complex binding to DNA[146]. The ubiquitination state of FANCI also assumes a vital role in regulating release of the ID complex from dsDNA since FANCI recruits the deubiquitinating enzyme USP1-UAF1[147], which can deubiquitinate $FANCD2^{Ub}$-FANCI, but not $FANCD2^{Ub}$-$FANCI^{Ub}$, to prevent DNA trapping of the ID complex at non-productive DNA damage sites[138,146]. It is also important to highlight the importance of the ATR/CHK1 and ATM/CHK2 signalling cascades in maintenance of the intra-S-phase checkpoint, which is essential to permit sufficient time for DNA repair orchestrated by the FA pathway, and the role of these cascades in phosphorylating a plethora of chromatin-bound factors promoting the stability of DNA replication forks and DNS repair[27]. For example, ATR kinase directly phosphorylates FANCI, providing an important molecular switch that promotes monoubiquitination of the ID complex[148,149]. Monoubiquitination of FANCD2-FANCI plays a key role in facilitating interaction with downstream DNA repair proteins including FANCP/SLX4 (a scaffold protein and master regulator of the ERCC1-FANCQ/ERCC4/XPF, MUS81-EME1/2 and SLX 1 nucleases), the nuclease FAN1 and a series of DNA repair proteins (including FANCS/BRCA1, FANCN/PALB2, FANCD1/BRCA2, and FANCJ/BACH/BRIP1)[2].

Additionally, FANCD2-FANCI appears to harbour additional non-canonical FA pathway roles including during cytokinesis where FANCD2 (and FANCA) are required to maintain the stability of DNA at common fragile sites including FRA3B and FRA16D[150], and downregulation of inappropriate NHEJ through interaction with Ku proteins[2], consistent with the observation that FANCD2-deficient cells exhibit inappropriate recruitment of DNA-PKcs at sites of DNA replication stress[131].

Critically, FA pathway activation also occurs in response to DNA replication stress in the absence of ICLs. For example, hydroxyurea which generates replication stress through depletion of the deoxyribonucleotide pool elicits FA pathway activation[151-153], however various mechanistic responses may ensue influenced by the degree of replication stress apparent. Under low levels of replication stress, the firing of new and dormant DNA replication origins is suppressed and restart of existing stalled replication forks is promoted through the distinct function of non-ubiquitinated FANCD2 in recruiting BLM helicase[154]. Non-ubiquitinated FANCD2 also binds and inhibits the MCM2-7 helicase complex, promoted by ATR-mediated phosphorylation of FANCD2, to restrain DNA synthesis. Conversely, in the context of high replication stress, FANCD2 and FANCI function in co-ordination with the FA core complex to stabilise replication forks and promote replication restart. Here the core complex proteins FANCA, FANCC, FANCJ, FANCM function together with monoubiquitinated FANCD2 and the Fanconi anaemia associated protein BOD1L (biorientation of chromosomes in cell division protein 1-like) to bind the nascent strand of DNA, providing protection from MRE-11 and DNA2-mediated nucleolytic degradation[2,27]. Additionally, monoubiquitinated FANCD2 and the downstream FA proteins FANCS/BRCA1 and FANCD1/BRCA2 chaperone and protect ssDNA loaded with FANCR/RAD51 at stalled replication forks[27].

Downstream proteins functioning within the FA pathway

In the context of stalled replication forks at the site of an ICL, monoubiquitinated ID complex acts as a landing pad for downstream DNA repair proteins and helps orchestrate an intricate process at the intersection of multiple divergent DNA repair pathways whereby DNA is incised by structure-specific nucleases to release the ICL from one of the parental strands ('unhooking'), before translesion synthesis proteins are co-opted to bypass the defect, restoring an intact DNA duplex, which in turn is then used as template to facilitate HR-

mediated repair of the DSB in the adjacent DNA duplex, as summarised in Figure 1.7 and subsequent sections.

1.4.5 Fanconi anaemia

Phenotypically, germline homozygous or compound heterozygous mutations in any Fanconi anaemia gene (with the exceptions of FANCB which demonstrates X-linked inheritance and FANCR which revealed penetrance with a dominant negative mutation) result in a rare disorder of chromosomal stability characterised by physical abnormalities, bone marrow failure (BMF) and an exquisite predisposition to developing cancer. First described by the Swiss paediatrician Guido Fanconi in 1927[155], the incidence of Fanconi anaemia is estimated to be approximately three per million with a heterozygote frequency in the region of 1 in 300 in Europe[156], however substantially higher carrier frequencies have been reported in specific ethnic groups which may harbour founder mutations including Ashkenazi Jews (carrier frequency ~1 in 89) and Afrikaners (~1 in 83). Although rare, this condition represents the commonest cause of inherited BMF.

Clinical features and diagnosis

The majority of patients with Fanconi anaemia display detectable congenital abnormalities including: skeletal abnormalities (~71%) such as radial ray defects including hypoplasia of the thumb; aberrant skin pigmentation such as café au lait spots or patches of hypopigmentation (~64%); short stature (~63%); microphthalmia (~38%); renal and urinary tract defects (~34%), and; male genital abnormalities (~20%). Less commonly, significant developmental delay and structural abnormalities of the gastrointestinal tract, heart, hearing apparatus and/or central nervous system can occur[157]. However, approximately 30% of patients have no apparent physical abnormality as a neonate, which may contribute to a delay of diagnosis until features associated with BMF become evident.

The characteristic chromosomal hypersensitivity of cells from patients with FA towards drugs which induce DNA interstrand crosslinks, such as mitomycin C (MMC) or diepoxybutane (DEB), underpins the key diagnostic test for FA[156]. Exposure of cells to either MMC or DEB during the chromosomal breakage assay elicits a substantial increase in the number of chromosomal breaks in FA cells[158], relative to non-FA cells, and classical tri and quadri-radial figures[159] as a result of the failure of interstrand crosslink resolution. Although the testing of peripheral blood lymphocytes is usually sufficient to confirm the diagnosis, around 20% of patients may, interestingly, develop somatic reversion of the pathogenic allele within

haematological cells resulting in a false negative or equivocal test result. In these cases, repeating the test using skin fibroblasts usually helps to resolve the diagnosis[159]. Flow cytometry can also be used to help confirm the diagnosis since cells from FA patients demonstrate constitutive delay in progression through G2 phase of the cell cycle and this is disproportionately exaggerated following exposure to cross linking agents resulting in detectable G2 arrest relative to non-FA cells[160]. However, flow cytometry is less useful as a diagnostic test once myelodysplastic syndrome (MDS) or acute myeloid leukaemia (AML) has developed. More recently, the advent of next generation sequencing has shown demonstrable diagnosis utility in the work-up of patients with suspected FA[161] and is likely to be used early in the diagnostic pathway in the future. However, maintaining both functional and genetic testing modalities is likely to be advantageous.

Bone marrow failure and haematological malignancy

Patients with FA develop BMF with onset of pancytopenia at a median age of 7 years old[162,163]. Early definitive treatment is crucial and consists of stem cell transplantation (SCT), of which transplant from a matched sibling donor (if available) represents the most successful option with 3-year overall survival rates of approximately 80%[164,165]. Due to the hypersensitivity of FA cells to DNA alkylating agents and irradiation typically used during myeloablation prior to transplant, intensity-reduced conditioning regimens, including the use of fludarabine (a purine analogue which inhibits DNA synthesis by interfering with ribonucleotide reductase and DNA polymerase) have been developed specifically for patients with FA[159]. SCT for patients who have already developed cytogenetic abnormalities or overt MDS/AML can be particularly challenging, highlighting the importance of early transplant, ideally before such features develop. Although survival rates are improving, BMF (including complications of therapy to manage BMF) and malignancy represent the main causes of mortality. Haematological malignancies represent the most common cancers observed with a reported cumulative incidence of AML as high as 20% by age 40 (700-fold higher than the general population). The cumulative incidence of MDS is approximately 40% at an age of 50 years old (6000-fold higher than the general population)[166,167].

1.4.6 Solid tumours and Fanconi anaemia

Cancer in FA

Patients with FA also have a substantially increased risk of solid malignancies including: head and neck squamous cell carcinomas (with a risk 600-fold increased risk relative to the general population) which tend to be more aggressive than in non-FA patients and metastasize early; oesophageal carcinomas (2000-fold increased risk); vulval carcinomas (3000-fold increased risk), and; cervical carcinomas[166,168]. The risk of other types of cancer is also increased including hepatocellular carcinoma, liver adenomas, Wilms tumour, neuroblastoma, breast cancer and intrinsic brain tumours[159]. Medulloblastoma is the most commonly reported brain tumour in the context of FA[169,170], however the development of glioblastoma has been reported in a 3-year old patient in the context of biallelic FANCD1/BRCA2 mutations[171].

Cancer predisposition syndromes

Germline monoallelic mutations in FA pathway genes do not cause Fanconi anaemia (excluding the previously mentioned exceptions), but can substantially increase the lifetime risk of developing cancer, highlighting a tumour suppressive role of intact FA pathway function since the development of cancer is often associated with corresponding loss of heterozygosity[27]. Heterozygous mutations in FANCS/BRCA1 or FANCD1/BRCA2 are well established to cause clinical autosomal dominant hereditary breast and ovarian/fallopian tube cancer (HBOC) syndrome with concomitant increase in the risk of pancreatic, stomach and prostate cancers. However, heterozygous mutations in FANCJ/BRIP1, FANCN/PALB2, FANCM, FANCA, FANCO/RAD51C, FANCC and FANCG also appear to be associated with increased risk of a number of cancers including breast, ovarian and pancreatic malignancies, but with each mutation appearing to confer a divergent spectrum of tissue specificity[27].

1.4.7 Related DNA damage repair pathways

An exhaustive discussion of all DNA damage repair pathways is not possible within the confines of this thesis, however adapted summaries and details of a comprehensive review for each of the main processes are provided below.

1.4.7.1 Homologous recombination

The homologous recombination (HR) pathway represents a complex, high fidelity mechanism of DNA DSB repair. However, given its reliance on a homologous DNA sequence (duplicate DNA strand on a sister chromatid), DNA repair via HR is only possible during S and G2 phases of the cell cycle, when sister chromatids are available to act as repair templates. The process of HR is summarised below and useful reviews have been published by Sung P & Klein H (2006)[172] and Lord C & Ashworth A (2016)[173].

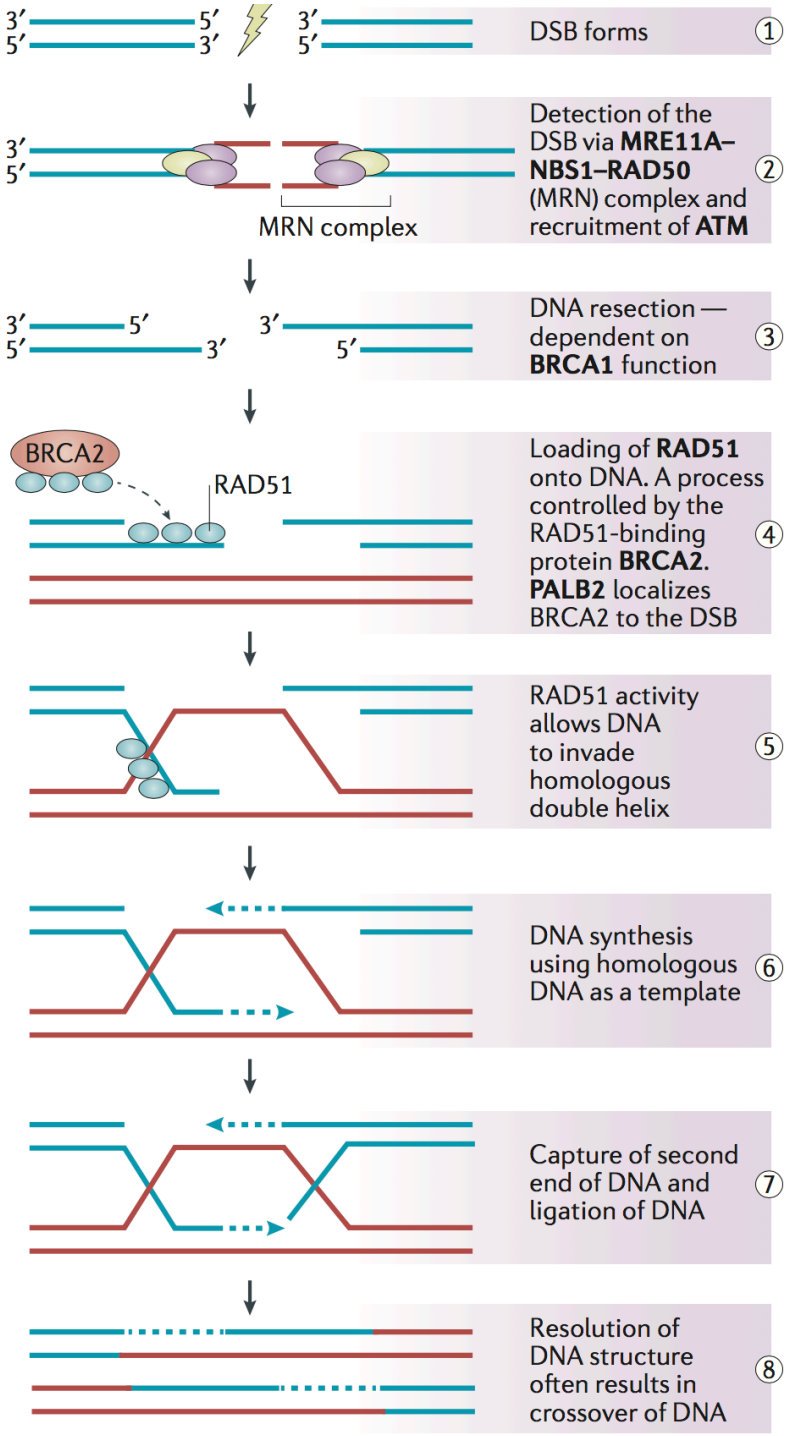


Figure 1.8: A schematic model for homologous recombination – The sequential steps of HR DNA repair are detailed above. *Adapted from Lord et al. (2016)*[173].

1.4.7.2 Non homologous end joining

In contrast to HR, the non-homologous DNA end joining (NHEJ) pathway provides DSB repair capabilities throughout the cell cycle since a homologous sister chromatid is not required, permitting repair to a range of DNA-end configurations. However, the flexibility and rapidity of NHEJ is provided at the expense of fidelity. The process of NHEJ is

summarised below and useful reviews have been published by Chang et al. (2017)[174] and Scully et al. (2019)[175].

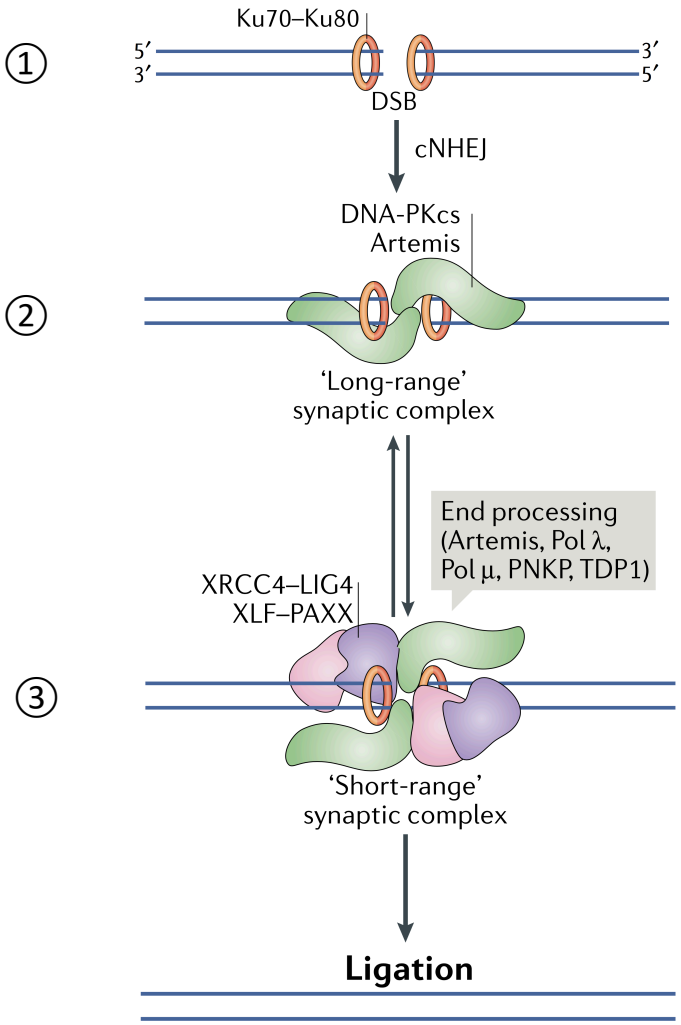


Figure 1.9: A schematic model for non-homologous end joining – The Ku70-80 heterodimer binds to DSBs to promote DNA DSB repair by classical non-homologous end joining (cNHEJ) (1). Activated DNA-PKcs plays an apical role in the co-ordination of cNHEJ by recruiting downstream NHEJ proteins such as Artemis, DNA polymerase, XRCC4, XLF and DNA Ligase IV, as well as γH2AX (a well-established marker of DSBs which also recruits further DSB repair proteins). A 'long-range' synaptic complex is formed by the incorporation of phosphorylated DNA-PKcs and Artemis (2). This can reversibly form a 'short-range' synaptic complex which permits the activity of DNA end processing and ligation enzymes (3). Multiple rounds of nucleotide additions and deletions often occur before ligation of the resultant DNA ends, and the product of NHEJ is generally error-prone, often resulting in the deletion and/or addition of base pairs. *Adapted from Scully et al (2019)*[175].

1.4.7.3 Mismatch repair

Mismatch repair (MMR) improves the fidelity of DNA replication via degradation of a strand of newly synthesized DNA containing a base-base mismatch, allowing DNA polymerase another chance to generate an error-free DNA strand complimentary to the template sequence. The process of MMR is summarised below, and useful reviews have been published by Jiricny J (2006)[3,176].

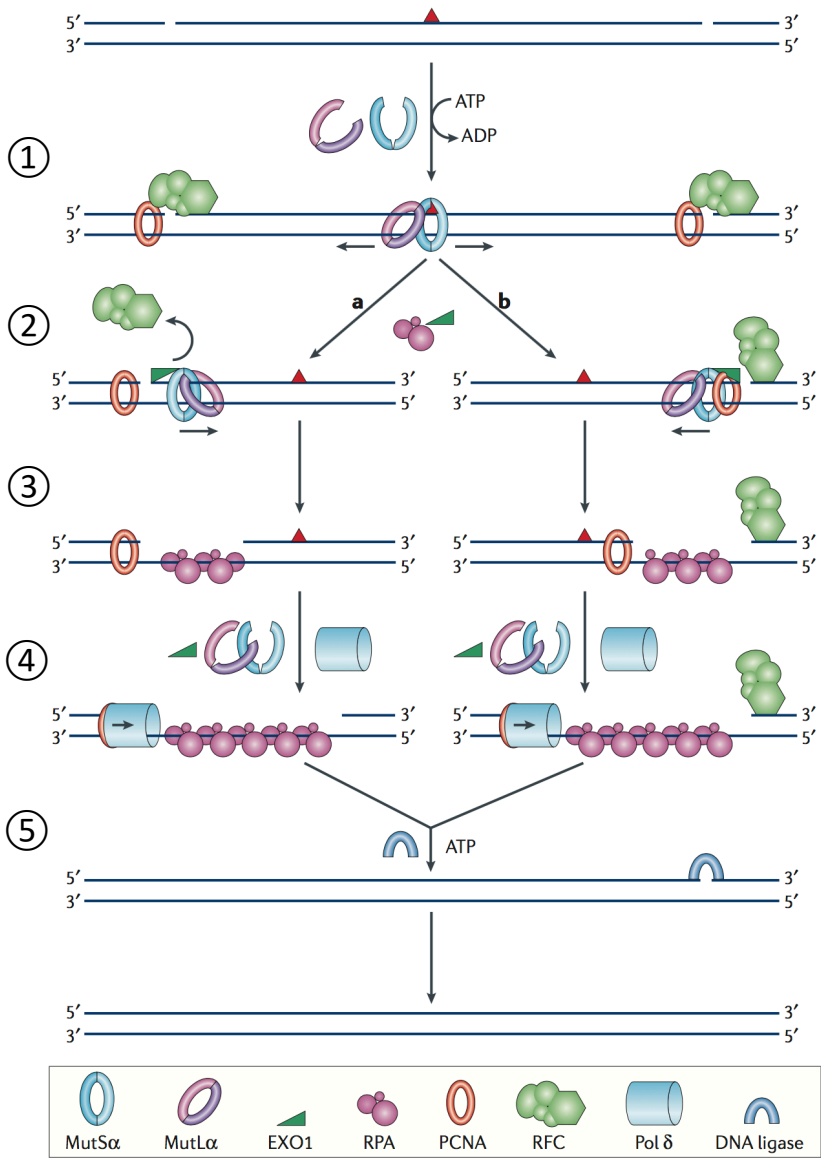


Figure 1.10: A schematic model for DNA mismatch repair – MutSα (or MutSβ) binds to the DNA mismatch (red triangle) then recruits MutLα resulting in the ternary complex undergoing an ATP-driven conformational switch which releases the sliding clamp from the mismatch site (1).

Clamps that diffuse upstream encounter replication factor C (RFC) bound to the 5′ terminus of the strand break and displace it to load exonuclease-1 (EXO1), which is activated to begin degradation of the strand in a 5′→3′ direction (2a).

Conversely, clamps that diffuse downstream encounter a proliferating cell nuclear antigen (PCNA) molecule bound at the 3′ terminus of the strand break then recruit and activate EXO1 resulting in degradation of the region between the original discontinuity and the mismatch. (RFC at the 5′ terminus of the discontinuity prevents degradation in the 5′→3′ direction (away from the mismatch) (2b).

Replication protein A (RPA) stabilizes the single-stranded gap (3).

DNA polymerase δ (Pol δ) loads at the 3′ terminus of the discontinuity and carries a bound PCNA molecule. The complex fills the DNA gap (4).

DNA ligase I seals the remaining nick to complete the repair process (5). *Adapted from Jiricny (2006)* [3].

1.4.7.4 Base excision repair

This pathway corrects specific damage caused by oxidation, deamination or alkylation of a DNA base. One of several specific DNA glycosylases detects and removes the damaged base leaving an apurinic/apyrimidinic (AP) site which is further processed using either a short- or long-patch repair process. The process of base excision repair (BER) is illustrated below and useful reviews have been published by David S et al. (2007)[177] and Krokan H & Bjoras (2013)[178].

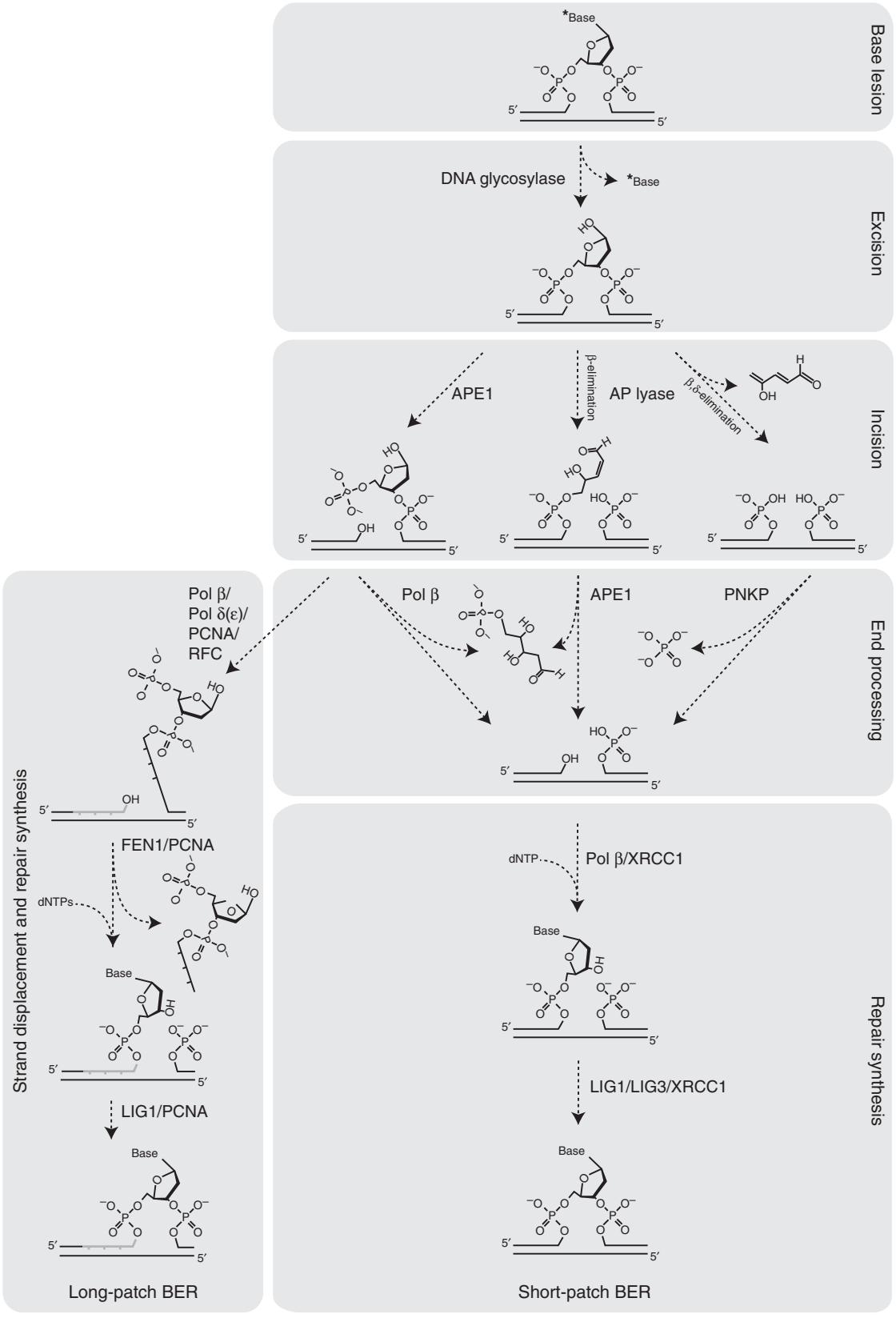


Figure 1.11: A summary of base excision repair. A variety of DNA glycosylase enzymes excise specific damaged DNA bases to leave an AP site. With respect to temozolomide induced lesions, N-methylpurine-DNA glycosylase (MPG) efficiently removes N^3-methlyadenine and N^7-methylguanine. Subsequently, the AP site is cleaved before filling of the single strand gap and ligation as mediated by either long-patch or short-patch repair processes. *Adapted from Krokan H & Bjoras (2013)*[178].

1.4.7.5 Nucleotide excision repair

Nucleotide excision repair (NER) is able to remove a wide variety of structurally unrelated DNA lesions. The process can be activated by DNA helix distortions associated with structural changes to nucleotides, or by stalling of RNA polymerase II due to a DNA lesion during transcript elongation. The role of NER downstream of the FA pathway in the context of ICL repair is illustrated in Figure 1.7A and a detailed review has been published by Marteijn et al. (2014)[179].

1.4.8 Synthetic lethality and sensitivity

The term, synthetic lethality encompasses a concept in which simultaneous mutation in, or functional aberration of, the product of two genes causes cell death; but in isolation, either change is survivable[180,181]. Synthetic sensitivity expands this concept to include scenarios in which aberration in function of the genes results in impaired cell growth or proliferation, promoting lethal effects in the presence of additional insults such as ionizing radiation or cytotoxic chemotherapy[1]. The term 'synthetic sensitivity or lethality' (SSL) can be used to amalgamate these related concepts. Although major advancements in the generation of RNAi libraries and more recent development of CRISPR/Cas9 gene editing have undoubtedly advanced our ability to uncover SSL relationships[182,183], perhaps the most successful implementation of an SSL strategy in cancer treatment – targeted killing of *BRCA2*-deficient tumours using inhibitors of PARP1[184] [185] – was derived from hypothesis-driven research rooted in a fundamental understanding of the molecular pathways concerned and relevant interplay between them, rather than broad screening techniques.

1.4.9 Molecular interplay within the overall DDR

Glioblastoma cells within a single tumour can demonstrate remarkable heterogeneity in their DNA damage response (DDR)[186], and consequently exhibit varying resistance profiles. This plays a key role in understanding treatment failure, as some groups of cells will always resist therapy. Since the DDR is an interconnected collection of pathways that repair DNA, with multiple parts able to repair any particular defect, it is perhaps not convincing that blocking any single pathway will produce a comprehensively effective treatment. As the FA pathway is selectively active in glioblastoma it represents a highly attractive starting point for new strategies, because inhibiting this pathway should affect glioblastoma, but not healthy brain tissue where the pathway lies dormant. However, due to inherent functional

redundancy within the overall DDR, interactions between various related pathways may need to be considered in order to generate a new effective treatment paradigm.

Numerous interactions between the FA pathway and other DDR elements have been previously characterised[187]. For example, ataxia telangiectasia mutated (ATM) and ataxia telangiectasia Rad3-related (ATR) protein kinases phosphorylate components of the FA core complex (see Figure 1.12) after being activated in response to stalled DNA replication forks and DNA damage[188]. Additionally, components of the FA pathway have also been shown to promote activation of ATR[189], and the FA pathway acts to prevent deleterious non-homologous DNA end joining activity[131]. Poly(ADP-ribose) polymerase 1 (PARP1); a ubiquitously present nuclear enzyme activated by DNA single strand breaks and involved in base excision repair, is also present at stalled replication forks. PARP1 facilitates the repair of DNA single-strand breaks[190,191], and has been shown to be hyperactivated in replicating BRCA2/FANCD1 defective cells to compensate for a lack of HR-mediated repair[192], a process promoted by the FA pathway[131,193]. ATM is mainly activated by DNA double-strand breaks and has been shown to phosphorylate FANCD2, a process which is implicated in activation of the S-phase checkpoint in a cascade distinct from the main FA pathway[188]. Clearly, there is a staggering degree of molecular interplay between the FA pathway and other elements of the overall DNA damage response (as illustrated in Figure 1.12).

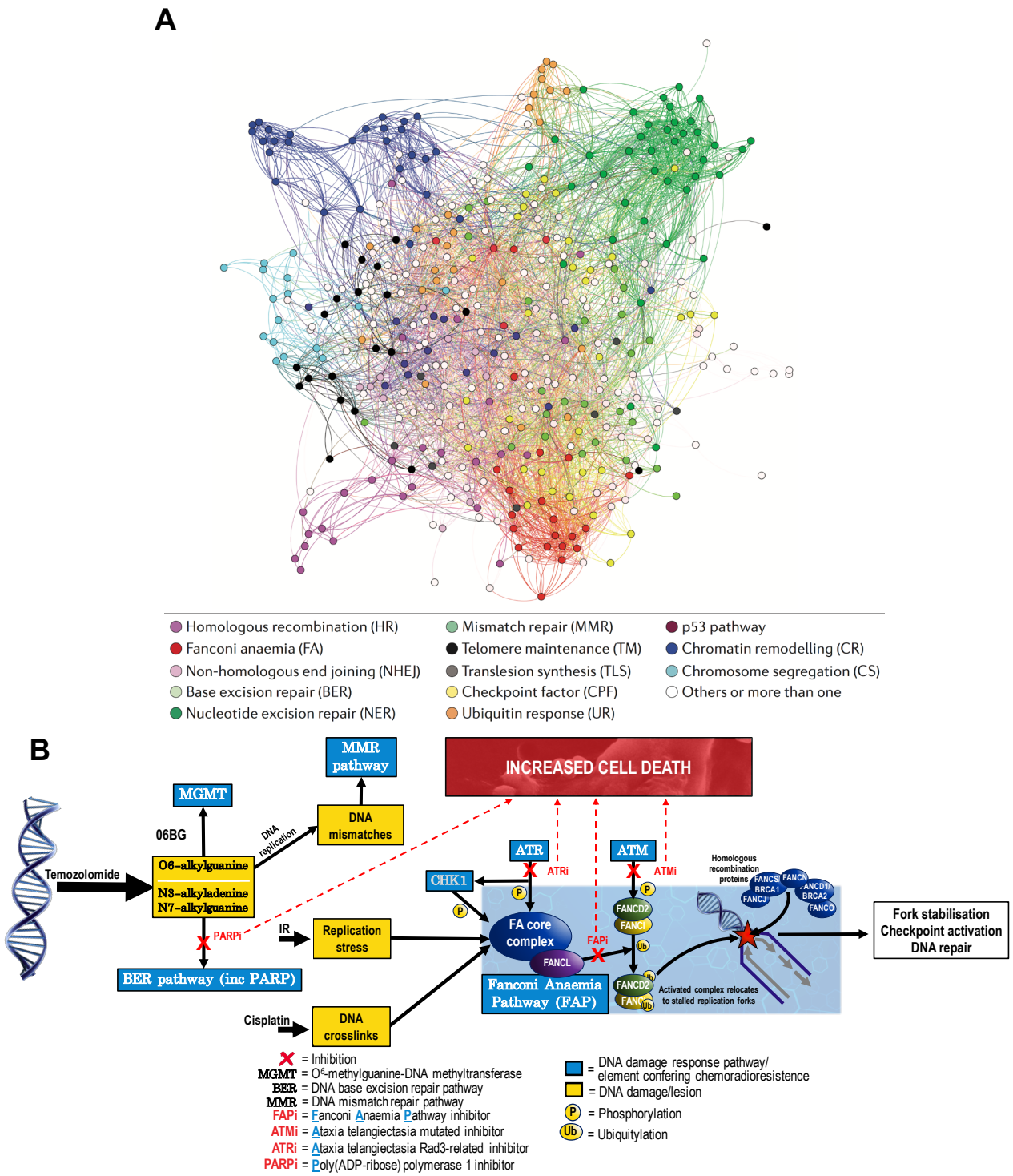


Figure 1.12: Global and FA pathway-related interactions within the DNA damage response – A. A network view of the DNA damage response demonstrating the complexity of interaction between proteins within the DDR, generated using only experimentally derived protein-protein interactions extracted from the STRING database. *Adapted from Pearl et al (2015)*[1] B. A schematic representation of functional interactions between the FA pathway and other key components of the DDR. Chemotherapy induces specific DNA lesions (highlighted yellow), which evoke a multifaceted DDR in attempt to repair DNA and permit replication. Ionising radiation causes a plethora of SSBs and DSBs which can impede DNA synthesis during S-phase resulting in replication stress and activation of the FA pathway. In glioblastoma, constituents of the DNA damage response (highlighted blue) facilitate treatment resistance. Targeting these molecules should impair DNA repair following chemoradiotherapy, leading to increased glioblastoma cell death (red arrows). MMR-dependent processing of methylation damage may give rise to persistent single-strand gaps and DSBs, permitting accumulation of DNA damage which may lead to indirect activation of the FA pathway via increased replication stress (not shown) and also engender increased cell death.

1.5 Rationale for combination targeting of the DDR in glioblastoma

1.5.1 Parallel targeting of the DDR

The principle of using combination inhibition to overwhelm overarching phenotypic delinquency within the DDR of cancerous cells, rather than selecting ever smaller subgroups by targeting a single mutation, is a highly attractive and a widely applicable aspiration for future therapeutic strategies. Although there has been intense research into the development of small-molecule inhibitors of DDR proteins[194], only a handful of studies have examined combined inhibition of multiple DDR elements simultaneously in glioblastoma.

Building on evidence suggesting that ATM inhibition and PARP inhibition each individually possess some utility in sensitising glioblastoma stem-like cells (GSC) to radiotherapy[195,196], Ahmed *et al*. (2015)[197] investigated parallel inhibition of the DNA damage response targets: ATM, ATR, CHK1 and PARP1, in primary, patient-derived glioblastoma cell lines. Firstly, this study demonstrated that these targets were upregulated in the inherently treatment resistant subpopulation, GSCs, compared to bulk populations – highlighting the importance of multiple DDR pathways, and the potential for functional redundancy within the DDR, to contribute to the treatment refractory nature of glioblastoma. Secondly, Ahmed *et al*. demonstrated that combined inhibition of PARP1 and ATR resulted in a profound radiosensitisation of GSCs, with effects greater than any single inhibitor used in isolation. Although these results highlight dual DDR inhibition as an appealing therapeutic strategy, the lack of any *in vivo* data, or data using more clinically predictive 3D models[108], in this study is a clear limitation.

Work by Signore *et al*. (2014)[198] further supports the rationale of combination inhibition of the DNA damage response as a therapeutic strategy in glioblastoma. Simultaneous multi-pathway inhibition with UCN-01 (a staurosporin derivative used as a CHK1 inhibitor) resulted in profound retardation of GSC growth in both *in vitro* and *in vivo* (subcutaneous and intracranial mouse) models. This study then utilized reverse-phase protein microarrays and kinase inhibitor library screening to identify combined inhibition of PDK1 and CHK1 with UCN-01 as the likely culprit for the observed therapeutic efficacy. Although this study is highly informative, the lack of target specificity with a drug such as UCN-01 severely limits potential clinical utility due to the high likelihood of dose-limiting toxicities mediated by off-

target effects. Nevertheless, this work does provide further proof of concept for combinatorial approaches.

Additionally, Rasmussen *et al.* (2016)[199] have demonstrated that epigenetic down-regulation of the DDR and induction of oxidative stress via histone deacetylase (HDAC) inhibition with vorinostat combined with the PARP inhibitor olaparib reduced glioblastoma cell survival, induced apoptosis, and impaired cell cycle progression. Clearly, novel combination therapies which abrogate DDR-mediated treatment resistance in glioblastoma have the potential to lead to an effective putative treatment paradigm. Preclinical research investigating dual DDR inhibition in extra-cranial malignancies also support such a paradigm, including in: pancreatic cancer (CHK1 and PARP inhibition)[200]; lymphoma (CHK2 and PARP inhibition)[201]; breast cancer (CHK1 and PARP)[202]; breast and ovarian cancer (ATR and PARP inhibition)[203], and; lung cancer (ATM and PARP inhibition)[204].

1.5.2 Integrative strategies based on the Fanconi anaemia pathway

Consideration of the parallels between glioblastoma and another rapidly mutating, difficult to treat disease is highly informative. Countless monotherapies tested as a therapeutic solution for HIV were met by abject failure. Only the introduction of combination antiretroviral treatment changed the prognosis of this disease from a death sentence, to a stable chronic disease[205]. Glioblastoma is a devastating, incurable disease characterised by considerable heterogeneity, inevitable recurrence following treatment, and death. Strategic manipulation of the DDR may hold a key to effective future therapies, however given the degree of cross-communication and functional redundancy observed within the DDR, combination approaches are likely required in order to optimize therapeutic responses and tackle treatment resistance. The FA pathway provides a highly attractive exploitable therapeutic window since it remains dormant in healthy brain, but is reactivated in around 90% of glioblastoma[22]; it provides the ideal foundation for combinatorial strategies exploiting the DDR in glioblastoma. To date, no published study has purposefully examined the therapeutic potential of combining specific inhibition of the FA pathway with simultaneous inhibition of a related DDR target in glioblastoma, however an emerging theoretical basis is beginning to make such an approach increasingly appealing in the struggle to improve survival for patients with glioblastoma. The aims of this study are therefore as follows.

1.6 Study aims

1.6.1 Aims of the study

To determine whether simultaneous small molecule inhibition of the FA pathway and an interconnected DDR target (PARP, ATR, or ATM) has greater therapeutic potential than strategies which use a single DDRi. Then further validate dual targeting of the FA and related DDR pathways using more clinically-predictive 3D GSC cultures.

1.6.2 Hypotheses

Parallel inhibition of both the FA pathway and an interconnected DDR target (PARP, ATR or ATM) can efficiently:

1) Sensitise glioblastoma cells to the effects of chemo- and radiotherapy, and/or;
2) Mediate glioblastoma cell death in the absence of conventional therapies (potential synthetic lethality).

1.6.3 Objectives

As such, the objectives were to:

1) Confirm FA pathway inhibition using commercially available and novel small molecules.
2) Validate and quantify the ability of single DDRi (FAPi, PARPi, ATRi and ATMi) to sensitise glioblastoma cells to conventional DNA damaging therapies.
3) Generate and validate clinically- and surgically-relevant patient-derived 2D and 3D GSC *in vitro* models to facilitate robust evaluation of combinatorial approaches.
4) Establish the relevance of FA pathway expression within inherently treatment resistant GSC subpopulations.
5) Assess the effects of FA pathway-based DDRi combinations on clinically-relevant GSC models.
6) Evaluate the therapeutic potential of FA pathway-based DDRi combinations to enhance the efficacy of standard-of-care chemotherapy (temozolomide) and radiotherapy in clinically-relevant GSC models.

Collectively, the desired outcome of these studies was to identify novel combinatorial treatment strategies which exhibit demonstrable preclinical efficacy against glioblastoma

and merit investment to translate further within late preclinical and/or early clinical studies towards our ultimate goal of improving outcomes for patients.

Chapter 2 – Materials & methods

2 CHAPTER 2 – Materials & methods

MATERIALS

2.1 General laboratory equipment

Table 2.1: General laboratory equipment.

Item	Company
Balance	Metla
Centrifuge (5430)	Eppendorf
Centrifuge (5810 R)	Eppendorf
Centrifuge (Heraeus MegaFuge 16)	Thermo Fisher Scientific
Centrifuge (S415 R)	Eppendorf
Class II Biological Safety Cabinet (Airstream)	ESCO
Colony Counter	Stuart Scientific
Confocal Immunofluorescence Microscope (Zeiss LSM880 AiryScan)	Carl Zeiss
Dri-Block® (DB-2D)	Techne
Electric Pipet Controller	FisherBrand™
Electrophoretic Transfer Cell	Bio-Rad
FACSCalibur™	BD Biosciences
Film Processor (Mibolta SRX101A)	Konica
Fluorescent Microscope (Eclipse TE200)	Nikon
Haemocytometer (Improved Neubauer AC1000)	Hawksley
Heat Block	Grant Instruments
Incubator (Tissue Culture)	Sanyo
Incubator with Integrated Cooling System (CCL-170 – dedicated TTFields Tissue Culture)	ESCO
Inovitro™ Tumour Treating Fields Delivery System	Novocure
Light Microscope	Optika
Mini Gel Tank (Invitrogen)	Thermo Fisher Scientific
Mini Gyro-rocker	Stuart®

Mini-Cell Electrophoresis System (XCell SureLock™)	Thermo Fisher Scientific
Mini-PROTEAN tetra cell	Bio-Rad
Multi-channel Pipettes – P10, P20, P1000	Gilson
NanoDrop ND 1000 Spectrophotometer	NanoDrop Technologies
pH Meter (Model 3510)	Jenway
Pipet Aid	Drummond
Pipettes – P2, P10, P20, P200, P1000	Gilson
PowerPac™ Basic Power Supply	Bio-Rad
Real-Time PCR platform (Applied Biosystems 7900)	Thermo Fisher Scientific
Repetman™ Electronic Pipette	Gilson
Scanner (Expression 1680 Pro)	Epson
Shaking Platform	Stovall Life Science
Shaking Platform (Corning LSE™ Orbital Shaker)	Corning
Spectrophotometric Plate Reader	Thermo Fisher Scientific
Thermal Cycler (S1000)	Bio-Rad
Vacuum Aspirator (Gilson Safe Aspiration Station)	Gilson
Vertical Electrophoresis Unit (Hoefer SE250)	Amersham Biosciences
Vortex	Fisons Scientific Equipment
Water Bath (JB Aqua 18 Plus)	Grant Instruments

2.1 Consumables

Table 2.2: Consumables.

Item	Company
0.22µm Syringe Filter Unit (Millex-GP, ployethersulfone, 3mm, gamma sterilized)	Merck Millipore
Cell Scraper – 25cm	Sartedt
Centrifuge Tubes – 15ml	Corning
Centrifuge Tubes – 50ml	FisherBrand™
Coverglass – 22 x 22mm	Menzel-Glazer
Coverglass – 22 x 50mm	Menzel-Glazer

Cryovials (CryoPure White) – 1.8ml	Sarstedt
Culture Plates – 3D Alvetex™ 12 well	Reprocell
Disposable Serological Pipettes – 5ml, 10ml & 25ml	FisherBrand™
Eppendorfs – 0.2ml, 0.5ml, 1.5ml & 2ml	Sarstedt
Filter Tips – 0.1-10µl, 2-20µl, 2-200µl, 100-1000µl	Biosphere®
Filter Tips – 0.1-10µl, 2-20µl, 2-200µl, 100-1000µl	Starlab
Gel Loading Tips	Starlab
Glass Bottles	Fisher Scientific
Immu-Mount (Shandon™)	Thermo Scientific
Microlance Needles	Becton Dickinson
Microscope Slides	Thermo Scientific
Optical Adhesive Film (MicroAmp™)	Thermo Fisher Scientific (4311971)
PCR Tubes – 200µl	Starlab
Pipette Tips – 2-200µl, 100-1000µl	Sarstedt
Pyrex Glassware	Fisher Scientific
QAIshredder Tubes (50)	Qiagen (79654)
Reagent Reservoir – 50ml	Corning
Refill Tips	Sarstedt
Repetman™ Sterile Pipet Tips – 1.25ml, 5ml, 12.5ml	Gilson
RNeasy Mini Kit	Qiagen (74104)
Round Tissue Culture Dishes – 10cm	Cellstar
Sterile Syringes – 1ml, 5ml, 10ml (Plastipak™)	BD Biosciences
Tissue Culture Flasks (Nunclon™ Delta Surface EasYFlask™) – 25cm^2, 75cm^2	Fisher Scientific
Tissue Culture Treated Plates – 24 & 96 well	Corning
Tissue Culture Treated Plates – 6 well	Costar
Universal Tubes	Sterilin

X-Ray Film (Fuji Medical Super RX)	Fujifilm

2.2 Sterilisation

Glassware was washed utilising RBS detergent, then rinsed in cold water followed by distilled water before being dried at 80°C. Glassware was then either hot air sterilised at 180°C or autoclaved using an MP24 Rodwell autoclaver. Solutions requiring sterilisation including PBS and distilled water were also autoclaved. Autoclaving was performed at a pressure of 15 pounds per square inch (psi) and temperature of 120°C for 15 mins.

Solutions to be used in tissue culture, such as those containing chemotherapeutic agents or DDR inhibitors, were filter sterilised using a 5ml syringe and a Millex GP filter unit (0.22µm pore size).

2.3 Purified water

Type 1 ultra-pure deionised water (ddH2O) was produced using a Triple Red System.

2.4 Reagents

Table 2.3: Reagents.

Item	Company (Product Code)
1,4-dithiothreitol (DTT)	Sigma (DTT-RO)
30% Acrylamide Mix	Geneflow (A2-0084)
5X siRNA Buffer	Dharmacon (B-002000-UB-100)
Accutase™ StemPro™ Cell Dissociation Reagent	Invitrogen (A11105-01)
Acetic Acid	Fisher Scientific (A38-212)
Advanced DMEM/F-12 (Dulbecco's Modified Eagle Medium/Ham's F-12)	Invitrogen (12634028)
Ammonium Persulfate (APS)	Thermo Fisher Scientific (17874)
Amphotericin B (Fungizone)	Gibco (15290)
B-27 Supplement (50x) Serum Free	Invitrogen (17504-044)
Benzonase Nuclease	Novagen (70664-3)
Bovine Serum Albumin (BSA)	Sigma (A2153)
Calcium Chloride	Sigma (499609)

Dimethyl Sulfoxide (DMSO)	Fisher Scientific (D/4120/PB08)
Dulbecco's Modified Eagle Medium (DMEM) with 4.5 g/L Glucose, with L-Glutamine	Lonza (BE12-604F)
EGF Recombinant Human Protein	Invitrogen (PHG0313)
Ethanol	Fisher Scientific (AC615090010)
Ethylenediaminetetraacetic acid (EDTA)	Sigma (1233508)
FGF Recombinant Human Protein	Invitrogen (PHG0263)
Foetal Calf Serum	Lonza (BE12-60F4)
Heparin Sodium Salt	Sigma (H3393-10KU)
HiMark™ Pre-stained Protein Standard (Ladder)	Thermo Fisher Scientific (LC5699)
High-Capacity RNA-to-cDNA™ Kit	Thermo Fisher Scientific (4387406)
Hydrochloric acid (HCL) 37%	Fisher Scientific (A144-500LB)
Industrial methylated spirit (IMS)	Fisher Scientific
L-Glutamine-200mM (100x)	Invitrogen (25030081)
Matrigel® Growth Factor Reduced (GFR) Basment Membrane Matrix LDEV-Free (Corning®)	BD Biosciences (354230)
Methanol	Fisher Scientific (A452SK-4)
Methylene blue	Sigma-Aldrich (M9140)
Milk Powder	Marvel
Minimum Essential Medium (MEM)	Invitrogen (10370-047)
MTT (3-(4,5-dimethylthiazol-2-yl)-2,5-diphenyltetrazolium bromide)	Sigma (M2128)
N-2 Supplement (100x) Serum Free	Invitrogen (17502-048)
Nitrocellulose Membrane (Protran®)	VWR (10600010)
NuPAGE™ 4-12% Bis-Tris Protein Gels –1.5 mm, 10 well	Thermo Fisher Scientific (NP0335BOX)
NuPAGE™ 4-12% Bis-Tris Protein Gels –1.5 mm, 15 well	Thermo Fisher Scientific (NP0336BOX)
NuPAGE™ LDS Sample Buffer (4X)	Thermo Fisher Scientific (NP0007)
NuPAGE™ MOPS SDS Running Buffer (20X)	Thermo Fisher Scientific (NP0001)
NuPAGE™ Transfer Buffer (20X)	Thermo Fisher Scientific (NP0006)
NuPAGE™ Tris-Acetate SDS Running Buffer (20X)	Thermo Fisher Scientific (LA0041)

Oxoid PBS Tablet	Thermo Fisher Scientific (BR0014)
Paraformaldehyde (PFA) – 4% solution in PBS	Santa Cruz Biotechnology (SC-281692)
Penicillin-Streptomycin (10,000U/ml)	Invitrogen (15140122)
Phosphatase Inhibitor Tablets (PhosSTOP™)	Sigma (4906845001)
PierceECL Western Blotting Substrate	Thermo Fisher Scientific (32106)
Potassium Chloride	Sigma (P9333)
Propidium Iodide	Sigma (P4864)
Protease Inhibitor Cocktail (cOmplete™ ULTRA Tablets Mini *EASYpack*)	Sigma (5892970001)
Protein Assay Dye Reagent Concentrate	Bio-Rad (500-0006)
RNase A	Sigma (10109142001)
RNase H	New England BioLabs (M0297S)
SeeBluePlus2 Prestained Standard (Ladder)	Thermo Fisher Scientific (LC5925)
Sodium chloride	Sigma (S7653)
Sodium Citrate	Sigma (1613859)
Sodium Dodecyl Sulphate (SDS)	Sigma (L3771-500G)
Sodium Hydroxide (NaOH) Pellets	Sigma (S5881)
Sorbitol	Sigma (S1876)
Sucrose	Sigma (S7903)
SYBR® Gold Nucleic Acid Gel Stain	Thermo Fisher Scientific (S11494)
TaqMan™ Universal PCR Master Mix (No AmpErase™ UNG)	Applied Biosystems (4324018)
Tris Base	Sigma (TRIS-RO)
Tris Hydrochloride	Sigma (10812846001)
Triton™ X-100	Sigma-Aldrich
Trypsin (0.5g/l trypsin, 0.2g/l versene (EDTA))	Lonza (17-161E)
TWEEN® 20	Sigma (P1379)
Visualiser™ Western Blot Detection Kit	Thermo Fisher Scientific (10553414)

β-Mercaptoethanol	Thermo Fisher Scientific (M/P200/05)

2.5 Inhibitors and cytotoxic agents

Table 2.4: Inhibitors and cytotoxic agents.

Item	Description	Solvent	Company
AZD0156	Selective inhibitor of ATM	DMSO	Selleckchem (S8375)
AZD6738	ATP-competitive inhibitor of ATR	DMSO	Selleckchem (S7693)
Cisplatin	DNA crosslinking agent	0.9% saline (NaCl)	Sigma (BP809)
Curcumin	Inhibits FA pathway	DMSO	Sigma (C1386)
DDN	Inhibits FA pathway	DMSO	Sigma (343420)
EF-24	Inhibits FA pathway	DMSO	Sigma (E8409)
KU55933	Inhibits ATM-mediated phosphorylation	DMSO	Sigma (SML1109)
Olaparib (*Lynparza; AZD-2281*)	PARP catalytic inhibition & PARP trapping potency >> veliparib	DMSO	Adooq Bioscience (A10111)
Ouabain	Inhibits FA pathway; Na+/K+ ATPase inhibitor	DMSO	Sigma (O3125)
TAK-243 (MLN7243)	Inhibits ubiquitin-activating enzymes	DMSO	Aobious (AOB87172)
Temozolomide	Mono-directional alkylating agent	DMSO	Sigma (T2577)
VE-821	ATP-competitive inhibitor of ATR	DMSO	Adooq Bioscience (A11605)
Veliparib (*ABT-888*)	PARP catalytic inhibition & PARP trapping potency << olaparib	DMSO	ApexBio (A3002)

2.6 Proprietary compounds

Table 2.5: Proprietary compounds.

Item	Solvent	Company
***Novel FA pathway inhibitors**: inhibit FANCL-mediated monoubiquitination of FANCD2*		
E41	DMSO	Concept Life Sciences (previously known as Peakdale)
F69	DMSO	As above
F73	DMSO	As above
F73-ethyl	DMSO	As above

F76	DMSO	As above
M66	DMSO	As above
nFAPi 4 (*E41*)	DMSO	TUoS Department of Chemistry
nFAPi 5	DMSO	As above
nFAPi 10	DMSO	As above

These compounds are currently subject to ongoing commercialisation processes. Consequently, details relating to chemical structures and the drug development process are pre-IP protected at present. These details are expected to be made available as soon as permissible, once agreed by all relevant stakeholders.

2.7 Primary antibodies

Table 2.6: Primary antibodies.

Antigen	Raised in*	Protein Size (kDa)	Application & Dilution	LOT no.(s)†	Company
β-Actin	Rabbit	42	WB 1:2000	No. 4969 Lot 7	Cell Signalling (4969)
β-Actin	Mouse	42	WB 1:2000	GR231973-7	Abcam (ab8226)
β-Actin	Mouse	42	WB 1:2000	E1017	Santa Cruz (sc-47778)
γH2AX (Ser139)	Mouse	14	IF (3D) 1:250	No. 9718 Lot 12	Cell Signalling (9718)
γH2AX (Ser139)	Mouse	14	WB 1:500 IF (3D) 1:250	2854975 3015339	Millipore (JBW301)
αPAR (binding reagent)	Rabbit‡	range	WB 1:1000	-	Millipore (MABE1016)
ATM	Mouse	350	WB 1:1000	B0614	Santa Cruz (sc-23921)
ATR	Goat	317	WB 1:1000	F0614	Santa Cruz (sc-1887)
BRCA1	Mouse	220	WB 1:1000	K0515	Santa Cruz (sc-6954)
BRCA2	Mouse	384	WB 1:1000	2770661	Calbiochem (OP95)
CD133 (Prominin)	Rabbit	97	WB 1:1000 IF (3D) 1:250	GR3205713-2	Abcam (ab216323)
CHK1	Mouse	54	WB 1:1000	124M4813V	Sigma (C9358)

CHK2	Rabbit	61	WB 1:1000	No. 2662S Lot 5	Cell Signalling (2662S)
DNA-PKcs	Mouse	460	WB 1:1000	GR52152-1	Abcam (ab1832)
DNA-PKcs	Rabbit (polyclonal)	460	WB 1:500	H2611	Santa Cruz (sc-9051)
FANCD2	Mouse	166	IF 1:1000 WB 1:1000	GR127154-10	Abcam (ab12450)
FANCD2	Rabbit	166	IF 1:1000	GR125860-1 (discontinued by manufacturer)	Abcam (ab2187)
FANCD2	Mouse	166	IF 1:1000 WB 1:1000	D0516 B0216 B0216	Santa Cruz (sc-20022)
FANCI	Rabbit (polyclonal)	149	WB 1:1000	GR145193-1	Abcam (ab15346)
FANCL	Rabbit (polyclonal)	43	WB 1:1000	GR75476-1	Abcam (ab94458)
MGMT	Mouse	26	WB 1:1000	GR66526-1	Abcam (ab39253)
Nestin	Mouse	176	WB 1:1000 IF (3D) 1:250	GR108589-3	Abcam (ab6142)
PARP1	Mouse	116	WB 1:1000	B2317	Santa Cruz (sc-8007)
pATM (Ser1981)	Rabbit	350	WB 1:1000	GR125270-3	Abcam (ab81292)
pCHK1 (Ser345)	Rabbit	54	WB 1:500	No. 133D3 Lot 15	Cell Signalling (133D3)
pCHK2 (Thr68)	Rabbit	61	WB 1:500	No. 13C1 Lot 12	Cell Signalling (13C1)
pDNA-PKcs (Ser2056)	Rabbit	460	WB 1:1000	GR296008-1	Abcam (ab18192)
S9.6 (R-loop)	Mouse	n/a	IF 1:500	n/a	ATCC (HB-8730)
SOX2	Mouse	34	WB 1:500	D1118	Santa Cruz (sc-365823)
Vimentin	Mouse	54	IF (3D) 1:250	A1518	Santa Cruz (sc-373717)

*Monoclonal antibody unless stated otherwise. †LOT no. colour denotes usage in Sheffield (blue) or Glasgow (grey). ‡PAR-binding reagent (His-tagged recombinant protein fused to rabbit Fc tag which is expressed in and purified from Rosetta™ (DE3)pLysS strain of E. coli[206]).

2.8 Secondary antibodies

Table 2.7: Secondary antibodies.

Secondary Antibody	Application & Dilution	LOT no.(s)	Company
Cy3® Goat Anti-Rabbit	IF 1:1000	434573	Invitrogen (A10520)
Alexa Fluor® 594 Goat Anti-Mouse	IF 1:1000 IF (3D) 1:250	1524907 1579585 1696463	Life Technologies (A11005)
Alexa Fluor ® 488 Goat Anti-Mouse	IF 1:1000	1572559	Life Technologies (A-11304)
Alexa Fluor ® 488 Goat Anti-Rabbit	IF 1:1000 IF (3D) 1:250	1275894	Life Technologies (A-11034)
Alexa Fluor ®594 Goat Anti-Rabbit	IF 1:1000	1844440	Life Technologies (A-11012)
Polyclonal Goat Anti-Mouse IgG, HRP-Linked	WB 1:1000	20039214 20062696	Dako (P0447)
Polyclonal Swine Anti-Rabbit IgG, HRP Linked	WB 1:1000	20025274 20058714	Dako (P0399)

2.9 TaqMan™ gene expression probes for quantitative PCR

Table 2.8: TaqMan™ gene expression probes for quantitative PCR.

Gene	Assay ID	Fluorescent Reporter Dye	Company
GAPDH	Hs02758991_g1	FAM	ThermoFisher
FANCA	Hs01116668_m1	FAM	ThermoFisher
FANCC	Hs00984545_m1	FAM	ThermoFisher
FANCE	Hs00222482_m1	FAM	ThermoFisher
FANCL	Hs01015745_m1	FAM	ThermoFisher
FANCD2	Hs00276992_m1	FAM	ThermoFisher
FANCI	Hs00383049_m1	FAM	ThermoFisher
FANCS (BRCA1)	Hs01556193_m1	FAM	ThermoFisher
FANCD1 (BRCA2)	Hs00609073_m1	FAM	ThermoFisher
NESTIN	Hs04187831_g1	FAM	ThermoFisher
SOX2	Hs01053049_s1	FAM	ThermoFisher
CD133 (PROM1)	Hs01009259_m1	FAM	ThermoFisher
GFAP	Hs00909233_m1	FAM	ThermoFisher

2.10 Standard solutions

Table 2.9: Standard solutions.

Standard solutions
1.0M Tris pH 8.0: 131.14 g tris base dissolved in 600ml ddH2O. HCl was added until pH 8.0 was reached. ddH2O made the solution up to 1000ml.
10% APS: 1g APS dissolved in 10ml ddH2O.
10% SDS: 50g SDS dissolved in 500ml ddH2O.
10X TBS: 24.2g Tris-Base and 80g NaCl dissolved in 300ml ddH2O. HCl was added until pH 7.6 was reached and ddH2O made the solution up to 1000ml.
1M DTT: 1.54g DTT dissolved in 10ml ddH2O.
5% BSA: 25g BSA dissolved in 500ml PBS.
5% Marvel Milk: 10g Marvel milk powder dissolved in 200ml PBS-T.
500mM EDTA: 146.12g EDTA dissolved in 1000ml ddH2O.
5M NaCl: 146g NaCl dissolved in 500ml ddH2O.
70% Ethanol: 700ml ethanol and 300ml ddH2O.
70% Methanol: 700ml methanol and 300ml ddH2O.
Block buffer: 1.5g BSA (3%) and 50µl Tween-20 (0.1%) made up to 50ml with 4x SSC.
Comet alkaline Unwinding Solution: 4g NaOH pellets and 2.5ml 20mM EDTA (included in comet assay kit) made up to 500ml with ddH2O.
Comet Electrophoresis Buffer: 8g NaOH pellets and 2ml 500mM EDTA made up to 1000ml with ddH2O.
Methylene Blue (0.4%): 2g methylene blue dissolved in 500ml 70% or 100% methanol.
NuPage MOPS SDS Running Buffer: 25ml NuPage MOPS SDS Running Buffer (20X) in 475ml ddH2O.
NuPage Transfer Buffer: 50ml NuPage Transfer Buffer (20X), 750ml ddH2O and 200ml methanol.
PBS-T: 500µl TWEEN 20 dissolved in 500ml PBS.
PBS: 1 Oxoid PBS tablet dissolved in 100ml ddH2O and sterilised by autoclaving.
SSC (4x): 175.3g NaCl (3M), 88.2g sodium citrate (0.3M) and ddH2O made the solution up to 1000ml and pH to 7 with HCl.
TBS-T: 500µl TWEEN 20 dissolved in 500ml TBS.
TE buffer pH 7.5: 10mM TRIS HCl pH 7.5 with 1mM EDTA.

METHODS

2.11 Established human cell line culture

2.11.1 Procurement of established cell lines

T98G cells, U87 cells and LN18 cells were purchased from American Type Culture Collection (ATCC) and U138 cells were taken from lab stocks originally purchased from ATCC. U251 cells were a gift kindly provided by Professor Susan Short (Leeds Institute of Cancer and Pathology).

2.11.2 Cell culture

All experiments involving cell lines and handling of live cells were performed in a Class II sterile laminar flow hood using sterile plasticware and solutions (detailed in Section 2.1: Materials). Laminar flow hood working surfaces were cleaned meticulously with industrial methylated spirit (IMS) before and after procedures and aseptic technique was maintained throughout to minimise the risk of contamination.

2.11.3 Growth conditions

Unless otherwise specified, cell lines were propagated as adherent monolayers in flat sided flasks of 75cm^2 containing 10ml DMEM with 10% FCS in a humidified incubator at: 37°C, 5% CO_2 and 21% O_2. Cells were routinely passaged roughly every 3-5 days, dependent on the cell line. STR profiling was performed on commonly used established cell lines by Dr Anil Ganesh. All cell lines were routinely tested for mycoplasma infection (typically each month whilst being cultured) and were not passaged beyond 15-20 times after thawing in order to avoid phenotypic drift.

2.11.4 Serial passaging of established cell lines

Cells were passaged once a confluency of approximately 70-80% was reached based on microscopic appearance. Spent medium was gently aspirated off before the cell monolayer was washed twice with PBS to remove any residual medium and debris. Cell monolayers were then treated with trypsin-Versene/EDTA (1ml to glioblastoma cell lines, 2ml to non-glioblastoma cell lines) and returned to an incubator until the cells started to detach from the growth surface (typically: ~2-3mins U87, LN18, U251, HeLa, HeLa Silencix cells; ~3-4mins T98G. Tissue culture flasks were gently agitated after removing from the incubator then 8-9ml warm media was added to inactivate trypsin and dilute the cell suspension. Cells

were agitated to provide a single cell suspension which was then used to seed new flasks in a ratio of 1:5-1:10. All cell lines were routinely tested for mycoplasma infection and, for all experiments, cells with a passage number below 30 (and usually below 20) were used in order to avoid phenotypic drift. Cells were discarded beyond this point.

2.11.5 Counting cells

Cells were detached from monolayers using trypsin-Versene/EDTA (as above) then made up to a 10ml single cell suspension by adding warmed media and passing the suspension through a 10ml pipette 5-6 times. Then 10µl of single cell suspension was added to the chamber of a haemocytometer and the number of cells in each quadrant was counted. The mean cell count 'C' of the 4 quadrants was calculated and the number of cells per ml suspension was equal to C x 10^4.

2.11.6 Cryopreservation

Cells were detached from the flask using trypsin-Versene/EDTA and diluted with media (as above) then centrifuged at 180xg for 2 minutes before the media was discarded. Cell pellets were resuspended in 3ml/75cm^2 flask of premixed 'cryopreservative media' (DMEM with 10% FCS + 10% DMSO). 1ml aliquots were placed in labelled cryovials and initially stored at -80C before transfer to liquid nitrogen for long-term storage.

2.11.7 Thawing cells

Cryovials were removed from liquid nitrogen storage and thawed rapidly in a 37°C water bath. Once thawed, the cell suspension was immediately transferred to a 25cm^2 flask containing 7ml medium. Cells were allowed to adhere overnight and medium was changed the following day. Cells were cultured as above and transferred to a 75cm^2 flask once 70-80% confluence was reached.

2.12 Primary patient-derived cell line culture

2.12.1 Procurement of the 'Cambridge' patient-derived glioblastoma stem cell lines

The G1, G7, E2 and S2 cell lines were kindly gifted by Professor Colin Watts (University of Birmingham, Brain Cancer Programme Chair) and Professor Anthony Chalmers (University of Glasgow, Chair of Clinical Oncology). These lines were originally derived from freshly resected glioblastoma specimens by Professor Watts' former laboratory in Cambridge.

Tissue samples were obtained in accordance with local ethics guidelines. Anonymised tissue was mechanically minced in modified phosphate buffered saline solution (PBS) prior to enzymatic digestion. Single cells were then isolated by filtration through a 40μm filter (Falcon, UK) and washed with 10ml red blood cell lysis buffer. Live cells were quantified by trypan blue exclusion, seeded at standard density of 15,000 cells/cm^2 in stem media (defined below) and allowed to form primary aggregates. These were collected and plated, without dissociation, onto extracellular matrix (ECM) coated flasks (ECM 1:10 dilution, Sigma, UK) and allowed to form a primary monolayer. As the primary monolayer approached confluence cells were dissociated by incubation with Accutase (Life Technologies) at room temperature and washed with PBS. The cell viability was assessed by light microscopy and cells were reseeded onto ECM-coated flasks at a density of 150 cells/cm^2 to generate the secondary monolayer. To generate subsequent monolayers cells were seeded at standard density 15,000 cells/cm^2 at each passage. Cell numbers were expanded in this fashion and aliquots frozen at -80°C in media with 10% DMSO as a cryoprotectant before being transferred to liquid nitrogen. 'Cambridge' patient-derived lines received by our team had also undergone a limited number of passages and cryopreservation in the Chalmers' laboratory (Glasgow) before transfer to Sheffield.

2.12.2 Derivation of 'Sheffield' patient-derived glioblastoma stem cell lines

The 'Sheffield' newly patient-derived GSC lines (OX-1 to OX10) were generated as follows and in accordance with local Research Ethics Committee (REC) approval (REC 11-YH-0319). Patients were consented for research preoperatively (by the author) and underwent surgery within the A-Floor theatre complex – Royal Hallamshire Hospital (RHH), Sheffield Teaching Hospitals NHS Foundation Trust (STH). Fresh glioblastoma tissue surplus to histological requirements resected by the operating surgeon (see Table 2.10) was collected intraoperatively (by the author) whilst surgery was ongoing and transferred immediately to the Collis laboratory (G-Floor, The University of Sheffield Medical School), which is co-located in the same building as RHH.

Table 2.10: List of Neurosurgeons providing brain tumour specimens for research.

Name	Initial	Role	Subspecialty
Mr Shungu Ushewokunze	SOU	Consultant Neurosurgeon	Neuro-Oncology; Paediatrics
Mr David Jellinek	DAJ	Consultant Neurosurgeon (retired); Previous Neuro-oncology MDT Lead	Neuro-Oncology
Mr Yahia Al-Tamimi	YAT	Consultant Neurosurgeon; Current Neuro-oncology MDT Lead	Neuro-Oncology; Skull Base
Mr Saurabh Sinha	SS	Consultant Neurosurgeon	Neuro-Oncology; Pituitary; Paediatrics
Mr Geza Mezei	GM	Consultant Neurosurgeon	Neuro-Oncology; Radiosurgery
Mr Veejay Bagga	VB	Speciality Registrar	N/A
Mr Daniel Brown	DB	Speciality Registrar	N/A
Mr Farouk Olubajo	FO	Speciality Registrar	N/A

Fresh tissue specimens for research were pseudonymised – with removal of any patient identifiable information and assignment of a unique identifier (e.g. STH913031) – then transferred in a universal specimen container with no additives, enclosed within a sealed pathology specimen bag. In the laboratory, tissue samples were washed thoroughly with warm (37°C) phosphate buffered saline (PBS). All excess PBS was aspirated and tumour specimens greater than 5x5mm were divided prior to further processing. Specimens were then mechanically dissociated using two scalpels. Accutase™ (5ml) warmed to (37°C) was added to provide enzymatic dissociation and the suspension was pipetted up and down to provide further disaggregation prior to incubation at 37°C for 30 mins. The enzymatic dissociation step was repeated until cells were well dissociated with the majority visible as single cells (typically 60-90 mins). Stem media (5ml) was added and the suspension transferred to a Falcon tube, mixed well then filtered through a 100µM cell strainer. Cell suspension was then centrifuged at 1000rpm for 5 minutes. Following aspiration of the supernatant, cells were re-suspended in 5ml stem media and transferred to a T25 flask kept upright (non-adherent conditions) and incubated at 37°C for 24-48 hours to allow the formation of primary aggregates. These were collected and transferred without dissociation into Matrigel™-coated flasks (T25) to form a primary monolayer. Cells were washed with PBS and had stem media replaced daily to gently remove red blood cells and debris. Once confluent, cells were transferred to two T25 flasks or one T75 flask to generate a secondary

monolayer (Figure 2.1). Cells continued to be expanded and aliquots cryopreserved as described below.

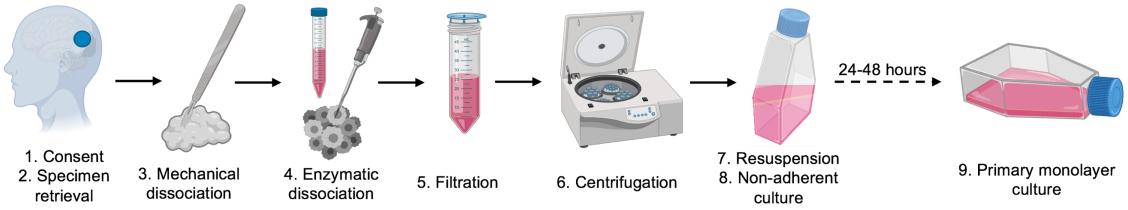


Figure 2.1: Schematic diagram of primary, patient-derived glioblastoma stem cell line generation.

2.12.3 *Parallel 'Sheffield' patient-derived glioblastoma stem cell lines to model resected & residual disease*

Dependent on specific anatomical considerations of individual cases, surgical resection occasionally provides a large *en-bloc* specimen (e.g. partial lobectomy) that includes portions of infiltrated brain that would not otherwise be resected (Figure 2.2A). This tissue may prove crucial in modelling and understanding residual disease in glioblastoma. *En-bloc* specimens were hemisected whilst in the operating theatre to ensure suitable specimens for both routine histopathology and research, each containing tumour mass and adjacent infiltrated brain tissue. In the laboratory, specimen for research was macroscopically divided to provide tissue from the tumour core and adjacent infiltrated brain, along with tissue from the intervening region (edge/intermediate sample). Subsequently, Sheffield GSC lines were generated from each tissue sample in parallel as described above.

2.12.4 *Parallel 'Sheffield' patient-derived glioblastoma stem cell lines to model random intra-tumoural heterogeneity*

Since glioblastoma is characterised by extensive intra-tumoural heterogeneity[13,15], the capability to establish whether or not biological differences between resected and residual disease models are systematic and distinct from an expected degree of molecular and functional heterogeneity of cells *within* all high-grade gliomas would be appealing. Consequently, additional parallel (i.e. multiple GSC lines from the same patient) primary GSC lines were generated from large tumour only specimens using macrodissection and random sampling (Figure 2.2B) prior to cell line derivation as described previously. These parallel GSC lines are intended to model the expected degree of intra-tumoural heterogeneity *within* the parental tumour and, in addition to utility in the functional cell-based study of intra-tumoural heterogeneity, these could serve as useful control

(comparison) models to ascertain if the properties of residual disease models are genuinely unique.

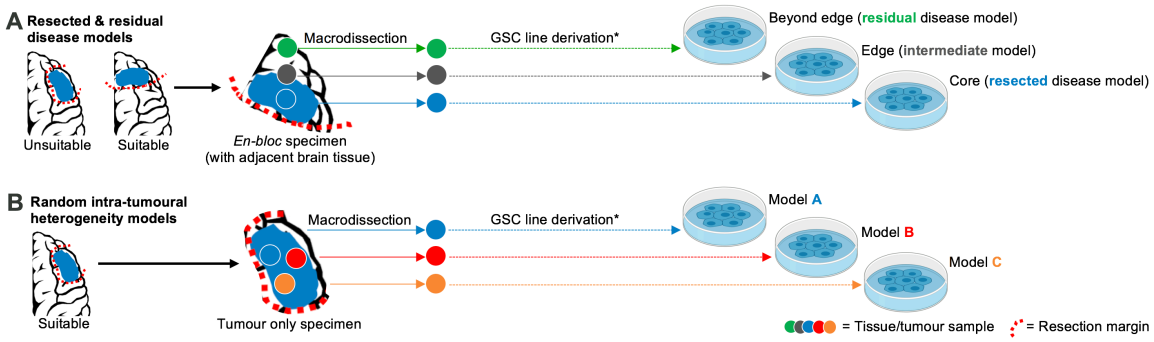


Figure 2.2: Schematic representation of parallel patient-derived glioblastoma stem cell line derivation – A. **Generation of resected and residual GSC models**. Requires suitable en-bloc surgical specimens containing tumour and adjacent brain tissue. B. **Generation of random intra-tumoural heterogeneity models**. Derived from large tumour only specimens (i.e. containing no adjacent brain tissue). *Following macrodissection of a specimen into discrete tissue-tumour samples, multiple GSC lines were derived (as described previously) in parallel.

2.12.5 Propagation of patient-derived glioblastoma stem cell lines

GSC cultures were maintained in stem cell enriching conditions using 'stem media'. This consisted of Adv DMEM F12 medium supplemented with 1% B27, 0.5% N2, 4µg/ml heparin, 20ng/ml epidermal growth factor (EGF), 20ng/ml fibroblast growth factor (FGF), 1% L-glutamine, 1% penicillin-streptomycin and 0.1% amphotericin B. Monolayer GSC cultures were seeded onto Matrigel™-coated plastic tissue culture flasks or plasticware. To coat tissue culture flasks or other plasticware, 1ml aliquot(s) of Matrigel™ were first defrosted on ice until liquid then diluted 1:40 with cold Adv DMEM F12 media (without additives) and mixed well using a chilled disposable pipette. Matrigel™:media solution was then applied to the cell facing surface of plasticware using a Repetman™ with a chilled disposable Repetman™ tip, with gentle rocking to ensure even coverage. Plasticware was then incubated at 37°C for 60 minutes to allow the Matrigel™ to solidify. Subsequently, excess solution was aspirated of and discarded. Matrigel™-coated plasticware was either used immediately, or stored in a refrigerator for up to 1 week with any plates/lids taped securely closed. Table 2.11 details the volume of 1:40 Matrigel™-media added to coat the range of plasticware used to culture patient-derived cell lines.

Table 2.11: Matrigel™ coating plasticware.

Plasticware	Volume Matrigel™-media added (μL)
75cm^2 Tissue Culture Flasks	2500/flask
25cm^2 Tissue Culture Flasks	1500/flask
6-Well Tissue Culture Treated Plates	500/well
12-Well 3D Alvetex™ Tissue Culture Plates	500/well
24-Well Tissue Culture Treated Plates (including with glass coverslips)	250/well

Neurosphere cultures did not require Matrigel™ coated plasticware. Cells were passaged when 70-80% confluency from microscopic appearance was reached. Media was aspirated off and the cell monolayer washed with PBS to remove any remaining medium and debris. Cell monolayers were then treated with 0.5ml Accutase™ and incubated at 37°C for 2-3 minutes to detach cells from the Matrigel™ coating, then the flask was gently agitated. Fresh stem media (4.5ml) was added, and the cell suspension mixed well. Cells were then distributed into new flasks with further stem media added (to make up to 10ml) and mixed well. Passage number was recorded.

2.12.6 Generation of paired tumour bulk populations

Differentiated tumour 'bulk' cultures were derived from GSC cultures by propagating in differentiating media for at least 5 passages. Differentiating 'bulk' media consisted of MEM, supplemented with 10% FCS, 1% L- glutamine, 1% penicillin-streptomycin and 0.1% amphotericin B. Tumour bulk cultures were grown as adherent monolayers on Matrigel™-coated flasks and Matrigel™-coated plasticware was used for all assays to minimise experimental variation between stem and bulk populations.

2.12.7 Growth conditions for patient-derived glioblastoma cells

Unless otherwise specified, cell lines were propagated as adherent monolayers in flat sided 75cm^2 tissue culture flasks containing 10ml complete stem media (GSC) or bulk media in a humidified incubator at: 37°C, 5% CO_2 and 21% O_2. Once primary, patient-derived cell lines had been successfully established, media was replaced every 2-3 days and cells were routinely passaged roughly every 5-10 days, dependent on the cell line.

2.12.8 Serial passaging of patient-derived glioblastoma cells

Cells were passaged once confluence of approximately 70-80% was reached based on microscopic appearance. Spent medium was gently aspirated off before the cell monolayer was washed twice with PBS to remove any residual medium and debris. Cell monolayers were then treated with Accutase™ (0.5ml) – in contrast to trypsin-Versene/EDTA used for established cell lines – and incubated at 37°C until cells started to detach (typically: ~1-3mins GSCs; ~3-6mins differentiated bulk glioblastoma cells). Tissue culture flasks were gently agitated after removing from the incubator then 9.5ml warm media was added. Cells were agitated to provide a single cell suspension which was then used to seed new flasks in a ratio of 1:5-1:10. All cell lines were routinely tested for mycoplasma infection (typically each month whilst being cultured). The risk of cell line misidentification was reduced by never using working with more than one patient-derived cell line in the safety cabinet simultaneously, thorough cleaning in-between switching cell lines and regular evaluation using light microscopy with comparison to early images. For all experiments, low passage number cells were used (maximum 20, but more commonly 5 to 15).

2.12.9 Counting patient-derived glioblastoma stem cells

Cells were detached from monolayers using Accutase™ (0.5ml) – in contrast to trypsin-Versene/EDTA used for established cell lines – then made up to a 5ml single cell suspension by adding warmed media and passing the suspension through a 5ml pipette 5 times to form a single cell suspension. Then 10µl of single cell suspension was added to the chamber of a haemocytometer and the number of cells in each quadrant was counted. The mean cell count 'C' of the 4 quadrants was calculated and the number of cells per ml suspension was equal to C x 10^4.

2.12.10 Cryopreservation of patient-derived glioblastoma stem cell lines

Cells were detached from monolayers (as previously described) and centrifuged for 5min at 1000rpm before discarding the supernatant. Cells were then re-suspended in cryopreservative medium (Adv DMEM F12 without supplements + 10% DMSO, premixed immediately before use) using 3ml media per 75cm^2 flask. Aliquots (1ml) were placed in labelled cryovials (Corning) and initially stored at -80°C for at least 24 hours within a Mr Frosty™ freezing container, to achieve a cooling rate close to -1°C/minute. Subsequently cryovials were transferred to liquid nitrogen for long-term storage.

2.12.11 Thawing cells

Cryovials were removed from liquid nitrogen and thawed rapidly in a 37°C water bath. The thawed cell suspension was then transferred to a 25cm^2 flask containing 9ml of stem media. Cells were allowed to adhere overnight and the media was replaced the following day.

2.13 MTT cell viability assay

In this assay, a tetrazolium salt 3-(4,5-dimethylthiazol-2-yl)-2,5-diphenyltetrazolium bromide – usually referred to as MTT, is used to provide a quantitative colorimetric correlate of mammalian cell survival and proliferation[207]. Water-soluble MTT is reduced by viable, actively metabolic cells to produce insoluble purple formazan crystals. Since dead cells are unable to metabolise MTT, optical density at the 540nm absorbance peak (OD_{540}) of the purple formazan product, which is solubilised using DMSO, represents a direct correlate of viable cell number in a well optimised assay.

2.13.1 MTT cell viability assay in established cell lines

Cells were seeded in a 96-well plate at densities determined during assay optimisation (see Figure 2.3), or previously optimised densities, in 100µl media per well and incubated for 24 hours prior to treatment. Plating densities for established cell lines are detailed in Table 2.12. To establish this, cells were plated at increasing density (from 0, 100, doubling up to 102,400/well) then incubated overnight without treatment before completion of the assay. Subsequent experiments were planned to provide results within the boundaries of the linear OD_{540}-cell number relationship (Figure 2.3A). Since subsequent assays using treatments would be incubated for several days (to allow adequate time for treatment effects to be revealed), it was important to establish an appropriate plating density that would provide OD_{540} close to the apex of the linear OD_{540}-cell number relationship by the end of the 6-day incubation period. Cells were plated at increasing densities and incubated for 6- and 7-days to determine optimal plating densities (Figure 2.3B).

Table 2.12: MTT cell plating densities.

Cell Line	Plating Density (cells/well)
U87	1.00 x 10^3
T98G	0.75 x 10^3
LN18	1.50 x 10^3
U251	1.20 x 10^3

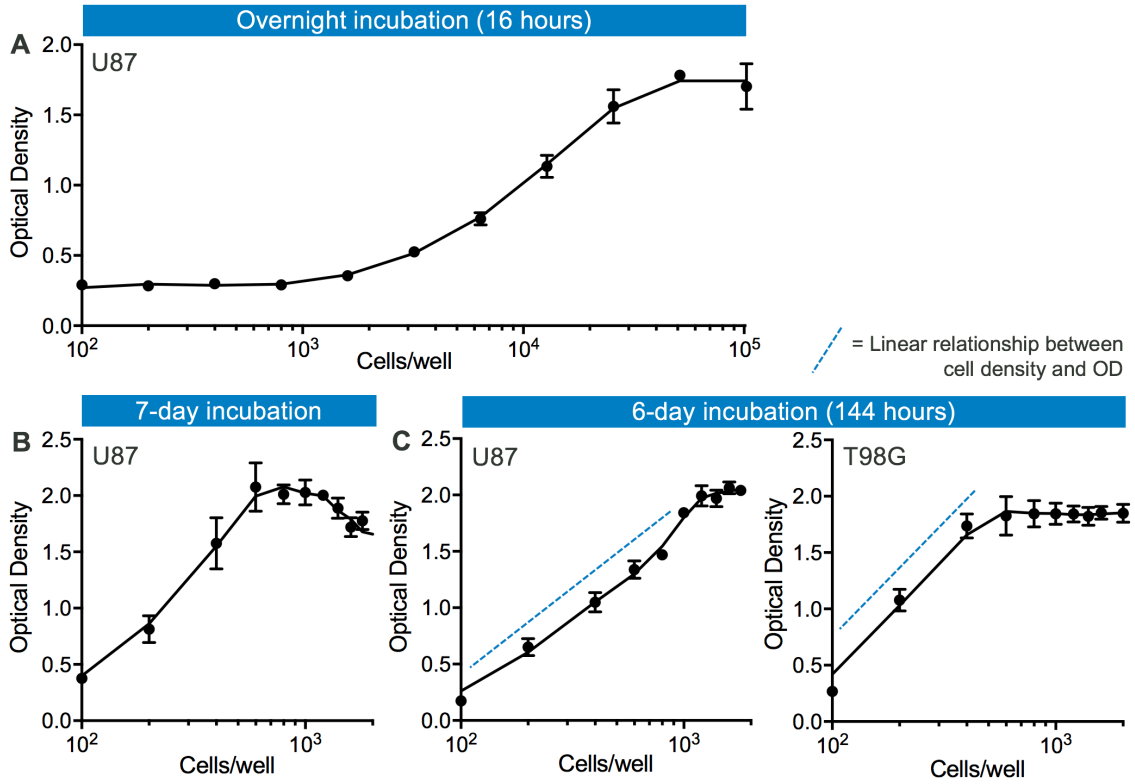


Figure 2.3: Example of cell number optimisation for the MTT cell viability assay using established glioblastoma cells – A. **Standard curve demonstrating the relationship between cell number and optical density.** U87 glioblastoma cells were plated at increasing density then incubated overnight before completion of the assay to provide a standard curve demonstrating the relationship between cell number and optical density. B-C. **Determination of optimal plating density.** Cells were plated ay increasing densities and incubated as indicated to determine optimal plating densities. Each optimisation experiment was performed in triplicate.

DDRi and DNA damaging agents were added by dilution of a stock solution to 20x the intended final concentration using media (except where otherwise specified), before adding 5µl of 20x drug solution or an equivalent concentration of DMSO to the defined wells. In assays determining the ability of DDR inhibitors to chemosensitise, the relevant chemotherapeutic agent was added 1 or 8 hours after DDR inhibition (as specified in results) to allow optimal target inhibition prior to the induction of exogenous DNA damage. Time periods were based on previous optimisation work by A. Patil (data not shown) and/or time-course data presented within this thesis. In contrast, for assays assessing combination DDR therapies (in the absence of chemotherapy), treatment with DDR inhibitors occurred simultaneously since we expected these therapeutic strategies rely on exacerbating the

effects of the ongoing, constitutively elevated levels of endogenous DNA damage and/or replication stress in cancerous and cancer stem cells[208,209]. Following treatment, cells were incubated for a further 5 days. Subsequently 50μl/well of MTT in PBS (3mg/ml) was added and cells were incubated for a further 3 hours at 37°C. The media was then gently removed using a multi-channel pipette and the purple formazan product was dissolved in 200μl/well of DMSO. Optical density values at 540nm (close to the maximal absorbance of the formazan product) were determined using a Multiskan FC spectrophotometric plate reader and percentage cell viability for each condition was calculated by comparison to DMSO-treated controls.

2.13.2 MTT heatmap meta-analysis

For each treatment condition, mean cell viability values for each established glioblastoma cell line (U87, U251, T98G, LN18) were calculated by combining data from individual experiments. Therefore temozolomide alone response values reflected the average across multiple sets of independent experiments for each cell line (typically 15+ independent experimental repeats), whilst values for temozolomide in combination with a particular DDRi were derived from 3+ independent experimental repeats. Using GraphPad Prism, a matrix of treatment conditions was constructed (temozolomide +/- FAPi or PARPi or ATRi or ATMi) stratified by cell line and a gradient colour scheme was applied with full green corresponding to cell viability of 100% and full red corresponding to a reduction in cell viability to 50% or less.

2.14 Clonogenic survival assay

The clonogenic survival assay provides a highly sensitive means of determining of cell survival following exposure to potentially cytotoxic agents including chemotherapy and ionising radiation. The assay measures viable cells that have demonstrated functional survival by maintaining the propensity for at least 5-6 rounds of replication to produce a colony[210,211].

2.14.1 Clonogenic set up and treatments

Single cell suspensions were prepared and counted (as above) then diluted with media to produce either 1 cell/μl or 10 cell/μl suspension as required. Cells were then seeded into 6-well plates (established cell lines) or Matrigel™-coated 6-well plates, at various densities

whilst maintaining a total volume of 2ml media in each well of the 6 well plates. Cells were plated in triplicate for each experimental condition and higher seeding densities were used for plates scheduled to receive treatment with irradiation or temozolomide chemotherapy as the example in Table 2.13-14 demonstrates. These values were derived from our previous optimisation studies (chemotherapy) and by Professor Anthony Chalmers Laboratory (radiotherapy).

Table 2.13: Seeding densities for G1, G7 & E2 glioblastoma stem cell lines treated with radiotherapy.

IR dose (Gy)	Cells/Well	Volume Cell Suspension (µl/well)	Volume Media (µl/well)
0, 1 & 2	300	300	1700
3	500	500	1500
4	800	800	1200
5	1000	1000	1000

Table 2.14: Seeding densities for G1, G7 & E2 glioblastoma stem cell lines treated with temozolomide chemotherapy.

Temozolomide dose (µM)	Cells/Well	Volume Cell Suspension (µl/well)	Volume Media (µl/well)
0	300	300	1700
5	750	750	1250
10	1500	1500	500
15	1750	1750	250
20 & 25	2000	2000	0

Plates were then incubated overnight (16 hours) to enable the cells to adhere. Subsequently, media was aspirated from the plates and replaced with 2ml media containing DDR inhibitor(s) at the final intended concentration or DMSO of equivalent concentration for control wells. Plates were then incubated for 1 hour prior to treatment with radiotherapy or temozolomide - exposure of individual plates to 1, 2, 3, 4 and 5 Gy of radiation was undertaken during each assay with 0 Gy control plates receiving sham irradiation; 50mM temozolomide stocks (in DMSO) were diluted using media to 20x final intended concentration with additional DMSO added to ensure equivalent % DMSO concentration across the various doses (including 0µM temozolomide) then 100µl/well was added. At 2 hours post-irradiation, or 120 hours post-temozolomide, drug/media was completely aspirated off the plates and replaced with 2ml of fresh media that did not contain drug or DMSO. After this, plates were incubated for a total of 21 days post-

irradiation/temozolomide to allow adequate colony formation prior to staining and counting.

TTFields treatments

For treatments with TTFields cells were seeded onto Matrigel™-coated glass coverslips within wells of a 24-well plate at a density of 5 x 10^4 cells/well. Plates were incubated overnight (16 hours) to enable the cells to adhere before the coverslips were transferred to ceramic dishes used for treatment within the Inovitro™ TTFields delivery system (see Chapter 4 – Section 4.4.1). Cells designated for both TTFields treatment and sham treatment (untreated) were transferred to ceramic dishes to avoid experimental variation. Within the Inovitro™ system, alternating electrical fields were delivered at the FDA approved frequency of 200kHz[70] for 48 hours. Treatments were delivered within a temperature controlled incubator with an integrated cooling system to maintain strict incubation at 37°C (measured directly by the 4 temperature probes integrated into each cell culture dish within the Inovitro™ system). Subsequently, cells were detached using Accutase and counted using a haemocytometer to establish TTFields-mediated growth inhibition. For clonogenic studies, cells were reseeded to 6-well plates at a density of 300 cells/well prior to staining and counting.

2.14.2 Clonogenic staining and counting

Following the 21-day incubation period, media was removed from the plates and methylene blue (0.4%) was used to stain the colonies. Following 60 minutes incubation at room temperature, methylene blue was removed and any excess was washed from the plates by gentle submersion in tepid water. The colonies (greater than 50 cells) were counted and the plating efficiency (PE) was calculated by the average number of colonies counted on the DMSO treated control plates divided by the number of cells plated. The survival fraction (SF) was then calculated by the number of colonies counted/number of colonies plated multiplied by the PE.

2.15 3D Alvetex™ clonogenic survival assay

Traditional 2D cell culture models present a limited representation of the 3-dimensional complexity and spatial orientation of cancerous cells within patient tumours. The interconnectedness of glioblastoma cells in 3-dimensions has been demonstrated to play

an important role in therapeutic resistance[212], highlighting a need to replicate this 3D orientation of cells during *in vitro* experiments. More recently, a novel 3D Alvetex™ cell culture system customised to model treatment resistant glioblastoma stem cells has been demonstrated to recapitulate key histological features of glioblastoma and more reliably predict clinical response when compared to conventional 2D models[106,108]. This 3D Alvetex™ glioblastoma stem cell model was pioneered by Dr Natividad Gomez-Roman and Professor Anthony Chalmers (The University of Glasgow), through NC3Rs-funded research aiming to provide a clinically-relevant, animal-free alternative to rodent xenograft studies used in glioblastoma research. During a 6-week Royal College of Surgeons funded research training secondment, I received comprehensive training in use of the 3D Alvetex™ model, prior to implementation of the model to generate data in Sheffield[213,214].

2.15.1 Preparation of 3D Alvetex™ plates

12-well 3D Alvetex™ plates (Figure 2.4) were prepared in a class II biological safety cabinet. On a new plate, 1ml of 70% ethanol per well was added then aspirated off after 1-2 minutes. This step removes a thin protective coating from the Alvetex™ (polystyrene) tissue culture scaffolds to render them hydrophilic. Subsequently, Alvetex™ scaffolds were Matrigel™ coated, as described above (Section 2.13.5). Once coated and excess Matrigel™:media had been aspirated, prepared Matrigel™-coated 12-well Alvetex™ 3D tissue culture plates could be stored at 4°C for up to 14-days. However, prepared plates were typically used (cells seeded) within 24 hours of preparation and plates from the same batch prepared were used for all conditions within each experimental repeat to minimise any technical variation.

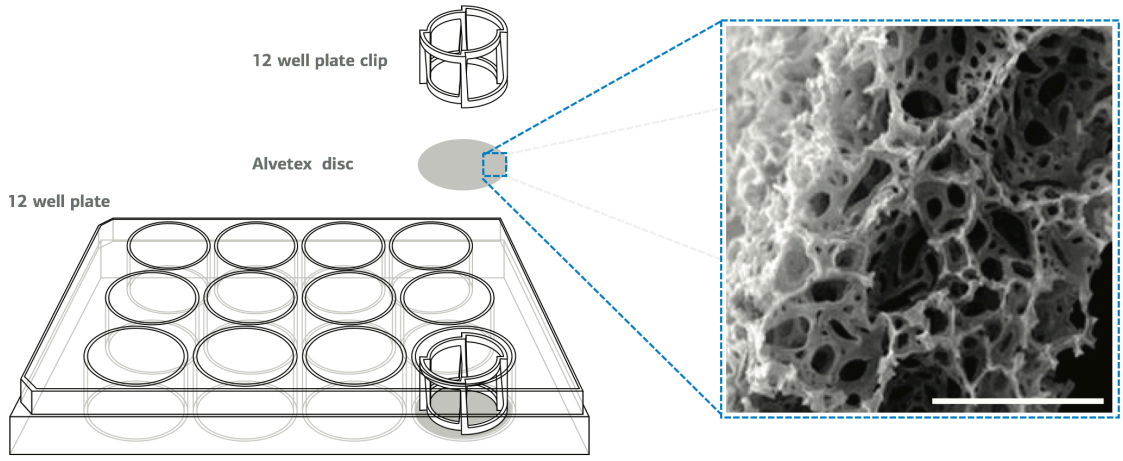


Figure 2.4: 3-dimensional Alvetex™ 12-well plate diagram – Plates consist of 12 Alvetex™ (polystyrene) scaffolds each secured within a well by a plate clip (to avoid floatation of the scaffold). The inset displays the 3D Alvetex™ scaffold ultrastructure observed by scanning electron microscopy (scale bar - 100µM). *Adapted from Reprocell.com*[215].

2.15.2 3D clonogenic set up and treatments

Cells were seeded and treated as described above for 2D clonogenic experiments (see Section 2.14.1). As Alvetex™ scaffolds are delicate, additional care was taken during aspiration steps avoid any damage/tears to the scaffolds.

2.15.3 3D clonogenic staining and counting

Following the 21-day incubation period, 200μL/well of MTT reagent (10mg/ml in PBS) was added to plates which were then incubated for 4 hours at 37°C in the dark. Importantly, in 3D clonogenic studies, MTT is used only to provide colony specific staining (since methylene blue can also discolour the Alvetex™ scaffolds) and the formazan product is not solubilised to estimate cellular activity or viability (Figure 2.5). Subsequently, media with MTT was aspirated off the scaffolds, plastic 12-well plate clips (see Figure 2.4) were removed, and 100μL/well of 4% paraformaldehyde was added. Plates were incubated at room temperature for 15 minutes to allow fixation of the colonies, before removal of the excess paraformaldehyde. Plates with stained colonies could be foil wrapped and stored at 4°C for up to 14 days, but were typically counted within 72 hours. Colonies were counted and the plating efficiency and surviving fractions were calculated as above. However, as it is not possible to visualise individual cells within the translucent 3D scaffolds using light microscopy, we estimated that any MTT-stained cluster of cells that is visible within the scaffold without magnification contains more than approximately 50 cells. This methodology has previously been previously validated by the Chalmers Laboratory. Additionally, we have tested this counting procedure using multiple assessors and found it to provide high inter-rater reliability, as demonstrated in Figure 2.6 below.

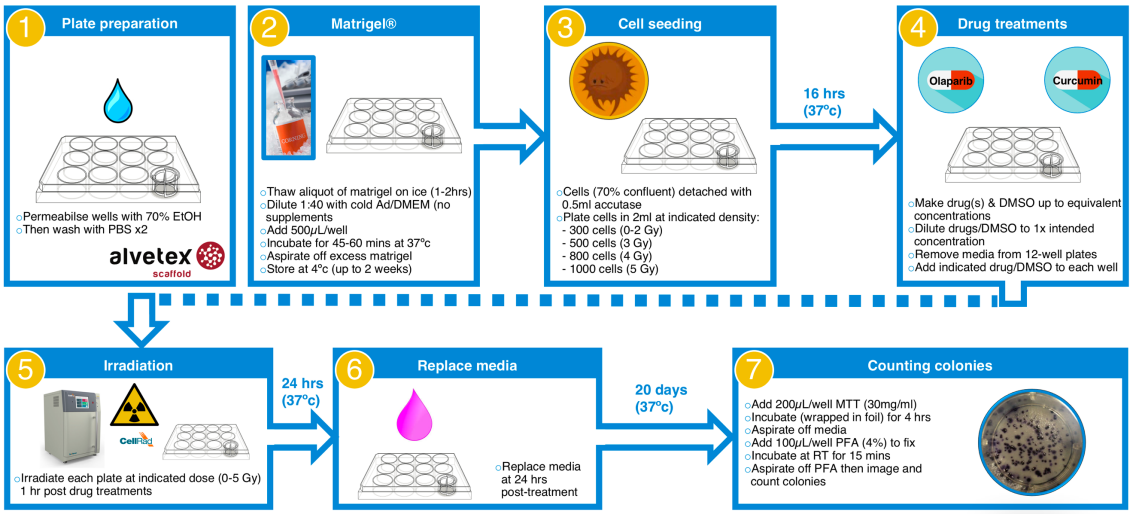


Figure 2.5: Flowchart protocol for a typical 3-dimensional clonogenic experiment – Example: combined inhibition of the FA pathway and PARP, using curcumin and olaparib, respectively prior to irradiation.

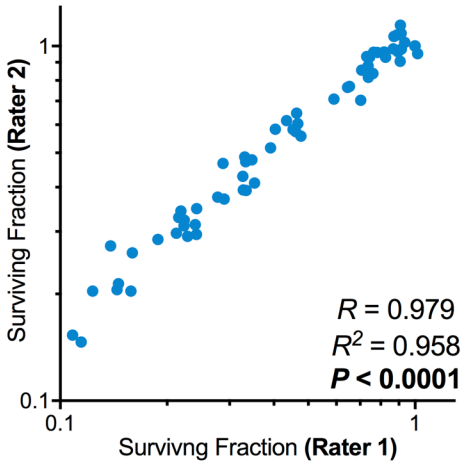


Figure 2.6: Inter-rater reliability of 3-dimensional clonogenic experiments – Results from 72 wells scored independently by 2 assessors (Rater 1, Ola Rominiyi; Rater 2, Dawoud Dar). Surviving fractions for each well (Rater 1 vs Rater 2) and demonstrate a strong, statistically significant Pearson correlation co-efficient (R^2). This optimisation experiment was performed in triplicate.

2.16 Immunoblotting

2.16.1 Protein extraction and quantification

Media was removed from cells that had previously been seeded (and treated where indicated) into 6-well plates, then wells were washed twice in ice cold PBS. Subsequently, 100µl of lysis buffer (see Table 2.15) was added to each well. Cells were harvested from each using a cell scraper, transferred to labelled eppendorfs, vortexed and then left to lyse on ice for 30 minutes, further vortexing each eppendorf at 15 then 30 minutes. Eppendorfs containing lysates were then centrifuged at 15,000r.c.f for 15 minutes at 4°C and the supernatant was transferred into newly labelled eppendorfs, which were kept on ice.

Table 2.15: Lysis buffer.

Reagent	Stock Concentration	Volume Added to Make 5ml Lysis Buffer
50mM Tris pH 8.0	1M	250µl
200mM NaCl	5M	200µl
1% Triton X-100	100%	50µl
1mM DTT	1M	5µl
1mM EDTA	500mM	10µl
Benzonase nuclease	25U/ml	10µl
Phosphostop™ & Complete EDTA Free Protease Inhibitor Tablet	½ tablet each*	2.5ml
ddH2O	-	1.98ml

**One Phosphostop tablet and one Complete EDTA Free Protease Inhibitor Tablet were dissolved together in 5ml ddH2O, then 2.5ml of the solution was used in the lysis buffer. The remaining 2.5ml was frozen at -20°C for future use.*

To quantify the protein in each extract, 1µl of protein lysate and then 39µl of ddH2O were added to wells of a 96 well, in triplicate. Protein Assay Dye Reagent Concentrate (BioRad) was then diluted 1:5 with ddH2O and 200µl/well was added. Optical Density (OD) was read at 595nm on a Multiskan FC Thermo Scientific spectrophotometer. The protein standard curves, which were made using known concentrations of bovine serum albumin (BSA), were used to quantify protein concentration by solving the linear quadratic equation y = mx + c, where m is the slope gradient and c is the y-intercept.

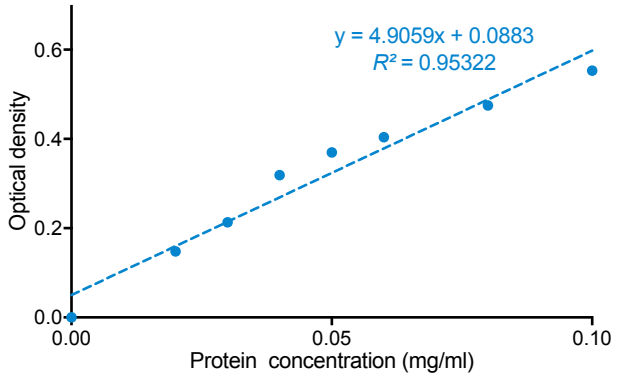


Figure 2.7: BSA standard curve – The standard curve created from standard solutions of known BSA concentrations was extrapolated to calculate lysate protein concentrations.

Once each lysate had been quantified, 25µl NuPage LDS Sample Buffer with 5mM DTT (1µl DTT per 100µl) was added to each sample. Samples were then, vortexed, heat-treated for 5 minutes at 95°C and then stored at -80°C until required.

2.16.2 Protein extraction from 3D Alvetex™ scaffolds

As cells grow within the pores of scaffolds in the 3D Alvetex™ model, protein extraction was more challenging, with lower yields and required a modified approach. Typically, 2-3 wells of a 12-well 3D Alvetex™ plate were used for each experimental condition to provide sufficient protein. After removal of media, wells were washed twice with ice cold PBS (as above), then left to rest on an incline for 1 minute and further aspirated to remove any residual PBS. Subsequently, 100µl lysis buffer was added to each well and plates were left to rest on ice for 20 minutes, before transfer to a shaking platform for 10 minutes (at approximately 200rpm). Plates were then transferred to ice and left to rest on an incline for 1 minute before lysates were aspirated and transferred to labelled eppendorfs. Following this, the procedures for 2D and 3D experiments were equivalent.

2.16.3 SDS-PAGE & protein transfer

Except where otherwise specified, NuPAGE 4-12% Bis-Tris or 3-8% Tris-Acetate gels were used for electrophoresis. Lysate (with LDS NuPAGE Sample Buffer) volumes calculated (as above) to provide 50µg of protein was loaded on to the gels. SeeBluePlus2 Prestained Standard (for Bis-Tris gels) or HiMark™ Pre-stained Protein Standard (for Tris-Acetate gels) were loaded using 10µl alongside the protein samples as a molecular weight reference. Any empty wells were loaded with 5µl of 4x NuPAGE LDS Loading Buffer. The samples were electrophoresed at 140-150V for 90-120 minutes in an XCell SureLock™ Electrophoresis Mini-Cell or Invitrogen Mini Gel Tank using 1x NuPAGE MOPS (for Bis-Tris gels) or 1x NuPAGE Tris-Acetate (for Tris-Acetate gels) as appropriate. Subsequently, protein within the gels was transferred to nitrocellulose membranes at 100V for 120 minutes in Mini PROTEAN Tetra Cells using 1x NuPAGE transfer buffer.

2.16.4 Immunodetection

All incubation steps took place on a shaking platform (approximately 30rpm). Nitrocellulose membranes were blocked for 30 minutes in 5% milk (Marvel) dissolved in PBS-T. Membranes were then divided, based on the expected location of proteins of interest, then incubated with primary antibodies overnight at 4°C. The next day, membranes were washed 3 times (10 minutes each + intervening washes) in PBS-T, before incubation with appropriate secondary antibodies conjugated to HRP at a concentration of 1:1000. Membranes were washed a further 3 times in PBS-T, then visualised using Pierce ECL western blotting

substrate. In dark conditions, membranes were exposed to medical x-ray film, then films were developed using a Konica SRX 101A Processor.

2.16.5 Calculation of FANCD2 L:S ratios

To quantify the degree of FA pathway activation the normalised ratio of Ub-FANCD2 (L) to FANCD2 (S) (normalised to DMSO only treated cells) was calculated for each treatment as previously described[216] and shown beneath the relevant bands. Briefly, films were scanned at a resolution of 1600 dpi or higher then loaded into ImageJ for densitometry analysis. Measurement criteria were set *(• Analyse → Set measurements → ✓ 'Mean grey value' (only)),* then the rectangular selection tool was used to create a region of interest large enough to contain the whole of the largest band in a row, but without overlapping adjacent bands. The region of interest template was saved *(• File → Save as → ✓ 'Selection')* then used to perform serial measurement of each band in the row *(• 'Command + M')*. The process was repeated for all conditions and in each row sequentially - Ub-FANCD2 (L), FANCD2 (S) and β-actin – and background measurements for each lane were taken. Measurement values were then transferred to an Excel spreadsheet. Inverted background values (255-background measurement) were subtracted from inverted Ub-FANCD2 and FANCD2 protein values (255-protein) to establish a net protein value. Then net protein values for Ub-FANCD2 and FANCD2 in each lane were adjusted using the corresponding net protein value for β-actin (net protein/net loading control) to provide relative quantification of Ub-FANCD2 and FANCD2. Subsequently the relative quantification of Ub-FANCD2 (L) was divided by relative quantification of FANCD2 (S) to provide the L:S ratio. All values were then divided by the L:S ratio of the DMSO only control to provide normalised L:S ratios (**L:S ratio (n)**). Where specifically mentioned, an additional bespoke measure – **L:S ratio (nt)** was also calculated to adjust for large changes in the quantity of total FANCD2. To derive this measure, L:S ratios were multiplied by net protein measurements for total FANCD2 (Ub-FANCD2 + FANCD2) then normalised to DMSO only controls.

2.17 Immunofluorescence

2.17.1 2-dimensional immunofluorescence in established and primary patient-derived cell lines

2.17.1.1 Seeding cells and treatments

Cells were seeded onto sterile coverslips in 24-well plates at a density of 5 x 10^4 cells/well. Prior to seeding, for experiments with established glioblastoma cell lines (U87 and T98G), coverslips were acid etched in a glass container using 1M HCl with agitation overnight, then washed with ddH2O three times, before being washed in 100% ethanol for 1 hour then air-dried inside a tissue culture Class II Biological Safety Cabinet. For experiments with primary glioblastoma cell lines, coverslips were washed in 100% ethanol overnight, then air-dried inside a tissue culture Class II Biological Safety Cabinet, before being placed into 24-well plates and coated with Matrigel™ as described above. Cells were then incubated for 48 hours to promote reliable adhesion to the coverslips prior to treatment. Subsequently, cells were treated as specified in the results then incubated at 37°C for 24 hours (unless otherwise specified) before further processing.

2.17.1.2 Immunostaining

Following treatments, media was aspirated and cells were washed carefully with cold PBS two times. Extraction buffer containing 0.5% Triton X-100 (100µl in 20ml) and 3% BSA (0.6g in 20ml) in PBS was added to promote cell membrane permeabilisation and prevent non-specific antibody binding, respectively. After incubation in extraction buffer for 5 minutes at room temperature, cells were washed 3 times with PBS. Cells were then fixed using 4% PFA for 10 minutes before washing 3 times with PBS. Primary antibody at the required concentration (see Table 2.6) was added (200µl/well) and cells were incubated for 2 hours at room temperature. After removal of the primary antibody and 3 further gentle washes with PBS, secondary antibody with DAPI (both 1:1000 in PBS with 3% BSA) was added to each well (200µl). Following incubation at room temperature for 1 hour with protection from light, the final washes with PBS (x3) were administered then the coverslips were mounted onto microscope slides using Shandon Immu-Mount medium (Thermo Fisher Scientific). Slides were protected from light and left overnight to dry.

2.17.1.3 Immunofluorescence microscopy

Except where otherwise specified, microscopy was performed on a Nikon Eclipse T200 inverted microscope (Melville), equipped with a Hamamatsu Orca ER camera and a 200W metal arc lamp (Prior Scientific) using a 100x objective lens.

2.17.1.4 Quantification of foci

Images were captured and analysed using Volocity software (Improvision). Image settings including exposure, gain and offset were kept constant between experimental conditions for each repeat. Cells were scored either positive ($\geq$5 foci) or negative (<5 foci) for nuclear foci, or the number of individual foci counted in each cell nucleus was recorded. Eight or more fields across each slide and more than 100 cells were analysed for each experimental condition. Three independent repeats of the experiment were completed. Means and SEM were produced for each condition where possible.

2.17.2 Confocal immunofluorescence in customised 3D Alvetex™ scaffolds

2.17.2.1 Seeding cells and treatments

12-well 3D Alvetex™ plates were prepared and impregnated with Matrigel™ as previously described. Primary, patient-derived glioblastoma stem cells were then seeded at a density of 2.5 x 10^4 cells/well in a volume of 2ml media per well. Cells were incubated at 37°C for 96 hours prior to treatments (where indicated) as described in the results. Subsequently, cells were incubated for a further 24 hours prior to processing.

2.17.2.2 Fixation of cells within 3D Alvetex™ scaffolds and immunostaining

Media was aspirated and scaffolds washed twice with cold PBS. Cells were fixed using 2% PFA in PBS (200µl/well) for 15 minutes. PFA was then aspirated, PBS added, and plates could be stored at 4°C until immunostaining (up to 7 days).

PBS was aspirated from the wells and scaffolds were incubated at room temperature in 1ml/well of 0.5% Triton X-100 (100µl in 20ml) for 15 minutes. Then, Triton X-100 was discarded and scaffolds were washed 3 times with PBS-T (5 minutes per wash on shaking platform at approximately 30rpm). Blocking solution (5% BSA in PBS-T) was then added (1ml/well) and plates were incubated at room temperature on a shaking platform for a further 15 minutes. Subsequently, each scaffold was removed from 12-well plates – taking

care to ensure orientation of each scaffold was maintained (as most cells are present in the upwards-facing half of the scaffolds) – and divided into 6 segments to minimise the quantity of antibody used. The required number of scaffold segments were then placed directly onto 80µl droplets of primary antibody in blocking solution (concentration 1:100-1:250, as indicated) within labelled sections of parafilm covering a bed of wet tissue (to prevent drying out) on trays maintained on a flat surface. Trays were covered and incubated at 4°C for 48 hours. New labelled trays with droplets of secondary antibody conjugated with fluorescent marker (1:400) and DAPI (1:400) in blocking solution were prepared. Scaffold segments from the first tray were then washed sequentially in three small beakers containing blocking solution (washing 3 times in each) – again, taking care to maintain scaffold orientation. The edge of each segment was blotted on tissue paper, to remove excess blocking solution, before being placed directly onto the corresponding droplet of secondary antibody/DAPI solution on the new tray. Scaffold segments were then covered and incubated at room temperature for 1 hour. Scaffold segments were then washed in blocking solution as above and mounted directly onto 15µl droplets of Immu-Mount (Shandon™) mounting media on labelled glass slides, whilst maintaining orientation (cell-seeded side facing upwards). A further 15µl droplet of mounting media was placed on top of scaffold segments then coverslips were gently applied and the edges sealed with coverslip sealant. Slides were protected from light and allowed to dry overnight. Slides were then stored at 4°C for up to 1 week (but typically 1-3 days) prior to imaging.

2.17.2.3 Confocal immunofluorescence microscopy

Microscopy was performed on a Carl Zeiss LSM880 AiryScan Confocal microscope using a 63x objective lens. Z-stacks of stained immunofluorescent cells were obtained with a minimum of 10 sections per stack. Microscope settings were kept constant between all experimental conditions. For foci analysis, the number of individual foci visible within each cell nucleus was counted manually and analysed as described above.

2.17.3 R-loop (RNA:DNA hybrid) immunostaining and confocal immunofluorescence

Primary GSCs were seeded to Matrigel™-coated glass coverslips as described in Section 2.17.1.1 then incubated at 37°C for 24 hours before treatment as specified in the results. Cells were then incubated for a further 6 hours prior to fixation with 100% methanol (-20°C) then permeabilization with 100% acetone. Subsequently, cells were blocked using SSC

blocking buffer for 20 minutes at room temperature. For slides treated with RNaseH - 2U per 400µl blocking buffer was applied to slides during the blocking phase. Slides were stained using the S9.6 antibody to bind RNA:DNA hybrids (1 hour incubation at room temperature). After removal of the primary antibody and 3 gentle washes with 4x SSC, secondary antibody with DAPI (both 1:1000 in SSC blocking buffer) was added to each well (200µl). Following incubation at room temperature for 1 hour with protection from light, the final washes with 4x SSC (x3) were administered then the coverslips were mounted onto microscope slides using Shandon Immu-Mount medium (Thermo Fisher Scientific). Slides were protected from light and left overnight to dry. Confocal microscopy was performed on a Carl Zeiss LSM880 AiryScan Confocal microscope using a 63x objective lens.

2.17.4 RNA:DNA hybrid image analysis

Images were analysed by calculation of the S9.6 mean fluorescence intensity (MFI) for each cell nucleus[217,218], using ImageJ. Briefly, a Gaussian blur was applied to the DAPi image *(• Process → Filter → Gaussian blur → 'Sigma 4' → 'ok')*, then nuclei were segmented *(• Image → Adjust → Threshold → ✓'Dark background' & ✓'Otsu' → 'Apply')*. Where required, holes in segmented nuclei were filled *(• Process → Binary → Fill holes)*, then cells in contact with each other were segregated using the watershed function *(• Process → Binary → Watershed)*. Subsequently, regions of interest were designated using the analyse particles function to exclude objects at the edges of the image and objects too small to represent an intact *nucleus (• Analyse → Analyse particles → ✓'size 50 – infinity' & ✓'Exclude edges')*, then regions of interest were applied to the corresponding S9.6 image *(• Image → Overlay → from ROI manager)* and the nuclear MFI was measured *(• Image → Measure)*.

2.18 TaqMan™ RT-PCR

2.18.1 RNA extraction

Cells were plated in 6-well plates and incubated at 37°C until 70% confluent before harvesting. Qiagen RNeasy Mini Kits were used to extract RNA. Briefly, media was removed from cultured cells and cells were washed twice with ice cold PBS. PBS was aspirated and 350µl RLT buffer was added to each well. Cells were dislodged using a cell scraper and transferred to labelled QIAshredder columns before being centrifuged at 8000r.c.f for minutes (4°C). Purple columns were discarded and 350µl of 70% ethanol was added to the supernatant, which was then transferred to an RNeasy Minispin column and centrifuged for

15 seconds. Flow through was discarded and 700µl of RW1 buffer was added to each column, which were then centrifuged for a further 15 seconds. This process was repeated twice with 500µl of RPE buffer, with centrifugation steps of 15 seconds and then 2 minutes. Flow through was discarded at each step, then an additional centrifugation step for 1 minute was used to remove any excess ethanol. Following this, 50µl RNase free water per sample was added and these were centrifuged for 1 minute to elute the RNA. Total RNA levels in each sample were quantified using the NanoDrop ND 1000 Spectrophotometer; this quantifies absorbance a wavelength of 260nm to establish the concentration of RNA in each sample, and the ratio of sample absorbance at 260/280 was used to confirm purity (absence of contaminants such as protein or phenol, which absorb strongly at/near 280nm) with ratios ~2.0 deemed to represent 'pure' RNA[219]. After RNA quantification, samples were either used immediately, or stored at -80°C.

2.18.2 Reverse transcription

RNA samples were reverse transcribed using the High-Capacity RNA-to-DNA™ Kit (Applied Biosystems™) – reagents detailed in Table 2.16. The RT reaction was prepared on ice. For a 20µl reaction, a volume of sample required to provide 1µg of RNA (determined above) was added to reagents from the Kit and made up to 20µl with RNase free water. Samples were then placed processed in an Thermal Cycler (S1000) (BioRad) with settings for the reverse transcription PCR reaction applied (see Table 2.17) to facilitate the conversion of RNA to cDNA. Samples containing cDNA were then used immediately for quantitative PCR (qPCR).

Table 2.16: Reverse transcription reaction mix.

Component (order added)	Volume per reaction	Constituents
(1) RNase free water	Q.S. to 20µl	
(2) RT Buffer Mix	10µl	*dNTPs*
		Random Octamers
		Oligo dT-16
(3) RNA sample	up to 8µl	
(4) RT Enzyme Mix	2µl	*MuLV*
		RNase Inhibitor Protein

Table 2.17: Reverse transcription PCR programme for cDNA.

Step	Temperature (°C)	Minutes
1	25	5
2	48	60
3	95	5
4	4	-

2.18.3 Real time qPCR – relative mRNA expression

cDNA samples generated from extracted RNA were used in triplicate reactions for each probe on a 384-well PCR plate. Each reaction consisted of: 2µl cDNA, 5µl TaqMan™ Universal PCR Mastermix, 2.5µl ddH_2O and 0.5µl of probes (specific probes used detailed in Table 2.8). GAPDH was probed as a control for each sample. The plate was sealed using optical adhesive film (MicroAmp™) and loaded onto a 7900HT Fast Real-Time PCR System to perform quantitative PCR. The system was set to report 18S FAM with repeats of 40 cycles. Double delta Ct ($2^{-\Delta\Delta Ct}$) analysis was used to determine relative gene expression using an average *Ct* value from the triplicate runs. For example, to detect differences in expression between primary, patient-derived glioblastoma stem cells and differentiated bulk cells:

$$\Delta Ct = Mean\ Control\ (GAPDH)\ Probe\ Ct - Mean\ Gene\ Probe\ Ct$$

$$\Delta Ct\ Expression = 2^{-\Delta Ct}$$

Then, to calculate fold-change expression in GSCs relative to bulk cells:

$$\Delta\Delta Ct = \frac{\Delta Ct\ Expression\ (Stem)}{\Delta Ct\ Expression\ (Bulk)}$$

2.19 Flow cytometry and analysis of cell cycle distribution

2.19.1 Sample preparation and PI staining

Cells were plated in 6-well plates, treated, and collected at various time points as specified in the results. Media was removed and cells were washed twice in PBS before 500µl/well of Accutase™ was added. Both media and PBS washes were retained. Following detachment, cells were collected in 500µl/well of PBS which was added to the media and PBS washes in 15ml Falcon tubes labelled for each condition. This was then centrifuged at 1,200rpm for 3 minutes. The supernatant was discarded, leaving a cell pellet to which 1ml of ice cold 70% ethanol was slowly added (whilst gently mixing on vortex) to aid the fixation of cells in single

suspension. Cells were left to fix overnight before excess ethanol was spun off and cells washed in PBS twice – centrifuging at 1,200rpm for 3 minutes and carefully discarding the supernatant at each stage. Subsequently, 5µl of RNAaseA (1µg/µl stock) was added to added to each sample and incubated at room temperature for 15 minutes to allow the degradation of RNA, whilst leaving DNA intact. After this, samples were protected from the light with foil and 200µl PI (50µg/ml stock) was added to each sample. Samples were incubated for at least 15 minutes (but typically overnight at 4°C) to allow the intercalation of PI with DNA, prior to flow cytometric analysis.

2.19.2 FACSCalibur flow cytometric analysis

Samples were processed using a BD FACSCalibur system with a minimum of 10,000 cells per sample and the data was analysed using FlowJo (Version 10) software. Analysis of the FS and SS parameters was used to gate single cells, excluding both cellular debris and doublet cells. Additionally, a 488nm laser was utilised to excite PI, with the resultant emission detected using channel FL-1 (530nm emission filter). A cumulative histogram based on PI emission data and the number of cell/events was plotted in FlowJo. Cells in G_2 or early M-phase of the cell cycle were identified by a peak with PI signal intensity roughly double that of the first (G_1) peak – representative of duplex and singular intracellular DNA content, respectively. Indicative of a range of intracellular DNA content quantities, the PI intensity of S-phase cells demonstrated a range of amplitudes between the G_1 and G_2 peaks. Cell cycle profiling algorithms within FlowJo were used to quantify the number of cells in each phase of the cell cycle. For each experiment, identical gating and analysis parameters were applied to each experimental condition to avoid bias.

2.20 Single cell gel electrophoresis: alkaline comet assay

The alkaline comet was used to detect single and double strand DNA breaks, thereby providing a direct representation of DNA damage which does not rely on the integrity of DDR processes for detection (in contrast to the detection of γH2AX foci for example). In brief, cells were embedded in agarose and lysed in detergent and high salt conditions to leave residual bodies of supercoiled DNA referred to as nucleoids. The assay uses alkaline conditions to promote the relaxation of tightly coiled DNA within nucleoids. Under electrophoresis, this allows negatively charged DNA to be drawn out towards the anode. A greater frequency of DNA breaks promotes further migration of DNA which, once a

fluorescence stain is applied, can be used to visualise and quantify DNA comet 'tails'[220] as a measure of DNA damage.

2.20.1 Alkaline comet assay procedure

Cells were seeded in 6-well plates at a density if 2.5 x 10^5 (i.e. 25 x 10^4) incubated at 37°C overnight. Subsequently, cells were treated, then processed at various time points as indicated in the results. Cells were processed using a Trevigen comet assay kit according to the manufactures instructions. Briefly, media from the wells was discarded and the cells washed with warmed PBS twice to remove any debris. Accutase was then added to each well (500µl/well) and cells incubated at 37°C for 2-3 minutes until detached. After this, 5ml of warmed PBS was added to each well and the cell suspension transferred to labelled 15ml Falcon tubes. Samples were centrifuged at 1,000rpm for 3 minutes and the supernatant discarded. Cell pellets were re-suspended in 1ml warm PBS and the concentration of cells in each suspension was quantified using a haemocytometer. Samples were then diluted to a concentration of 1 x 10^5 cells/ml by the addition of further warmed PBS and maintained in water bath set at 37°C as slides were prepared.

For each sample, 30µl cell suspension (after inverting x5 to mix well) and 250µl of LMagrose were added to labelled eppendorfs and mixed well. Cells suspended in agarose were added to Trevigen comet slides as 100µl discs (x2) and stored flat at 4°C for 30 minutes to solidify. Subsequently, slides were lysed in buffer containing (Triton- X100 and 2.5M NaCl) for 1 hour at 4°C. After this, the remaining DNA nucleoids suspended in agarose were submerged in alkaline unwinding buffer (see Table 2.9) for 1 hour before exposure to electrophoresis for 30 minutes at 21V, whilst maintaining a constant current at 0.3amps (by adjusting the volume of electrophoresis buffer). Slides were submerged in ddH_2O twice (5 minutes each) to remove any residue, before submerging in 70% ethanol for 5 minutes then incubating at room temperature to dry. The DNA was then stained using SYBR Gold nucleic acid gel stain (1:30,000) in TE buffer using 100µl for each agarose disc and allowing to stain for 30 minutes (protected from light) before tilting to remove excess and further incubation at room temperature until dry. Once dry, slides were stored at 4°C until imaged (typically within 1-3 days).

2.20.2 Image acquisition and analysis

A minimum of 100 cells per experimental condition were imaged using the FITC channel and 20x lens on a Nikon Eclipse TE200 Fluorescent Microscope. Images were analysed using TriTek Comet Score software (AMSBiotechnology, 2010). The percentage DNA in the comet tail (Equation 2.1) was used as a primary measure of DNA damage. Additionally, comet tail moment (Equation 2.2), which adjusts for the length of comet tails was used as a secondary measure of DNA damage severity.

$$DNA_t\ (\%) = 100 \times (I_t / I_c)$$

Equation 2.1: Percentage of DNA in comet tail – Where DNA_t = percentage DNA in comet tail; I_t = comet **t**ail intensity, and; I_c = total **c**omet intensity.

$$M_t = DNA_t\ (\%) \times L_t$$

Equation 2.2: Comet tail moment – Where Mt = tail moment; DNA_t = percentage DNA in comet tail, and; L_t = comet tail length.

2.21 Statistical analysis

All *in vitro* experimental procedures consisted of at least 3 independent biological repeats (containing 3-8 technical replicates per group depending on the assay) and appropriate negative and/or positive controls unless otherwise stated. Tests of normality (e.g. Shapiro-Wilk) were used to assess generated data sets prior to inferential statistics to confirm differences between test and control groups using appropriate statistical tests such as Mann-Whitney U-test (if normality was not apparent) or Student's t-test (if normality was apparent) as specified in the results, with *p*-values <0.05 used to determine statistically significant biological differences while accounting for multiple testing where required. Inferential statistical analysis was performed using GraphPad Prism (Version 7), except where otherwise specified. Special consideration must be given to the analysis of clonogenic assays, which is detailed below.

2.21.1 Clonogenic survival curve fitting and analysis

For clonogenic studies using irradiation, survival curves were fitted to the data using the linear quadratic (LQ) model where the magnitude of radiation-induced cell killing (i.e. reduction in SF) is described by combining a linear component (α), which is proportional to radiation dose, and quadratic component (β) which is proportional to the square of the dose

– highlighted below. The LQ model is used widely in radiation oncology and radiobiology research and can also applied to derive α/β ratios which describe the sensitivity of tissues to radiotherapy fraction size[221].

$$SF = exp^{-(\alpha \bullet d + \beta \bullet d\text{^}2)}$$

Equation 2.3: The linear-quadratic (LQ) model – Where SF = surviving fraction; α = linear term constant (Gy^{-1}); β = quadratic term constant (Gy^{-1}), and; *d* = dose of the radiotherapy fraction (Gy)[221].

Where required, survival curves fitted using non-linear regression with application of the LQ model in GraphPad Prism were then extrapolated at defined surviving fractions (typically at a SF of 0.37 unless otherwise stated) in test and control conditions. Extrapolated drug doses were used to calculate sensitiser enhancement ratios (*SER*) for each DDRi or DDRi combination; these represent the fold-change in radiation dose that would be required to provide an equivalent reduction in SF in the absence of the radiosensitising (DDRi) agent. For example, if a compound with a $SER_{0.37}$ of 2.0 was removed, double the IR dose would be required to achieve the same SF. $SER_{0.37}$ was calculated as described in Equation 2.4.

$$SER_{0.37} = d_{0.37}\ (\text{DMSO}) \ / \ d_{0.37}\ (\text{DDRi})$$

Equation 2.4: Calculation of sensitiser enhancement ratios – Where SER = sensitiser enhancement ratio, and; *d* = dose of the radiotherapy.

For clonogenic studies using temozolomide chemotherapy, survival curves were fitted to the data using non-linear regression with four parameters applied in GraphPad Prism ('[inhibitor] vs response – variable slope (four parameters)') as described in Equation 2.5 below.

$$SF = SF_{MIN} + (SF_{MAX} - SF_{MIN})/(1 + ((d^h)/(LD_{50}{}^h)))$$

Equation 2.5: Non-linear regression for temozolomide clonogenic studies – Where SF = surviving fraction; *d* = dose of the temozolomide chemotherapy (μM); LD50 = dose (μM) temozolomide required to portend SF of 0.50, and; *h* = hill slope, referring to the gradient (unitless).

In both radiotherapy and chemotherapy clonogenic experiments, curves fitted to data for each experimental condition were compared and analysed to establish whether any observed biological differences in treatment response were statistically significant. To compare curves, a pairwise extra sum-of-squares F test was used (GraphPad Prism) which compares the goodness-of-fit of alternate models to each experimental condition with a

null hypothesis that a simpler model, in which the same model parameters can be fitted to each experimental condition, was correct. Consequently, a statistical threshold of $P < 0.05$ was deemed to represent a significant difference, representing a high likelihood that different model parameters were required to ascribe fitted curves to data from each experimental group (whilst using the same model).

Chapter 3 – Exploiting single DDR targets

3 CHAPTER 3 – Exploiting single DDR targets in glioblastoma to confer chemosensitisation

3.1 Introduction

Therapeutic resistance and eventual disease progression in glioblastoma are universal. Although incorporated into current standard-of-care treatment, the addition of the DNA alkylating agent temozolomide to surgical resection and post-operative radiotherapy in a large phase III clinical trial only improved median progression-free survival by 1.9 months (from 5.0 to 6.9 months) in patients with newly diagnosed glioblastoma[10,11]. O^6-methylguanine (O^6-meG) is the most toxic DNA lesion induced by temozolomide chemotherapy. Expression of MGMT, the enzyme responsible for direct removal of O^6-meG, is associated with temozolomide response and patient survival. Hypermethylation of the *MGMT* gene promotor region is present in ~45% of patients with glioblastoma, portending reduced MGMT expression and enhanced response to temozolomide chemotherapy[94]. However, even responders with low ('negative') MGMT levels eventually succumb to the disease. Consistent with the finding that anti-cancer effects of temozolomide are substantially mediated through futile cycling of DNA mismatch repair (MMR) processes in an attempt to resolve the mispairing of thymine with O^6-methylguanine[119], the acquisition of loss of function mutations in MMR genes has been demonstrated to endow gliomas with temozolomide resistance[222,223]. Predictably, MMR defects in gliomas can be readily inferred by the presence of characteristic hypermutation with increases in tumour mutational burden (often several orders of magnitude), and enrichment of the C:G>T:A mutational signature, in addition to identifiable inactivating mutations in MMR pathway components[224]. However, longitudinal genomic profiling of gliomas at the time of first surgery and disease progression/recurrence revealed only 16% of *IDH* wild type gliomas exhibit alkylating treatment-associated hypermutation. Even in *IDH* mutant gliomas, rates of hypermutation were revealed to be 47% and 25% for non-co-deleted (astrocytomas) and 1p/19q co-deleted (oligodendrogliomas), respectively[223]. Therefore, a clear need exists to define and exploit other DDR processes contributing to temozolomide resistance since MGMT expression and loss of MMR do not explain therapeutic resistance in the majority of cases.

3.1.1 The Fanconi anaemia (FA) pathway in glioblastoma

Recent studies by MacLeod *et al.* (2019)[225] highlight a critical role of FA pathway genes in temozolomide resistance. Using genome-wide CRISPR-Cas9-based functional approaches

they revealed that, after treating primary glioblastoma cells with high-dose temozolomide (LD_{90}) for 28-37 days, gRNAs targeting core MMR genes including *MLH1*, *MSH2*, *MSH6* and *PMS2* were significantly enriched, thus corroborating a pivotal role of MMR loss in temozolomide sensitivity. However, during negative selection screens in which glioblastoma cells were treated with a sublethal dose of temozolomide (LD_{20}) for a similar duration, loss of genes incorporated in gene ontology (GO) terms for the FA pathway/interstrand crosslink repair followed by homologous recombination (HR) were most significantly implicated in temozolomide sensitivity[225]. Additional specific validation confirmed *FANCA* knock out via CRISPR-Cas9 gene editing enhanced the sensitivity of a patient-derived glioblastoma cell line to temozolomide chemotherapy[225]. The potential for variability in temozolomide resistance mechanisms employed by glioma cells, and the balance of intrinsic and acquired mechanisms, to be influenced by temozolomide dose is intriguing. Not least because the best available studies suggest that, following treatment, temozolomide doses within the CNS are likely to be relatively low (discussed in detail in Section 3.5.1), which would support an important role of the FA pathway in modulating temozolomide response in patients. Although these studies by MacLeod *et al.* provide the most unbiased evidence of FA pathway implication in temozolomide resistance, they are by no means the first to reveal this phenomenon.

Chen *et al*. (2007)[20] were the first to clearly demonstrate robust activation of the FA pathway (FANCD2 monoubiquitination) in response DNA damage induced by temozolomide chemotherapy, the mono- and bidirectional alkylating agent BCNU, and IR, in established glioblastoma cells (U87). Additionally, using isogenic FA pathway deficient (FANCF deficient) and proficient ovarian cancer cell lines, Chen *et al.* confirmed increased FANCD2 nuclear foci formation, in addition to dose- and time-dependent monoubiquitination of FANCD2, in response to temozolomide in FA proficient cells. FA deficient cells failed to demonstrate similar activity. In the context of glioma, the studies explored the relative sensitivities of 9 established glioblastoma cell lines to temozolomide and BCNU, to reveal that the only naturally occurring FA pathway deficient line within the panel exhibited substantially greater susceptibility to both alkylating chemotherapies, notwithstanding the notable limitation of comparing sensitivities across cell lines with entirely different genetic backgrounds. Subsequently, these studies established that suppression of FANCD2 using siRNA enhanced the sensitivity of U87 (MGMT negative) glioblastoma cells to both temozolomide and BCNU, whilst addition of the MGMT inhibitor O^6-benzylguanine to

BCNU-treated T98G (MGMT expressing/positive) cells further reduced cell survival, suggesting that FANCD2 and MGMT are not epistatic, but rather FANCD2 mediated resistance to alkylating chemotherapy is furnished independently of well characterised MGMT-dependent mechanisms. Finally, inhibition of the FA pathway using curcumin (5μM) in U87 cells was also demonstrated to enhance BCNU sensitivity, however the effects of curcumin on temozolomide sensitivity were not established[20]. Overall, therefore, these studies implicated the FA pathway as an MGMT-independent mechanism of resistance to alkylating chemotherapy in glioblastoma, highlighting key FA pathway players (including FANCD2 and FANCF) as appealing therapeutic targets.

Later studies by Kondo *et al.* (2011)[21] were the first to establish the therapeutic potential of targeting a downstream FA pathway gene in glioblastoma. Suppression of FANCD1/BRCA2 in A172 established glioblastoma cells using siRNA was demonstrated to significantly augment ACNU (nimustine, a DNA cross-linking agent) and temozolomide-induced reductions in clonogenic survival and cell growth (as assessed by MTS assay). Additionally, using a range of paired isogenic FA proficient/deficient non-glioma cell lines (cultured mouse embryonic fibroblasts *FANCA*$^{-/-}$, *FANCC*$^{-/-}$, *FANCA*$^{-/-}$*C*$^{-/-}$, *FANCD2*$^{-/-}$ cells and their parental cells; Chinese hamster ovary and lung fibroblast cells *FANCD1/BRCA2mt*, *FANCG*$^{-/-}$ and their parental cells) Kondo *et al.* revealed loss of a gene within any FA pathway key functional group: core complex (*FANCA, FANCC, FANCG*); ID complex (*FANCD2*), and; downstream (*FANCD1/BRCA2*) dramatically enhanced ACNU sensitivity, whereas within this cell line panel, the influence of these on temozolomide sensitivity was more nuanced. *FANCG*$^{-/-}$ or *FANCD1/BRCA2mt* status both conferred hypersensitivity to temozolomide, whilst *FANCD2*$^{-/-}$ status moderately enhanced temozolomide sensitivity relatively to parental cells. Conversely, *FANCA*$^{-/-}$, *FANCC*$^{-/-}$ and *FANCA*$^{-/-}$*C*$^{-/-}$ status had no substantial impact on temozolomide sensitivity[21]. Therefore, although the majority of studies performed by Kondo *et al.* were not glioma-specific, they do allude to potential differences in the roles of various FA pathway constituents in resolving temozolomide- vs ACNU-induced DNA damage. With respect to temozolomide-induced DNA damage, the studies suggest that not all FA pathway targets should be considered equal in the race to enhance current therapy. The fact that loss of a core complex (*FANCG*) gene and a downstream (*FANCD1/BRCA2*) gene both conferred substantial temozolomide sensitisation does perhaps support canonical, rather than, or in addition to, non-canonical FA roles in resolving the plethora of primary and secondary DNA lesions induced by temozolomide

chemotherapy. However, even these detailed studies by Kondo *et al.* left the relevance of many key FA pathway genes to temozolomide response unexplored.

More recently, work from our laboratory (Patil *et al.* 2014)[22] explored therapeutic relevance of the FA pathway in glioma. Using immunohistochemical staining these studies demonstrated an absence of FANCD2 positivity in healthy brain tissue (from tissue microarray) and WHO grade I tumours (including schwannomas). Conversely, increasing glioma grade was associated with a stepwise increase in FANCD2 protein expression with around 90% of all WHO grade IV glioma (glioblastoma) exhibiting clear FANCD2 expression. These studies established, for the first time in primary patient-derived glioblastoma cultures, that temozolomide exposure robustly activated the FA pathway (FANCD2 monoubiquitination and nuclear foci formation), in addition to confirming this phenomenon in established U87 glioblastoma cells and its absence in constitutively FA deficient U138 glioblastoma cells. The studies also provided the most extensive published evidence to date that chemical inhibition of the FA pathway using either curcumin (5μM), its monoketone analogue EF-24 (31nM), or its menadione analogue DDN (30nM) sensitised both MGMT negative (U87) and MGMT positive (T98G) glioblastoma cells to temozolomide chemotherapy[22]. These data are also consistent with Chen *et al.*[20] (above), that suggested FA-mediated temozolomide resistance was independent of MGMT activity.

In interpreting these studies, it is important to consider the various mechanisms of action unrelated to the DDR that curcumin may exhibit. For example, curcumin is widely established to exhibit anti-oxidant properties including through: promoting the activity of superoxide dismutase[226-228], catalase and glutathione peroxidase[229]; directly scavenging reactive oxygen and reactive nitrogen species[227], and; the inhibition of reactive oxygen species generating enzymes including cyclooxygenase and lipoxygenase[230]. Curcumin may also modulate cell cycle progression and apoptosis including through promoting upregulation of p53[231-234]. Additionally, curcumin has been reported to exhibit a range of anti-migratory, anti-angiogenic and immune modulatory effects[231].

Given the pleiotropic nature of curcumin (discussed further in Section 3.6.3), the possibility that temozolomide sensitisation might have been mediated through unexamined FA pathway independent mechanisms represents an important criticism of the studies by Patil *et al.* 2014[22]. Additionally, corroboration with the use of curcumin analogues rather than

structurally dissimilar crude chemical inhibitors of the FA pathway (such as TAK-243 (see Chapter 5 – Section 5.3.2) or ouabain (see Chapter 5 – Section 5.3.1) for example) may have increased the risk of a common, non-FA pathway-mediated mechanism conferring chemosensitisation with these compounds. Importantly however, the studies found that temozolomide response following sensitisation with curcumin or EF-24 in FA proficient U87 cells was of similar magnitude to the inherent temozolomide sensitivity observed in constitutively FA deficient U138 cells. Furthermore, after generating isogenic U87 FANCD2 proficient and deficient stable shRNA expressing clones, Patil *et al.* established that, relative to untreated FANCD2 proficient cells, FANCD2 deficiency or chemical inhibition appeared to enhance temozolomide sensitivity by an equivalent magnitude. The addition of curcumin treatment to FANCD2 deficient cells did not provide additional sensitisation and the addition of EF-24 or DDN to FANCD2 deficient U87 cells provided very little additional temozolomide sensitisation[22]. Together, these results strongly implicated FA pathway inhibition as the mechanistic basis for enhanced temozolomide efficacy when combined with curcumin, EF-24 or DDN, rather than any shared non-FA mediated effect of these compounds. In summary, these studies expound a striking differential in FA pathway expression between normal brain and high-grade gliomas which presents a therapeutic window that could be exploited pharmacologically, both in the contexts of MGMT expressing and non-expressing tumours, to improve the efficacy of current chemotherapy.

3.1.2 PARP, ATR and ATM as chemosensitisation targets in glioblastoma

PARP1 inhibition to confer temozolomide chemosensitisation

The most abundant DNA lesions inflicted by temozolomide are N^7-methylguanine (N^7-meG) and N^3-methyladenine (N^3-meA)[235]. These are readily resolved by base excision repair (BER) and therefore appear to contribute less to the overall anti-cancer effects of temozolomide than the highly cytotoxic lesion O^6-meG[7]. However, the role of PARP1 in binding to DNA and providing a scaffold that recruits BER proteins[209] raised the possibility that PARP inhibition might enhance the effects of temozolomide by disrupting BER[236] resulting in unresolved N^7-meG/N^3-meA adducts and elevated replication stress[237]. Interestingly however, Gupta *et al.* (2019)[237] demonstrated that siRNA-mediated knockdown of N-methylpurine DNA glycosylase (MPG) or XRCC1, both indispensable components of functional BER in this context, did not influence temozolomide response in established U251 temozolomide-resistant glioblastoma cells[237] (cells endowed with acquired resistance by culturing and passaging over 8 weeks in the presence of escalating concentrations of

temozolomide 30-300μM[238]) – suggesting any potential sensitising effects of PARP inhibition do not result from impaired BER and are therefore more likely to be associated with cellular responses to the O^6-meG lesion.

Consistent with this observation, earlier studies by Gupta *et al.* (2016)[239] established that sensitisation to temozolomide using the PARP inhibitor veliparib may be associated exclusively with *MGMT* promotor region hypermethylation, suggesting implication of the O^6-meG lesion in PARPi-mediated sensitisation to alkylating chemotherapy and that only tumours that are inherently sensitive to temozolomide might derive additional benefit from the addition of veliparib. This large 'preclinical trial' incorporated the use of 28 patient-derived glioblastoma orthotopic xenograft models (treating between 8-10, and on occasion 20 mice per model per treatment group) to compare survival in mice receiving either temozolomide alone or the combination of temozolomide with veliparib. Out of 20 *MGMT*-hypermethylated patient-derived xenograft (PDX) models, 5 demonstrated significantly improved survival following combination treatment with an average extension in median survival by 87 days (range = 20-150 days). Conversely, of 5 clearly *MGMT*-unmethylated PDX models, none demonstrated a survival advantage of receiving the combination of temozolomide with veliparib compared to temozolomide alone[239]. Additionally, Gupta *et al.* revealed that hypermethylated cell lines which responded to the combination showed elevated expression of key DDR signalling kinases including pCHK1 and pCHK2 (relative to unmethylated xenografts), and that in these models it was possible to reverse survival advantages conferred by the combination of temozolomide and veliparib by overexpressing *MGMT*[239]. However, despite the herculean efforts of Gupta *et al.* in completing such an extensive preclinical trial, the fact that responses for only 5 MGMT-unmethylated models were compared to responses for 20 MGMT-methylated models (of which only 5 showed survival benefit with the addition of PARP inhibition) means that the potential for veliparib-mediated temozolomide sensitisation in unmethylated (MGMT expressing) tumours cannot be completely excluded on the basis of the data presented, even if such a phenomenon was just as prevalent as observed in the context of *MGMT*-hypermethylation. Furthermore, the fact that only 5 out of 20 MGMT-methylated models demonstrated survival benefit with the combination of temozolomide plus veliparib alludes to a degree of heterogeneity in the molecular and/or other pathophysiological determinants of PARP inhibitor sensitisation to temozolomide. Given that the persistence of bulky O^6-meG lesions, which are not directly removed in the absence of MGMT, result in elevated DNA replication stress[240,241], and

replication fork stability and recovery is influenced by a number of DDR players including PARP, but also the HR protein RAD51, the FA protein FANCD2, and those implicated in both processes including FANCS/BRCA1 and FANCD1/BRCA2 proteins, the integrity of some of these other DDR processes may underpin the heterogenous preclinical success of PARP inhibitor mediated temozolomide sensitisation. At least theoretically, this would also support the use of adding an additional DDR inhibitor to maximise replication fork collapse and/or failure of resultant DNA DSB resolution, potentially resulting in more pronounced neoplastic cell death across a wider range of tumours.

ATR or ATM inhibition to confer temozolomide chemosensitisation

Given that temozolomide-induced O^6-meG lesions elicit DNA replication stress and DSBs (discussed above), it seems rational that apical DDR kinases involved in the resolution of these, ATR and ATM, respectively, might co-operate to limit the cytotoxicity of temozolomide in cancer cells. Interestingly, activation of both ATR and ATM following temozolomide chemotherapy occurs in an MMR-dependent manner[242], again highlighting the centrality of highly cytotoxic O^6-meG (over N^7-meG and N^3-meA, which do not activate MMR). Additionally, Eich *et al.* (2013)[243] demonstrated that siRNA mediated knockdown of either ATR or ATM significantly sensitised established LN229 (MGMT negative) glioblastoma cells to temozolomide. Interestingly, the degree of sensitisation conferred by ATR knockdown was more than double that observed in the absence of ATM, implicating impaired resolution of DNA replication stress as a key driver of sensitisation. Furthermore, simultaneous ATR and ATM knockdown did not provide any additional sensitisation relative to ATR alone. Stable transfection of LN229 cells to express MGMT abolished ATR– , ATM– , and ATR/ATM–loss mediated sensitisation to temozolomide, and the sensitisation of these cells could be rescued (and even further augmented) by pre-treatment with the MGMT inhibitor O^6-BG. Finally, these excellent studies illustrated that although the downstream targets CHK1 and CHK2 (classically/canonically phosphorylated by ATR and ATM, respectively), are both activated in MGMT negative (but not in MGMT expressing) LN229 cells transfected with control siRNA or siATM followed by temozolomide exposure, knockdown of ATR abolished temozolomide-induced phosphorylation of H2AX and both CHK1 and CHK2 phosphorylation[243]. Together the studies by Eich *et al.* establish a framework whereby the kinases ATR and ATM are relevant in cellular responses to temozolomide only in the context of MGMT deficiency due to the failure of primary resolution of toxic O6-MeG lesions. Within this response, ATR is primarily activated by O6-

MeG-induced secondary lesions which invoke H2AX phosphorylation (including stalled replication forks), whereas ATM may only be required somewhat downstream after O6-MeG/T mispairs lead to multiple futile cycles of MMR and DNA DSBs[243]. Indeed, more recent studies by Jackson *et al.* (2019)[244] have confirmed: substantially heightened temozolomide sensitivity; ATR-CHK1 axis activation, and; ATR inhibitor (ATRIN-119 and VX-970) -mediated temozolomide sensitisation in LN229 (constitutively) MGMT deficient cells, relative to LN229 that stably express MGMT. Additionally, these studies were able to demonstrate *in vivo* efficacy of ATR inhibition using VX-970 as a strategy to enhance temozolomide response in MGMT-deficient (LN229 and a primary glioblastoma cell line) mouse flank xenografts.

3.1.3 Development and clinical translation of pharmacological inhibitors of the FA pathway and interconnected DDR processes

Inhibitors of the Fanconi anaemia pathway

Although there are over 290 clinical trials actively recruiting patients diagnosed with a glioblastoma to evaluate new therapeutic approaches (clinicaltrials.gov), none are currently assessing the clinical potential of FA pathway inhibition. This likely reflects a lack of compounds for which robust data is available confirming target inhibition, appropriate pharmacokinetic/pharmacodynamic (PK/PD) properties, and evidence of preclinical anti-cancer efficacy. Although *in vitro* efficacy data is available for the crude FA pathway inhibitor curcumin as a chemosensitising agent in glioma[20,22], similar *in vivo* preclinical data has not yet been generated and the pharmacokinetic properties of curcumin may not support translation to clinical trials. A Phase I dose escalation study of curcumin in patients with advanced colorectal cancer previously demonstrated that relatively high doses, up to 3.6g per day administered orally, were safe and resulted in detectable plasma levels of curcumin and its glucuronide and sulphate metabolites, but with low concentrations in the 10nM range[245]. Higher oral doses of curcumin up to 8g per day have been assessed alongside gemcitabine in patients with advanced pancreatic cancer, however such high oral doses appear to be unpalatable, with 29% of patients requiring dose reduction due to intractable abdominal discomfort or pain[246]. Given the poor oral bioavailability of curcumin, it seems unlikely that sufficient concentrations could be achieved within the CNS and intratumourally to inhibit the FA pathway in glioblastoma using this route of administration. A Phase 0 type clinical trial (NCT01712542) in which 15 patients with a glioblastoma received oral curcumin prior to surgery with subsequent measurement of intratumoural curcumin concentration

within the resection specimens was reported to have been completed in May 2013[247]. However, methods associated with the study findings, published by Dützmann *et al.* in 2016[248], appear to have evolved somewhat to use a combination of curcuminoid compounds incorporated into micelles to improve bioavailability with oral administration. Following the preoperative administration of 70mg micellar curcuminoids (containing 57.4mg curcumin, 11.2mg demethoxycurcumin and 1.4mg bis-demthoxycurcumin) three times daily for 4 days to 10 patients, they reported mean curcumin intratumoural and serum concentrations of 56pg/mg of tissue and 253ng/ml, respectively. These equate to concentrations of ~152 pM (intratumoural) and 688nM (serum) (curcumin MW = 368.38g/mol) – so whilst the micellar preparation represents a substantial improvement over previous studies with respect to plasma levels, both these and particularly CNS concentrations remain likely too low to restrain FA pathway activity, highlighting the need for alternative and novel methodologies of curcumin administration (discussed in Section 3.6.3) and the development of more potent and selective FA pathway inhibitors. Relevant to the latter, novel compounds which specifically bind and inhibit FANCL are currently under development in Sheffield (see Section 3.3). Additionally, a number of groups are also working to develop novel inhibitors of FA pathway components including strategies targeting: the FA core complex – FANCM (Voter *et al.* (2016)[249]), FANCT/FANCL-mediated FANCD2 monoubiquitination (Cornwell *et al.* (2019)[250]); ID complex associated processes – USP1 (Mistry *et al.* (2013)[251]), and; downstream FA constituents – including FANCS/BRCA1 inhibition using a peptide molecule (Pessetto *et al.* (2012)[252]), or targeting FANCR/RAD51 (King *et al.* (2017)[253]). Most recently, Sharp *et al.* (2020)[254] developed a high-throughput, cell-free methodology which utilised 11 recombinant proteins (ubiquitin, ubiquitin activating enzyme, FANCT, FANC-B-L-100, FANC-C-E-F, FANCI, FANCD2) and dsDNA to detect compounds which reduced chemi-luminescent signal resulting from FANCD2 monoubiquitination within a proximity assay. Through screening 9,067 compounds this methodology identified 11 which were also confirmed to reduce FANCD2 monoubiquitination (but not PCNA ubiquitination) on immunoblotting and demonstrate some selectivity towards killing *BRCA1*-deficient cells as a monotherapy, during orthogonal testing. However, none of these compounds were able to significantly inhibit the formation of FANCD2 foci[254] therefore their status as *bona fide* FA pathway inhibitors is questionable. Of all the compounds discussed above, none appear ready or suitable for clinical translation. Nevertheless, this area of research is expected to progress rapidly over the coming years towards the ultimate aim of producing a novel, first-in-class, specific FA pathway inhibitor

suitable for clinical application as either a sensitiser for chemo- and radiotherapy, and/or as a monotherapy in the context of cancers with an underlying molecular vulnerability via a synthetic lethal approach[255], similar to the application of PARP inhibitors in *BRCA*-deficient cancers[184,185].

In contrast to the FA pathway, numerous inhibitors of PARP, ATR and ATM have either been approved clinically for usage in other (non-glioma) cancer types and/or are under evaluation in clinical trials to treat high-grade gliomas.

PARP inhibitors

Four PARP inhibitors – olaparib, niraparib, rucaparib and talazoparib – have received FDA approvals to date, in a number of therapeutic contexts including: refractory *BRCA1/2*-mutant ovarian cancer[256-259]; maintenance therapy for advanced ovarian cancer following complete or partial response to platinum-based chemotherapy (irrespective of *BRCA1/2* status)[260-262]; metastatic, HER2-negative breast cancers with *BRCA1/2* mutations[263]; germline *BRCA1/2*-mutant metastatic pancreatic cancer (olaparib)[264], and; olaparib has recently gained FDA approval for use in *BRCA1/2*- or *ATM*-mutant (HRR gene mutated) metastatic castration-resistant prostate cancer[265] following a priority review process. Although PARP inhibitors are yet to receive clinical approvals in the context of glioblastoma, numerous clinical trials to support such applications are underway. These are summarised in Table 3.1. Anecdotally, there have also been discussions around the potential for a clinical trial combining a PARP and ATR inhibitor to treat glioblastoma, however no such trial has yet been registered, and may be unlikely until outcomes from some of the larger ongoing PARP inhibitor trials are known.

ATR inhibitors

Although no ATR inhibitors are currently in clinical trials for glioblastoma, a first-in-human Phase I dose escalation trial (NCT02264678/D5330C00004) has assessed the safety and tolerability of administering the ATR inhibitor AZD6738 alongside either carboplatin, olaparib or the immune checkpoint inhibitor durvalumab to treat advanced solid malignancies (not including primary brain tumours). The trial established that all three ATRi incorporating combinations are feasible and demonstrated some evidence of preliminary efficacy[266,267]. It will be exciting to observe AZD6738 or similar ATR inhibitors enter clinical trials to treat glioblastoma in the near future.

ATM inhibitors

Two potent, selective, BBB-penetrant ATMi inhibitors (AZD32 and AZD1390) have recently been developed[268,269], and should support clinical studies to evaluate the efficacy of ATM inhibition in glioblastoma. Indeed, a Phase I clinical trial (NCT03423628) is currently underway (see Table 3.2).

The more rapid progress in terms of development and clinical evaluation of PARP, ATM and ATR inhibitors (relative to FA pathway inhibitors), raises a hope that once a novel FA pathway inhibitor is suitable for first-in-man clinical trials, DDRi inhibitors within the other classes may have received regulatory approval(s) in the context of glioblastoma, and/or have more robust clinical data available, paving the way for future combinatorial studies assessing simultaneous FA and related DDR pathway inhibition. In the meantime however, studies presented in this thesis represent some of the first steps towards building a preclinical evidence base to support such anti-cancer strategies. In this Chapter, the potential of crude and novel (under development) compounds to inhibit the FA pathway and provide chemosensitisation to standard-of-care temozolomide treatment is assessed. The chemosensitising abilities of chemical inhibitors for PARP1, ATR and ATM are also independently validated, to provide a foundation for subsequent studies.

Table 3.1: PARP inhibitor trials in high-grade glioma.

Summary of key PARP inhibitor in high-grade glioma clinical trials - completed and ongoing					
Trial (ref) **& Indication**	**Design & n** (rec dates)	**Treatment(s)**	**1° Endpoint**	**2° Endpoint(s)**	**Results/Remarks & Conclusions**
Phase I studies					
NCT00770471 [(270)] **nGBM** Veliparib (ABT-888), Radiation Therapy, and Temozolomide in Treating Patients with Newly Diagnosed Glioblastoma Multiforme.	Phase I Single arm 24 patients (2009-2012)	VELI + IR + TMZ	Phase I: VELI MTD. Phase II: OS (with VELI MTD)	A) Safety/toxicity. B) Pharmacokinetics.	• Following initial safety groups and planned dosing steps, 3/6 pts (50%) had DLTs (2 thrombocytopenia, 1 neutropenia) with 10mg BD VELI+R+TMZ → accrual discontinued. • VELI at this dose with standard dosing regimen of IR+TMZ deemed not tolerable. • Further development of appropriate dosing regimen needed.
NCT01390571[(271,272)] **rGBM** Olaparib and Temozolomide in Treating Patients with Relapsed Glioblastoma (**OPARATIC**).	Phase 0/I Single arm 48 patients (2011-2017)	Stage I: OLAP for 3/7 prior to surgery then usual Rx. Stage II: Escalating OLAP 3/7 prior to surgery then OLAP + TMZ post-op.	Phase 0: Tumour penetration via BBB/BTB. Phase I: Safety.	A) BBB disruption/permeability. B) Preliminary anti-tumour activity of OLAP + TMZ.	• OLAP detected in 73/74 tumour specimens from 27 pts, mean conc. 588nM (range = 97-1374nM). • Mean tumour margin:core ratio = 1.2 (0.2-3.9). • Mean tumour:plasma ratio = 0.25 (0.01-0.9). • 24/35 pts (67%) AEs$^{(G3-4)}$. • 45% PFS at 6m F/U. • OLAP penetrates tumour core/margins and is safe with extended low-dose TMZ.
NCT01294735 [(273)] **rGBM / rMelanoma / solid cancers** Niraparib (MK-4827) Given With Temozolomide in Participants With Advanced Cancer.	Phase I Single arm 19 patients (2011-2012)	NIRA + TMZ	No. of DLTs.	A) ORR within 30 days of last dose & 2m intervals. B) PFS.	• MTD & RP2D = 40mg OD NIRA with 150mg/m^2 TMZ. • 2/10 pts (20%) had Grade 4 thrombocytopenia at this dose. • 1 PR (glioblastoma) & 2 SD out of 16 evaluable pts. • NIRA tolerable in combination with TMZ.
nGBM [(274)] Two parallel phase I studies of olaparib and radiotherapy or olaparib and radiotherapy plus temozolomide in patients with newly diagnosed glioblastoma, with treatment stratified by MGMT status (**PARADIGM-2**).	Phase I Parallel Estimated patients: 25-40 methylated; 19-28 unmethylated (2016-2020)	Methylated: OLAP + IR + TMZ Unmethylated: OLAP + IR	Safety/toxicity (MTD & optimum scheduling).	A) Define DLTs (+/- TMZ)	• MGMT methylated dosing schedule = OLAP (dose escalation) with IR and concomitant TMZ, then 4 weeks OLAP with maintenance TMZ started *after* completing OLAP. • Trial **ongoing** – recruitment ends December 2020.
Phase I/II studies					
NCT01026493 [(275)] **rGBM** A Randomized Phase I/II Study of Veliparib (ABT-888) in Combination with Temozolomide in Recurrent (Temozolomide Resistant) Glioblastoma (**RTOG0929**).	Phase I/II Randomised 225 patients: 151 BEV naïve (BEV-N); 74 BEV refractory (BEV-R)	Arm 1: VELI + TMZ 75mg/m^2 (both 21/28 day cycle) Arm 2: VELI + TMZ 150mg/m^2 (both 5/28 day cycle)	Phase I: MTD. Phase II: PFS at 6m.	A) ORR. B) OS.	• Myelosuppression AE$^{(G3-4)}$ in 20% of pts. • PFS at 6m = 17.0% (BEV-N) & 4.4% (BEV-R) – median PFS ~ 2m (95% CI, 1.9-2.1m) in both groups. • Median OS = 10.3m (8.4-12.0m, BEV-N) & 4.7m (3.5-5.6m, BEV-R). • Concluded addition of VELI "did not significantly improve PFS at 6m" relative to historic controls.

	(2009-2017)				• Note: MGMT status was not included or analysed.
NCT01514201 ((276,277)) **DIPG** Veliparib, Radiation Therapy, and Temozolomide in Treating Younger Patients With Newly Diagnosed Diffuse Pontine Gliomas: a Paediatric Brain Tumor Consortium Study.	Phase I/II Single arm 65 patients (2012-2018)	VELI + IR + TMZ	Phase I: RP2D/DLTs. Phase II: OS.	A) PFS. B) Pseudo-progression. C) Pharmacokinetics.	• VELI RP2D was 65mg/m^2 BD. • Day 4 average VELI (65mg/m^2) plasma C_{max} = 3μM. • VELI DLTs inc: intratumoural haemorrhage (1 pt, Grade 2); rash (2 pts, Grade 3); neurological (1 pt, Grade 3). • Additional intrapatient TMZ dose escalation could not be tolerated. • OS at 1yr and 2yr = 37.2% and 5.3% respectively. • Accrual stopped early due to futility at interim analysis.
NCT02116777 ((278)) **Solid & haematological cancers** Talazoparib and Temozolomide in Treating Younger Patients With Refractory or Recurrent Malignancies.	Phase I/II Single arm 40 patients (2014-2018)	TALA + TMZ	Phase I: MTD/RP2D; Safety/toxicity; Pharmacokinetics Phase II: ORR (Ewing/PNET).	A) ORR all solid tumours (RECIST).	• RP2D = TALA 600μg/m^2 BD on day 1 then OD days 2-6/28 with TMZ 30mg/m^2 day 2-6/28 cycle. • Majority of patients had Ewing sarcoma (EWS), but one patient with a malignant glioma experienced a PR. • During Phase II, no response observed out of 10 EWS pts. • No efficacy in EWS but may warrant further study in CNS tumours.
NCT03150862 ((279)) **nGBM / rGBM** Pamiparib (BGB-290) With Radiation and/or Temozolomide (TMZ) in Newly Diagnosed or Recurrent Glioblastoma.	Phase Ib/II Parallel Estimated patients: 116 (2017-2021)	nGBM (unmethylated) Arm 1: PAMI + IR Arm 2: PAMI + IR + TMZ rGBM (un- & methylated) Arm 3: PAMI + TMZ	Phase I: Safety/toxicity. Phase II: Disease response/control.	A) Pharmacokinetics. B) PFS. C) OS. D) ORR.	• RP2D for Arm 1 = PAMI 60mg BD for 6 weeks alongside IR. • RP2D for Arm 3 = PAMI 60mg BD day 1-28 + TMZ 60mg/m^2 7/28 day cycle. • Well tolerated – no Grade 4/5 toxicities; Grade 3 – Arm 1 - nausea (2%), Arm 2 - decreased WBC count (11%). Arm 3 none. • PAMI + IR + TMZ well tolerated – trial **ongoing** – recruitment ends October 2021, final results awaited.
NCT03212742 ((280)) **Unresectable HGG** Study of Concomitant Radiotherapy with Olaparib and Temozolomide in Unresectable High-Grade Gliomas Patients (**OLA-TMZ-RTE-01**).	Phase I/IIa Sequential Estimated patients: 79 (2017-2022)	OLAP + IR + TMZ	Phase I: RP2D for both IR-period and maintenance period. Phase II: OS.	A) PFS. B) ORR. C) Neurocognitive function. D) Morphological and functional MRI findings.	• Dosing schedule = OLAP (IR-period dose) with IR and concomitant TMZ, then 4 weeks OLAP at same dose → then maintenance TMZ started alongside daily OLAP (maintenance dose). • Trial **ongoing** – expected completion June 2022.
Phase II studies					
NCT02974621 **rGBM** Cediranib Maleate and Olaparib Compared to Bevacizumab in Treating Patients With Recurrent Glioblastoma.	Phase II Randomised Estimated patients: 70 (2017-2020)	Arm 1: OLAP + cediranib Arm 2: BEV	PFS.	A) OS. B) Safety/toxicity. C) Circulating biomarkers (inc DDR and cytokines)	• Dosing schedule = OLAP BD on day 1-28/28 cycle with cediranib OD on day 1-28/28 cycle. • Trial **ongoing** – recruitment ends May 2020, results awaited.
NCT03233204 **Solid tumours with DDR defects** Phase 2 Subprotocol of Olaparib in Patients With Tumors Harbouring	Phase II Single group assignment	OLAP only	ORR.	A) PFS. B) Safety/toxicity. C) Pharmacokinetics.	• Patient subprotocol assignment from within the overall paediatric MATCH study(281) – based on actionable mutations. • Eligible actionable mutations not defined at trial registration.

Defects in DNA Damage Repair Genes (**NCI-COG Paediatric MATCH (Molecular Analysis for Therapy Choice)**).	Estimated patients: 49 (2017-2024)				• Dosing schedule = OLAP BD on day 1-28/28 cycle. • Changes in tumour genomic profile monitored using ctDNA. • Trial **ongoing** – recruitment ends September 2024.
NCT03212274 **rGlioma (WHO Grade II-IV) / Cholangiocarcinoma / Solid Tumours with IDH1/2 Mutation** Olaparib in Treating Patients With Advanced Glioma, Cholangiocarcinoma, or Solid Tumours with IDH1 or IDH2 Mutations.	Phase II Single arm Estimated patients: 145 (2018-2020)	OLAP only	ORR (3 cohorts) A) Glioma B) Cholangio C) Other solid tumours	A) PFS. B) OS. C) Safety/toxicity. D) Exploratory objectives inc correlation between baseline 2HG and response.	• Dosing schedule = OLAP BD on day 1-28/28 cycle. • Builds on preclinical studies demonstrating 'BRCAness' with IDH1/2 mutation and elevated 2HG[45]. • Trial **ongoing** – recruitment ends July 2020, results awaited.
NCT03581292 **nHGG (H3K27M$^-$ BRAFV600$^-$)** Veliparib (ABT-888), Radiation Therapy, and Temozolomide in Treating Patients With Newly Diagnosed Malignant Glioma Without H3 K27M or BRAFV600 Mutations.	Phase II Single arm Estimated patients: 115 *age 3-25* (2018-2024)	VELI + IR + TMZ	PFS.	A) ORR. B) OS.	• Dosing schedule = daily VELI BD during chemoradiotherapy phase then 4 weeks after completion → daily VELI BD + maintenance TMZ on days 1-5/28 cycle. • Incorporates longitudinal assessment of ctDNA. • Exploratory objectives inc: relationship between BRCA1/2 alternations and features of HRD (inc. large scale translocations, mutational signature 3); penetrance of HRD genes inc. HR genes, FA genes, ATM, CHK2, and MMR genes. • Trial **ongoing** – recruitment ends October 2024.
NCT04221503 **rGBM** Evaluating the Efficacy and Safety of Niraparib and Tumor-Treating Fields in Recurrent Glioblastoma (**Niraparib/TTFields**).	Phase II Parallel Estimated patients: 30 (2019-2025)	All patients receive NIRA + TTFields Cohort 1: surgical resection indicated Cohort 2: resection not indicated	Disease control (CR/PR or SD)	A) Safety/toxicity. B) ORR. C) PFS. D) OS.	• Cohort 1: initiate and continue TTFields for 5-7 days prior to starting NIRA. • Cohort 2: receive TTFields for 5-7 before planned resection, then post-operative therapy as above. • Builds on preclinical studies demonstrating 'BRCAness' induced by TTFields[72-74]. • Trial **ongoing** – expected completion September 2021.
NCT03561870 **rHGG (IDH^{mut})** Olaparib in Recurrent IDH-mutant High Grade Gliomas (**OLAGLI**).	Phase II Single arm Estimated patients: 35 (2020-2021)	OLAP only	PFS.	n/a	• Dosing schedule = OLAP 300mg BD on days 1-28/28 cycle. • Based on preclinical studies demonstrating 'BRCAness' with IDH1/2 mutation and elevated 2HG[45]. • Trial **ongoing** – expected completion September 2021.
NCT03991832 **IDH^{mut} Solid Tumours** Olaparib and Durvalumab in Patients With IDH-Mutated Solid Tumors (**MEDI 4736**).	Phase II Parallel Estimated patients: 78 (2020-2022)	All pts receive OLAP + durvalumab Cohort 1: Glioma Cohort 2: Cholangio Cohort 3: Other solid tumours	ORR.	A) PFS. B) OS. C) Safety/toxicity.	• Dosing schedule = OLAP BD on days 1-28/28 cycle + durvalumab (anti-PD-L1 therapy) on day 1/28 cycle. • Based on preclinical studies demonstrating 'BRCAness' with IDH1/2 mutation and elevated 2HG[45]. • Trial **ongoing** – recruitment ends September 2022, expected completion September 2023.

Phase II/III studies					
NCT02152982 **nGBM (MGMT promoter hypermethylated)** Temozolomide With or Without Veliparib in Treating Patients With Newly Diagnosed Glioblastoma Multiforme.	Phase II/III RCT Estimated patients: 440 (2014-2021)	After SoC IR and concomitant TMZ: Arm 1: VELI + TMZ Arm 2: PLACEBO + TMZ	OS.	A) 'Interaction' with TTFields (for pts receiving this). B) PFS. C) ORR. D) Safety/toxicity. E) QoL.	• Patients permitted to receive TTFields alongside trial therapies. No other additional therapies permitted. • Studies will also assess whether genetic/epigenetic alternations to DDR genes influence outcomes. • Trial **ongoing** – expected completion January 2021.
Abbreviations: rGBM = recurrent GBM; nGBM = newly diagnosed GBM; rHGG = recurrent high-grade glioma; DIPG = diffuse intrinsic pontine glioma; IR = radiotherapy; TMZ = temozolomide; TTF = tumour treating fields; OLAP = olaparib; NIRA = niraparib; PAMI = pamiparib; VELI = veliparib; TALA = talazoparib; SoC = standard-of-care; Rx = treatment; OS = median overall survival; PFS = median progression-free survival; MTD = maximum tolerated dose; RP2D = recommended Phase II dose - highest dose with acceptable toxicity (producing a rate of around 20% DLTs); SD = stable disease; CR = complete response; PR = partial response; ORR = overall response rate (proportion of patients with a PR or CR); F/U = follow-up; QoL = quality of life; DLTs = dose limiting toxicities; AEs = adverse events; AEs$^{(G3-4)}$ = grade 3-4 adverse events; SAEs = severe adverse events.					

Table 3.2: ATM inhibitor trials in high-grade glioma.

Summary of key ATM inhibitor in high-grade glioma clinical trials - ongoing					
Trial (ref) **& Indication**	**Design &** **n** (rec dates)	**Treatment(s)**	**1° Endpoint**	**2° Endpoint(s)**	**Remarks & Conclusions**
Phase I studies					
NCT03423628 [(282,283)] **nGBM / rGBM / Brain Metastases** Safety and Tolerability of AZD1390 Given With Radiation Therapy in Patients With Brain Cancer.	Phase I Parallel Estimated patients: 132 (2018-2020)	AZD1390 + SoC IR: nGBM: IMRT 60 Gy over 6 weeks rGBM: IMRT 35 Gy over 2 weeks Mets: WBRT 30 Gy over 2 weeks	Safety/toxicity	A) EFS. B) ORR. C) Pharmacokinetics.	• Dosing schedule = AZD1390 administered in 3 'cycles' – (1) 1 dose prior to starting IR; (2) intermittent if continuous administration during IR; (3) 2-weeks adjuvant ATMi after IR. • Based on preclinical studies demonstrating BBB penetration and improved survival with AZD1390 in mouse models[(268)]. • Trial **ongoing** – expected completion April 2022.
Abbreviations: rGBM = recurrent GBM; nGBM = newly diagnosed GBM; IR = radiotherapy; IMRT = intensity-modulated radiation therapy; WBRT = whole brain radiotherapy; SoC = standard-of-care; EFS = event free survival; ORR = overall response rate (proportion of patients with a PR or CR).					

3.2 Inhibition of key DDR targets sensitises established glioblastoma cell lines to DNA damaging therapy

3.2.1 Inhibition of the DNA damage response following DNA damaging therapy

In order to confirm the inhibition of key DDR processes, MGMT negative (U87) and MGMT positive (LN18) glioblastoma cell cultures were exposed to DNA damaging therapy following pre-treatment with: inhibition of the FA pathway using curcumin, a compound well-established to down regulate FA pathway activity[20,22,284,285], or PARP inhibition using olaparib[286]. Western blot analysis demonstrated evidence of reduced DDR target activity with both of the compounds tested (Figure 3.1). Compound doses for ATR inhibition using VE-821 or ATM inhibition using KU55933 were based on previously published studies using these compounds[238,243,287,288].

Considering the FA pathway, treatment with temozolomide chemotherapy (100μM) produced a notable induction of FANCD2 monoubiquitination in both U87 and LN18 cells, as expected. Furthermore, treatment with increasing concentrations of curcumin prior to temozolomide provided a dose-dependent reduction in monoubiquitinated FANCD2 (Ub-FANCD2), with maximal effects most evident in MGMT expressing LN18 glioblastoma cells. Interestingly, pre-treatment with curcumin reduced not only Ub-FANCD2 levels, but also appeared to reduce the protein expression of non-ubiquitinated FANCD2 at higher doses, particularly in LN18 cultures (Figure 3.1A).

Since PARP1 is a key mediator of DNA single strand break (SSB) repair[289] and SSBs are the most abundant DNA lesion generated by irradiation[290], ionising radiation (5 Gy) was used during the confirmation of olaparib activity. Both U87 and LN18 cells demonstrated baseline protein expression of PARP1. Furthermore, DMSO treated cells demonstrated functional PARP1 catalytic activity as confirmed by detectable PAR chains of variable molecular weight. Treatment with olaparib was confirmed to inhibit PAR polymerisation (Figure 3.1B). Although there was subtle evidence of dose dependency, even the lowest doses of olaparib used (0.5-1μM) substantially abrogated PARylation in both untreated and IR treated cells.

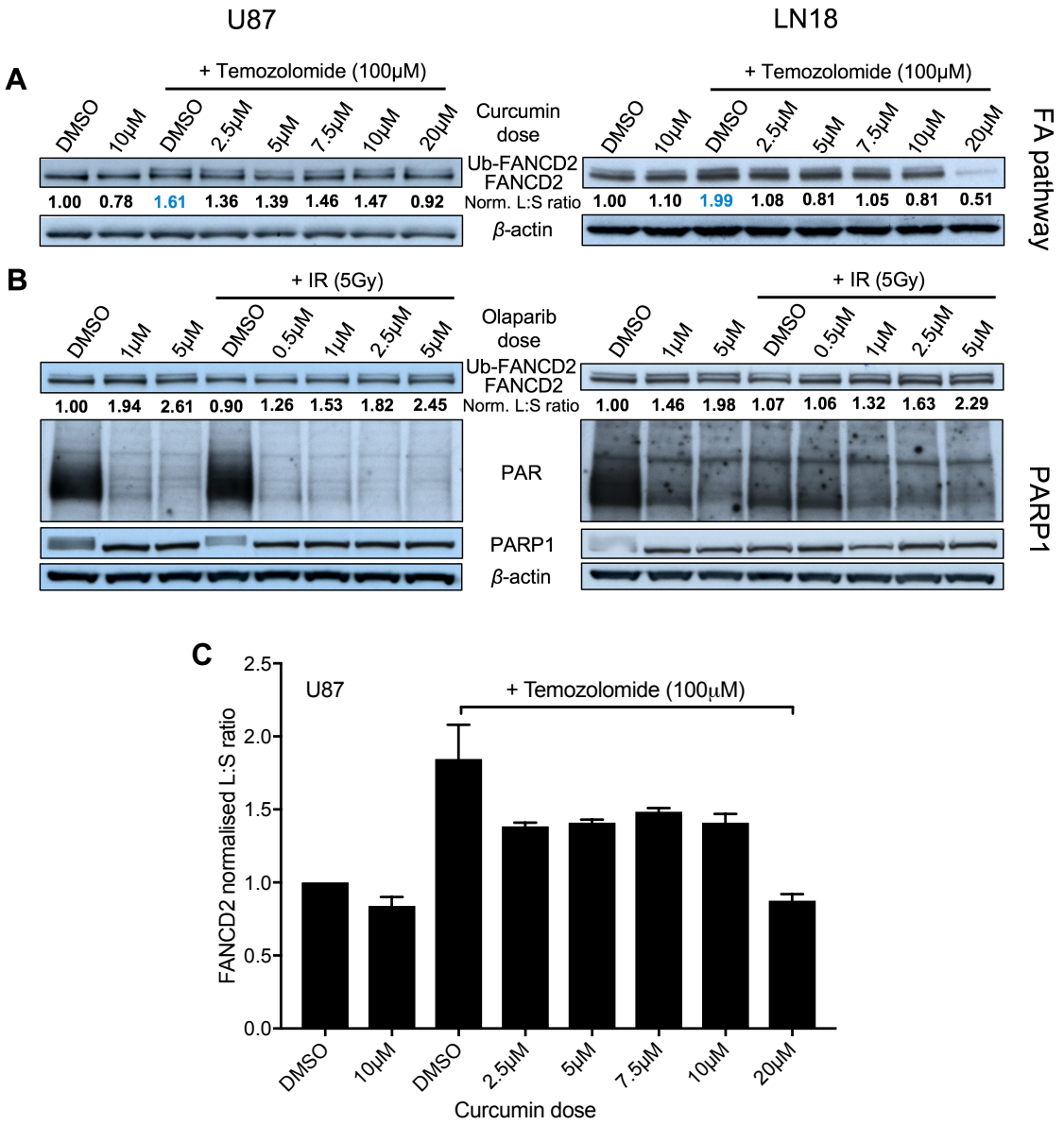


Figure 3.1: Inhibition of FANCD2 monoubiquitination and PARylation in established glioblastoma cell lines – U87 (MGMT negative) or LN18 (MGMT positive) glioblastoma cells were plated for 24 hours prior to exposure to the indicated DDRi then DNA-damaging temozolomide chemotherapy or radiotherapy 1 hour later. Cells were incubated for a further 16 hours (chemotherapy blots) or 2 hours (radiotherapy blots) prior to lysis and Western blotting. Blots confirm pharmacological inhibition of: **A.** The FA pathway, using curcumin; **B.** PARP1, using olaparib. To determine FA pathway activation, the normalised ratio of Ub-FANCD2 (L) to FANCD2 (S) (normalised to DMSO only treated cells) was calculated for each treatment as previously described[216] and shown beneath the relevant bands. Numbers in **blue** indicate maximal FA pathway activation following temozolomide exposure. Each Western blot was performed in 2 independent experimental repeats. **C.** Comparison of quantification of FANCD2 normalised L:S ratios in U87 cells treated with curcumin prior to temozolomide exposure – data represents 2 independent experimental repeats. *(Data shown was produced by Mr D Dar working directly under my direct supervision).*

3.2.2 Inhibition of the FA pathway, PARP1 and ATR sensitise established glioblastoma cultures to temozolomide chemotherapy

After confirming target inhibition with the above compounds, studies were undertaken to establish whether the inhibition of key DDR processes might confer sensitisation to temozolomide, the chemotherapeutic agent used most commonly to treat glioblastoma. MGMT expression, as delineated by promotor region methylation status, is a major

determinant of clinical outcome following treatment with the temozolomide-incorporating Stupp regimen in patients[10,94]. As such, a panel of temozolomide sensitive (MGMT negative; U87 and U251) and relatively temozolomide resistant (MGMT positive; T98G and LN18) glioblastoma cell lines were used to reflect a spectrum of temozolomide susceptibility and evaluate the potential of putative strategies targeting a single, key DDR process to enhance therapeutic response to chemotherapy. The applied dose of each DDRi agent was selected on the basis of single agent Western blot dose-response studies above (Figure 3.1), dose-response optimisation studies assessing the effects of each compound on cell viability (see Figure 3.2) and consideration of previously published studies[22,197,238,243,287,288], to establish a dose for each compound that demonstrated minimal toxicity as a monotherapy whilst maintaining robust inhibitory activity.

As anticipated, MGMT negative U87 and U251 cells generally demonstrated greater sensitivity to temozolomide relative to MGMT positive T98G and LN18 cells (Figure 3.3). The relative effects of each DDRi used in combination with temozolomide chemotherapy are summarised in Figure 3.3.

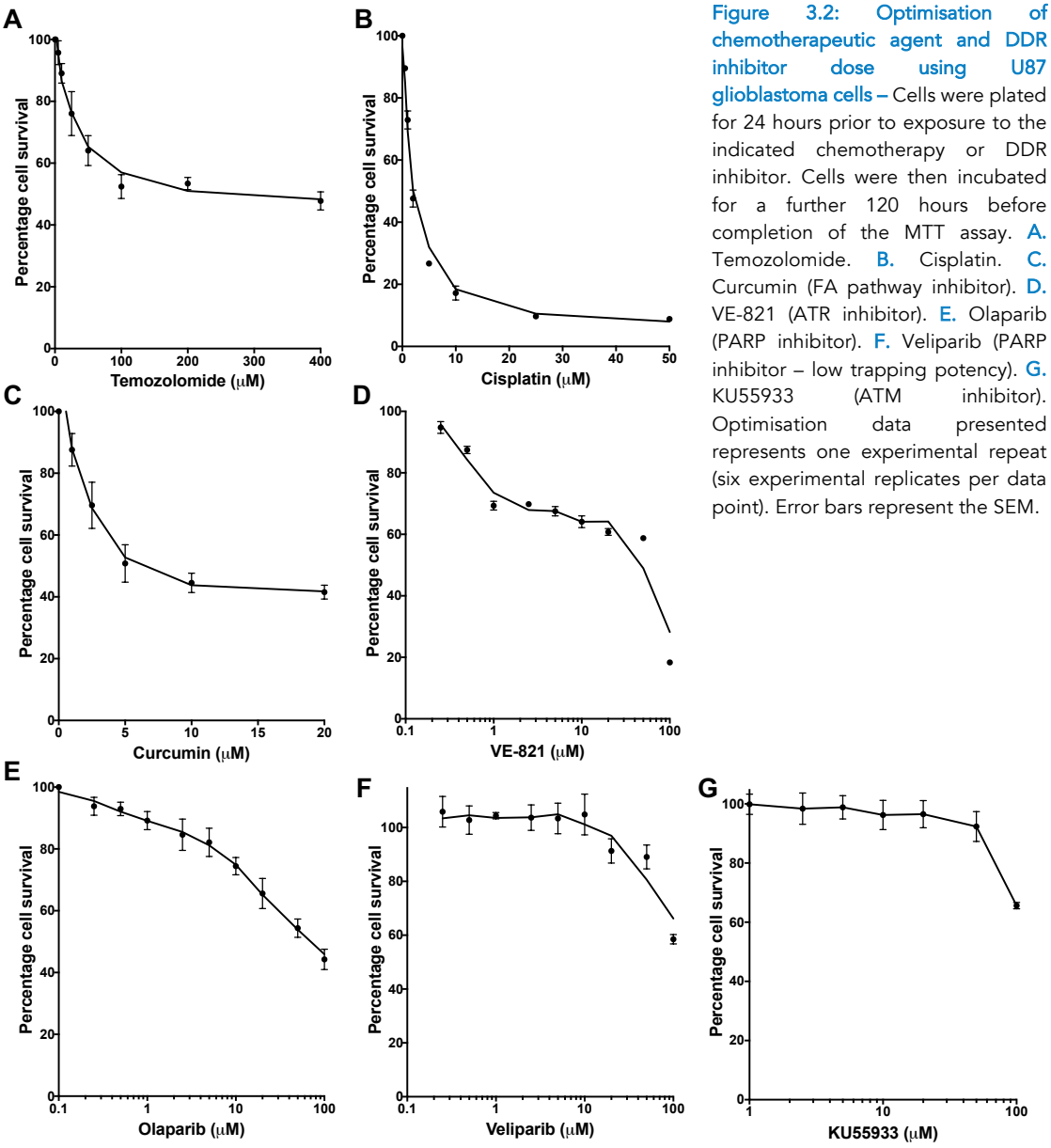


Figure 3.2: Optimisation of chemotherapeutic agent and DDR inhibitor dose using U87 glioblastoma cells – Cells were plated for 24 hours prior to exposure to the indicated chemotherapy or DDR inhibitor. Cells were then incubated for a further 120 hours before completion of the MTT assay. **A.** Temozolomide. **B.** Cisplatin. **C.** Curcumin (FA pathway inhibitor). **D.** VE-821 (ATR inhibitor). **E.** Olaparib (PARP inhibitor). **F.** Veliparib (PARP inhibitor – low trapping potency). **G.** KU55933 (ATM inhibitor). Optimisation data presented represents one experimental repeat (six experimental replicates per data point). Error bars represent the SEM.

3.2.3 Effects of Fanconi anaemia pathway inhibition with curcumin on temozolomide response

U87 glioblastoma cells treated with curcumin prior to temozolomide chemotherapy were significantly more sensitive (Figure 3.3A-B). Given that these cells have previously been demonstrated to actively express FA pathway proteins and curcumin has been demonstrated to inhibit the monoubiquitination of FANCD2 (a key step in the FA pathway), this data corroborates the previously identified therapeutic potential of FA pathway inhibition in glioblastoma[22]. Pre-treatment with curcumin also sensitised T98G cultures to temozolomide (further corroborating Patil *et al.* (2014)[22]) and LN18 cultures, providing new data to support this therapeutic strategy. However, surprisingly, no clear temozolomide-sensitisation was observed using curcumin in U251 cultures.

3.2.4 Effects of PARP inhibition on temozolomide response

Inhibition of PARP with olaparib consistently sensitised U87 glioblastoma cells to the effects of temozolomide throughout the range of treatment doses used (Figure 3.3). Interestingly, treatment with veliparib did not appear to confer similar sensitisation, except at the highest dose of temozolomide used (100μM). Differential effects of these drugs sharing a common target may reflect known divergence in the ability of each to 'trap' PARP. Indeed the efficacy of various PARP inhibitors is not predicated on catalytic inhibition of PARylation alone, but is instead influenced by their differing effects at the PARP1 helical domain which permit allosteric changes. These changes modulate the affinity and duration of PARP1 binding at DNA strand breaks to generate lesions which become toxic through cell cycle progression[291]. PARP1 is unable to be released from DNA (hence 'trapped') until the PARP inhibitor dissociates from the active site, permitting the utilisation of NAD+ and autoPARylation which allows PARP to be released from DNA and the assembly of downstream SSB DNA repair factors[292,293]. Consequently, an inhibitor possessing greater PARP trapping potency might be expected to sensitise cancer cells to DNA damaging therapies more reliably. Since olaparib is reported to trap PARP much more potently than veliparib[294,295], data here suggests greater PARP trapping potency may translate to increased sensitisation of U87 glioblastoma cells to temozolomide, at least at lower temozolomide doses. Indeed, olaparib sensitised all MGMT negative (U87 and U251) and MGMT positive (T98G and LN18) glioblastoma cells to 12.5μM temozolomide whereas veliparib failed to sensitise cells to this dose of temozolomide. However, at the highest dose of temozolomide used (100μM), both inhibitors demonstrated chemosensitising effects, underlining the overall potential of PARP inhibition as a novel therapeutic strategy in GBM management. However, the failure of veliparib to sensitise MGMT positive cell lines (T98G and LN18) even at relatively high temozolomide doses (50μM) suggests MGMT status might influence response to PARP inhibitor-mediated temozolomide sensitisation only in the context of weakly PARP trapping compounds.

3.2.5 Effects of ATR and ATM inhibition on temozolomide response

Inhibition of ATR using the potent and selective inhibitor VE-821[296] markedly enhanced the sensitivity of U87, T98G and LN18 glioblastoma cells to temozolomide chemotherapy – but effects in U251 cells were less pronounced (Figure 3.3). Conversely, ATM inhibition using

KU55933 elicited marked sensitisation to temozolomide chemotherapy in U251 cells only, perhaps reflecting MGMT-independent differences in the genetic contexts of these cell lines.

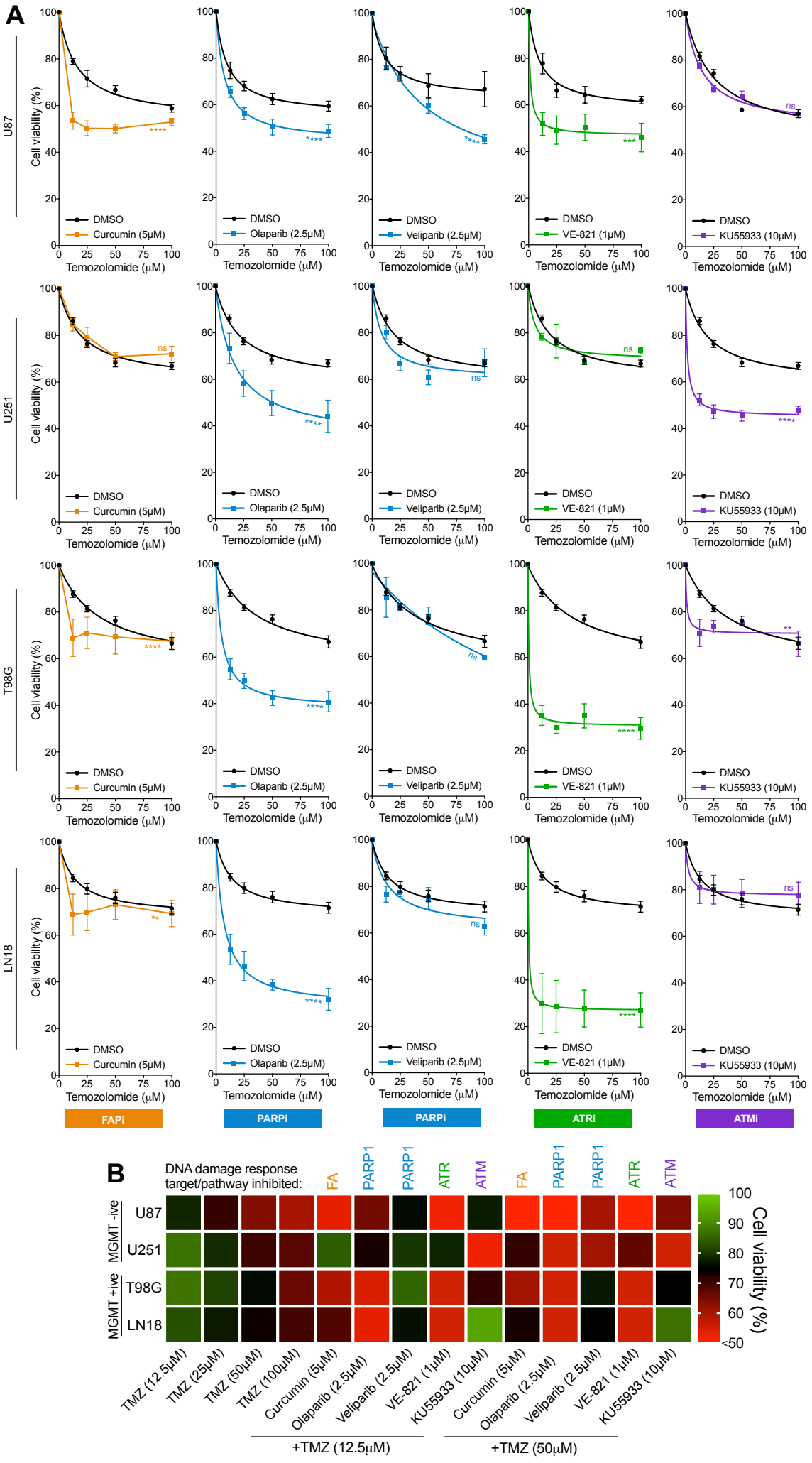

A
U87
U251
T98G
LN18
Cell viability (%)
Temozolomide (μM)
DMSO
Curcumin (5μM)
Olaparib (2.5μM)
Veliparib (2.5μM)
VE-821 (1μM)
KU55933 (10μM)
ns
FAPi
PARPi
PARPi
ATRi
ATMi
B
DNA damage response target/pathway inhibited:
FA
PARP1
PARP1
ATR
ATM
FA
PARP1
PARP1
ATR
ATM
MGMT -ive
MGMT +ive
U87
U251
T98G
LN18
Cell viability (%)
100
90
80
70
60
<50
TMZ (12.5μM)
TMZ (25μM)
TMZ (50μM)
TMZ (100μM)
Curcumin (5μM)
Olaparib (2.5μM)
Veliparib (2.5μM)
VE-821 (1μM)
KU55933 (10μM)
Curcumin (5μM)
Olaparib (2.5μM)
Veliparib (2.5μM)
VE-821 (1μM)
KU55933 (10μM)
+TMZ (12.5μM)
+TMZ (50μM)

Figure 3.3: Targeting the DNA damage response in established glioblastoma cultures to enhance temozolomide response – MGMT negative (U87 and U251) and MGMT positive (T98G and LN18) glioblastoma cells were plated for 24 hours prior to exposure to the indicated DDRi then DNA-damaging temozolomide chemotherapy 8 hours later. Cells were incubated for a further 120 hours before the MTT assay was used to compare cell viability. **A.** Drug response data for established glioblastoma cultures. **B.** Heatmap summarising the effects of temozolomide alone, and in combination with the indicated DDRi, on glioblastoma cell viability. Each cell line – DDRi data set illustrated represents the mean of at least 3 independent experiments. Error bars represent the SEM.

(Data shown in A-B was produced by the author [U87, 3 repeats; U251, T98G and LN18, 2 repeats] and the following students working under my direct supervision: Miss Nikita Lad [U251, T98G and LN18, 2 repeats – excluding the TMZ + veliparib combination in LN18 cells], and; Mr Dawoud Dar [LN18 TMZ + veliparib only combination, 3 repeats).

3.2.6 Inhibition of the FA pathway, PARP1 and ATR sensitise U87 glioblastoma cultures to DNA crosslinking chemotherapy

Effects of Fanconi anaemia pathway inhibition with curcumin on cisplatin response

As interstrand crosslinks are considered the primary DNA lesion resolved by canonical activation of the FA pathway[2], we sought to establish whether chemosensitisation was maintained during treatment with the platinum-based bi-directional alkylating agent cisplatin. Indeed, in U87 glioblastoma cultures, treatment with the FA pathway inhibitor curcumin prior to cisplatin treatment demonstrated a substantial reduction in cell viability even at a relatively low cisplatin dose (Figure 3.4).

Effects of PARP1, ATR and ATM inhibition on cisplatin response

Interestingly, in U87 glioblastoma cells, olaparib failed to sensitise to cisplatin therapy whilst pre-treatment with veliparib demonstrated a significant, albeit modest, reduction in cell viability (Figure 3.4). This partially reverses the trend in chemosensitising potential observed between olaparib (more potent PARP trapping ability) and veliparib (less potent PARP trapping ability) when these PARPi were combined with temozolomide chemotherapy (Section 3.2.4). Similar to the effects of ATR inhibition on temozolomide-induced DNA damage (Section 3.2.5), potent chemosensitisation was observed with the combination of VE-821 and cisplatin. In contrast, ATM inhibition with KU55933 antagonised the effects of cisplatin on cell viability.

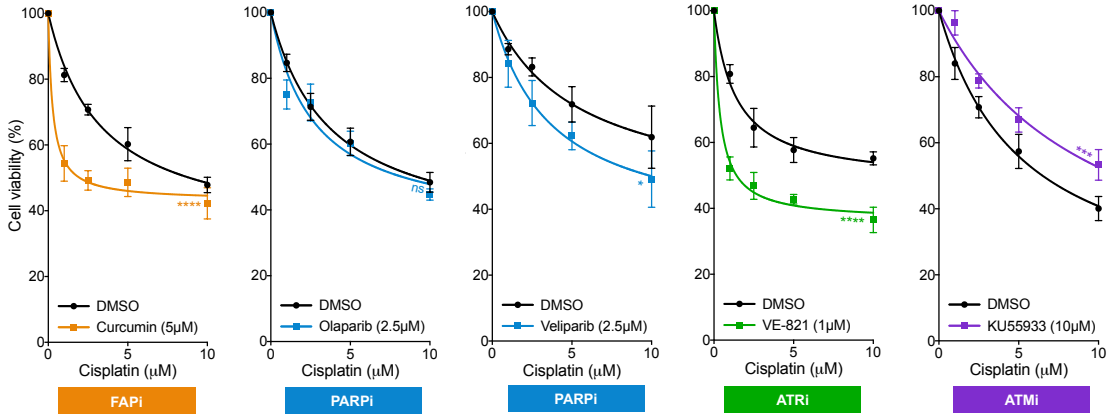


Figure 3.4: Inhibition of the FA pathway, PARP1 and ATR sensitise established U87 glioblastoma cultures to crosslinking chemotherapy – U87 glioblastoma cells were plated for 24 hours prior to exposure to the indicated DDRi then DNA-crosslinking cisplatin chemotherapy 8 hours later. Cells were incubated for a further 120 hours before the MTT assay was used to compare cell viability. Data points shown are the mean from 3 independent experiments with error bars representing the SEM.

Together, these data suggest pharmacological targeting of the FA DNA damage repair pathway or a key interconnected DDR process might represent an appealing therapeutic strategy to render glioblastoma more susceptible to currently available chemotherapies. However, in the context of brain tumours, curcumin is not well suited to clinical use for a plethora of reasons including: poor absorption; poor bioavailability with extensive first pass metabolism; poor penetration of the blood brain barrier, and; a number of non-FA pathway-related, pleiotropic effects[245,297,298]. As such, the ongoing preclinical development of novel, specific compounds which target the FA pathway at our institution provides a key opportunity to generate putative therapeutic strategies suitable for clinical translation.

3.3 Novel, specific compounds to inhibit the FA pathway (nFAPi) as a therapeutic strategy

3.3.1 The development of nFAPi

Work has recently been undertaken at our institution (Department of Chemistry, The University of Sheffield) to develop compounds which effectively inhibit the FA pathway and could be suitable for the clinic, representing a prime example of hypothesis-driven drug design. Briefly, since FANCL plays a critical role in FA pathway activation through its E3 ligase activity (resulting in the monoubiquitination of FANCD2 and FANCI)[299,300], its x-ray crystallographic structure[301,302] was interrogated to identify putative binding pockets. A novel in-house compound libraries containing ~2000 drug-like molecules was utilised. Compounds within this bespoke library were based on previous drugs used to treat neurological conditions and were synthesised in Dr Beining Chen's laboratory. Compound

structures were docked into predicted binding pockets of FANCL using fpocket and Accelrys's Discovery Studio binding site tool. *In silico* analyses were performed to predict and rank the binding affinity of each molecule to various pockets of FANCL. From these analyses, 12 compounds were predicted to have FANCL binding capacity. These candidate molecules (novel FA pathway inhibitors; nFAPi) were subsequently validated in the laboratory for ability to inhibit FANCL activity[303]. Internal data produced by A. Patil (previous PhD student) confirmed strong FA pathway inhibition with 3 of these first-generation compounds that belong to the same chemical family. More recently, screening of 38 analogue compounds has revealed several with potentially more potent activity as part of early structure-activity relationship (SAR) analyses[304]. The previously assessed LD_{50} of some of these compounds in combination with temozolomide is presented in Table 3.3 (data produced by previous PhD student Abhijit Patil). These compounds are currently being assessed further in on-going biochemical and target engagement studies (Collis & Chen, unpublished). Importantly, these nFAPi remain within an active drug development process with their novel chemistry protected by agreements designed to provide a temporary safeguard as the potential of this intellectual property is investigated further and the compounds continue to be refined.

Table 3.3: Summary of previously established sensitisation activity during early SAR studies.

Previously established sensitisation activity derived from MTT studies	
nFAPi codename	**LD_{50} with 25μM TMZ (nM)***
E41	216.8
F73	80.5
F76	25.1
M66	27.7
F69	3.9
* LD_{50} values derived from MTT studies in U87 glioblastoma cells (3 experimental repeats)	

3.3.2 Cell-free evaluation of nFAPi compound activity

Initial confirmation of the biochemical activity of nFAPi compounds was conducted in collaboration with our Melbourne-based collaborators (Dr Wayne Crismani, Dr Michael Sharp and Dr Andrew Deans) using a cell-free, AlphaScreen™-based assay. Briefly, the AlphaScreen™ assay relies on the conjugation of molecules of interest to hydrogel-coated beads which act as a 'donor' or 'acceptor' of singlet oxygen (Figure 3.5A)[305]. Following laser excitation and conversion of ambient oxygen to a more excited singlet state within the donor bead, the nanoscale-limited diffusion of singlet oxygen (no further than 200nm) ensures fluorescent emissions following reaction with a chemiluminescer in the acceptor

bead only occur when the molecules of interest physically interact. In this experiment, a cell-free reaction in the presence of the proteins E1, E2 and BL100 subcomplex with acceptor/donor bead bioconjugated FANCD2 (within the ID2 complex) and ubiquitin were used to produce an 'Alpha' signal increase specific to FANCD2 ubiquitination.

On initial evaluation of these experimental compounds, two nFAPi (E41 and M66) reduced the rate of alpha signal increase and maximum alpha signal relative to DMSO (Figure 3.5B). As expected, the clearly detectable reduction in alpha screen signal observed with each nFAPi (approximately 35% after 240 minutes) was smaller than the extensive and sustained reduction observed using the assay positive control TAK243, which inhibits the E1 enzyme, ubiquitin activating enzyme (UAE) responsible for charging >99% of cellular ubiquitin, resulting in profound pathway-agnostic intracellular abrogation of ubiquitination[306]. Further evaluation of 5 nFAPi nine days later demonstrated similar reduction in alpha screen signal in the presence of F69, F76 and M66 (Figure 3.5C), relative to DMSO. However, at this time, E41 failed to clearly reproduce the reduction in alpha signal observed on Day 1. Additionally, F73 did not demonstrate any clear reduction in alpha signal.

Taken together, the capability of some of these novel compounds to restrain increases in alpha signal supports their ability to inhibit FANCD2 monoubiquitination. However, the lack or loss of this ability by Day 10 after solubilisation in DMSO perhaps suggests this capability may be lost relatively quickly. Indeed, further testing of the several nFAPi after Day 10 using AlphaScreen assays failed to demonstrate any further activity (data not shown), including a loss of M66 activity (the only nFAPi confirmed to maintain consistent inhibition of FANCD2 ubiquitination between day 1 and day 10).

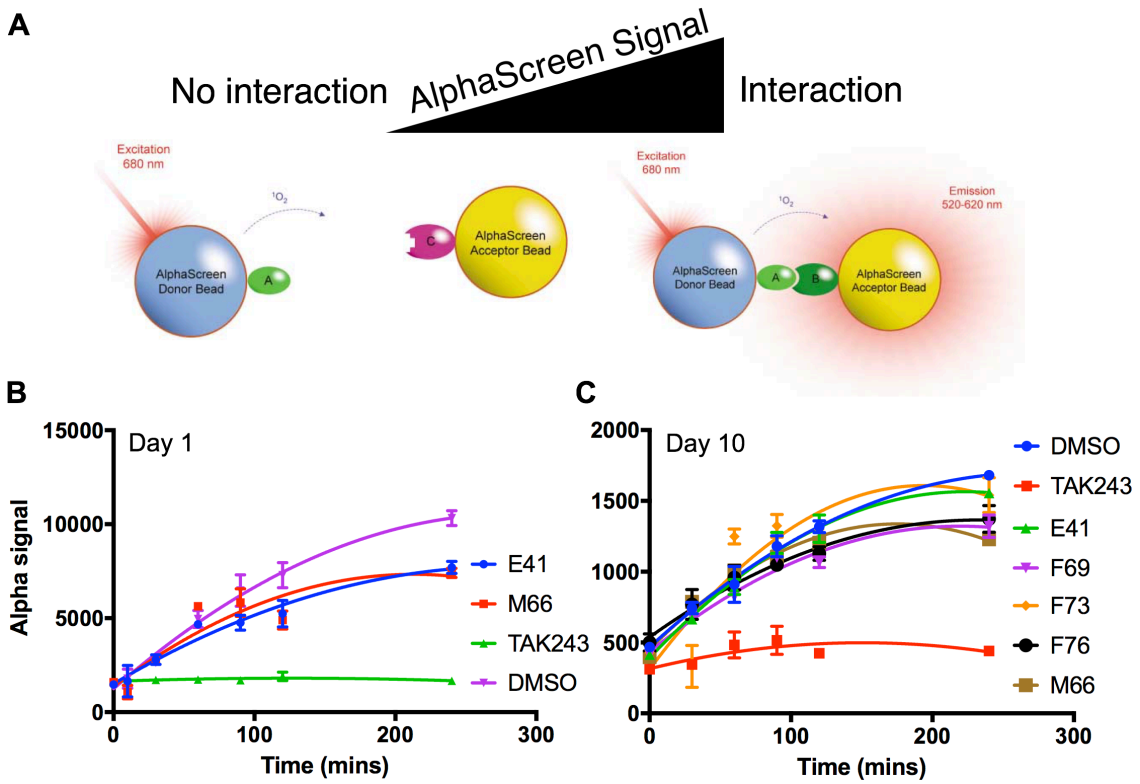


Figure 3.5: Novel compounds targeting FANCL reduce FANCD2 monoubiquitination in cell-free AlphaScreen assay – A. Schematic representation of the AlphaScreen™ assay (Adapted from AlphaScreen™ Principles[305]). B. Initial AlphaScreen™ assay to assess inhibition of FANCD2 monoubiquitination with E41 and M66. C. Repeat AlphaScreen™ assay to assess inhibition of FANCD2 monoubiquitination using 5 second generation nFAPi. Data points shown represent the mean from experimental replicates with error bars representing the SEM. *(Data shown is provided courtesy of Dr Wayne Crismani, Dr Michael Sharp and Dr Andrew Deans – St Vincent's Institute Medical Research, Melbourne, Australia).*

3.3.3 Curcumin and nFAPi reduce temozolomide-induced FANCD2 foci formation and FANCD2 monoubiquitination

Next, we aimed to establish whether nFAPi are capable of reducing key quantifiable markers of FA pathway activity in response to DNA damage within a cellular context. These studies (Figure 3.1A) and previous studies have demonstrated that the FA pathway is activated in response to alkylating chemotherapies used to treat glioblastoma including temozolomide[20,22],[21]. Additionally, inhibition of the FA pathway with commercially available inhibitors sensitises glioblastoma cells to temozolomide chemotherapy (see Figure 3.3 and Patil *et al.* (2014)[22]) and an emerging body of evidence confirms that FA-deficient cells appear to be more sensitive to alkylating chemotherapy than FA-proficient cells[20-22]. Consequently, confirmation of the ability to reduce FA pathway activity represents a key step in the early preclinical evaluation of these novel, targeted compounds.

Using an immunofluorescence approach, exposure of glioblastoma cells to temozolomide chemotherapy (50μM) led to a robust induction of FANCD2 nuclear foci formation.

Furthermore, treatment of cells with nFAPi (5μM) for 8 hours prior to temozolomide exposure provided a significant reduction in FANCD2 nuclear foci formation, which was comparable to that observed in curcumin treated cells (Figure 3.6A-B).

Additionally, nFAPi treatment resulted in moderately reduced FANCD2 monoubiquitination following temozolomide exposure in U87 glioblastoma cultures (Figure 3.6C). Together, these data confirm nFAPi are capable of restraining fundamental, quantifiable features of FA pathway activation in cell-free and cellular contexts. Therefore, investigation of the postulated therapeutic potential of nFAPi was carried out.

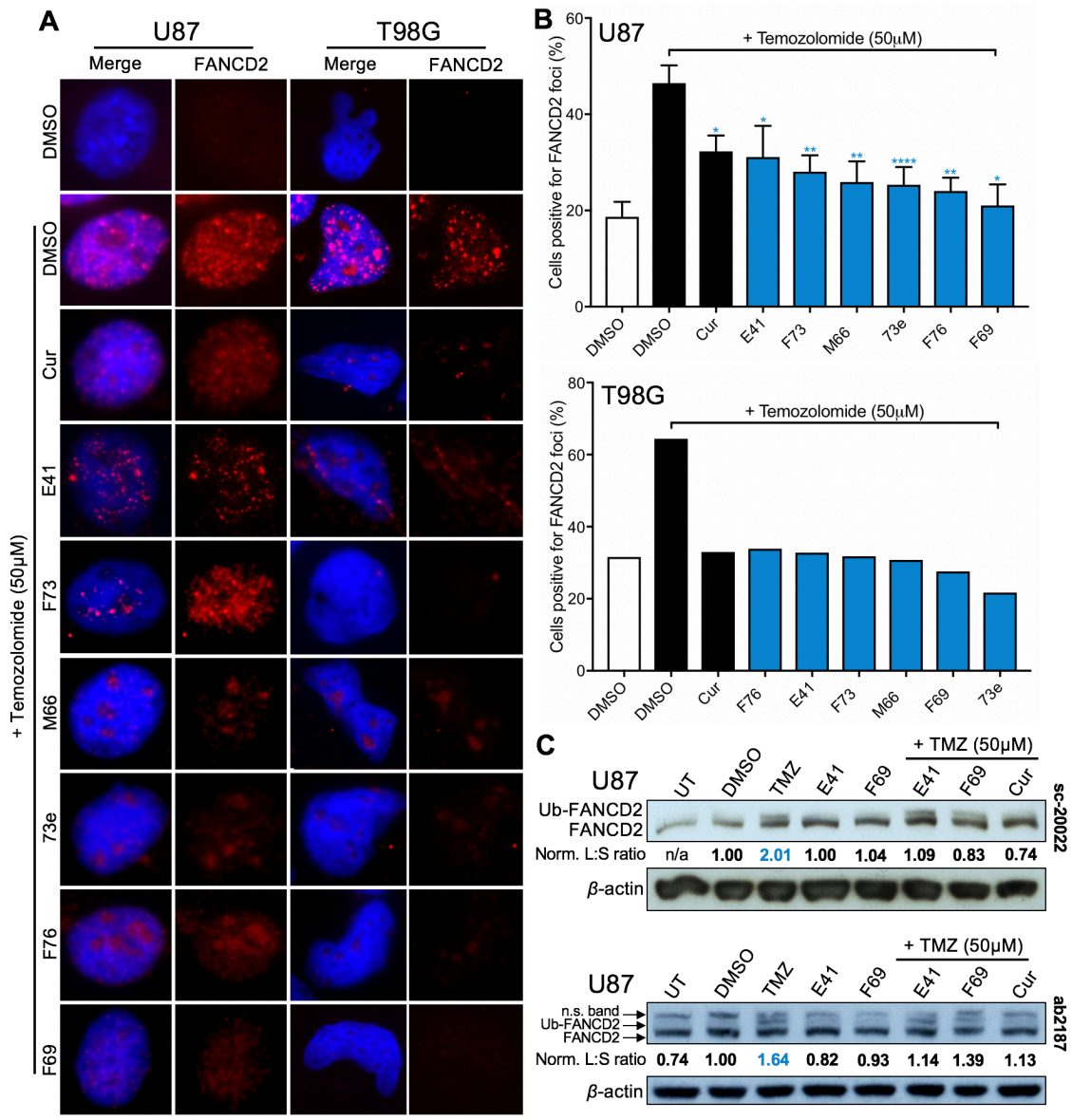


Figure 3.6: Novel specific FA pathway inhibitors reduce temozolomide-induced FANCD2 foci formation and FANCD2 monoubiquitination in established glioblastoma cultures – MGMT negative U87 and MGMT positive T98G glioblastoma cells were plated for 24 hours prior to exposure to the indicated nFAPi/FAPi (each at 5μM) then DNA-damaging temozolomide chemotherapy 8 hours later. Cells were then incubated for a further 16 hours before being fixed (for immunofluorescence) or lysed (for Western blot). **A.** Immunofluorescence detection of FANCD2 nuclear foci in U87 and T98G glioblastoma cultures – representative images. **B.** Immunofluorescence quantification of FANCD2 nuclear foci in U87 and T98G glioblastoma cultures. **C.** Western blots showing FANCD2 protein expression (both independent experimental repeats with two different antibodies are presented) and actin (loading control) expression in U87 cells. To determine FA pathway activation, the normalised ratio of Ub-FANCD2 (L) to FANCD2 (S) (normalised to DMSO only treated cells) was calculated for each treatment as previously described[216] and shown beneath the relevant bands. Data shown in 3.5A-B are from 3 independent experiments in U87 cells and 1 independent experiment in T98G cells.

3.3.4 Evaluation of the effects of nFAPi on temozolomide sensitivity

Here, we aimed to determine whether nFAPi sensitised glioblastoma cells to temozolomide in a manner analogous to commercial compounds previously shown to affect FA pathway activity. Doses of the compounds used were selected based on the above data (see Figure 3.6) and dose optimisation work performed by a previous PhD Student (Abhijit Patil). Early testing of initial nFAPi (nFAPi4, 5 & 10) demonstrate some ability to sensitise U87

glioblastoma cells to temozolomide chemotherapy, however this effect dissipated on repeat testing (Figure 3.7A).

The availability of nFAPi analogues provided further opportunities to assess the therapeutic potential of this collection of compounds. Importantly, a dose of 5μM nFAPi alone (i.e. in the absence of temozolomide) did not cause any significant reduction in U87 cell viability and ~5% reduction in T98G cell viability (data not shown). Similar to the initial nFAPi compounds, early testing of the nFAPi analogues appeared to increase the sensitivity of U87 glioblastoma cells, with maximal sensitisation at 25μM temozolomide (Figure 3.7B). However, on repeated comprehensive evaluation these compounds failed to sensitise U87 and T98G glioblastoma cultures to temozolomide chemotherapy (Figure 3.7C). Of note, repeated testing in Figure 3.7C was completed using compound newly solubilised in DMSO after earlier repeated testing using previously solubilised 10mM DMSO stocks of the compound stored at -20°C and -80°C did not demonstrate further sensitisation to temozolomide in U87, T98G and HeLa cells (data not shown). The MTT assay used to infer cell viability had previously been optimised (see Methods – Figure 2.3). However, to avoid missing any subtle sensitising effect of second generation nFAPi due to the selected assay parameters, for example, as a result of doses of temozolomide alone (theoretically) producing cell viabilities close the lower limit of assay detection, we re-tested the compounds on U87 cell cultures using a higher seeding density (1.80×10^3 rather than the 1.00×10^3 cells/well typically seeded). As expected, the reduction in U87 cell viability observed with temozolomide alone was reduced at this higher cell density, however no ability of nFAPi to chemosensitise was observed in this context (Figure 3.8). Together, these results led us to speculate that the compounds may have degraded in powder form, or may quickly degrade once solubilised in DMSO. However, HPLC testing of the compounds solubilised in DMSO over a range of time points from immediately to 1 month did not demonstrate any evidence of compound degradation or structural change (data not shown). Additionally, varying the nFAPi pre-treatment duration (1-8 hours) and solubilisation of the compounds in PBS, DMEM, DMEM with 10% FCS or ethanol did not reveal any further potential to sensitise established cultures to temozolomide chemotherapy (data not shown). However, since these compounds remain within an active preclinical drug development process, future iterations of nFAPi may demonstrate more consistent and potent chemosensitisation.

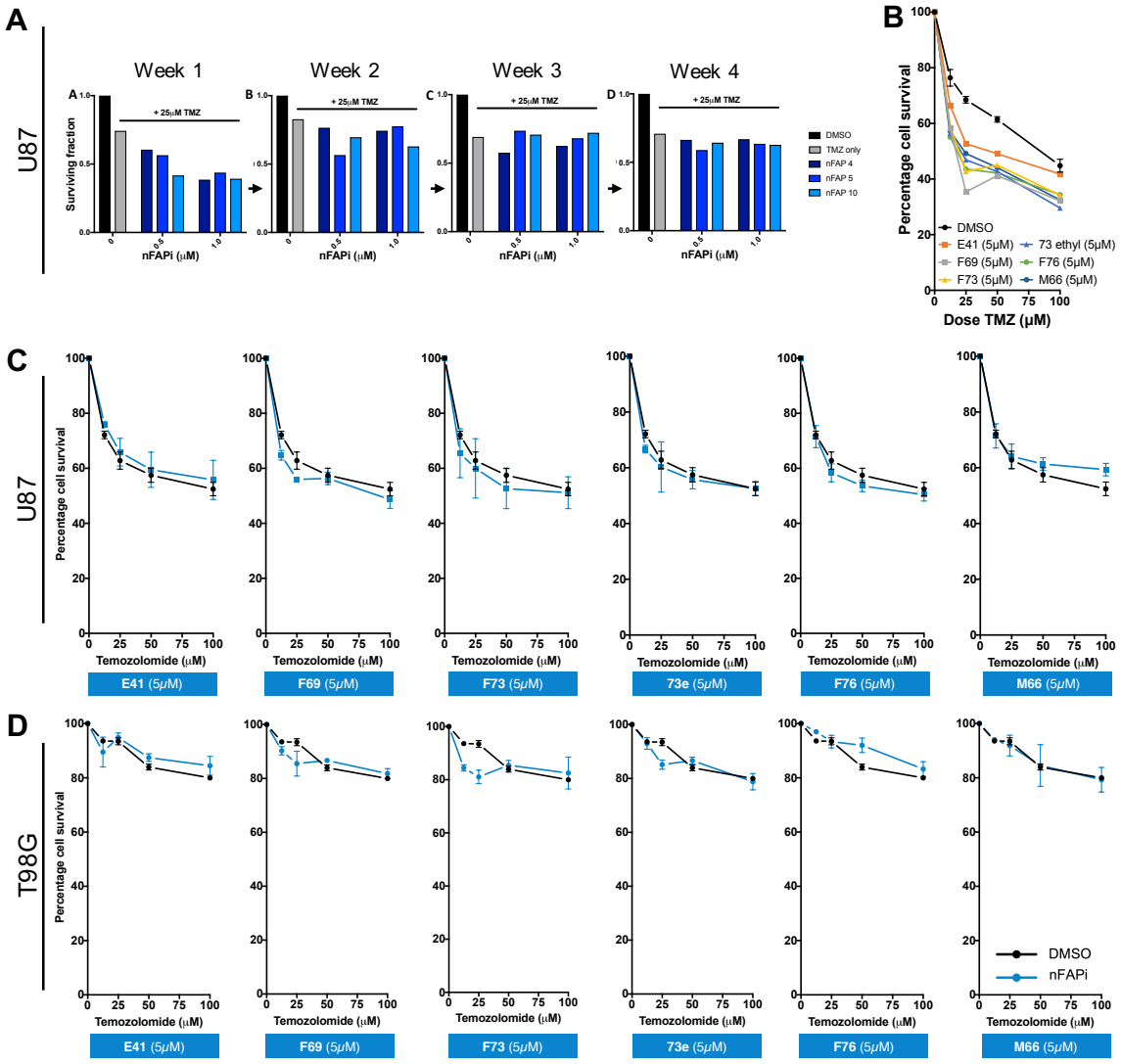


Figure 3.7: Assessing the putative therapeutic effects of novel specific FA pathway inhibitors as a strategy to sensitise established glioblastoma cultures to temozolomide chemotherapy – MGMT negative U87 and MGMT positive T98G glioblastoma cells were plated for 24 hours prior to exposure to the indicated nFAPi then DNA-damaging temozolomide chemotherapy 8 hours later. Cells were then incubated for a further 120 hours before completion of the MTT assay **A.** Viability assays performed on consecutive weeks using U87 glioblastoma cells treated with DMSO (control) or temozolomide following pre-treatment with first generation nFAPi as indicated. The nFAPi compounds in these experiments had been solubilised in DMSO and aliquoted on week 1 then stored at -20°C. Data from the 4 repeat experiments were not combined as a general trend towards loss of chemosensitisation over time was observed. **B.** Initial viability assays performed on U87 cells using nFAPi analogues synthesized by an industrial collaborator, Concept Life Sciences (Peakdale). Data points represent the mean value of experimental replicates within 1 independent experiment. **C.** Comprehensive assessment of nFAPi analogues in combination with temozolomide in U87 and T98G cells. Data shown in 3.6C are from 3 independent experiments in U87 cells (i.e. from repeats 2-4) completed after 3.6B and 3 independent experiments in T98G cells. Within these experiments, curcumin was also reassessed in combination with temozolomide, as a positive control within the assay, and continued to demonstrate significant chemosensitisation as expected (data not shown).

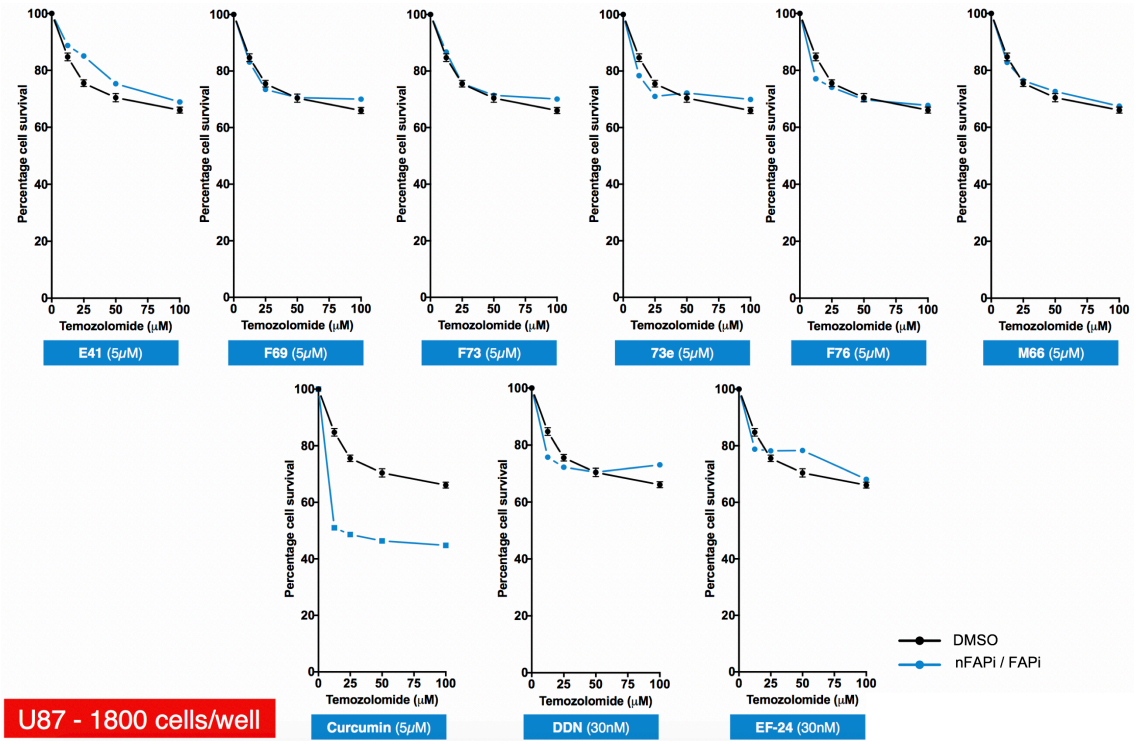


Figure 3.8: Assessing the putative therapeutic effects of novel specific FA pathway inhibitors as a strategy to sensitise established glioblastoma cultures to temozolomide chemotherapy – MGMT negative U87 glioblastoma cells were plated at a density of 1,800 cells/well for 24 hours prior to exposure to the indicated nFAPi or crude FAPi (curcumin, DDN, EF-24) then DNA-damaging temozolomide chemotherapy 8 hours later. Cells were then incubated for a further 120 hours before completion of the MTT assay. Data presented represents one experimental repeat (six experimental replicates per data point). Error bars represent the SEM.

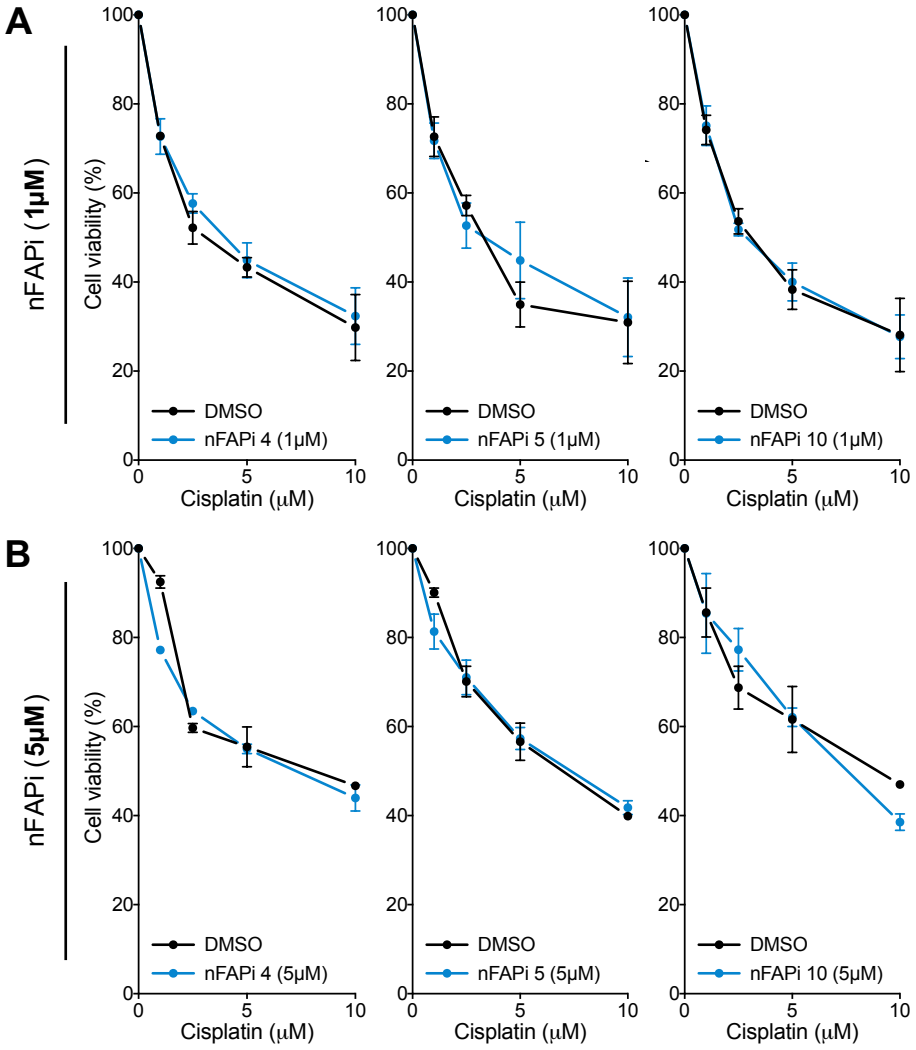


Figure 3.9: Assessing the putative therapeutic effects of novel specific FA pathway inhibitors as a strategy to sensitise established glioblastoma cultures to cisplatin chemotherapy – MGMT negative U87 glioblastoma cells were plated for 24 hours prior to exposure to the indicated nFAPi then cisplatin chemotherapy 8 hours later. Cells were then incubated for a further 120 hours before completion of the MTT assay. Viability after exposure to either: A. 1μM, or; B. 5μM nFAPi. Data presented represents two experimental repeats. Error bars represent the SEM.

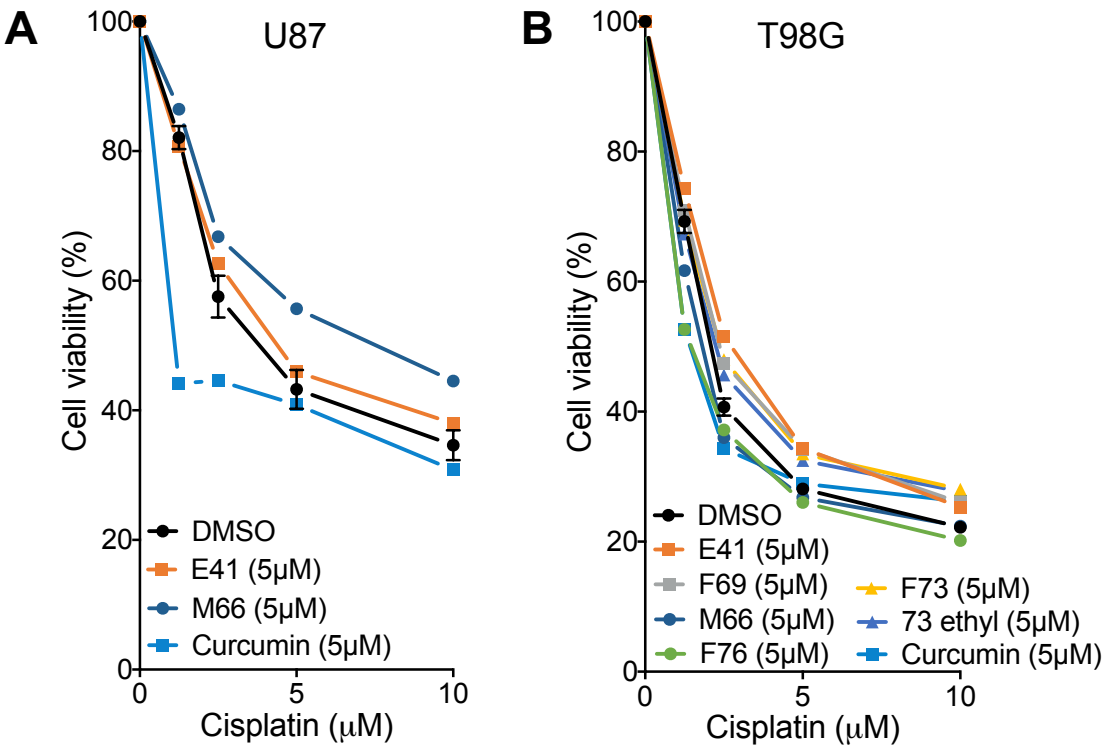


Figure 3.10: Assessing the putative therapeutic effects of (second generation) novel specific FA pathway inhibitors as a strategy to sensitise established glioblastoma cultures to cisplatin chemotherapy – Established glioblastoma cells were plated for 24 hours prior to exposure to the indicated nFAPi or curcumin then cisplatin chemotherapy 8 hours later. Cells were then incubated for a further 120 hours before completion of the MTT assay. **A.** U87 glioblastoma cells. **B.** T98G glioblastoma cells. Data presented represents one experimental repeat. Error bars represent the SEM for cisplatin chemotherapy.

3.4 Developing DDR-based combinatorial approaches to treat glioblastoma

Next, we aimed to begin establishing an evidence base to support the overarching concept of simultaneously targeting the FA pathway and an interconnected DNA damage response process to treat cancer (see Chapter 1 – Section 1.4.7). Throughout the studies so far, curcumin had demonstrated reliable inhibition of FANCD2 monoubiquitination (Figure 3.1), inhibition of FANCD2 nuclear foci formation (Figure 3.6) and chemosensitisation to temozolomide chemotherapy (Figure 3.3). In contrast, although substantial reduction in temozolomide-induced FANCD2 nuclear foci formation had been confirmed with all 6 nFAPi tested (Figure 3.6), the effect of these compounds on FANCD2 monoubiquitination was of a lesser magnitude than that conferred by curcumin at an equivalent 5μM dose (Figure 3.6) and the effect of nFAPi on chemosensitisation had been inconsistent (Figure 3.7). Consequently, in studies investigating the effect of reducing the activity of DDR processes or targets in parallel, we primarily used curcumin as an FA pathway inhibitor tool compound.

For simplicity, these early studies investigating combined DDR targeting were completed in the absence of DNA damaging chemotherapy or radiotherapy.

3.4.1 *Combined targeting of DDR processes in tandem (proof-of-concept using HeLa Silencix cells)*

Firstly, to test the general concept of whether combined targeting of interlinked DDR processes *within* the FA pathway in tandem might present an appealing anti-cancer strategy, we utilised *BRCA1/2*-deficient and proficient HeLa Silencix™ cell lines (tebu-bio). These lines were produced via the non-viral transfection of HeLa cells with a replicative pEBV-derived plasmids which remain as independent replicons and consistently express shRNAs over a long duration to provide stable gene silencing for months to over a year[307].

Both *BRCA1*-deficient and *BRCA2*-deficient HeLa SilenciX™ cells demonstrated lower clonogenic plating efficiency (i.e. clonogenic potential in the absence of treatment; Figure 3.11A). Inhibition of the FA pathway using curcumin portended dose-dependent reduction in clonogenic survival in all HeLa SilenciX™ cell lines, however *BRCA1*- and *BRCA2*-deficient cells demonstrated substantially more pronounced sensitivity to curcumin (Figure 3.11B). Furthermore, the magnitude of increased sensitivity conferred by FA pathway inhibition in *BRCA1*- and *BRCA2*-deficient cells was similar that observed with the PARP1 inhibitor, veliparib (Figure 3.11C). Further work using these cell lines, however, was prohibited by inconsistent BRCA1/2 expression in them (data not shown).

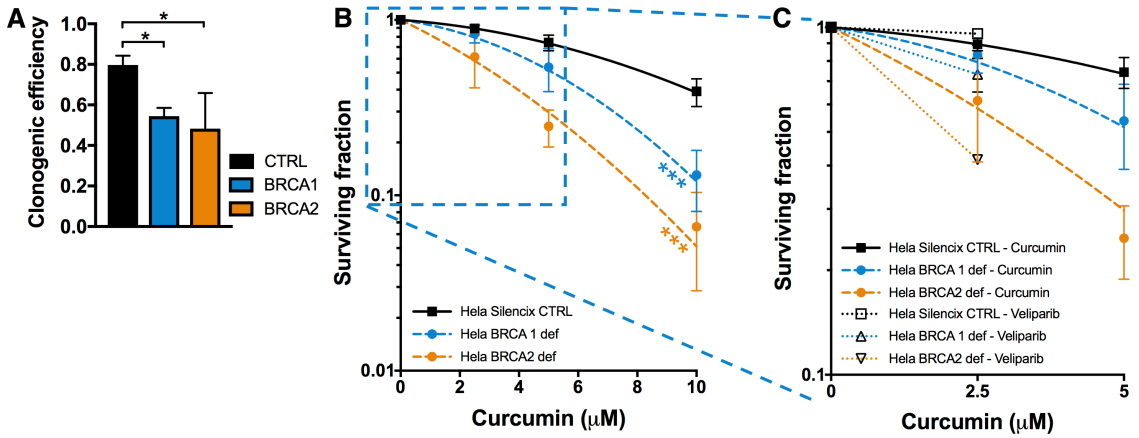


Figure 3.11: *BRCA1*-deficient and *BRCA-2* deficient cells are sensitive to the FA pathway inhibitor curcumin – Isogenic *BRCA1/2*-deficient/proficient HeLa SilenciX™ cells were seeded 16 hours prior to exposure to the indicated doses of curcumin. Cells were then incubated for a further 2 weeks before colonies were stained. **A.** Clonogenic efficiency of HeLa SilenciX™ control, *BRCA1*-deficient, and *BRCA2*-deficient cells. **B.** Clonogenic survival of following continuous exposure to curcumin. **C.** Inset of clonogenic survival data from 3.7B (0-5μM curcumin) with positive control (veliparib 2.5μM) data presented. Veliparib used as a positive control in view of the well-established hypersensitivity of *BRCA*-deficient cells to PARP inhibition[184,185]. Data presented represents 3+ independent experiments with error bars representing the SEM.

3.4.2 *Combined inhibition of the FA pathway and PARP1 in the absence of conventional DNA damaging therapy*

There are no drugs which directly target homologous recombination (HR) available in the clinic. However, PARP inhibitors have received multiple regulatory approvals for use in the context of HR-deficient cancers, often as a result of *BRCA1/2*-deficiency (see Section 3.1.3), to exploit the concept of synthetic lethality between these genes. Furthermore, *BRCA1/2*-deficient tumours also upregulate FANCD2 and this may confer PARP inhibitor resistance by facilitating DNA replication fork stabilisation[255]. Since glioblastoma demonstrate constitutively high expression and activity of FANCD2[22] representing a potential oncogenic dependency, and PARP inhibition activates the FA pathway (see Figure 3.1), we postulated that combined inhibition of the FA pathway and PARP in glioblastoma might provide an efficacious therapeutic strategy, even in the absence of exogenous DNA damaging therapy.

In U87 glioblastoma cells treated with an escalating dose of the PARP inhibitor olaparib, inhibition of the FA pathway resulted in further significant reduction in cell viability (Figure 3.12). The effect of parallel FA pathway and PARP inhibition, even with 5μM of curcumin and olaparib, demonstrated a greater reduction in cell viability than that typically observed when U87 glioblastoma cells are exposed to 100μM temozolomide. Taken together, these results suggest that combinatorial strategies designed to exploit interconnected DDR processes in parallel may represent an appealing therapeutic avenue towards more effective treatments for glioblastoma.

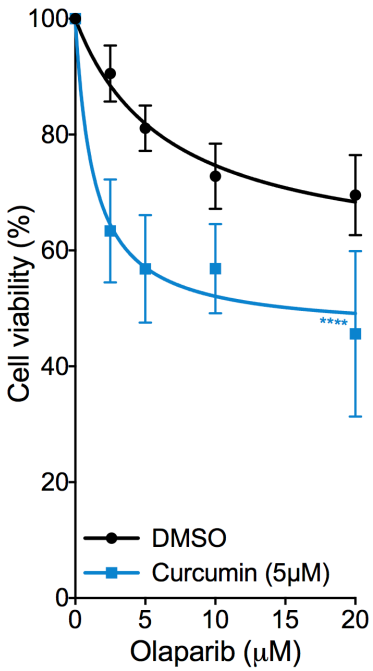


Figure 3.12: Combined inhibition of the FA pathway and PARP as a treatment strategy in the absence of conventional DNA damaging therapy – U87 glioblastoma cells were plated for 24 hours prior to exposure to an escalating dose of the PARP inhibitor olaparib +/- simultaneous FA pathway inhibition with curcumin. Cells were then incubated for a further 120 hours before completion of the MTT assay. Data presented represents 3 independent experiments with error bars representing the SEM.

3.5 Summary of key findings

Inhibition of key DDR targets to sensitise glioblastoma

- Temozolomide chemotherapy robustly activates the FA pathway in both MGMT negative U87, and MGMT positive LN18 established glioblastoma cells.
- Treatment with curcumin prior to DNA damaging therapy inhibits FANCD2 monoubiquitination in a dose dependent manner, and limits the formation of FANCD2 nuclear foci in U87 and LN18 cells.
- Olaparib inhibits PARylation in established glioblastoma cells at sub-micromolar concentrations and evokes FANCD2 monoubiquitination in a dose-dependent manner (both in the presence and absence of IR), implicating the FA pathway in responses to PARP inhibitor therapy and as a putative route of PARPi therapeutic resistance.
- FA pathway inhibition with curcumin sensitises U87 and inherently mono-alkylating therapy-resistant MGMT positive (T98G and LN18) cells to temozolomide.
- PARP inhibition with olaparib sensitised all established glioblastoma cell lines (U87, U251, T98G and LN18) to temozolomide, whereas equivalent doses of veliparib demonstrated little sensitisation (except in U87 cells), potentially highlighting the therapeutic importance of PARP trapping potency in addition to catalytic activity.
- Cell lines tested demonstrated mutually exclusive sensitisation profiles to ATR and ATM inhibition with U87, T98G and LN18 glioblastoma cells displaying profound chemosensitisation with VE-821 (ATRi), whereas U251 cells were resistant to the effects of ATRi but markedly susceptible to ATMi-mediated chemosensitisation using KU55933.

Novel inhibitors of the FA pathway as a therapeutic strategy

- Novel compounds developed in Sheffield limit FANCD2 monoubiquitination and significantly reduce FANCD2 nuclear foci formation following temozolomide.
- Limited chemosensitising potential of nFAPi has been illustrated, however this appears to be inconsistent and these compounds continue to be refined as part of an active drug development process.

DDR-targeted combinatorial strategies

- *BRCA1*- and to a greater extent, *BRCA2*-deficient HeLa SilenciX™ cells demonstrate heighted sensitivity to monotherapy with curcumin, highlighting loss of *BRCA1/2* as a potential genetic biomarker to predict favourable response to FA pathway inhibition.
- In the absence of chemotherapy, simultaneously targeting the FA pathway and PARP, using curcumin and olaparib demonstrated high efficacy in U87 glioblastoma cells and reduced viability by a similar magnitude as observed with high doses of temozolomide.

3.6 Discussion

3.6.1 General Study limitations

A broad investigation of the use of commercially available and novel compounds to target key DDR pathways and sensitise glioblastoma to temozolomide chemotherapy has been documented. Experiments were carefully designed to ensure the data presented above were robust and relevant. Nevertheless, limitations of the study exist; important limitations are detailed below and should be considered alongside the study results to facilitate faithful interpretation and application of the data.

The use of established cell lines

All lines used during the *in* vitro studies above were commercially available, previously established cell lines cultured in DMEM supplemented with 10% FCS. Use of these established models provided a number of advantages including the availability of well-established growth conditions, cell line characteristics and, within the Collis laboratory, the availability of previous internal assay optimisation data for some of these lines. However, the source and stated clinicopathological origins of commercially available cell lines cannot always be assumed to be reliable, as exemplified by recent notification of the misidentification of the U87 glioblastoma cell line – which, although derived using tumour tissue from a 44-year old female in 1966[308], U87 cells within the ATCC repository were later found to possess divergent molecular characteristics including a Y chromosome, resulting in ATCC being required to update the clinical information pertaining to this cell line in its repository and the lines designation as a cell line of unknown patient origin, despite confirmation that it likely does represent a *bona fide* human glioblastoma cell line[309,310]. Furthermore, in the context of glioblastoma, it is critical to highlight that the spectrum of molecular aberrations observed in commonly used established lines may not reflect those observed in patient tumours and more recently patient-derived, primary glioblastoma cell lines at low passage[97]. Indeed, the expansive study of somatic mutations, copy number alternations and methylation status across 29 tumour types (11,289 primary tumours) and 1,001 cancer cell lines reflecting the spectrum of cancers by Iorio *et al.* (2016)[97] demonstrated that in most types of cancer, oncogenic alterations in patient tumours tend to be conserved across established cell lines. However, glioblastoma (in addition to renal clear cell carcinoma and pancreatic carcinoma) represents an exception to this phenomenon with demonstrable discordance between clinically-relevant 'cancer functional events'

detected in primary tumours and established cell lines. Although copy number aberrations were the predominant molecular events in both (>80% samples), primary tumours were dominated by deleted recurrently aberrant copy number segments (RACS), whereas the majority of established cell lines demonstrated amplified RACS, highlighting the failure of established glioblastoma cell lines to recapitulate key molecular features of patient tumours. Consequently, the molecular features and associated pharmacogenomic assumptions regarding established glioblastoma cell lines used in these investigations may provide only a limited prediction of expected results on future clinical translation.

This limitation highlights the importance of more clinically-relevant research models to aid preclinical glioblastoma research, including the generation and use of early-passage, primary patient-derived glioblastoma stem-like cell (GSC) models[99,100] and surgically-relevant models under development[311,312] to reflect the characteristic spatiofunctional heterogeneity of glioblastoma[13-15,313] (both discussed below and in subsequent chapters).

Limitations of the MTT assay

We emphasize that selection of the MTT assay to assess therapeutic response in these studies reflected a need to assess many DDRi-chemotherapy combinations in multiple cell lines. Extensive use of this assay this could be criticised since the MTT assay provides a measure of metabolic activity in viable, metabolically active cells[207], rather than detecting cell survival/death or the capacity of cells to divide and recapitulate a colony of cancerous cells following treatment. However, in a well optimised assay, as confirmed in these studies (see Chapter 2 – Figure 2.3), metabolic activity indicated by the OD_{540} of the purple formazan product of MTT reduced by viable living cells, remains proportional to cell number. Therefore, inferences regarding cell survival can meaningfully be extrapolated from this data. However, it is important to consider potential scenarios in which the proportionality between OD_{540} and cell number might not be maintained. For example, increased non-specific, intracellular but extra-mitochondrial reduction of MTT in treatment groups represents a previously identified confounding factor[314]. Some compounds or treatments may also interfere with formazan production by the succinate dehydrogenase enzyme[315,316]. Evidence that treatment with irradiation notably alters the metabolic activity of surviving cells suggests assessment of radiation response using the MTT assay might represent another scenario in which proportionality between OD_{540} and cell number is difficult to maintain[316,317]. This tallies with the authors experience of implausible cell number

optimisation curves when glioblastoma cell lines were exposed to either 0 Gy or 5 Gy ionizing radiation (data not shown) and numerous reports of challenging data interpretation, and divergence in percentage survival relative to colony forming methods, when using the MTT assay to assess radiotherapy response[318,319]. Consequently, DDRi-radiotherapy combination treatments were not evaluated during these studies, but are explored in depth within an evaluation of combinatorial radiosensitising strategies in Chapter 5, using clonogenic survival assays which are broadly considered the 'gold-standard' *in vitro* assay in establishing radiation response.

Relevance of temozolomide chemotherapy doses

Following surgery, patients with newly diagnosed glioblastoma typically receive a temozolomide dose of 75mg per m^2 of body surface area (BSA) per day, 7 days per week for 6 weeks alongside radiotherapy, followed by six 5-day cycles of adjuvant temozolomide administered every 28 days at a dose of 150-200mg per m^2 BSA[10,11]. The most detailed study to date of temozolomide concentration in the plasma and CSF of human patients following oral administration demonstrated peak plasma concentrations in the region of 10μg/ml (~52μM; temozolomide MW = 194.151g/mol) with peak CSF temozolomide concentrations of 1.9μg/ml (~9.8μM) and a CSF:plasma area under the concentration-time curve (AUC) ratio of 0.20 (20%)[320]. Since glioblastoma are typically intraparenchymal, rather than interventricular tumours, the concentration of temozolomide within or close to tumour tissue in patients is likely more representative of the final drug concentration that cancerous cells are exposed to. Indeed, research using intracerebral microdialysis catheters implanted into peritumoural brain tissue at the time of surgery revealed a mean peak intraparenchymal temozolomide concentration of 0.6 ± 0.3μg/ml (~1.5-4.6μM) with a AUC brain:plasma ratio of 0.17 (17%) following the analysis of dialysate and plasma from 7 patients receiving a single oral dose of temozolomide (150mg/m^2)[321]. Such values suggest higher values within the range of temozolomide concentrations used *in vitro* during these studies (0-100μM) may not be representative of the concentrations glioblastoma cells are typically exposed to within patients. Arguably, evaluation of temozolomide concentrations above 50μM may lack physiological relevance, with greater coverage of concentrations between 0-20μM representing a more translational ideal. However, reassuringly multiple DDRi (curcumin, olaparib and VE-821) appeared to demonstrate robust chemosensitisation at the lowest temozolomide dose evaluated in these studies (12.5μM). Additionally, it is important to emphasize that neither of the previous human *in vivo* pharmacokinetic studies of

temozolomide (above) successfully measured the concentration of the drug's active metabolite MTIC. Therefore, since the conversion of temozolomide to MTIC is spontaneous and does not require hepatic activation[321], the presence of temozolomide conversion within non-neoplastic cells throughout the body during *in vivo* studies and the absence of this phenomenon within reductionist unicellular *in vitro* studies suggests that assuming analogous effects of even identical temozolomide concentrations in cell culture vs human *in vivo* studies may represent a false equivalence.

Taking such limitations into account, the studies presented in this chapter provide meaningful insight to effective putative strategies to therapeutically target the DNA damage response in glioblastoma

3.6.2 nFAPi require further development

The role of FA pathway proteins as multifunctional regulators of genomic integrity in response to a variety of DNA replication impeding lesions suggests these proteins could represent compelling targets for the development of anti-cancer drugs. A number of naturally occurring and synthetic compounds have been reported to inhibit or downregulate FA pathway activity (as detailed in Section 3.1.3), and a number of groups are actively developing small molecule inhibitors which target the FA pathway. However, to date, no such molecules have progressed to early-phase clinical trials. Here, we have demonstrated that novel compounds developed in Sheffield which target FANCL (nFAPi) possess the ability to reduce FANCD2 monoubiquitination (in cell-free and cell-based assays, Figures 3.4 and 3.5, respectively) and reduce the localisation FANCD2 into discrete foci at sites of DNA damage following chemotherapy (Figure 3.6). Both events represent well-established, quantifiable markers of FA pathway activity mediated by FANCL, and therefore provide evidence of nFAPi intracellular activity. To date, only one group has published data demonstrating small-molecule inhibitors of FANCL[250]. These studies, by Cornwell *et al.* (2019)[250], utilised a cell-free, high-throughput homogenous time-resolved fluorescence (HTRF) screening assay based on the relative ability of ~10,000 compounds to reduce ubiquitination of GST-tagged $FANCL_{RING}$ (E3 ligase) domain by the E2 (UBE2T) carrying Cy5-labelled ubiquitin, as detected by close proximity with the anti-GST Tb cryptate mediating fluorescence via excitation of the Tb cryptate donor resulting in fluorescence resonance energy transfer (FRET) to the Cy5 acceptor. Prioritisation of the screen primary hits demonstrated 5 compounds (designated CU1, CU2, CU9, CU10 and CU12) capable of

abrogating the ubiquitination of $FANCL_{RING}$ at 100μM in cell-free assays. Importantly, each of these compounds appear structurally distinct from nFAPi under development in Sheffield (Sheffield nFAPi structures not shown in view of ongoing development and commercialisation processes). CU10 and CU12 were deprioritised due to lack of target selectivity, since they also prevented the ubiquitination of UBE1 and FANCT (UBE2T). In cell-based assays, Cornwell *et al.* (2019)[250] found that none of the 3 remaining compounds, used at a 100μM concentration, were able to inhibit HU-induced monoubiquitination of FANCD2. Furthermore, CU1 and CU2 were capable of reducing FANCD2 monoubiquitination and the formation of HU- and cisplatin-induced FANCD2 nuclear foci in U2OS cells, but only when using extremely high doses of each compound - 200μM and 500μM, respectively. In contrast, data presented in this Chapter confirms that all 6 Sheffield nFAPi tested (E41, F73, F73-ethyl, M66, F76 and F69) were able to significantly reduce the formation of temozolomide-induced FANCD2 nuclear foci formation in U87 glioblastoma cells (Figure 3.6A-B) at a comparatively low concentration of 5μM. Additionally, when two Sheffield nFAPi were further evaluated by western blot (at 5μM concentration) both demonstrated the ability to reduce FANCD2 monoubiquitination in U87 cells (Figure 3.6C), albeit modestly. It is challenging to make robust comparisons between our study and Cornwell *et al.* (2019)[250] about the relative potency of FA pathway inhibitors evaluated on account of methodological differences, including different methods of scoring FANCD2 foci, and differences in the cell lines used. However, given that the FA pathway is known to be highly expressed and active in glioblastoma, including in U87 cells, it is likely that Sheffield nFAPi represent the most potent bespoke small-molecules specifically targeting FANCL-mediated ubiquitination of FANCD2 described to date – at least in terms of their inhibitory capacity.

Despite these results, it was not possible to confirm consistent chemosensitisation using either the initial nFAPi identified in our previous screens (nFAPi 4/E41, 5 and 10) or nFAPi analogues (F73, F73-ethyl, M66, F76 and F69) – see Figure 3.7. This was unexpected given that previous studies have confirmed inhibition of the FA pathway (both through RNA interference or the use of commercially available molecules to reduce FA pathway activation) sensitises glioblastoma cells to alkylating chemotherapies including temozolomide[20-22] and non-glioblastoma cell lines, including: mouse embryonic fibroblasts, lung fibroblasts, Chinese hamster ovary (CHO) cells[21] and multiple myeloma[322]. Since previous internal data from the Collis Laboratory and the data presented here confirm

Sheffield nFAPi compounds represent *bona fide* inhibitors of the FA pathway, with demonstrable activity in cell-free (Figure 3.5) and cell-based (Figure 3.6) assays, the inability to consistently demonstrate robust sensitisation to temozolomide chemotherapy is particularly enigmatic (Figure 3.7). In contrast to some FA pathway inhibitors under development by other research groups[250,252] it is clear that Sheffield nFAPi are capable of permeating cells to exert intracellular effects even at low micromolar concentrations. Particularly in the context temozolomide, which ultimately results in a plethora of SSBs and DSBs with associated replication stress as a result of O^6-methylguanine directing the misincorporation of thymine during DNA synthesis causing persistent futile cycling of the DNA mismatch repair (MMR) machinery[7], it is possible that chemosensitisation observed in previous studies could be mediated through non-canonical functions of FA pathway proteins such as the roles of FANCD2-I in the: abrogation of inappropriate NHEJ through interaction with Ku proteins, DNA-PKcs or DNA ligase IV[131,193,323,324], and; stabilisation of DNA replication forks[325,326]. However, this would not explain the inability to demonstrate nFAPi sensitisation to the widely used crosslinking chemotherapeutic cisplatin (see Supplementary Figures 3.3 & 3.4).

The possibility that nFAPi loose activity over time, either before and/or following solubilisation, may represent a more likely explanation. Indeed, this would help interpret discordant cell viability data which, with both sets of nFAPi used, demonstrated evidence of temozolomide sensitisation in an early experiment(s) that appeared to dissipate on repeat evaluation. This hypothesis is further supported by internal data at the Collis laboratory in the years before these PhD studies suggesting nFAPi activity at nanomolar concentrations (data not shown). This was not reproducible in these more recent studies. Additionally, the independent experience of our Melbourne-based collaborators, where use of a cell-free AlphaScreen-based assay to detect FANCD2 monoubiquitination, found that E41 lost activity within 10 days of being solubilised in DMSO, after having demonstrated ~35% reduction in FANCD2 monoubiquitination on initial evaluation, supports this hypothesis. Although M66 did maintain activity over a 10-day period in this cell-free assay, subsequent evaluation of all nFAPi tested in AlphaScreen-based assays beyond 10 days could no longer demonstrate a reduction in FANCD2 monoubiquitination. It is difficult to reconcile suspected loss of nFAPi compound activity in cell-free and cell-based chemosensitisation assays with the lack of demonstrable compound degradation on serial LC/MS over a 1-month duration (data not shown) following solubilisation in DMSO. Nevertheless, in

retrospect, the serial structural evaluation using LC/MS would have benefited from a longitudinal control known to be of robust stability, and therefore subtle degradation of the nFAPi over time and/or longer durations cannot be entirely excluded. In any respect, it is clear that Sheffield nFAPi require further evaluation and development. Such studies are ongoing, including: the re-synthesis of high-grade compounds; confirmation of biophysical FANCL target engagement using nano-isothermal titration calorimetry (nano-ITC)[327,328] and cellular thermal shift assay (CETSA)[329], and; the application of iterative medicinal chemistry approaches to optimise DMPK properties of subsequent generations of nFAPi and improve the potency and specificity of lead compounds. In view of this actively progressing drug development process and the unsuitability of currently available nFAPi for further cell-based investigation, due to inconsistent effects, the crude but well established FA pathway inhibitor curcumin[20,22,284,285] was used in subsequent combinatorial studies as a tool FAPi compound.

3.6.3 Targeting the DNA damage response represents an appealing therapeutic strategy in glioblastoma

The Fanconi anaemia pathway

The therapeutic effects of targeting a number of key DDR processes in established glioblastoma cultures have been characterised. In targeting the FA pathway, curcumin was confirmed to reduce temozolomide-induced FANCD2 monoubiquitination in both MGMT negative cells (U87) and MGMT positive cells (LN18) (Figure 3.1). Although, higher doses of curcumin pre-treatment (10-20μM) were required to elicit a marked reduction in FANCD2 monoubiquitination, lower doses of curcumin were also able to reduce FA pathway activation, and this was confirmed orthogonally by demonstrating that curcumin at a 5μM concentration was able to reduce the organisation of FANCD2 into discrete nuclear foci following temozolomide chemotherapy (Figure 3.6). Together, these results confirm that curcumin is a legitimate inhibitor of FA pathway activity, consistent with previous studies[20-22]. Since higher doses of curcumin elicited substantial toxicity to established cultures as monotherapy (Figure 3.2), a lower concentration of 5μM was selected for studies assessing the effect of curcumin in combination with chemotherapy on cell viability.

The addition of curcumin sensitised both MGMT negative (U87) and MGMT positive (LN18 and T98G) glioblastoma cultures to temozolomide (Figure 3.3), suggesting that FA pathway inhibition might represent an appealing therapeutic strategy irrespective of status for the

principle known molecular biomarker predictive of temozolomide response[94]. Strikingly, curcumin did not modify temozolomide sensitivity in U251 (MGMT negative) glioblastoma cultures, in direct contrast to other cell lines tested. It is tempting to speculate that such divergence in response might be attributable to differences in the FA pathway in U251 cells, or disparities in the genomic context of these cells more broadly, including the status of interconnected DDR pathways. However further investigation would be required to confirm such hypotheses, particularly since no published studies investigating the FA pathway or its inhibition in glioblastoma appear to have interrogated U251 cells.

Despite its use as a crude FA pathway inhibitor/tool compound in these studies, the pleiotropic nature of curcumin represents an unavoidable criticism. Indeed, studies suggest curcumin may elicit a range of effects in glioblastoma cell lines including modulation of: cell cycle (via induction of p21 and p53, and inhibition of cyclin D1), apoptosis (via decreases in bcl-2, bcl-xl, and activation of caspases), invasiveness (via inhibition of MMP secretion), autophagy, and survival pathways including JAK/STAT3, EGFR, PI3K/AKT and NF-kβ[330-337]. Interestingly however, at least some of these may be connected with the effects of curcumin on FA pathway activity. For example, curcumin inhibits the NF-kβ-pathway kinase IKK which has previously been demonstrated to interact with the FA core complex[338] and can potentially modulate FA pathway activity independent of its kinase activity[285,339]. Perhaps more concerning is the potential that curcumin may suppress DNA damage response processes other than the FA pathway. For example, Ogiwara *et al*. (2013)[340] reported that curcumin suppresses NHEJ, HR and ATR-CHK1 mediated checkpoint activation. However, these studies did not assess FA pathway activity, and at least some of the findings reported are consistent with FA pathway (inhibition)-mediated effects, such as downregulation of FANCS/BRCA1. Additionally, previous research comparing isogenic FANCD2 proficient and deficient U87 glioblastoma cells confirmed that FANCD2 deficient cells demonstrate heightened sensitivity to temozolomide that was equivalent in magnitude to temozolomide sensitisation elicited by curcumin pre-treatment in the context of FANCD2 proficient cells. Furthermore, the addition of curcumin pre-treatment in the context of FANCD2 deficient U87 cells did not provide further increase in temozolomide sensitivity[22], supporting inhibition of the FA pathway as the primary and perhaps sole route by which curcumin is able to sensitise glioblastoma cells to temozolomide chemotherapy. Additionally, our data also illustrate that curcumin elicits robust sensitisation of U87 glioblastoma cultures to

interstrand crosslink-inducing treatment with cisplatin, further supporting a centrality of the FA pathway in any chemosensitisation provided by curcumin.

Finally, translation of FA pathway manipulation into the clinic is limited by the presently available pharmacological inhibitors that are recognised to have widely pleiotropic effects (discussed above) and unsuitable pharmacokinetic and pharmacodynamic properties. The *in vivo* benefits of curcumin are limited by limited mucosal absorption, poor aqueous solubility and first-pass metabolism[341]. The ongoing development of nFAPi and recently established *in vivo* testing of novel FA pathway inhibitors at our institution is intended to produce compounds with greater target specificity and PK/PD profiles that are more suitable for clinical applications. However, in the meantime, additional tools could aid the translation of curcumin into the clinic despite a suboptimal PK/PD profile including: nano-encapsulation[341]; conjugation with a monoclonal antibody[342]; use of magnetic nanoparticles and MRI to provide tumour-specific delivery[343,344]; or local delivery via intra-thecal[345], intra-(resection)cavity[346] or convection-enhanced intra-parenchymal approaches[347,348].

Targeting PARP, ATR and ATM

Confirming the potential of single DDR target inhibition with PARP, ATR and ATM inhibition to sensitise glioblastoma cells to DNA damaging therapy was a necessary precursor to testing the effects of these in combination with FA pathway inhibition (see Chapter 5). The data presented here showing that olaparib sensitised all cell lines in the panel to temozolomide, compliment previous studies demonstrating its therapeutic potential in glioblastoma[196,349]. We could not demonstrate convincing temozolomide sensitisation using veliparib (except at the highest temozolomide doses tested which may not be physiologically relevant – see Section 3.5.1), a finding which seems to contrast work by Gupta *et al.* (2014)[350] and Barazzuol *et al.* (2013)[351], however direct comparison is challenging as Barazzuol *et al.* tested veliparib sensitisation (using a higher dose of 5μM) with combined radiation and low-dose temozolomide (but not temozolomide alone) with only modest, albeit statistically significant, effects observed. Gupta *et al* demonstrated chemosensitisation in 6 different glioblastoma cell lines, but did not test U87 or LN18 cells. Furthermore, Gupta *et al.* demonstrated more potent temozolomide sensitisation (i.e. detectable at lower doses of temozolomide) when using veliparib doses of 10μM and 30μM (10 to 30-times the dose required to abrogate the catalytic activity of PARP1 as

demonstrated by the loss of PAR), which may underscore the primacy of PARP1 trapping, rather than inhibition per se, in mediating temozolomide sensitivity. Interestingly, Gupta *et al.* also found that the sensitising effects of PARP inhibitor therapy were more pronounced in MGMT positive (temozolomide resistant) cells, a finding that is supported by our olaparib data at lower doses of temozolomide (see Figure 3.3A, 12.5μM). However, of critical importance, studies by Gupta *et al.* using temozolomide-resistant glioblastoma murine xenograft models found that the concentrations of veliparib required to provide sensitisation *in vivo* could not be achieved using a tolerable dosing regimen. Since olaparib and veliparib are both under investigation in actively recruiting clinical trials (see Table 3.1), the clinical potential of each in glioblastoma may become clear in the near future. However, the success or failure of clinical trials testing PARP inhibition (or any other DDRi) as a single DDRi agent in glioblastoma may not necessarily determine whether these drugs are likely to provide benefit in combination with FA pathway inhibitors (see Chapter 5).

Eich *et al.* (2013)[243] demonstrated that the abrogation of ATR, but not ATM, activity in glioblastoma cell lines using siRNA resulted in significant sensitisation to temozolomide. Our results were similar, demonstrating that pharmacological ATR inhibition sensitised 3/4 cell lines to temozolomide, whereas ATM inhibition sensitised the only glioblastoma cell line that was not responsive to ATR inhibition (U251). Consistent with data presented here, studies by Nadkarni *et al.* (2012)[238] suggest MGMT expressing glioblastoma cell lines are not susceptible to sensitisation using ATMi since high levels of MGMT directly repair toxic O^6-methylguanine lesions, preventing deleterious downstream sequelae including the formation of DNA DSBs. However, Nadkarni *et al.* (2012)[238] were able to demonstrate temozolomide sensitisation in U87 and U251 cells using the ATM inhibitor KU55933 at an equivalent concentration (10μM). Although consistent with our findings in U251 cells, it is difficult to reconcile their data with the complete lack of temozolomide sensitisation we observed using KU55933 to inhibit ATM in U87 cells.

Concerning responses to irradiation, ATM inhibition with KU55933 has been previously demonstrated to potently radiosensitise glioblastoma cell lines and overcome the radioresistance of glioblastoma stem-like cells[195] and is a more potent sensitiser of GSCs than ATR inhibition[197]. Given that standard present therapy for glioblastoma includes radiotherapy and chemotherapy, a combination DDRi strategy inhibiting two targets such as ATM or ATR and the FAP pathway to optimise both radiosensitisation and

chemosensitisation, respectively, would be particularly appealing (investigated in Chapter 5).

3.6.4 Recapitulating therapeutic resistance in vitro

A number of issues are shared by our work to date and those foundational studies interrogating the FA pathway in glioblastoma by Chen *et al*. (2007)[20], Kondo *et al*. (2011)[21] and Patil *et al*. (2014)[22]. Firstly, given increasing evidence that a subpopulation of glioblastoma cells possess an up-regulated DNA damage response and capacity for unlimited self-renewal, often termed glioblastoma stem-like cells, are thought to be disproportionately responsible for the inherently treatment resistant nature of this disease[18,352,353] – confirmation that pharmacological FA pathway inhibition is able to effectively sensitise this cellular fraction is urgently needed. To date, no data to this effect has been published. Secondly, these studies do not address how the intertumoural (i.e. inter-patient) and extensive intratumoural heterogeneity of glioblastoma[13-15] is likely to influence the ability of FA pathway inhibition to sensitise cells to temozolomide broadly and enduringly. Thirdly, these studies lack the use of more physiologically representative, *in vivo* models of glioblastoma such as mouse orthotopic patient-derived xenograft models. Clearly, such models are more costly and time-consuming. A pragmatic solution might incorporate use of a recently pioneered 3D glioblastoma cell culture system which utilises an Alvetex® (polystyrene) scaffold – this model was demonstrated to recapitulate key histological features of glioblastoma and better predict the *in vivo* efficacy of temozolomide, bevacizumab and erlotinib when compared to conventional 2D cultures[108]. Our development of more clinically-relevant 2D and 3D GSC models to overcome some of these issues and evaluation of FA pathway targeting in these therapeutically recalcitrant models are detailed in the following chapters.

3.6.5 Assessing therapeutic strategies incorporating DDRi combinations and DNA damaging therapy

Two landmark studies have demonstrated *BRCA1 and BRCA2*-deficient tumours possess up-regulated FA pathway activity, which appears to be required to limit replication fork progression and genomic instability in the context of *BRCA* loss[255],[153]. In both studies, FANCD2 was determined to be essential for cell survival in the absence of *BRCA1/FANCS* or *BRCA2/FAND1*, with FANCD2 knock down using siRNA resulting in increased cell death.

Using stable isogenic *BRCA1/2*-deficient/proficient HeLa SilenciX™ cell lines, data presented here confirms for the first time that pharmacological inhibition of the FA pathway using curcumin is associated with substantially heightened sensitivity in *BRCA1* and *BRCA2* deficient cell lines demonstrating a 3-fold and 5-fold increase in clonogenic cell death after treatment with 10μM, respectively (Figure 3.11). It is therefore tempting to consider that our work may support the hypothesis presented by Kais *et al*. (2016)[255] and Michl *et al*. (2016)[153] that the relationship between *BRCA1/2* and *FANCD2* (and perhaps other FA pathway constituents) may be synthetic lethal, with our studies suggesting that synthetic lethality could be exploited in the clinic by targeting the FA pathway pharmacologically. More generally, these findings provide further proof-of-concept that therapeutic manipulation of DDR targets in combination represents an effective therapeutic strategy[1] (see Chapter 1 – Figure 1.12), and one that might even reduce the need for conventional chemo- and radiotherapy in the future.

Considering combination DDRi targeted approaches specifically in glioblastoma, there are a limited number of studies available in the literature presently (summarised in Chapter 1 – Section 1.5.1). However, to date, none have explored the effects of combining FA pathway inhibition with inhibition of either PARP, ATR, or ATM. Considering there is evidence that: FANCD2 overexpression has been established as a molecular feature of gliomas which increases with tumour grade[22]; *BRCA1* mutated breast cancer cell lines overexpress FANCD2 which is associated with therapeutic resistance to PARP inhibition[255], and; PARP inhibition robustly stimulates FA pathway activity in a dose dependent manner (see Figure 3.1). We hypothesized FA pathway inhibition with curcumin should abrogate intrinsic PARP inhibitor resistance mediated by high levels of FANCD2 expression in glioblastoma. Our results demonstrating the therapeutic efficacy of combined FA pathway and PARP inhibition provide encouraging support for this hypothesis (Figure 3.12), but will need replicating in additional clinically-relevant glioblastoma models (explored in Chapter 4), and the effect of this combination in the presence of DNA damaging therapy remains to be determined (investigated in Chapter 5). Furthermore, our single DDRi studies using inhibitors of ATR and ATM provide an appropriate foundation for these compounds to be evaluated in combination with inhibition of the FA pathway (explored in Chapter 5).

Chapter 4 – Development and validation of clinically-relevant GSC models

4 CHAPTER 4 – Development and validation of clinically-relevant glioblastoma stem cell models

4.1 Introduction

The failure of preclinical research over many decades to portend substantial improvements in patient survival for cancers of unmet need[59], including glioblastoma, implies that commonly used preclinical models do not fully reflect the complexities of tumour cell biology and therapeutic resistance. Therefore, efforts to increase the clinical relevance of laboratory research models may not only enhance our understanding of difficult to treat cancers, but also improve the predictive value of preclinical studies to delineate therapeutic strategies which might confer meaningful benefit for patients. To enhance traditional models, both the cellular constitution and surrounding microenvironmental niches need to be considered to facilitate appropriate model selection, refinement and application. The importance of modelling inherently treatment resistant cancer stem cells and the *in vitro* 2D and 3D models in which these subpopulations can be utilised are therefore discussed further below.

4.1.1 Cancer stem cell theory

Not all cancer cells are equal

Cancer stem cell theory presupposes that all neoplastic cells within a given patient's cancer do not possess equivalent potential to recapitulate a given tumour/cancer with such events governed in a purely random manner. But rather that, like normal tissue, the functional organisation of cells within a tumour assembles within an invariant hierarchy, at the apex of which lie cancer stem cells (CSCs)[354]. Whilst varying definitions of the scope of what constitutes a CSC can attract some controversy, the classic, functionally-defined triad of: self-renewal; sustained proliferative potential, and; ability to recapitulate the tumour cell hierarchy, are essential to enable faithful reproduction of the entire repertoire of functional diversity present within the original tumour[352]. The earliest evidence supporting existence of a subpopulation of cancer cells that possess these features was established in haematological malignancies. Whilst it was clear that the vast majority of acute myeloid leukaemia (AML) cells demonstrated limited proliferative capacity, a rare fraction of cells were reproducibly identified to possess characteristic features of 'stemness'[355-358]. By injecting patient-derived AML cells into the tail vein of sublethally irradiated severe combined immune-deficient (SCID) mice, Lapidot and Dick *et al.* (1994)[359] established that

approximately 1 in 250,000 cells were able to initiate leukaemia with sustained cellular proliferation and reproduction of the broad repertoire of human donor leukaemic cell phenotypes in the murine host. Importantly, AML-inducing potential was not distributed equally amongst xenotransplanted cells with engraftment and proliferation governed in a purely stochastic manner. Rather the $CD34^+CD38^-$ fraction of AML cells appeared to contain a sizable proportion of cells with the potential to successfully engraft, whereas the $CD34^-$ and $CD34^+CD38^+$ fractions contained no cells with these properties. Further studies by Bonnet and Dick *et al.* (1997)[360] confirmed that injections containing on average just 3.2 $CD34^+CD38^-$ 'leukaemia-initiating cells' were not only able to demonstrate sustained proliferation on transplantation to non-obese diabetic (NOD) SCID mice, but were able to differentiate *in vivo* producing large numbers of $CD38^+$ and $CD33^+$ cells. Additionally, serial transplantation of the engrafted human AML cells into a second murine host successfully recapitulated the disease with an estimated 30- to 100-fold expansion of $CD34^+CD38^-$ 'leukaemia-initiating cells' in the bone marrow of primary mice over a 6 week period – indicating these cells possessed an exquisite capacity for self-renewal. These landmark studies revealed undeniable parallels between the cardinal features of normal tissue stem cells – sustained proliferative capacity, self-renewal and multipotency – and the primitive leukaemia-initiating cells, paving the way for characterisation of these rare and functionally important neoplastic cellular fractions as CSCs. It seems plausible that oncogenic events occurring in primitive, multipotent normal stem cells replete with the ability to self-renew and produce a range of differentiated neoplastic progeny would represent a more likely route to the development of cancer than oncogenic events occurring in more differentiated normal cells. Theoretically, healthy differentiated cells would, during the process of carcinogenesis, need to de-differentiate to establish a multipotent CSC base capable of producing the multifaceted hierarchical cellular architecture observed in most cancers. Importantly however, designation as a CSC does not depend on knowledge or proof that a cancer is initiated by oncogenic transformation from a normal tissue stem cell as the cell of origin[352,360].

4.1.2 Cancer stem cells in glioblastoma and other brain tumours

CSCs were subsequently discovered in a range of solid malignancies including breast[361], prostate[362], colorectal[363,364], pancreatic[365] and lung cancer[366], head and neck cancers[367], and sarcomas[368]. However, brain tumours were the first solid cancer in which CSCs were revealed. Ignatova *et al.* (2002)[369] established that, similar to neural stem cells isolated from

the subventricular zone and hippocampus of adult brains, cortical glial tumours contained a population of cells which exhibited single cell clonogenicity in non-adherent, serum-free conditions with supplementation using the pleiotropic growth factors EGF, FGF2 and insulin, forming neurospheres (discussed further in Section 4.1.3). The intermediate cytoskeletal filament nestin, which is associated with neural and progenitor cells in the developing CNS[370], was detected abundantly in these putative CSCs. Importantly, clones derived from a single CSC were readily expandable and contained cells which expressed the stemness marker nestin, in addition to cells which expressed the neuronal markers neuron-specific enolase (NSE) and neuronal ß-III tubulin, or the glial marker glial fibrillary acidic protein (GFAP), thus demonstrating the proliferative ability of CSCs and inherent capability to generate heterogeneous progeny across multiple lineages. However, in a clear sign of the abnormal programme of differentiation associated with CSC progeny, cells also frequently demonstrated overlapping co-immunopositivity for neuronal and glial markers, in contrast to neural stem cells in which positivity for ß-III tubulin or GFAP were mutually exclusive.

Subsequent landmark studies by Singh *et al.* (2003, 2004)[16,371] established the importance of the neural stem cell surface marker CD133 in the identification and isolation of brain tumour CSCs. Freshly dissociated glioblastoma and medulloblastoma tumour samples were confirmed to form neurospheres following culture in non-adherent, serum-free culture conditions with EGF and bFGF supplementation. Furthermore, primary neurospheres demonstrated avid positivity for CD133 and nestin. Further investigation of the clonogenicity of brain tumour cells following magnetic sorting based on CD133 status revealed that $CD133^+$ populations demonstrated sustained proliferation as neurospheres in serum-free conditions, whilst in the same conditions, $CD133^-$ cells adhered to the culture dishes and failed to proliferate[16]. Furthermore, compelling *in vivo* experiments revealed the orthotopic intracranial injection of as few as 100 $CD133^+$ brain tumour (glioblastoma and medulloblastoma) cells into NOD-SCID mice was able to generate brain tumours which were successfully re-transplanted into a second murine cohort, with both primary and secondary xenotransplanted tumours recapitulating key histological and immunohistochemical features of the original patient tumour. Meanwhile, orthotopic injection of even 100,000 $CD133^-$ cells into NOD-SCID mice failed to produce a tumour[16]. Studies by Galli *et al.* (2004)[17] independently corroborated the self-renewal capacity of human glioblastoma CSCs though successful serial orthotopic transplantation in

immunocompromised mice, whilst Hemmati *et al*. (2003)[372] confirmed the ability of neurosphere-forming cells from paediatric gliomas and medulloblastomas to robustly express nestin and, following repeated dissociation to a single cell suspension, serially reclone neurospheres replete with cells possessing characteristics of multiple lineages. Considered together, these studies strongly support the existence of a cellular fraction in high-grade glial brain tumours that exhibit sustained proliferation, self-renewal and multipotency, and functionally, these cells represent *bona fide* brain tumour CSCs. Their existence should be no more controversial than that of leukaemic stem cells, which has been accepted for over two decades[352,359,360].

Glioblastoma stem cell terminology

The terminology used to refer to CSC within or derived from brain tumours is often variable and inconsistent; this may have contributed to misunderstandings and controversies within the literature. In the context of glioblastoma, many terminologies have been used including: glioblastoma/glioma initiating cell (reflecting the capacity of these cells to form tumours following implantation); glioblastoma/glioma stem-like (reflecting the reality that although these cells possess similarities to normal tissue stem cells, key differences exist such as organised, tightly controlled regulation of self-renewal in normal stem cells relative to the delinquency of these processes in CSCs), and; glioblastoma/glioma stem cells (GSCs)[352,354], which is the term applied in this thesis to reflect populations functionally enriched for glioblastoma cancer stem cells, whilst accepting there is currently no single marker, or even combination of markers capable of flawlessly segregating GSC and non-stem glioblastoma cell populations[373]. Additionally, in this thesis, glioblastoma cell populations exposed to differentiating (serum-containing) media to deplete GSC populations are referred to as tumour 'bulk' cell populations – since these cells represent those most abundant in patient tumours.

GSC features and microenvironmental interplay

GSCs are enriched for a range of cellular markers including CD133[16,371], nestin[374], SOX2[375], OLIG2[13,376], NANOG[377], ALDH[378], CD15 (SSEA-1)[379] and integrin $\alpha 6$[380], and represent a major driver of intratumoural heterogeneity through constant flux between a spectrum of multipotent microstates at positions of highest entropy atop the cancer cell hierarchy in glioblastoma[373]. Functionally, this means that reciprocal interplay between GSCs and the microenvironment in which they reside may serve to 'sculpt' diversity within the cancer cell

hierarchy by providing 'attractor states' towards various programmes of differentiation. Since the microanatomical topography within which these tumours reside is not uniform, each specific microenvironmental niche provides unique and regionally differential cues that mould spatiofunctional intratumoural heterogeneity and, by virtue of enhanced diversity (and capacity for diversity), increase the likelihood of at least some cells possessing intrinsic therapeutic resistance. The oxygen-rich perivascular niche, the hypoxic-necrotic tumour core, and the invasive leading edge of a growing tumour each represent key microenvironmental niches which serve as attractor states, influencing the properties and differentiation programmes if GSCs which reside within them. The reader is referred to Prager *et al.* (2020)[373] for an excellent up-to-date review of these and other GSC attractor states, however brief summaries are provided below.

Within the perivascular niche, vascular endothelial cells (ECs) support the maintenance of glioblastoma cell 'stemness' though a range of mechanisms including NOTCH, SHH and nitric oxide (NO) signalling cascades[381-383]. Conversely, GSCs produce high levels of proangiogenic factors including VEGF which help to sustain and drive proliferation of the tumour vasculature[384], safeguarding a consistent nutrient supply. MMP9 is highly expressed in the perivascular niche, which likely contributes to the invasive properties of GSCs[385] – often reported to migrate along blood vessels to infiltrate healthy brain tissue[386,387]. Interestingly, TGF-ß is also highly expressed in the perivascular niche, with abrogation of this previously demonstrated to reduce IR-induced phosphorylation of ATM and p53, and radiosensitise glioma cells in both *in vitro* neurosphere culture and *in vivo* mouse flank xenografts[388], highlighting specific mechanisms by which the perivascular GSC niche might promote radioresistance.

Hypoxic-necrotic tumour regions are characterised by high expression of HIF-1 and HIF-2[389], with chronic elevation of HIF-2α implicated in the activation of signalling pathways which facilitate the maintenance of stemness including SOX2, OCT4 and KLF4[390,391]. GSCs residing in regions of tumour hypoxia are reported to assume a more quiescent phenotype, which confers substantial therapeutic resistance in the face of conventional chemotherapy and radiotherapy[102,392].

Finally, GSCs at the tumour invasive edge, perhaps unsurprisingly, appear to be enriched for cells with high functional invasive potential within *in vitro and in vivo* assays[102,393]. These

GSCs release cell surface integrins to facilitate migration[394] and display enhanced capacity to cleave through extracellular matrix using matrix metalloproteinases including MMP2, MMP9 and ADAMT17[395,396]. The expression of mediators of epithelial-mesenchymal transition in GSCs, including TWIST1-SOX2 signalling, N-cadherin, STAT3 and NF-kβ contribute to this invasive, locally metastatic phenotype[393,397-400], which underpins the surgical recalcitrance of glioblastoma, in contrast to, for example, WHO grade I pilocytic astrocytomas which can be cured by gross total surgical resection[401].

Importantly, GSCs demonstrate unique features of aberrant DDR signalling which confer therapeutic resistance including to radiotherapy[18] and chemotherapy[19]. These features are discussed in Chapter 1 – Section 1.5.1.

Given that GSCs appear to orchestrate intratumoural heterogeneity and the therapeutic recalcitrance of glioblastoma, it seems rational to specifically target these subpopulations to establish more effective therapeutic strategies. Discovery science seeking to identify and evaluate such therapeutic strategies may benefit from the use of *in vivo* models including murine patient-derived orthotopic xenograft models of glioblastoma[113], since these models are able to retain a broad physiologically representative repertoire of important microenvironmental cues. However, such models do harbour inherent limitations, such as the lack of immune-mediated microenvironmental cues in immunodeficient mouse strains (such as BALB/c) commonly used in xenograft studies, and the potential for mouse-specific evolution of implanted human glioma cells[114]. Additionally, *in vivo* preclinical glioblastoma studies are extremely costly and relatively low-throughput (see Chapter 1 – Table 1.1). Therefore, although reductionist, 3D *in vitro* models which are able to faithfully recapitulate key features of the native environment of GSCs within parental tumours may represent an incredibly useful tool to identify multiple promising GSC-targeting therapeutic strategies and prioritise these for further preclinical and/or early clinical translation[311].

4.1.3 3-dimensional glioblastoma stem cell models

Scaffold/matrix-based culture systems

Hydrogels (natural and synthetic)

A number of synthetic hydrogels have been used in an attempt to replicate the features and composition of the glioblastoma microenvironment. These include various collagen proteins[402,403], hyaluronic acid[402,404], chondroitin sulphate polysaccharides[405], alginates[406]

and chitosan[406]. The synthetic nature of these compounds provides the advantage of tightly controlled composition with negligible batch-to-batch variation. However, such simplicity also represents an inherent disadvantage, since each presents an exceedingly unidimensional, reductionist 3D culture environment for glioblastoma cells.

In contrast, Matrigel™ (Corning), Cultrex™ (Trevigen) and Geltrex™ (Gibco) each provide branded variations of a natural, animal-derived basement membrane substrate for 3D cell culture. All three are derived from mouse sarcomas and provide a complex blend of collagen and laminin, which may be more biologically-relevant than synthetic, single component hydrogels[407]. These natural hydrogels can also be used to provide a viscous cell suspension for animal injection to produce flank or orthotopic brain tumours[106]. However their biological nature contributes to potential issues with animal/mouse specific constituents, limited shelf-life and the potential for detectable batch-to-batch variation, which renders it challenging to define the exact composition of substrates used within and between experiments.

Nevertheless, Matrigel™ is reported to be the most widely used substrate for the culture of patient-derived glioblastoma cells, whether in 2D models where Matrigel™ is used to provide a thin coating to tissue culture plasticware, or in 3D models where the gel can used to coat hard scaffolds (see below), or form 'beads' or 'plugs' of the Matrigel™ alone, within which cells are suspended and cultured[106]. Sarcoma-derived, purified laminin can be used in similar contexts to Matrigel™ to support GSC growth[100]. However, it is subject to similar limitations, for example Sigma confirm that 'the purity of this product is not determined'[408]. Interestingly, studies by Storch *et al.* (2010)[409] suggest that 3D culture within a laminin-rich extracellular matrix, such as Matrigel™ or laminin, not only influences cellular morphology, but influences the distribution of IR-induced DNA double strand breaks (DSBs) between regions of euchromatin and heterochromatin (2:1 in 2D culture vs 1:1 in 3D culture and mouse xenograft tumours), reflecting more physiological maintenance of chromatin condensation with increased levels of heterochromatin in 3D culture which was associated with reduced overall numbers of DSBs, relative radioresistance and enhanced susceptibility to histone deacetylase inhibition.

Hard scaffolds (Alvetex™)

The Alvetex™ polystyrene scaffold-based system has been used to generate 3D cultures for a range of normal cells including neurones and glial cells[410,411] and cancer types including melanona[412], colorectal cancer[413], pancreatic cancer[414], as well as primary[415,416] and metastatic breast cancer[417]. In the earliest studies incorporating this technology for the 3D culture of glioblastoma cells, Alvetex™ scaffolds were primarily applied as an assay of migration or invasion with immunohistochemical staining of sectioned scaffolds or immunofluorescence imaging of confocal z-stack images used to assess the depth to which cells infiltrated into the scaffolds[418,419]. More recently, Gomez-Roman *et al.* (2017)[108] pioneered the use of 3D Alvetex™ scaffolds to perform a wider range of assays using patient-derived glioblastoma cells including protein and RNA extraction, and robust 3D clonogenic survival assays. These scaffolds are coated with Matrigel™, similar to 2D GSC culture, prior to cell seeding and therefore share common limitations such as the potential for added variability resulting from challenges in constraining the exact composition of Matrigel™. It is also challenging to liberate cells from within the scaffold therefore, whilst a substantial proportion can be liberated to enable protein or RNA/DNA extraction, the scaffolds may not be as appropriate for applications such as FACS[106]. Nevertheless, Gomez-Roman *et al.* found the organisation of patient-derived glioblastoma cells cultured within the 3D Alvetex™ architecture was able to recapitulate key histological features of patient tumours including regions of high cellularity, invasion, hypoxia and proliferation with elevated Ki67 staining. Furthermore, relative to traditional 2D culture, GSC culture within the 3D scaffolds modified the RNA expression of a spectrum of genes with cytoskeletal, extracellular region and cell membrane receptor activity functions. These findings underlined the wide-ranging phenotypic differences between cells in 2D vs 3D culture, and perhaps begin to provide some rationale for the study's most striking finding – that patient-derived GSCs cultured in 2D or 3D were observed to exhibit important differences in responses to various pharmacotherapies, with the response of 3D GSCs aligning more closely with outcomes observed in clinical trials[108].

Suspension (non-scaffold) -based culture systems

Neurosphere culture

The generation of neurospheres (also referred to as tumourspheres or tumour spheroids) relies on the ability of glioblastoma cells to self-aggregate into 3D spherical structures whilst proliferating in non-adherent culture conditions. Renewable, or serial, neurosphere formation is considered a hallmark of GSC cells[420], and numerous studies have

demonstrated robust expression of stem cell markers in GSC cultured as neurospheres[99,369,371]. The use of neurospheres in suspension as a 3D culture system has numerous advantages, including the relative speed of establishment and low cost (since expensive substrates such as Matrigel™ and scaffolds can be avoided). GSC neurosphere cultures conserve key genomic and phenotypic features of parental tumours[421] relative to 2D cultures using serum-containing media. However, Al-Mayhani *et al.* (2008)[99] were able to establish the long-term propagation of patient-derived GSC cultures using a combination of 3D neurosphere and 2D adherent monolayer culture (both in serum-free media) and demonstrate similar expression of stem cell markers (including nestin and CD133) and robust tumourigenicity *in vivo* following 2D monolayer culture. Rahman *et al.* (2015)[101] and Pollard *et al.* (2009)[100] also demonstrated similar robust stem cell marker expression in 3D neurosphere and 2D adherent cultures using a laminin-rich substrate. However, the physiologically-relevant and potentially advantageous regional heterogeneity generated, particularly in larger neurospheres with substantial oxygen and nutrient gradients contributing to central necrosis also limits the specificity of evaluating responses in GSCs. Indeed, relative to adherent culture, neurospheres were revealed to express higher levels of differentiation markers including GFAP, O4 and TuJ-1[100], highlighting the issue of excessive spontaneous differentiation of GSCs sequestered deep within the neurosphere, beyond the diffusion limits EGF and FGF used to supplement stemness sustaining serum-free media.

Tumouroid and organoid

Tumour organoids (or 'tumouroids') consist of larger aggregations of GSCs compared to neurospheres. Although there is no universally accepted size definition that provides qualification as a tumour organoid, these are typically expected to measure multiple millimetres in diameter. Hubert *et al.* (2016)[102] established tumour organoids by suspending freshly derived glioblastoma cells in Matrigel™ to form small (20µl) beads which were solidified by incubation at 37°C for one hour prior to static culture in serum-free 'stem' media for 4 days before transfer to an orbital shaker for further propagation. Using this methodology, tumour organoids were demonstrated to exhibit a proliferative outer rim containing SOX2, OLIG2 and TLX-expressing GSCs, encasing a necrotic core. Interestingly, however, relatively quiescent GSCs were scantily dispersed amongst bulk glioblastoma cells throughout the organoid core. The model could be used to typify differential therapeutic responses based on stemness, with $SOX2^{+}$ GSCs displaying radioresistance to 3 Gy IR

relative to bulk glioblastoma cell populations within the same organoid. Importantly, orthotopic patient-derived xenograft tumours generated via organoid implantation were reported to be more representative of the parental tumour compared to those generated using neurosphere cultures[102]. However, tumour organoids still lack a spectrum of microenvironmental cues observed *in vivo*, including from healthy brain tissue.

More recently, groups including Ogawa *et al.* (2018)[105] and Linkous *et al.* (2019)[104] have developed glioma cerebral organoid (GLICO) models which incorporate 'normal' cells in the form of human embryonic stem cells (hESCs) or induced pluripotent stem cells (iPSCs), in conditions which promote neuroectodermal expansion with the formation of neural rosettes containing proliferative zones of neural stem cells. These cerebral organoids can then be co-cultured with patient-derived glioblastoma cells which invade and proliferate within the 'mini brain'[104]. Alternatively, Ogawa *et al.* also used a CRISPR-Cas9 based strategy in which a TP53 sgRNA plasmid was co-electroporated with HRasG12V-expressing homologous recombination donor vector ($HRas^{G12V}$-tdTomato p53 exon HA) to simultaneously disrupt TP53 resulting in a truncated non-functional protein, and introduce oncogenic HRas – the combination of which resulted in neoplastic transformation with infiltrative putative tumour cells that exhibited gene expression profiles consistent with mesenchymal subtype human glioblastoma and progressively overwhelmed the GLICO[105]. Perhaps the most resounding endorsement of GLICOs as a preclinical model of glioblastoma was recently published by Pine *et al.* (2020)[103] who performed a parallel comparison of glioma neurospheres, tumour organoids, GLICOs (using patient-derived GSCs) and patient-derived orthotopic xenografts generated from 5 patients, using single-cell RNA-sequencing to compare the transcriptomes of these models with each other and parental tumours (characterised by scRNA-seq and bulk tumour RNA-seq). Ultimately, Pine *et al.* revealed that GLICOs were the model most enriched for neural progenitor-like cell subpopulations, which exhibit a strong stemness capacity, and clustered closer to the transcriptomes of primary tumour samples than neurospheres and tumour organoids, suggesting GLICOs may provide modelling comparable to xenograft studies for many applications at a fraction of the cost and time[103]. However, for many early preclinical applications such evaluating combination drug responses, the use of GLICOs may still be relatively cumbersome and low-throughput. Additionally, these GLICOs still only incorporate a very limited repertoire of cell types (normal neural and glioma cells) and have not yet been shown to recapitulate clinical trial response unlike the 3D GSC Alvetex™ system[108].

Microfluidic glioblastoma-on-a-chip culture

These models employ microfluidics based-culture (cancer-on-a-chip) technology and 3D bioprinting to assemble neoplastic and, potentially, a range of non-neoplastic cell types in specific and highly reproducible configurations. Yi & Jeong *et al.* (2019)[109] recently developed a bioprinted human-glioblastoma-on-a-chip system which consists of a gas-permeable silicone chamber printed on a glass slide which incorporates an inner ring of human umbilical vein endothelial cells (HUVECs) to provide a vascular/perivascular context, filled with patient-derived glioblastoma cells, both bioprinted using a suspension made from porcine brain-derived extracellular matrix. This compartmentalised system was able to generate a radial oxygen gradient and recapitulate the peripherally invasive and centrally necrotic clinical features of glioblastoma[109]. Furthermore, therapeutic response to radiotherapy and temozolomide chemotherapy in a number of these models using metabolic activity as a surrogate of treatment response was reported to correlate with clinical survival in a patient-specific manner[109]. However, the doses of temozolomide used to elicit a response were incredibly high (250μM and 950μM) demonstrating a lack of clinical relevance[110] (see discussion of CSF and intratumoural temozolomide concentrations in patients, Chapter 3 – Section 3.6.1) and suggesting this model is not likely to be particularly useful for drug testing (at least in its current form).

Overall, a broad selection of *in vitro* models exist (see Chapter 1 – Table 1.1) to support preclinical glioblastoma research, each with specific advantages and caveats. Considered collectively, more complex models may be better suited to the later stages of *in vitro* evaluation of therapeutic strategies and interrogation of nuanced multicellular biology, particularly where known microenvironmental interactions are expected to be relevant, and can feasibly be replicated. Conversely, less complex, more efficient models are likely to be beneficial in basic and early translational preclinical studies such as the evaluation of multiple combinatorial therapeutic strategies. In this Chapter the generation and validation of multiple patient-derived glioblastoma models is reported with application of a customised 3D Alvetex™ scaffold-based system that is considered to provide a favourable combination of biological relevance and acceptable throughput for early-stage preclinical studies.

4.2 Validation of 2D and 3D scaffold-based Cambridge patient-derived glioblastoma stem cell models

4.2.1 Propagation and validation of Cambridge-derived GSCs

The derivation and propagation of glioblastoma cells under serum-free conditions has been demonstrated to enrich for GSC populations which more closely resemble genetic and phenotypic features of primary tumours, relative to cells propagated in serum containing media[98,421]. The G1, G7, E2 and S2 primary, patient-derived GSC lines derived in Cambridge by Colin Watts' laboratory have been previously characterised and used by multiple groups to facilitate preclinical glioblastoma research[99,108,208,422]. These lines were kindly provided by Professor Colin Watts (University of Birmingham) and Professor Anthony Chalmers (University of Glasgow) and continued to be successfully propagated in serum-free 'stem' media (Figure 4.1) using Matrigel™-coated plasticware (see Methods – Section 2.14.5). As a key characteristic of 'stemness'[16,99,423], we independently confirmed that transfer of each Cambridge patient-derived GSC line to non-adherent culture conditions (using Matrigel™-free plasticware) led to robust neurosphere formation (Figure 4.1) within days. Additionally, as previously described[108,195,197,208], change of culture conditions to permit serum exposure promoted clear phenotypic changes observable at a macroscopic level. These changes were consistent with transition towards a more differentiated ('non-stem') phenotype and included a 'flattening out' of gross morphological features (Figure 4.1) and subjectively greater adherence to Matrigel™-coated plasticware.

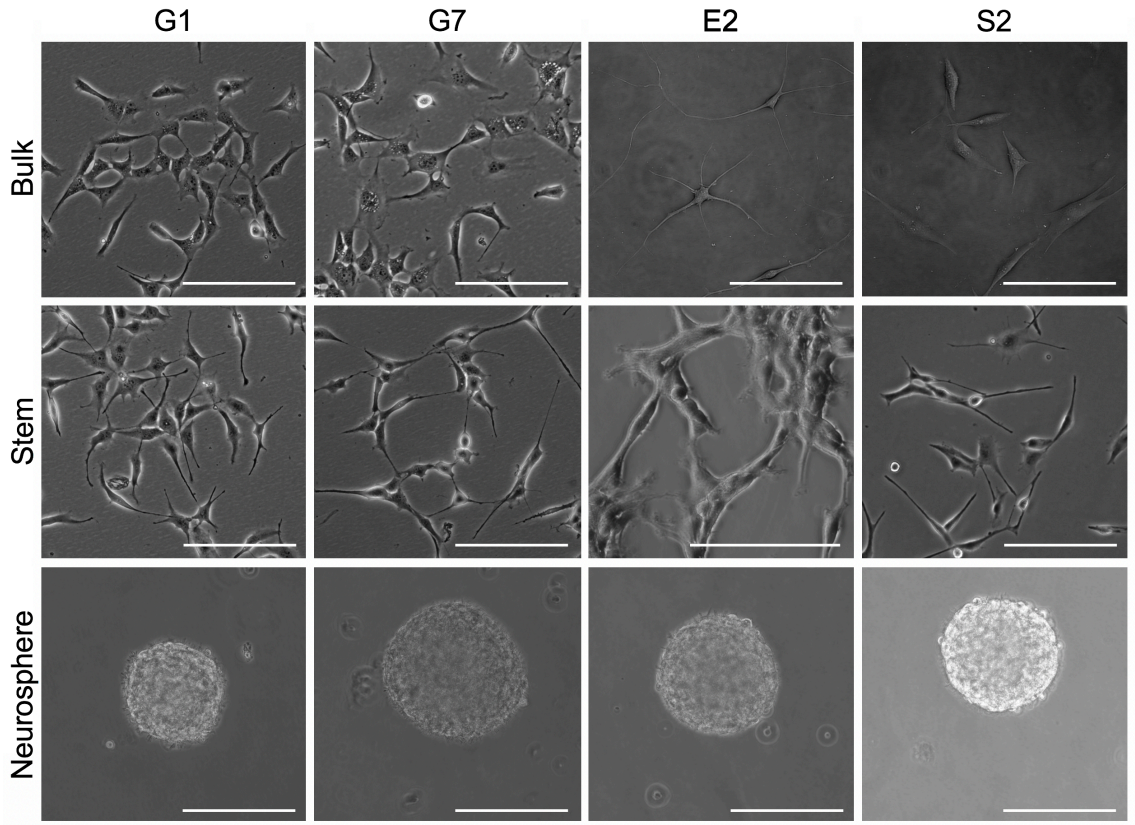


Figure 4.1: Cambridge primary, patient-derived glioblastoma stem cell lines – Representative brightfield light microscopy images (20x magnification) of 4 primary GSC lines (G1, G7, E2 and S2) derived from patients undergoing surgical resection of a glioblastoma in Cambridge. The images illustrate each cell line propagated in: culture media containing serum to promote differentiation to represent tumour 'bulk' cells (*top row*); serum-free media supplemented with EGF and FGF ('stem' media) to enrich for GSCs (*middle row*), and; GSCs cultured in non-adherent conditions to elicit neurosphere formation (*bottom row*). Scale bars = 200μm.

4.2.2 Putative stem cell marker expression in 2D and 3D GSC models

Although robust putative stem cell marker expression with the Cambridge patient-derived GSC lines used in these studies has previously been reported[99,197], these properties were briefly reassessed following receipt of the lines in our laboratory as a quality control check prior to embarking on extensive studies (as detailed in Chapter 5). As expected, G1 GSCs demonstrated 2.2-fold higher nestin mRNA expression (p=0.0003, unpaired t-test) and 2.9-fold higher SOX2 mRNA expression (p=0.0066), relative to matched tumour bulk cells (Figure 4.2A). Considering G7 GSCs, these appeared to express on average 6.2-fold higher expression of nestin mRNA relative to matched tumour bulk cells (Figure 4.2B). Although nestin expression in G7 GSCs was consistently higher than in bulk cells on repeated evaluation, notable variability in the magnitude of this difference (SD=7.0) may have contributed to an absence of statistical significance (p=0.2692). Moreover, SOX2 demonstrated no clear evidence of elevated mRNA expression in G7 GSCs relative to bulk cells (average 1.3-fold difference, p=0.3687).

The use of a Alvetex™ scaffold-based 3D GSC model (see Methods – Section 2.15) was implemented in the Collis Laboratory, following an RCS-funded research training secondment in Professor Anthony Chalmers' Laboratory (University of Glasgow) completed by the author. Cambridge GSCs embedded within this 3D architecture have previously been reported to robustly express nestin and SOX2[108]. Using confocal immunofluorescence of G7 GSCs within the scaffolds, we independently confirmed the protein expression of nestin; in addition to visualising expression of the putative stem cell markers CD133 and vimentin within Alvetex™-embedded GSCs, which is the first time reported for these cells within the 3D scaffold architecture (Figure 4.2C-D).

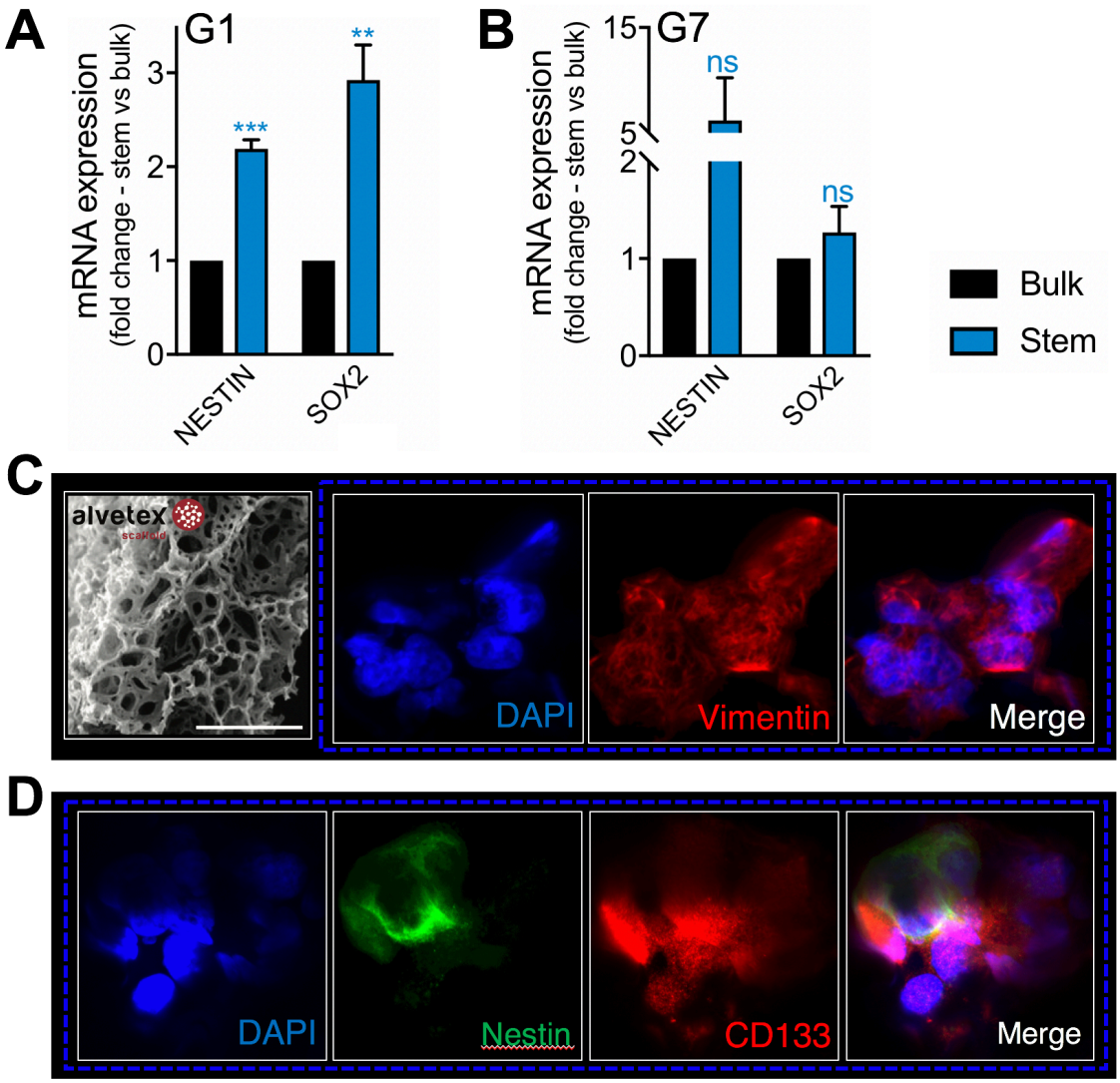


Figure 4.2: Stem cell marker expression in Cambridge primary, patient-derived glioblastoma stem cell lines – A-B. TaqMan™ RT-PCR analysis of nestin and SOX2 gene expression in untreated G1 (A), and G7 (B) patient-derived GSCs and matched bulk populations. Bulk cells had been propagated in serum-containing culture media for 5+ passages prior to the investigation. Cells were plated then incubated for 24 hours prior to RNA extraction. Data points shown represent the mean of 3 independent experiments. Error bars represent the SEM. C-D. Confocal immunofluorescence for the putative glioblastoma stem cell markers: vimentin (C); nestin and CD133 (D) in untreated 3D G7 GSCs. Cells were seeded into Alvetex™ scaffolds and incubated for 72 hours prior to fixation with paraformaldehyde then immunofluorescence processing. Cells were imaged using a Zeiss LSM880 AiryScan confocal microscope. Images (63x magnification) for visualisation were produced using the maximum intensity projection of Z-stacks. *Inset* (C) represents a scanning electron microscope image of the Alvetex™ scaffold polystyrene architecture – scale bar = 100µm (courtesy of Alvetex™, Reprocell).

4.2.3 *Comparison of GSC colony formation and IR response in 2D and 3D culture systems*

Next, we sought to confirm the clonogenicity of Cambridge GSCs in 2D and 3D culture conditions and establish reproducible measurement of response following DNA damaging therapy. In 2D conditions, S2 GSCs proliferated but failed to produce discrete colonies due to a highly migratory phenotype (data not shown). E2 GSCs formed loosely packed colonies which frequently overlapped, but were amenable to quantification (see Chapter 5 – Figure 5.17). G1 and G7 GSCs robustly formed more tightly packed colonies which were most suitable for accurate, reproducible quantification. As such, the clonogenicity of G1 and G7 GSCs was also assessed within the 3D Alvetex™ scaffold-based culture system. Comparison of these conditions revealed notably higher clonogenic plating efficiency in the 3D system for both G1 GSCs (0.424 vs 0.635, p=0.0128, unpaired t-test) and G7 GSCs (0.435 vs 0.673, p=0.0190, unpaired t-test) – see Figure 4.3A-B (*insets*). Additionally, G1 and G7 GSCs demonstrated moderately greater radiosensitivity in the 3D model (Figure 4.3) with dose modifying factors at SF 0.37 ($DMF_{0.37}$) of 1.27 (1.26-1.29, 95% CI) and 1.13 (1.10-1.19, 95% CI), respectively (p<0.0001 G1 GSCs and p=0.0006 G7 GSCs).

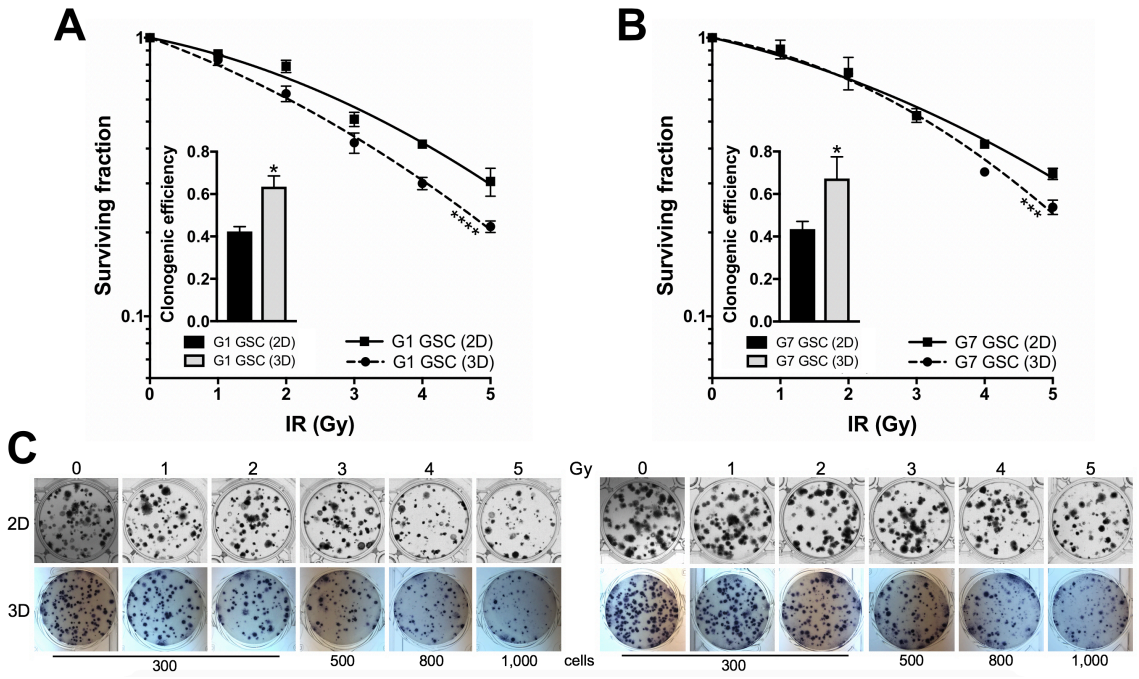


Figure 4.3: 2- and 3-dimensional colony formation and response to ionizing radiation in Cambridge patient-derived glioblastoma stem cells – G1 or G7 primary GSCs were seeded 24 hours prior to exposure to irradiation (0-5 Gy). Cells were incubated for a further 21 days, with media replacement 24 hours post irradiation. Subsequently, colonies were identified using incubation with MTT for 4 hours, then fixed with paraformaldehyde and quantified. **A-B.** Comparison of 2D and 3D Alvetex™ clonogenic survival curves in G1 GSCs (**A**), and; G7 GSCs (**B**) with clonogenic plating efficiency (*inset*). **C.** Representative images of 2D and 3D colonies in G1 (*left*) and G7 (*right*) GSCs. Data points shown represent the mean of 3 independent experiments. Error bars represent the SEM. Error bars not shown where these are smaller than the corresponding symbol. Note 2D and 3D clonogenic plates not to scale – internal diameter of wells in 2D (6-well) plates is 2.3-fold the diameter of 3D Alvetex™ scaffolds (34.8mm vs 15mm). Row titled 'cells' indicates the number of GSCs seeded per well.

4.3 Development of clinically- and surgically-relevant Sheffield patient-derived glioblastoma stem cell models

4.3.1 Derivation of Sheffield primary, patient-derived glioblastoma stem cell lines

To build a valuable resource to support these studies and future preclinical glioblastoma research we established the derivation of primary, patient-derived GSCs in Sheffield using fresh surgical specimens retrieved from the Royal Hallamshire Hospital, Department of Neurosurgery. Tumour samples were procured and processed as detailed in Chapter 2 (Methods – Section 2.12). Close proximity between the Collis laboratory (The University of Sheffield Medical School) and Neurosurgical Theatres at the Royal Hallamshire (which are co-located in the same building) and the presence of the author in theatre during the relevant surgical cases facilitated efficient and immediate transfer of fresh tumour research samples to the laboratory. This was reflected in excellent success rates for the derivation of primary GSC lines from 11/12 patients (92%) and propagation (including successful cryopreservation) of GSC lines from 10/12 patients (83%). In total 24 primary, patient derived GSC lines were generated and propagated from 26 fresh tumour samples (overall success rate = 92%), since multiple tumour samples from spatially divergent regions were used to generate parallel GSC lines from some patients (discussed below). Details on relevant clinicopathological features and molecular features pertaining to each parental tumour were also recorded. Collectively, the Sheffield primary GSC lines generated in these studies reflect a diverse range of clinical and pathological features as detailed in Table 4.1 (overleaf), and represent the foundation of our 'Sheffield Living Biobank' of clinically and surgically-relevant patient-derived models of glioblastoma. Representative images of individual Sheffield GSC lines are presented in Figure 4.4 and details on the derivation of parallel, surgically-relevant models are detailed in the following sections (Section 4.3.2 and 4.3.3).

Table 4.1: Towards a living biobank of patient-derived glioblastoma stem cell models – clinicopathological features of the Sheffield lines.

		Clinical			Histological		Molecular						Cell line		
No.	M-Name	Age	Sex	Location	Histology	WHO Grade	IDH1	MGMT	TERTp	1p/19q	Other	100K consent	Propagated	Cryo	Survived unthawing
1	**OX-1**	53	**M**	Right parietal	Glioblastoma	IV	wt (Seq)	NR	**mut** (c.-124C>T)	NR	IDH2 wt BRAF wt H3F3A wt HIST1H3B wt	✓	✓	✓	✓
2	**OX-2** (core)	71	**F**	Left frontal (large) – partial frontal lobectomy	Glioblastoma	IV	wt (IHC)	**Methylated** (MGMT -ive)	NR	NR	NR	✓	✓	✓	✓
3	**OX-2** (c+e)														
4	**OX-2** (edge)														
5	**OX-3**	74	**M**	Left temporal (infiltrative edge)	Glioblastoma	IV	wt (IHC)	'Equivocal' (Likely +ive)	NR	NR	NR	✓	✓	✓	✓
6	**OX-4**	45	**M**	Left fronto-parietal	Gliosarcoma (Recurrent)	IV	wt (Seq)	NR	**mut**	NR	IDH2 wt BRAF wt	✓	✓	✓	✓
7	**OX-5** (core)	76	**F**	Right frontal	Gliosarcoma	IV	wt (IHC)	Unmethylated (MGMT +ive)	NR	NR	NR	✗	✓	✓	✓
8	**OX-5** (c+e)														
9	**OX-5** (edge)														
10	**OX-6**	50	**M**	Right parietal	Glioblastoma	IV	wt (Seq)	Unmethylated (MGMT +ive)	wt	No co-del	**BRAF mut** (c.1799T>A; p.(Val600Glu) **1p36 del** IDH2 wt ATRX intact INI1 intact Vimentin expression +++	✓	✓	✗	N/A

Wildtype (wt) / unmethylated; mutant (mut) / methylated / structural aberration; not reported (NR); not yet tested (NT)

(Table 1 continued overleaf)

Table 4.1 (continued): Towards a living biobank of patient-derived glioblastoma stem cell models – clinicopathological features of the Sheffield lines.

		Clinical			Histological		Molecular						Cell line		
No.	M-Name	Age	Sex	Location	Histology	WHO Grade	IDH1	MGMT	TERTp	1p/19q	Other	100K consent	Propagated	Cryo	Survived unthawing
11	**OX-7**	61	**F**	Left frontal → corpus callosum	Glioblastoma	IV	wt (Seq)	Unmethylated (+ive)	wt (Seq)	No co-del	IDH2 wt BRAF wt H3F3A wt HIST1H3B wt	N/A	✓	✓	✓
12	**OX-8** (a)	68	**F**	Left frontal (large) but not partial lobectomy	Glioblastoma	IV	wt (IHC)	**Methylated** (MGMT -ive) by pyroseq	NR	NR	NR	N/A	✓	✓	✓
13	**OX-8** (b)														
14	**OX-8** (c)														
15	**OX-8** (d)														
16	**OX-8** (e)														
17	**OX-9** (a)	67	**M**	Left parietal	**Low-grade glioma** 'possible transformed areas on scan'	II	**mut** (IHC) R132H	**Promotor mut & Methylated** (MGMT -ive) by pyroseq	**mut** (Seq)	No co-del (1p loss only)	IDH2 wt BRAF wt H3F3A wt HIST1H3B wt GFAP +ive MAP2 +ive	N/A	✓	✓	✓
18	**OX-9** (b)														
19	**OX-9** (c)														
20	**OX-9** (d)														
21	**OX-10** (a)	34	**M**	Right occipito-parietal	Glioblastoma *(Patient has known diagnosis of NF1)*	IV	wt (Seq)	**Intermediate** (MGMT equivocal) by pyroseq	**mut** (Seq)	No co-del	**EGFR amplification** (84/100 cells) IDH2 wt BRAF wt H3F3A wt HIST1H3B wt	N/A	✓	✓	✓
22	**OX-10** (b)														
23	**AX-11** (a)	43	**M**	Right frontal (into corpus callosum) 5-ALA guided resection	Glioblastoma	IV	wt (Seq)	**Methylated** (MGMT -ive) by pyroseq	wt (Seq)	No co-del	ATRX wt IDH2 wt BRAF wt H3F3A wt HIST1H3B wt No EGFR amp PTEN intact	N/A	✓	✓	✓
24	**AX-11** (b)														
25	**AX-11** (c)														

Wildtype (wt) / unmethylated; mutant (mut) / methylated / structural aberration; not reported (NR); not yet tested (NT)

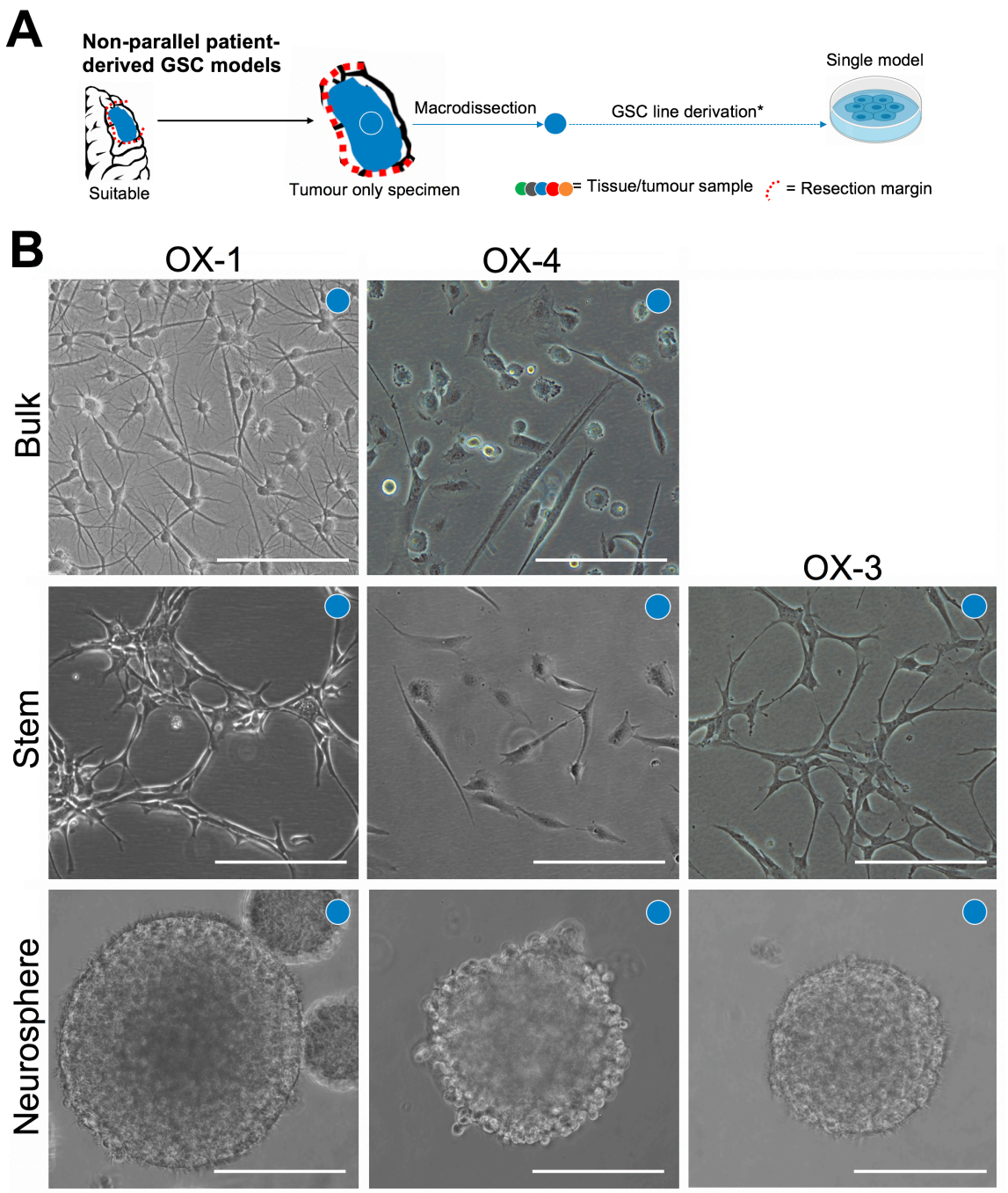


Figure 4.4: Derivation of Sheffield patient-derived glioblastoma stem cell lines – A. Schematic of non-parallel GSC model derivation; these represent a single GSC line generated from a patient's tumour. **B.** Representative brightfield light microscopy images (20x magnification) of 3 primary GSC models (OX-1, OX-3 and OX-4) derived from patients undergoing surgery for suspected high-grade glioma in Sheffield. The images illustrate cells derived from each patient propagated in: culture media containing serum to promote differentiation to represent tumour 'bulk' cells (*top row*); serum-free media supplemented with EGF and FGF ('stem' media) to enrich for GSCs (*middle row*), and; GSCs cultured in non-adherent conditions to elicit neurosphere formation (*bottom row*). Scale bars = 200μm.

Although detailed characterisation of Sheffield GSC lines is currently ongoing and incorporates key aspects of multiple recently awarded research grants, early assessment of these GSCs suggests robust mRNA expression of putative glioblastoma stem cell markers. For example, assessment of the Sheffield GSC lines OX-3 and OX-4 alongside Cambridge GSCs (with matched differentiated 'bulk' lines) and established commercial glioblastoma

cell lines revealed highest mRNA expression of nestin in both Sheffield GSC lines and highest SOX2 expression in OX-3 GSCs (Figure 4.5). This analysis confirmed an expected strong correlation in expression between the stem cell markers nestin and SOX2 (R^2=0.6923, p=0.0015) amongst a panel of 11 cell lines and alludes to a spectrum of 'stemness', within which: most established commercial lines demonstrate low-to-negligible relative stem cell marker expression; Cambridge primary cell lines demonstrate intermediate expression, with moderately lower expression in tumour bulk cells compared to GSCs, and; early passage Sheffield GSCs (less than passage 8) demonstrate high expression of at least 1 stem cell marker. An exception of these observations were the established U251 cell line which exhibited high nestin and SOX2 expression.

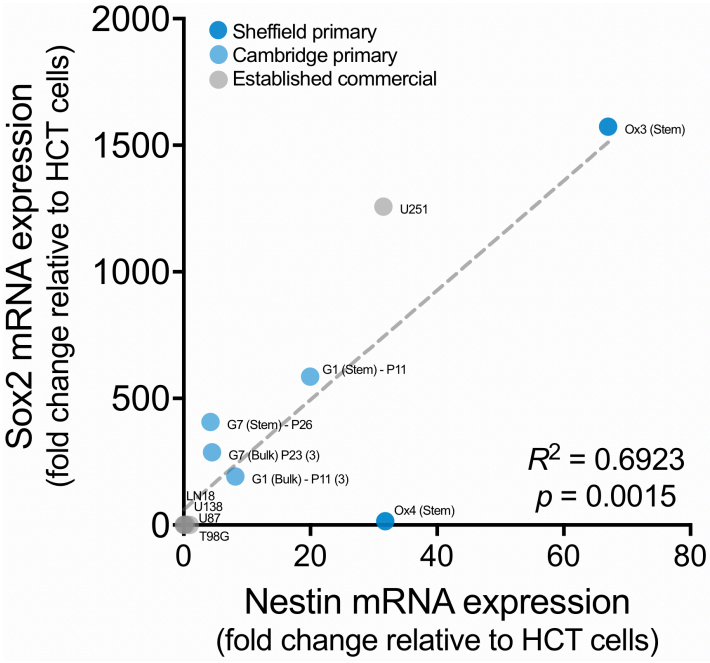


Figure 4.5: Comparison of stem cell marker expression in Sheffield primary GSCs, Cambridge primary cell lines and established commercial glioblastoma cell lines – TaqMan™ RT-PCR analysis of nestin and SOX2 gene expression in 11 untreated glioblastoma cell lines: Sheffield primary, patient-derived GSCs (OX-3 and OX-4) at early passage (<P8); Cambridge GSCs and matched bulk populations (G1 and G7 – passage number indicated), and; established glioblastoma cell lines (U87, U138, U251, LN18 and T98G). Bulk cells had been propagated in serum-containing culture media for 3 passages prior to the investigation. Nestin expression normalised to HCT116 (colorectal cancer) cell line to facilitate comparison across cell lines and highlight elevated nestin expression across all the primary glioblastoma lines relative to an established non-glioma cell line. Cells were plated then incubated for 24 hours prior to RNA extraction. Data points shown represent the mean of 3 experimental replicates.

4.3.2 Parallel 'Sheffield' GSCs to model random intra-tumoural heterogeneity

To facilitate future studies investigating genetic and/or functional heterogeneity in spatially distinct glioblastoma cell populations from *within* an individual patient's tumour, given the influence of heterogeneity on disease course in a range of cancers[424], we generated 'random intra-tumoural heterogeneity' models using multiple samples from the same

patient and deriving GSC lines in parallel as illustrated in Figure 4.6A. To date, 13 such GSC lines have been generated from 4 patients (OX-8A-E, OX-9A-D, OX-10A-B and AX-11A-C) – see Table 4.1 and Figure 4.6B. Further genetic and phenotypic characterisation of these models forms part of future planned studies.

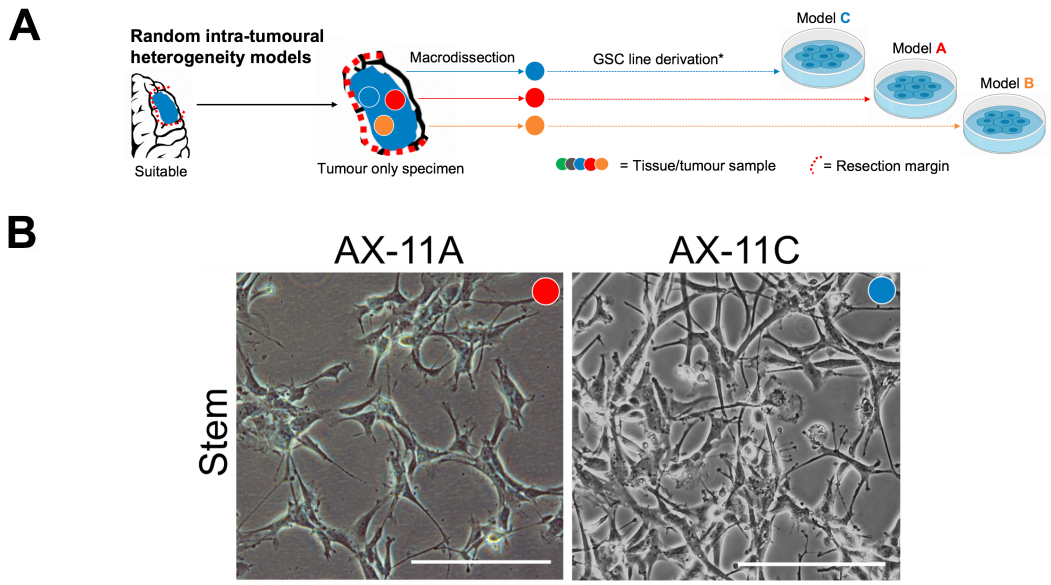


Figure 4.6: Derivation of Sheffield *ex vivo* random heterogeneity GSC models and representative pictures – A. Schematic of intra-tumoural heterogeneity model derivation. **B.** Representative brightfield light microscopy images (20x magnification) of the parallel primary GSC lines – AX-11A and AX-11C derived from separate regions of a single patient's tumour following surgery for a suspected high-grade glioma in Sheffield. The images illustrate each cell line propagated in serum-free media supplemented with EGF and FGF ('stem' media) to enrich for GSCs. Scale bars = 200μm.

4.3.3 Parallel 'Sheffield' GSCs to model resected and post-surgical residual disease

Translation of novel therapies for glioblastoma from the laboratory into clinical trials has relied heavily on cells derived from the bulk of patient tumours. However, it is clear from over 40 years of stagnant survival rates for patients with glioblastoma that the traditional paradigm of 2D *in vitro* studies using these cells followed by implantation into rodent xenograft models poorly predicts the treatment response of glioblastoma cells left behind after surgery in patients[425]. Additionally, increases in the number of targeted therapies available, and therefore potential therapeutic combinations, emphasise a need to apply efficient disease models that faithfully recapitulate the features and treatment response of post-surgical residual human glioblastoma. Consequently, a robust scientific and ethical rationale exists to develop a living biobank that represents post-surgical glioblastoma (in addition to typical resected disease) in patients.

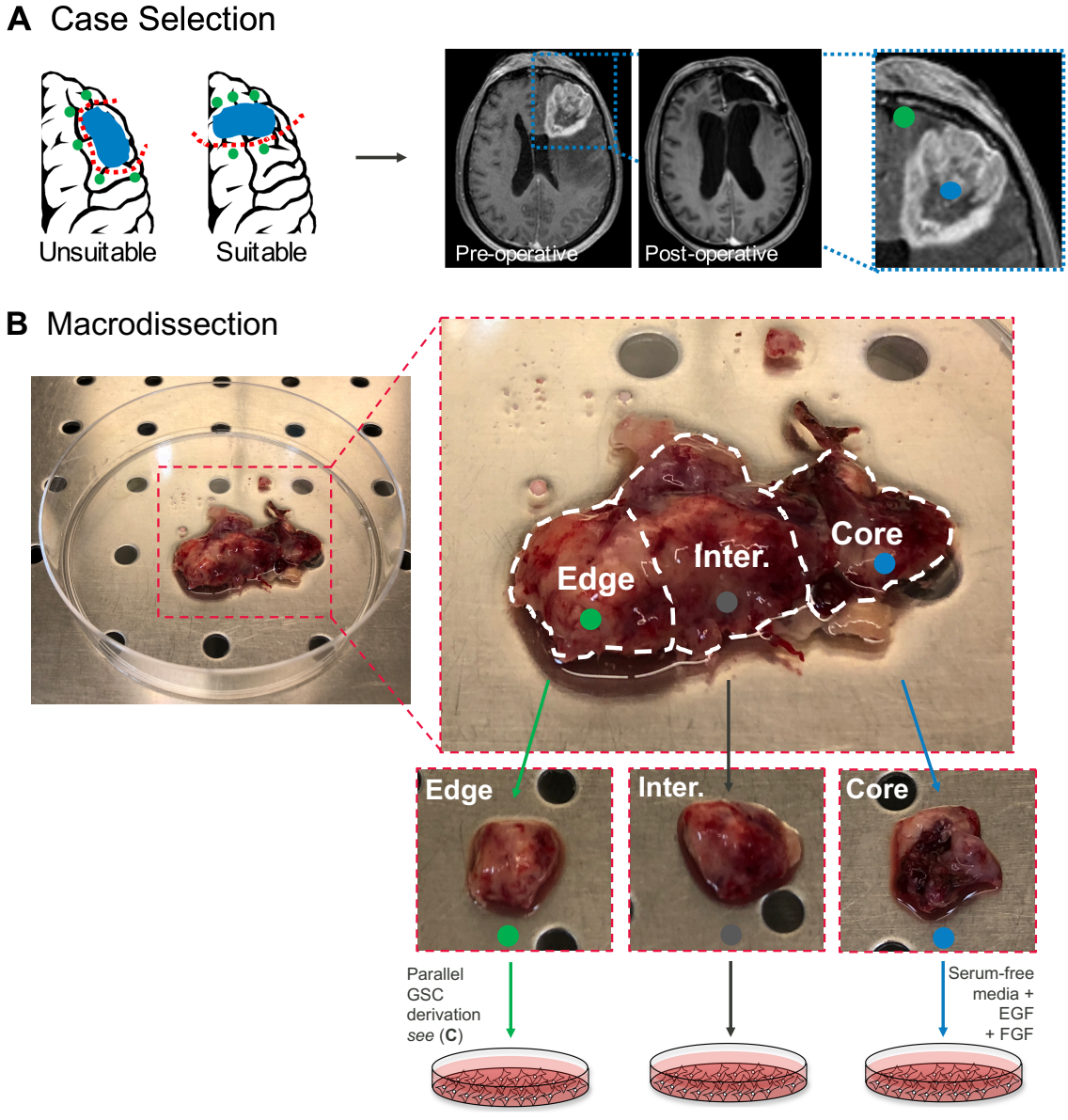
Recent studies have retrieved tissue from the bulk and immediate margins of patient tumours[15,313], but it is often technically and ethically challenging to retrieve tissue that is

more distant from the resected tumour mass. Additionally, sampling of more distal marginal glioblastoma cells using 5-aminolevulinic acid (5-ALA) fluorescence-guided approaches is limited by a low proportion of tumour/fluorescence in brain tissue that is more distant from the bulk of the tumour[313]. To overcome these challenges, a pragmatic methodology to efficiently model residual glioblastoma without the additional risk of taking biopsies from the resection cavity was developed.

Generation of Sheffield *ex vivo* resected and residual GSC models

Dependent on the anatomical considerations of individual cases, surgical resection occasionally provides a large *en-bloc* specimen (e.g. partial lobectomy) which includes portions of infiltrated brain that would not otherwise be resected (Figure 4.7A). This tissue may provide a crucial resource in modelling and understanding residual disease in glioblastoma. Such *en-bloc* specimens were hemisected in theatre (for pathology and research) along an axis to ensure both tumour and adjacent infiltrated brain tissue were present in each sample, before macrodissection of the research sample.

Whilst maintaining orientation, research samples were subdivided as illustrated (Figure 4.7B) to represent tumour core (resected model), infiltrative edge (residual disease model), and intermediate (inter) components for parallel GSC line derivation (Figure 4.7C).


A Case Selection
Unsuitable
Suitable
Pre-operative
Post-operative
B Macrodissection
Edge
Inter.
Core
Edge
Inter.
Core
Parallel GSC derivation see (C)
Serum-free media + EGF + FGF
C Parallel Derivation
Mechanical dissociation
Enzymatic dissociation (0 mins)
Enzymatic dissociation (90 mins)
Filtration...
(100µm)
Centrifugation
1000rpm (5 mins)
Day 1 appearance – 'dirty prep'
Resuspension

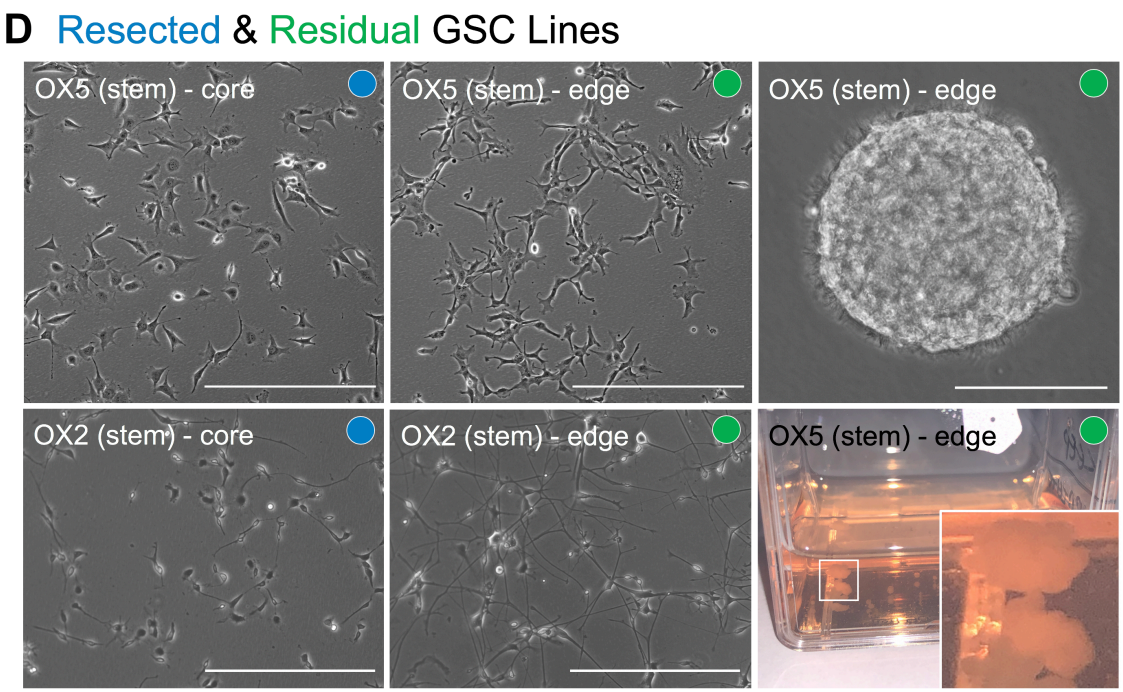


Figure 4.7: Derivation of Sheffield *ex vivo* resected and residual GSC models with representative pictures – A. Selection of patients undergoing partial lobectomy for glioblastoma – schematic representation of unsuitable and suitable planned resections (*left*) and suitable pre- and post-operative MRI (T1-weighted) following intravenous contrast (*right*). Regions within the tumour **core** (for **resected** model) and adjacent brain tissue affected by the infiltrative **edge** (for **residual** model) highlighted in *inset*. **B.** *En-bloc* specimen following hemi-section in theatre for clinical pathology and research (*left*) before macrodissection of the research specimen. Whilst maintaining orientation – the research specimen is subdivided as illustrated (*right*) to represent **core**, infiltrative **edge**, and **intermediate** (**inter.**) components for parallel GSC line derivation. **C.** Parallel derivation of patient-derived GSCs from **core** and edge of the *en-bloc* specimen – representative images. **D.** Representative brightfield light microscopy images (20x magnification) of Sheffield *ex vivo* **resected** and **residual** models. OX-5 and OX-2 **core** (*left column*) and **edge** (*middle column*) GSCs cultured as monolayers on Matrigel™-coated plasticware are demonstrated (scale bars = 500µm). *Right column* (*upper*) – representative image of OX-5 **edge** GSCs cultured in non-adherent conditions as 3-dimensional neurospheres (scale bar = 250µm), and; *right column* (*lower*) – representative photograph in non-adherent conditions (T25 flask) as larger 3-dimensional tumoroids following culture for 2 weeks. Scale bars = 200µm.

Analysis of the morphological features of resected and residual GSC lines cultured in 2D conditions found no significant differences in the mean number of protrusions per cell with 2.8 protrusions/cell observed with OX-5 core vs 3.3 protrusions/cell with OX-5 edge GSCs (p=0.0567) – see Figure 4.8A-C. Despite this however, OX-5 edge GSCs, which represent typical post-surgical residual disease, demonstrated a greater number of connecting tumour microtubes (TMs) and (1.8/cell compared to 0.7/cell in core GSCs, p=0.0005) and a higher proportion of GSCs with 3 or more connecting TMs (25% compared to 1% in core GSCs, p<0.0001) – see Figure 4.8D-E. Since the development of TM networks between glioma cells has been implicated in treatment resistance[212], these data imply that inherently greater connectivity of post-surgical residual disease may contribute to the therapeutic recalcitrance of glioblastoma observed in the clinic.

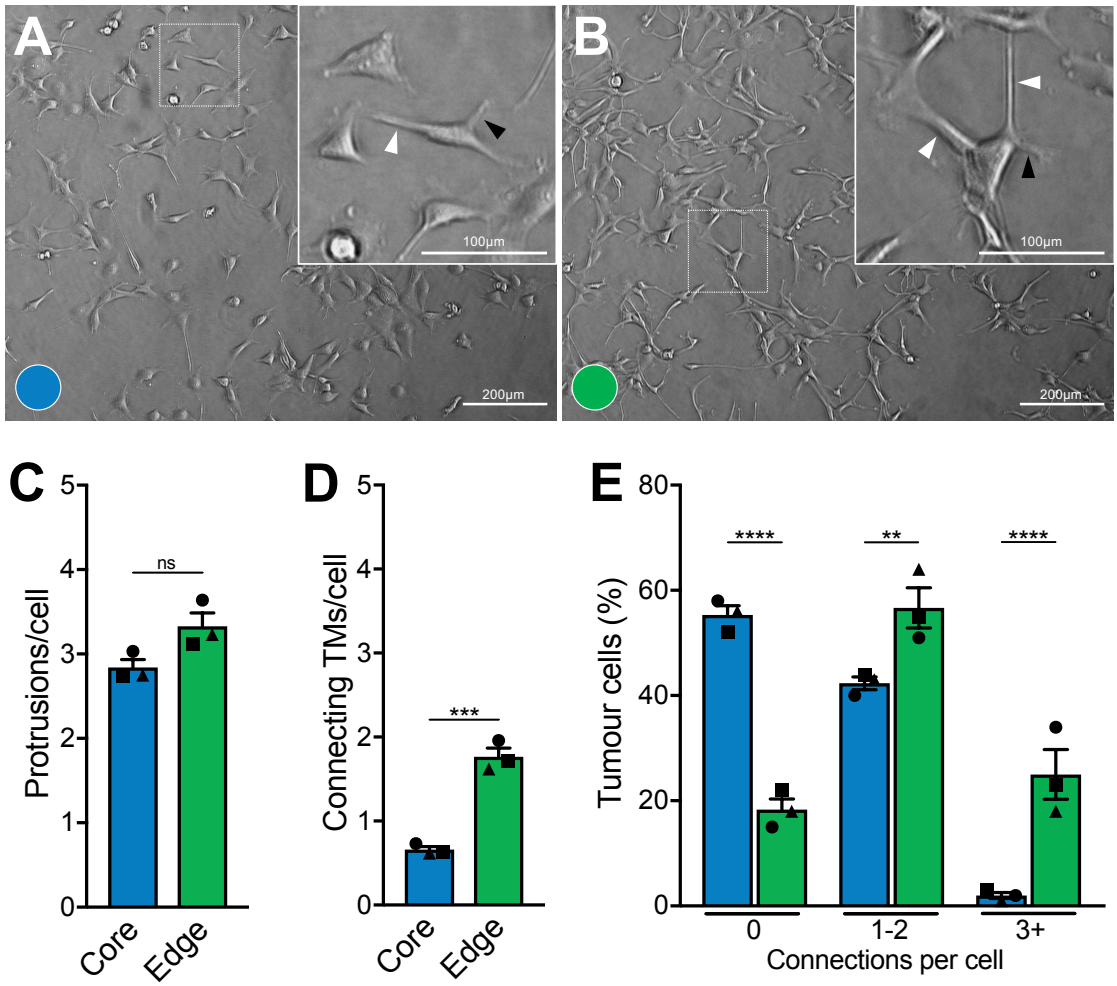


Figure 4.8: Differences in connecting tumour microtube formation between Sheffield *ex vivo* resected and residual GSC models – Untreated OX-5 core and OX-5 edge GSCs, to reflect resected and typically residual disease, were seeded at a density of 20,000 cells per well in 2D conditions then incubated for 3 days. Subsequently, cells were imaged using phase contrast microscopy and morphological features were quantified. A-B. Representative images of OX-5 core (A) and OX-5 edge (B) GSCs. Typical cellular protrusions (black arrowheads) and protrusions that form connecting tumour microtubes (white arrowheads) are highlighted in each inset. C. Mean protrusions per cell. D. Mean connecting TMs per cell. E. Number of connecting TMs per cell. Data points shown represent the mean of 3 independent experiments. Error bars represent the SEM.

The utility of these lines in 2D culture conditions (Figure 4.7D and Figure 4.9) and the customised 3D Alvetex™ scaffold-based architecture (Figure 4.9) was confirmed. Interestingly, very early passage Sheffield resected and residual GSCs appeared extremely migratory and exhibited poor clonogenic plating efficiency in 2D culture conditions, despite extensive cell proliferation. However, resected and residual models within the 3D culture system demonstrated much improved clonogenicity (Figure 4.9) with a 3.4-fold increase in 3D OX-5 core P3 ($p<0.0001$) and 2.1-fold increase in OX-5 edge P3 GSCs ($p=0.0008$), relative to 2D conditions. This was consistent with the enhanced clonogenic efficiency of G1 and G7 GSCs in 3D conditions (see Figure 4.3), but the magnitude of 3D vs 2D differential observed with OX-5 core and edge was substantially greater.

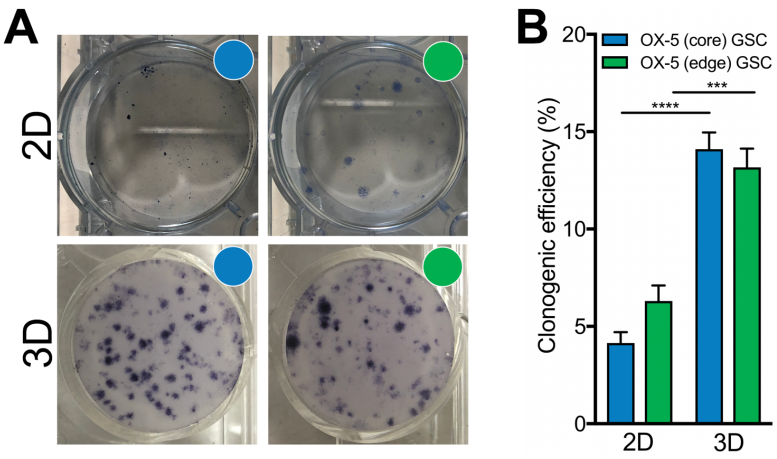


Figure 4.9: 2- and 3-dimensional colony formation with Sheffield *ex vivo* resected and residual GSC models – Untreated OX-5 core and OX-5 edge GSCs, to reflect resected and typically residual disease, were seeded at a density of 1,000 cells per well in 2D or 3D culture conditions (as indicated) then incubated for 21 days. Subsequently, colonies were identified using 0.04% methylene blue in 100% methanol to stain and fix 2D colonies, or incubation with MTT for 4 hours to reveal 3D colonies followed by paraformaldehyde fixation prior to quantification. A. Representative images, and; B. Comparison of clonogenic plating efficiency for OX-5 core and OX-5 edge GSCs in 2D and 3D Alvetex™ scaffold-based conditions. Data points shown represent the mean of 3 independent experiments. Error bars represent the SEM. Note 2D and 3D clonogenic plates not to scale – internal diameter of wells in 2D (6-well) plates is 2.3-fold the diameter of 3D Alvetex™ scaffolds (34.8mm vs 15mm).

Putative stem cell marker expression in resected and residual GSC models

Since glioblastoma exhibit intractable therapeutic resistance and are universally fatal, we hypothesised that GSC lines generated from the infiltrative tumour edge within *en-bloc* specimens to reflect post-surgical residual (normally 'left behind') disease would demonstrate greater mRNA expression of putative stem cell markers – since these are associated with resistance to radiotherapy[18], chemotherapy[426], and rapid tumour repopulation following treatment[19]. If validated, this hypothesis would, at least in part, explain the failure of promising therapies evaluated in preclinical studies using glioblastoma cell lines generated from typically resected tumour cells to translate to improved patient survival in clinical trials – since cells left behind after surgery are responsible for disease progression and death. Therefore the question of whether resected cells and typically left behind (residual) cells are equivalent is of paramount translational importance.

Firstly, we assessed the mRNA expression of nestin in OX-5 core and OX-5 edge GSCs and matched bulk cultures (propagated in culture media containing serum for 5+ passages), alongside G1 primary cells. As expected, OX-5 core, OX-5 edge and G1 GSCs demonstrated greater nestin mRNA expression compared to matched bulk cell populations ($p<0.0001$) – see Figure 4.10A. In contrast, there was no demonstrable divergence in nestin mRNA expression between OX-5 edge GSCs and OX-5 core GSCs ($p=0.9556$). Similarly, there was no significant difference in nestin mRNA expression between OX-5 edge bulk and

OX-5 core bulk cells (p=0.1070). Since these findings were inconsistent with our original hypothesis (above), we investigated expression of the additional commonly used glioblastoma stem cell markers CD133 and SOX2 in OX-5 GSCs, in addition to reassessing the expression of nestin. Validating the previous assessment, both OX-5 edge GSCs and OX-5 core GSCs demonstrated equivalent levels of nestin mRNA expression. However, in contrast, OX-5 edge GSCs demonstrated higher expression of SOX2 mRNA (1.6-fold higher, p=0.0274) and profoundly higher mRNA expression of the archetypal GSC marker CD133[16] (9.7-fold higher, p=0.0033) relative to core GSCs from the same patient (Figure 4.10B). These findings require further validation at the protein level and in additional resected and residual GSC models. Nevertheless, they support the previously unreported possibility that infiltrative GSCs typically left behind after surgery may exhibit greater 'stemness' and associated inherent therapeutic resistance compared to cells normally resected (and used in preclinical research). This hypothesis would be consistent with data from the landmark study by Bao *et al*. (2006)[18] which demonstrated that GSCs, designated on the basis of CD133 positivity, displayed enhanced radioresistance associated with increased expression and activation of key DDR proteins including ATM, CHK2 and CHK1. To investigate this hypothesis further, we have begun to quantify the differentials in mRNA expression of DDR genes between resected and residual GSC models. Strikingly, preliminary data suggests residual model GSCs may exhibit elevated mRNA expression of key DDR genes including ATM, ATR and FANCD1/BRCA2 (Figure 4.11), however, further study is required to validate these potentially important differences. Taken together, these findings suggest that preclinical evaluation of future novel strategies to treat glioblastoma should incorporate assessment of efficacy in models that faithfully recapitulate unique features of post-surgical residual disease.

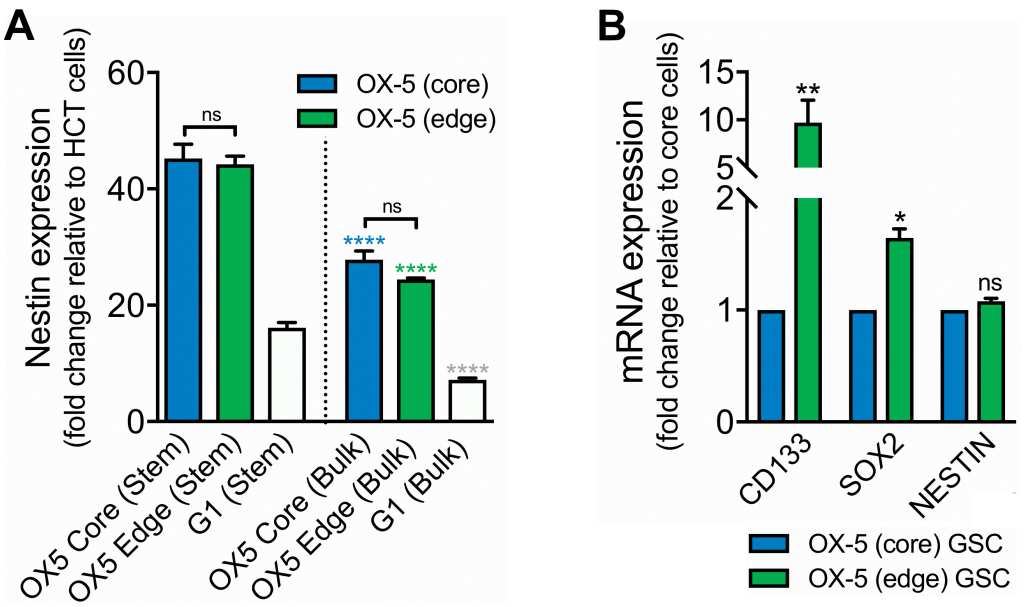


Figure 4.10: Stem cell marker expression in Sheffield *ex vivo* resected and residual GSC models – A. TaqMan™ RT-PCR analysis of nestin in untreated OX-5 core and OX-5 edge GSCs with matched bulk populations, to reflect resected and typically residual disease, respectively. These were evaluated for stem cell marker mRNA expression alongside G1 GSCs with matched bulk populations. Nestin expression normalised to HCT116 (colorectal cancer) cell line to facilitate comparison across cell lines and highlight elevated nestin expression across all the primary glioblastoma lines relative to an established non-glioma cell line. Asterisks (*/*/*) denote statistical significance of nestin expression in bulk cells compared to the corresponding GSC line. **B.** TaqMan™ RT-PCR analysis of CD133, SOX2 and nestin in untreated OX-5 core and OX-5 edge GSCs. Asterisks (*) denote statistical significance of stem cell marker mRNA expression in edge (residual model) stem cells compared to core (resected model) stem cells. In all experiments (A-B) cells were plated then incubated for 24 hours prior to RNA extraction. All data points shown represent the mean of 3 independent experiments. Error bars represent the SEM.

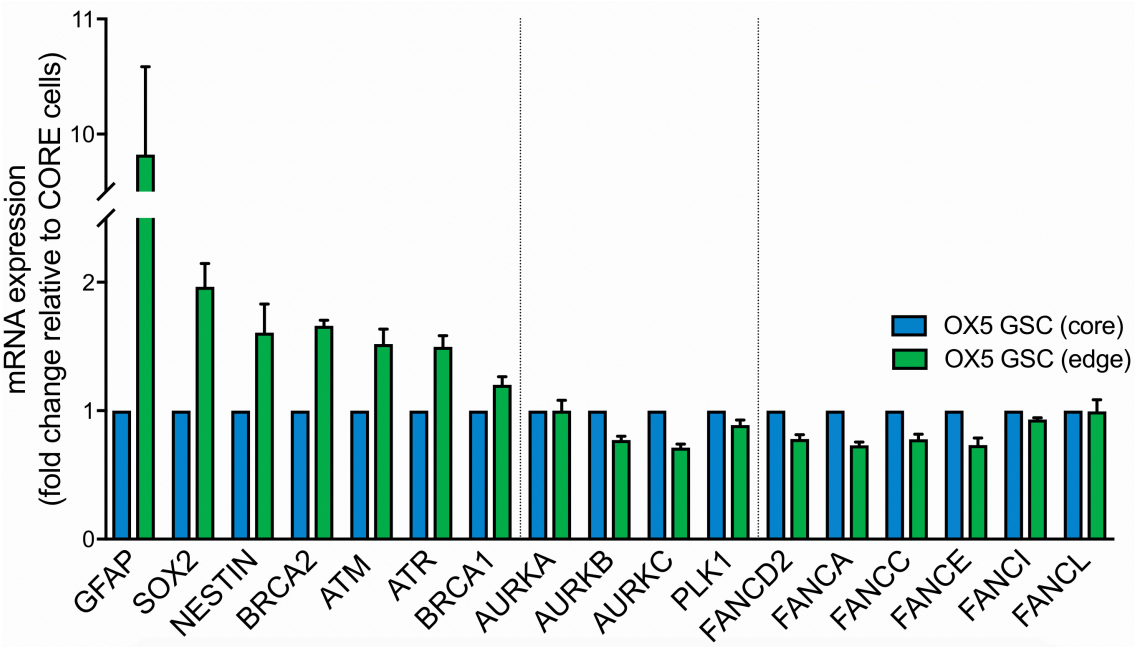


Figure 4.11: Expression of DDR and 'stemness' genes in Sheffield *ex vivo* resected and residual GSC models – A. TaqMan™ RT-PCR analysis of untreated OX-5 core and OX-5 edge GSCs, to reflect resected and typically residual disease, respectively. Cells were plated then incubated for 24 hours prior to RNA extraction. Data points shown represent the mean of 3 experimental replicates. Error bars represent the SEM. *Data shown were produced by Miss Aurelie Vanderlinden working under my direct supervision.*

4.4 Early development of a 3D *ex vivo* scaffold-based system to assess tumour treating fields and replace animal studies

4.4.1 Model development and TTFields delivery via Inovitro™

Since tumour treating fields (TTFields) represents an entirely new therapeutic modality that has been proven to extend overall survival in patients with newly diagnosed glioblastoma[427] and may modify aspects of the DDR[72-74], we aimed to develop a 3D scaffold-based model which could replace the use of traditional 2D models and animal models to evaluate the effects of TTFields, and assess TTFields + DDRi combinations in future studies. After establishing a collaboration with Novocure™, the patent holder and sole global producer of clinical TTFields technology, Inovitro™ preclinical TTFields research equipment was installed in the Collis laboratory in late 2019, with early studies confirming demonstrable efficacy against GSCs (Figure 4.12).

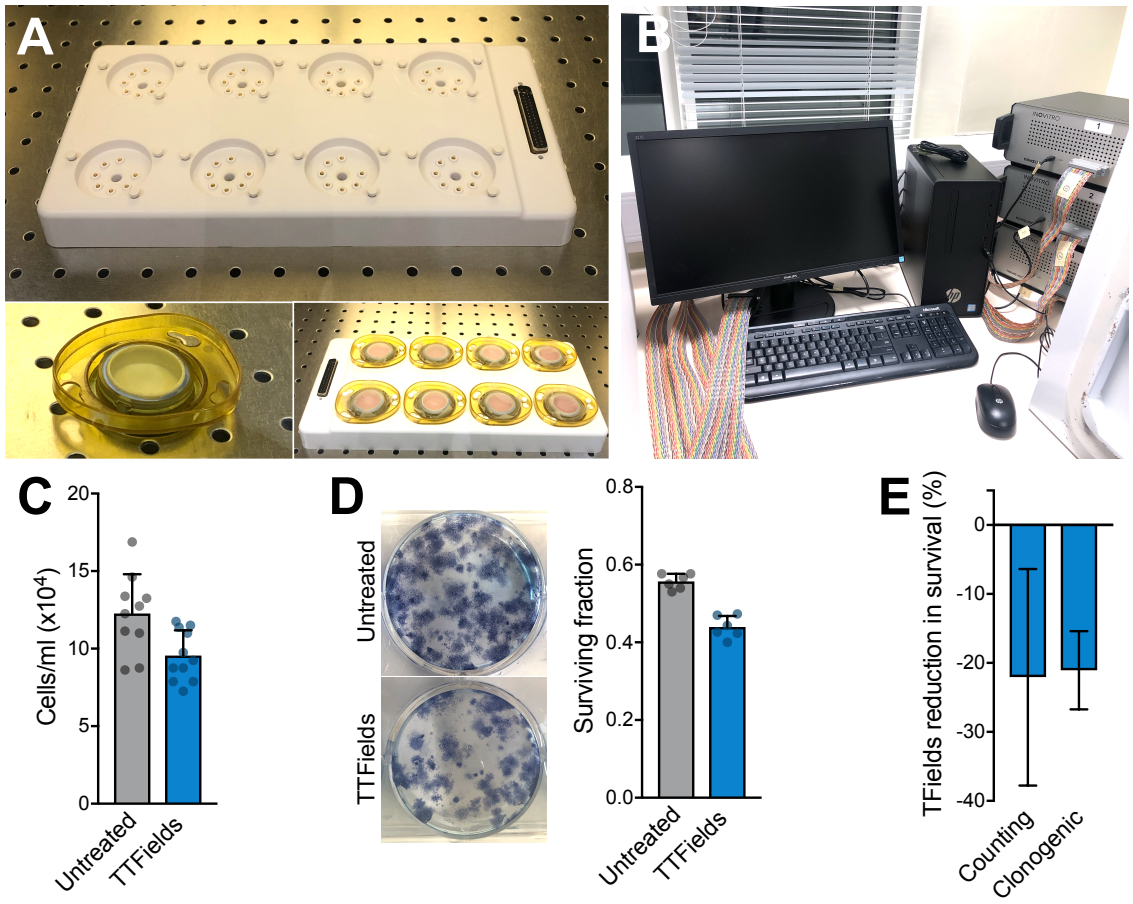


Figure 4.12: Inovitro™ preclinical TTFields delivery equipment and early efficacy – A. Base plate for TTFields delivery with a single ceramic dish (*inset – lower left*) and ceramic dishes loaded after seeding cells (*inset – lower right*). **B.** TTFields generators with flat cables (for attachment to baseplates) and dedicated desktop computer with Inovitro™ software. **C-D.** Survival of G1 GSCs receiving sham (untreated) or TTFields for 48 hours at 200 kHz established by cell counting (**C**) and clonogenic assay after reseeding surviving cells (**D**). **E.** Comparison of reduction in survival estimated by cell counting vs clonogenic survival assay with 95% confidence intervals. Note: although both methods demonstrate ~20% reduction in GSC survival following a 48 hour treatment exposure, in line with modest single modality efficacy of TTFields observed in previous studies[72-74], the clonogenic assay appears to be associated with reduced variability. Graph bars represent the mean of experimental replicates which are individually superimposed (grey/blue dots). Error bars represent the SD (**C-D**) or the 95% confidence interval as indicated (**E**). Treatment duration was based on our previous characterisation of

G1 and G7 GSC proliferation rates (data not shown). *Data shown were produced by Miss Aurelie Vanderlinden and the author working together.*

During typical *in vitro* preclinical TTFields studies, researchers seed cells onto 2D glass or plastic coverslips which are subsequently placed within ceramic dishes of the Inovitro™ system for TTFields delivery. Since the internal diameter of ceramic dishes used with Inovitro™ is ~15mm, it is usually not possible to seed sufficient cells for robust 2D clonogenic studies to cover slips (without resulting in substantially overlapping colonies and/or a cell monolayer) without reseeding cells. Therefore, recent studies have relied on counting and/or reseeding cells after delivery of TTFields[72,73], which is likely to represent an important source of experimental variability and potential contamination. As colonies generated within the customised Alvetex™ scaffold-based system used in this thesis grow in 3-dimensions with smaller colony diameters compared to the same cell line in 2D conditions (see Figure 4.3C – note 2D/3D images not to scale, internal diameter of wells in 2D 6-well plates is 2.3-fold greater than the diameter of 3D Alvetex™ scaffolds), we hypothesised that application of the 3D scaffold within Inovitro™ would enable TTFields clonogenic studies without the need to reseed cells and the inherent variability associated with this. Furthermore, preclinical TTFields studies which leveraged the heightened clinical-relevance and predictive value of 3D scaffold-based models[108] might have the potential to replace/reduce some TTFields animal studies in the future. Figure 4.13 provides a schematic representation of the concept of an *ex vivo* 3D GSC scaffold-based TTFields culture and delivery system.

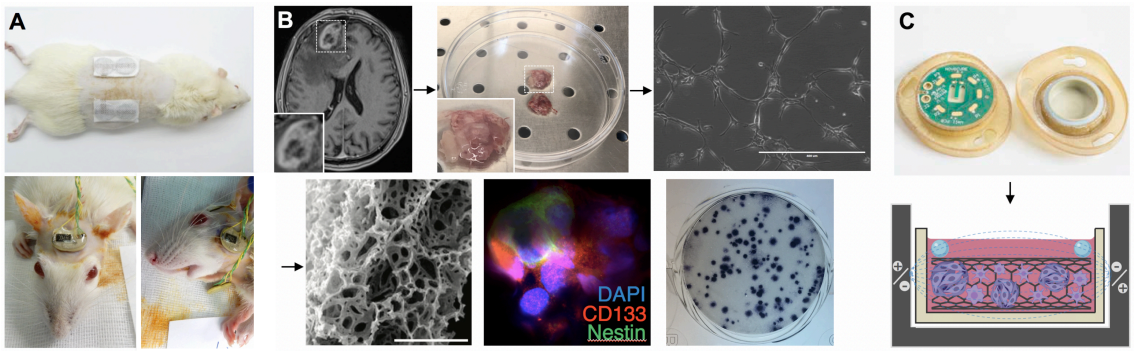


Figure 4.13: Conceptual representation of an *ex vivo* 3D scaffold-based TTFields culture and delivery system to replace animal studies – A. Representative TTFields transducer array placement on dorsal (*upper*) and cranial (*lower*) Sprague Dawley rat skin during typical animal studies (images courtesy of Novocure™). **B.** Representative steps to generate a 3D *in vitro* replacement model: UPPER – preoperative T1-weighted MRI of a right frontal glioblastoma prior to surgical resection (*left*); surgical specimen (*middle*) – which is dissociated and cultured in serum-free media to maintain GSCs; bright-field microscope image of patient- derived GSCs in 2D conditions (*right*); LOWER – scanning electron micrograph image of 3D Alvetex™ scaffold into which cells would be seeded following Matrigel™ coating (*left*); representative immunofluorescence detection of stem cell markers of GSCs within the 3D scaffold (*middle*); representative well from stained 3D clonogenics (*right*). C. Ceramic dish into which scaffolds are inserted and TTFields delivered via Inovitro™ – back and front sides (*upper*); schematic of TTFields generation by Inovitro™ and delivery to 3D scaffold-based GSCs within the ceramic dish (*lower*).

Confocal z-stack images of an 3D Alvetex™ scaffold (kindly provided by Frederique Tholozan, REPROCELL Europe Ltd) were used to generate a 3-dimensional scaffold render to which the physical properties of its constituent material polystyrene were attributed *in silico*. In collaboration with Novocure™ computer simulations were used to approximate the delivery of TTFields to 3D Alvetex™ scaffolds (Figure 4.14A-B). These simulations predicted 3D Alvetex™ scaffolds would permit acceptable TTField intensities to facilitate preclinical therapeutic studies. Interestingly, comparison with Novocure's simulations of TTFields delivery to mouse brain and human brain suggested that, unlike in mouse brain which exhibited uniform TTField intensities throughout, simulations within the 3D scaffold recapitulate characteristic spatial heterogeneity in TTField intensities observed in human brain simulations (Figure 4.14A-B). To facilitate efficient *in vitro* model development, the use of LN18 established glioblastoma cells with 3D Alvetex™ scaffolds was optimised (Figure 4.14C). Subsequently, the delivery of TTFields delivery to LN18 cells embedded within Alvetex™ scaffolds was confirmed by our collaborators at Novocure™ to reduce cell viability using the XTT assay (Figure 4.14D) and further investigation of therapeutic TTFields delivery to customised 3D models is ongoing within the Collis laboratory.

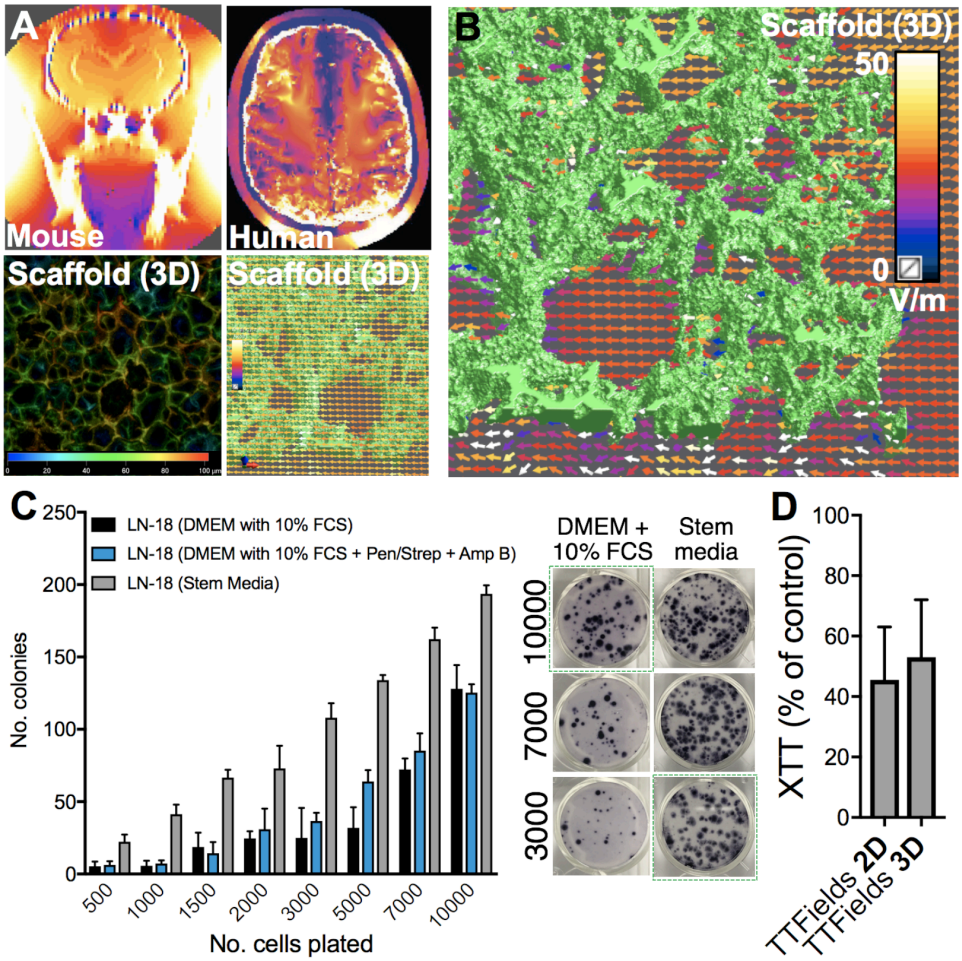


Figure 4.14: Feasibility of TTFields delivery to cells within a 3D culture system – A. *UPPER – In silico* simulation of TTFields to mouse (*left*), and; human (*right*) brain; *LOWER* – confocal Nile red depth map of 3D Alvetex™ scaffold used to generate *in silico* mesh (*left*); *in silico* prediction of TTField delivery [to media] above scaffold (*right*). B. Simulation of TTFields delivery **within** 3D scaffold *in silico* – coloured arrows denote directionality & field intensity (0-50V/m). **Note: 3D scaffolds permit acceptable TTField intensities and, unlike mouse models, reflect spatial heterogeneity observed in human simulations**. C. Optimisation of established glioblastoma cell line (LN18) 3D colony formation *in vitro*. D. Effective *in vitro* delivery of TTFields to LN18 glioblastoma cells within the 3D scaffold. *In silico simulation (A-B) and XTT data (D) provided courtesy of Novocure™. Confocal z-stack images of an 3D Alvetex™ scaffold (A) kindly provided by Frederique Tholozan, REPROCELL Europe Ltd.*

4.5 Summary of key findings

Validation of 2D and 3D Cambridge patient-derived glioblastoma stem cell (GSC) models

- GSCs can be effectively propagated in serum-free media with evidence of neurosphere formation in non-adherent conditions and differentiation after serum exposure.
- Nestin and SOX2 mRNA expression was elevated in G1 GSCs, relative to differentiated 'bulk' cells.
- G7 GSCs may express elevated nestin mRNA but this did not reach statistical significance.
- G7 GSCs cultured within 3D Alvetex™ scaffolds demonstrate protein expression of putative stem cell markers including nestin, CD133 and vimentin.
- Compared to traditional 2D culture, use of a 3D scaffold-based architecture enhanced the clonogenic plating efficiency of G1 and G7 GSCs by 33% and 35%, respectively.
- G1 and G7 GSCs demonstrated marginally increased radiosensitivity within the 3D culture system – with $DMF_{0.37}$ of 1.27 and 1.13, respectively.

Clinically- and surgically-relevant Sheffield patient-derived GSC models

- A foundational resource of 24 primary GSC lines from 11 patients with linked clinical and molecular data has been established to support current and future studies.
- Early passage Sheffield GSCs demonstrate high stem cell marker mRNA expression relative to matched bulk populations, Cambridge GSCs and established lines.
- Random intra-tumoural heterogeneity models have been developed using parallel GSC derivation from spatially distinct samples within an individual patient's tumour.
- Novel *ex vivo* resected and residual models have been developed, based on GSC derivation from tumour and adjacent infiltrated brain in partial lobectomy specimens.
- First evaluation of a post-surgical residual disease model (OX-5 edge GSCs) reveals divergent properties relative to a matched resected disease model including elevated CD133, SOX2 and early evidence of differential DDR gene expression.

Early development of a 3D scaffold-based system to assess tumour treating fields (TTFields) – in collaboration with Novocure

- TTFields delivered via Inovitro™ exhibit efficacy against G1 GSCs cultured in 2D conditions demonstrable by both cell counting and clonogenic survival, but the latter is associated with reduced variability.

- *In silico* simulations predict Alvetex™ scaffolds permit acceptable TTField intensities and reflect spatial heterogeneity observed in human simulations (unlike mouse brain simulations).
- *In vitro*, optimised culture of LN18 glioblastoma cells within 3D Alvetex™ scaffolds with TTFields delivery via the Inovitro™ system demonstrates therapeutic efficacy.

4.6 Discussion

The preclinical models validated during these studies underpin investigations presented in Chapter 5 which aim to develop new, more effective combinatorial strategies to treat glioblastoma. Additionally, the newly developed clinically- and surgically-relevant *ex vivo* models presented in this Chapter currently support multiple ongoing glioblastoma research projects and are expected to provide a foundational resource for future work, contributing to the establishment of a vibrant brain tumour research ecosystem in Sheffield and beyond.

4.6.1 General Study Limitations

Prolonged neurosphere culture vs early transfer to Matrigel™ substrate

Serum-free conditions have previously been established to enrich for glioma cell phenotypes that more faithfully represent associated parental tumours[421,428]. The Cambridge protocol for cell line derivation by Fael Al-Mayhani *et al.* (2009)[99], with the potential to reliably generate patient-derived lines which robustly express putative glioblastoma stem cell markers and retain key molecular features of each parental tumour, relied on short-term neurosphere culture prior to transferring intact spheroids onto ECM-coated plasticware to facilitate monolayer culture. Although the Cambridge protocol, which we adapted, does not specify the duration required for short-term neurosphere culture to permit the formation of primary aggregates, durations of between 24-48 hours were used in our studies before transferring spheroids to monolayer culture. Thus, a maximum limit of 48 hours primary neurosphere culture was enforced for the generation of all primary lines even if substantial primary spheroids were not easily visible in the milieu of cellular material and debris (typically extensive as the use of RBC lysis buffer was avoided in contrast to Fael Al-Mayhani *et al.* (2009)[99] to avoid any potential effects on tumour cells – 'dirty prep' – see Figure 4.7C). Our decision to avoid the longer-term propagation of patient-derived glioblastoma cells as neurospheres is potentially subject to criticism since, using comparative genomic hybridization, De Witt Hamer *et al.* (2008)[98] previously demonstrated the genomic profiles of neurospheres tended to cluster closer to parental tumours than those of primary glioma monolayer cultures when subjected to unsupervised hierarchical clustering. However, this study[98] was substantially flawed by the maintenance of primary cells in serum-containing media, which may have contributed to failure of glioblastoma stem cell preservation[421] and therefore substantial changes in the clonal/subclonal cellular heirachy[429] with more substantial (less ecologically valid) effects of culture media-based

selection. Additionally, short-term neurosphere culture followed by further propagation and expansion of glioblastoma cells as a monolayer in serum-free media was revealed by Fael Al-Mayhani *et al.* (2009)[99] to dramatically enhance the success rate of establishing primary cultures. This statistic represents an important consideration given the precious, irreplaceable nature of each individual patient's glioma specimen; a statistic that, surprisingly, was not reported in the study by De Witt Hamer *et al.* (2008)[98]. Our excellent success rate in establishing and propagating primary cultures in 24/26 (92%) individual samples, is identical to Fael Al-Mayhani *et al.* (2009)[99] (22/24 samples, 92%), and is substantially greater than other previous studies[371,423] and partially validates the use of monolayer GSC culture following only a brief period for neurosphere formation. Furthermore, confirmation of putative stem cell marker expression in Sheffield GSCs expanded as adherent monolayers (Figures 4.5 and 5.10) and studies by Rahman *et al.* (2015)[101] support this choice of protocol, whilst studies by Pollard *et al.* (2009)[100] suggested even a brief period of neurosphere culture (prior to propagation as an adherent monolayer) may not be required to establish *bona fide* primary GSC lines which demonstrate robust stem cell marker expression and reflect patient-specific features.

Physiological relevance of culture systems used

In patients, glioblastoma cells exist amongst a myriad of microenvironmental cues and gradients (as discussed in Section 4.1.2), the collective effects of which are impossible to replicate flawlessly *in vitro*. Consequently, whilst considering data generated using the 2D and 3D models investigated within this Chapter, it is imperative to consider key limitations associated with their physiological relevance and how these may influence results.

Firstly, all patient-derived GSCs used were cultured in Advanced DMEM/F-12 (Gibco) which contains a D-glucose (dextrose) concentration of 17.5mM (manufacturers website/product sheet) – almost 4-times normal brain concentrations (4.5 ± 0.5 mM) as measured by ^{1}H-magenetic resonance spectroscopy in healthy human subjects[430]. Since glucose concentration can exert a range of influences on glioblastoma cells[106,431], and of specific relevance, glucose restriction has been demonstrated to promote features consistent with stemness, including enhanced mRNA expression of *SOX2*, *NANOG*, *OCT4*, and expansion of the CD133^{+} GSC subpopulation[432], the relatively high glucose concentrations used in our studies may have partially diminished the stem characteristics and associated therapeutic recalcitrance of GSC models applied. However, the D-glucose concentration of

Advanced DMEM/F-12 used in these studies remains lower than in more commonly used DMEM/Advanced DMEM (25mM)[106,431,432], and may therefore represent a viable compromise to enable the efficient GSC expansion required to evaluate a range of therapeutic compounds and combinations, given that reduced glioblastoma cell proliferation rates are associated with glucose deprivation[433].

Secondly, 2D and 3D Alvetex™ scaffold-based models used in this Chapter are not likely to generate the heterogeneous oxygen and pH gradients observed *in vivo*. For example, Gomez-Roman *et al.* (2017)[108] previously demonstrated low-to-undetectable levels of hypoxia (via pimonidazole staining and direct measurement) throughout scaffolds embedded with G7 GSCs (also used in our 3D studies) – although E2 GSCs did demonstrate observable pimonidazole staining in 20% of scaffold sections, indicating some cell line specific variability. In contrast, studies by Hubert *et al.* (2016)[102] elegantly illustrate profound regional hypoxia within glioblastoma tumour organoids which is most pronounced towards the core of these 3D structures. Hypoxia elicits a range of intercellular effects and profoundly modulates radiosensitivity[434]. In the context of glioblastoma, hypoxia has been demonstrated to elevate levels of VEGF and lead to a more radioresistant GSC phenotype[107]. Interestingly, two co-existing, diametrically opposed GSC subpopulations have been described based on an oxygen-rich perivascular niche subpopulation, and a relatively quiescent subpopulation within the hypoxic niche[102] (see Section 4.1.2). More complex 3D culture systems that enable greater regional heterogeneity, such as neurosphere and organoid/GLICO cultures, also invariably portend greater difficulty in establishing which cellular subpopulations and/or microenvironmental niches a particular experimental therapy is effective against. Indeed, such models even permit notable spontaneous differentiation of GSCs towards the core of structures[100,435] making it challenging to ascertain if therapies are genuinely effective against treatment resistant cancer stem cells, rather than tumour bulk cells. In contrast to the impenetrable core of these aggregoid 3D models, culture of GSCs within 3D Alvetex™ scaffolds permits more homogenous percolation of 'stemness'-maintaining culture media and appears to permit more uniform protein expression of GSC markers (our images including Figure 4.2C-D and Gomez-Roman *et al.* (2017)[108]). So, for precisely the same reasons a reductionist approach of 3D GSC culture using Alvetex™ scaffolds may detract from physiological-relevance due to a lack of substantial resource and nutrient gradients, this approach may also render these scaffolds an invaluable tool to model the specific killing of treatment resistant, infiltrative

nutrient-rich perivascular niche GSC populations in early preclinical studies, before promising therapeutic candidates and strategies are translated to more complex models.

Thirdly, Matrigel™ used as an adherent substrate within both 2D and 3D models in these studies contains a rich mixture of collagen, laminin and ECM-associated growth factors[106,407]. In contrast, ECM in the brain is rich in proteoglycans (including heparan sulphate) and the glycosaminoglycan hyaluronic acid, with relatively low collagen and laminin expression[436] compared to the ECM of most extra-cranial tissues. Thus the inability of Matrigel™ to precisely reflect brain-specific ECM composition, combined with the inherently high stiffness of polystyrene used to form the coated Alvetex™ scaffolds[106] may have influenced key phenotypic features of GSCs within the 3D scaffold-based model such as proliferation and migration[437], with implications including the effects of these on colony formation in the 3D model. Interestingly however, since laminin is abundant within the cerebral vasculature[106], the use of Matrigel™ might be more appropriate to represent the perivascular niche, within which a subset of GSCs typically reside (discussed above). Additionally, Matrigel™ can also suffer from batch-to-batch variability, in view of its origins, having been extracted from murine Engelbreth–Holm–Swarm (EHS) sarcomas[407]. To minimise the effects of variability in our studies, growth factor reduced (GFR) Matrigel™ was used, with a consistent concentration of growth factors (EGF and FGF) added directly to the media, to promote more reproducible culture conditions. Furthermore, every effort was taken to ensure Matrigel™ from the same batch was used to coat plasticware within a single experiment. Nevertheless, the inability to ensure an identical composition of Matrigel™ throughout this these studies is a noted concern, particularly when attempting to consider or compare experiments completed at different times.

Finally, model validation and development in these studies did not extend to the generation of multicellular models. Even some of the most complex *in vitro* 3D multicellular culture systems reported[438-442] cannot simultaneously replicate the plethora of interactions and features afforded by various cell types present in the *in vivo* scenario, such as effects of: the BBB[443]; immune system[444]; interaction with healthy glia[445], and; glioma-neuronal synapses[446,447]. Clearly, the culture systems employed in our studies are orientated towards early preclinical development of therapeutic strategies that require mid-high throughput applications, accepting the key role of more complex, ideally *in vivo* models, such as

patient-derived orthotopic xenografts, for the future validation of promising strategies identified.

Towards more comprehensive validation and characterisation

Cambridge GSC lines were confirmed to propagate effectively in serum-free 'stem' media conditions used in these studies, retain the capacity to form neurospheres, and demonstrate gross morphological changes consistent with differentiation following serum exposure (Figure 4.1). Although elevated nestin and SOX2 mRNA expression was confirmed in G1 GSCs relative to bulk cells, validating the enhanced 'stemness' of the GSCs in this matched pair, greater variability in expression data generated for G7 primary cells prevented similar confirmation using this patient-derived line (Figure 4.2A-B). Further validation of the 'stemness' properties of the Cambridge GSCs, and G7 GSC in particular, would have been ideal. However, such properties in these cell lines have been previously confirmed by Fael Al-Mayhani *et al.* (2009)[99], Carruthers *et al.* (2015)[195] and Ahmed *et al.* (2015)[197] – with the latter two of these studies undertaken in the Chalmers laboratory, from which we were a direct recipient of these cell lines. Additionally, protein expression of the putative GSC markers CD133, nestin and vimentin was confirmed in G7 GSC cultured within 3D Alvetex™ scaffolds, validating the maintenance of stem features in 3D culture conditions as previously reported in scaffold-based[(108)], neurosphere[(99,100)], and organoid-based systems[(102)].

Validating and characterising a range of additional features pertaining to the Cambridge primary GSC lines may have helped further inform studies presented in this thesis. For example: additional confirmation of stem cell markers (including CD133, SOX2, nestin, OLIG2) at the mRNA and protein level in additional cell lines in both 2D and 3D conditions; characterisation of proliferation rates[(99)], and; characterisation of migration and invasiveness. However, even more extensive profiling of these Cambridge GSC lines would not resolve limitations arising from the relatively paucity of associated clinical information available, and the challenge of obtaining such details. Consequently, we agreed it more desirable to allocate resources to building a collection of primary, patient-derived GSC lines in Sheffield, rather than more extensive characterisation of the existing Cambridge lines. In addition to avoiding the duplication inherent with validating aspects of characterisation completed in other laboratories for the Cambridge GSCs, beginning the development of a Sheffield-based resource provides the advantage of comprehensive, detailed and contemporaneous access to the clinical features associated with each patient-derived GSC line, including:

demographics; tumour pathology and molecular features; pre- and post-operative imaging; treatment, clinical course and survival. As an example, overall survival data for patients whose specimens were also used to successfully generate primary GSC lines is illustrated in Figure 4.15 below. As our living biobank continues to expand, linked patient data such as this will be invaluable to help better understand patient-specific differences in therapeutic response. However, this strategic decision to divert time towards building a Sheffield-based resource also resulted in a greater reliance on previous characterisation of the Cambridge GSCs, used extensively during these studies, whilst the development and characterisation of Sheffield patient-derived GSCs remains ongoing.

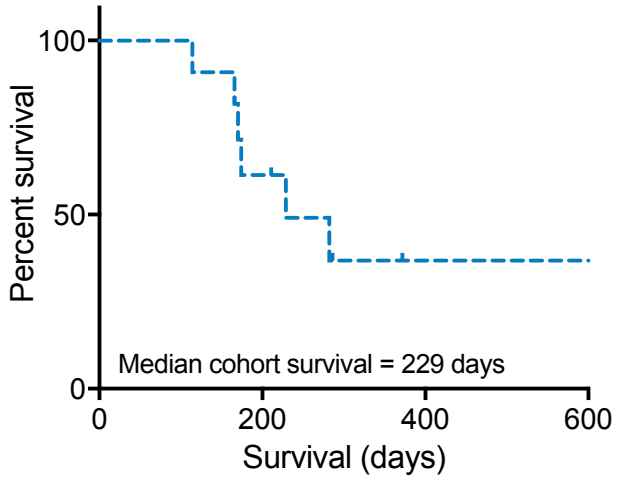


Figure 4.15: The Sheffield Living Biobank cohort survival – Kaplan-Meier survival analysis of 11 patients undergoing surgical resection of a glioma in Sheffield whose specimens were also used to generate primary GSC lines. Histological tumour grades include 10 patients with WHO grade IV tumours (glioblastoma) and 1 patient with a WHO grade II astrocytoma (see Table 1 for additional histological and molecular details).

4.6.2 Differences in IR response between 2D and 3D GSCs

Our comparison of radiation response between GSCs cultured in 2D and 3D conditions revealed marginally greater radiosensitivity in 3D conditions (with $DMF_{0.37}$ of 1.27 and 1.13 in G1 and G7 GSCs, respectively – see Figure 4.3). In contrast, Gomez-Roman *et al.* (2017)[108] did not detect any significant difference in radiosensitivity between G7 GSCs in 2D and 3D conditions, but did find that R10 GSCs (not evaluated in our studies) displayed greater radiosensitivity in 3D conditions, and G1 GSCs were not evaluated in this study. Importantly, these studies cannot represent a direct comparison since Gomez-Roman *et al.* (2017)[108] used additional 'stem' media supplementation with VEGF, which has recently been implicated in 3D scaffold embedded GSC radioresistance, but with no similar influence on 2D GSC cultures[(107)]. This study[(107)] revealed that, specifically in 3D conditions, VEGF/AKT signalling was associated with an upregulation of homologous recombination machinery, as evidenced by increased numbers of RAD51 foci following IR exposure, and suggests that the radioresistance of GSCs used in our studies could have been further enhanced by VEGF supplementation. Again, this would have promoted a 3D model more consistent with the

microenvironment of perivascular niche GSCs, where VEGF is abundant[448]. Additional methodological differences may also have contributed to these discordance assessments of 2D vs 3D radiosensitivity, including differences in cell line passage number and differential thresholds for counting colonies in 3D culture – since, due to the translucency of Alvetex™ scaffolds, it is not possible to directly examine colonies using light microscopy and count cells to establish minimum colony size/number of cells.

4.6.3 Developing the Sheffield Living Biobank of clinically- and surgically-relevant glioblastoma models

Establishment of the Sheffield Living Biobank represents the creation of a foundational resource which is expected to enrich (and be enriched by) multiple ongoing and future glioma studies. Living biobanks of *ex vivo* models for other cancer types including ovarian[449] and liver[450] cancer have been able to recapitulate patient-specific histological features, molecular landscapes and therapeutic sensitivities – alluding to the future potential of these resources to encompass patient-specific *in vitro* cancer avatars used to evaluate a range of therapeutic options and inform more individualised treatment options. Although characterisation of patient-specific GSC models within the Sheffield Living Biobank is at an early stage, Sheffield GSCs tested to date (including OX-3, OX-4, OX-5) have demonstrated high putative stem cell marker mRNA expression relative to matched bulk populations, Cambridge GSCs[99] and established lines (Figures 4.5 and 4.10). Further focused characterisation of these models is needed to confirm the maintenance of key molecular features observed in each parental tumour (Table 4.1) including IDH1/2, MGMT methylation, TERT promotor, and BRAF status. Additionally, recently secured funding will allow more global characterisation of these *ex vivo* models and their associated parental tumours using WGS/WES and RNAseq. Combined with the future availability of WGS data for patients recruited into the national 100,000 Genomes Project with a matched GSC line(s), our ongoing studies are expected to help develop an excellent resource to enhance glioma studies and help understand patient-specific responses to therapy.

Random intratumoural heterogeneity models generated during these studies using multiple samples from *within* a single patient's tumour, and post-surgical residual disease models using samples from the tumour and adjacent infiltrated brain from a single patient's *en bloc* partial lobectomy specimen, to derive GSC lines in parallel (Figures 4.6 & 7) are expected to support future studies interrogating features of regional heterogeneity and if these

features can be successfully maintained *ex vivo*. These models complement previous studies which utilised multi-region surgical sampling to illustrate that spatially distinct samples from within a single tumour exhibited variability in the prevalence of key genetic events including loss of PTEN, loss of CDKN2A/B and EGFR gain/amplification[15]. A recent study by Spiteri *et al*. (2018)[313] which incorporated fluorescence-guided sampling of more distant infiltrative and subventricular zone glioblastoma cells supports a hypothesis of genetically distinct tumour subclones which arise early in the evolution of glioblastoma demonstrating a greater functional capacity to invade deeper into normal brain and therefore be more likely to represent disease left behind after surgery (residual disease)[424,451]. The parallel *ex vivo* primary, patient-derived lines developed and presented in this Chapter build on these prior studies by establishing models suitable to interrogate whether and how previously observed intra-tumoural spatial genetic heterogeneity will translate to functional heterogeneity, including intracellular responses to DNA damaging IR and temozolomide treatments (which represent standard of care adjuvant management for patients with glioblastoma) and subclonal divergence in therapeutic sensitivity. Crucially, post-surgical residual disease cannot be considered equivalent to glioblastoma at the time of recurrence, which may harbour a range of genomic changes following chemoradiotherapy[223]. We demonstrate for the first time that distant infiltrative GSCs derived from brain parenchyma adjacent to the contrast-enhancing tumour within partial lobectomy specimens exhibit elevated stem cell marker mRNA expression (Figure 4.10B), with the potential for divergent DDR expression (Figure 4.11), both of which are likely to have implications for the responsiveness of residual GSC models to current therapy. These results are consist with the study of glioblastoma tumour organoids by Hubert *et al*. (2016)[102], which identified a higher proportion of SOX2+ cells at the rim of organoids relative to the core, and unpublished work recently presented at the Society for Neuro-Oncology (SNO) Annual Meeting (November 2019) confirming higher stem cell marker expression in cell lines derived from resection cavity samples relative to those near the centre of the tumour. However, our novel pragmatic methodology using rare *en bloc* partial lobectomy specimens provides the opportunity to interrogate more distant infiltrative cells, and thus maximise the chance of defining quantitative differences and qualitative nuances between resected and typically residual disease. Developing a more detailed understanding of treatment naive post-surgical residual disease, and how this may differ from resected disease (which forms the basis of current glioblastoma models), is likely to provide useful insights informing more effective treatment of glioblastoma in the newly diagnosed setting.

4.6.4 Ongoing preclinical TTFields 3D model development

Our progress in customising 3D Alvetex™ scaffold-based models represent some of the first studies to establish more clinically-relevant 3D *in vitro* TTFields culture and delivery systems. A limited number of recent studies have applied TTFields to glioma neurospheres as a 3D culture model. Chang *et al.* (2017)[452] used representative brightfield microscopy images to highlight changes in neurosphere size/shape and infer efficacy alongside quantitative traditional 2D studies[(452)], perhaps highlighting the challenges of robust quantification of therapeutic response in 3D culture systems. In a subsequent study, Chang *et al.* (2018)[453] used fluorescence and bioluminescence imaging to interrogate the effects of TTFields in established U87 cells transfected with lentiviruses expressing a fusion protein of GFP and firefly luciferase. Although temporal quantification of neurosphere fluorescence demonstrated a reduction at 24 hours following TTFields therapy, the size of this effect is relatively subtle and may reflect an inherent lack of sensitivity associated with using fluorescence intensity quantification from 2D images to infer the growth dynamics of a 3D structure. Furthermore, the suitability of bioluminescence imaging to quantify the therapeutic effects of TTFields can be excluded since, paradoxically, neurospheres treated with TTFields demonstrated increased photon flux, which was confirmed to be associated with a transient TTFields-induced increase in cell membrane permeability. Arguably, 3D Alvetex™ scaffold-based clonogenicity may represent a more suitable, sensitive and reproducible methodology to quantify the therapeutic effects of TTFields and assess the capability of cells post-treatment to recapitulate a given tumour of tumour clone. Certainly, our assessment of inter-rater reliability (Chapter 2 – Figure 2.6) and 3D clonogenic data presented in Figure 4.3, Figure 4.9, and extensively in the following Chapter, support the application of our customised scaffold-based 3D model to TTFields studies to generate robust and highly reproducible data. Of great interest, a 3D multi-channel microfluidic culture platform to assess the effects of TTFields has recently been developed by Pavesi *et al.* (2016)[454]. This system allowed established non-brain cancer cell lines (MDA-MB-321, breast adenocarcinoma, and; A549, lung adenocarcinoma) to grow in a central channel within a type I collagen suspension whilst flanked by fluidic channels supplied with culture medium on either side. Use of the model was able to establish potential efficacy of TTFields in cancer cell lines with no similar effect on endothelial cells when tested in the model. However, efficacy was determined by a reduction in cancer cell density, with clonogenicity unestablished. Therefore, our ongoing development of a customised Alvetex™-scaffold-

based 3D culture and TTFields delivery system is expected to provide a valuable tool for the neuro-oncology research community.

Collectively, the validation of existing and generation of new clinically- and surgically-relevant glioblastoma models reported in this Chapter are expected to support preclinical glioblastoma research at our institution, and potentially elsewhere, over the next few years.

Chapter 5 – FA pathway-based DDR targeted combinations

5 CHAPTER 5 – FA pathway-based DDR targeted combinations to enhance chemotherapy and radiotherapy response in glioblastoma stem cells

5.1 Introduction

5.1.1 A new foundation for DNA damage response targeted combinations

Failure to substantially improve survival rates for patients diagnosed with glioblastoma over the last 40 years[59] implies a paradigmatic shift in the types of strategies developed and trialled to overcome therapeutic resistance is desperately needed. Although optimising the extent of surgical resection[83,455], the addition of temozolomide chemotherapy[10,11], and recent introduction of TTFields therapy[76,427] each incrementally improve survival, disease recurrence remains universal. The propensity of glioblastoma to escape immunosurveillance has limited progress in the development of effective immunotherapies compared to other types of cancer[456], and numerous molecularly targeted therapies including against EGFR (rindopepimut), VEGF (bevacizumab) and integrins (cilengitide) have failed to improve patient survival in large clinical trials[91].

Although radiotherapy remains the single most effective adjuvant therapy for glioblastoma[457], recent post-mortem studies revealing brainstem infiltration of glioblastoma cells from distant supratentorial disease[458] suggest that fractionated focal irradiation to the gross tumour volume with a 2-3cm margin as delivered within the current standard-of-care Stupp regimen for patients with newly diagnosed glioblastoma is not sufficient to abrogate extensive, early disease infiltration. Strategies which both maximise local tumour cell killing and have the potential to demonstrate high CNS-wide efficacy are urgently needed.

The rationale to develop FA pathway-based DDR targeted combinations as a novel anti-glioma strategy is broad and compelling. Firstly, since DNA damaging radiotherapy and chemotherapy continue to represent the cornerstone of adjuvant treatment, strategies which substantially enhance, rather than aim to supplant, these modalities are more likely to gain clinical acceptance and be integrated into patient care. Secondly, extensive intratumoural heterogeneity associated with glioblastoma[13-15,313] support a high likelihood of intrinsically resistant and/or the acquisition of subclones which are resistant to selective

pressures applied by any single targeted therapy (see Chapter 1 – Section 1.4.7). Thirdly, recalcitrant GSC subpopulations demonstrate heightened DDR activity which underpin radio- and chemoresistance[18,19] (see Chapter 1 – Section 1.5.1), however the extensively interconnected nature of DDR networks[1] almost certainly endow GSCs with a degree of functional redundancy to support resolution of therapy-induced DNA damage even in-spite of single DDRi strategies. Finally, although there is a risk that combination therapies may portend greater toxicity, strategies based on targeting the FA pathway – a fundamental DDR process required for the resolution of replication fork impeding lesions which has previously been shown to be inactive in normal brain, but re-activated in glioblastoma[22] – might provide a robust basis for safe, cancer-selective combination DDR-targeting therapies.

In this Chapter, the first evaluation of FA pathway-based DDR-targeted combinations in clinically-relevant patient-derived GSC models are presented as potential strategies to radiosensitise and chemosensitise glioblastoma towards substantial enhancement of locoregional and pan-CNS efficacy, respectively.

RESULTS

5.2 Clinical relevance of FA pathway gene expression in gliomas

5.2.1 FA pathway functional groups are highly expressed in gliomas and associated with poor survival

The FA pathway is frequently activated in response to DNA strand breaks, replication arrest, and other cytotoxic secondary lesions induced by alkylating and cross-linking chemotherapeutic agents[2,129,130]. Patients who suffer from Fanconi anaemia, typically as a result of biallelic inactivation of one of currently 22 FA pathway genes, are exquisitely sensitive to a number of chemotherapeutic agents including interstrand cross-link (ICL) inducing therapies[131]. Since, adjuvant therapies commonly used in the clinical setting to treat patients with a high-grade glioma (radiotherapy and temozolomide) have also been demonstrated to activate the FA pathway[20-22], and we have previously demonstrated high levels of FANCD2 protein expression in high grade gliomas (Patil *et al*. 2014[22]), we hypothesised that the expression of FA pathway genes may be related to intrinsic therapeutic resistance and disease course.

FA pathway mRNA expression and glioma grade

Using transcriptomic data from 329 glioma patients retrieved from a web-based repository (REMBRANDT database), the mRNA expression of FA pathway genes in patient samples from grade IV glioma (glioblastoma), grade II-III glioma, or normal tissue were categorised into the following broad functional groups: **core complex** (*FANCA, FANCB, FANCC, FANCE, FANCF, FANCG/XRCC9, FANCL, FANCM, FANCT/UBE2T and FANCP/SLX4*); **ID complex** (*FANCD2* and *FANCI*), and; **downstream** FA pathway effectors (*FANCD1/BRCA2, FANCJ/BRIP1, FANCN/PALB2, FANCO/RAD51C, FANCR/RAD51, FANCS/BRCA1, FANCU/XRCC2, FANCV/REV7/MAD2L2, FANCW/RFWD3, FANCQ/ERCC4/XPF*). Analysis of the mean FA pathway functional group mRNA expression within patient samples revealed consistently elevated expression in glioma tissue relative to normal (non-neoplastic) samples (Figure 5.1). Importantly, the mRNA expression of each FA pathway functional group was significantly higher in glioblastoma samples compared to lower grades of glioma (grade I-III), consistent with a relationship between tumour aggressiveness and FA pathway expression.

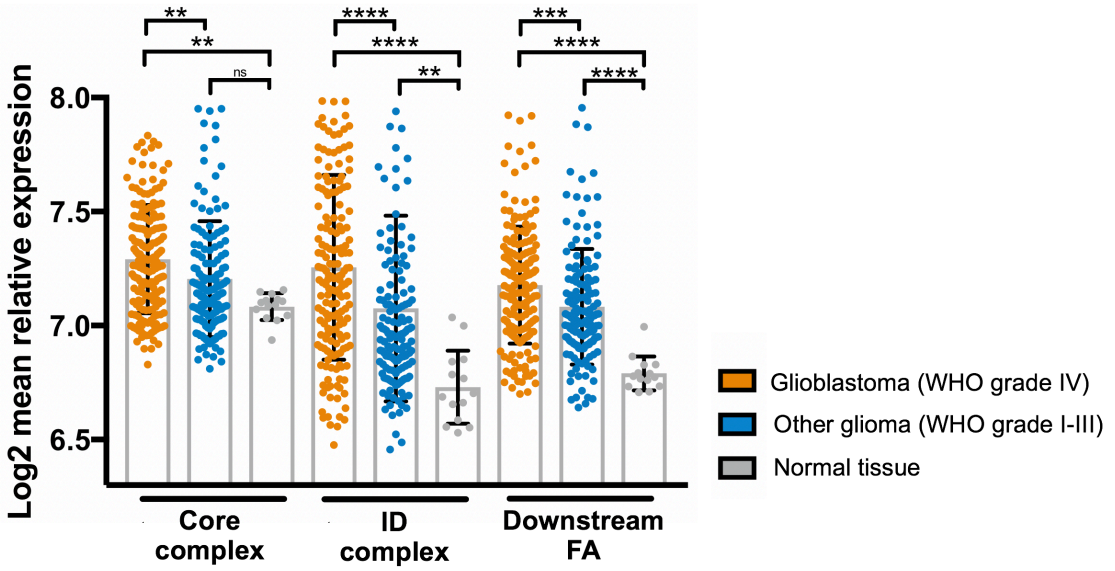


Figure 5.1: mRNA expression of FA pathway genes increases with glioma grade – Comparative analysis of FA pathway functional group expression data for patients (n=329) in the REMBRANDT database. Glioblastoma (WHO grade IV) demonstrate significantly greater expression than WHO grade I-III gliomas, for each functional group (p=0.0015, <0.0001, 0.009 for core complex, ID complex and downstream FA genes respectively), and normal tissue (p=0.0013, <0.0001, and <0.0001 respectively). Fourteen normal tissues samples are available in the data set. Each data point represents mean expression data for the genes that comprise a functional FA sub-complex for an individual patient (error bars represent +/- SD).

Canonical association of FA pathway functional groups

If the products of FA genes function within an active, canonical DDR process in gliomas, one would expect patients demonstrating high mRNA expression of a particular FA pathway functional group to similarly exhibit elevated expression of the remaining functional groups, since these are schematically interlinked. Indeed, correlative analysis of mean mRNA expression data confirmed strong (i.e. correlation co-efficients between 0.6-0.79[459]), statistically significant correlations between the 3 canonically associated FA pathway functional groups in patients with glioblastoma and grade I-III gliomas (Figure 5.2). Consistent with a glioma-specific importance of FA pathway activity, no correlation between the mRNA expression of FA functional groups was observed in patients with normal tissue samples. Therefore, the strong correlation between the expression of canonically associated groups of FA pathway genes observed in gliomas is indicative of a functional DDR pathway in these tumours.

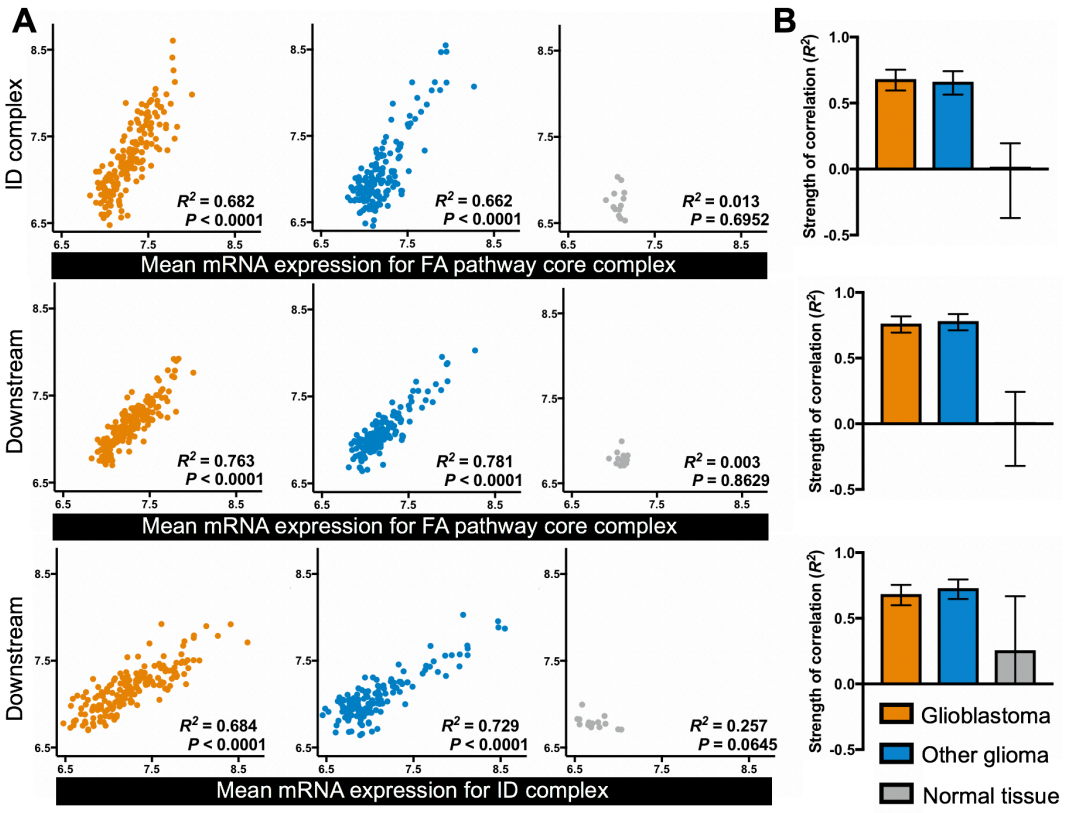
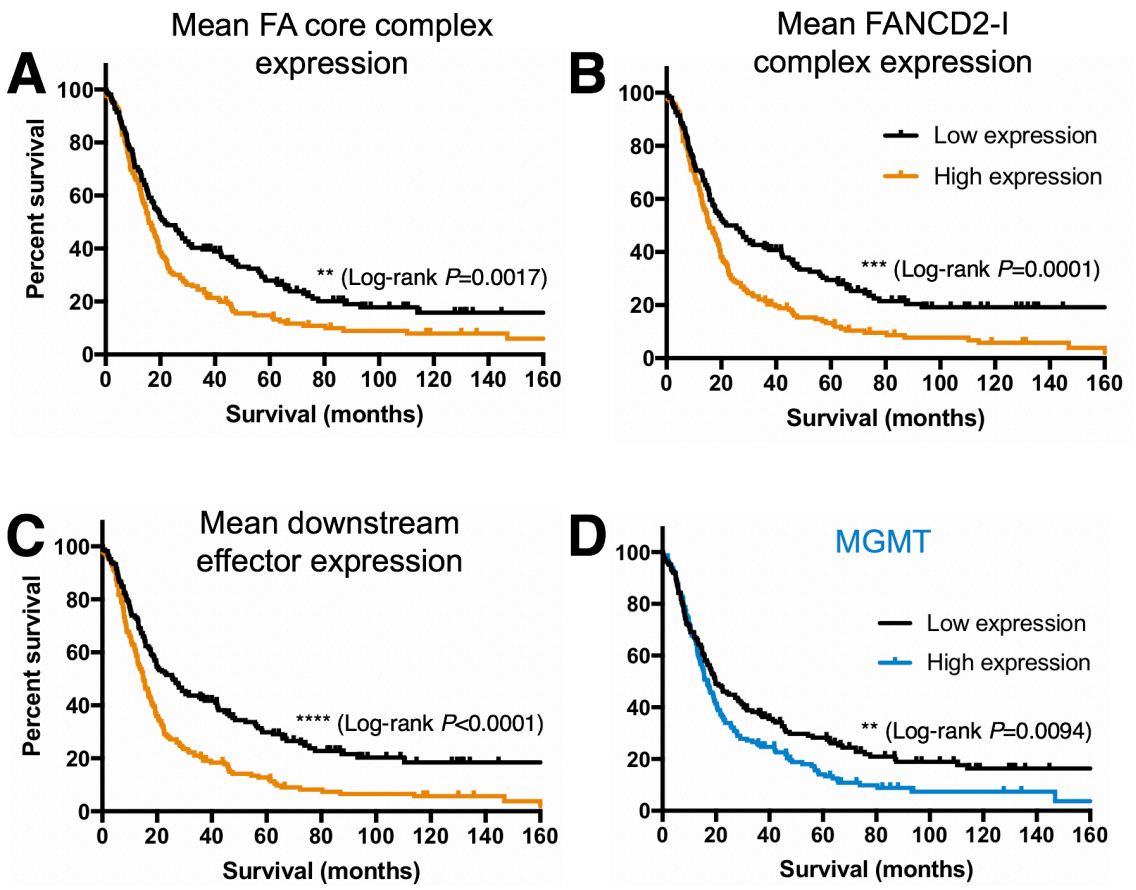


Figure 5.2: Canonical association of mRNA expression levels for FA pathway functional complexes is apparent in gliomas – A-B. Correlative analysis (A) and strength of Pearson correlation coefficients – R^2 (B) for FA pathway functional group mean mRNA expression data pertaining to patients with a glioma (n=329) in the REMBRANDT database. Expression data for the functional groups demonstrate significant positive correlations (between core vs ID complex; core vs downstream, and; ID complex vs downstream mean mRNA expression), consistent with canonical activity, in glioblastoma (grade IV gliomas) and grade I-III gliomas but not in normal tissue. Values = log2 mean relative expression. Error bars represent 95% confidence intervals for strength of correlation (R^2).

FA pathway expression and patient survival

Since DNA damaging treatments represent a cornerstone of current clinical management for patients with a glioma and the FA pathway plays a fundamental role in facilitating DNA damage repair, we hypothesised that the expression of FA pathway genes would influence therapeutic resistance and, as a consequence, patient survival. To investigate this further, survival data for all patients in the REMBRANT cohort were dichotomized on the basis of FA pathway functional group mRNA expression. This analysis demonstrated significant associations between high FA pathway expression (core complex, ID complex and downstream FA genes) and poor survival that were comparable to that with expression of the established prognostic glioma biomarker MGMT (Figure 5.3). The association between high expression and poor survival demonstrated a greater putative effect with genes known to function more distally in the FA pathway. For example, high mRNA expression of core complex genes, ID complex genes and downstream FA genes were associated with 5.8, 6.3 and 10.9 month reductions in median overall survival, respectively (Figure 5.3E). Importantly, analysis including only patients with a WHO grade IV glioma (glioblastoma) did not reveal any statistically significant association between the expression of FA pathway genes and overall survival (data not shown). Together, these data suggest that, rather than holding any specific utility to stratify patients with a grade IV glioma into prognostic groups, the prevalence of high FA pathway expression in gliomas increases with tumour grade, representing a potentially exploitable feature of more aggressive cancer biology which is pervasive in the most challenging to treat tumours.



E

	Five-year overall survival			
	Core	**ID**	**Downstream**	**MGMT**
Low expression	27.1%	28.7%	29.1%	28.3%
High expression	14.0%	12.6%	12.0%	14.1%
Δ 5-year survival	***13.1%***	***16.1%***	***17.1%***	***14.2%***
	Median overall survival (months)			
Low expression	21.7	21.9	25.9	19.8
High expression	15.9	15.6	15.0	16.7
Δ median survival	***5.8***	***6.3***	***10.9***	***3.1***
	Overall survival hazard ratio (log-rank - high/low expression)			
Hazard ratio	1.45	1.59	1.73	1.36
95% CI	(1.14-1.84)	(1.25-2.01)	(1.36-2.10)	(1.07-1.72)

Figure 5.3: High mRNA expression of FA pathway functional groups is associated with poor overall survival in glioma patients – A-C. Kaplan-Meier survival analysis of patients with a glioma (all grades) in the REMBRANDT cohort dichotomised by high/low expression (cut off at median mRNA expression value) of: core complex genes (A); ID complex genes (B); downstream FA genes (C), and; expression of the well-established prognostic biomarker MGMT as a positive control (D). E. Comparison of 5-year and median overall survival values.

5.2.2 *Glioblastoma stem cells demonstrate elevated FA pathway gene expression relative to bulk populations*

Within brain tumours, previous studies have identified cellular subpopulations of cancer stem cells (CSCs) which demonstrate 'stem-like' properties including substantially heightened capacity for self-renewal and the ability to recapitulate the cellular phylogenetic hierarchy of an original tumour[16,460] (Detailed discussion in Chapter 4 - Section 4.1.1-2). In the context of grade IV glioma, glioblastoma stem cells (GSC) – as pragmatically (if imperfectly) defined by the presence of stemness markers including CD133[16,373], nestin[373,429] and SOX2[373,461] – are reported to exhibit up to 1,000 times the tumorigenicity of matched non-stem ('bulk') populations[35]. Furthermore, GSC demonstrate enhanced therapeutic resistance to current DNA damaging treatments, with heightened expression and capacity of key DDR mechanisms including activation of the ATM-CHK2 axis and ATR-CHK1 reported, that are postulated to underlie the recalcitrant nature of GSC subpopulations[18]. However, to date no previous studies have investigated the FA DNA damage repair pathway specifically in treatment resistant GSC subpopulations. As such, we speculated that, consistent with their heightened resistance to temozolomide and irradiation (both of which activate the FA pathway[20-22]), GSCs might exhibit constitutively high expression of FA pathway genes.

Using matched primary, patient-derived GSCs and tumour bulk cells (propagated in media enriched with FCS to facilitate differentiation – see Chapter 2 – Section 2.12.6 and Chapter 4 – Figure 4.1) TaqMan™ RT-PCR analysis revealed significantly elevated mRNA expression of FA pathway genes in G1 GSCs (7 of 8 genes) and G7 GSCs (2 of 8 genes, but with a general trend towards increased expression in the other 6 genes) relative to bulk populations (Figure 5.4). Interestingly, genes implicated in the ID complex and downstream FA pathway were generally more highly expressed than core complex genes – a finding consistent with lower 5-year and median overall survival with high ID complex or downstream FA expression (relative to high core complex expression) in patient samples (see Figure 5.3E). It is therefore tempting to consider that the lower survival rates observed in cohorts stratified by high distal (ID and downstream) FA pathway gene expression might be mediated through particularly high expression in treatment resistant GSC subpopulations within patient tumours.

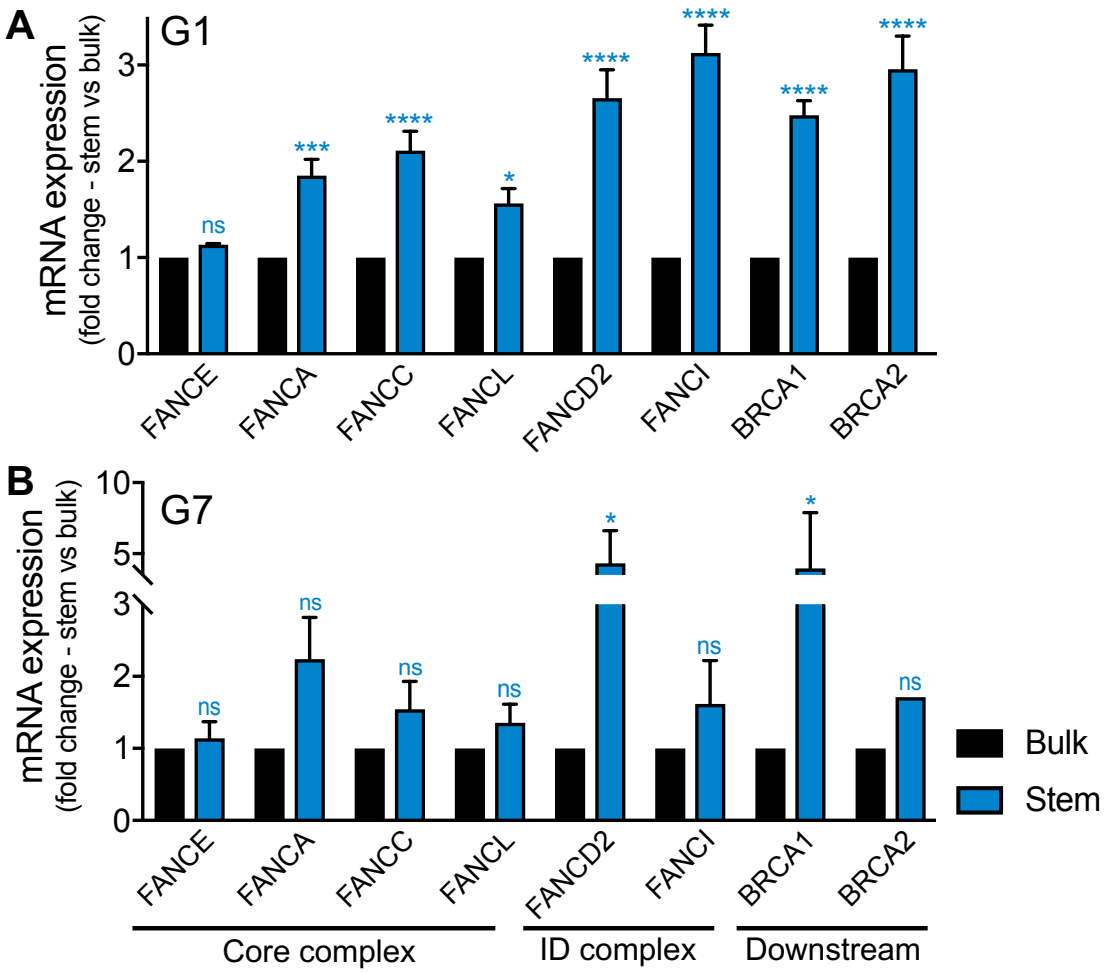


Figure 5.4: FA pathway mRNA expression is elevated in patient-derived glioblastoma stem cells – A-B. TaqMan™ RT-PCR analysis of FA pathway gene expression in untreated G1 (A), and G7 (B) patient-derived glioblastoma stem cells and matched bulk populations. Cells were plated then incubated for 24 hours prior to RNA extraction. Data points shown represent the mean of 3 independent experiments. Error bars represent the SEM.

5.2.3 Activation kinetics of the FA pathway and other key DDR processes in glioblastoma stem cells

Next, we aimed to characterise the magnitude and duration of FA pathway activation following DNA damaging therapy in GSCs. Following exposure to temozolomide chemotherapy, both G1 and G7 patient-derived GSCs demonstrated a detectable increase in FANCD2 monoubiquitination within 30 minutes, which was sustained for at least 24 hours. Compared to untreated cells, the peak fold increase in Ub-FANCD2 in proportion to the abundance of non-ubiquitinated FANCD2 – as described by the normalised L:S ratio – was 1.61 and 2.39 in G1 and G7 GSC, respectively. Additionally, FANCL (the FA core complex E3 ligase), FANCI (the heterodimeric partner of FANCD2 within the ID complex), and the downstream homologous recombination proteins FANCS/BRCA1 and FANCD1/BRCA2 were all detectable in primary GSCs. However, the abundance of FANCD1/BRCA2, and to

a lesser extent FANCS/BRCA1 and FANCI appeared to decrease following treatment with temozolomide for greater than 12-18 hours (Figure 5.5).

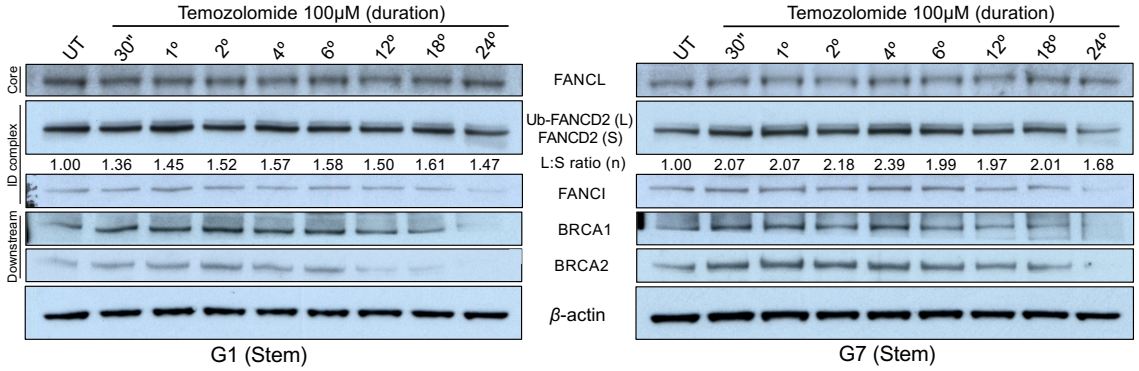


Figure 5.5: The dynamics of FA pathway activation following temozolomide chemotherapy in 2D patient-derived glioblastoma stem cells – G1 or G7 glioblastoma stem cells were plated for 24 hours prior to treatment with temozolomide chemotherapy (100μM) at various time points and further incubated to provide the indicated duration of exposure, excluding untreated (UT) controls. Cells were subsequently lysed and Western blotting performed. To determine FA pathway activation, the normalised ratio of Ub-FANCD2 (L) to FANCD2 (S) (normalised to DMSO only treated cells) was calculated for each treatment as previously described[216] and shown beneath the relevant bands. Each blot represents a single independent experiment due the nature of performing a time course over 24 hours.

In order to rationally develop FA pathway-based DDRi combinations it was also necessary to establish the integrity of related DDR process activation following DNA damaging therapy. Western blot analysis confirmed enhanced phosphorylation of key DDR proteins following exposure to temozolomide chemotherapy. Activation of the ATM-CHK2 axis was confirmed through increased phosphorylation of ATM at serine 1981 (pATM S1981) and CHK2 at threonine 68 (pCHK2 Thr68). Additionally, increased phosphorylation of DNA-PKcs at serine 2056 (pDNA-PKcs S2056) was evident. Activation of the ATM-CHK2 axis and DNA-PKcs, both processes integral to efficient DNA DSB repair, was evident within 30 mins of exposure to temozolomide and long-lasting (at least 12-18 hours), with maximal activation around 4-6 hours post treatment. ATR-CHK1 axis activation was demonstrable within 30-60 minutes, as established by increased CHK1 phosphorylation at serine 345 (pCHK1 S345) and appeared to last at least 12 hours. Additionally, both G1 and G7 GSCs continued to exhibit detectable PAR levels throughout the duration of treatment, consistent with intact PARP1 catalytic activity (Figure 5.6). Interpretation of any potential changes in the degree of PARP1 protein expression however, is more challenging, since the specific antibody used has been reported within our Department to lose antigenic epitope specificity during conditions of DNA damage (personal communication – Dr Helen Bryant).

In summary, these data confirm that both G1 and G7 GSCs demonstrate activity of FANCL, PARP1, ATR and ATM – all of which are functional during conventional DNA damaging

therapy, including robust FANCD2 monoubiquitination (by FANCL), ATM-CHK2 axis activation and ATR-CHK1 axis activation. Consequently, both patient-derived GSC lines were deemed to be appropriate cells for the evaluation of FA pathway based DDRi combinations which incorporate these targets.

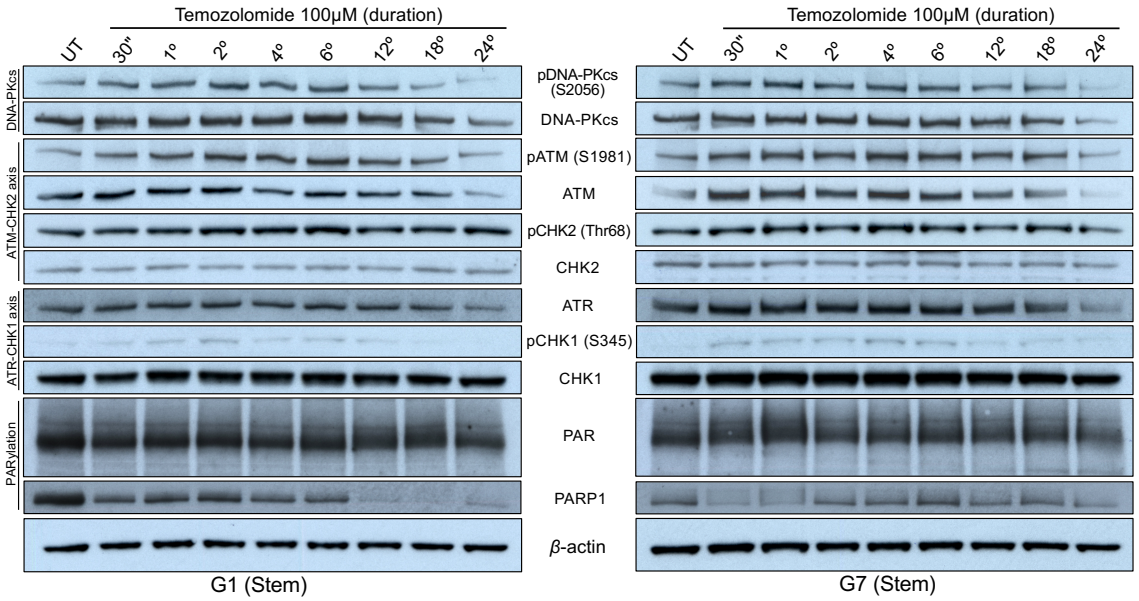


Figure 5.6: The dynamics of related DNA damage response processes following temozolomide chemotherapy in 2D patient-derived glioblastoma stem cells – G1 or G7 glioblastoma stem cells were plated for 24 hours prior to treatment with temozolomide chemotherapy (100μM) at various time points and further incubated to provide the indicated duration of exposure, excluding untreated (UT) controls. Cells were subsequently lysed and Western blotting performed. Each blot represents a single independent experiment due the nature of performing a time course over 24 hours.

5.3 Targeting the FA pathway to overcome inherent therapeutic resistance in glioblastoma stem cells

After establishing that elevated FA pathway expression is associated with aggressive, high-grade tumour biology, poor patient survival, and treatment resistant GSC subpopulations, we reasoned that pharmacological inhibition of the FA pathway should represent an effective therapeutic strategy to overcome the recalcitrant nature of GSCs. Below, the therapeutic potential of ouabain (a medication previously used to treat heart failure), F76 (a novel inhibitor of the FA pathway, nFAPi) and curcumin (a compound previously established to affect FA pathway activity) to inhibit the FA pathway in established and clinically-relevant glioblastoma stem cell models are assessed.

5.3.1 *The 'heart failure' medication ouabain inhibits the FA pathway and potently radiosensitises glioblastoma cell cultures*

The cardiac glycoside ouabain binds and inhibits cellular Na^+/K^+-ATPase enzymes which are essential for life[288]. Given this mechanism, it is unsurprising that ouabain exhibits a narrow therapeutic index with the potential for substantial toxicity and even lethality in supra-optimal doses[462]. Despite this, ouabain has traditionally been used to treat heart failure for decades due to the positive cardiac inotropic effects of inhibiting Na^+/K^+-ATPase enzymes[463]. Interestingly, a previously published drug screen of 1280 compounds in the LOPAC1280 chemical library by Jun *et al.* (2013)[464] identified ouabain as an effective inhibitor of the FA pathway in U2OS osteosarcoma cells[19]. In view of this, and the potential advantages of repurposing a drug that has previously been used in the clinic, we sought to establish whether ouabain might effectively inhibit the FA pathway in glioblastoma cells and elicit a sensitising effect to DNA damaging therapy.

Establishing an optimal dose for studies using ouabain

Preliminary investigations using the MTT cell viability assay revealed the exposure of 4 established glioblastoma cultures (U87, U251, LN18 and T98G) to ouabain for 120 hours (5 days) resulted in substantial toxicity with LD_{50} values between 58-140nM (See Figure 5.7A). As expected, reducing the duration of ouabain exposure to 24 hours minimised cytotoxicity, providing LD_{50} values more amenable to combinatorial studies (LD_{50} values between 256nM and 7.2μM, see Figure 5.7B). Due to the considerable cost of Matrigel™ coating 96-well plates to optimise the use of GSCs in MTT cell viability assays, clonogenic survival assays were preferred to assess GSC survival following ouabain monotherapy. Patient-derived G7 GSCs were initially exposed to ouabain for 120 hours resulting in a profound reduction in clonogenic survival in both 2D and 3D conditions (Figure 5.8A). Further studies exposing G1 and G7 GSC to ouabain for 24 hours in 2D conditions established LD_{50} values of 200nM and 187nM respectively. These values were used to inform studies assessing the effect of ouabain on FA pathway inhibition, to help identify a dose capable of reducing the monoubiquitination of FANCD2, but without impractical toxicity.

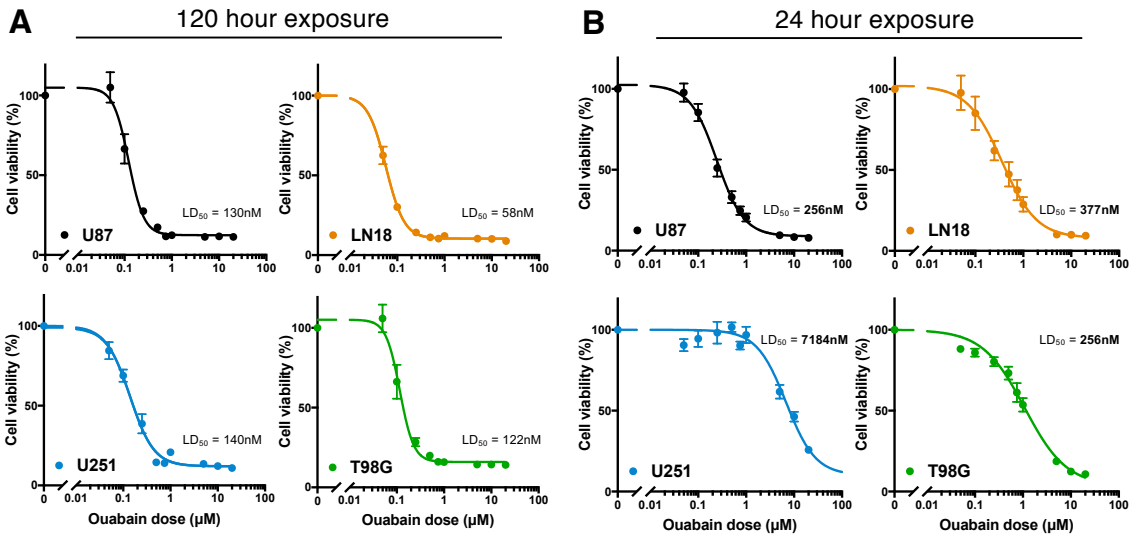


Figure 5.7: Ouabain effect on cell viability in established glioblastoma cultures following 24 hour and 120 hour exposure – U87, LN18, U251 or T98G glioblastoma cells were plated for 24 hours prior to exposure to either DMSO (0μM) or various doses of ouabain (50nM to 20μM). Cells were incubated for a further 120 hours before the MTT assay was used to compare cell viability. For the shorter exposure time, media was replaced at 24 hours post treatment. Data points shown are the mean from 3 independent experiments with error bars representing the SEM. A-B. Cell viability after: (A) Ouabain exposure for 120 hours; (B) Ouabain exposure for 24 hours. Data points shown represent the mean of 3 independent experiments. Error bars represent the SEM. *(Data shown were produced by Mr Dawoud Dar working under my direct supervision).*

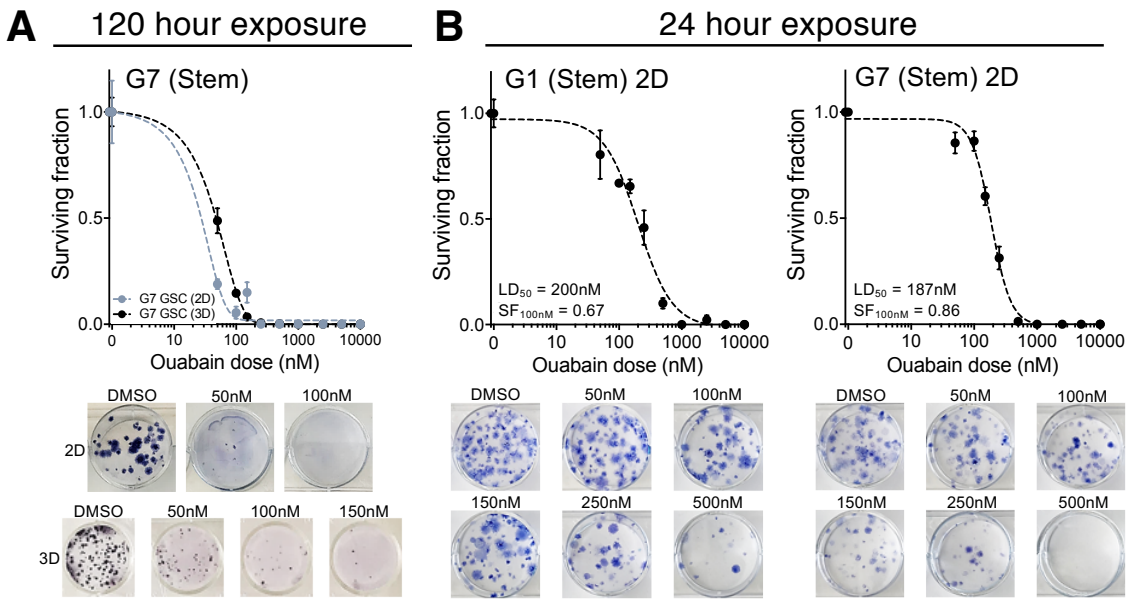


Figure 5.8: Ouabain effect on clonogenic survival in primary, patient-derived glioblastoma stem cells following 24 hour and 120 hour exposure – G1 or G7 GSCs were seeded 24 hours prior to exposure to either DMSO (0μM) or various doses of ouabain (50nM to 10μM). Cells were incubated for a further 21 days. For the shorter exposure time, stem media was replaced at 24 hours post treatment. Subsequently, colonies were stained and quantified. A-B. Clonogenic survival curves (*upper*) and representative images (*lower*) after: (A) Ouabain exposure for 120 hours in G7 GSCs; (B) Ouabain exposure for 24 hours in G1 and G7 GSCs. Data points shown represent the mean of 3 experimental replicates from one independent experiment. Error bars represent the SEM. Error bars not shown where these are smaller than the corresponding symbol. *(Data shown were produced by Miss Aurelie Vanderlinden working under my direct supervision).*

Ouabain inhibits the FA pathway in glioblastoma cells

Treatment of established (U87) and primary, patient-derived GSC (G1 and G7) cultures with ouabain reduced DNA damage-induced FANCD2 monoubiquitination following temozolomide exposure (Figure 5.9). The effect of ouabain on preventing FA pathway activation appeared to be dose-dependent, however, with even relatively low doses of ouabain able to mediate a substantial reduction in temozolomide-induced FANCD2 monoubiquitination (250nM in U87 cells and G7 GSCs; 100nM in G1 GSCs). Interestingly, 100nM ouabain did not reduce FANCD2 monoubiquitination in G7 GSCs (Supplementary Figure 5.1), highlighting patient-specific differences in GSC susceptibility to ouabain-mediated inhibition of the FA pathway. Consistent with studies by Jun *et al.* (2013)[464], ouabain exposure was also observed to reduce the overall protein expression of FANCD2, which is likely to further restrain FA pathway activity, as indicated by very low L:S ratio (nt) values (which reflect L:S ratios adjusted for the total FANCD2 abundance relative to untreated cells).

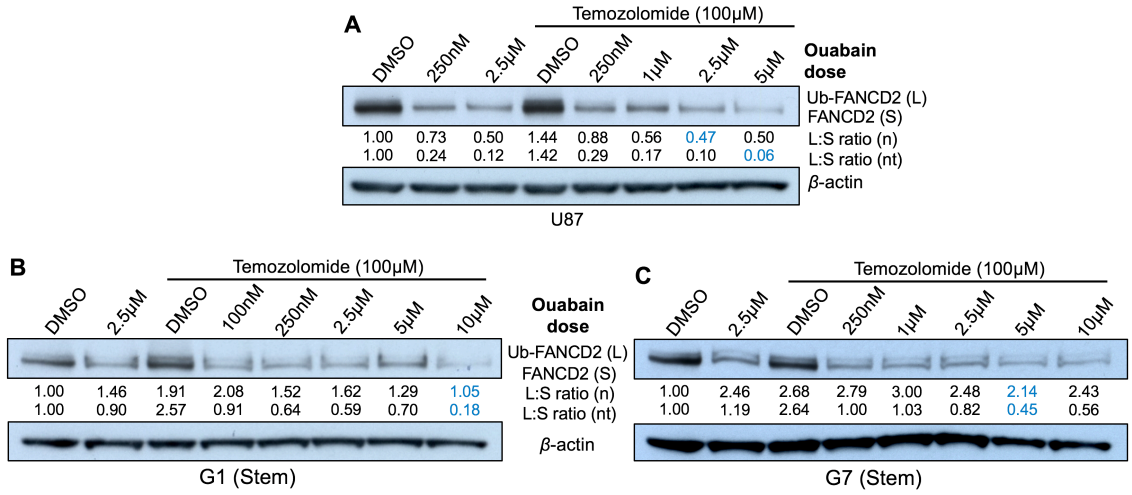


Figure 5.9: The 'heart failure' medication ouabain inhibits the FA pathway in 2D established and primary, patient-derived glioblastoma stem cells – Established U87 cells or G1/G7 primary GSCs were plated for 24 hours prior to exposure to the indicated doses of ouabain or DMSO then DNA-damaging temozolomide chemotherapy 1 hour later. Cells were incubated for a further 16 hours prior to lysis and Western blotting. Blots confirm pharmacological inhibition in: A. U87 glioblastoma cells; B. G1 GSCs, and; C. G7 GSCs. The signal intensity ratio of monoubiquitinated FANCD2 (Ub-FANCD2) to FANCD2 was calculated to determine L:S ratios. L:S ratios were normalised to the DMSO only (0μM temozolomide) control (n). Then normalised L:S ratios were adjusted for the total FANCD2 intensity (Ub-FANCD2 + FANCD2) to provide a comparable measure of FA pathway inhibition (nt). Using these measures, the data demonstrate potent FA pathway activation following temozolomide exposure, which is inhibited by ouabain administration 1 hour prior to chemotherapy (values indicating most effective inhibition highlighted in blue). Each Western blot was performed in 2 independent experimental repeats. *(Data shown in A and B were produced by Mr D Dar and Miss Aurelie Vanderlinden, respectively – both working under my direct supervision; C was produced by the author).*

Ouabain as a potent radiosensitiser in glioblastoma

Optimised doses were used to evaluate the potential of ouabain as a radiosensitising agent using an established glioblastoma cell line and more clinically-relevant primary, patient-derived GSCs. We found that U87 glioblastoma cells tended to form loosely-packed, overlapping colonies leading to unreliable quantification (data not shown) – we therefore transitioned to use LN18 cells as the established glioblastoma cell line of choice. These cells exhibited an LD_{50} of 377nM following 24 hours of ouabain exposure (Figure 5.7B) and reliably form discrete colonies. Furthermore, since our clonogenic assays using temozolomide as a DNA damaging therapy were based on a 5 day drug (DDRi and chemotherapy) exposure (a duration over which ouabain was highly toxic), and experimental designs using differing exposure durations for DDRi and chemotherapy would unacceptably increase the assay complexity and cost, radiotherapy was used to induce DNA damage in combination clonogenic studies.

Ouabain exposure from 1 hour prior to irradiation elicited potent radiosensitation (Figure 5.10) with $SER_{0.37}$ (representing the fold change in IR needed to portend a SF of 0.37 in absence of the specified radiosensitising agent – see Methods – Section 2.21.1) of 2.36 (2.03-2.73, 95% CI) and 1.87 (1.67-2.66, 95% CI) in LN18 and G1 GSCs, respectively. Additional preliminary data suggests the combination of ouabain with radiotherapy may substantially augment IR-induced DNA DSBs as detected by γH2AX foci in G1 GSCs (Figure 5.11). Taken together these data support the potential of ouabain, a medication that has previously been used in patients for the treatment of heart failure, to be repurposed as a robust radiosensitiser for the treatment of glioblastoma. Although the emerging clinical potential of ouabain to inhibit the FA pathway and enhance current DNA damaging therapies is clearly exciting and will be investigated further in the Collis laboratory, from a mechanistic perspective, ouabain has also been recently demonstrated to inhibit NHEJ DNA double strand break repair[465]. As such, subsequent studies as part of this project investigated the potential of curcumin and the novel FA pathway inhibitor (F76) to sensitise glioblastoma to current DNA damaging therapies.

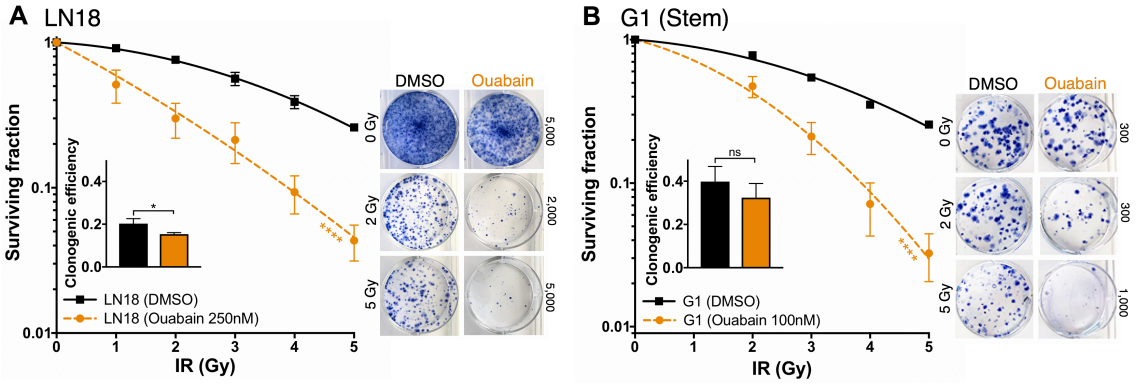


Figure 5.10: The cardiac glycoside ouabain sensitises 2D established and primary, patient-derived glioblastoma cultures to radiotherapy – Established LN18 cells or G1 primary GSCs were seeded 24 hours prior to exposure to the indicated doses of ouabain or DMSO then irradiated 1 hour later. Cells were incubated for a further 14 days (LN18) or 21 days (G1 GSCs), with media replacement 24 hours post treatment. Subsequently, colonies were stained and quantified. **A.** Clonogenic survival with clonogenic (plating) efficiency (*inset*) and representative images in LN 18 cells, and; **B.** G1 GSCs. Data points shown represent the mean of 3 independent experiments. Error bars represent the SEM. *(Data shown in A and B were produced by Mr Dawoud Dar and Miss Aurelie Vanderlinden, respectively – both working under my direct supervision).*

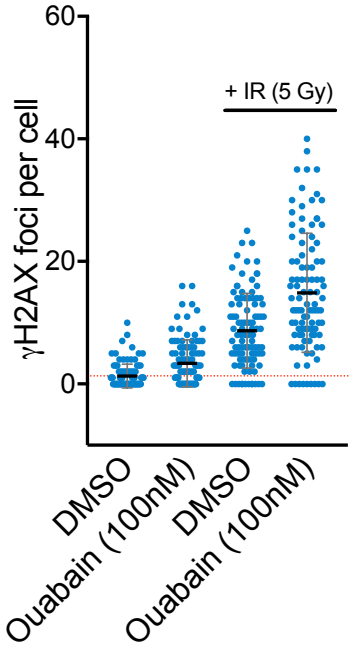


Figure 5.11: The 'heart failure' medication ouabain augments radiation-induced γH2AX foci formation in glioblastoma stem cells – G1 primary GSCs were seeded onto Matrigel™ coated coverslips 24 hours prior to exposure to DMSO (control) or ouabain (crude FA pathway inhibitor, 100nM). GSCs were then irradiated 2 hour post DDRi treatment. Cells were incubated for a further 18 hours prior to fixation and immunofluorescence processing. Data represents the quantification of γH2AX foci per nucleus for 400 individual cells (100 cells per experimental condition) in one independent experiment. The mean number of foci per nucleus is indicated for each condition (black bar) and error bars represent the SD. Red dashed line indicates the mean γH2AX foci per nucleus for control (DMSO only) GSCs. Statistical comparisons between groups were not performed on this preliminary data. *(Data shown were produced by Miss Aurelie Vanderlinden working under my direct supervision).*

5.3.2 The effects of novel FA pathway inhibitor F76 on FA pathway activation and radiosensitivity in glioblastoma stem cells

In view of previous concerns that nFAPi may lose activity over time, particularly after solubilisation in DMSO (see Chapter 3 – Section 3.6.2), F76 was solubilised immediately before application in exposures delivered to GSCs. The exposure of G7 GSCs to non-toxic doses of F76 (see Figure 5.12) prior to irradiation elicited a dose-dependent reduction in FANCD2 monoubiquitination (Figure 5.13A), confirming activity of the novel compound in inhibiting this key quantifiable marker of FA pathway activation. To date, the only previously

reported novel specific inhibitors of FANCL required doses >200μM to reduce DNA damage-induced monoubiquitination of FANCD2[250]. Further evaluation of our compound F76 as a novel FA pathway inhibitor, which specifically binds and inhibits FANCL, alongside other compounds known to reduce FANCD2 monoubiquitination confirmed robust activity in GSC with doses less than 10μM (Figure 5.13).

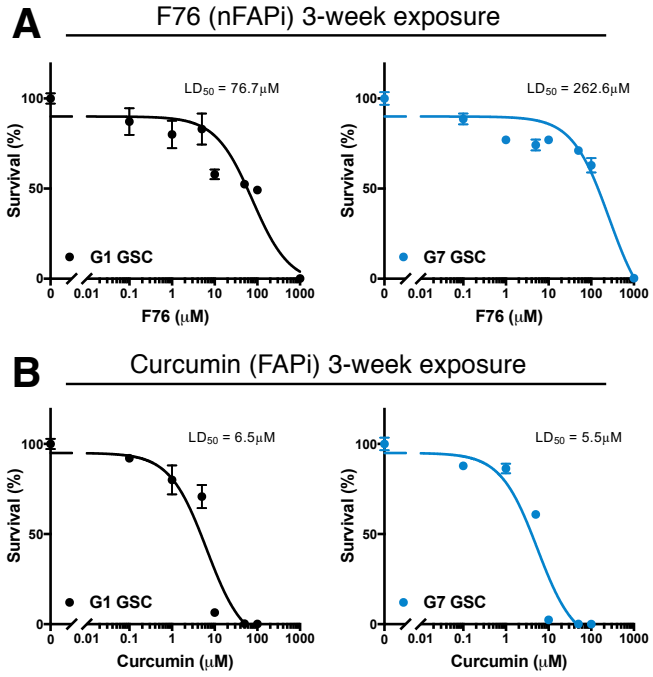


Figure 5.12: Maximal effect of the novel FA pathway inhibitor F76 and curcumin on clonogenic survival in 2D primary, patient-derived glioblastoma stem cells – G1 or G7 primary GSCs were seeded 24 hours prior to exposure to DMSO (control), F76 (novel FANCL inhibitor) or curcumin (crude FA pathway inhibitor, 5μM). Cells were incubated for a further 21 days without media replacement to provide maximal drug exposure. Subsequently, colonies were stained and quantified. A-B. Clonogenic dose-response following maximal exposure to F76 (A), and curcumin (B). Data points shown represent the mean of 3 experimental replicates from one independent experiment. Error bars represent the SEM. Error bars not shown where these are smaller than the corresponding symbol.

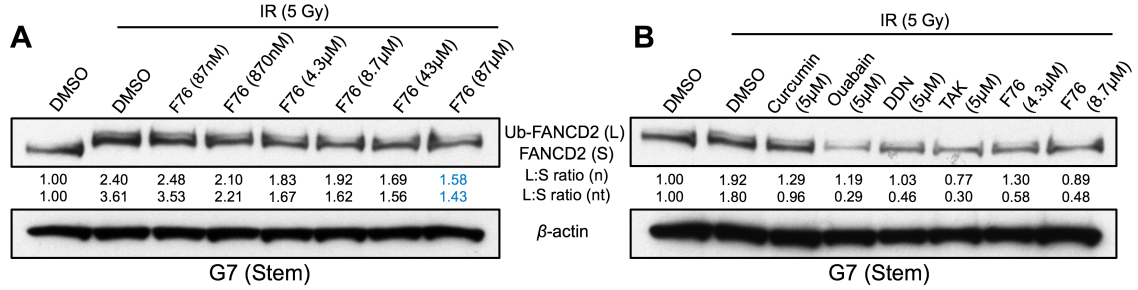


Figure 5.13: The novel FA pathway inhibitor F76 reduces FANCD2 monoubiquitination in 2D primary, patient-derived glioblastoma stem cells following DNA damage – G7 primary GSCs were plated for 24 hours prior to exposure to the indicated doses of F76, DMSO, or positive controls (curcumin, ouabain, DDN, TAK-243) then irradiation 1 hour later. Cells were incubated for a further 16 hours prior to lysis and Western blotting. A. F76 dose-response (values indicating most effective inhibition highlighted in blue). B. Inhibition with F76 in comparison to compounds known to reduce FANCD2 monoubiquitination. Each blot represents a single independent experiment.

Subsequently, the radiosensitising potential of F76 was assessed. In G1 GSC, the combination of F76 (4.3μM) treatment with IR (5 Gy) elicited a modest, albeit statistically significant reduction in surviving fraction from 0.297 (IR alone) to 0.233 (p=0.0052, ANOVA) – see Figure 5.14. The crude FA pathway inhibitor curcumin (5μM), used as a positive control, also demonstrated a significant radiosensitising effect (SF with curcumin

pretreatment = 0.177, $p<0.0001$, ANOVA). In contrast, inhibition of the FA pathway using F76 (4.3μM) in G7 GSCs failed to demonstrate a radiosensitising effect (SF with IR alone = 0.267 vs F76 with IR = 0.260, $p=0.9635$, ANOVA). However, even the positive control curcumin only demonstrated a trend towards radiosensitisation in G7 GSCs during these assays (SF with curcumin pretreatment = 0.197, $p=0.0599$, ANOVA).

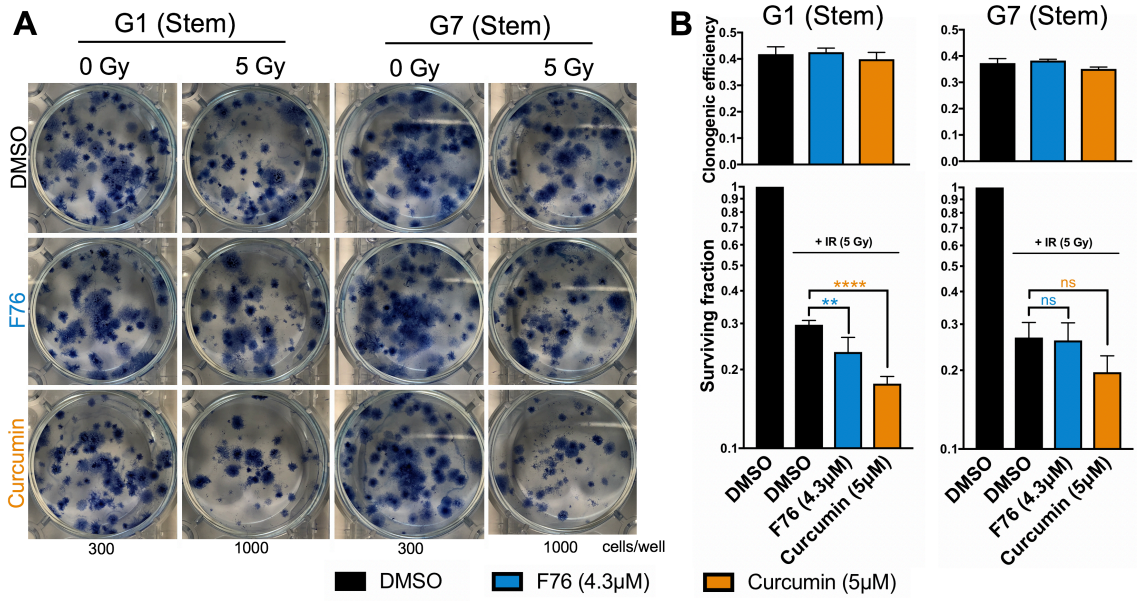


Figure 5.14: Effects of the novel FA pathway inhibitor F76 on radiosensitivity in 2D primary, patient-derived glioblastoma stem cells – G1 or G7 primary GSCs were seeded 24 hours prior to exposure to F76 (4.3μM), curcumin (5μM) or DMSO then irradiated 1 hour later. Cells were incubated for a further 21 days, with media replacement 24 hours post treatment. Subsequently, colonies were stained and quantified. **A.** Representative images. **B.** Clonogenic (plating) efficiency (*upper*) and clonogenic survival (*lower*). Data points shown represent the mean of 3 independent experiments. Error bars represent the SEM.

5.3.3 Inhibition of the FA pathway in glioblastoma stem cells using curcumin

Previous studies detailed in this thesis confirmed that curcumin reliably inhibits the FA pathway in established glioblastoma cultures (Chapter 3 – Figure 3.1 & 3.5). However, the effects of curcumin on FA pathway activity in GSCs has not been described to date. Given earlier findings presented here that high expression of FA pathway genes is associated with more aggressive tumour biology with poor patient survival (Figure 5.3), and that treatment resistant GSC subpopulations more highly express FA pathway genes relative to tumour 'bulk' cells (Figure 5.4), establishing the effects of curcumin on FA pathway activation in GSCs became highly important.

In these studies, treatment of G1 and G7 GSCs with curcumin elicited dose-dependent reductions in temozolomide and IR-induced FANCD2 monoubiquitination. Furthermore,

higher curcumin doses also appeared to reduce the protein expression of total FANCD2 both in the presence and absence of DNA damaging therapy (Figure 5.15).

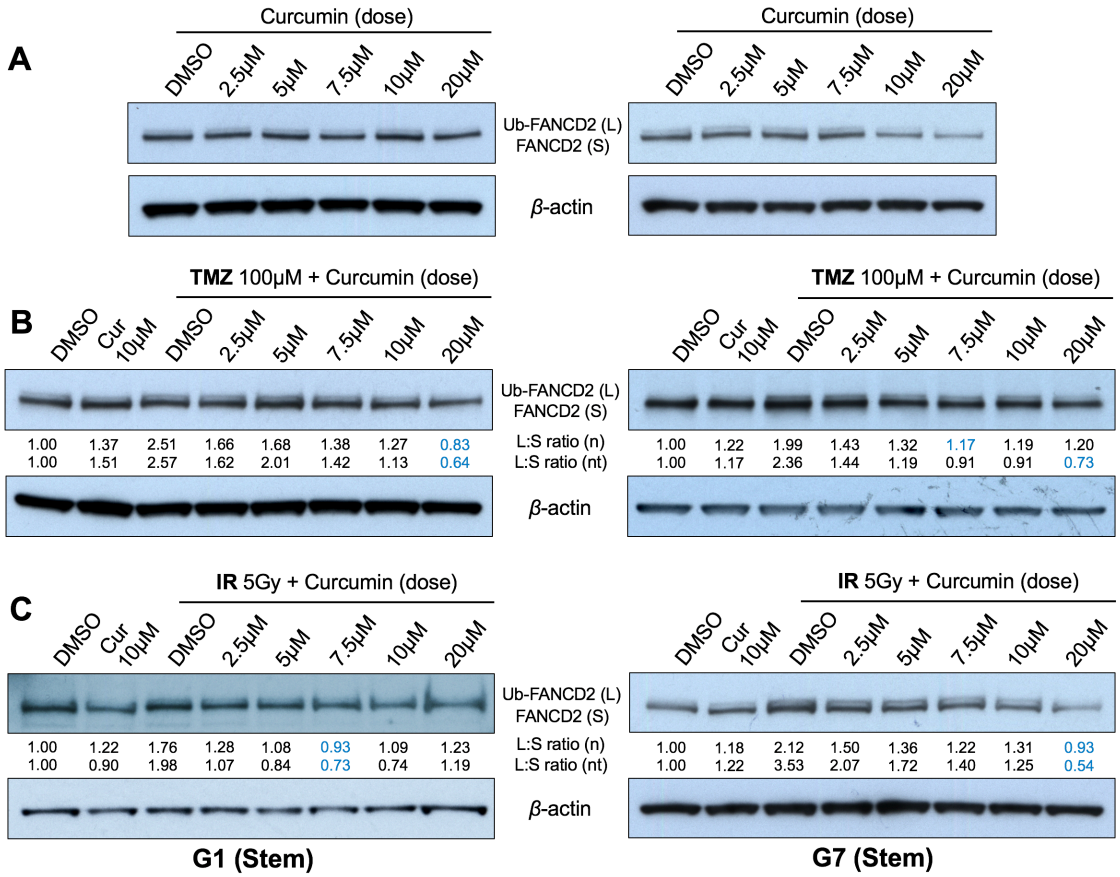


Figure 5.15: Curcumin inhibits the FA pathway in 2D primary, patient-derived glioblastoma stem cell cultures – G1 or G7 primary GSCs were plated for 24 hours prior to exposure to the indicated doses of curcumin or DMSO (control) then, where indicated, DNA damaging treatment with temozolomide (100μM) or irradiation (5 Gy) 1 hour later. Cells were incubated for a further 16 hours prior to lysis and Western blotting. **A-B.** Effects of curcumin on FANCD2 and FANCD2-Ub (in the absence of chemo- or radiotherapy) in G1 and G7 GSC, respectively. **C-D.** Effects of curcumin on temozolomide-induced monoubiquitination of FANCD2 in G1 and G7 GSC, respectively. **E-F.** Effects of curcumin on IR-induced FANCD2 monoubiquitination in G1 and G7 GSC, respectively. Values indicating most effective inhibition **highlighted in blue**. Each blot represents a single independent experiment *(Data shown in C (G1 only) were produced by Miss Aurelie Vanderlinden working under my direct supervision; the remaining data were produced by the author).*

Of the various compounds assessed to inhibit the FA pathway in glioblastoma, curcumin was selected for further combinatorial studies in 2D and clinically-relevant 3D patient-derived models, in view of consistent confirmation of its ability to reduce FA pathway activation and data to support chemo- and radiosensitisation in GSCs and established glioblastoma cell cultures. In view of this, the use and timing of curcumin in relation to radiotherapy in 3D Alvetex™ scaffold-based clonogenic studies was optimised. Using a bespoke measure termed 'L:S ratio (nt)' which adjusts normalised L:S ratios for total FANCD2 intensity – based on the rational assumption that complete absence of total FANCD2 (FANCD2 + Ub-FANCD2) would abrogate FA pathway activity – the data confirm

that curcumin administrated 1 hour prior to irradiation provided optimal reduction in FA pathway activity (2.5-fold reduction in L:S ratio (nt), from 6.2 to 2.5) – see Figure 5.16.

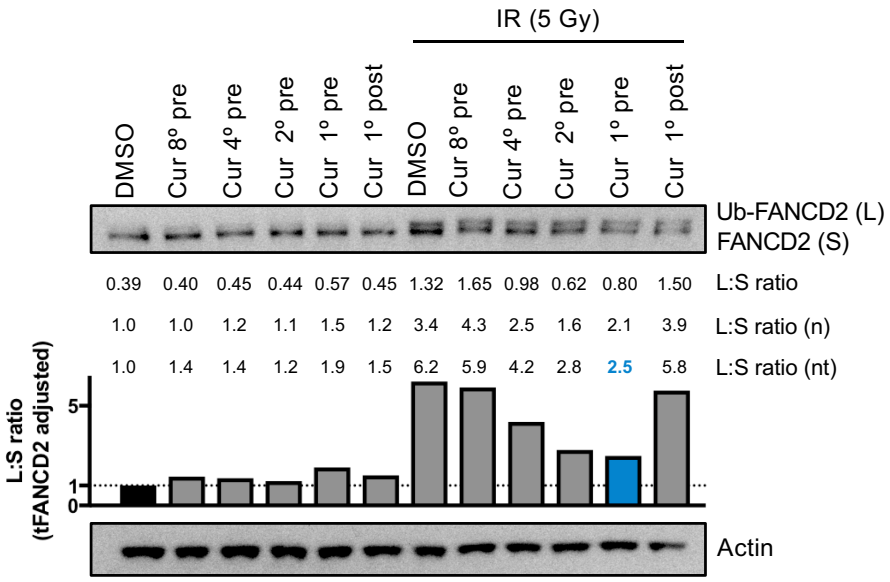


Figure 5.16: Optimising FA pathway inhibition using curcumin following DNA damage in 3D scaffold-based glioblastoma stem cell cultures – G7 primary GSCs were seeded in duplicate at a density of 2.5 x 10^4/scaffold then incubated for 4 days prior to treatments. Cells embedded within the 3D scaffolds were then exposed to DMSO or curcumin (5μM) at various time points to provide the indicated treatment durations in relation to irradiation (5 Gy). Cells were incubated for a further 16 hours. Scaffolds were then lysed on a shaking platform to liberate protein and Western blotting was performed. The signal intensity ratio of monoubiquitinated FANCD2 (Ub-FANCD2) to FANCD2 was calculated using ImageStudio Lite (Li-Cor) to determine L:S ratios. L:S ratios were normalised to the DMSO (0 Gy) control (n). Then normalised L:S ratios were adjusted for the total FANCD2 intensity (Ub-FANCD2 + FANCD2) to provide a comparable measure of FA pathway inhibition (nt). Using this measure, the data demonstrate potent FA pathway activation following irradiation with 5 Gy (L:S ratio (nt) = 6.2), which is inhibited most efficiently with curcumin administration 1 hour prior to irradiation (L:S ratio (nt) = 2.5 – highlighted in blue).

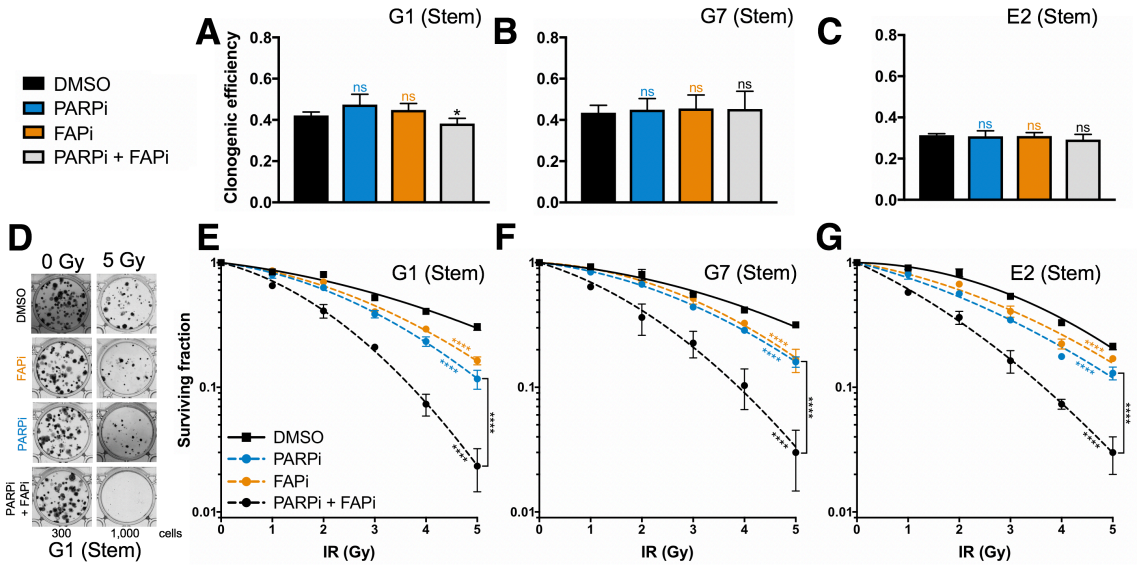
5.4 Combined FA pathway and PARP inhibition to enhance chemotherapy and radiation response

5.4.1 Radiosensitisation with combined FA pathway and PARP1 inhibition in 2D and 3D scaffold-based primary, patient-derived glioblastoma stem cell models

In the pursuit of substantially more effective anti-cancer strategies to tackle glioblastoma, there is a strong rationale to combine different classes of DDR-response targeted therapies. For example, functional redundancy within DDR networks represents an established concept[1] as cancerous cells often exhibit an overreliance on a reduced repertoire of DDR processes[209]. Similarly, GSCs demonstrate elevated FA pathway expression (Figure 5.4), and glioblastoma cells also harbour high expression of PARP1[466] – potentially alluding to a dependency on these DDR mechanisms. As such, we hypothesised that inhibiting both the FA pathway and PARP1 simultaneously would elicit more substantial radio- and chemosensitisation than either single DDR inhibitor.

2-dimensional models

Exposure of GSC to low dose DDRi treatments with either the FA pathway inhibitor curcumin (5μM), PARP1 inhibition with olaparib (1μM), or a combination of these compounds (curcumin 5μM + olaparib 1μM) did not reduce clonogenic (plating) efficiency (i.e. clonogenic surviving fraction in the absence of radiotherapy), with the exception of a very modest reduction in G1 GSCs (p=0.0389) – see Figure 5.17A-C. Consistent with previous findings (see Figure 5.14), FAPi with curcumin demonstrated a moderate radiosensitising effect in G1 primary, patient-derived GSCs ($SER_{0.37}$ = 1.27 (1.27-1.28, 95% CI)), in addition to G7 GSCs ($SER_{0.37}$ = 1.19 (1.18-1.22, 95% CI)) and E2 GSCs ($SER_{0.37}$ = 1.27 (1.23-1.30, 95% CI)) – see Figure 5.17D-H. Pretreatment of GSCs with the PARPi olaparib provided robust radiosensitisation in all three GSC lines tested: G1 ($SER_{0.37}$ = 1.40 (1.37-1.45, 95% CI)); G7 ($SER_{0.37}$ = 1.29 (1.28-1.30, 95% CI)), and; E2 ($SER_{0.37}$ = 1.45 (1.43-1.46, 95% CI)). Interestingly, combined FA pathway and PARP1 inhibition with curcumin and olaparib elicited profound radiosensitisation in all GSC lines tested: G1 ($SER_{0.37}$ = 2.08 (1.96-2.32, 95% CI)); G7 ($SER_{0.37}$ = 2.08 (1.84-2.88, 95% CI)), and; E2 ($SER_{0.37}$ = 2.06 (1.93-2.33, 95% CI)) – and reduced clonogenic survival significantly more than PARP inhibition alone. Therefore in all 3 primary GSC lines evaluated, $SER_{0.37}$ achieved with the PARPi + FAPi combination was greater than the product of the $SER_{0.37}$ achieved with each DDRi used a single agent radiosensitiser. These data suggest combined FA pathway and PARP1 inhibition represents a highly appealing potential strategy to overcome the inherent therapeutic recalcitrance of GSCs and improve treatment response. As such, this combinatorial strategy was evaluated further using a 3D Alvetex™ scaffold-based model in view of this models clinical-relevance and demonstrable ability to better predict the outcome of clinical trials than conventional 2D cultures[106,108,311].



H

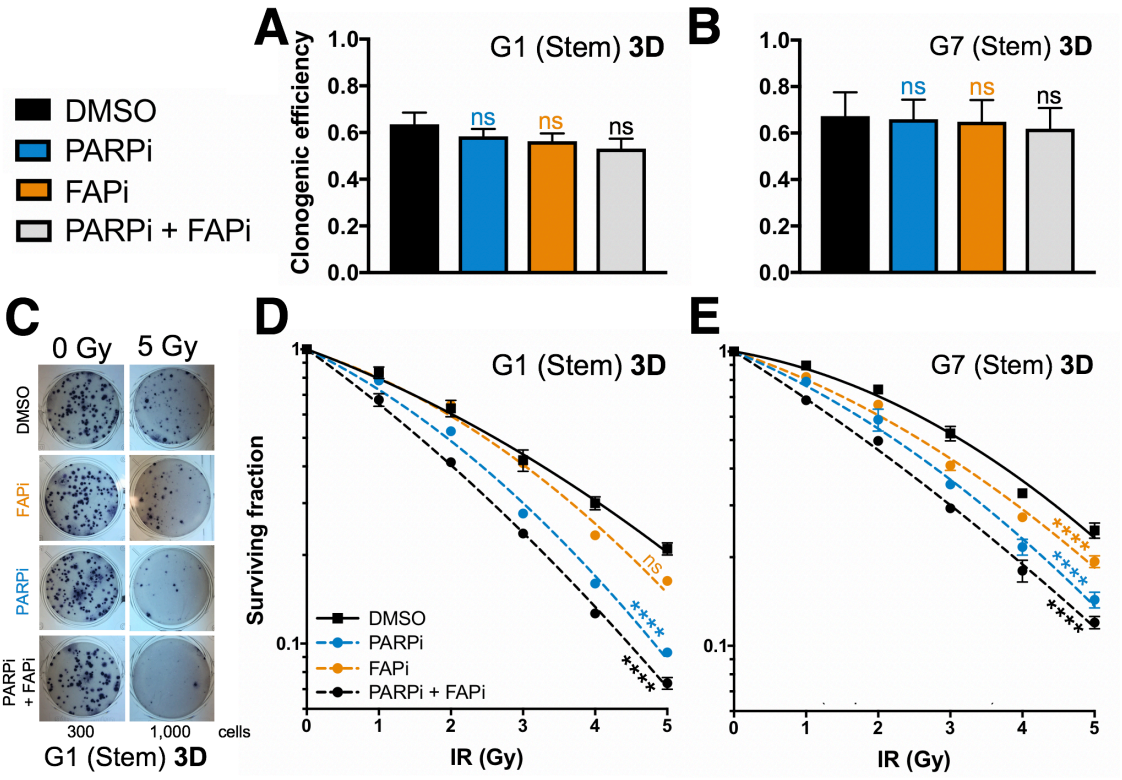
	G1		G7		E2	
	$SER_{0.80}$ (95% CI)	$SER_{0.37}$ (95% CI)	$SER_{0.80}$ (95% CI)	$SER_{0.37}$ (95% CI)	$SER_{0.80}$ (95% CI)	$SER_{0.37}$ (95% CI)
FAPi	**1.21** (1.21-1.22)	**1.27** (1.27-1.28)	**1.22** (1.12-1.81)	**1.19** (1.18-1.22)	**1.42** (1.37-1.60)	**1.27** (1.23-1.30)
PARPi	**1.41** (1.30-1.97)	**1.40** (1.37-1.45)	**1.40** (1.54-1.77)	**1.29** (1.28-1.30)	**1.64** (1.59-1.78)	**1.45** (1.43-1.46)
PARPi + FAPi	**2.31** (1.66-NC)	**2.08** (1.96-2.32)	**3.64** (1.69-NC)	**2.08** (1.84-2.88)	**4.17** (2.38-NC)	**2.06** (1.93-2.33)

Figure 5.17: Combined FA pathway and PARP inhibition enhances radiosensitisation in 2D primary, patient-derived glioblastoma stem cells – G1, G7 or E2 primary GSCs were seeded 24 hours prior to exposure to DMSO (control), FAPi (curcumin, 5μM), PARPi (olaparib, 1μM) or the combination of PARPi + FAPi (curcumin 5μM + olaparib 1μM) administered simultaneously. GSCs were then irradiated 1 hour post DDRi treatments. Cells were incubated for a further 21 days, with media replacement 24 hours post irradiation. Subsequently, colonies were stained and quantified. A-C. Clonogenic (plating) efficiency following treatment with DMSO, FAPi, PARPi or the combination (at 0 Gy radiation) in G1 GSCs (A); G7 GSCs (B), and; E2 GSCs (C). D. Representative images of colonies following DDRi treatments at 0 Gy and 5 Gy irradiation in G1 GSCs. E-G. Clonogenic survival curves in G1 GSCs (E); G7 GSCs (F), and; E2 GSCs (G). H. Sensitiser enhancement ratios for single and combination DDRi strategies. **Note:** p53 status of G7 and E2 GSCs has previously been confirmed as wild-type by Sanger sequencing[467], whilst status of G1 GSCs remains unknown. NC = not able to compute. Data points shown represent the mean of 3 independent experiments. Error bars represent the SEM.

3-dimensional scaffold-based models

Similar to the above 2D studies, exposure to FAPi with curcumin (5μM), PARPi with olaparib (1μM) or a combination of these compounds (curcumin 5μM + olaparib 1μM) did not notably reduce the clonogenic efficiency of G1 or G7 GSCs embedded within 3D Alvetex™ scaffolds (Figure 5.18A-B). In contrast to the above 2D studies, curcumin use as a single DDRi failed to significantly radiosensitise G1 GSCs ($SER_{0.37}$ = 1.05 (1.01-1.09, 95% CI) – see Figure 5.18C-D and F, however, analysis of radiosensitisation at 5 Gy alone demonstrated a modest reduction in SF with curcumin treatment prior to IR (mean SF 0.210 vs 0.163, p=0.0198). Curcumin also demonstrated modest but statistically significant radiosensitisation in G7 GSCs ($SER_{0.37}$ = 1.15 (1.14-1.15, 95% CI) – see Figure 5.18E. Olaparib demonstrated robust radiosensitisation in both G1 GSCs ($SER_{0.37}$ = 1.32 (1.26-1.32, 95% CI) and G7 GSCs ($SER_{0.37}$ = 1.30 (1.28-1.33, 95% CI). Importantly, the combination of FA pathway and PARP1 inhibition with curcumin and olaparib provided the greatest degrees of radiosensitisation observed in the 3D scaffold-based model - G1 GSCs $SER_{0.37}$ = 1.57

(1.52-1.61, 95% CI) and G7 GSCs $SER_{0.37}$ = 1.51 (1.50-1.51, 95% CI). Although the effect of combined DDRi on radiosensitivity was not as dramatic as observed in 2D models, use of combined FA pathway and PARP1 inhibition retained a statistically significant benefit over the best single radiosensitiser tested (PARPi vs PARPi + FAPi, p<0.0001 G1 and G7 GSCs, sum of squares F-test) – Figure 5.18D-F.



F

	G1		G7	
	$SER_{0.80}$ (95% CI)	$SER_{0.37}$ (95% CI)	$SER_{0.80}$ (95% CI)	$SER_{0.37}$ (95% CI)
FAPi	**0.95** (0.86-1.01)	**1.05** (1.01-1.09)	**1.38** (1.37-1.40)	**1.15** (1.14-1.15)
PARPi	**1.20** (1.06-1.29)	**1.32** (1.26-1.32)	**1.63** (1.54-1.77)	**1.30** (1.28-1.33)
PARPi + FAPi	**1.82** (1.75-1.84)	**1.57** (1.52-1.61)	**2.62** (2.44-2.89)	**1.51** (1.50-1.51)

Figure 5.18: Combined FA pathway and PARP inhibition enhances radiosensitisation in 3-dimensional Alvetex™ scaffold-based glioblastoma stem cell models – G1 or G7 primary GSCs were seeded 24 hours prior to exposure to DMSO (control), FAPi (curcumin, 5μM), PARPi (olaparib, 1μM) or the combination of PARPi + FAPi (curcumin 5μM + olaparib 1μM) administered simultaneously. GSCs were then irradiated 1 hour post DDRi treatments. Cells were incubated for a further 21 days, with media replacement 24 hours post irradiation. Subsequently, colonies were identified using incubation with MTT for 4 hours, then fixed with paraformaldehyde and quantified. A-B. Clonogenic (plating) efficiency following treatment with DMSO, FAPi, PARPi or the combination (at 0 Gy radiation) in G1 GSCs (A), and; G7 GSCs (B). C. Representative images of colonies following DDRi treatments at 0 Gy and 5 Gy irradiation in G1 GSCs. D-E. 3D Alvetex™ clonogenic survival curves in G1 GSCs (D), and; G7 GSCs (E). The clonogenic survival curve fits for radiosensitisation with PARPi alone vs PARPi + FAPi in both G1 and G7 GSCs demonstrated the combination elicits significantly greater radiosensitisation (p<0.0001, Sum of squares F-test). F. Sensitiser enhancement ratios for single and combination DDRi strategies. Data points shown represent the mean of 3 independent experiments. Error bars represent the SEM. Note: error bars are not shown where these are smaller than the corresponding symbol.

Use of 3D scaffold-based models to derive α/β ratios

The responses of tumour cells following radiotherapy are commonly described using a linear-quadratic model (see Methods – Section 2.21.1) which incorporates a linear term constant (α value) and a quadratic term constant (β value). Consequently, the ratio of these values – the α/β ratio – provides a description of the sensitivity of specific tumours or tissues to radiotherapy fraction size in the clinic[221]. Most cancers, and acutely responding normal tissues (those susceptible to rapidly occurring adverse effects of radiotherapy, such as the skin or oral mucosa) exhibit high α/β ratios of 10 or greater, which are indicative of a lower sensitivity to radiotherapy fraction size (i.e. even smaller fractions of radiotherapy mediate substantial cell death)[221]. Conversely, tissues with low α/β ratios, such as the CNS, lung and kidneys are less susceptible to the adverse effects of radiotherapy and partially underlie the basis by which a tissue-sparring therapeutic index can be achieved/modified by varying radiotherapy fractionation parameters.

Since intercellular communication/contact has been demonstrated to influence therapeutic response in glioblastoma[212,468], and GSCs in the Alvetex™ scaffold-based model are orientated throughout 3-dimensions in a way that is more reflective of patient's tumour histology[108] (with greater opportunity for intercellular connections to form), we considered that analysis of our 3D clonogenic data would provide robust α/β ratios (relative to traditional 2D *in vitro* models), which better describe the way in which patient tumours might respond to these therapies. Interestingly, G1 and particularly G7 3D GSCs demonstrated lower α/β ratios than would be expected with typical tumours (α/β ratios 9.5 and 2.5, respectively) – see Figure 5.19. This is likely to reflect the inherent radioresistance of GSCs[18,195,197] and could be interlinked with the potential slow-cycling and/or quiescent nature of some cancer stem cell subpopulations[469], although the quiescence of GSCs is controversial and potentially variable[373]. Neither the use of curcumin (α/β ratios 4.2 and 6.4 in G1 and G7 GSCs, respectively) or olaparib (α/β ratios 6.5 and 7.3 in G1 and G7 GSCs, respectively) as a single radiosensitiser modified the α/β ratios of GSC to a value that would be indicative of cancers that respond acutely and substantially to radiotherapy (i.e. α/β ratio >/>>10), despite even the robust radiosensitisation provided by olaparib exposure in both models. Remarkably, simultaneous FA pathway and PARP1 inhibition with the combination of curcumin and olaparib was uniquely able to elicit α/β ratios >10 in GSCs (15.8 and 23.1 in G1 and G7 GSCs, respectively). Together, these data suggest that combined FA pathway and PARP1 inhibition may fundamentally alter the dynamics of GSC response to irradiation

and may have meaningful implications for predicted response to various radiotherapy fractionation schedules if such DDRi combinatorial strategies progress towards clinical studies.

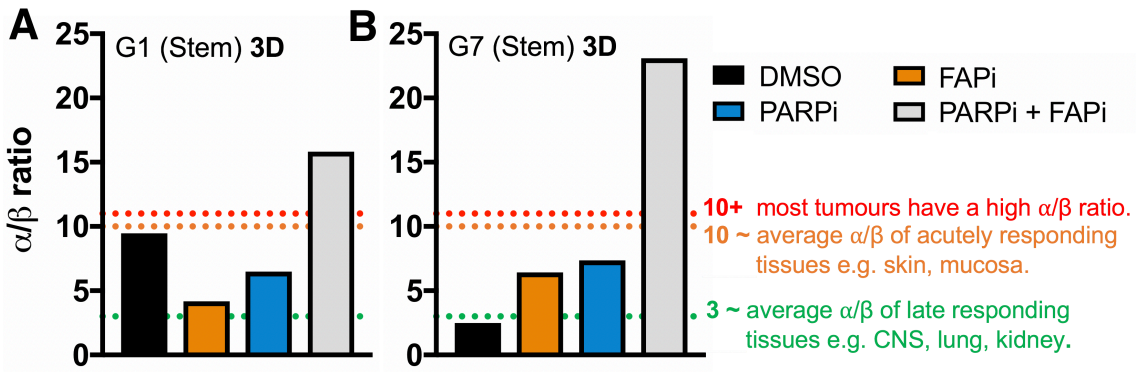


Figure 5.19: Combined FA pathway and PARP inhibition modifies α/β ratios in 3-dimensional Alvetex™ scaffold-based glioblastoma stem cell models – A-B. α/β ratios derived from curves fitted to clonogenic survival data (3 independent repeats , Figure 5.18) using a linear-quadratic model in G1 GSCs (A), and; G7 GSCs (B).

5.4.2 Combined FA pathway and PARP1 inhibition augments radiation-induced DNA damage

Next we sought to establish how this combined DDRi strategy might influence levels of DNA damage in GSCs under treatment. Initially, G7 GSCs cultured within a 3D Alvetex™ scaffold-based architecture were lysed 16 hours after treatment with proteinaceous lysates liberated from the scaffolds mechanically using agitation before further investigation using immunoblotting. As expected, GSCs treated with 1μM of the PARP inhibitor olaparib demonstrated complete abrogation of PAR formation in the context of monotherapy and combination therapies. Interestingly, PARP inhibition elicited robust monoubiquitination of FANCD2 as illustrated by normalised L:S ratios of 1.86 and 3.12 in the absence and presence of IR (5 Gy), respectively (Figure 5.20). This observation is consistent with dose dependent FA pathway activation following PARPi in established U87 and LN18 2D cultures reported earlier in this thesis (Chapter 3 – Figure 3.1), and confirms the phenomenon of parallel DDR pathway activation after PARPi therapy in a clinically-relevant, patient-derived 3D GSC culture system.

Relative abundance of the DNA damage marker γH2AX (H2AX phosphorylated at serine 139) – normalised to β-actin – was used to quantify and compare residual DNA damage following exposure to the various combinatorial strategies at 16 hour post-treatment. Treatment with IR (5 Gy) alone induced a 1.38-fold increase in γH2AX to control GSCs. The

addition of either PARPi or FAPi treatment followed by IR enhanced DNA damage with 1.63- and 1.81-fold increases in the relative abundance of γH2AX. However, the greatest increase in γH2AX (2.09-fold) was observed in GSCs treated with a combined PARPi + FAPi followed by IR (Figure 5.20). These results suggest combined FA pathway and PARP inhibition represents an effective strategy to maximise radiation induced DNA damage, however the presence of γH2AX in cell lysates cannot be used to confirm the abundance of specific DNA lesions, such as DSBs, within a cellular context.

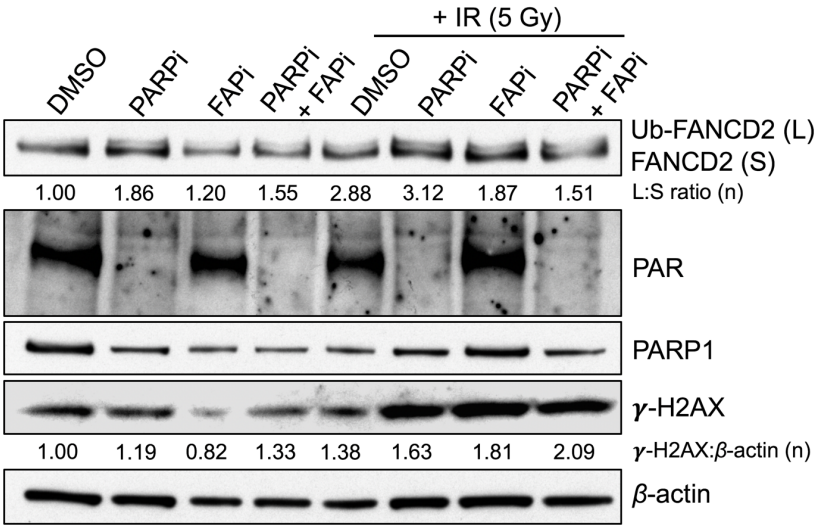


Figure 5.20: Combined FA pathway and PARP inhibition enhance radiation-induced γH2AX in 3-dimensional Alvetex™ scaffold-based glioblastoma stem cell models – G7 primary GSCs were seeded into Alvetex™ scaffolds 72 hours prior to exposure to DMSO (control), PARPi (olaparib, 1μM), FAPi (curcumin, 5μM), or the PARPi + FAPi combination (curcumin 5μM + olaparib 1μM) administered simultaneously. GSCs were then irradiated 1 hour post DDRi treatments. Cells embedded within the scaffolds were incubated for a further 16 hours prior to lysis and Western blotting. L:S ratios. To determine FA pathway activation, the normalised ratio of Ub-FANCD2 (L) to FANCD2 (S) (normalised to DMSO only treated cells) was calculated for each treatment as previously described[216] and shown beneath the relevant bands. The relative abundance of γH2AX was established by calculating the ratio of γH2AX to loading control (β-actin) for each treatment condition then normalising these values to control GSCs. This blot represents a single independent experiment.

Although pan-nuclear staining of the DNA damage marker γH2AX can represent DNA replication stress, the presence of DNA DSBs is well described to initiate localised recruitment of γH2AX with these molecules coalescing at sites of DNA damage to form foci of γH2AX as a specific and early event in the cellular response to DBSs, which facilitates the retention of multiple key downstream DDR factors[470-472]. Confocal immunofluorescence microscopy was therefore used to detect nuclear foci comprised of γH2AX in G7 GSCs cultured within a 3D Alvetex™ scaffold-based architecture. In GSCs treated with IR alone, the quantity of γH2AX foci/cell observed was equivalent to untreated cells (mean 1.6/cell untreated vs 2.4/cell γH2AX foci, p=0.0817), suggesting a resolution of DSBs to constitutive or near constitutive levels within 24 hours. However, GSCs treated with PARPi or the combination of PARPi + FAPi prior to IR exhibited an increase in γH2AX foci – mean 2.8/cell

(p=0.0009) and 6.7/cell (p<0.0001), respectively (Figure 5.21). Importantly, the radiosensitising PARPi + FAPi combination yielded a 2.4-fold increase in the mean number of γH2AX foci/cell, relative to PARPi with olaparib as a single sensitising DDRi – a result that was highly statistically significant (p<0.0001) and underlines the potential value of such DDRi combinations.

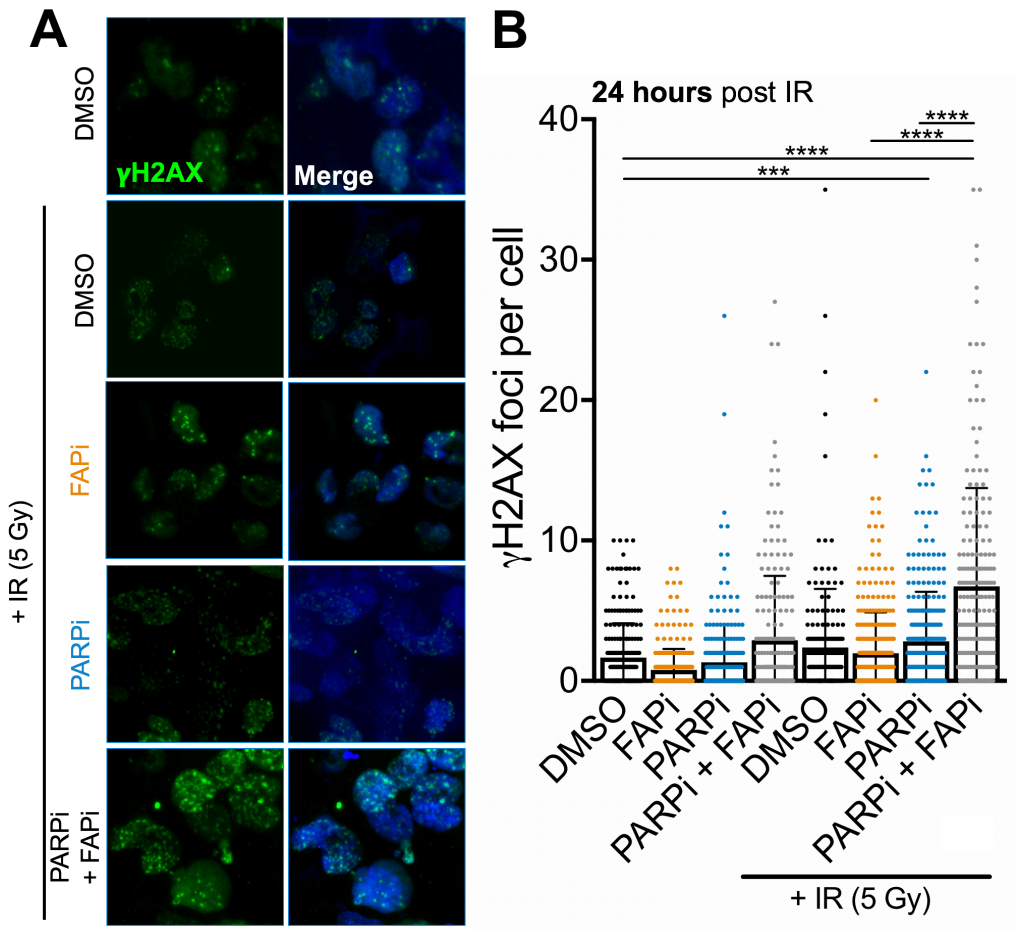


Figure 5.21: Combined FA pathway and PARP inhibition delays resolution of radiation-induced γH2AX foci in G7 3-dimensional Alvetex™ scaffold-based glioblastoma stem cell models – G7 primary GSCs were seeded into Alvetex™ scaffolds 72 hours prior to exposure to DMSO (control), FAPi (curcumin, 5μM), PARPi (olaparib, 1μM) or the combination of PARPi + FAPi (curcumin 5μM + olaparib 1μM) administered simultaneously. GSCs were then irradiated 1 hour post DDRi treatments. Cells embedded within the scaffolds were incubated for a further 24 hours prior to fixation with paraformaldehyde then immunofluorescence processing. Cells were imaged using a Zeiss LSM880 AiryScan confocal microscope. Images (63x magnification) for visualisation and quantification were produced using the maximum intensity projection of multiple slice Z-stacks. Only cells with a nucleus captured in its entirety within a Z-stack were used of quantification of γH2AX. A. Representative images. B. Immunofluorescence quantification. Data represents the quantification of individual nuclear γH2AX foci in 2,027 cells (>/>>200 cells/condition) over 2 independent experiments. Error bars represent the SD.

5.4.3 Effects of combined FA pathway and PARP1 inhibition on temozolomide sensitivity in 3D scaffold-based primary, patient-derived glioblastoma stem cell models

In studies assessing chemosensitisation, GSCs were exposed to therapeutic compounds for a duration of 120 hours (in contrast to 24 hours for radiosensitisation studies), therefore we felt it prudent to reassess the effects of each DDRi under investigation on clonogenic plating efficiency. With this extended duration of DDRi exposure, the combination of curcumin (5μM) and olaparib (1μM) modestly reduced clonogenic efficiency in G1 GSCs from 0.55 (DMSO) to 0.46 (combination), p=0.0013 (Figure 5.22A). In contrast, there was no statistically significant reduction in clonogenic efficiency with the DDRi combination in G7 GSCs (Figure 5.22B). As a single agent DDRi, neither curcumin or olaparib significantly reduced clonogenic efficiency in either cell line.

Remarkably, in contrast to established glioblastoma cell line studies (Chapter 3 – Figure 3.3), inhibition of the FA pathway using curcumin in clinically-relevant 3D GSC models failed to sensitise cells to temozolomide chemotherapy (Figure 5.22C-E). Furthermore, olaparib sensitised G7 GSCs (p=0.0014) but failed to provide significant chemosensitisation throughout the dose range tested in G1 GSCs (p=0.1159). However considering cells treated with the highest dose of temozolomide evaluated (25μM), olaparib elicited a degree of chemosensitisation (p=0.0402). Consistent with the radiosensitisation findings in 2D and 3D GSC cultures, in both G1 and G7 GSCs, the combination of curcumin and olaparib provided modestly but significantly greater chemosensitisation than olaparib alone (p=0.0158 and p=0.0013, respectively - sum of squares F-test).

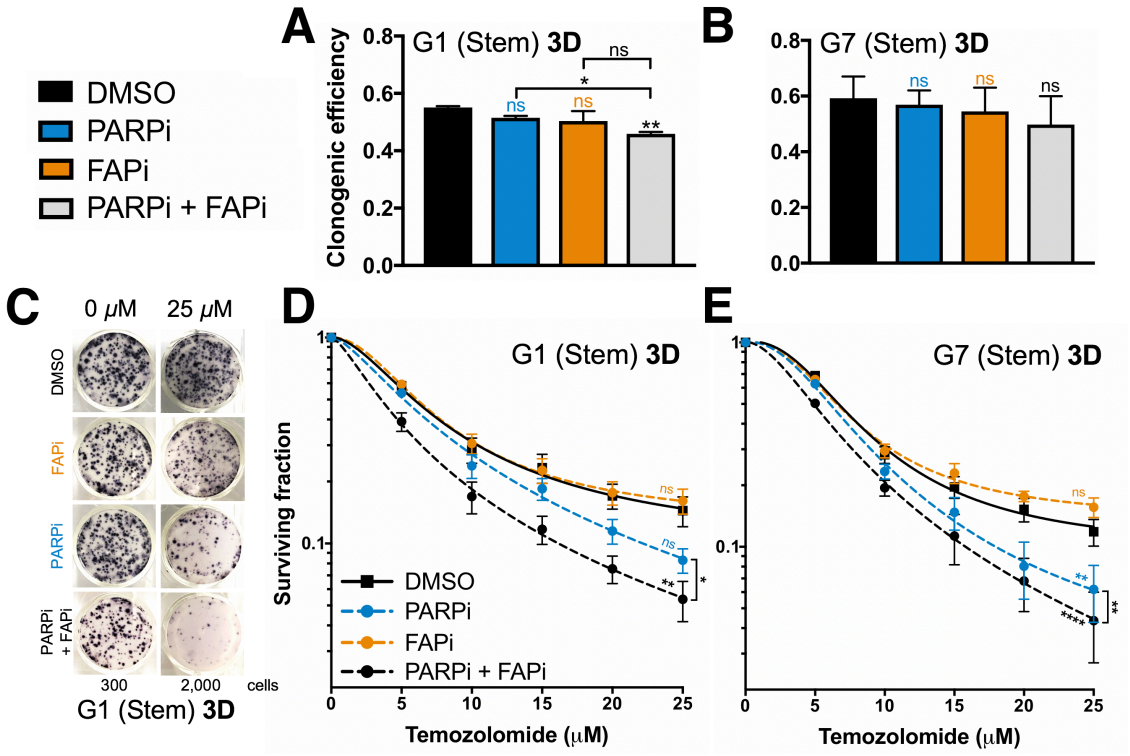


Figure 5.22: Combined FA pathway and PARP inhibition enhances temozolomide sensitisation in 3-dimensional Alvetex™ scaffold-based glioblastoma stem cell models – G1 or G7 primary GSCs were seeded 24 hours prior to exposure to DMSO (control), FAPi (curcumin, 5μM), PARPi (olaparib, 1μM) or the combination of PARPi + FAPi (curcumin 5μM + olaparib 1μM) administered simultaneously. GSCs were then treated with the indicated doses of temozolomide chemotherapy 1 hour post DDRi treatments. Cells were incubated for a further 21 days, with media replacement 120 hours post treatment. Subsequently, colonies were identified using incubation with MTT for 4 hours, then fixed with paraformaldehyde and quantified. **A-B.** Clonogenic (plating) efficiency following treatment with DMSO, FAPi, PARPi or the combination (at 0μM temozolomide) in G1 GSCs (**A**), and; G7 GSCs (**B**). **C.** Representative images of colonies following DDRi treatments at 0μM and 25μM temozolomide in G1 GSCs. **D-E.** 3D Alvetex™ clonogenic survival curves in G1 GSCs (**D**), and; G7 GSCs (**E**). Data points shown represent the mean of 3 independent experiments. Error bars represent the SEM. Error bars not shown where these are smaller than the corresponding symbol.

5.5 Combined FA pathway and ATM or ATR inhibition to enhance chemotherapy and radiation response

5.5.1 Radiosensitisation with combined FA pathway and ATR or ATM inhibition in 3D scaffold-based primary, patient-derived glioblastoma stem cell models

Ionizing radiation delivered at a dose of 2 Gy will produce an average of 2,000 SSBs and 80, substantially more toxic, DSBs per cell[473,474], resulting in activation of both the ATR-CHK1 axis and ATM-CHK2 axis. These are extensively interlinked with the FA pathway, as previously discussed (Chapter 1 – Section 1.4.7). Consequently, we hypothesised that simultaneous inhibition of the FA pathway with either ATR or ATM would substantially increase the sensitivity of GSCs to radiotherapy.

Inhibition of ATR and ATM kinases

The potent, selective inhibitors AZD6738 and AZD0156 were selected to target the ATR-CHK1 axis and ATM-CHK2 axis, respectively[204,288,475,476]. In 2D GSCs, ATR inhibition with AZD6738 effectively abolished constitutive levels of CHK1 phosphorylation at serine 345 in untreated cells and robustly inhibited IR-induced CHK1 phosphorylation in a dose dependent manner (Figure 5.23A). Similarly, relative to untreated GSCs, ATM inhibition with AZD0156 abolished constitutive phosphorylation of ATM at serine 1981 and CHK2 at threonine 68. Furthermore, despite robust activation of the ATM-CHK2 axis following treatment with IR (5 Gy), primary GSCs treated with AZD0156 demonstrated clear abrogation of IR-induced ATM and CHK2 phosphorylation in a dose-dependent manner (Figure 5.23B). Partial overlap in DNA DSB repair substrate specificity between activated ATM and DNA-PKcs, for example with H2AX and 53BP1 phosphorylation, is well established[477-479]. Furthermore, DNA-PKcs can be activated by both ATM mediated transphosphorylation at threonine 2609, and via autophosphorylation at the PQR cluster around serine 2056 with differential effects[480-483]. Therefore, in order to exclude ATM-independent off-target effects of AZD0156 on DNA-PKcs, its phosphorylation site serine 2056 was also assessed. Although higher doses of AZD0156 (5μM in G1 GSCs and ≥1μM G7 GSCs) reduced the abundance of pDNA-PKcs (S2056) following IR, submicromolar doses which potently inhibited IR-induced phosphorylation of ATM and CHK2 had no demonstrable effect on DNA-PKcs phosphorylation, consistent with the previously reported ATM-specificity of AZD0156 at effective doses[204].

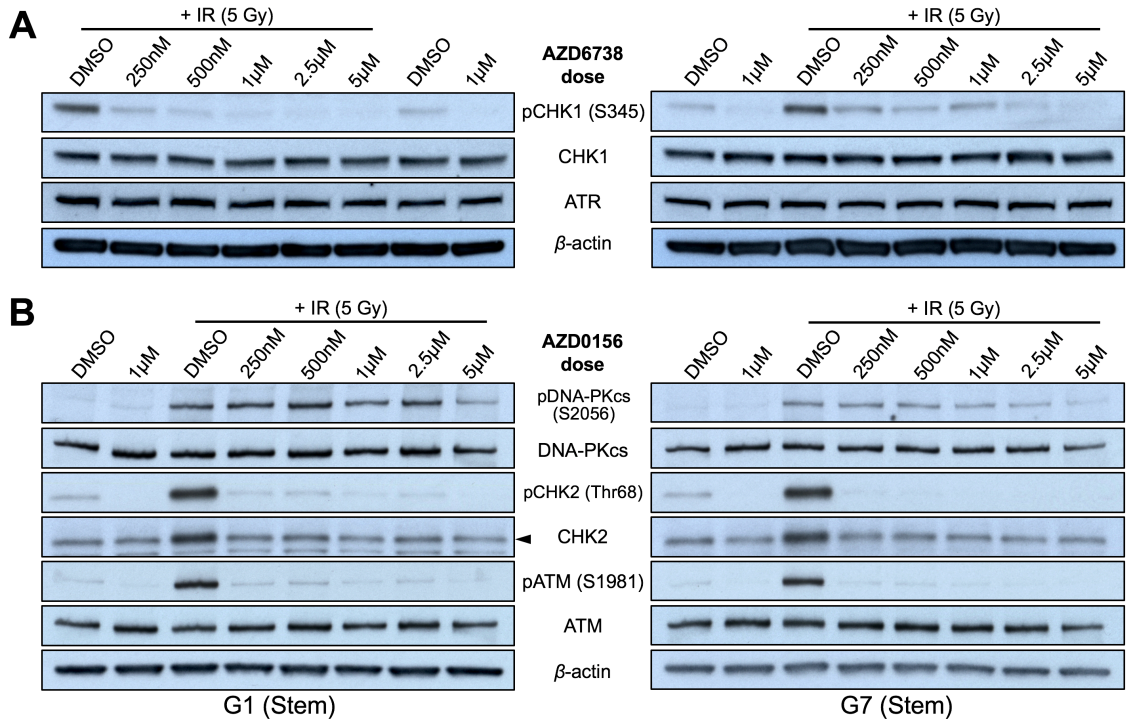
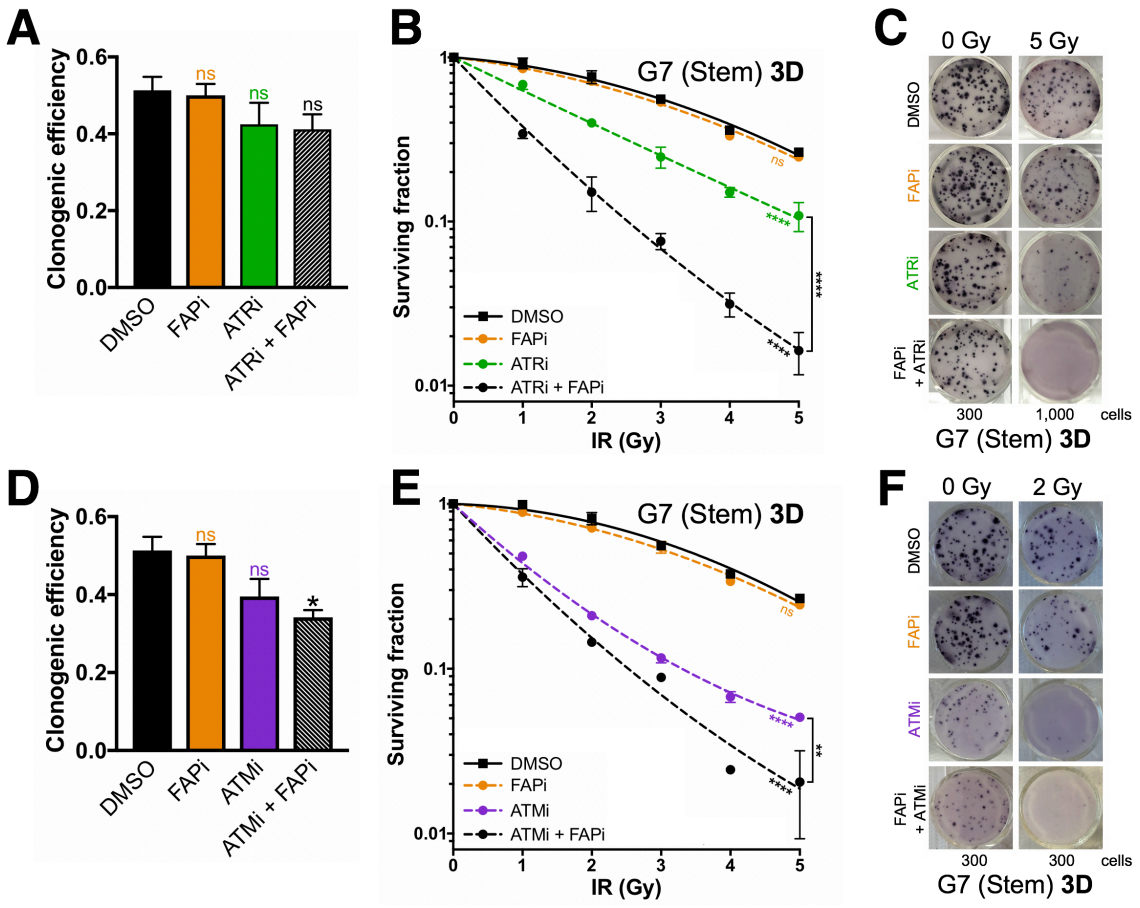


Figure 5.23: Inhibition of ATR and ATM in 2D primary, patient-derived glioblastoma stem cell cultures – G1 or G7 primary GSCs were plated for 24 hours prior to exposure to the indicated doses of AZD6738 (ATR inhibitor), AZD0156 (ATM inhibitor) or DMSO (control) then, DNA damaging treatment with irradiation (5 Gy) 1 hour later. Cells were incubated for a further 4 hours prior to lysis and Western blotting. **A.** Effects of AZD6738 on CHK1 phosphorylation at serine 345 in G1 and G7 GSCs, respectively. **B.** Effects of AZD0156 on ATM phosphorylation at serine 1981 and CHK2 phosphorylation at threonine 68 in G1 and G7 GSCs. The presence of IR-induced, ATM-independent, autophosphorylation of DNA-PKcs at serine 2056 was used to confirm drug specificity, with no demonstrable off-target inhibition of DNA-PKcs when using submicromolar concentrations of AZD0156. Each blot represents a single independent experiment *(Data shown were produced by Miss Aurelie Vanderlinden working under my supervision).*

Radiosensitisation with curcumin and AZD6738 (ATR inhibitor)

3-Dimensional scaffold-based clonogenic studies were performed in G7 GSCs but not G1 GSCs due to the high cost of performing large combinatorial studies using the Alvetex™ system. Neither FA pathway inhibition with curcumin (5μM), ATR inhibition with AZD6738 (1μM), or a combination of the two, significantly reduced clonogenic efficiency in G7 GSCs (Figure 5.24A). In the context of radiotherapy, as expected, AZD6738 provided robust radiosensitisation with $SER_{0.37}$ 1.89 (1.88-1.90, 95% CI). Interestingly, despite a lack of radiosensitisation observed using curcumin as a lone DDRi, the combination of curcumin and AZD6738 provoked an extraordinary degree of radiosensitivity with $SER_{0.37}$ 3.23 (3.03-3.49, 95% CI) – Figure 5.24B-C & G. In fact, the degree of radiosensitisation observed was of similar magnitude to our positive control which consisted of simultaneous PARP and ATR inhibition (see Supplementary Figure 5.2), since this represents the most potently radiosensitising DDRi combination previously reported in GSCs[197,208]. However, in contrast to combined PARPi + ATRi which demonstrated significant cytotoxicity in the absence of IR (see Supplementary Figure 5.2A), the similar degree of radiosensitisation achieved with ATRi

+ FAPi whilst not significantly reducing clonogenic plating efficiency (i.e. in the absence of radiotherapy) suggest this combination might hold appealing potential to maximise CNS tumour response aided by locoregional delivery of radiotherapy in the clinic and minimise the risk of extra-cranial adverse effects associated with systemic exposure such as bone marrow failure.



G

	G7	
	$SER_{0.80}$ (95% CI)	$SER_{0.37}$ (95% CI)
FAPi	**1.20** (1.09-1.29)	**1.04** (1.02-1.08)
ATRi	**2.69** (2.61-2.81)	**1.89** (1.88-1.90)
ATRi + FAPi	**6.50** (4.71-30.43)	**3.23** (3.03-3.49)
ATMi	**5.32** (4.76-7.35)	**2.81** (2.75-2.91)
ATMi + FAPi	**7.29** (4.94-NC)	**3.25** (2.95-3.64)

Figure 5.24: Combined FA pathway and ATR or ATM inhibition enhances radiosensitisation in G7 3-dimensional Alvetex™ scaffold-based glioblastoma stem cell models – G7 primary GSCs were seeded 24 hours prior to exposure to DMSO (control), FAPi (curcumin, 5μM), ATRi (AZD6738, 1μM), ATMi (AZD0156, 0.5μM) or the combination of ATRi + FAPi (AZD6738 1μM + curcumin 5μM) + or ATMi + FAPi (AZD0156 0.5μM + curcumin 5μM) administered simultaneously. GSCs were then irradiated 1 hour post DDRi treatments. Cells were incubated for a further 21 days, with media replacement 24 hours post irradiation. Subsequently, colonies were identified using incubation with MTT for 4 hours, then fixed with paraformaldehyde and quantified. A. Clonogenic (plating) efficiency following treatment with DMSO, FAPi, ATRi or ATRi + FAPi (at 0 Gy radiation) in G7 GSCs. B. 3D Alvetex™ clonogenic survival curves in G7 GSCs treated with FAPi and/or ATRi and IR, then; C. Representative images. D. Clonogenic (plating) efficiency following treatment with DMSO, FAPi, ATMi or ATMi + FAPi (at 0 Gy radiation) in G7 GSCs. E. Survival curves in G7 GSCs treated with FAPi and/or ATMi and IR, then; F. Representative images. Data generated from 3 independent experiments. Error bars represent the SEM. Error bars not shown where these are smaller than the corresponding symbol. G. Sensitiser enhancement ratios for single and combination DDRi strategies. Note - ATRi and ATMi studies were performed simultaneously, but survival curves are presented separately for clarity.

Radiosensitisation with curcumin and AZD0156 (ATM inhibitor)

As expected, treatment of G7 GSCs with AZD0156 elicited substantial radiosensitisation with $SER_{0.37}$ 2.81 (2.75-2.91, 95% CI). The combination of FA pathway inhibition with curcumin and ATMi with AZD0156 reduced clonogenic efficiency in the absence of

radiotherapy, and provided a significant increase in radiosensitisation relative to AZD0156 alone (p=0.0019, curcumin + AZD0156 $SER_{0.37}$ 3.25 (2.95-3.64, 95% CI)) - Figure 5.24D-G. Nevertheless, relative to single DDRi use, the gain in therapeutic response gained with curcumin + AZD0156 was not as marked as with curcumin + AZD6738 (ATRi).

5.5.2 The effects of combined FA pathway and ATR or ATM inhibition on temozolomide sensitivity in 3D scaffold-based primary, patient-derived glioblastoma stem cell models

In contrast to 24-hour exposures (above), exposure to curcumin and/or AZD6738 or AZD0156 for 120 hours in the absence of chemotherapy appeared to yield more variable effects on clonogenic efficiency (Figure 5.25A & D). This greater degree of baseline variability in the data may, at least partially, account for the lack of detectable statistically significant reductions in clonogenic efficiency with the various DDRi evaluated, with the exception of combined FA pathway and ATR inhibition with AZD6738 (p=0.0477, ANOVA).

Temozolomide sensitivity with curcumin and AZD6738 (ATR inhibitor)

As expected from earlier studies (Section 5.4.3), inhibition of the FA pathway with curcumin failed to sensitise 3D G7 GSC to temozolomide chemotherapy (Figure 5.25B & E). In contrast, ATR inhibition using AZD6738 generated marked chemosensitisation to temozolomide, p<0.0001, sum of squares F-test (Figure 5.25B-C). The combination of curcumin with AZD6738 also induced profound chemosensitisation relative to DMSO treated cells (p<0.0001, sum of squares F-test). Analysis of curves fitted to the entire dose-response relationship (temozolomide doses 0-25μM) revealed the addition of curcumin did not provide any statistically significant benefit compared to AZD6738 as a single DDRi (p=0.4194, sum of squares F-test). However, it is possible that this may reflect a lack of benefit with the DDRi combination at higher temozolomide doses, since isolated analysis at temozolomide doses of 5μM and 10μM (concentrations closest to those previously reported in CSF[320] and peritumoural tissue[321]) suggest enhanced killing of GSCs with the DDRi combination (relative to AZD6738 as a single DDRi) at these lower concentrations of chemotherapy – p=0.0016 (mean SF 0.159 vs 0.068) and p=0.0276 (mean SF 0.060 vs 0.032), respectively (paired t tests).

Temozolomide sensitivity with curcumin and AZD0156 (ATM inhibitor)

Similarly, inhibition of ATM with AZD0156 or treatment with the combination of curcumin and AZD0156 both provided substantial sensitisation to temozolomide (p<0.0001, sum of squares F-test – Figure 5.25E-F), but with no significant advantage of using the DDRi combination over ATMi alone. Perhaps with the exception of the low dose of 5μM temozolomide, where isolated analysis suggested some benefit of combined curcumin with AZD0156 over AZD0156 alone – p=0.0369, paired t test (mean SF 0.368 vs 0.242).

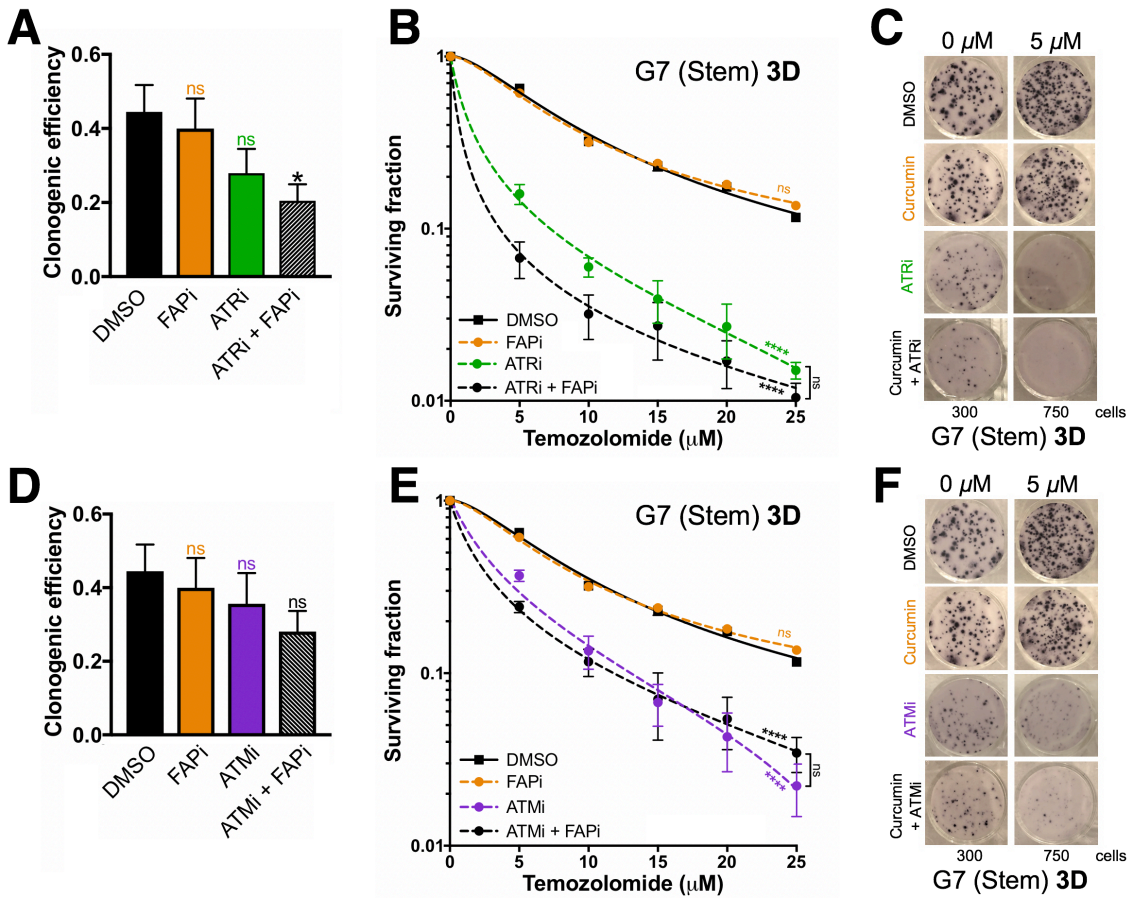


Figure 5.25: The effects of combined FA pathway and ATR or ATM inhibition on temozolomide sensitivity in G7 3-dimensional Alvetex™ scaffold-based glioblastoma stem cell models – G7 primary GSCs were seeded 24 hours prior to exposure to DMSO (control), FAPi (curcumin, 5μM), ATRi (AZD6738, 1μM), ATMi (AZD0156, 0.5μM) or the combination of ATRi + FAPi (AZD6738 1μM + curcumin 5μM) + or ATMi + FAPi (AZD0156 0.5μM + curcumin 5μM) administered simultaneously. GSCs were then treated with temozolomide chemotherapy (0-25μM) 1 hour post DDRi treatments. Cells were incubated for a further 21 days, with media replacement 120 hours post treatments. Subsequently, colonies were identified using incubation with MTT for 4 hours, then fixed with paraformaldehyde and quantified. A. Clonogenic (plating) efficiency following treatment with DMSO, FAPi, ATRi or ATRi + FAPi (at 0μM temozolomide) in G7 GSCs. B. 3D Alvetex™ clonogenic survival curves in G7 GSCs treated with FAPi and/or ATRi and temozolomide, then; C. Representative images. D. Clonogenic (plating) efficiency following treatment with DMSO, FAPi, ATMi or ATMi + FAPi (at 0μM temozolomide) in G7 GSCs. E. Survival curves in G7 GSCs treated with FAPi and/or ATMi and temozolomide, then; F. Representative images. Data generated from 3 independent experiments. Error bars represent the SEM. Error bars not shown where these are smaller than the corresponding symbol. Note - ATRi and ATMi studies were performed simultaneously, but survival curves are presented separately for clarity.

5.6 The effects of FA pathway-based DDRi combinations on DNA strand breaks, replication stress and cell cycle progression

5.6.1 Combined FA pathway and PARP or ATR inhibition augments radiation-induced DNA damage and delays repair in glioblastoma stem cells

The alkaline comet assay (single-cell gel electrophoresis) was used to provide a global measure of DNA strand breaks (SSBs and DSBs) at single cell resolution. Since the relative amount of DNA in each comet tails is indicative of DNA break frequency[220], the percentage of DNA within the comet tail associated with each nucleoid was used as a primary measure to compare the relative abundance of DNA strand breaks between conditions. Additionally, tail moment, which incorporates the intensity and length of fluorescence from DNA stained in the comet tail[220], was used as an auxiliary measure (presented in Figure 5.27).

DNA strand breaks at 1 hour

At 1 hour post IR/sham, DDRi monotherapy using either curcumin- (5μM) mediated FA pathway inhibition, PARP inhibition with olaparib (1μM), or ATR inhibition with AZD6738 (1μM) failed to increase DNA damage relative to DMSO treated cells (control). Similarly, combined PARPi + FAPi did not augment measures of DNA damage. However, the combination of ATRi + FAPi elicited a modest but significant increase in the mean proportion of comet tail DNA (31.6%, (95% CI = 28.6-34.7%)) relative to control GSCs (25.4% (23.3-27.5%)), p=0.0286; and comet tail moment (65.7a.u. (95% CI = 57.3-74.2a.u.) vs 35.4a.u. (23.3-27.5a.u.)), p<0.0001 – see Figure 5.26A & Figure 5.27A, respectively. As expected, compared to control GSCs, cells treated with IR (5 Gy) demonstrated increased tail DNA (37.3% (34.6-40.0), p<0.0001) and tail moment (61.1a.u. (54.5-67.8), p<0.0001), however the addition of FAPi, PARPi, ATRi or the combinations (PARPi + FAPi and ATRi + FAPi) as a radiosensitising strategy were unable to further augment the proportion of fragmented DNA in comet tails compared to GSCs treated with IR alone at this early timepoint. Interestingly however, analysis of tail moment data revealed treatment with the DDRi combinations prior to IR increased this measure of DNA damage – PARPi + FAPi (81.6a.u. (72.0-91.1), p=0.0006) and ATRi + FAPi (81.3a.u. (73.5-89.0), p=0.0012) – relative to GSCs treated with IR alone.

DNA strand breaks at 6 hours

Assessment of DNA damage at 6 hours post IR/sham revealed the most striking differences between treatment conditions. In the absence of IR, GSCs treated with FAPi or ATRi (but not PARPi) demonstrated a substantial increase in both measures of DNA damage (p<0.0001) relative to control GSCs (see Figure 5.26B & Figure 5.27B). The combination of ATRi + FAPi did not confer additional DNA damage over ATRi alone as assessed by tail DNA, but did confer a subtle increase in tail moment (59.0a.u. (95% CI = 51.6-66.5) vs 78.8a.u. (69.4-88.2a.u.) with the combination, p=0.0130). More remarkably, the combination of PARPi + FAPi elicited a substantial increase in DNA damage that was greater than the additive effects of each DDRi individually (p<0.0001), both in terms of comet tail DNA and tail moment. After 6 hours, GSCs treated with IR did not harbour significantly elevated DNA damage relative to control GSCs (19.4% (95% CI = 17.1-21.7%) vs 23.9% (21.5-26.2%) tail DNA with IR, p=0.3695). However, all three single DDRi radiosensitising strategies increased comet tail DNA: FAPi (34.7% (32.2-37.2%), p<0.0001); PARPi (29.9% (29.9-36.2%), p=0.0002); ATRi (44.8% (41.9-47.7%), p<0.0001). The incorporation of PARPi or ATRi within an FAPi-based combination profoundly augmented DNA damage further with a clear shift towards the majority of GSCs demonstrating more fragmented DNA within comet tails than intact supercoiled DNA within nucleoid bodies (see Figure 5.26B). GSCs treated with PARPi + FAPi demonstrated mean tail DNA of 54.2% (51.7-56.7%) whilst the ATRi + FAPi combination conferred mean tail DNA of 59.8% (57.0-62.5%); both significantly more DNA damaging strategies than radiosensitisation using each constituent DDRi alone (p<0.0001).

DNA strand breaks at 24 hours

Strikingly, at 24 hours post IR/sham only GSCs treated with FAPi-based DDRi combinations as a radiosensitising strategy continued to harbour elevated comet tail DNA relative to control GSCs (13.23% (95% CI = 11.6-14.8%)) and GSCs treated with IR only (14.5% (13.1-16.0%)), with mean tail DNA of 22.1% (19.7-24.5%) with PARPi + FAPi before IR (p<0.0001) and 19.9% (18.1-21.7%) in GSCs treated with ATRi + FAPi before IR (p<0.0001) – see Figure 5.26C. Although treatment with FAPi or PARPi as a single radiosensitiser did maintain some elevation of tail moment at 24 hours post IR, these effects were subtle and significantly less potent than use of the PARPi + FAPi combination (Figure 5.27C)

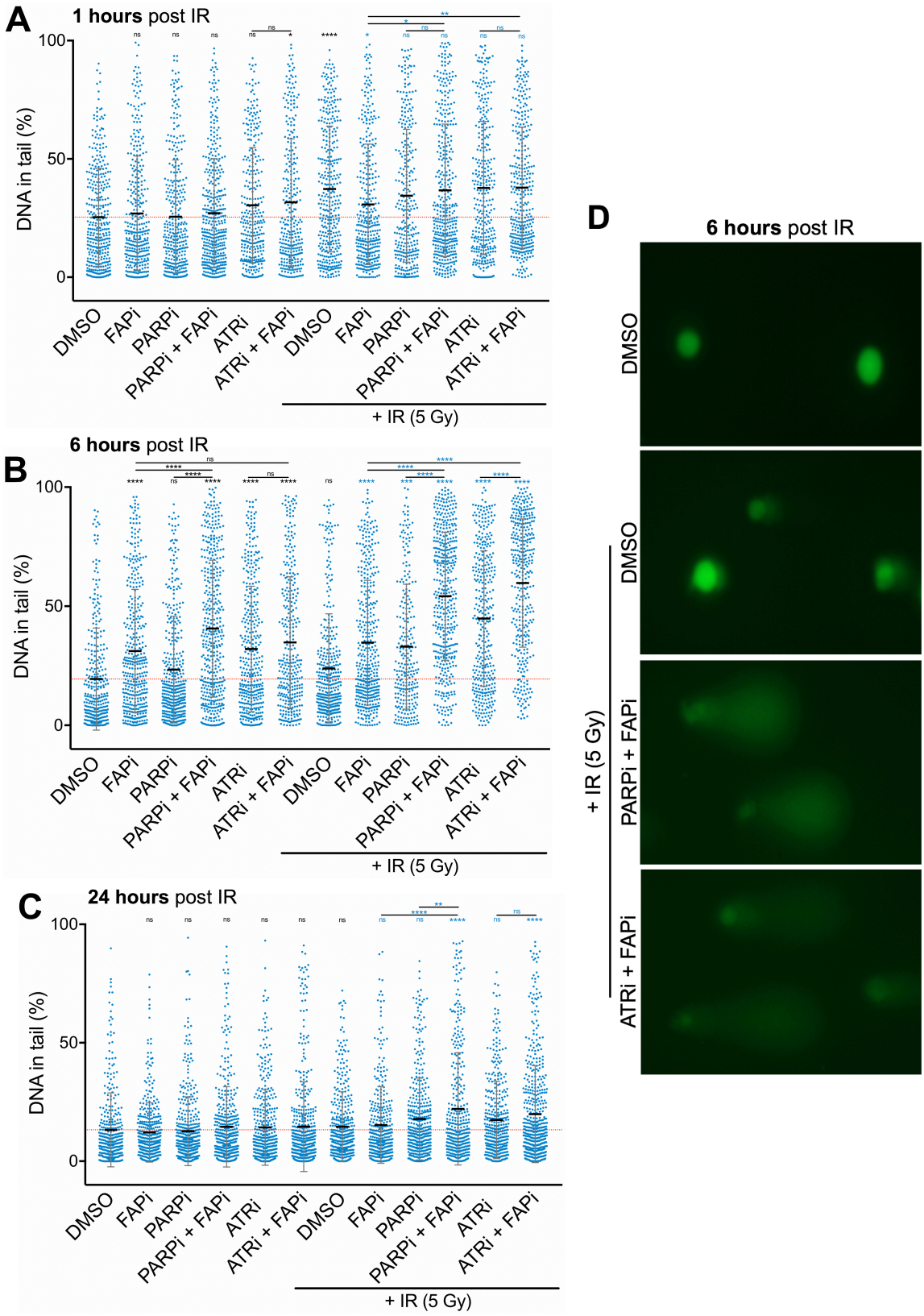


Figure 5.26: Combined FA pathway and PARP or ATR inhibition augment DNA damage and delay repair in 2D G7 primary, patient-derived glioblastoma stem cells (percentage DNA in tail) – G7 primary GSCs were plated then incubated overnight prior to exposure to DDRi treatments: FAPi (curcumin 5μM); PARPi (olaparib 1μM); ATRi (AZD6738 1μM); PARPi + FAPi (olaparib 1μM + curcumin 5μM); ATRi + FAPi (AZD6738 1μM + curcumin 5μM), or; DMSO. GSCs were then irradiated (or exposed to sham irradiation) 1 hour post DDRi treatments. Cells were incubated for a further 1, 6 or 24 hours as indicated prior to completion of single cell gel electrophoresis as described previously (see Methods – Section 2.23.1). **A-C.** Percentage of DNA in comet tail at 1 (**A**), 6 (**B**) and 24 (**C**) hours post-IR/sham. **D.** Representative images of DMSO-treated G7 GSCs -/+ IR and GSCs treated with FA pathway-based DDRi combinations prior to IR. Data represents the quantification of percentage DNA in the comet tail of nucleoid bodies for 5,042 individual cells over 3 independent

experiments. Mean tail DNA is also indicated for each condition (black bar) and error bars represent the SD. Red dashed line indicates mean tail DNA for control (DMSO only) GSCs. Statistical comparisons between groups using ANOVA with Sidak correction to adjust for multiple hypothesis testing. Black asterisks (*) indicate significant difference relative to control GSCs, or between groups not treated with IR where indicated. Blue asterisks (*) indicate significant difference relative to GSCs treated with DMSO + IR (5 Gy), or between groups treated with IR where indicated.

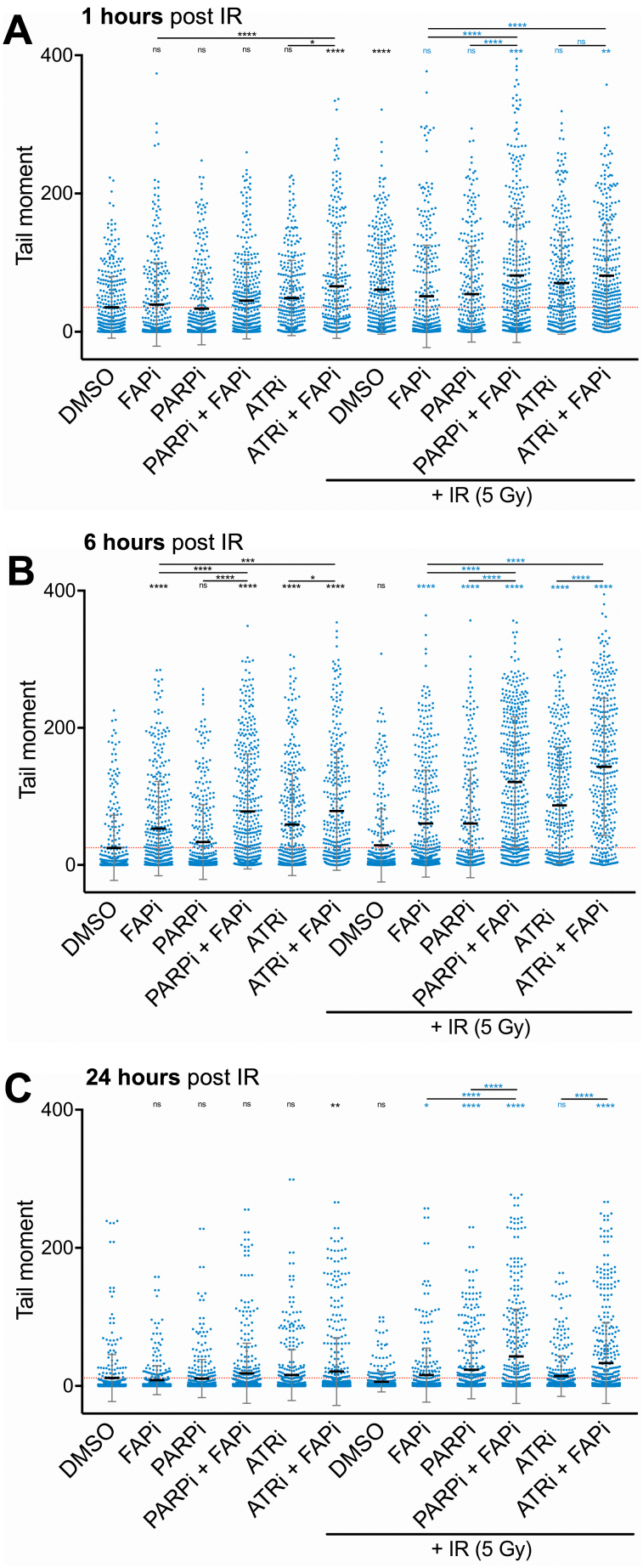


Figure 5.27: Combined FA pathway and PARP or ATR inhibition augment DNA damage and delay repair in 2D G7 primary, patient-derived glioblastoma stem cells (comet tail moment) – G7 primary GSCs were plated then incubated

overnight prior to exposure to DDRi treatments: FAPi (curcumin 5μM); PARPi (olaparib 1μM); ATRi (AZD6738 1μM); PARPi + FAPi (olaparib 1μM + curcumin 5μM); ATRi + FAPi (AZD6738 1μM + curcumin 5μM), or; DMSO. GSCs were then irradiated (or exposed to sham irradiation) 1 hour post DDRi treatments. Cells were incubated for a further 1, 6 or 24 hours as indicated prior to completion of single cell gel electrophoresis as described previously (see Methods – Section 2.23.1). A-C. Quantification of comet tail moment at 1 (A), 6 (B) and 24 (C) hours post-IR/sham. Data represents tail moment quantification of nucleoid bodies for 5,042 individual cells over 3 independent experiments. Mean tail moment is also indicated for each condition (black bar) and error bars represent the SD. Red dashed line indicates mean tail moment for control (DMSO only) GSCs. Statistical comparisons between groups using ANOVA with Sidak correction to adjust for multiple hypothesis testing. Black asterisks (*) indicate significant difference relative to control GSCs, or between groups not treated with IR where indicated. Blue asterisks (*) indicate significant difference relative to GSCs treated with DMSO + IR (5 Gy), or between groups treated with IR where indicated

In summary, these data reveal that G7 GSCs resolve radiation-induced DNA damage to baseline levels within 6 hours of exposure. In contrast, the use of a DDRi (FAPi, PARPi or ATRi) augments constitutive and radiation-induced DNA damage for at least 6 hours, whilst treatment with the combination of either PARPi + FAPi or ATRi + FAPi results in profound elevation of DNA damage at 6 hours which, in the context of radiosensitisation, continues to confer persistently elevated DNA damage for at least 24 hours (Figure 5.28).

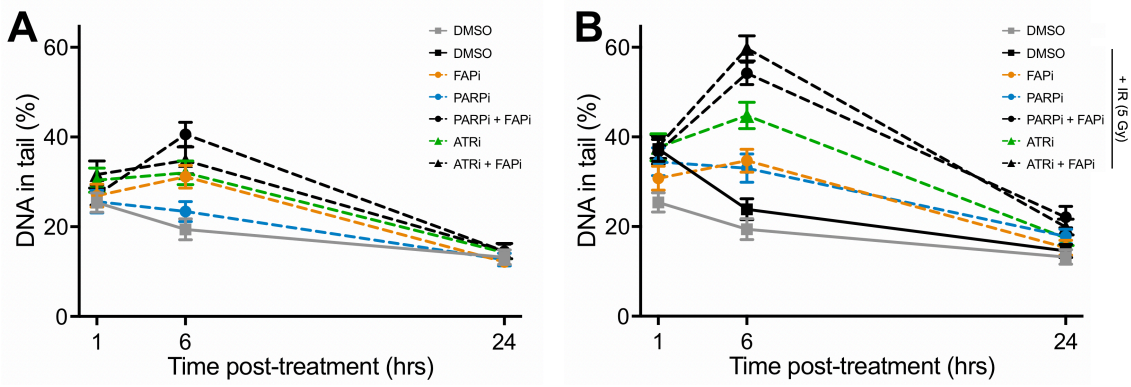


Figure 5.28: Summary of the kinetics of DNA damage and repair in 2D G7 primary, patient-derived glioblastoma stem cells treated with FA pathway based DDRi combinations – A-B. Summary of single cell gel electrophoresis data for G7 GSCs at 1, 6 and 24 hour points following exposure to sham – 0 Gy (A), or IR – 5 Gy (B).

5.6.2 *The effects of combined FA pathway and PARP or ATR inhibition on replication-transcription conflicts in glioblastoma stem cells*

Following exposure to radiotherapy, these studies (see Figure 5.28B) and previous studies[467] confirm primary GSCs harbour a maximum burden of DNA strand breaks at around 1 hour post IR. Therefore, evidence of an increase in DNA strand breaks between 1 to 6 hours post IR in the context of some DDRi-radiotherapy combinations suggests these strategies prevent the early, efficient repair of IR-induced DNA damage causing progressive accumulation of strand breaks and/or continued generation of additional strand breaks for at least 6 hours. Although FAPi, as a single DDRi radiosensitising strategy, was associated

with an increase in DNA strand breaks between 1 hour and 6 hours post IR, the maximum burden of DNA damage at 6 hours was not greater than in GSCs treated with IR alone at 1 hour, therefore it is possible the results observed with FAPi primarily represent a modification of DNA repair kinetics rather than substantial generation of additional DNA damage. Conversely, combining IR with ATRi or either of the PARPi + FAPi or ATRi + FAPi combinations engendered a remarkable increase in additional DNA damage between 1 to 6 hours that was over and above maximal DNA damage observed in GSCs treated with IR alone at 1 hour. Recently, GSCs have been reported to exhibit high levels of constitutive DNA replication stress relative to bulk counterparts[208]. Additionally, increased expression of long neural genes in both neural progenitor cells and GSCs appears to be associated with an elevated propensity for replication-transcription collisions, resulting in the generation of replication stress associated DNA DSBs[208,484]. Consequently, we reasoned that high basal replication stress may represent an inherently exploitable vulnerability within GSC biology and therefore we hypothesized the modulation of DNA replication fork stability and kinetics afforded by specific DDRi and/or DDRi combinations might increase the likelihood of additional replication-transcription conflicts resulting in the increased burden of DNA strand breaks observed above and providing a mechanistic basis for the exquisite preclinical efficacy of these therapeutic strategies reported earlier in this Chapter. Therefore, in order to investigate the burden of replication-transcription conflicts in GSCs exposed to a range of therapeutic strategies, immunofluorescence staining for RNA:DNA hybrids (S9.6) in G7 GSCs was performed at 6 hours post IR/sham.

Specificity of immunofluorescence staining for RNA:DNA hybrids

Both hydroxyurea (HU) and the pyrimidine nucleoside, thymidine, are well established inducers of DNA replication stress[485] and should therefore increase the frequency of collisions between replication and transcription machineries as a function of reduced replication fork velocities. As expected, treatment of G7 GSCs with either of these compounds – used as experimental positive controls in this context – substantially increased the intensity of S9.6 staining for RNA:DNA hybrids: DMSO (median S9.6 nuclear mean fluorescence intensity (MFI) 58.13a.u. (IQR = 42.82-82.55a.u.)); HU-treated (83.9a.u.(47.5-126.5a.u.)); thymidine-treated (193.2a.u. (167.3-221.4a.u.)). Furthermore, the application of RNaseH, which specifically degrades RNA hybridised with DNA, reduced the nuclear MFI of S9.6 staining to a low level (34.7a.u. (25.2-43.4a.u.)) and abrogated the effects of HU (31.8a.u. (24.9-40.1a.u.)) – see Figure 5.29. Together, these data support a robust

experimental workflow, with compounds known to induce high-levels of DNA replication stress generating a high degree of RNA:DNA hybrids, as expected, and abolition of S9.6 staining following the addition of RNaseH confirming the fluorescence detected is highly specific for RNA:DNA hybrids (Figure 5.29).

Effects of DDRi on RNA:DNA hybrids (in the absence of IR)

At 6 hours post sham (0 Gy), GSCs treated with either FAPi or PARPi demonstrated a moderate or subtle reduction in S9.6 nuclear MFI, respectively. Interestingly, the effects of combined PARPi + FAPi did not reflect the sum of each individual DDR inhibitor's negative effects, but rather was equivalent with DMSO-treated GSCs (**control** - 50.5a.u. (IQR = 31.6-78.5a.u.)). Additionally, whilst ATRi alone did not significantly modify the intensity of S9.6 staining at 6 hours relative to control GSCs (50.8a.u. (29.0-84.8a.u.)), the combination of ATRi + FAPi elicited a remarkable increase RNA:DNA hybrids (85.9a.u. (58.1-113.1a.u.)), $p<0.0001$) – see Figure 5.30A & C.

Effects of DDRi-radiotherapy combinations on RNA:DNA hybrids

Relative to control GSCs, cells treated with IR (5 Gy) demonstrated a reduction in RNA:DNA hybrids at 6 hours (43.6a.u. (IQR = 27.4-59.6a.u.), $p<0.0001$). Compared to these GSCs treated with DMSO + IR, the addition of either FAPi or PARPi as single DDRi radiosensitising strategies appeared to have diametrically opposed effects causing an increase (71.1a.u. (47.2-113.7a.u.), $p<0.0001$) or decrease (32.3a.u. (17.0-62.2a.u.), $p<0.0002$) in the intensity of S9.6 staining, respectively. The combination of PARPi + FAPi as a radiosensitising strategy portended effects somewhat intermediate between those of PARPi and FAPi as single DDRi radiosensitisers, and was therefore similar to GSCs treated with DMSO + IR (47.1a.u. (33.9-63.8a.u.), $p=0.0722$.). In contrast, although the use of ATRi as a single radiosensitising strategy significantly reduced the intensity of S9.6 immunofluorescence staining (34a.u. (23.3-52.5a.u.), $p=0.0003$), the effects of combining ATRi + FAPi did not reflect the net sum these as individual radiosensitisers but instead evoked a substantial increase in S9.6 staining (90.9a.u. (47.3-153.2a.u.), $p<0.0001$ – relative to DMSO + IR-treated GSCs) – see Figure 5.30B-C. In the context of radiosensitisation the increase in S9.6 staining with ATRi + FAPi was significantly greater than that observed using FAPi as a single radiosensitiser ($p=0.0038$). However, use of the ATRi + FAPi combination with IR did not appear to portend significantly greater S9.6 staining relative to ATRi + FAPi treated cells in the absence of IR ($p=0.8391$). Perhaps indicating that additional exogenously delivered DNA damage is a

prerequisite to achieve a substantial increase in FAPi-mediated collisions between DNA replication and transcription in GSCs, and the addition of ATRi can remove the need for conventional DNA damaging therapy, potentially through destabilising stalled replication forks to generate additional DNA DSBs, permitting global origin firing, and allowing inappropriate progression through cell cycle checkpoints resulting in more frequent collisions between the apparatus of DNA replication and transcription[208].

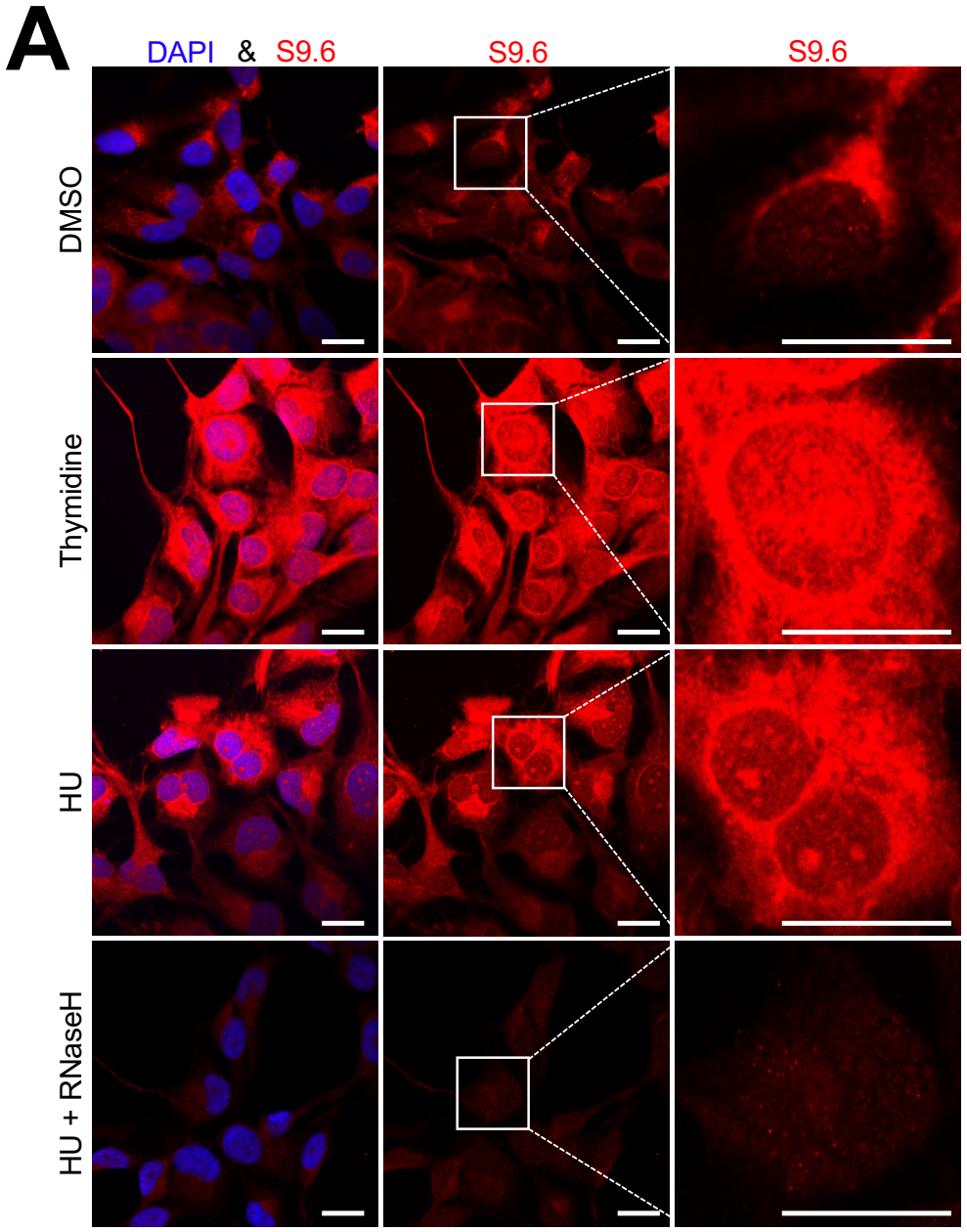


Figure 5.29: Specificity of S.9.6 staining for RNA:DNA hybrids and effects of replication stress-inducing positive controls – G7 primary GSCs were plated then incubated for 24 hours prior to exposure to either DMSO or the positive control treatments (HU 2mM or thymidine 3mM). GSCs were then exposed to sham irradiation 1 hour post DDRi treatments. Subsequently, cells were incubated for a further 6 hours as indicated prior to fixation and processing for RNA:DNA hybrids (see Methods – Section 2.17.3-4). Cells were imaged using a Zeiss LSM880 AiryScan confocal microscope (63x magnification). Scale bars = 20µm. **A.** Representative immunofluorescent staining for RNA:DNA hybrids using S9.6 antibody and DAPI to reveal the specificity of S.9.6 staining for RNA:DNA hybrids and effects of replication stress-inducing positive controls. **B.** Quantification of S9.6 nuclear mean fluorescence intensity (MFI). Data represents the quantification of segmented nuclei for 669 individual cells over 1 independent experiment (performed alongside Figure 5.30) to confirm assay robustness.

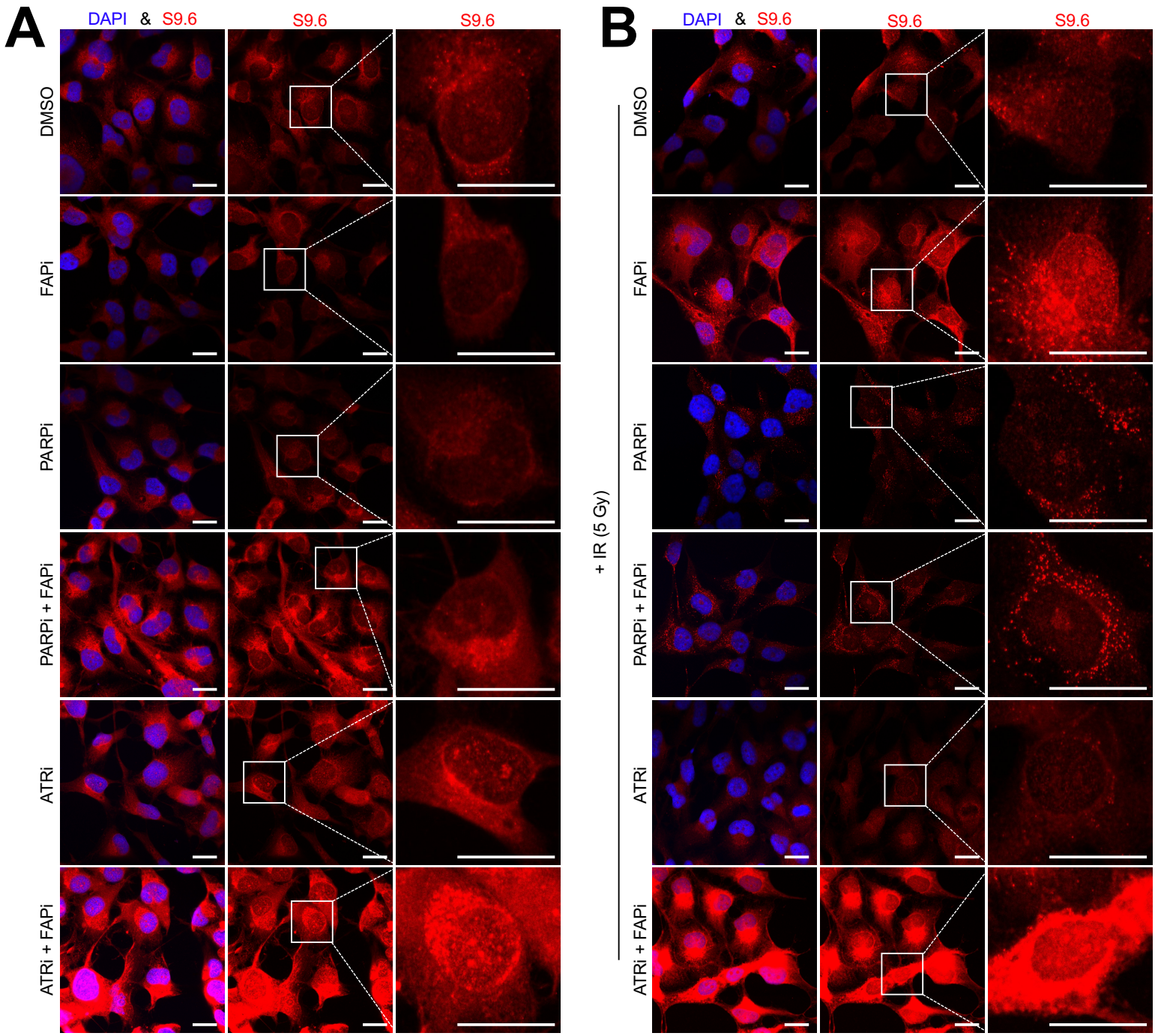


Figure 5.30: Combined FA pathway and ATR inhibition generates additional RNA:DNA hybrids in 2D G7 primary, patient-derived glioblastoma stem cells – (Figure continued overleaf).

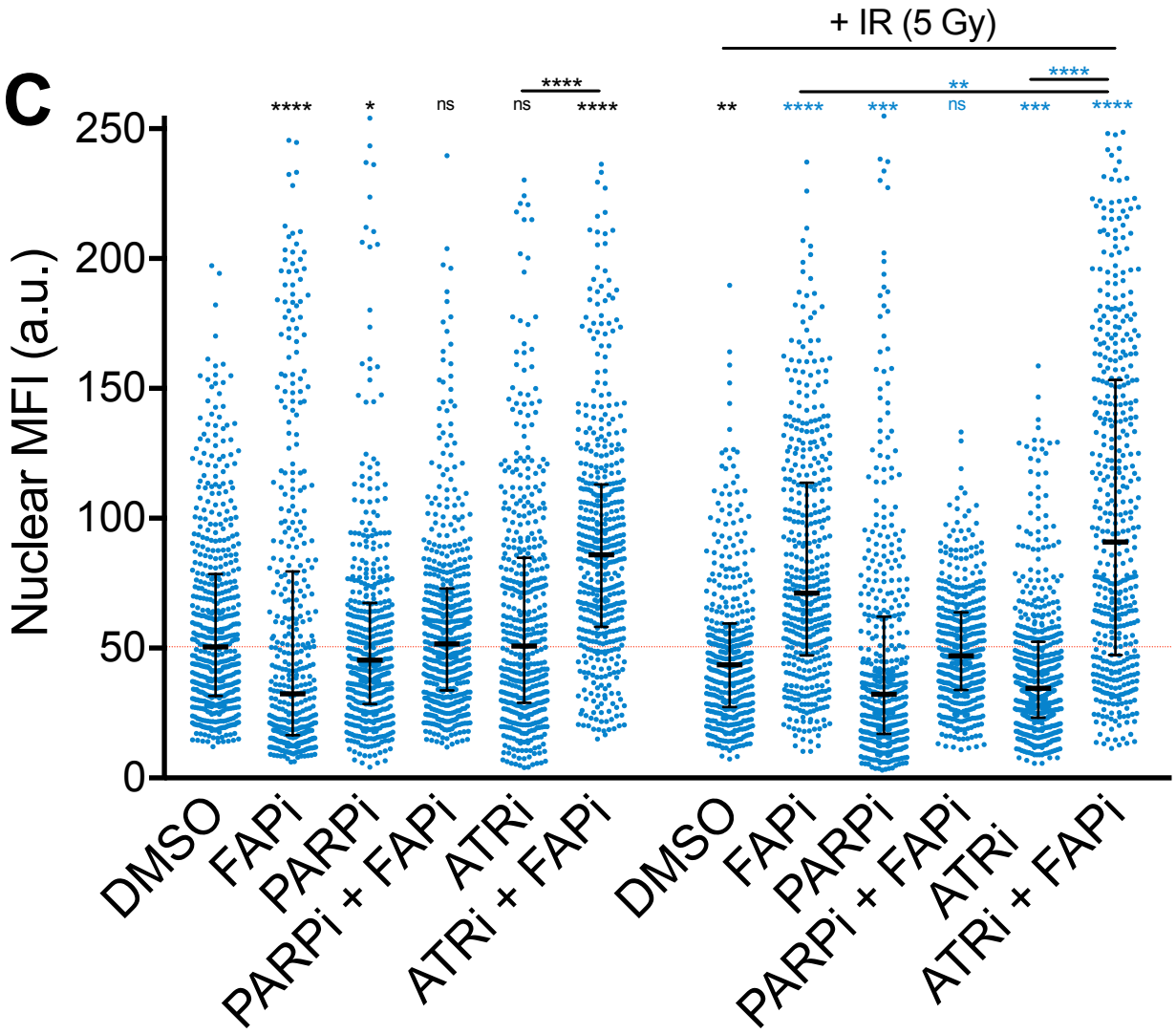


Figure 5.30: Combined FA pathway and ATR inhibition generates additional RNA:DNA hybrids in 2D G7 primary, patient-derived glioblastoma stem cells – (Figure continued from previous page) G7 primary GSCs were plated then incubated for 24 hours prior to exposure to either DMSO, positive control treatments (HU 2mM or thymidine 3mM – see Figure 5.29), or DDRi treatments: FAPi (curcumin 5μM); PARPi (olaparib 1μM); ATRi (AZD6738 1μM); PARPi + FAPi (olaparib 1μM + curcumin 5μM); ATRi + FAPi (AZD6738 1μM + curcumin 5μM). GSCs were then irradiated (or exposed to sham irradiation) 1 hour post DDRi treatments. Cells were incubated for a further 6 hours as indicated prior to fixation and processing for RNA:DNA hybrids (see Methods – Section 2.17.3-4). Cells were imaged using a Zeiss LSM880 AiryScan confocal microscope (63x magnification). Scale bars = 20μm. A-C. Representative immunofluorescent staining for RNA:DNA hybrids using S9.6 antibody and DAPI to reveal the: A. Effects of DDRi 6 hours following sham (0 Gy) treatment; B. Effects of DDRi 6 hours following irradiation with 5 Gy. C. Quantification of S9.6 nuclear mean fluorescence intensity (MFI). Data represents the quantification of segmented nuclei for 6,155 individual cells over 3 independent experiments (with the exception of thymidine, HU and RNaseH control data which was performed over 1 independent experiment to confirm assay robustness – see Figure 5.29). The distribution of nuclear MFI data for each condition was found to deviate significantly from a normal distribution ($p<0.0001$, Shapiro-Wilk normality test), therefore the median S9.6 nuclear MFI is indicated for each condition (black bar) and error bars represent the inter-quartile range (IQR). Red dashed line indicates median S9.6 nuclear MFI for control (DMSO only) GSCs. Nonparametric statistical comparisons between groups were performed using Kruskal-Wallis test with the Benjamini, Krieger and Yekutieli method used to correct for multiple hypothesis testing. Black asterisks (*) indicate significant difference relative to control GSCs, or between DDRi groups not treated with IR where indicated. Blue asterisks (*) indicate significant difference relative to GSCs treated with DMSO + IR (5 Gy), or between DDRi groups treated with IR where indicated.

Considered together, these data support a model where increased DNA replication stress induction resulting from replication-transcription conflicts constitute a putative mechanistic basis underpinning the high preclinical efficacy of ATRi + FAPi combinatorial strategies. Conversely however, although PARPi + FAPi based combinatorial strategies have demonstrable preclinical efficacy against primary GSCs (see Figures 5.13-15 & 5.18) and generate additional DNA damage (Figure 5.20), including increased DNA strand breaks (Figures 5.22-23) and specifically, an increased propensity for DNA DSBs (Figure 5.21), durable generation of additional replication-transcription conflicts at 6 hours post-IR/sham does not appear to contribute to the mechanism-of-action for this combination.

5.6.3 The effects of combined FA pathway and PARP or ATR inhibition on cell cycle progression in glioblastoma stem cells

Enhanced activation of cell cycle checkpoints has been previously reported as a feature of GSCs and may contribute to intrinsic therapeutic resistance[18,195,197]. Consequently, we hypothesized that the observed preclinical efficacy of FA pathway-based DDRi combinations might, in part, also be mediated by the modulation of cell cycle checkpoint kinetics. Consequently, the cell cycle profiles of GSCs at 6 and 24 hours post treatment were examined by incubation with PI and subsequent flow cytometry. Quantification of the estimated proportion of cells in G1, S and G2M phases for G7 GSCs are presented in Figure 5.31. Additionally, representative cell cycle profiles for G1 and G7 GSCs are illustrated in Figure 5.32.

Effects of DDRi on cell cycle progression (in the absence of IR)

Interestingly, despite earlier confirmation that DDRi strategies under evaluation generate additional DNA damage at the 6 hour timepoint (with the exception of PARPi – see Figures 5.22-23), these data reveal that in the absence of irradiation, treatment with FAPi, ATRi, PARPi or the combinations of PARPi + FAPi or ATRi + FAPi did not modify cell cycle progression in G7 GSCs at 6 or 24 hours.

Effects of DDRi-radiotherapy combinations on cell cycle progression

Following irradiation (5 Gy), G7 GSCs demonstrated accumulation of cells in G2/M with 33.7% (95% CI = 22.8-44.6%) of cells at 6 hours (vs 17.1% (10.1-24.1%) DMSO + 0 Gy control at 6 hours, p=0.0124), and 41.6% (40.7-42.6%) of cells at 24 hours (vs 23.4% (21.4-25.4%) DMSO + 0 Gy control at 6 hours, p<0.0001) consistent with an intact G2/M checkpoint

portending robust arrest – see Figure 5.31-32. Considering the various DDRi combinations assessed alongside IR, none appeared to generate noteworthy changes in cell cycle progression at 6 hours post IR. However, by 24 hours GSCs treated with PARPi prior to irradiation demonstrated heightened G2/M arrest relative to IR alone (56.0% (44.1-67.9%), p=0.0005), whilst the addition of FAPi did not significantly modulate this effect. ATRi treatment prior to irradiation resulted in abrogation of the G2/M checkpoint with only 23.1% (15.1-31.11%) of GSCs in G2/M phase, significantly less than GSCs treated with IR alone (p<0.0001), and equivalent to DMSO + 0 Gy control GSCs. Again the addition of FAPi did not modify this effect.

Taken together, these data demonstrate that in combination with IR, PARPi exacerbate G2/M arrest whilst ATRi result in loss of the G2/M checkpoint with cell cycle arrest in G1-phase. However, incorporating these targeted therapies into a FAPi based DDRi combination does not modify their effects on cell cycle progression and therefore, the additional preclinical efficacy observed with these combinations is not achieved through changes in cell cycle kinetics. Nevertheless, the effects of additional DNA damage generated by DDRi combinations (PARPi + FAPi, ATRi + FAPi) might be exacerbated by PARPi/ATRi-mediated modification of cell cycle kinetics, for example inappropriate progression through the G2/M checkpoint with ATRi despite a plethora of unresolved DNA damage engendered by the ATRi + FAPi combination. This would certainly be consistent with the dramatic decrease in clonogenic survival observed using ATRi + FAPi as a radiosensitising DDRi combination (see Figure 5.24).

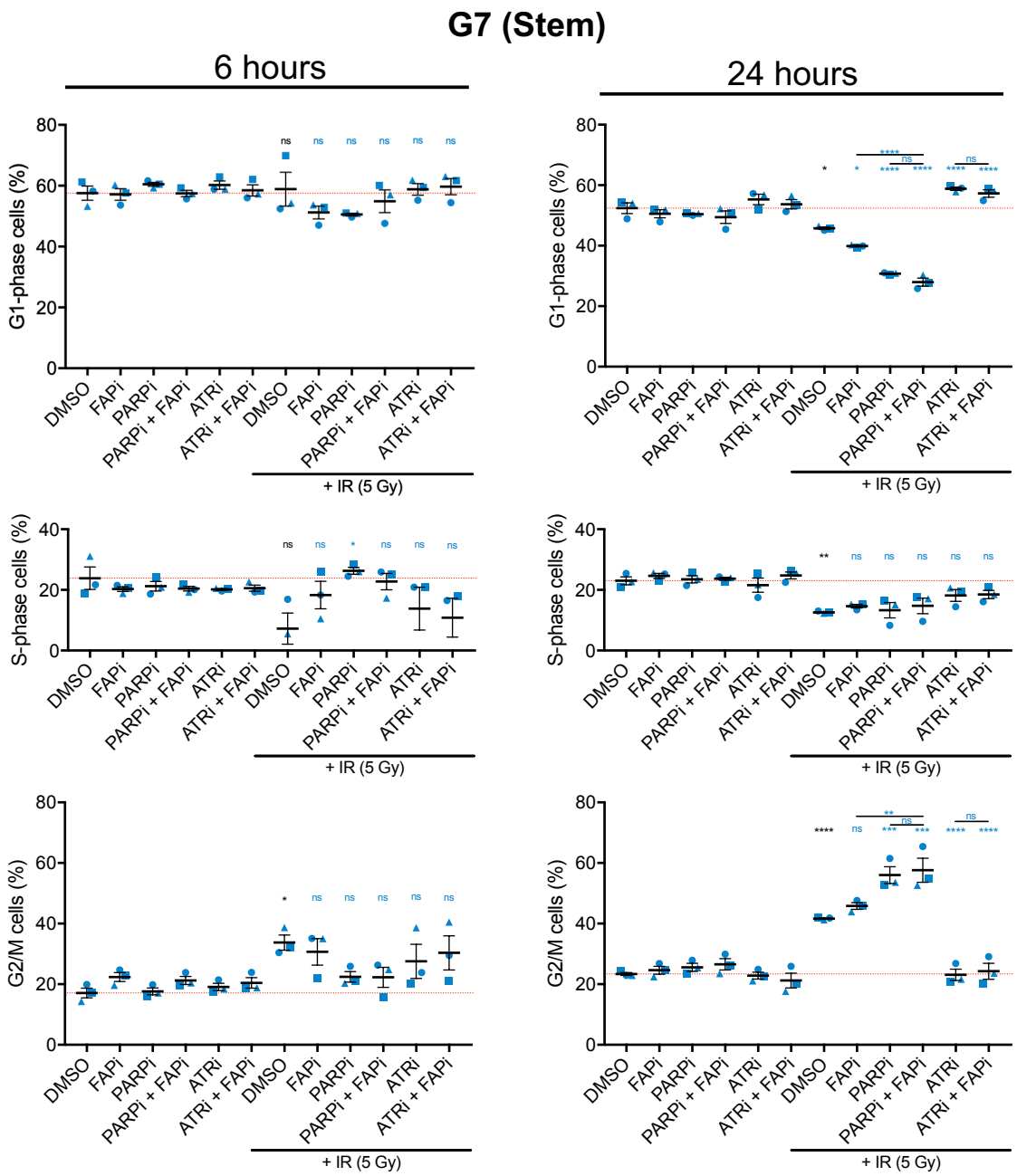


Figure 5.31: The effects of FA pathway, PARP and ATR inhibition on cell cycle progression in 2D G7 primary, patient-derived glioblastoma stem cells – G7 primary GSCs were plated then incubated for 24 hours prior to exposure to either DMSO or DDRi treatments: FAPi (curcumin 5μM); PARPi (olaparib 1μM); ATRi (AZD6738 1μM); PARPi + FAPi (olaparib 1μM + curcumin 5μM); ATRi + FAPi (AZD6738 1μM + curcumin 5μM). GSCs were then irradiated (or exposed to sham irradiation) 1 hour post DDRi treatments. Cells were incubated for a further 6 or 24 hours as indicated prior to PI staining and flow cytometry analysis (see Methods – Section 2.19). Quantification of cell cycle phase. Data represents the mean 3 independent experiments (black bars) with each consecutive experiments denoted by the blue symbols. Error bars represent the SEM. Red dashed line indicates mean tail DNA for control (DMSO only) GSCs. Statistical comparisons between groups using ANOVA with Sidak correction to adjust for multiple hypothesis testing. Black asterisks (*) indicate significant difference relative to control GSCs, or between groups not treated with IR where indicated. Blue asterisks (*) indicate significant difference relative to GSCs treated with DMSO + IR (5 Gy), or between groups treated with IR where indicated. **Note:** p53 status of G7 has previously been confirmed as wild-type by Sanger sequencing[467], whilst status of G1 GSCs remains unknown.

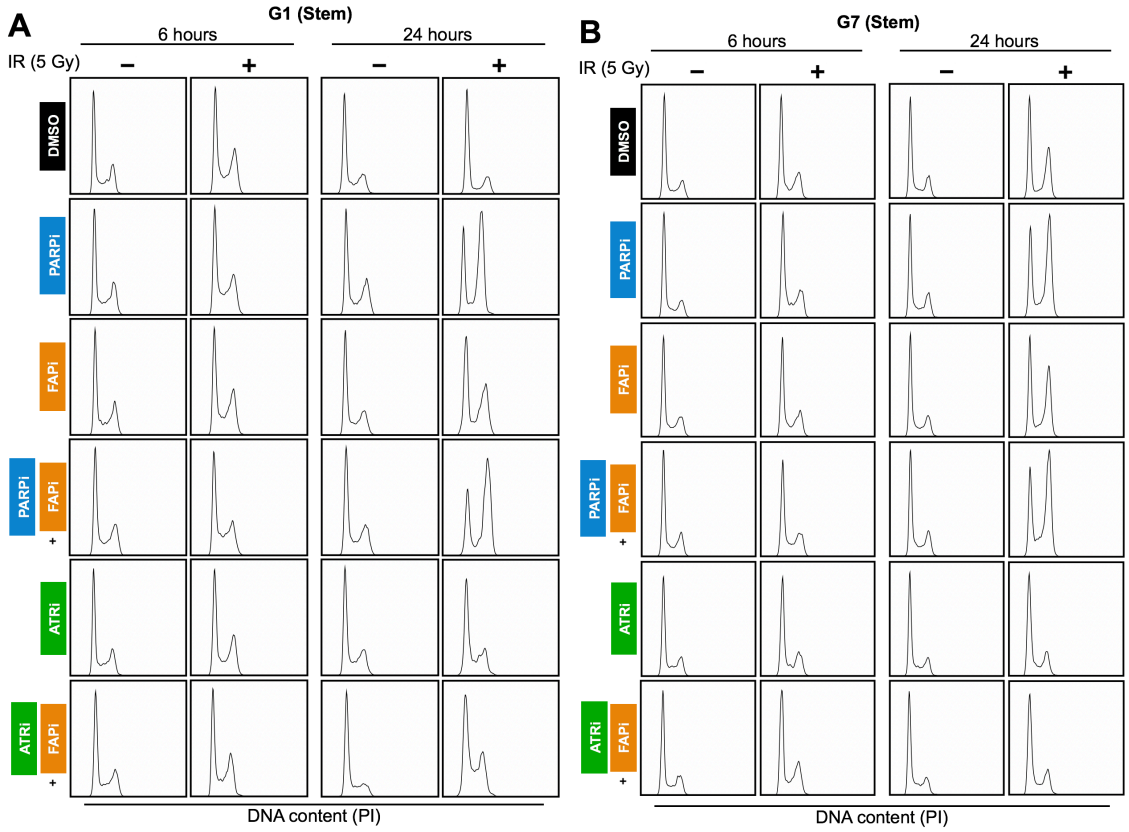


Figure 5.32: The effects of FA pathway, PARP and ATR inhibition on cell cycle progression in 2D G1 and G7 primary, patient-derived glioblastoma stem cells (representative cell cycle profiles) – G1 and G7 primary GSCs were plated then incubated for 24 hours prior to exposure to either DMSO or DDRi treatments: FAPi (curcumin 5μM); PARPi (olaparib 1μM); ATRi (AZD6738 1μM); PARPi + FAPi (olaparib 1μM + curcumin 5μM); ATRi + FAPi (AZD6738 1μM + curcumin 5μM). GSCs were then irradiated (or exposed to sham irradiation) 1 hour post DDRi treatments. Cells were incubated for a further 6 or 24 hours as indicated prior to PI staining and flow cytometry analysis (see Methods – Section 2.20).

5.7 Summary of key findings

The FA pathway in patients and primary, patient-derived glioblastoma models

- The mRNA expression of FA pathway genes increases with aggressiveness of glioma grade and high expression is associated with worse patient survival.
- In glioblastoma, FA pathway gene expression is elevated within inherently treatment resistant glioblastoma stem cell (GSC) subpopulations, relative to tumour 'bulk' cells.
- Following treatment with DNA damaging temozolomide chemotherapy GSCs activate the FA pathway within 30 minutes and maintain activation for at least 24 hours.

Targeting the FA pathway in clinically-relevant models of glioblastoma

- The cardiac glycoside ouabain inhibits the FA pathway and sensitises established glioblastoma cultures and GSCs to radiotherapy.
- The novel compound F76 inhibits FANCD2 monoubiquitination in a dose-dependent manner and sensitises G1, but not G7, GSCs to radiotherapy.
- Curcumin inhibits both IR and temozolomide-induced FA pathway activation in a dose-dependent manner and radiosensitises 2D (G1 & G7) and 3D (G7 only) GSCs.

Combined targeting of the FA pathway and PARP to enhance therapeutic response

- Simultaneous inhibition of the FA pathway (FAPi) and PARP (PARPi) enhances radiosensitisation in 2D and 3D patient-derived GSC models.
- Combined PARPi + FAPi modifies the α/β ratios of 3D GSC models to values more consistent with tumours/tissues which respond acutely to radiotherapy.
- In the context of radiosensitisation, combined PARPi + FAPi maintains high DNA damage for at least 6 hours, with persistently elevated damage including DSBs for at least 24 hours.
- In the context of temozolomide-induced DNA damage, combined PARPi + FAPi confers a modest benefit over PARPi alone in 3D G1 and G7 GSCs.

Combined targeting of the FA pathway and ATR/ATM to enhance therapeutic response

- Simultaneous FAPi and inhibition of ATR (ATRi) represents a profoundly radiosensitising DDRi combination in 3D G7 GSCs.
- Combined ATRi + FAPi portends substantially elevated IR-induced DNA damage for at least 24 hours in G7 GSC, which greater than either single DDRi at 6 and 24 hours.
- ATRi profoundly sensitises 3D G7 GSC to temozolomide chemotherapy.
- Relative to ATRi alone, combined ATRi + FAPi does not further enhance sensitisation throughout the range of temozolomide doses evaluated, but does enhance sensitisation at temozolomide concentrations expected within the CSF (~10μM) and peritumoural brain tissue (≤5μM).
- Inhibition of ATM (ATMi) potently radiosensitises 3D G7 GSC, however the addition of simultaneous FAPi provides additional sensitisation.
- ATMi potently sensitises 3D G7 GSC to temozolomide, but simultaneous FAPi provides no further sensitisation (except at 5μM temozolomide).

Effects of FA pathway-based DDRi combinations on RNA:DNA hybrids and cell cycle progression

- The PARPi + FAPi combination does not appear to modulate RNA:DNA hybrid frequency at 6 hours post IR or sham.
- In the absence of radiotherapy, the combination of ATRi + FAPi elicits a marked increase in RNA:DNA hybrids.
- Combined with radiotherapy, both single DDRi with FAPi, or the combination of ATRi + FAPi generate a substantial increase in RNA:DNA hybrids, however the latter is significantly more potent in this regard.
- Using the ATRi + FAPi combination, equivalent generation of RNA:DNA hybrids was observed irrespective of whether or not radiotherapy was added.
- The PARPi + FAPi combination does not appear to modulate RNA:DNA hybrid frequency at 6 hours post IR or sham.
- At 24 hours post-radiotherapy, PARPi evokes robust G2/M cell cycle arrest, whereas ATRi completely abrogates the G2/M checkpoint leading to cell cycle arrest in G1-phase – however, the addition of FAPi to either of these strategies does not further modulate cell cycle dynamics.

5.8 Discussion

5.8.1 General Study limitations

Potential pleiotropic effects of compounds used to inhibit the FA pathway

In this chapter, 3 distinct drugs were used as tool compounds to inhibit the FA pathway, namely: curcumin; a novel, specific FANCL inhibitor F76, and; the cardiac glycoside, ouabain. Theoretically, an ideal compound for use in these studies would reliably inhibit the FA pathway at low-nanomolar concentrations, exhibit no toxicity as a monotherapy, and engender no off-target (i.e. non-FA pathway mediated) effects. Unfortunately, no such compound currently exists. Consequently, the data generated throughout this Chapter must be interpreted in the context of the potential promiscuity of the FA pathway inhibitors utilised. Although, curcumin is well-known and used as an FA pathway inhibitor in research[20,284,285,464], it exerts a range of non-FA pathway/DDR-mediated effects which are discussed at length in Chapter 3 – Section 3.6.3), and its mechanism of action on the FA pathway is currently unknown. However, it is important to emphasize that previous research from our laboratory demonstrated that curcumin conferred chemosensitivity to U87 glioblastoma cells in a FANCD2-dependent manner[22], supporting the centrality of this DDR process in the therapeutic potential of curcumin. In contrast, the effects of F76 should be notably FA pathway specific since this compound is a product of an ongoing drug development process to identify compounds that bind to FANCL with consequent abrogation of its E3 ligase activity and therefore FANCD2 monoubiquitination. Studies in the Collis laboratory have shown that 3 related compounds in this chemical series exhibit temozolomide sensitisation through FA pathway dependent mechanisms, and preliminary unpublished data demonstrates potential target engagement of F76 with FANCL in CETSA studies. Furthermore, internal data within our laboratory confirms nFAPi do not modulate the DDR via ATM- or ATR-mediated mechanisms, however more comprehensive exclusion of potential 'off-target' effects with F76 and related nFAPi is ongoing and these compounds are subject to other flaws which are discussed in detail in Chapter 3 – Section 3.6.2). Finally, ouabain has also been reported to exert a number of intracellular effects which are not or not likely to be mediated by FA pathway inhibition. The potential pleiotropic effects of ouabain are discussed in detail below. As these studies were translationally driven, we aimed to use compounds with the potential for future clinical implementation within novel anti-cancer therapeutic strategies, however the use of additional molecular techniques such as RNA interference studies might have added further confidence that beneficial therapeutic

effects of targeting the FA pathway were mediated exclusively through FA pathway-based mechanisms. Notably, we highlight that, although feasible[486,487], primary patient-derived GSCs may be challenging to transfect with RNAi. Indeed the use of FANCL-targeted siPOOLs™ siRNA (consisting of a pool of 30 different sequences of siRNA to the target gene, siTOOLs Biotech) at typical concentrations of 1nM and 3nM (which were extremely effective in established T98G glioblastoma cells) did not deplete FANCL in primary GSCs (data not shown), therefore robust development of the optimal conditions for such studies is needed. Nevertheless, we emphasize that the use of 3 structurally divergent compounds (curcumin, ouabain, F76), with each confirmed to inhibit FA pathway activity in these studies and sensitise some or all models tested to DNA-damaging therapy, provides strong support for targeting the FA pathway as a therapeutic strategy to counteract the inherent therapeutic resistance of GSCs.

The intracellular effects of ouabain

To the best of our knowledge, these studies represent the first to confirm ouabain is able to inhibit the FA pathway (Figure 5.9 & Supplementary Figure 5.1) and potently radiosensitise both established glioblastoma cells and primary GSCs (Figure 5.10) at sublethal doses (Supplementary Figures 5.1-2). Nevertheless, the potential of ouabain as a radiosensitiser more generally has been established for over 30 years. A report by Lawrence et al (1988)[488], demonstrated its ability to modify the radiation response of A549 lung adenocarcinoma cells, but with no similar effect on normal lung fibroblasts, highlighting a potential to enhance the therapeutic index of IR[488]. Despite this early report, it is not entirely clear which mechanism(s) are primarily responsible for the therapeutic and radiosensitising effects of ouabain.

Traditionally, ouabain has been used in the clinic to treat heart failure and in this context exerts positive inotropic effects on cardiac myocytes by rapid inhibition of Na^+/K^+-ATPase enzymes. The interaction of ouabain with these critical membrane-bound sodium pumps perturbs intra-extracellular sodium gradients and therefore, indirectly, the activity of Na^+/Ca^{2+}-exchangers resulting in elevated cytosolic Ca^{2+} and increased myocyte contractility[489]. However it is clear that, in interacting with Na^+/K^+-ATPase pumps and fundamentally perturbing cellular Na^+ and Ca^{2+} gradients, ouabain may have numerous effects[490-493]. For example, Yang *et al.* (2018)[494] recently assessed the effects of ouabain as a monotherapy on established U87 glioblastoma cells. Using cell viability assays, they

reported an LD_{50} value of 450nM which is not too dissimilar from the range of values we report for established glioblastoma cell lines (U87 LD50 = 256nM; all established lines 256-7184nM – Figure 5.7). Yang *et al.* (2018)[494] reported that ouabain treatment repressed AKT/mTOR signalling with reductions in the level of p-AKT, p-mTOR and HIF-1α[494]. Although postulated, the studies by Yang *et al.* (2018)[494] did not provide evidence to confirm reduced AKT/mTOR signalling as the cause of reduced cell viability and migration observed in the studies. Interestingly, although Yang *et al.* (2018)[494] did not assess any combination with IR, the depletion of HIF-1α by ouabain treatment observed in their studies might provide an alternative (i.e. non-FA pathway-related) mechanistic route to radiosensitisation[495,496]. However, importantly Yang *et al.* (2018)[494] found that treatment with ouabain at a 500nM concentration was not sufficient to significantly reduce protein levels of HIF-1α in glioblastoma cells, indeed the lowest dose demonstrated to reduce HIF-1α was 2.5μM. Since our studies demonstrate robust FA pathway inhibition and radiosensitisation using lower ouabain doses of 100-250nM, even accounting for differences between cell lines, it seems unlikely that ouabain-mediated reduction in HIF-1α would provide an adequate explanation for the observed radiosensitising effect.

Ouabain has also been demonstrated to globally reduce protein synthesis with reduced ^{3}H-valine incorporation following exposure to concentrations ≥200nM for 4 hours[488]. Speculatively, these effects might explain the reduction in both monoubiquitinated and non-ubiquitinated FANCD2 observed following ouabain exposure. However since, doses of cycloheximide which repressed ^{3}H-valine incorporation more profoundly failed to provide similar radiosensitisation to ouabain[488], it is unlikely that the FA pathway inhibition and enhanced radiosensitivity we report with ouabain occurs as a result of reduced protein synthesis. Perhaps more relevant is the recent identification of ouabain as a 'hit' in a screen of 1,540 compounds for NHEJ inhibitors by Du et al. (2018)[465]. This screen used a CRISPR/Cas9-based system to produce a DSB in the gene loci of hypoxanthine guanine phosphoribosyltransferase (HPRT) or heparin-binding EGF-like growth factor (HBEGF) then used high-resolution melting (HRM) analysis (a PCR-based method for detecting DNA sequence variation) to quantify mutational frequency – which was used as a surrogate to reflect NHEJ activity, which is typically considered to repair DSBs with low fidelity. Critically, this screening methodology did not segregate the relative effects of compounds on canonical Ku-dependent NHEJ (cNHEJ), or alternative NHEJ (alt-NHEJ, also known as mutagenic-NHEJ), which is widely regarded as more error prone than cNHEJ[497].

Furthermore, the screening methodology in no way excluded compounds which also reduced high-fidelity DSB repair by HR. Indeed, further investigation by Du *et al.* (2018)[465] using reporter assays revealed that ouabain evoked a substantially greater reduction in HR activity (~60-70% reduction) than in NHEJ (~20% reduction). Given that, numerous downstream FA proteins are directly implicated in HR (FANCD1/BRCA2, FANCJ/BRIP1, FANCN/PALB2, FANCO/RAD51C, FANCR/RAD51, FANCS/BRCA1, FANCU/XRCC2)[27] and siRNA mediated depletion of FA core complex (FANCA, FANCC, FANCG, FANCL) and ID complex (FANCD2) genes has been demonstrated to simultaneously reduce both HR and alt-NHEJ DSB repair capacity within the same cells using a bi-functional reporter assay[497], it seems plausible that broader effects of ouabain on the DDR and radiosensitivity are mediated primarily by its effects on the FA pathway. This would be consistent with previous studies which highlight a role of the FA pathway in orchestrating DSB repair pathway 'choice', for example through preventing engagement of DNA-PKcs to suppress inappropriate cNHEJ[131].

Furthermore, a potential mechanistic basis for the FA pathway inhibition observed with ouabain has been revealed which is dependent on p38 and transduced through Na^+/K^+-ATPase effects on the SRC-Ras-Raf-MAPK cascade[498]. This is strongly supported by the work of Jun *et al.* (2013)[464] which demonstrated that ouabain exposure elicited the phosphorylation of JNK, ERK and p38 within 5 minutes of exposure, whilst simultaneous inhibition of p38 with SB203580 completely reversed the inhibitory effects of ouabain on FANCD2 monoubiquitination. Taken together, the above studies and our data suggest that, whilst the effects of ouabain are clearly pleiotropic in nature, influence of the FA pathway may well play a central role in ouabain-mediated radiosensitisation.

Selection and application of glioblastoma stem cell models

Although 2D and particularly 3D primary, patient-derived GSC models are regarded to be more biologically- and clinically-relevant than traditional 2D established cell cultures (discussed in Chapter 4 – Section 4.1) for preclinical glioma research, the implementation of these models is not without limitation.

Firstly, the propagation and use of primary GSCs is associated with considerably high costs. In particular the use of: Matrigel™ (£445 per 10ml) as a substrate to ensure GSCs adhere to plasticware; the supplements B27 (£637 per 100ml) and N2 (£563 per 50ml), and; growth

factors EGF (£293 per 100μg) and FGF (£411 per 100μg), to promote GSC growth in serum-free media and promote the stem cell phenotype[99,100], contribute to the expensive nature of experiments with primary GSCs, particularly experiments with high media and plasticware consumption such as clonogenic studies. Additionally, for 3D studies, the use of Alvetex™ scaffolds (£2,176 per box of 80x 12-scaffold plates) added further considerable cost to these studies. These financial considerations and the range of therapeutic combinations evaluated during these studies (FAPi +/- PARPi +/- IR/TMZ and FAPi +/- ATRi/ATMi +/- IR/TMZ and ATRi + PARPi +/- IR) limited the number of cell lines that could be used to typically 1-2 for 3D studies and 1-3 for 2D studies. In view of these constraints, we typically used a single, optimised dose of each DDRi in conjunction with a dose range of radiotherapy or temozolomide chemotherapy. The lack of response data for multiple DDRi doses in conjunction with temozolomide precluded meaningful calculation of a Combination Index (CI) as per the Chou-Talalay method[499] or further visualisation and interrogation of synergy using software tools such as the Combenefit platform[500]. Nevertheless, using clinically-relevant patient-derived models, our studies provide highly informative and interesting data that describe the therapeutic effects of pharmacologically inhibiting multiple key DDR processes on chemosensitivity across a range of temozolomide concentrations which reflect those expected within the CNS of patients. Additionally, through fitting data from IR-based experiments to a linear-quadratic model, we were able to generate $SER_{0.37}$ values, as an established measure of radiosensitising potential[195,197,208], for each DDRi and DDRi combination evaluated.

During experiments comparing the features of GSCs to bulk tumour cell populations (see Figure 5.4), the propagation of patient-derived glioblastoma cells in MEM + 10% FCS in order to elicit a more differentiated phenotype akin to 'bulk' cells remains a source of potential criticism. We (and other groups[99,100,108,195]) have confirmed that these conditions (serum-free media with EGF and FGF for GSC vs serum-containing media) promote high and low expression of putative stem cell factors in GSC and bulk tumour cells, respectively (see Chapter 4 – Figures 4.2 & 4.10B). Nevertheless, it is not inconceivable that differences in the expression of FA pathway genes between GSCs and bulk cells, for example, could be mediated by uncharacterised effects of propagating these cell populations in culture media with different properties, rather than by the well characterised effects of each media on stemness. In conjunction to the approach used here, some studies have used FACS to sort primary glioblastoma cells on the basis of well-established stem cell markers such as CD133

to enable further interrogation of the properties of 'stem' (e.g. CD133+) and 'non-stem/bulk' (e.g. CD133-) glioblastoma cells using identical culture media[208]. It may have been informative to apply such an approach in parallel during these studies, however sorting glioblastoma cells in this way may represent an even more limited approach, since there is no good, single universal marker for GSCs[354]. Furthermore, glioblastoma cells exhibit substantial plasticity[501], and therefore may not remain stable along the spectrum of 'stemness' even after sorting for a particular feature or marker. Considering these, the use of differential media in these studies to consistently promote stemness in GSCs and differentiation in bulk cells may be more informative than commonly used alternative methodologies.

5.8.2 Emerging clinical relevance of the FA pathway in glioblastoma

These studies support a biological relevance of the FA pathway in gliomas, with more aggressive grade IV glioma (glioblastoma) exhibiting higher expression of FA pathway genes than lower grades of glioma, which in turn express higher levels than normal brain tissue (Figure 5.1). This finding is consistent with previous work by Patil *et al.* (2014)[22] which used immunohistochemistry to demonstrate increasing protein expression of FANCD2 with increasing glioma grade. Similarly, Rasmussen *et al.* (2016)[502] demonstrated that FANCS/BRCA1 protein expression increased in parallel with glioma grade. However, the analysis presented in this thesis expands the relevance of the FA pathway in gliomas to a transcriptional level and underlines the relevance of FA genes within 3 functionally defined groups (core complex; ID complex; downstream). The observations that all 3 functional groups exhibit highest FA expression in glioblastoma (Figure 5.1), and that the co-expression of FA functional groups demonstrate high correlation in gliomas but no correlation in normal tissue (Figure 5.2) support a notion that the entire, canonical FA pathway retains importance in gliomas, rather than important functions being mediated by additional non-canonical effects of a single or a sub-set of FA pathway genes.

Critically, we also demonstrate for the first time that high mRNA expression of FA pathway genes is a feature of GSCs (Figure 5.4), with the implication that the FA pathway may contribute to therapeutic resistance in patients mediated through intra-tumoural heterogeneity similar to the role of elevated pATM/pCHK2 and pCHK1 in inherently recalcitrant GSC subpopulations identified in the landmark paper by Bao *et al.* (2006)[18]. Importantly, we confirm that high expression of FA pathway genes in glioblastomas is

associated with worse patient survival (Figure 5.3), highlighting an important and underreported link between the FA pathway and biologically aggressive disease with gliomas.

In the clinic, post-surgical management for glioblastoma consists of daily 2 Gy fractions of radiotherapy given 5 days per week for 6 weeks (to deliver 10 Gy/week – 60 Gy in total) alongside continuous daily temozolomide (75mg/m^2 body-surface area) 7 days a week until the completion of radiotherapy, followed six 28-day cycles of higher dose temozolomide therapy (150-200mg/m^2 body-surface area) where chemotherapy is delivered in 5 day blocks interspersed between 23-day periods to allow the recovery of normal tissues[10,11]. Consequently, our time-course data which demonstrates rapid FANCD2 monoubiquitination within 30 minutes of exposure to temozolomide with sustained elevation of pathway activity for at least 18 hours (Figure 5.5) suggests the FA pathway is likely to be persistently activated in GSCs within patient (residual) tumours during the initial 6 weeks of adjuvant therapy. Consequently, combinatorial strategies aiming to abrogate FA pathway activity on a daily basis during this temporal therapeutic window may be particularly effective. In contrast, during the subsequent months of adjuvant temozolomide, treatment with an FA pathway inhibitor might only be indicated for 5-6 days in every 28 day cycle alongside the administration of chemotherapy. Additionally, with respect to radiotherapy response, our data illustrates the combination of PARPi + FAPi substantially increases α/β ratios in clinically-relevant 3D GSC models (Figure 5.18-15). This supports the potential use of FA pathway-based DDRi combinations to modify the radiobiology of recalcitrant GSC subpopulations towards a more acutely responding phenotype. Although not directly evaluated in these studies, the substantial shift in α/β ratios raises an encouraging possibility that strategies incorporating PARPi + FAPi with fractionated radiotherapy might demonstrate even greater efficacy whilst helping substantially widen the therapeutic index between neoplastic and healthy tissue. Overall, these results, and those describing the kinetics of interconnected DDR processes (Figure 5.6) should help inform some of the practicalities (such as dose scheduling, intensity and radiotherapy fractionation) associated with the clinical translation of DDR-targeting strategies investigated within this thesis.

On the whole, these studies and previous work[22] describe elevated FA pathway expression and activity in glioblastoma. However, it is clear that a prominent FA pathway is not a cancer-

associated feature within a modest proportion of cases – for example, some tumours demonstrate FA pathway mRNA expression values similar to or less than those observed in normal tissue (Figure 5.1-2). Interrogation of the status of all 22 known FA pathway genes in glioblastoma within the TCGA cohort[32,60] via cBioportal suggests 37.8% of patient tumour samples (603 samples) harbour at least 1 FA pathway molecular alteration. Approximately 2.7% of tumours demonstrate somatic mutations, some of which may be associated with loss-of-function. Furthermore, 2.0% of tumours demonstrate low mRNA expression of an FA pathway gene, 1.0% demonstrate low expression of an FA pathway protein, and 5.0% demonstrate multiple FA pathway alterations (Figure 5.33). Given the findings presented in this thesis which suggest simultaneous FAPi and PARPi may represent a potent chemo/radiosensitising combination and FAPi with ATRi or ATMi both represent exquisitely radiosensitising combinations (discussed further below), it is likely that constitutive loss of or low FA pathway activity in a subset of glioblastoma might predispose these particular tumours to heighted sensitivity to PARPi, ATRi or ATMi in the clinic as a single DDRi strategy to enhance responses to current DNA damaging therapies. Many foundations required for the clinical translation of such strategies are already in place, for example: despite low penetration of intact BBB, olaparib has been demonstrated to readily cross the blood-tumour barrier (BTB) and penetrate the core and margin of patient's specimens in sufficient concentration to inhibit PARP (OPARATIC trial[272]); the ATRi inhibitor used in these studies, AZD6738, demonstrates effective BBB penetration[475], and; more recently developed ATM inhibitors, such as AZD1390 which display excellent BBB penetration and efficacy in orthotopic xenograft models, have become available[268]. In view of this, further studies to explore the utility of surrogate measures of low FA pathway activity such as: low gene expression; failure of FANCD2 monoubiquitination (as previously observed in the U138 glioblastoma cell line[22]), or; reduced formation of FANCD2 foci in response to DNA damage, as predictive biomarkers for PARPi/ATRi/ATMi-mediated chemo- and radiosensitisation in patients with glioblastoma would be incredibly informative and could rapidly support clinical trial stratification and advances in patient care for molecularly defined subgroups. Early validation of such biomarkers could incorporate assessment of their ability to accurately predict *ex vivo* therapeutic efficacy as planned in our recently funded studies (see Chapter 6 – Section 6.2.4).

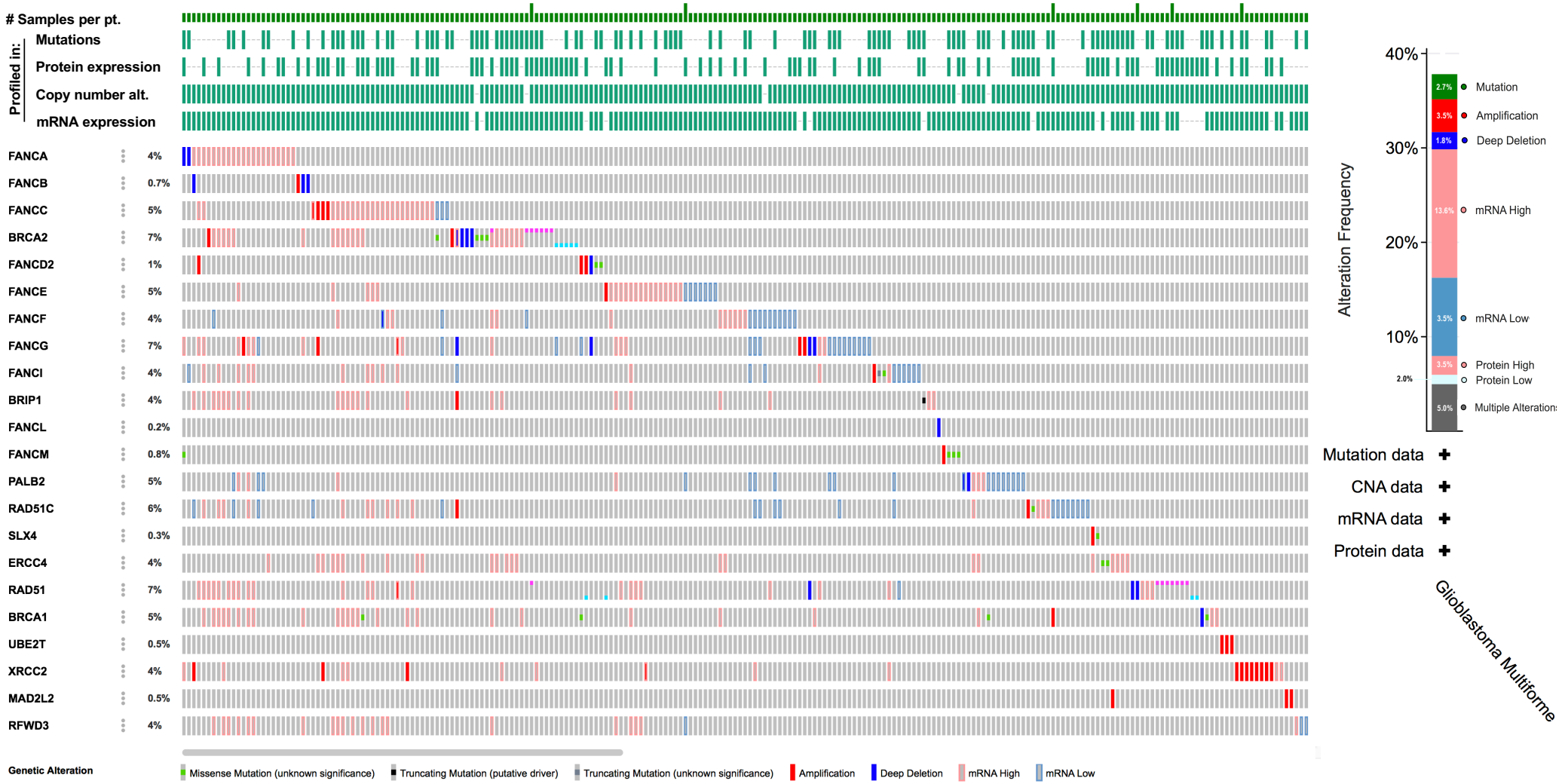


Figure 5.33: FA pathway molecular alterations in 603 glioblastoma samples (TCGA cohort) – OncoPrint and molecular alteration frequency of all 22 known FA pathway genes in 603 glioblastoma samples (from 591 patients). Adapted from cBioPortal for Cancer Genomics (www.cbioportal.org).

5.8.3 *FA pathway-based, DDR-targeting combinations as a novel therapeutic strategy for glioblastoma*

Previous studies that analysed the expression of key DDR proteins in clinical specimens have revealed high levels of FA pathway proteins (FANCD2[22], FANCS/BRCA1[502]), pCHK1[503], pCHK2[503], pATM[503], and PARP1[466] in glioblastoma. Furthermore, treatment resistant GSC populations have been demonstrated to express elevated pCHK1, pCHK2 and pATM[18] (which is consistent with our findings in Figures 5.6 and 5.19). Data presented in this Chapter extends the concept of GSC-specific elevation of DDR expression to the FA pathway, demonstrating that FANCA, FANCC, FANCL, FANCD2, FANCI, FANCS/BRCA1 and FANCD1/BRCA2 mRNA were significantly raised in at least 1 patient-derived GSC line relative to bulk populations (Figure 5.4). This finding is consistent with recent work by King *et al.* (2017)[253] which identified greater than expected immunohistochemical co-staining between cells positive for FANCR/RAD51 and the putative GSC markers SOX2 and nestin. Importantly though, investigation of genes implicated in the FA core complex, ID complex and downstream in our studies confirm the association between GSCs and the FA pathway is not exclusive to downstream factors with known HR functions (FANCR/RAD51, FANCS/BRCA1, FANCD1/BRCA2), and is therefore more likely to be associated with canonical FA pathway function, which is apparent in glioblastoma (Figure 5.2). Therefore, considered in context with previous research, these studies support the FA pathway and interconnected DDR players including PARP1 and the ATR-CHK1 and ATM-CHK2 axes as viable and exploitable therapeutic targets to eradicate GSCs.

The effects of FA pathway inhibition on GSC sensitivity to current adjuvant therapies

Previous studies have demonstrated that inhibition of the FA pathway in established[20-22], patient-derived[22], and patient-derived GSC models[225] can sensitise high-grade gliomas to alkylating chemotherapy including temozolomide. Furthermore, proteosomal-mediated degradation of FANCD2 using the plant derivate celastrol has recently been shown to enhance the sensitivity of paediatric high-grade gliomas to the ICL-inducing therapy carboplatin[504], and small-molecule inhibition of FANCR/RAD51 has been confirmed to radiosensitise GSCs[253,505]. Considered collectively, these studies suggest FA pathway inhibition as a therapeutic strategy may be capable of enhancing the sensitivity of glioblastoma cells to a range of deleterious DNA lesions induced by current adjuvant treatments. Furthermore, these studies are consistent with our findings that demonstrated 3 structurally distinct pharmacological compounds that inhibit FANCD2 monoubiquitination

were able to evoke radiosensitisation in GSCs (with the exception of F76 in G7 cells) – see Figures 5.8, 5.10 and 5.13. However, the use of 2D cell viability and survival assays represents a common feature of these experiments and the previous studies above. Interestingly, when the potential of FA pathway inhibition using curcumin was assessed in more clinically-relevant 3D Alvetex™ scaffold-based GSC models, which have previously been shown to better predict therapeutic efficacy in clinical trials compared to conventional 2D models[106,108], no consistent sensitisation to radiotherapy (Figures 5.14 and 5.20) or temozolomide chemotherapy (Figures 5.18 and 5.21) was observed. To refute the possibility that curcumin might bind to the polystyrene architecture of the scaffold, leaving less free drug available, or not reach cells embedded within the scaffold, we assessed the effects of curcumin on FA pathway activation in GSCs treated within the 3D model. Crucially, the dose of curcumin used in 3D clonogenic studies was confirmed to substantially reduce FANCD2 monoubiquitination of GSCs within these 3D architectures (Figures 5.13 & 5.17), therefore the lack of chemo- or radiosensitisation observed in 3D clonogenic studies (which is entirely in contrast to 2D studies presented here and reported previously in high-grade gliomas[20-22,225,253,504,505], and other types of cancer[285,497,506,507]) are likely to reflect genuine biological differences in therapeutic sensitisation mediated by FA pathway inhibition between traditional 2D and clinically-relevant 3D GSC cultures. Interestingly, our results in 3D studies are consistent with findings from multicellular organisms, since Collis *et al.* (2006)[508] previously observed that although loss-of-function FANCD2 mutations in the nematode *C. elegans* conferred increased sensitivity to ICL-inducing therapies (cisplatin and UV radiation), these did not modify radiosensitivity and the effect of monofunctional alkylating chemotherapies such as temozolomide was not evaluated. Speculatively, resistance to chemo- and radiosensitisation through FA pathway inhibition might occur as a result of the physical opportunity afforded to GSCs to form greater numbers of intercellular connections in 3D conditions – since the formation of more 'connected' networks has been shown to provide enhanced therapeutic resilience[212]. Nevertheless, a lack of efficacy using FA pathway inhibition in more biologically-relevant 3D models, despite encouraging 2D data, underlines a potential need for combinatorial strategies which incorporate multiple DDRi to optimise therapeutic response.

Simultaneous FA pathway and PARP inhibition as a therapeutic strategy

Our results in clinically-relevant, patient-derived 3D GSC models reveal that inhibition of the FA pathway represents a potent strategy to optimise the radiosensitisation (Figure 5.18)

and chemosensitisation (Figure 5.22) achieved with the PARP1 inhibitor olaparib; a drug which is NICE and FDA approved for use in ovarian, breast, pancreatic and prostate cancer, and is currently being combined with radiotherapy with or without temozolomide (dependent on MGMT status) in the ongoing PARADIGM-2 clinical trial for patients with glioblastoma[274] (see Chapter 3 – Table 1.1). To the best of our knowledge, no previous studies have assessed the potential of combined DDRi with simultaneous FA pathway and PARP1 inhibition to radio- or chemosensitise high-grade gliomas or other types of cancer. As such, these studies present an entirely novel combinatorial approach to tackle the inherent therapeutic recalcitrance of GSCs. Previous studies have however, highlighted the therapeutic potential of reducing the expression of FA pathway proteins and PARP1 in parallel, or inhibiting one of this pair in the context of genetic deficiency of the other to achieve substantial anti-cancer responses predicated on the concept of synthetic lethality.

It should be emphasized that the landmark studies demonstrating the potential of synthetic lethal approaches to improve cancer therapy by Bryant *et al.* (2005)[184] and Farmer *et al.* (2005)[185] are based on enhanced PARP inhibitor sensitivity within a context of deficiency in the HR and downstream FA genes *FANCS/BRCA1* and *FANCD1/BRCA2*. More recently, this concept was extended by Kais *et al.* (2016)[255] demonstrating that *BRCA1/2*-deficient cells exhibit an enhanced reliance on FANCD2 to stabilize DNA replication forks, with overexpression of FANCD2 able to confer PARP inhibitor resistance in this genetic context. Interestingly, HR restoration as a mechanism of PARPi resistance in these *BRCA1/2*-deficient cells was excluded since IR-induced foci formation of FANCR/RAD51, a marker of HR functionality, remained impaired despite FANCD2 overexpression. Therefore, FANCD2 and more proximal FA pathway genes/proteins may influence PARPi sensitivity though replication fork dependent mechanisms which are independent of downstream FA proteins that function in HR DNA repair, in addition to classical enhancement of PARPi sensitivity though 'BRCAness' induction dependent on reduced HR activity, since the depletion of key proximal FA pathway genes including FANCA, FANCC, FANCD2, FANCG and FANCL have been demonstrated to substantially reduce the HR (and alt-NHEJ) mediated repair of I-SceI-induced DNA DSBs using a dual GFP/RFP reporter system[497]. Additionally, our finding that olaparib exposure in patient-derived GSCs elicits FANCD2 monoubiquitination (Figures 3.1 & 5.16) is consistent with increased FANCD2 foci formation following PARPi recently observed by Sharp *et al.* (2020)[254], and a recent CRISPR screen which identified multiple FA pathway genes (including *FANCA*, *FANCC*, *FANCE*, *FANCM*, *FANCT*, *FANCS/BRCA1* and

FANCD1/BRCA2) as determinants of sensitivity to the highly PARP trapping inhibitor talazoparib in non-glioblastoma cell lines (HeLa, RPE1-hTERT, and the hemizygous *BRCA1* mutant line SUM149PT)[509]. These further corroborate a relative interdependence between the FA pathway and PARP. Furthermore, Rasmussen *et al.* (2016)[199] demonstrated that use of the HDAC inhibitor suberoylanilide hydroxamic acid (SAHA), which downregulated the expression FANCS/BRCA1 and FANCR/RAD51, augmented PARP inhibitor sensitivity in patient-derived GSCs. Although few are specific to glioblastoma, these studies considered collectively would suggest that after a plethora of DNA SSBs and DSBs are generated using current adjuvant therapies (immediately with IR and mediated through repetitive futile cycles of MMR in the context of temozolomide-induced O^6-meG lesions), PARP inhibition biases the proportion of strand breaks towards more deleterious DSBs through abrogation of SSBR mechanisms. The greater burden of DNA DSBs relies on template-dependent HR repair and the template-independent alt-NHEJ and cNHEJ mechanisms. However, simultaneous downregulation of the FA pathway enables the inappropriate engagement of cNHEJ proteins at damaged DNA replication forks[131], and promotes a damaging trifecta of reduced replication fork stability, HR and alt-NHEJ. This is consistent with our findings that combined PARPi + FAPi augmented and substantially delayed the repair of IR-induced DNA damage in patient-derived GSCs (Figures 5.22-23 & Figure 5.27) and resulted in significantly more persistent DSBs 24 hours after IR in clinically-relevant 3D models (Figure 5.21). Within this conceptual framework, a model can be proposed where the combination of PARPi + FAPi results in slower DNA repair kinetics with greater reliance on more mutagenic and potentially deleterious cNHEJ and a greater proportion of unresolved DSBs following DNA damaging therapy, which likely underpin the substantial preclinical efficacy of this novel therapeutic strategy in patient-derived GSCs (Figures 5.13-15 and 5.18).

Simultaneous inhibition of the FA pathway and the apical DDR serine/threonine protein kinases ATR and ATM

Strikingly, our studies also reveal that inhibition of the FA pathway alongside ATR inhibition represents a profoundly radiosensitising strategy in patient-derived 3D GSC models (Figure 5.24), which delivers a degree of sensitisation approaching the most potently radiosensitising DDRi combination reported to date (PARPi + ATRi[197,208]), but with a substantially lower effect on cell survival in the absence of IR (Supplementary Figure 5.2) – which, in view of the locoregional nature of radiotherapy, raises the possibility of therapeutic strategies integrating the ATRi + FAPi combination portending lower systemic toxicity.

Although no previous studies have systematically assessed simultaneous FA pathway and ATR inhibition as a strategy to evoke radio- or chemosensitisation, recent functional CRISPR/Cas9 screens allude to a co-dependency between these important DDR processes[510-512]. Wang *et al.* (2019)[510] demonstrated that loss of *FANCD2*, *FANCD1/BRCA2*, *FANCR/RAD51* or *FANCN/PALB2* were each associated with heightened sensitivity to the highly selective ATR inhibitor AZD6738 (also used in our studies) in the majority of cancer cell lines tested (293A, kidney; HCT116, colon; MCF10A, breast). Independently, Hustedt *et al.* (2019)[511] analysed sensitising mutations to VE-821 and AZD6738 in multiple cell lines (HCT116, HeLa, and RPE1-hTERT *TP53-/-* cells) and demonstrated significant cellular component gene ontology enrichment for 'Fanconi anaemia nuclear complex genes'.

In addition to the above comprehensive CRISPR/Cas9 screens, more focussed hypothesis-driven research by Chen *et al.* (2009)[513] has previously established that FA deficient cells demonstrate enhanced sensitivity to both siRNA mediated silencing of *CHK1* and pharmacological inhibition of CHK1 (using Gö6976 and UCN-01), further supporting a potential co-dependency between the ATR-CHK1 axis and the FA pathway. Such a relationship is perhaps unsurprising given the extensive interplay between ATR signalling and the FA pathway as detailed. Firstly, FANCM binds DNA at sites of replication impeding DNA damage in a manner dependent on its phosphorylation by ATR[139]. Secondly, the ATR-CHK1-CDC25C signalling axis is crucial to maintain a robust G2/M checkpoint and permit adequate time to facilitate canonical FA pathway (i.e. core complex – ID complex) orchestrated DNA repair[27]. Thirdly, independent of FA core complex recruitment and canonical FA pathway activity, the DNA translocase activity of FANCM associated with its N-terminal region DEAH box helicase domain is indispensable for the generation of an efficient ATR-CHK1 axis signalling response to replication stress and DNA damage, required to facilitate replication fork stabilisation and appropriate activation of the intra-S phase and G2/M checkpoints[189]. Further downstream, ATR-dependent phosphorylation of FANCI at clustered Ser/Thr-Gln motifs is required to facilitate ID complex monoubiquitination[148,514]; whilst the recently identified FA pathway gene FANCW/RFWD3[515] facilitates the repair of stalled DNA replication forks and HR progression through polyubiquitinating RPA and RAD51 in an ATR and ATM-dependent manner[516-518]. Finally, monoubiquitination-dependent FANCD2 association with the MCM2-MCM7 replicative helicase is facilitated by ATR signalling in response to replication stress[152]. Given that GSCs have been

demonstrated to exhibit high levels of constitutive replication stress, associated with more frequent replication-transcription collisions due to elevated expression of long neural genes[208], and exhibit heightened FA pathway and ATR-CHK1 axis signalling (discussed previously), it is tempting to speculate that, relative to the bulk of tumour cells, GSC subpopulations may be uniquely sensitive to combined ATRi + FAPi – similar to the differential (stem vs bulk) effects observed with PARPi + ATRi[208]. This would certainly be supported by the marked increase in RNA:DNA hybrids we observe following the treatment of G7 GSCs with the combination of ATRi + FAPi in both the presence and absence of IR (Figure 5.30).

Previously, Kennedy *et al.* (2007)[519] demonstrated embryonic lethality with combined ATM and FANCG knockout when interbreeding mice and hypersensitivity to ATM inhibition in FA pathway deficient tumour cells, but did not assess the effects of this combination on radio- or chemosensitivity. Our findings, that the addition of FA pathway inhibition enhanced ATM-mediated radiosensitisation (and sensitisation to temozolomide at 5μM) in patient-derived 3D GSCs, but to a lesser extent than with ATR-mediated sensitisation (Figures 5.20 and 5.21) might reflect the importance of replication stress in the therapeutic effects conferred by some FA pathway based DDRi combinations. However further studies to assess RNA:DNA hybrid formation with the ATMi + FAPi combination, DNA replication fork kinetics, and the relative contributions of HR/cNHEJ/alt-NHEJ following treatment with various FA pathway-based DDRi combinations would be particularly appealing.

Overall, our studies have identified and support the preclinical-clinical translation of 3 novel FA pathway based combinatorial strategies (PARPi + FAPi; ATRi + FAPi; ATMi + FAPi) to enhance the sensitivity of glioblastoma to current chemoradiotherapy used in the clinic and eradiate recalcitrant GSC populations (summarised in Figure 5.34). Considering this work in the context of previous studies (discussed above), which predict synthetic lethality using each of these combinations in extracranial cancers, perhaps a more general concept should be emphasised. That synthetic lethal relationships involving DDR genes might robustly predict synthetic sensitivity to current DNA damaging adjuvant therapies. Therefore, these relationships should be increasingly exploited to build more comprehensive, cancer-selective and efficacious combinatorial strategies, which can be rapidly (and ethically) integrated into the framework of current treatment regimens, to overcome inherent

complex therapeutic resistance associated with glioblastoma and improve patient outcomes.

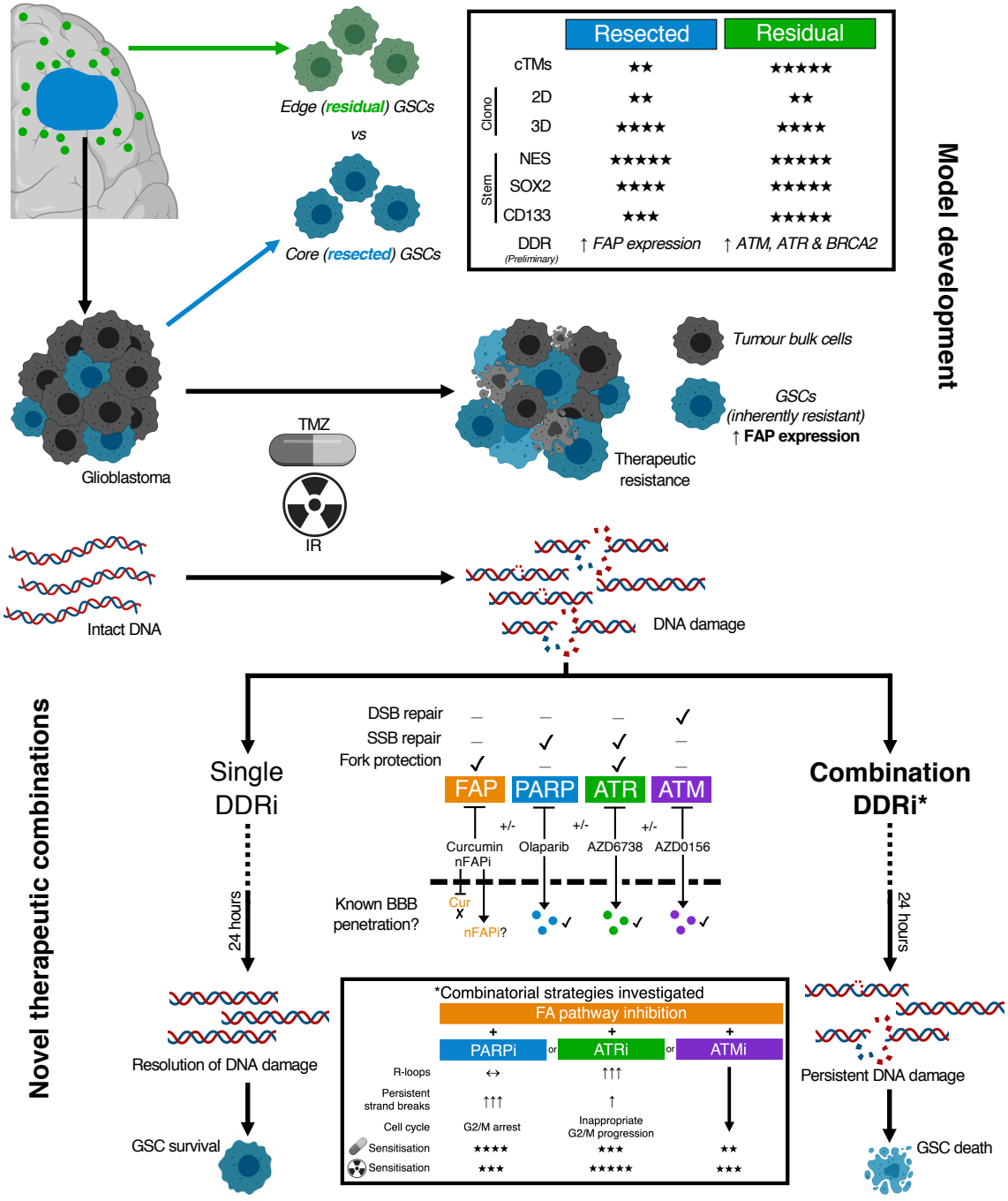
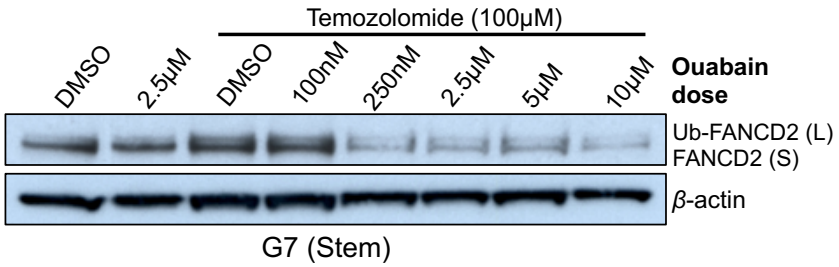
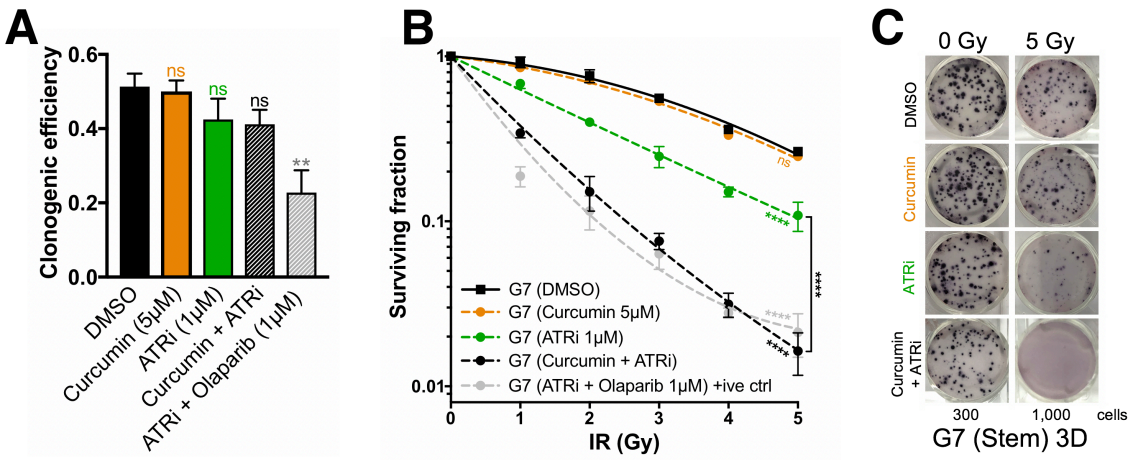


Figure 5.34: Schematic summary of models developed and FA pathway-based DDRi combinations investigated – The studies have generated clinically- and surgically-relevant patient-derived GSC models to investigate features of spatiofunctional intratumoural heterogeneity *ex vivo* (see Chapter 4). These include novel 'resected' and 'residual' models which underpin future studies aiming to better understand the recalcitrant nature of GSCs typically left behind after surgery ('Model development' – *top*). Additionally, these studies highlight 3 FA pathway-based combinatorial strategies (PARPi + FAPi; ATRi + FAPi; ATMi + FAPi) which each provide additional chemo- and radiosensitisation of GSCs relative to single DDRi sensitising strategies (Chapter 5). These combinatorial strategies are expected to provide new ways to overcome elevated DDR activity and inherent therapeutic resistance in difficult-to-treat GSC subpopulations ('Novel therapeutic combinations' – *bottom*). Abbreviations: cTMs = connecting tumour microtubes (↑cTMs associated with enhanced therapeutic resistance[212]); Clono = clonogenic efficiency; Stem = stem cell marker expression (↑ stem cell and DDR marker expression associated with enhanced therapeutic resistance[18,19]).

5.9 Supplementary figures



Supplementary Figure 5.1: The 'heart failure' medication ouabain inhibits the FA pathway in G7 glioblastoma stem cells at 250nM but not at 100nM – Established U87 were plated for 24 hours prior to exposure to the indicated doses of ouabain or DMSO then DNA-damaging temozolomide chemotherapy 1 hour later. Cells were incubated for a further 16 prior to lysis and Western blotting. *(Data shown were produced by Miss Aurelie Vanderlinden working under my direct supervision).*



Supplementary Figure 5.2: Combined FA pathway and ATR inhibition provides similar radiosensitisation to combined inhibition of PARP and ATR, but with less toxicity in the absence of irradiation in G7 3-dimensional Alvetex™ scaffold-based glioblastoma stem cell models – G7 primary GSCs were seeded 24 hours prior to exposure to DMSO (control), curcumin (crude FA pathway inhibitor, 5μM), AZD6738 (ATR inhibitor, 1μM), the combination of curcumin (5μM) + AZD6738 (1μM), olaparib (PARP inhibitor, 1μM), or the combination of olaparib (1μM) + AZD6738 (1μM) administered simultaneously. GSCs were then irradiated 1 hour post DDRi treatments. Cells were incubated for a further 21 days, with media replacement 24 hours post irradiation. Subsequently, colonies were identified using incubation with MTT for 4 hours, then fixed with paraformaldehyde and quantified. A. Clonogenic (plating) efficiency following indicated treatments at 0 Gy radiation in G7 GSCs. B. 3D Alvetex™ clonogenic survival curves in G7 GSCs, then; C. Representative images. Data generated from 3 independent experiments. Error bars represent the SEM. Error bars not shown where these are smaller than the corresponding symbol. Note – these graphs include data presented in Figure 5.24 but with the addition of PARPi + ATRi positive control data, which was omitted from the main Figure for clarity.

Chapter 6 – Conclusions and future studies

6 CHAPTER 6 – Conclusions and future studies

6.1 Conclusions

Glioblastoma continues to represent an unmet clinical need[59] with a dismal prognosis for patients diagnosed today. Whether aiming to sensitise to conventional chemo-radiotherapy, or act as a chemo- or radiation-sparing strategy, new DDR targeted therapies will need to overcome the highly adaptive resistance mechanisms glioblastoma employ to prevent their eradication[373]. There is an issue, given the extensive intratumoural heterogeneity of glioblastoma[13,15,32,65] and inherently treatment resistant GSCs within these tumours[18,426], that any single targeted therapy may in fact be 'too targeted' leading to inevitable resurgence of resistant subclones and tumour repopulation. Consequently, targeting multiple DDR constituents in parallel bares the potential provide new effective treatment paradigms that might help prevent disease progression by counteracting complex and overarching phenotypic delinquency within the DDR of cancerous cells.

Given that normal tissue toxicity can represent an even greater challenge when dealing with combination therapies, the differential in FA pathway activity between normal brain and glioblastoma[22] presents a critically useful therapeutic window that may form a basis for constructing safe and efficacious combinations of DDR inhibitors. An overall framework is emerging in which there is clearly extensive interconnections between various DDR pathways[1], and yet cancer cells have lost function in some of these pathways during the process of carcinogenesis and become overly reliant on others[209]. It was therefore hypothesized that FA pathway-based combinatorial targeting of the DDR in glioblastoma would represent an effective therapeutic strategy, by virtue of the narrowed repertoire of active pathways and reduced degree of functional redundancy within the DDR of cancer cells. Considering the data reported and discussed throughout the preceding chapters, this thesis represents a meaningful early step towards novel combination therapies targeting the DDR. It is fully expected that novel findings and research models generated during these studies will contribute to important and urgently needed advances in the treatment of glioblastoma which, at present, remains a death sentence.

Firstly, this thesis aimed to confirm whether pharmacological targeting of the FA pathway or an interconnected DDR process has the potential to enhance the therapeutic response of glioblastoma to DNA damaging treatments, as a single DDRi strategy (Objectives 1-2).

Using established glioblastoma cell lines, activation of the FA pathway following standard of care temozolomide chemotherapy was demonstrated through both robust induction of FANCD2 nuclear foci formation (Figure 3.6) and FANCD2 monoubiquitination (Figure 3.1, Figure 3.6, Figure 5.9). Both these metrics of FA pathway activity were downregulated by exposing glioblastoma cells to the naturally occurring compound curcumin and such treatment increased the susceptibility of a panel of glioblastoma cell lines to temozolomide, as predicted on the basis of previous studies (Figure 3.3)[20-22]. Additionally, single DDR target inhibition of PARP1 elicited sensitisation to temozolomide in all established glioblastoma cell lines tested whilst inhibition of either ATR or ATM revealed an intriguing pattern of chemosensitisation whereby the target largely implicated in cellular responses to DNA single strand breaks, ATR (and PARP1 inhibition at low doses of temozolomide), provided robust chemosensitisation in 3 of 4 established glioblastoma cell lines in the panel including both MGMT positive (T98G, LN18) and negative (U87) cells. Conversely, only the MGMT negative U251 glioblastoma cells demonstrated resistance to temozolomide sensitisation mediated by ATRi (and PARPi at low doses of temozolomide), but were susceptible to profound temozolomide chemosensitisation with inhibition of ATM. Thus the potential of using a single DDRi to enhance the efficacy of temozolomide has been established (Figure 3.3). Furthermore, potential cell line specific differences in response to therapeutic strategies incorporating a single DDRi with DNA damaging therapy have been revealed, with the implication that the genomic and phenotypic context of an individual cancer may influence how effective such strategies are in the clinic.

Secondly, since the biological relevance of established glioblastoma cell lines is commonly questioned, this thesis aimed to validate the use of patient-derived glioblastoma stem cells in 2D and 3D models, and develop a novel resource of *ex vivo* models with the potential to recapitulate the spatiofunctionally heterogeneous features of glioblastoma[15,313] (Objectives 3-4), including the nuances of disease more likely to be left behind after surgery (residual disease). Although the cancer stem cell hypothesis can attract controversy[460], investigation of the expression of putative stem cell markers in primary lines generated by Colin Watts' laboratory (Cambridge) confirmed elevated mRNA expression of nestin and SOX2 in 'GSC' populations propagated in serum-free conditions, relative to bulk cells switched to and propagated in (5+ passages) serum-containing media (Figure 4.2). G7 GSCs embedded within a customised Alvetex™ scaffold-based architecture also readily exhibited protein expression of the stem cell markers CD133, nestin and vimentin (Figure 4.2). However,

during the studies, resources were diverted away from replicating detailed stem vs bulk characterisation of Cambridge GSCs (which have previously been characterised[15,99,195,197,422] and for which limited clinical information was available), and towards the development of potentially more clinically- and surgically relevant models of patient-derived glioblastoma. As such, the Sheffield Living Biobank of patient-derived glioblastoma models was established which, to date, consists of 22 primary GSC lines from 11 patients with linked clinical and molecular data (Table 1). These include parallel *ex vivo* random intratumoural heterogeneity models whereby multiple GSC lines were generated from spatially distinct regions of a single patient's tumour (Figure 4.6), and novel matched resected and post-surgical residual models which leverage adjacent tumour infiltrated brain in rare *en bloc* partial lobectomy specimens (which contain cells that would be left behind in other operative scenarios – see Figure 4.7). Evaluation of the features of Sheffield GSCs confirmed these lines can be effectively propagated in serum-free media, readily form neurospheres in non-adherent conditions (Figure 4.4, Figure 4.6, Figure 4.7), and exhibit elevated mRNA expression of putative stem cell markers including nestin relative to differentiated bulk populations (Figure 4.5, Figure 4.10). A novel utility of the 3D Alvetex™ scaffold-based model has been highlighted, in that early passage Sheffield GSC lines were frequently too migratory to form colonies in traditional 2D conditions, but use of the 3D architecture supported robust colony formation (Figure 4.9), potentially permitting future *ex vivo* therapeutic assessment using patient-derived cell lines which otherwise would not be amenable to reliable use with the 'gold-standard' clonogenic assay[467]. Remarkably, early assessment of divergent properties between *ex vivo* resected and residual models revealed the first infiltrative edge GSC line interrogated (OX-5 edge) demonstrated 1.6-fold higher SOX2 and 9.7-fold higher CD133 mRNA expression relative to a matched residual GSC line (Figure 4.10B). Since high CD133 expressing GSCs have been linked with elevated DDR activity and therapeutic resistance for over a decade[18], our findings in post-surgical residual disease models might have substantial implications for future treatment strategies. Finally, studies in collaboration with Novocure™ revealed TTFields were predicted (*in silico*) and confirmed (*in vitro*) to be deliverable to glioblastoma cells within scaffold-based 3D models (Figure 4.13, Figure $.14), which could form a basis for more clinically predictive cell-based TTFields research in the future.

Thirdly, this thesis aimed to establish whether dual inhibition of key DDR processes including the FA pathway might substantially enhance the susceptibility of cancer to current chemo-

and radiotherapy, through the application of clinically-relevant 2D and 3D patient-derived glioblastoma stem cell models (Objectives 5-6). Corroborating previous work which demonstrated elevated protein expression of FANCD2 in high-grade glioma specimens (relative to low-grade gliomas and benign tissue)[22], this thesis established elevated mRNA expression of FA pathway genes in glioblastoma (WHO grade IV glioma) through analysis of the REMBRANT database (Figure 5.1, Figure 5.2). Furthermore, amongst all grades of glioma, high expression of FA pathway genes was associated with a greater reduction in survival than the well-established prognostic biomarker MGMT (Figure 5.3), and patient-derived primary cultures GSCs were revealed for the first time to exhibit high FA pathway mRNA expression relative to bulk populations (Figure 5.4). Together, these findings underline an important role of the FA pathway in therapeutic recalcitrance and death.

In 2D models, inhibition of the FA pathway with either curcumin (Figure 5.15, Figure 5.17), the cardiac glycoside ouabain (Figure 5.9, Figure 5.10. Figure 5.11), or (to a lesser extend) the novel inhibitor F76 radiosensitised GSCs (Figure 5.13, Figure 5.14). However, when the use of curcumin was also evaluated in 3D models no consistent radiosensitisation could be achieved (Figure 5.18, Figure 5.24), thus further highlighting differential responses of GSCs in 2D and more biologically-relevant 3D models that had been noted earlier in Chapter 4 (Figure 4.3) and previous studies[107,108]. In clinically-relevant 3D GSC models, simultaneous inhibition of the FA pathway (FAPi) and PARP or ATR enhanced chemosensitisation at low doses of temozolomide compared to a single DDRi (Figure 5.22, Figure 5.25). Furthermore, combined PARPi + FAPi or ATMi + FAPi conferred radiosensitisation whilst combined ATRi + FAPi led to a profoundly radiosensitising effect (Figure 5.18, Figure 5.24). The comparison of α/β ratio enhancement suggests dual-DDRi strategies fundamentally alter the DDR of GSCs (Figure 5.19), whilst single cell gel electrophoresis & immunofluorescence studies suggest FA pathway based DDRi combinations profoundly delay the resolution of IR-induced DNA strand breaks at 6 hours post-treatment, with increased persistent DNA double strand breaks at 24 hours (Figure 5.21, Figure 5.26, Figure 5.27, Figure 5.28). Additionally, the ATRi + FAPi combination engenders substantial generation of RNA:DNA hybrids (Figure 5.30), providing a mechanistic basis for enhanced replication stress and DNA damage. In conclusion, simultaneously targeting the FA pathway and interconnected DDR processes represents an appealing therapeutic strategy to overcome the biological complexity, heterogeneity, and intractable treatment resistance which are inherent features of glioblastoma. This represents successful completion of the final, most important thesis

aim and supports further studies to expeditiously translate FA pathway-based DDRi combinations towards the clinic. Additionally, given that at least 7-10% of patients with a glioblastoma exhibit FA pathway aberrations suggestive of reduced activity (see Figure 5.33), in the future, the constitutive somatic lack of FA pathway function in some tumours, could serve as a novel predictive biomarker for patient response to PARPi, ATRi or ATMi currently in clinical trials.

Further studies are required to reveal detailed mechanistic understanding of the exceedingly potent sensitisation to DNA damaging therapy achieved with some FA pathway-based DDRi combinations. Additionally, given the striking modulation of α/β ratios observed with dual DDRi strategies, additional work to characterise the efficacy and therapeutic index of these strategies in conjunction with fractionated radiotherapy would be particularly appealing. The incorporation of such experiments into currently ongoing and planned future studies is expected to inform and enhance the clinical translatability of data generated during this thesis.

6.2 Future studies

Studies and activity throughout this thesis were approached with broader appreciation of the need to help expand the breadth and depth of brain tumour research at our institution. In part, this was motivated by clear geographical disparity in opportunities for patients to access novel therapies and interventions in our region. For example, interventions delivered by two recently established national multi-centre trials (Tessa Jowell BRAIN-MATRIX and FUTURE-GB) were not locally accessible to patients within South Yorkshire since Sheffield did not achieve participating status in these studies. Furthermore, a dearth of established and funded clinical academic training opportunities for clinicians working in neurosurgery or neuro-oncology in Sheffield is, over the years, likely to have adversely impacted patient opportunity to access novel interventions locally. For example, at the time of writing, there are four current Academic Clinical Lecturers (ACL) in neurosurgery training in Cambridge (https://www.neurosurg.cam.ac.uk/departmental-staff/), yet Sheffield has never hosted an ACL in neurosurgery. As such, ongoing and future studies arising from this thesis represent important steps to establish and refine novel therapeutic strategies (and build a strong research team) ready for clinical translation in future Sheffield-led clinical trials with the potential to improve outcomes nationally/internationally, whilst ensuring regional

inequalities in patient access to novel therapies are addressed through the availability of access for local patients. Additionally, more active engagement (and collaboration) of Sheffield-based researchers within the glioblastoma research community should provide additional opportunities for local patients and enrich collaborative efforts to more effectively tackle this devastating disease.

6.2.1 Developing more effective FA pathway inhibitors to underpin single and combination DDRi strategies

This thesis demonstrates the therapeutic potential of anti-cancer strategies which incorporate inhibition of the FA pathway, however the lack of highly-selective, small molecule FA inhibitors suitable for clinical translation continues to pose a problem for researchers and patients. Although both curcumin and ouabain have been administered to patients and inhibit the FA pathway, their effects are pleiotropic and both exhibit suboptimal PK/PD profiles (as discussed in Chapter 3 and Chapter 5 respectively). Nevertheless, in both cases future 'Phase 0' clinical studies[520] in which drugs are administered preoperatively then drug concentration and target effects are evaluated within surgically resected tumour tissue to provide direct confirmation of FA pathway inhibition would be highly informative. This is a capability we hope to establish at our institution in the near future, and such studies would help establish the appropriateness of pursing clinical trials evaluating therapeutic strategies which incorporate curcumin or ouabain as DNA sensitising agents, and/or if more sophisticated modes of drug delivery such as: administration within magnetic nanoparticles[343,344]; intraparenchymal convection enhanced delivery[347,348]; implantable infusion pump[345], or; the use of technological adjuncts to transiently increase BBB permeability, including combined focused ultrasound and intravenous microbubbles[521,522] or use of TTFields[523,524].

Ideally, however, the ongoing drug development process and recently established *in vivo* testing of novel FA pathway inhibitors at our institution aims to produce compounds with greater target specificity and PK/PD profiles that are more suitable for clinical application. Recent funding from Artios secured by Dr Spencer Collis is currently being used to further refine, resynthesise and evaluate nFAPi, including: cell-free biochemical analyses; confirmation of target engagement (including CETSA assays), and; confirmation of potency in *ex vivo* primary 3D GSC models. These studies are expected to yield highly potent,

specific nFAPi suitable for clinical translation and subsequent application with efficacious combinatorial DDRi strategies including those revealed within this thesis.

6.2.2 Combining TTFields and inhibitors of the DNA damage response

The discovery of TTFields modulatory effects on DNA damage and highly-coordinated cellular DNA damage response (DDR) processes[73] presents a critical opportunity to develop more effective, rationally-designed TTFields-based therapeutic strategies. Emerging data suggests TTFields delays the resolution of IR- and chemotherapy-induced DNA lesions, potentially through reducing the efficiency of homologous recombination (HR) DNA repair[72] eliciting a 'BRCAness' phenotype[73] and through promoting replication stress[74]. The induction of such putative vulnerabilities within DNA damage repair machinery provides a rational and promising basis for multimodal therapeutic strategies which incorporate TTFields alongside novel drugs targeting the DDR to overwhelm mechanisms of treatment resistance in glioblastoma. For example, targeting the FA pathway or PARP in combination with TTFields could yield potential synthetic lethality akin to that demonstrated in HR-deficient tumours due to underlying BRCA1/2 mutations[153,184,185,255]. In collaboration with Novocure, such studies are currently ongoing. These are supported by a University of Sheffield Faculty PGT-PGR PhD Scholarship competitively awarded to Miss Aurelie Vanderlinden and by additional funding from the Sheffield NIHR Biomedical Research Centre. The studies are enriched by unique *ex vivo* patient-derived GSC models within our Sheffield Living Biobank and further development and application of the novel 3D Alvetex™ scaffold-based TTFields culture and delivery system established during this thesis (Chapter 4 – Section 4.4) is incorporated within the study plans.

6.2.3 Ex vivo 3D models of post-surgical residual disease to improve biological understanding and treatment

The novel, pragmatic methodology to generate parallel GSC lines from tumour tissue and adjacent infiltrated brain within *en bloc* partial lobectomy specimens and novel differences uncovered between these *ex vivo* models reflecting resected and typically post-surgical residual disease are likely to be clinically important and therefore require further interrogation. Funding recently awarded by The Brain Tumour Charity – Expanding Theories scheme will support the generation of further unique 3D resected and residual GSC models and detailed characterisation of differential features of residual disease as summarised in

Figure 6.1, including: stem cell marker expression; baseline response clinical standard of care chemo- and radiotherapy; focused functional analysis of DDR divergence (including strand break propensity, replication fork dynamics, and markers of DNA damage and pathway activity), and; divergence in constitutive and therapy-induced transcriptomic landscapes. Finally, these studies will establish whether differential features of the DDR in post-surgical residual disease can be specifically targeted to generate more efficacious therapeutic strategies.

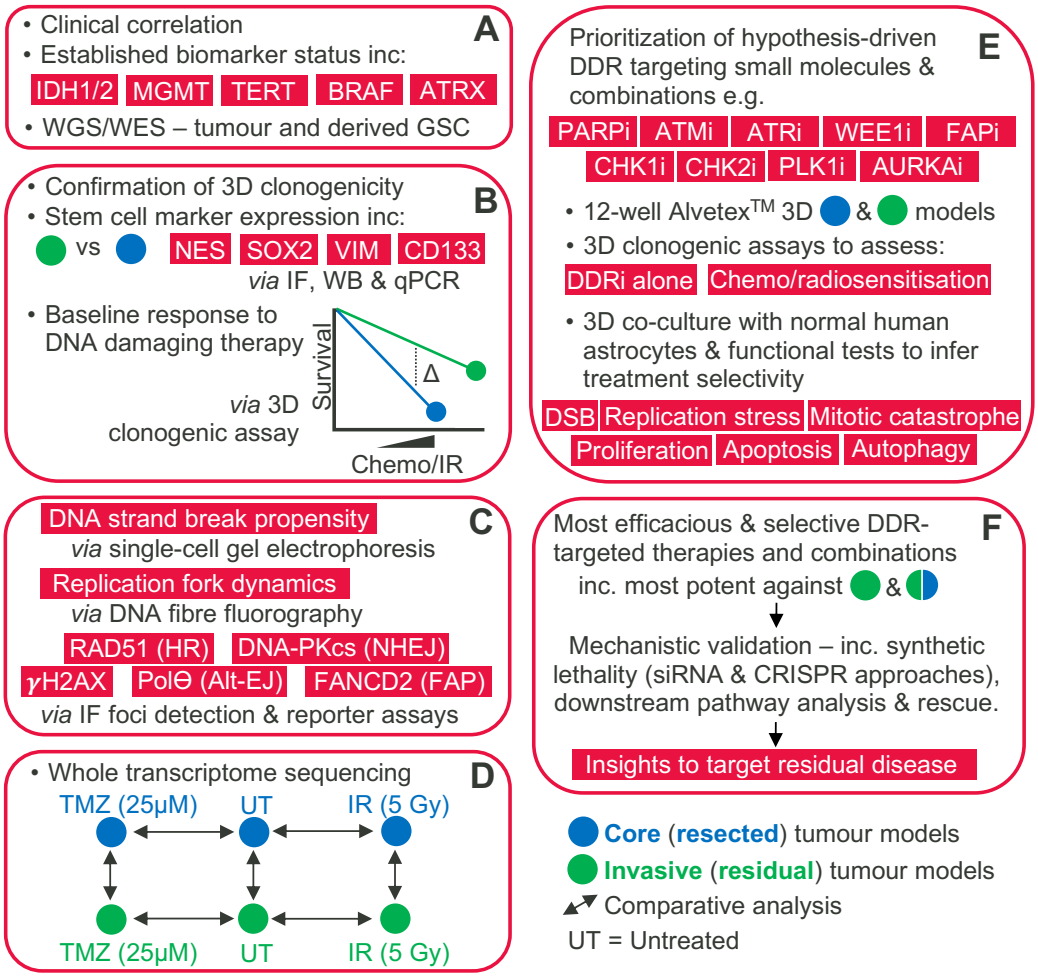


Figure 6.1: Schematic for planned studies using resected and residual 3D GSC models to evaluate therapeutic combinations targeting the DNA damage response – A. Clinical correlation and; **B.** Early characterisation of resected and residual 3D GSC models (A-B, Aim I). **C.** Detailed functional and; **D.** transcriptomic comparison of cellular responses to DNA damaging therapy in resected and residual models (C-D, Aim II). **E.** Investigation and; **F.** Prioritisation of DDR-targeting strategies to tackle residual disease (E-F, Aim III).

Additionally, funding recently awarded by the NC3Rs will support a PhD Studentship to further expand our Living Biobank of post-surgical residual glioblastoma models and validate these as an alternative to, in some contexts, replace animal studies as the current 'gate-keeper' to clinical translation. Animal studies have performed particularly poorly in this role for preclinical glioblastoma research, with no pharmacotherapy progressing through

laboratory-based studies providing definite improvements in patient overall survival since the introduction if temozolomide more than 15 years ago[10,525].

6.2.4 Ex vivo drug screening using human tissue to personalise cancer therapy and replace murine avatars

In addition to revealing novel DDR targeting combinations, studies during this thesis highlighted cell-line specific differences. For example, in 2D studies FA pathway inhibition with curcumin sensitised U87, T98G and LN18 established cultures in addition to G1 and G7 patient-derived GSCs to DNA damaging therapy, but conversely failed to sensitise U251 established cultures and had very modest effects on E2 patient-derived GSCs. These differences *allude* to the inevitability of differential patient responses in current and future clinical studies evaluating DDRi. Coupled with the substantial increase in potential therapeutic options worthy of assessing for each individual patient once combinatorial strategies are taken into account[311], there is a profound need to enhance choice of therapy in an individualised and evidence-based manner. The use of PDX models as a patient-specific test systems to evaluate and prioritise multiple treatments before providing patients and clinicians with an individualised list of options, has previously been highlighted. However, the use of animals in this context, as personalised 'avatars' is plagued by numerous limitations including: the number of animals (typically mice) required to test a range of therapies; exquisitely high cost; a lengthy duration before results are available, and; the potential for mouse-specific evolution of implanted human cancer cells[114,526-529].

As an alternative, in collaboration with Professor Thomas Helleday and Misvik Biology[530], we have proposed *ex vivo* single-cell drug response profiling, from henceforth referred to as '*ex vivo* screening', to replace the use of animal avatars and democratise phenotypically personalised medicine. Our methodology uses freshly, human patient-derived tissue from solid tumours and new technology to rapidly determine response to hundreds of treatment options and provide prioritised recommendations. In brief, fresh tumour tissue is disaggregated into a mixture of cancerous, immune and other normal microenvironmental cell types (see Figure 6.2). These are seeded to multi-well plates which are pre-coated with anti-cancer agents. Multi-parameter, ultra-high content microscopy and sophisticated image analysis algorithms are used to evaluate treatment response, and rapidly analyse interactions between cancerous cells and tumour microenvironment at single cell resolution, providing novel biological insights. We have recently secured funding from the NC3Rs (PhD

Studentship) to support studies using tumour tissue from patients with glioblastoma to demonstrate the feasibility of *ex vivo* screening to generate personalised therapeutic recommendations more quickly and comprehensively than possible using mouse avatars for drug screening. This high throughout platform is expected to accelerate the clinical translation of novel therapeutic strategies, including DDRi combinations, and directly inform future trials.

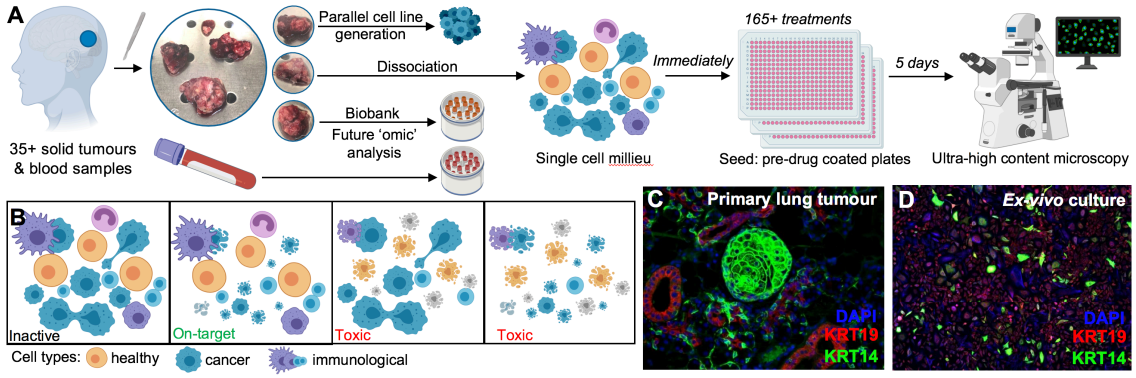


Figure 6.2: Schematic representation and feasibility of *ex vivo* single-cell drug response profiling for solid tumours – A. Schematic overview of *ex vivo* screening protocol. **B.** Schematic representation of differential drug responses. **C-D.** Representative confocal immunofluorescence images of tumour tissue from a lung cancer specimen (**C**) and dissociated passage-free *ex vivo* culture from the same tumour (**D**) demonstrating maintenance of heterogeneous cell populations.

6.2.5 Understanding and predicting patient-specific responses to therapy for glioblastoma

The studies presented in this thesis, current ongoing studies, and planned future studies are expected to deliver multiple promising therapeutic options suitable for clinical translation. However, an urgent need remains to define molecular biomarkers capable of predicting response to novel therapies near the cusp of clinical translation to ensure emerging clinical trials can pair patients with therapies most likely to achieve good responses in their specific tumour and avoid unnecessary/unwanted side effects. The advent of next generation sequencing and its increasing clinical application to profile tumours at genome-scale[32], including our participation in the 100,000 Genomes Project[531] and current ongoing studies at our institution (highlighted above), will facilitate greater integration of novel therapies into the clinic. However, predictive molecular biomarkers need to be defined for the cutting-edge therapeutic strategies currently being developed by our team and others. We have planned studies which leverage the Sheffield Living Biobank to facilitate genome-scale characterisation of patient tumours and associated GSC lines to identify molecular biomarkers with the potential to predict novel therapy response – through relating genomic

data with emerging patient-specific 3D GSC data generated in ongoing studies (as summarised in Figure 6.3) – and inform patient stratification in future clinical trials.

Such future patient stratification might occur in parallel, or as an alternative to, *ex vivo* phenotypic drug response profiling (see above).

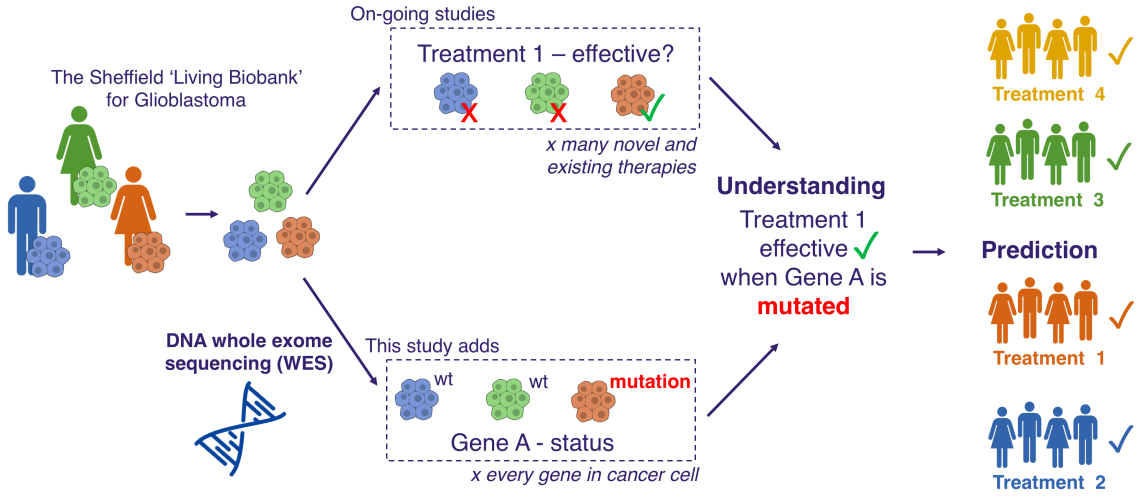


Figure 6.3: Schematic representation of studies using comprehensive genetic profiling of the Sheffield Living Biobank to understand and predict patient-specific responses to novel therapies – Patient-specific Sheffield GSC lines with linked clinicopathological data will be characterised using WES (or WGS, including patients recruited into the 100,000 Genomes Project). This genetic data will be analysed in conjunction with patient-specific 3D GSC novel therapy response data (e.g. response to nFAPi, response to PARPi + FAPi, response to TTFields) generated during ongoing studies (with generation of additional treatment response data using further patient-derived 3D GSC models where required) to establish pharmacogenomic predictions to help stratify future patients cohorts.

Overall, this thesis has established for the first time that FA pathway-based DDRi combinations can augment standard-of-care radiotherapy and chemotherapy to form highly effective therapeutic strategies and overcome the inherent treatment resistance of GSCs in preclinical models. The novel therapeutic strategies and clinically-relevant models developed during these studies are expected to underpin a burgeoning ecosystem of translational glioblastoma research at our institution towards the ultimate aim of reducing suffering and enhancing survival for patients diagnosed with this devastating disease.

References

7 References

1 Pearl, L. H., Schierz, A. C., Ward, S. E., Al-Lazikani, B. & Pearl, F. M. Therapeutic opportunities within the DNA damage response. *Nature Reviews Cancer* **15**, 166-180, doi:10.1038/nrc3891 (2015).

2 Ceccaldi, R., Sarangi, P. & D'Andrea, A. D. The Fanconi anaemia pathway: new players and new functions. *Nature Reviews Molecular Cell Biology* **17**, 337-349, doi:10.1038/nrm.2016.48 (2016).

3 Jiricny, J. The multifaceted mismatch-repair system. *Nature Reviews Molecular Cell Biology* **7**, 335-346, doi:10.1038/nrm1907 (2006).

4 Kee, Y. & D'Andrea, A. D. Expanded roles of the Fanconi anemia pathway in preserving genomic stability. *Genes & Development* **24**, 1680-1694, doi:10.1101/gad.1955310 (2010).

5 Office for National Statistics. *Deaths Registered in England and Wales*, <http://www.ons.gov.uk/ons/rel/vsob1/death-reg-sum-tables/2014/sb-deaths-first-release--2014.html.> (2014).

6 Burnet, N. G., Jefferies, S. J., Benson, R. J., Hunt, D. P. & Treasure, F. P. Years of life lost (YLL) from cancer is an important measure of population burden--and should be considered when allocating research funds. *British Journal of Cancer* **92**, 241-245, doi:10.1038/sj.bjc.6602321 (2005).

7 Erasimus, H., Gobin, M., Niclou, S. & Van Dyck, E. DNA repair mechanisms and their clinical impact in glioblastoma. *Mutation Research* (2016).

8 Messaoudi, K., Clavreul, A. & Lagarce, F. Toward an effective strategy in glioblastoma treatment. Part I: resistance mechanisms and strategies to overcome resistance of glioblastoma to temozolomide. *Drug Discovery Today* **20**, 899-905, doi:10.1016/j.drudis.2015.02.011 (2015).

9 Adamson, C. *et al.* Glioblastoma multiforme: a review of where we have been and where we are going. *Expert Opinion on Investigational Drugs* **18**, 1061-1083, doi:10.1517/13543780903052764 (2009).

10 Stupp, R. *et al.* Radiotherapy plus concomitant and adjuvant temozolomide for glioblastoma. *The New England Journal of Medicine* **352**, 987-996, doi:10.1056/NEJMoa043330 (2005).

11 Stupp, R. *et al.* Effects of radiotherapy with concomitant and adjuvant temozolomide versus radiotherapy alone on survival in glioblastoma in a randomised phase III study: 5-year analysis of the EORTC-NCIC trial. *The Lancet Oncology* **10**, 459-466, doi:10.1016/s1470-2045(09)70025-7 (2009).

12 Louis, D. N. *et al.* The 2016 World Health Organization Classification of Tumors of the Central Nervous System: a summary. *Acta Neuropathologica* **131**, 803-820, doi:10.1007/s00401-016-1545-1 (2016).

13 Patel, A. P. *et al.* Single-cell RNA-seq highlights intratumoral heterogeneity in primary glioblastoma. *Science* **344**, 1396-1401, doi:10.1126/science.1254257 (2014).

14 Piccirillo, S. G. *et al.* Genetic and functional diversity of propagating cells in glioblastoma. *Stem Cell Reports* **4**, 7-15, doi:10.1016/j.stemcr.2014.11.003 (2015).

15 Sottoriva, A. *et al.* Intratumor heterogeneity in human glioblastoma reflects cancer evolutionary dynamics. *Proceedings of the National Academy of Sciences of the United States of America* **110**, 4009-4014, doi:10.1073/pnas.1219747110 (2013).

16 Singh, S. K. *et al.* Identification of human brain tumour initiating cells. *Nature* **432**, 396-401, doi:10.1038/nature03128 (2004).

17 Galli, R. *et al.* Isolation and characterization of tumorigenic, stem-like neural precursors from human glioblastoma. *Cancer Research* **64**, 7011-7021, doi:10.1158/0008-5472.can-04-1364 (2004).

18 Bao, S. *et al.* Glioma stem cells promote radioresistance by preferential activation of the DNA damage response. *Nature* **444**, 756-760, doi:10.1038/nature05236 (2006).

19 Chen, J. *et al.* A restricted cell population propagates glioblastoma growth after chemotherapy. *Nature* **488**, 522-526, doi:10.1038/nature11287 (2012).

20 Chen, C. C., Taniguchi, T. & D'Andrea, A. The Fanconi anemia (FA) pathway confers glioma resistance to DNA alkylating agents. *Journal of Molecular Medicine* **85**, 497-509, doi:10.1007/s00109-006-0153-2 (2007).

21 Kondo, N. *et al.* FANCD1/BRCA2 Plays Predominant Role in the Repair of DNA Damage Induced by ACNU or TMZ (FANCD1/BRCA2 Repair of ACNU- or TMZ-DNA Damage). *PLoS ONE* **6**, e19659, doi:10.1371/journal.pone.0019659 (2011).

22 Patil, A. A. *et al.* FANCD2 re-expression is associated with glioma grade and chemical inhibition of the Fanconi Anaemia pathway sensitises gliomas to chemotherapeutic agents. *Oncotarget* **5**, 6414 (2014).

23 Deans, A. J. & West, S. C. DNA interstrand crosslink repair and cancer. *Nature Reviews Cancer* **11**, 467-480, doi:10.1038/nrc3088 (2011).

24 Bosch, P. C., Bogliolo, M. & Surrallés, J. Activation of the Fanconi anemia/BRCA pathway at low doses of ionization radiation. *Mutation Research. Genetic toxicology and environmental mutagenesis* **793**, 9-13, doi:10.1016/j.mrgentox.2015.06.010 (2015).

25 Wong, W. M. *et al.* Squamous cell carcinoma of the oral tongue in a patient with Fanconi anemia treated with radiotherapy and concurrent cetuximab: a case report and review of the literature. *Head & Neck* **35**, E292-298, doi:10.1002/hed.23155 (2013).

26 Kutler, D. I. *et al.* High incidence of head and neck squamous cell carcinoma in patients with Fanconi anemia. *Archives of otolaryngology--head & neck surgery* **129**, 106-112, doi:10.1001/archotol.129.1.106 (2003).

27 Niraj, J., Farkkila, A. & D'Andrea, A. D. The Fanconi Anemia Pathway in Cancer. *Annu Rev Cancer Biol* **3**, 457-478, doi:10.1146/annurev-cancerbio-030617-050422 (2019).

28 Ostrom, Q. T. *et al.* CBTRUS Statistical Report: Primary Brain and Central Nervous System Tumors Diagnosed in the United States in 2008-2012. *Neuro Oncol* **17 Suppl 4**, iv1-iv62, doi:10.1093/neuonc/nov189 (2015).

29 Zhu, Y. & Parada, L. F. The molecular and genetic basis of neurological tumours. *Nature reviews. Cancer* **2**, 616-626, doi:10.1038/nrc866 (2002).

30 van den Bent, M. J. Interobserver variation of the histopathological diagnosis in clinical trials on glioma: a clinician's perspective. *Acta neuropathologica* **120**, 297-304, doi:10.1007/s00401-010-0725-7 (2010).

31 Sturm, D. *et al.* Hotspot mutations in H3F3A and IDH1 define distinct epigenetic and biological subgroups of glioblastoma. *Cancer Cell* **22**, 425-437, doi:10.1016/j.ccr.2012.08.024 (2012).

32 Brennan, C. W. *et al.* The somatic genomic landscape of glioblastoma. *Cell* **155**, 462-477, doi:10.1016/j.cell.2013.09.034 (2013).

33 Ceccarelli, M. *et al.* Molecular Profiling Reveals Biologically Discrete Subsets and Pathways of Progression in Diffuse Glioma. *Cell* **164**, 550-563, doi:10.1016/j.cell.2015.12.028 (2016).

34 Suzuki, H. *et al.* Mutational landscape and clonal architecture in grade II and III gliomas. *Nat Genet* **47**, 458-468, doi:10.1038/ng.3273 (2015).

35 Cancer Genome Atlas Research, N. *et al.* Comprehensive, Integrative Genomic Analysis of Diffuse Lower-Grade Gliomas. *The New England Journal of Medicine* **372**, 2481-2498, doi:10.1056/NEJMoa1402121 (2015).

36 Reifenberger, G., Wirsching, H. G., Knobbe-Thomsen, C. B. & Weller, M. Advances in the molecular genetics of gliomas - implications for classification and therapy. *Nat Rev Clin Oncol* **14**, 434-452, doi:10.1038/nrclinonc.2016.204 (2017).

37 Wiestler, B. *et al.* Integrated DNA methylation and copy-number profiling identify three clinically and biologically relevant groups of anaplastic glioma. *Acta neuropathologica* **128**, 561-571, doi:10.1007/s00401-014-1315-x (2014).

38 Cohen, A. L., Holmen, S. L. & Colman, H. IDH1 and IDH2 mutations in gliomas. *Curr Neurol Neurosci Rep* **13**, 345, doi:10.1007/s11910-013-0345-4 (2013).

39 Xu, W. *et al.* Oncometabolite 2-hydroxyglutarate is a competitive inhibitor of alpha-ketoglutarate-dependent dioxygenases. *Cancer Cell* **19**, 17-30, doi:10.1016/j.ccr.2010.12.014 (2011).

40 Noushmehr, H. *et al.* Identification of a CpG island methylator phenotype that defines a distinct subgroup of glioma. *Cancer Cell* **17**, 510-522, doi:10.1016/j.ccr.2010.03.017 (2010).

41 Capper, D., Zentgraf, H., Balss, J., Hartmann, C. & von Deimling, A. Monoclonal antibody specific for IDH1 R132H mutation. *Acta neuropathologica* **118**, 599-601, doi:10.1007/s00401-009-0595-z (2009).

42 Amatangelo, M. D. *et al.* Enasidenib induces acute myeloid leukemia cell differentiation to promote clinical response. *Blood* **130**, 732-741, doi:10.1182/blood-2017-04-779447 (2017).

43 Foran, J. M. *et al.* Ivosidenib (AG-120) in Patients with IDH1-Mutant Relapsed/Refractory Myelodysplastic Syndrome: Updated Enrollment of a Phase 1 Dose Escalation and Expansion Study. *Blood* **134**, 4254-4254, doi:10.1182/blood-2019-123946 (2019).

44 Wang, Y. *et al.* Targeting therapeutic vulnerabilities with PARP inhibition and radiation in IDH-mutant gliomas and cholangiocarcinomas. *Sci Adv* **6**, eaaz3221, doi:10.1126/sciadv.aaz3221 (2020).

45 Sulkowski, P. L. *et al.* 2-Hydroxyglutarate produced by neomorphic IDH mutations suppresses homologous recombination and induces PARP inhibitor sensitivity. *Science translational medicine* **9**, eaal2463, doi:10.1126/scitranslmed.aal2463 (2017).

46 Watson, L. A., Goldberg, H. & Berube, N. G. Emerging roles of ATRX in cancer. *Epigenomics* **7**, 1365-1378, doi:10.2217/epi.15.82 (2015).

47 Flynn, R. L. *et al.* Alternative lengthening of telomeres renders cancer cells hypersensitive to ATR inhibitors. *Science (New York, N.Y.)* **347**, 273-277, doi:10.1126/science.1257216 (2015).

48 O'Rourke, J. J., Bythell-Douglas, R., Dunn, E. A. & Deans, A. J. ALT control, delete: FANCM as an anti-cancer target in Alternative Lengthening of Telomeres. *Nucleus* **10**, 221-230, doi:10.1080/19491034.2019.1685246 (2019).

49 Lovejoy, C. A. *et al.* Loss of ATRX, genome instability, and an altered DNA damage response are hallmarks of the alternative lengthening of telomeres pathway. *PLoS genetics* **8**, e1002772, doi:10.1371/journal.pgen.1002772 (2012).

50 Schwartzentruber, J. *et al.* Driver mutations in histone H3.3 and chromatin remodelling genes in paediatric glioblastoma. *Nature* **482**, 226-231, doi:10.1038/nature10833 (2012).

51 Obad, N. *et al.* Lack of functional normalisation of tumour vessels following anti-angiogenic therapy in glioblastoma. *J Cereb Blood Flow Metab* **38**, 1741-1753, doi:10.1177/0271678X17714656 (2018).

52 Fan, Q., Zhang, F., Barrett, B., Ren, K. & Andreassen, P. R. A role for monoubiquitinated FANCD2 at telomeres in ALT cells. *Nucleic acids research* **37**, 1740-1754, doi:10.1093/nar/gkn995 (2009).

53 Lyakhovich, A. *et al.* Fanconi anemia protein FANCD2 inhibits TRF1 polyADP-ribosylation through tankyrase1-dependent manner. *Genome integrity* **2**, 4, doi:10.1186/2041-9414-2-4 (2011).

54 Sarkar, J. *et al.* SLX4 contributes to telomere preservation and regulated processing of telomeric joint molecule intermediates. *Nucleic acids research* **43**, 5912-5923, doi:10.1093/nar/gkv522 (2015).

55 Jaunmuktane, Z. *et al.* Methylation array profiling of adult brain tumours: diagnostic outcomes in a large, single centre. *Acta Neuropathologica Communications* **7**, 24, doi:10.1186/s40478-019-0668-8 (2019).

56 Capper, D. *et al.* DNA methylation-based classification of central nervous system tumours. *Nature* **555**, 469-474, doi:10.1038/nature26000 (2018).

57 Hegi, M. E., Kleihues, P., Wen, P. Y. & Suvà, M. L. Toward methylation-based classification of central nervous system tumors. *Neuro Oncol* **20**, 579-581, doi:10.1093/neuonc/noy023 (2018).

58 Thakkar, J. P. *et al.* Epidemiologic and molecular prognostic review of glioblastoma. *Cancer Epidemiol Biomarkers Prev* **23**, 1985-1996, doi:10.1158/1055-9965.EPI-14-0275 (2014).

59 Cancer Research UK. *Tackle cancers with substantial unmet need: our research strategy*, <http://www.cancerresearchuk.org/funding-for-researchers/our-research-strategy/tackle-cancers-with-substantial-unmet-need> (2017).

60 Cancer Genome Atlas Research, N. Comprehensive genomic characterization defines human glioblastoma genes and core pathways. *Nature* **455**, 1061-1068, doi:10.1038/nature07385 (2008).

61 Ohgaki, H. & Kleihues, P. The definition of primary and secondary glioblastoma. *Clinical Cancer Research* **19**, 764-772, doi:10.1158/1078-0432.CCR-12-3002 (2013).

62 Aldape, K., Zadeh, G., Mansouri, S., Reifenberger, G. & von Deimling, A. Glioblastoma: pathology, molecular mechanisms and markers. *Acta neuropathologica* **129**, 829-848, doi:10.1007/s00401-015-1432-1 (2015).

63 Bai, H. *et al.* Integrated genomic characterization of IDH1-mutant glioma malignant progression. *Nat Genet* **48**, 59-66, doi:10.1038/ng.3457 (2016).

64 Verhaak, R. G. W. *et al.* Integrated Genomic Analysis Identifies Clinically Relevant Subtypes of Glioblastoma Characterized

by Abnormalities in PDGFRA , IDH1 , EGFR , and NF1. *Cancer Cell* **17**, 98-110 (2010).

65 Verhaak, R. G. W. *et al.* Integrated Genomic Analysis Identifies Clinically Relevant Subtypes of Glioblastoma Characterized by Abnormalities in PDGFRA , IDH1, EGFR, and NF1. *Cancer Cell* **17**, 98-110 (2010).

66 Sidaway, P. Glioblastoma subtypes revisited. *Nature Reviews Clinical Oncology* **14**, 587-587, doi:10.1038/nrclinonc.2017.122 (2017).

67 Wang, Q. *et al.* Tumor Evolution of Glioma-Intrinsic Gene Expression Subtypes Associates with Immunological Changes in the Microenvironment. *Cancer Cell* **32**, 42-56.e46, doi:10.1016/j.ccell.2017.06.003 (2017).

68 Lee, J. H. *et al.* Human glioblastoma arises from subventricular zone cells with low-level driver mutations. *Nature* **560**, 243-247, doi:10.1038/s41586-018-0389-3 (2018).

69 Prayson, R. *Histologic Classification of High-Grade Gliomas in Current Clinical Oncology: High-Grade Gliomas: Diagnosis and Treatment*. 3-35 (Humana Press, 2006).

70 Administration, T. U. S. F. a. D. *Premarket Approval (PMA): Optune*, <https://www.accessdata.fda.gov/scripts/cdrh/cfdocs/cfpma/pma.cfm?id=P100034S013> (2015).

71 *Premarket Approval (PMA): Optune*, <https://www.accessdata.fda.gov/scripts/cdrh/cfdocs/cfpma/pma.cfm?id=P100034S013> (2015).

72 Giladi, M. *et al.* Tumor treating fields (TTFields) delay DNA damage repair following radiation treatment of glioma cells. *Radiation Oncology* **12**, 206, doi:10.1186/s13014-017-0941-6 (2017).

73 Karanam, N. K. *et al.* Tumor-treating fields elicit a conditional vulnerability to ionizing radiation via the downregulation of BRCA1 signaling and reduced DNA double-strand break repair capacity in non-small cell lung cancer cell lines. *Cell Death & Disease* **8**, e2711, doi:10.1038/cddis.2017.136 (2017).

74 Karanam, N. K., Hao-Ding, L., Aroumougame, A. & Story, M. D. Tumor treating fields cause replication stress and interfere with DNA replication fork maintenance: Implications for cancer therapy. *Translational Research*, doi:10.1016/j.trsl.2019.10.003.

75 Stupp, R. *et al.* Effect of Tumor- Treating Fields Plus Maintenance Temozolomide vs Maintenance Temozolomide Alone on Survival in Patients With Glioblastoma: A Randomized Clinical Trial. *JAMA* **318**, 2306-2316, doi:10.1001/jama.2017.18718 (2017).

76 Stupp, R. *et al.* Maintenance Therapy With Tumor-Treating Fields Plus Temozolomide vs Temozolomide Alone for Glioblastoma: A Randomized Clinical Trial. *JAMA* **314**, 2535-2543, doi:10.1001/jama.2015.16669 (2015).

77 (The National Institute for Health and Care Excellence. *Brain tumours (primary) and brain metastases in adults. NICE guideline [NG99]*, <https://www.nice.org.uk/guidance/ng99> (2018).

78 Stupp, R. *et al.* NovoTTF-100A versus physician's choice chemotherapy in recurrent glioblastoma: a randomised phase III trial of a novel treatment modality. *European journal of cancer (Oxford, England : 1990)* **48**, 2192-2202, doi:10.1016/j.ejca.2012.04.011 (2012).

79 Rominiyi, O. *et al.* Tumour Treating Fields for the treatment of glioblastoma: new advances and future directions. *British Journal of Cancer (submitted)* (2020).

80 Lacroix, M. *et al.* A multivariate analysis of 416 patients with glioblastoma multiforme: prognosis, extent of resection, and survival. *Journal of Neurosurgery* **95**, 190-198, doi:10.3171/jns.2001.95.2.0190 (2001).

81 Prada, F. *et al.* Identification of residual tumor with intraoperative contrast-enhanced ultrasound during glioblastoma resection. *Neurosurgical Focus* **40**, E7, doi:10.3171/2015.11.focus15573 (2016).

82 Stummer, W. *et al.* Fluorescence-guided resection of glioblastoma multiforme by using 5-aminolevulinic acid-induced porphyrins: a prospective study in 52 consecutive patients. *Journal of Neurosurgery* **93**, 1003-1013, doi:10.3171/jns.2000.93.6.1003 (2000).

83 Stummer, W. *et al.* Fluorescence-guided surgery with 5-aminolevulinic acid for resection of malignant glioma: a randomised controlled multicentre phase III trial. *The Lancet. Oncology* **7**, 392-401, doi:10.1016/s1470-2045(06)70665-9 (2006).

84 Kuhnt, D. *et al.* Correlation of the extent of tumor volume resection and patient survival in surgery of glioblastoma multiforme with high-field intraoperative MRI guidance. *Neuro Oncol* **13**, 1339-1348, doi:10.1093/neuonc/nor133 (2011).

85 Ferraro, N. *et al.* The role of 5-aminolevulinic acid in brain tumor surgery: a systematic review. *Neurosurgical review* **39**, 545-555, doi:10.1007/s10143-015-0695-2 (2016).

86 Teixidor, P. *et al.* Safety and Efficacy of 5-Aminolevulinic Acid for High Grade Glioma in Usual Clinical Practice: A Prospective Cohort Study. *PLoS One* **11**, e0149244, doi:10.1371/journal.pone.0149244 (2016).

87 Alexander, J. *et al.* A novel methodology for in vivo endoscopic phenotyping of colorectal cancer based on real-time analysis of the mucosal lipidome: a prospective observational study of the iKnife. *Surgical endoscopy*, doi:10.1007/s00464-016-5121-5 (2016).

88 Balog, J. *et al.* Intraoperative tissue identification using rapid evaporative ionization mass spectrometry. *Science translational medicine* **5**, 194ra193, doi:10.1126/scitranslmed.3005623 (2013).

89 Livermore, L. J. *et al.* Rapid intraoperative molecular genetic classification of gliomas using Raman spectroscopy. *Neuro-Oncology Advances* **1**, doi:10.1093/noajnl/vdz008 (2019).

90 Depciuch, J. *et al.* Raman and FTIR spectroscopy in determining the chemical changes in healthy brain tissues and glioblastoma tumor tissues. *Spectrochimica Acta Part A: Molecular and Biomolecular Spectroscopy* **225**, 117526, doi:https://doi.org/10.1016/j.saa.2019.117526 (2020).

91 Stupp, R., Lukas, R. V. & Hegi, M. E. Improving survival in molecularly selected glioblastoma. *Lancet (London, England)* **393**, 615-617, doi:10.1016/s0140-6736(18)33211-2 (2019).

92 Bedard, P. L., Hansen, A. R., Ratain, M. J. & Siu, L. L. Tumour heterogeneity in the clinic. *Nature* **501**, 355-364, doi:10.1038/nature12627 (2013).

93 Phillips, H. S. *et al.* Molecular subclasses of high-grade glioma predict prognosis, delineate a pattern of disease progression, and resemble stages in neurogenesis. *Cancer Cell* **9**, 157-173, doi:10.1016/j.ccr.2006.02.019 (2006).

94 Hegi , M. E. *et al.* MGMT Gene Silencing and Benefit from Temozolomide in Glioblastoma. *New England Journal of Medicine* **352**, 997-1003, doi:10.1056/NEJMoa043331 (2005).

95 Vartanian, A. *et al.* GBM's multifaceted landscape: highlighting regional and microenvironmental heterogeneity. *Neuro Oncol* **16**, 1167-1175, doi:10.1093/neuonc/nou035 (2014).

96 Soeda, A. *et al.* The evidence of glioblastoma heterogeneity. *Scientific reports* **5**, 7979, doi:10.1038/srep07979 (2015).

97 Iorio, F. *et al.* A Landscape of Pharmacogenomic Interactions in Cancer. *Cell* **166**, 740-754, doi:10.1016/j.cell.2016.06.017 (2016).

98 De Witt Hamer, P. C. *et al.* The genomic profile of human malignant glioma is altered early in primary cell culture and preserved in spheroids. *Oncogene* **27**, 2091-2096, doi:10.1038/sj.onc.1210850 (2008).

99 Fael Al-Mayhani, T. M. *et al.* An efficient method for derivation and propagation of glioblastoma cell lines that conserves the molecular profile of their original tumours. *Journal of neuroscience methods* **176**, 192-199, doi:10.1016/j.jneumeth.2008.07.022 (2009).

100 Pollard, S. M. *et al.* Glioma stem cell lines expanded in adherent culture have tumor-specific phenotypes and are suitable for chemical and genetic screens. *Cell stem cell* **4**, 568-580, doi:10.1016/j.stem.2009.03.014 (2009).

101 Rahman, M. *et al.* Neurosphere and adherent culture conditions are equivalent for malignant glioma stem cell lines. *Anatomy & cell biology* **48**, 25-35, doi:10.5115/acb.2015.48.1.25 (2015).

102 Hubert, C. G. *et al.* A Three-Dimensional Organoid Culture System Derived from Human Glioblastomas Recapitulates the Hypoxic Gradients and Cancer Stem Cell Heterogeneity of Tumors Found In Vivo. *Cancer Research* **76**, 2465-2477, doi:10.1158/0008-5472.Can-15-2402 (2016).

103 Pine, A. R. *et al.* Tumor microenvironment is critical for the maintenance of cellular states found in primary glioblastomas. *Cancer Discovery*, CD-20-0057, doi:10.1158/2159-8290.CD-20-0057 (2020).

104 Linkous, A. *et al.* Modeling Patient-Derived Glioblastoma with Cerebral Organoids. *Cell Rep* **26**, 3203-3211.e3205, doi:10.1016/j.celrep.2019.02.063 (2019).

105 Ogawa, J., Pao, G. M., Shokhirev, M. N. & Verma, I. M. Glioblastoma Model Using Human Cerebral Organoids. *Cell Rep* **23**, 1220-1229, doi:10.1016/j.celrep.2018.03.105 (2018).

106 Caragher, S., Chalmers, A. J. & Gomez-Roman, N. Glioblastoma's Next Top Model: Novel Culture Systems for Brain Cancer Radiotherapy Research. *Cancers* **11**, doi:10.3390/cancers11010044 (2019).

107 Gomez-Roman, N. *et al.* Radiation responses of 2D and 3D glioblastoma cells: a novel, 3D-specific radioprotective role of VEGF/Akt signaling through functional activation of NHEJ. *Molecular Cancer Therapeutics*, molcanther.1320.2018, doi:10.1158/1535-7163.MCT-18-1320 (2019).

108 Gomez-Roman, N., Stevenson, K., Gilmour, L., Hamilton, G. & Chalmers, A. J. A novel 3D human glioblastoma cell culture system for modeling drug and radiation responses. *Neuro Oncol* **19**, 229-241, doi:10.1093/neuonc/now164 (2017).

109 Yi, H. G. *et al.* A bioprinted human-glioblastoma-on-a-chip for the identification of patient-specific responses to chemoradiotherapy. *Nature biomedical engineering* **3**, 509-519, doi:10.1038/s41551-019-0363-x (2019).

110 Gomez-Roman, N. & Chalmers, A. J. Patient-specific 3D-printed glioblastomas. *Nature biomedical engineering* **3**, 498-499, doi:10.1038/s41551-019-0379-2 (2019).

111 Oh, T. *et al.* Immunocompetent murine models for the study of glioblastoma immunotherapy. *Journal of translational medicine* **12**, 107-107, doi:10.1186/1479-5876-12-107 (2014).

112 Lenting, K., Verhaak, R., Ter Laan, M., Wesseling, P. & Leenders, W. Glioma: experimental models and reality. *Acta neuropathologica* **133**, 263-282, doi:10.1007/s00401-017-1671-4 (2017).

113 Aldape, K. *et al.* Challenges to curing primary brain tumours. *Nature Reviews Clinical Oncology*, doi:10.1038/s41571-019-0177-5 (2019).

114 Ben-David, U. *et al.* Patient-derived xenografts undergo mouse-specific tumor evolution. *Nat Genet* **49**, 1567-1575, doi:10.1038/ng.3967 (2017).

115 Holland, E. C. A mouse model for glioma: biology, pathology, and therapeutic opportunities. *Toxicologic pathology* **28**, 171-177, doi:10.1177/019262330002800122 (2000).

116 Lindahl, T. Instability and decay of the primary structure of DNA. *Nature* **362**, 709-715, doi:10.1038/362709a0 (1993).

117 Goldstein, M. & Kastan, M. B. The DNA damage response: implications for tumor responses to radiation and chemotherapy. *Annual review of medicine* **66**, 129-143, doi:10.1146/annurev-med-081313-121208 (2015).

118 Davar, D., Beumer, J. H., Hamieh, L. & Tawbi, H. Role of PARP inhibitors in cancer biology and therapy. *Current medicinal chemistry* **19**, 3907-3921 (2012).

119 Johannessen, T.-C. A., Bjerkvig, R. & Tysnes, B. B. DNA repair and cancer stem-like cells – Potential partners in glioma drug resistance? *Cancer Treatment Reviews* **34**, 558-567, doi:http://dx.doi.org/10.1016/j.ctrv.2008.03.125 (2008).

120 Wick, W. *et al.* MGMT testing--the challenges for biomarker-based glioma treatment. *Nat Rev Neurol* **10**, 372-385, doi:10.1038/nrneurol.2014.100 (2014).

121 Trivedi, R. N., Almeida, K. H., Fornsaglio, J. L., Schamus, S. & Sobol, R. W. The role of base excision repair in the sensitivity and resistance to temozolomide-mediated cell death. *Cancer Research* **65**, 6394-6400, doi:10.1158/0008-5472.can-05-0715 (2005).

122 Frosina, G. Overexpression of enzymes that repair endogenous damage to DNA. *European journal of biochemistry* **267**, 2135-2149 (2000).

123 El-Khamisy, S. F., Masutani, M., Suzuki, H. & Caldecott, K. W. A requirement for PARP-1 for the assembly or stability of XRCC1 nuclear foci at sites of oxidative DNA damage. *Nucleic acids research* **31**, 5526-5533 (2003).

124 Sherr, C. J. & Bartek, J. Cell Cycle–Targeted Cancer Therapies. *Annual Review of Cancer Biology* **1**, 41-57, doi:10.1146/annurev-cancerbio-040716-075628 (2017).

125 Lukas, J., Lukas, C. & Bartek, J. Mammalian cell cycle checkpoints: signalling pathways and their organization in space and time. *DNA Repair (Amst)* **3**, 997-1007, doi:10.1016/j.dnarep.2004.03.006 (2004).

126 Shiloh, Y. & Ziv, Y. The ATM protein kinase: regulating the cellular response to genotoxic stress, and more. *Nature Reviews Molecular Cell Biology* **14**, 197-210, doi:10.1038/nrm3546 (2013).

127 Marechal, A. & Zou, L. DNA damage sensing by the ATM and ATR kinases. *Cold Spring Harb Perspect Biol* **5**, doi:10.1101/cshperspect.a012716 (2013).

128 Carruthers, R. & Chalmers, A. in *Radiation Oncology* Vol. 1 (ed F. Wenz) 1-14 (Springer Nature, 2019).

129 Kennedy, R. D. & D'Andrea, A. D. The Fanconi Anemia/BRCA pathway: new faces in the crowd. *Genes & development* **19**, 2925-2940, doi:10.1101/gad.1370505 (2005).

130 Wang, A. T. & Smogorzewska, A. SnapShot: Fanconi anemia and associated proteins. *Cell* **160**, 354-354.e351, doi:10.1016/j.cell.2014.12.031 (2015).

131 Adamo, A. *et al.* Preventing nonhomologous end joining suppresses DNA repair defects of Fanconi anemia. *Molecular Cell* **39**, 25-35, doi:10.1016/j.molcel.2010.06.026 (2010).

132 Palovcak, A., Liu, W., Yuan, F. & Zhang, Y. Maintenance of genome stability by Fanconi anemia proteins. *Cell Biosci* **7**, 8, doi:10.1186/s13578-016-0134-2 (2017).

133 Ciccia, A. *et al.* Identification of FAAP24, a Fanconi anemia core complex protein that interacts with FANCM. *Molecular Cell* **25**, 331-343, doi:10.1016/j.molcel.2007.01.003 (2007).

134 Shakeel, S. *et al.* Structure of the Fanconi anaemia monoubiquitin ligase complex. *Nature* **575**, 234-237, doi:10.1038/s41586-019-1703-4 (2019).

135 Rajendra, E. *et al.* The genetic and biochemical basis of FANCD2 monoubiquitination. *Molecular Cell* **54**, 858-869, doi:10.1016/j.molcel.2014.05.001 (2014).

136 Huang, Y. *et al.* Modularized Functions of the Fanconi Anemia Core Complex. *Cell Reports* **7**, 1849-1857, doi:https://doi.org/10.1016/j.celrep.2014.04.029 (2014).

137 Pace, P. *et al.* FANCE: the link between Fanconi anaemia complex assembly and activity. *The EMBO journal* **21**, 3414-3423, doi:10.1093/emboj/cdf355 (2002).

138 van Twest, S. *et al.* Mechanism of Ubiquitination and Deubiquitination in the Fanconi Anemia Pathway. *Molecular Cell* **65**, 247-259, doi:10.1016/j.molcel.2016.11.005 (2017).

139 Castella, M. *et al.* FANCI Regulates Recruitment of the FA Core Complex at Sites of DNA Damage Independently of FANCD2. *PLoS genetics* **11**, e1005563, doi:10.1371/journal.pgen.1005563 (2015).

140 Hira, A. *et al.* Mutations in the gene encoding the E2 conjugating enzyme UBE2T cause Fanconi anemia. *Am J Hum Genet* **96**, 1001-1007, doi:10.1016/j.ajhg.2015.04.022 (2015).

141 Miles, J. A. *et al.* The Fanconi Anemia DNA Repair Pathway Is Regulated by an Interaction between Ubiquitin and the E2-like Fold Domain of FANCL. *J Biol Chem* **290**, 20995-21006, doi:10.1074/jbc.M115.675835 (2015).

142 Rickman, K. A. *et al.* Deficiency of UBE2T, the E2 Ubiquitin Ligase Necessary for FANCD2 and FANCI Ubiquitination, Causes FA-T Subtype of Fanconi Anemia. *Cell Rep* **12**, 35-41, doi:10.1016/j.celrep.2015.06.014 (2015).

143 Virts, E. L. *et al.* AluY-mediated germline deletion, duplication and somatic stem cell reversion in UBE2T defines a new subtype of Fanconi anemia. *Hum Mol Genet* **24**, 5093-5108, doi:10.1093/hmg/ddv227 (2015).

144 Chaugule, V. K. *et al.* Allosteric mechanism for site-specific ubiquitination of FANCD2. *Nat Chem Biol* **16**, 291-301, doi:10.1038/s41589-019-0426-z (2020).

145 Alcón, P. *et al.* FANCD2-FANCI is a clamp stabilized on DNA by monoubiquitination of FANCD2 during DNA repair. *Nat Struct Mol Biol* **27**, 240-248, doi:10.1038/s41594-020-0380-1 (2020).

146 Tan, W. *et al.* Monoubiquitination by the human Fanconi anemia core complex clamps FANCI:FANCD2 on DNA in filamentous arrays. *eLife* **9**, e54128, doi:10.7554/eLife.54128 (2020).

147 Yang, K. *et al.* Regulation of the Fanconi anemia pathway by a SUMO-like delivery network. *Genes & development* **25**, 1847-1858, doi:10.1101/gad.17020911 (2011).

148 Ishiai, M. *et al.* FANCI phosphorylation functions as a molecular switch to turn on the Fanconi anemia pathway. *Nat Struct Mol Biol* **15**, 1138-1146, doi:10.1038/nsmb.1504 (2008).

149 Sareen, A., Chaudhury, I., Adams, N. & Sobeck, A. Fanconi anemia proteins FANCD2 and FANCI exhibit different DNA damage responses during S-phase. *Nucleic acids research* **40**, 8425-8439, doi:10.1093/nar/gks638 (2012).

150 Howlett, N. G., Taniguchi, T., Durkin, S. G., D'Andrea, A. D. & Glover, T. W. The Fanconi anemia pathway is required for the DNA replication stress response and for the regulation of common fragile site stability. *Hum Mol Genet* **14**, 693-701, doi:10.1093/hmg/ddi065 (2005).

151 Chen, Y. H. *et al.* ATR-mediated phosphorylation of FANCI regulates dormant origin firing in response to replication stress. *Molecular Cell* **58**, 323-338, doi:10.1016/j.molcel.2015.02.031 (2015).

152 Lossaint, G. *et al.* FANCD2 binds MCM proteins and controls replisome function upon activation of s phase checkpoint signaling. *Molecular Cell* **51**, 678-690, doi:10.1016/j.molcel.2013.07.023 (2013).

153 Michl, J., Zimmer, J., Buffa, F. M., McDermott, U. & Tarsounas, M. FANCD2 limits replication stress and genome instability in cells lacking BRCA2. *Nat Struct Mol Biol* **23**, 755-757, doi:10.1038/nsmb.3252 (2016).

154 Chaudhury, I., Sareen, A., Raghunandan, M. & Sobeck, A. FANCD2 regulates BLM complex functions independently of FANCI to promote replication fork recovery. *Nucleic acids research* **41**, 6444-6459, doi:10.1093/nar/gkt348 (2013).

155 Fanconi, G. Familiaere infantile perniziosaartige Anaemie (pernizioeses Blutbild und Konstitution). *Jahrbuch Kinderheild* **117**, 257-280 (1927).

156 Tischkowitz, M. D. & Hodgson, S. V. Fanconi anaemia. *J Med Genet* **40**, 1-10, doi:10.1136/jmg.40.1.1 (2003).

157 Dokal, I. The genetics of Fanconi's anaemia. *Baillieres Best Pract Res Clin Haematol* **13**, 407-425, doi:10.1053/beha.2000.0085 (2000).

158 Auerbach, A. D. Fanconi anemia diagnosis and the diepoxybutane (DEB) test. *Experimental hematology* **21**, 731-733 (1993).

159 Dufour, C. How I manage patients with Fanconi anaemia. *Br J Haematol* **178**, 32-47, doi:10.1111/bjh.14615 (2017).

160 Dutrillaux, B., Aurias, A., Dutrillaux, A. M., Buriot, D. & Prieur, M. The cell cycle of lymphocytes in Fanconi anemia. *Hum Genet* **62**, 327-332, doi:10.1007/bf00304549 (1982).

161 Ghemlas, I. *et al.* Improving diagnostic precision, care and syndrome definitions using comprehensive next-generation sequencing for the inherited bone marrow failure syndromes. *J Med Genet* **52**, 575-584, doi:10.1136/jmedgenet-2015-103270 (2015).

162 Butturini, A. *et al.* Hematologic abnormalities in Fanconi anemia: an International Fanconi Anemia Registry study. *Blood* **84**, 1650-1655 (1994).

163 Auerbach, A. D. & Allen, R. G. Leukemia and preleukemia in Fanconi anemia patients. A review of the literature and report of the International Fanconi Anemia Registry. *Cancer Genet Cytogenet* **51**, 1-12, doi:10.1016/0165-4608(91)90002-c (1991).

164 Socié, G. *et al.* Transplantation for Fanconi's anaemia: long-term follow-up of fifty patients transplanted from a sibling donor after low-dose cyclophosphamide and thoraco-abdominal irradiation for conditioning. *Br J Haematol* **103**, 249-255, doi:10.1046/j.1365-2141.1998.00968.x (1998).

165 Dufour, C. *et al.* Stem cell transplantation from HLA-matched related donor for Fanconi's anaemia: a retrospective review of the multicentric Italian experience on behalf of AIEOP-GITMO. *Br J Haematol* **112**, 796-805, doi:10.1046/j.1365-2141.2001.02572.x (2001).

166 Alter, B. P., Giri, N., Pan, Y., Savage, S. A. & Pinto, L. A. Antibody response to human papillomavirus vaccine in subjects with inherited bone marrow failure syndromes. *Vaccine* **32**, 1169-1173, doi:10.1016/j.vaccine.2013.11.048 (2014).

167 Alter, B. P. *et al.* Malignancies and survival patterns in the National Cancer Institute inherited bone marrow failure syndromes cohort study. *Br J Haematol* **150**, 179-188, doi:10.1111/j.1365-2141.2010.08212.x (2010).

168 Alter, B. P. Fanconi's anemia, transplantation, and cancer. *Pediatr Transplant* **9 Suppl 7**, 81-86, doi:10.1111/j.1399-3046.2005.00440.x (2005).

169 Dewire, M. D. *et al.* Fanconi anemia and biallelic BRCA2 mutation diagnosed in a young child with an embryonal CNS tumor. *Pediatr Blood Cancer* **53**, 1140-1142, doi:10.1002/pbc.22139 (2009).

170 Hirsch, B. *et al.* Association of biallelic BRCA2/FANCD1 mutations with spontaneous chromosomal instability and solid tumors of childhood. *Blood* **103**, 2554-2559, doi:10.1182/blood-2003-06-1970 (2004).

171 Dodgshun, A. J., Sexton-Oates, A., Saffery, R. & Sullivan, M. J. Biallelic FANCD1/BRCA2 mutations predisposing to glioblastoma multiforme with multiple oncogenic amplifications. *Cancer Genet* **209**, 53-56, doi:10.1016/j.cancergen.2015.11.005 (2016).

172 Sung, P. & Klein, H. Mechanism of homologous recombination: mediators and helicases take on regulatory functions. *Nature Reviews Molecular Cell Biology* **7**, 739-750, doi:10. 1038/nrm2008 (2006).

173 Lord, C. J. & Ashworth, A. BRCAness revisited. *Nature reviews. Cancer* **16**, 110-120, doi:10.1038/nrc.2015.21 (2016).

174 Chang, H. H. Y., Pannunzio, N. R., Adachi, N. & Lieber, M. R. Non-homologous DNA end joining and alternative pathways to double-strand break repair. *Nature Reviews Molecular Cell Biology* **18**, 495-506, doi:10.1038/nrm.2017.48 (2017).

175 Scully, R., Panday, A., Elango, R. & Willis, N. A. DNA double-strand break repair-pathway choice in somatic mammalian cells. *Nature Reviews Molecular Cell Biology* **20**, 698-714, doi:10.1038/s41580-019-0152-0 (2019).

176 Jiricny, J. Postreplicative mismatch repair. *Cold Spring Harb Perspect Biol* **5**, a012633, doi:10.1101/cshperspect.a012633 (2013).

177 David, S. S., O'Shea, V. L. & Kundu, S. Base-excision repair of oxidative DNA damage. *Nature* **447**, 941-950, doi:10.1038/nature05978 (2007).

178 Krokan, H. E. & Bjoras, M. Base excision repair. *Cold Spring Harb Perspect Biol* **5**, a012583, doi:10.1101/cshperspect.a012583 (2013).

179 Marteijn, J. A., Lans, H., Vermeulen, W. & Hoeijmakers, J. H. Understanding nucleotide excision repair and its roles in cancer and ageing. *Nature Reviews Molecular Cell Biology* **15**, 465-481, doi:10.1038/nrm3822 (2014).

180 Kaelin, W. G., Jr. The concept of synthetic lethality in the context of anticancer therapy. *Nature reviews. Cancer* **5**, 689-698, doi:10.1038/nrc1691 (2005).

181 Nijman, S. M. Synthetic lethality: general principles, utility and detection using genetic screens in human cells. *FEBS letters* **585**, 1-6, doi:10.1016/j.febslet.2010.11.024 (2011).

182 Moutsatsos, I. K. & Parker, C. N. Recent advances in quantitative high throughput and high content data analysis. *Expert opinion on drug discovery* **11**, 415-423, doi:10.1517/17460441.2016.1154036 (2016).

183 Wang, T., Wei, J. J., Sabatini, D. M. & Lander, E. S. Genetic screens in human cells using the CRISPR-Cas9 system. *Science (New York, N.Y.)* **343**, 80-84, doi:10.1126/science.1246981 (2014).

184 Bryant, H. E. *et al.* Specific killing of BRCA2-deficient tumours with inhibitors of poly(ADP-ribose) polymerase. *Nature* **434**, 913-917, doi:10.1038/nature03443 (2005).

185 Farmer, H. *et al.* Targeting the DNA repair defect in BRCA mutant cells as a therapeutic strategy. *Nature* **434**, 917-921, doi:10.1038/nature03445 (2005).

186 Meyer, M. *et al.* Single cell-derived clonal analysis of human glioblastoma links functional and genomic heterogeneity. *Proceedings of the National Academy of Sciences of the United States of America* **112**, 851-856, doi:10.1073/pnas.1320611111 (2015).

187 Lopez-Martinez, D., Liang, C. C. & Cohn, M. A. Cellular response to DNA interstrand crosslinks: the Fanconi anemia pathway. *Cellular and molecular life sciences : CMLS* **73**, 3097-3114, doi:10.1007/s00018-016-2218-x (2016).

188 Wang, J. D., Sanders, G. M. & Grossman, A. D. Nutritional control of elongation of DNA replication by (p)ppGpp. *Cell* **128**, 865-875, doi:10.1016/j.cell.2006.12.043 (2007).

189 Collis, S. J. *et al.* FANCM and FAAP24 function in ATR-mediated checkpoint signaling independently of the Fanconi anemia core complex. *Molecular Cell* **32**, 313-324, doi:10.1016/j.molcel.2008.10.014 (2008).

190 Ji, Y. & Tulin, A. V. The roles of PARP1 in gene control and cell differentiation. *Current opinion in genetics & development* **20**, 512-518, doi:10.1016/j.gde.2010.06.001 (2010).

191 Krishnakumar, R. & Kraus, W. L. The PARP side of the nucleus: molecular actions, physiological outcomes, and clinical targets. *Molecular Cell* **39**, 8-24, doi:10.1016/j.molcel.2010.06.017 (2010).

192 Gottipati, P. *et al.* Poly(ADP-ribose) polymerase is hyperactivated in homologous recombination-defective cells. *Cancer Research* **70**, 5389-5398, doi:10.1158/0008-5472.can-09-4716 (2010).

193 Pace, P. *et al.* Ku70 corrupts DNA repair in the absence of the Fanconi anemia pathway. *Science (New York, N.Y.)* **329**, 219-223, doi:10.1126/science.1192277 (2010).

194 Curtin, N. J. DNA repair dysregulation from cancer driver to therapeutic target. *Nature reviews. Cancer* **12**, 801-817, doi:10.1038/nrc3399 (2012).

195 Carruthers, R. *et al.* Abrogation of radioresistance in glioblastoma stem-like cells by inhibition of ATM kinase. *Molecular oncology* **9**, 192-203, doi:10.1016/j.molonc.2014.08.003 (2015).

196 Venere, M. *et al.* Therapeutic targeting of constitutive PARP activation compromises stem cell phenotype and survival of glioblastoma-initiating cells. *Cell death and differentiation* **21**, 258-269, doi:10.1038/cdd.2013.136 (2014).

197 Ahmed, S. U. *et al.* Selective Inhibition of Parallel DNA Damage Response Pathways Optimizes Radiosensitization of Glioblastoma Stem-like Cells. *Cancer Research* **75**, 4416-4428, doi:10.1158/0008-5472.can-14-3790 (2015).

198 Signore, M. *et al.* Combined PDK1 and CHK1 inhibition is required to kill glioblastoma stem-like cells in vitro and in vivo. *Cell Death & Disease* **5**, e1223, doi:10.1038/cddis.2014.188 (2014).

199 Rasmussen, R. D., Gajjar, M. K., Jensen, K. E. & Hamerlik, P. Enhanced efficacy of combined HDAC and PARP targeting in glioblastoma. *Molecular oncology* **10**, 751-763, doi:10.1016/j.molonc.2015.12.014 (2016).

200 Vance, S. *et al.* Selective radiosensitization of p53 mutant pancreatic cancer cells by combined inhibition of Chk1 and PARP1. *Cell cycle (Georgetown, Tex.)* **10**, 4321-4329, doi:10.4161/cc.10.24.18661 (2011).

201 Hoglund, A., Stromvall, K., Li, Y., Forshell, L. P. & Nilsson, J. A. Chk2 deficiency in Myc overexpressing lymphoma cells elicits a synergistic lethal response in combination with PARP inhibition. *Cell cycle (Georgetown, Tex.)* **10**, 3598-3607, doi:10.4161/cc.10.20.17887 (2011).

202 Booth, L. *et al.* PARP and CHK inhibitors interact to cause DNA damage and cell death in mammary carcinoma cells. *Cancer biology & therapy* **14**, 458-465, doi:10.4161/cbt.24424 (2013).

203 Peasland, A. *et al.* Identification and evaluation of a potent novel ATR inhibitor, NU6027, in breast and ovarian cancer cell lines. *British Journal of Cancer* **105**, 372-381, doi:10.1038/bjc.2011.243 (2011).

204 Riches, L. C. *et al.* Pharmacology of the ATM Inhibitor AZD0156: Potentiation of Irradiation and Olaparib Responses Preclinically. *Molecular Cancer Therapeutics* **19**, 13, doi:10.1158/1535-7163.MCT-18-1394 (2020).

205 Calcagno, A., Di Perri, G. & Bonora, S. Treating HIV Infection in the Central Nervous System. *Drugs*, doi:10.1007/s40265-016-0678-9 (2017).

206 MerckMillipore_Anti-pan-ADP-ribose_binding_reagent. <http://www.merckmillipore.com/GB/en/product/Anti-pan-ADP-ribose-binding-reagent,MM_NF-MABE1016> (2019).

207 Mosmann, T. Rapid colorimetric assay for cellular growth and survival: application to proliferation and cytotoxicity assays. *Journal of immunological methods* **65**, 55-63, doi:10.1016/0022-1759(83)90303-4 (1983).

208 Carruthers, R. D. *et al.* Replication Stress Drives Constitutive Activation of the DNA Damage Response and Radioresistance in Glioblastoma Stem-like Cells. *Cancer Research* **78**, 5060-5071, doi:10.1158/0008-5472.Can-18-0569 (2018).

209 Helleday, T., Petermann, E., Lundin, C., Hodgson, B. & Sharma, R. A. DNA repair pathways as targets for cancer therapy. *Nature reviews. Cancer* **8**, 193-204, doi:10.1038/nrc2342 (2008).

210 Munshi, A., Hobbs, M. & Meyn, R. E. Clonogenic cell survival assay. *Methods in molecular medicine* **110**, 21-28, doi:10.1385/1-59259-869-2:021 (2005).

211 Puck, T. T. & Marcus, P. I. Action of x-rays on mammalian cells. *The Journal of experimental medicine* **103**, 653-666 (1956).

212 Osswald, M. *et al.* Brain tumour cells interconnect to a functional and resistant network. *Nature* **528**, 93-98, doi:10.1038/nature16071 (2015).

213 Rominiyi, O. *et al.* FA-based combinations to target the DNA damage response in glioblastoma. *Neuro Oncol* **20**, v358, doi:https://doi.org/10.1093/neuonc/noy130.066 (2018).

214 Rominiyi, O. *et al.* Preclinical evaluation of combinations targeting the DNA damage response in 2D and 3D models of glioblastoma stem cells [abstract]. *Neuro-Oncology* **20**, iii297, doi:https://doi.org/10.1093/neuonc/noy139.308 (2018).

215 Reprocell.com. *What is Alvetex?*, <https://www.reprocell.com/what-is-alvetex-i70> (2020).

216 Collis, S. J. *et al.* HCLK2 is essential for the mammalian S-phase checkpoint and impacts on Chk1 stability. *Nature cell biology* **9**, 391-401, doi:10.1038/ncb1555 (2007).

217 García-Muse, T. & Aguilera, A. R Loops: From Physiological to Pathological Roles. *Cell* **179**, 604-618, doi:10.1016/j.cell.2019.08.055 (2019).

218 Bhatia, V. *et al.* BRCA2 prevents R-loop accumulation and associates with TREX-2 mRNA export factor PCID2. *Nature* **511**, 362-365, doi:10.1038/nature13374 (2014).

219 ThermoScientific. *NanoDrop 1000 Spectrophotometer V3.8 User's Manual*, <http://tools.thermofisher.com/content/sfs/manuals/nd-1000-v3.8-users-manual-8%205x11.pdf> (2020).

220 Azqueta, A. & Collins, A. R. The essential comet assay: a comprehensive guide to measuring DNA damage and repair. *Archives of toxicology* **87**, 949-968, doi:10.1007/s00204-013-1070-0 (2013).

221 Brand, D. H. & Yarnold, J. R. The Linear-Quadratic Model and Implications for Fractionation. *Clinical oncology (Royal College of Radiologists (Great Britain))*, doi:10.1016/j.clon.2019.06.007 (2019).

222 Wang, J. *et al.* Clonal evolution of glioblastoma under therapy. *Nat Genet* **48**, 768-776, doi:10.1038/ng.3590 (2016).

223 Barthel, F. P. *et al.* Longitudinal molecular trajectories of diffuse glioma in adults. *Nature* **576**, 112-120, doi:10.1038/s41586-019-1775-1 (2019).

224 Daniel, P. *et al.* Temozolomide Induced Hypermutation in Glioma: Evolutionary Mechanisms and Therapeutic Opportunities. *Front Oncol* **9**, 41-41, doi:10.3389/fonc.2019.00041 (2019).

225 MacLeod, G. *et al.* Genome-Wide CRISPR-Cas9 Screens Expose Genetic Vulnerabilities and Mechanisms of Temozolomide Sensitivity in Glioblastoma Stem Cells. *Cell Rep* **27**, 971-986.e979, doi:10.1016/j.celrep.2019.03.047 (2019).

226 Banach, M. *et al.* Lipid, blood pressure and kidney update 2013. *Int Urol Nephrol* **46**, 947-961, doi:10.1007/s11255-014-0657-6 (2014).

227 Menon, V. P. & Sudheer, A. R. Antioxidant and anti-inflammatory properties of curcumin. *Adv Exp Med Biol* **595**, 105-125, doi:10.1007/978-0-387-46401-5_3 (2007).

228 Panahi, Y., Alishiri, G. H., Parvin, S. & Sahebkar, A. Mitigation of Systemic Oxidative Stress by Curcuminoids in Osteoarthritis: Results of a Randomized Controlled Trial. *J Diet Suppl* **13**, 209-220, doi:10.3109/19390211.2015.1008611 (2016).

229 Sahebkar, A., Serban, M.-C., Ursoniu, S. & Banach, M. Effect of curcuminoids on oxidative stress: A systematic review and meta-analysis of randomized controlled trials. *Journal of Functional Foods* **18**, 898-909, doi:https://doi.org/10.1016/j.jff.2015.01.005 (2015).

230 Lin, Y. G. *et al.* Curcumin inhibits tumor growth and angiogenesis in ovarian carcinoma by targeting the nuclear factor-kappaB pathway. *Clinical Cancer Research* **13**, 3423-3430, doi:10.1158/1078-0432.Ccr-06-3072 (2007).

231 Mansouri, K. *et al.* Clinical effects of curcumin in enhancing cancer therapy: A systematic review. *BMC Cancer* **20**, 791, doi:10.1186/s12885-020-07256-8 (2020).

232 Ranjan, D., Chen, C., Johnston, T. D., Jeon, H. & Nagabhushan, M. Curcumin inhibits mitogen stimulated lymphocyte proliferation, NFκB activation, and IL-2 signaling. *Journal of Surgical Research* **121**, 171-177, doi:https://doi.org/10.1016/j.jss.2004.04.004 (2004).

233 Liu, H. L., Chen, Y., Cui, G. H. & Zhou, J. F. Curcumin, a potent anti-tumor reagent, is a novel histone deacetylase inhibitor regulating B-NHL cell line Raji proliferation. *Acta pharmacologica Sinica* **26**, 603-609, doi:10.1111/j.1745-7254.2005.00081.x (2005).

234 Fujiwara, H. *et al.* Curcumin inhibits glucose production in isolated mice hepatocytes. *Diabetes Res Clin Pract* **80**, 185-191, doi:10.1016/j.diabres.2007.12.004 (2008).

235 Fu, D., Calvo, J. A. & Samson, L. D. Balancing repair and tolerance of DNA damage caused by alkylating agents. *Nature reviews. Cancer* **12**, 104-120, doi:10.1038/nrc3185 (2012).

236 Calabrese, C. R. *et al.* Anticancer chemosensitization and radiosensitization by the novel poly(ADP-ribose) polymerase-1 inhibitor AG14361. *Journal of the National Cancer Institute* **96**, 56-67, doi:10.1093/jnci/djh005 (2004).

237 Gupta, S. K. *et al.* PARP Inhibitors for Sensitization of Alkylation Chemotherapy in Glioblastoma: Impact of Blood-Brain Barrier and Molecular Heterogeneity. *Front Oncol* **8**, 670, doi:10.3389/fonc.2018.00670 (2018).

238 Nadkarni, A. *et al.* ATM inhibitor KU-55933 increases the TMZ responsiveness of only inherently TMZ sensitive GBM cells. *Journal of neuro-oncology* **110**, 349-357, doi:10.1007/s11060-012-0979-0 (2012).

239 Gupta, S. K. *et al.* Delineation of MGMT Hypermethylation as a Biomarker for Veliparib-Mediated Temozolomide-Sensitizing Therapy of Glioblastoma. *Journal of the National Cancer Institute* **108**, doi:10.1093/jnci/djv369 (2016).

240 Sarkaria, J. N. *et al.* Mechanisms of chemoresistance to alkylating agents in malignant glioma. *Clinical Cancer Research* **14**, 2900-2908, doi:10.1158/1078-0432.Ccr-07-1719 (2008).

241 D'Atri, S. *et al.* Involvement of the mismatch repair system in temozolomide-induced apoptosis. *Mol Pharmacol* **54**, 334-341, doi:10.1124/mol.54.2.334 (1998).

242 Caporali, S. *et al.* DNA damage induced by temozolomide signals to both ATM and ATR: role of the mismatch repair system. *Mol Pharmacol* **66**, 478-491, doi:10.1124/mol.66.3. (2004).

243 Eich, M., Roos, W. P., Nikolova, T. & Kaina, B. Contribution of ATM and ATR to the resistance of glioblastoma and malignant melanoma cells to the methylating anticancer drug temozolomide. *Molecular Cancer Therapuetics* **12**, 2529-2540, doi:10.1158/1535-7163.MCT-13-0136 (2013).

244 Jackson, C. B. *et al.* Temozolomide Sensitizes MGMT-Deficient Tumor Cells to ATR Inhibitors. *Cancer Research* **79**, 4331-4338, doi:10.1158/0008-5472.Can-18-3394 (2019).

245 Sharma, R. A. *et al.* Phase I Clinical Trial of Oral Curcumin. *Clinical Cancer Research* **10**, 6847, doi:10.1158/1078-0432.CCR-04-0744 (2004).

246 Epelbaum, R., Schaffer, M., Vizel, B., Badmaev, V. & Bar-Sela, G. Curcumin and gemcitabine in patients with advanced pancreatic cancer. *Nutrition and cancer* **62**, 1137-1141, doi:10.1080/01635581.2010.513802 (2010).

247 ClinicalTrials.gov. *Curcumin Bioavailability in Glioblastoma Patients*, <https://clinicaltrials.gov/ct2/show/NCT01712542?term=curcumin&cond=Glioma&draw=2&rank=1> (2012).

248 Dutzmann, S. *et al.* Intratumoral Concentrations and Effects of Orally Administered Micellar Curcuminoids in Glioblastoma Patients. *Nutrition and cancer* **68**, 943-948, doi:10.1080/01635581.2016.1187281 (2016).

249 Voter, A. F., Manthei, K. A. & Keck, J. L. A High-Throughput Screening Strategy to Identify Protein-Protein Interaction Inhibitors That Block the Fanconi Anemia DNA Repair Pathway. *Journal of biomolecular screening* **21**, 626-633, doi:10.1177/1087057116635503 (2016).

250 Cornwell, M. J. *et al.* Small-Molecule Inhibition of UBE2T/FANCL-Mediated Ubiquitylation in the Fanconi Anemia Pathway. *ACS Chemical Biology* **14**, 2148-2154, doi:10.1021/acschembio.9b00570 (2019).

251 Mistry, H. *et al.* Small-molecule inhibitors of USP1 target ID1 degradation in leukemic cells. *Molecular Cancer Therapuetics* **12**, 2651-2662, doi:10.1158/1535-7163.Mct-13-0103-t (2013).

252 Pessetto, Z. Y., Yan, Y., Bessho, T. & Natarajan, A. Inhibition of BRCT(BRCA1)-phosphoprotein interaction enhances the cytotoxic effect of olaparib in breast cancer cells: a proof of concept study for synthetic lethal therapeutic option. *Breast cancer research and treatment* **134**, 511-517, doi:10.1007/s10549-012-2079-4 (2012).

253 King, H. O. *et al.* RAD51 Is a Selective DNA Repair Target to Radiosensitize Glioma Stem Cells. *Stem Cell Reports* **8**, 125-139, doi:10.1016/j.stemcr.2016.12.005 (2017).

254 Sharp, M. F. *et al.* Methodology for the identification of small molecule inhibitors of the Fanconi Anaemia ubiquitin E3 ligase complex. *Scientific reports* **10**, 7959, doi:10.1038/s41598-020-64868-7 (2020).

255 Kais, Z. *et al.* FANCD2 Maintains Fork Stability in BRCA1/2-Deficient Tumors and Promotes Alternative End-Joining DNA Repair. *Cell Rep* **15**, 2488-2499, doi:10.1016/j.celrep.2016.05.031 (2016).

256 Ledermann, J. *et al.* Olaparib Maintenance Therapy in Platinum-Sensitive Relapsed Ovarian Cancer. *New England Journal of Medicine* **366**, 1382-1392, doi:10.1056/NEJMoa1105535 (2012).

257 Kaufman, B. *et al.* Olaparib monotherapy in patients with advanced cancer and a germline BRCA1/2 mutation. *Journal of clinical oncology : official journal of the American Society of Clinical Oncology* **33**, 244-250, doi:10.1200/jco.2014.56.2728 (2015).

258 Swisher, E. M. *et al.* Rucaparib in relapsed, platinum-sensitive high-grade ovarian carcinoma (ARIEL2 Part 1): an international, multicentre, open-label, phase 2 trial. *The Lancet. Oncology* **18**, 75-87, doi:10.1016/s1470-2045(16)30559-9 (2017).

259 Kristeleit, R. S. *et al.* Clinical activity of the poly(ADP-ribose) polymerase (PARP) inhibitor rucaparib in patients (pts) with high-grade ovarian carcinoma (HGOC) and a BRCA mutation (BRCAmut): Analysis of pooled data from Study 10 (parts 1, 2a, and 3) and ARIEL2 (parts 1 and 2). *Annals of Oncology* **27**, vi296, doi:10.1093/annonc/mdw374.03 (2016).

260 Mirza, M. R. *et al.* Niraparib Maintenance Therapy in Platinum-Sensitive, Recurrent Ovarian Cancer. *New England Journal of Medicine* **375**, 2154-2164, doi:10.1056/NEJMoa1611310 (2016).

261 Pujade-Lauraine, E. *et al.* Olaparib tablets as maintenance therapy in patients with platinum-sensitive, relapsed ovarian cancer and a BRCA1/2 mutation (SOLO2/ENGOT-Ov21): a double-blind, randomised, placebo-controlled, phase 3 trial. *The Lancet. Oncology* **18**, 1274-1284, doi:10.1016/s1470-2045(17)30469-2 (2017).

262 Coleman, R. L. *et al.* Rucaparib maintenance treatment for recurrent ovarian carcinoma after response to platinum therapy (ARIEL3): a randomised, double-blind, placebo-controlled, phase 3 trial. *Lancet (London, England)* **390**, 1949-1961, doi:10.1016/s0140-6736(17)32440-6 (2017).

263 Robson, M. *et al.* Olaparib for Metastatic Breast Cancer in Patients with a Germline BRCA Mutation. *The New England Journal of Medicine* **377**, 523-533, doi:10.1056/NEJMoa1706450 (2017).

264 Golan, T. *et al.* Maintenance Olaparib for Germline BRCA-Mutated Metastatic Pancreatic Cancer. *New England Journal of Medicine* **381**, 317-327, doi:10.1056/NEJMoa1903387 (2019).

265 Sandhu, S. K. *et al.* PROfound: Phase III study of olaparib versus enzalutamide or abiraterone for metastatic castration-resistant prostate cancer (mCRPC) with homologous recombination repair (HRR) gene alterations. *Annals of Oncology* **30**, ix188-ix189, doi:10.1093/annonc/mdz446.007 (2019).

266 Pilie, P. G., Tang, C., Mills, G. B. & Yap, T. A. State-of-the-art strategies for targeting the DNA damage response in cancer. *Nat Rev Clin Oncol* **16**, 81-104, doi:10.1038/s41571-018-0114-z (2019).

267 Yap, T. A. *et al.* Phase I modular study of AZD6738, a novel oral, potent and selective ataxia telangiectasia Rad3-related (ATR) inhibitor in combination (combo) with carboplatin, olaparib or durvalumab in patients (pts) with advanced cancers. *European Journal of Cancer* **69**, S2, doi:10.1016/S0959-8049(16)32607-7 (2016).

268 Durant, S. T. *et al.* The brain-penetrant clinical ATM inhibitor AZD1390 radiosensitizes and improves survival of preclinical brain tumor models. *Sci Adv* **4**, eaat1719-eaat1719, doi:10.1126/sciadv.aat1719 (2018).

269 Karlin, J. *et al.* Orally Bioavailable and Blood-Brain Barrier-Penetrating ATM Inhibitor (AZ32) Radiosensitizes Intracranial Gliomas in Mice. *Molecular Cancer Therapuetics* **17**, 1637-1647, doi:10.1158/1535-7163.Mct-17-0975 (2018).

270 Kleinberg, L. *et al.* Phase I adult brain tumor consortium (ABTC) trial of ABT-888 (veliparib), temozolomide (TMZ), and radiotherapy (RT) for newly diagnosed glioblastoma multiforme (GBM) including pharmacokinetic (PK) data. *Journal of Clinical Oncology* **31**, 2065-2065, doi:10.1200/jco.2013.31.15_suppl.2065 (2013).

271 Halford, S. E. R. *et al.* Results of the OPARATIC trial: A phase I dose escalation study of olaparib in combination with temozolomide (TMZ) in patients with relapsed glioblastoma (GBM). *Journal of Clinical Oncology* **35**, 2022-2022, doi:10.1200/JCO.2017.35.15_suppl.2022 (2017).

272 Hanna, C. *et al.* Pharmacokinetics, safety and tolerability of olaparib and temozolomide for recurrent glioblastoma: results of the phase I OPARATIC trial. *Neuro Oncol*, doi:10.1093/neuonc/noaa104 (2020).

273 Kurzrock, R. *et al.* A phase I study of niraparib in combination with temozolomide (TMZ) in patients with advanced cancer. *Journal of Clinical Oncology* **32**, 2092-2092, doi:10.1200/jco.2014.32.15_suppl.2092 (2014).

274 Fulton, B. *et al.* PARADIGM-2: Two parallel phase I studies of olaparib and radiotherapy or olaparib and radiotherapy plus temozolomide in patients with newly diagnosed glioblastoma, with treatment stratified by MGMT status. *Clin Transl Radiat Oncol* **8**, 12-16, doi:10.1016/j.ctro.2017.11.003 (2017).

275 Robins, H. I. *et al.* ATCT-27: NRG ONCOLOGY/RTOG 0929: A RANDOMIZED PHASE I/II STUDY OF ABT-888IN COMBINATION WITH TEMOZOLOMIDE IN RECURRENT TEMOZOLOMIDE RESISTANT GLIOBLASTOMA. *Neuro-Oncology* **17**, v7-v7, doi:10.1093/neuonc/nov206.27 (2015).

276 Baxter, P. A. *et al.* A phase I/II study of veliparib (ABT-888) with radiation and temozolomide in newly diagnosed diffuse pontine glioma: a Pediatric Brain Tumor Consortium study. *Neuro-Oncology*, doi:10.1093/neuonc/noaa016 (2020).

277 Baxter, P. A. *et al.* A phase I/II clinical trial of veliparib (ABT-888) and radiation followed by maintenance therapy with veliparib and temozolomide in patients with newly diagnosed diffuse intrinsic pontine glioma (DIPG): A Pediatric Brain Tumor Consortium Interim Report of Phase I Study. *Journal of Clinical Oncology* **33**, 10053-10053, doi:10.1200/jco.2015.33.15_suppl.10053 (2015).

278 Schafer, E. S. *et al.* Phase 1/2 trial of talazoparib in combination with temozolomide in children and adolescents with refractory/recurrent solid tumors including Ewing sarcoma: A Children's Oncology Group Phase 1 Consortium study (ADVL1411). *Pediatr Blood Cancer* **67**, e28073, doi:10.1002/pbc.28073 (2020).

279 Piotrowski, A. *et al.* ACTR-39. PAMIPARIB IN COMBINATION WITH RADIATION THERAPY (RT) AND/OR TEMOZOLOMIDE (TMZ) IN PATIENTS WITH NEWLY DIAGNOSED OR RECURRENT/REFRACTORY (R/R) GLIOBLASTOMA (GBM); PHASE 1B/2 STUDY UPDATE. *Neuro-Oncology* **21**, vi21-vi22, doi:10.1093/neuonc/noz175.081 (2019).

280 Lesueur, P. *et al.* Phase I/IIa study of concomitant radiotherapy with olaparib and temozolomide in unresectable or partially resectable glioblastoma: OLA-TMZ-RTE-01 trial protocol. *BMC Cancer* **19**, 198, doi:10.1186/s12885-019-5413-y (2019).

281 Parsons, D. W. *et al.* Identification of targetable molecular alterations in the NCI-COG Pediatric MATCH trial. *Journal of Clinical Oncology* **37**, 10011-10011, doi:10.1200/JCO.2019.37.15_suppl.10011 (2019).

282 Reddy, V. P. *et al.* Abstract 4868: A preclinical PK/PD model based on a mouse glioblastoma survival model for AZD1390, a novel, brain-penetrant ATM kinase inhibitor, to predict the inhibition of DNA damage response induced by radiation and the human efficacious dose. *Cancer Research* **79**, 4868, doi:10.1158/1538-7445.AM2019-4868 (2019).

283 CRUK. *A trial of AZD1390 and radiotherapy for some types of brain tumour*, <https://www.cancerresearchuk.org/about-cancer/find-a-clinical-trial/a-trial-of-azd1390-and-radiotherapy-for-some-types-of-brain-tumour#undefined> (2020).

284 Landais, I., Sobeck, A., Stone, S., LaChapelle, A. & Hoatlin, M. E. A novel cell-free screen identifies a potent inhibitor of the Fanconi anemia pathway. *Int J Cancer* **124**, 783-792, doi:10.1002/ijc.24039 (2009).

285 Landais, I. *et al.* Monoketone analogs of curcumin, a new class of Fanconi anemia pathway inhibitors. *Molecular cancer* **8**, 133, doi:10.1186/1476-4598-8-133 (2009).

286 Lord, C. J., Tutt, A. N. & Ashworth, A. Synthetic lethality and cancer therapy: lessons learned from the development of PARP inhibitors. *Annual review of medicine* **66**, 455-470, doi:10.1146/annurev-med-050913-022545 (2015).

287 Pires, I. M. *et al.* Targeting radiation-resistant hypoxic tumour cells through ATR inhibition. *British Journal of Cancer* **107**, 291-299, doi:10.1038/bjc.2012.265 (2012).

288 Frosina, G., Marubbi, D., Marcello, D., Vecchio, D. & Daga, A. The efficacy and toxicity of ATM inhibition in glioblastoma initiating cells-driven tumor models. *Critical reviews in oncology/hematology* **138**, 214-222, doi:10.1016/j.critrevonc.2019.04.015 (2019).

289 Ray Chaudhuri, A. & Nussenzweig, A. The multifaceted roles of PARP1 in DNA repair and chromatin remodelling. *Nature reviews. Molecular Cell biology* **18**, 610-621, doi:10.1038/nrm.2017.53 (2017).

290 Lomax, M. E., Folkes, L. K. & O'Neill, P. Biological Consequences of Radiation-induced DNA Damage: Relevance to Radiotherapy. *Clinical Oncology* **25**, 578-585, doi:https://doi.org/10.1016/j.clon.2013.06.007 (2013).

291 Zandarashvili, L. *et al.* Structural basis for allosteric PARP-1 retention on DNA breaks. *Science (New York, N.Y.)* **368**, eaax6367, doi:10.1126/science.aax6367 (2020).

292 Murai, J. *et al.* Rationale for poly(ADP-ribose) polymerase (PARP) inhibitors in combination therapy with camptothecins or temozolomide based on PARP trapping versus catalytic inhibition. *J Pharmacol Exp Ther* **349**, 408-416, doi:10.1124/jpet.113.210146 (2014).

293 Pommier, Y., O'Connor, M. J. & de Bono, J. Laying a trap to kill cancer cells: PARP inhibitors and their mechanisms of action. *Science translational medicine* **8**, 362ps317, doi:10.1126/scitranslmed.aaf9246 (2016).

294 Murai, J. *et al.* Trapping of PARP1 and PARP2 by Clinical PARP Inhibitors. *Cancer Research* **72**, 5588-5599, doi:10.1158/0008-5472.CAN-12-2753 (2012).

295 Murai, J. *et al.* Identification of novel PARP inhibitors using a cell-based TDP1 inhibitory assay in a quantitative high-throughput screening platform. *DNA Repair (Amst)* **21**, 177-182, doi:10.1016/j.dnarep.2014.03.006 (2014).

296 Reaper, P. M. *et al.* Selective killing of ATM- or p53-deficient cancer cells through inhibition of ATR. *Nat Chem Biol* **7**, 428-430, doi:10.1038/nchembio.573 (2011).

297 Lopresti, A. L. The Problem of Curcumin and Its Bioavailability: Could Its Gastrointestinal Influence Contribute to Its Overall Health-Enhancing Effects? *Advances in Nutrition* **9**, 41-50, doi:10.1093/advances/nmx011 (2018).

298 Tomeh, M. A., Hadianamrei, R. & Zhao, X. A Review of Curcumin and Its Derivatives as Anticancer Agents. *International journal of molecular sciences* **20**, 1033, doi:10.3390/ijms20051033 (2019).

299 Garcia-Higuera, I. *et al.* Interaction of the Fanconi anemia proteins and BRCA1 in a common pathway. *Molecular Cell* **7**, 249-262, doi:10.1016/s1097-2765(01)00173-3 (2001).

300 Gregory, R. C., Taniguchi, T. & D'Andrea, A. D. Regulation of the Fanconi anemia pathway by monoubiquitination. *Seminars in cancer biology* **13**, 77-82, doi:10.1016/s1044-579x(02)00102-5 (2003).

301 Cole, A. R., Lewis, L. P. & Walden, H. The structure of the catalytic subunit FANCL of the Fanconi anemia core complex. *Nat Struct Mol Biol* **17**, 294-298, doi:10.1038/nsmb.1759 (2010).

302 Hodson, C., Purkiss, A., Miles, J. A. & Walden, H. Structure of the human FANCL RING-Ube2T complex reveals determinants of cognate E3-E2 selection. *Structure* **22**, 337-344, doi:10.1016/j.str.2013.12.004 (2014).

303 Patil, A. A. *et al. Inhibition of the Fanconia anaemia pathway in glioblastoma multiforme (Poster Abstract)* (Yorkshire Cancer Research (ASM), 2016).

304 Patil, A. A. *et al.* Fanconi Anaemia small molecule inhibitors potentiate temozolomide cytotoxicity in high-grade gliomas. (Currently embargoed due to university IP protection and patenting processes.).

305 PerkinElmer. *Alpha Screen*, <https://www.perkinelmer.com/Content/RelatedMaterials/Brochures/BRO_AlphaScreen2004.pdf> (2018).

306 Hyer, M. L. *et al.* A small-molecule inhibitor of the ubiquitin activating enzyme for cancer treatment. *Nature medicine* **24**, 186-193, doi:10.1038/nm.4474 (2018).

307 Normand, N. SilenciX cell lines for valuable insights into cellular pathways. *Nature Methods* **5**, iii-iv, doi:10.1038/nmeth.f.208 (2008).

308 Ponten, J. & Macintyre, E. H. Long term culture of normal and neoplastic human glia. *Acta pathologica et microbiologica Scandinavica* **74**, 465-486, doi:10.1111/j.1699-0463.1968.tb03502.x (1968).

309 Allen, M., Bjerke, M., Edlund, H., Nelander, S. & Westermark, B. Origin of the U87MG glioma cell line: Good news and bad news. *Science translational medicine* **8**, 354re353, doi:10.1126/scitranslmed.aaf6853 (2016).

310 Dolgin, E. Venerable brain-cancer cell line faces identity crisis. *Nature* **537**, 149-150, doi:10.1038/nature.2016.20515 (2016).

311 Rominiyi, O., Al-Tamimi, Y. & Collis, S. J. The 'Ins and Outs' of Early Preclinical Models for Brain Tumor Research: Are They Valuable and Have We Been Doing It Wrong? *Cancers* **11**, doi:10.3390/cancers11030426 (2019).

312 Rominiyi, O. *et al.* TMOD-39. EX-VIVO 3-DIMENSIONAL MODELS OF POST-SURGICAL RESIDUAL DISEASE IN HUMAN GLIOBLASTOMA. *Neuro-Oncology* **21**, vi271-vi271, doi:10.1093/neuonc/noz175.1138 (2019).

313 Spiteri, I. *et al.* Evolutionary dynamics of residual disease in human glioblastoma. *Annals of oncology : official journal of the European Society for Medical Oncology*, doi:10.1093/annonc/mdy506 (2018).

314 Jo, H. Y. *et al.* The Unreliability of MTT Assay in the Cytotoxic Test of Primary Cultured Glioblastoma Cells. *Exp Neurobiol* **24**, 235-245, doi:10.5607/en.2015.24.3.235 (2015).

315 Zidek, Z., Jansa, P. & Kmonickova, E. Activation of respiratory complex II by interferon-gamma and its inhibition by pyrimidine derivatives. *Neuro endocrinology letters* **35 Suppl 2**, 141-148 (2014).

316 Rai, Y. *et al.* Mitochondrial biogenesis and metabolic hyperactivation limits the application of MTT assay in the estimation of radiation induced growth inhibition. *Scientific reports* **8**, 1531, doi:10.1038/s41598-018-19930-w (2018).

317 Reid, P. *et al.* Experimental investigation of radiobiology in head and neck cancer cell lines as a function of HPV status, by MTT assay. *Scientific reports* **8**, 7744, doi:10.1038/s41598-018-26134-9 (2018).

318 Slavotinek, A., McMillan, T. J. & Steel, C. M. Measurement of radiation survival using the MTT assay. *European Journal of Cancer* **30**, 1376-1382, doi:https://doi.org/10.1016/0959-8049(94)90189-9 (1994).

319 Buch, K. *et al.* Determination of cell survival after irradiation via clonogenic assay versus multiple MTT Assay--a comparative study. *Radiation oncology (London, England)* **7**, 1-1, doi:10.1186/1748-717X-7-1 (2012).

320 Ostermann, S. *et al.* Plasma and cerebrospinal fluid population pharmacokinetics of temozolomide in malignant glioma patients. *Clinical Cancer Research* **10**, 3728-3736, doi:10.1158/1078-0432.Ccr-03-0807 (2004).

321 Portnow, J. *et al.* The neuropharmacokinetics of temozolomide in patients with resectable brain tumors: potential implications for the current approach to chemoradiation. *Clinical Cancer Research* **15**, 7092-7098, doi:10.1158/1078-0432.Ccr-09-1349 (2009).

322 Yarde, D. N. *et al.* Targeting the Fanconi anemia/BRCA pathway circumvents drug resistance in multiple myeloma. *Cancer Research* **69**, 9367-9375, doi:10.1158/0008-5472.Can-09-2616 (2009).

323 Howard, S. M., Yanez, D. A. & Stark, J. M. DNA damage response factors from diverse pathways, including DNA crosslink repair, mediate alternative end joining. *PLoS genetics* **11**, e1004943, doi:10.1371/journal.pgen.1004943 (2015).

324 Bunting, S. F. *et al.* BRCA1 functions independently of homologous recombination in DNA interstrand crosslink repair. *Molecular Cell* **46**, 125-135, doi:10.1016/j.molcel.2012.02.015 (2012).

325 Zhu, J. *et al.* FANCD2 influences replication fork processes and genome stability in response to clustered DSBs. *Cell cycle (Georgetown, Tex.)* **14**, 1809-1822, doi:10.1080/15384101.2015.1036210 (2015).

326 Liang, Z. *et al.* Binding of FANCI-FANCD2 Complex to RNA and R-Loops Stimulates Robust FANCD2 Monoubiquitination. *Cell Reports* **26**, 564-572.e565, doi:10.1016/j.celrep.2018.12.084 (2019).

327 Velazquez-Campoy, A. & Freire, E. Isothermal titration calorimetry to determine association constants for high-affinity ligands. *Nature Protocols* **1**, 186-191, doi:10.1038/nprot.2006.28 (2006).

328 Su, H. & Xu, Y. Application of ITC-Based Characterization of Thermodynamic and Kinetic Association of Ligands With Proteins in Drug Design. *Frontiers in pharmacology* **9**, 1133, doi:10.3389/fphar.2018.01133 (2018).

329 Jafari, R. *et al.* The cellular thermal shift assay for evaluating drug target interactions in cells. *Nature Protocols* **9**, 2100-2122, doi:10.1038/nprot.2014.138 (2014).

330 Mercer, R. W., Tyler, M. A., Ulasov, I. V. & Lesniak, M. S. Targeted Therapies for Malignant Glioma: Progress and Potential. *BioDrugs : clinical immunotherapeutics, biopharmaceuticals and gene therapy* **23**, 25-35 (2009).

331 Sarvjeet, S. & Ashok, K. Biological Effects of Curcumin and Its Role in Cancer Chemoprevention and Therapy. *Anti-Cancer Agents in Medicinal Chemistry* **6**, 259-270, doi:http://dx.doi.org/10.2174/187152006776930918 (2006).

332 Cheng, A. L. *et al.* Phase I clinical trial of curcumin, a chemopreventive agent, in patients with high-risk or pre-malignant lesions. *Anticancer research* **21**, 2895-2900 (2001).

333 Gao, X. *et al.* Curcumin differentially sensitizes malignant glioma cells to TRAIL/Apo2L-mediated apoptosis through activation of procaspases and release of cytochrome c from mitochondria. *Journal of experimental therapeutics & oncology* **5**, 39-48 (2005).

334 Kim, S. Y., Jung, S. H. & Kim, H. S. Curcumin is a potent broad spectrum inhibitor of matrix metalloproteinase gene expression in human astroglioma cells. *Biochem Biophys Res Commun* **337**, 510-516, doi:10.1016/j.bbrc.2005.09.079 (2005).

335 Nagai, S. *et al.* Inhibition of cellular proliferation and induction of apoptosis by curcumin in human malignant astrocytoma cell lines. *Journal of neuro-oncology* **74**, 105-111, doi:10.1007/s11060-004-5757-1 (2005).

336 Woo, M. S. *et al.* Curcumin suppresses phorbol ester-induced matrix metalloproteinase-9 expression by inhibiting the PKC to MAPK signaling pathways in human astroglioma cells. *Biochem Biophys Res Commun* **335**, 1017-1025, doi:10.1016/j.bbrc.2005.07.174 (2005).

337 Gerstner, E. R., Sorensen, A. G., Jain, R. K. & Batchelor, T. T. Anti-vascular endothelial growth factor therapy for malignant glioma. *Curr Neurol Neurosci Rep* **9**, 254-262 (2009).

338 Otsuki, T. *et al.* Fanconi anemia protein complex is a novel target of the IKK signalsome. *Journal of cellular biochemistry* **86**, 613-623, doi:10.1002/jcb.10270 (2002).

339 Burke, J. R. *et al.* BMS-345541 is a highly selective inhibitor of I kappa B kinase that binds at an allosteric site of the enzyme and blocks NF-kappa B-dependent transcription in mice. *J Biol Chem* **278**, 1450-1456, doi:10.1074/jbc.M209677200 (2003).

340 Ogiwara, H. *et al.* Curcumin suppresses multiple DNA damage response pathways and has potency as a sensitizer to PARP inhibitor. *Carcinogenesis* **34**, 2486-2497, doi:10.1093/carcin/bgt240 (2013).

341 Zanotto-Filho, A. *et al.* The curry spice curcumin selectively inhibits cancer cells growth in vitro and in preclinical model of glioblastoma. *J Nutr Biochem* **23**, 591-601, doi:10.1016/j.jnutbio.2011.02.015 (2012).

342 Langone, P. *et al.* Coupling to a glioblastoma-directed antibody potentiates antitumor activity of curcumin. *Int J Cancer* **135**, 710-719, doi:10.1002/ijc.28555 (2014).

343 Yallapu, M. M. *et al.* Novel curcumin-loaded magnetic nanoparticles for pancreatic cancer treatment. *Molecular Cancer Therapuetics* **12**, 1471-1480, doi:10.1158/1535-7163.Mct-12-1227 (2013).

344 Yallapu, M. M. *et al.* Curcumin-loaded magnetic nanoparticles for breast cancer therapeutics and imaging applications. *International journal of nanomedicine* **7**, 1761-1779, doi:10.2147/ijn.S29290 (2012).

345 Chen, J. J. *et al.* Intrathecal curcumin attenuates pain hypersensitivity and decreases spinal neuroinflammation in rat model of monoarthritis. *Scientific reports* **5**, 10278, doi:10.1038/srep10278 (2015).

346 Smith, S. J. *et al.* Overall survival in malignant glioma is significantly prolonged by neurosurgical delivery of etoposide and temozolomide from a thermo-responsive biodegradable paste. *Clinical Cancer Research*, clincanres.3850.2018, doi:10.1158/1078-0432.CCR-18-3850 (2019).

347 Vogelbaum, M. A. & Aghi, M. K. Convection-enhanced delivery for the treatment of glioblastoma. *Neuro-Oncology* **17**, ii3-ii8, doi:10.1093/neuonc/nou354 (2015).

348 Jahangiri, A. *et al.* Convection-enhanced delivery in glioblastoma: a review of preclinical and clinical studies. *Journal of Neurosurgery* **126**, 191-200, doi:10.3171/2016.1.Jns151591 (2017).

349 Karpel-Massler, G. *et al.* PARP inhibition restores extrinsic apoptotic sensitivity in glioblastoma. *PLoS One* **9**, e114583, doi:10.1371/journal.pone.0114583 (2014).

350 Gupta, S. K. *et al.* Discordant in vitro and in vivo chemopotentiating effects of the PARP inhibitor veliparib in temozolomide-sensitive versus -resistant glioblastoma multiforme xenografts. *Clinical Cancer Research* **20**, 3730-3741, doi:10.1158/1078-0432.CCR-13-3446 (2014).

351 Barazzuol, L. *et al.* Evaluation of poly (ADP-ribose) polymerase inhibitor ABT-888 combined with radiotherapy and temozolomide in glioblastoma. *Radiation oncology (London, England)* **8**, 65, doi:10.1186/1748-717x-8-65 (2013).

352 Lathia, J. D., Mack, S. C., Mulkearns-Hubert, E. E., Valentim, C. L. L. & Rich, J. N. Cancer stem cells in glioblastoma. *Genes & development* **29**, 1203-1217, doi:10.1101/gad.261982.115 (2015).

353 Bradshaw, A. *et al.* Cancer Stem Cell Hierarchy in Glioblastoma Multiforme. *Front Surg* **3**, 21, doi:10.3389/fsurg.2016.00021 (2016).

354 Gimple, R. C., Bhargava, S., Dixit, D. & Rich, J. N. Glioblastoma stem cells: lessons from the tumor hierarchy in a lethal cancer. *Genes & development* **33**, 591-609, doi:10.1101/gad.324301.119 (2019).

355 Sawyers, C. L., Denny, C. T. & Witte, O. N. Leukemia and the disruption of normal hematopoiesis. *Cell* **64**, 337-350, doi:https://doi.org/10.1016/0092-8674(91)90643-D (1991).

356 Keinänen, M., Griffin, J. D., Bloomfield, C. D., Machnicki, J. & de la Chapelle, A. Clonal Chromosomal Abnormalities Showing Multiple-Cell-Lineage Involvement in Acute Myeloid Leukemia. *New England Journal of Medicine* **318**, 1153-1158, doi:10.1056/NEJM198805053181803 (1988).

357 Fearon, E. R., Burke, P. J., Schiffer, C. A., Zehnbauer, B. A. & Vogelstein, B. Differentiation of Leukemia Cells to Polymorphonuclear Leukocytes in Patients with Acute Nonlymphocytic Leukemia. *New England Journal of Medicine* **315**, 15-24, doi:10.1056/NEJM198607033150103 (1986).

358 Griffin, J. D. & Lowenberg, B. Clonogenic cells in acute myeloblastic leukemia. *Blood* **68**, 1185-1195 (1986).

359 Lapidot, T. *et al.* A cell initiating human acute myeloid leukaemia after transplantation into SCID mice. *Nature* **367**, 645-648, doi:10.1038/367645a0 (1994).

360 Bonnet, D. & Dick, J. E. Human acute myeloid leukemia is organized as a hierarchy that originates from a primitive hematopoietic cell. *Nature medicine* **3**, 730-737, doi:10.1038/nm0797-730 (1997).

361 Al-Hajj, M., Wicha, M. S., Benito-Hernandez, A., Morrison, S. J. & Clarke, M. F. Prospective identification of tumorigenic breast cancer cells. *Proceedings of the*

National Academy of Sciences of the United States of America **100**, 3983-3988, doi:10.1073/pnas.0530291100 (2003).

362 Collins, A. T., Berry, P. A., Hyde, C., Stower, M. J. & Maitland, N. J. Prospective identification of tumorigenic prostate cancer stem cells. *Cancer Research* **65**, 10946-10951, doi:10.1158/0008-5472.Can-05-2018 (2005).

363 O'Brien, C. A., Pollett, A., Gallinger, S. & Dick, J. E. A human colon cancer cell capable of initiating tumour growth in immunodeficient mice. *Nature* **445**, 106-110, doi:10.1038/nature05372 (2007).

364 Ricci-Vitiani, L. *et al.* Identification and expansion of human colon-cancer-initiating cells. *Nature* **445**, 111-115, doi:10.1038/nature05384 (2007).

365 Li, C. *et al.* Identification of pancreatic cancer stem cells. *Cancer Research* **67**, 1030-1037, doi:10.1158/0008-5472.Can-06-2030 (2007).

366 Tirino, V. *et al.* The role of CD133 in the identification and characterisation of tumour-initiating cells in non-small-cell lung cancer. *European journal of cardio-thoracic surgery : official journal of the European Association for Cardio-thoracic Surgery* **36**, 446-453, doi:10.1016/j.ejcts.2009.03.063 (2009).

367 Prince, M. E. *et al.* Identification of a subpopulation of cells with cancer stem cell properties in head and neck squamous cell carcinoma. *Proceedings of the National Academy of Sciences of the United States of America* **104**, 973-978, doi:10.1073/pnas.0610117104 (2007).

368 Wu, C. *et al.* Side population cells isolated from mesenchymal neoplasms have tumor initiating potential. *Cancer Research* **67**, 8216-8222, doi:10.1158/0008-5472.Can-07-0999 (2007).

369 Ignatova, T. N. *et al.* Human cortical glial tumors contain neural stem-like cells expressing astroglial and neuronal markers in vitro. *Glia* **39**, 193-206, doi:10.1002/glia.10094 (2002).

370 Lendahl, U., Zimmerman, L. B. & McKay, R. D. CNS stem cells express a new class of intermediate filament protein. *Cell* **60**, 585-595, doi:10.1016/0092-8674(90)90662-x (1990).

371 Singh, S. K. *et al.* Identification of a cancer stem cell in human brain tumors. *Cancer Research* **63**, 5821-5828 (2003).

372 Hemmati, H. D. *et al.* Cancerous stem cells can arise from pediatric brain tumors. *Proceedings of the National Academy of Sciences of the United States of America* **100**, 15178-15183, doi:10.1073/pnas.2036535100 (2003).

373 Prager, B. C., Bhargava, S., Mahadev, V., Hubert, C. G. & Rich, J. N. Glioblastoma Stem Cells: Driving Resilience through Chaos. *Trends in Cancer*, doi:10.1016/j.trecan.2020.01.009.

374 Jin, X., Jin, X., Jung, J. E., Beck, S. & Kim, H. Cell surface Nestin is a biomarker for glioma stem cells. *Biochem Biophys Res Commun* **433**, 496-501, doi:10.1016/j.bbrc.2013.03.021 (2013).

375 Annovazzi, L., Mellai, M., Caldera, V., Valente, G. & Schiffer, D. SOX2 expression and amplification in gliomas and glioma cell lines. *Cancer genomics & proteomics* **8**, 139-147 (2011).

376 Ligon, K. L. *et al.* Olig2-regulated lineage-restricted pathway controls replication competence in neural stem cells and malignant glioma. *Neuron* **53**, 503-517, doi:10.1016/j.neuron.2007.01.009 (2007).

377 Zbinden, M. *et al.* NANOG regulates glioma stem cells and is essential in vivo acting in a cross-functional network with GLI1 and p53. *The EMBO journal* **29**, 2659-2674, doi:10.1038/emboj.2010.137 (2010).

378 Rasper, M. *et al.* Aldehyde dehydrogenase 1 positive glioblastoma cells show brain tumor stem cell capacity. *Neuro Oncol* **12**, 1024-1033, doi:10.1093/neuonc/noq070 (2010).

379 Son, M. J., Woolard, K., Nam, D. H., Lee, J. & Fine, H. A. SSEA-1 is an enrichment marker for tumor-initiating cells in human glioblastoma. *Cell stem cell* **4**, 440-452, doi:10.1016/j.stem.2009.03.003 (2009).

380 Lathia, J. D. *et al.* Integrin alpha 6 regulates glioblastoma stem cells. *Cell stem cell* **6**, 421-432, doi:10.1016/j.stem.2010.02.018 (2010).

381 Zhu, T. S. *et al.* Endothelial cells create a stem cell niche in glioblastoma by providing NOTCH ligands that nurture self-renewal of cancer stem-like cells. *Cancer Research* **71**, 6061-6072, doi:10.1158/0008-5472.Can-10-4269 (2011).

382 Charles, N. *et al.* Perivascular nitric oxide activates notch signaling and promotes stem-like character in PDGF-induced glioma cells. *Cell stem cell* **6**, 141-152, doi:10.1016/j.stem.2010.01.001 (2010).

383 Becher, O. J. *et al.* Gli activity correlates with tumor grade in platelet-derived growth factor-induced gliomas. *Cancer Research* **68**, 2241-2249, doi:10.1158/0008-5472.Can-07-6350 (2008).

384 Jain, R. K. *et al.* Angiogenesis in brain tumours. *Nature reviews. Neuroscience* **8**, 610-622, doi:10.1038/nrn2175 (2007).

385 Brooks, M. D., Sengupta, R., Snyder, S. C. & Rubin, J. B. Hitting Them Where They Live: Targeting the Glioblastoma Perivascular Stem Cell Niche. *Current pathobiology reports* **1**, 101-110, doi:10.1007/s40139-013-0012-0 (2013).

386 McCoy, M. G. *et al.* Endothelial cells promote 3D invasion of GBM by IL-8-dependent induction of cancer stem cell properties. *Scientific reports* **9**, 9069, doi:10.1038/s41598-019-45535-y (2019).

387 Giese, A. & Westphal, M. Glioma invasion in the central nervous system. *Neurosurgery* **39**, 235-250; discussion 250-232, doi:10.1097/00006123-199608000-00001 (1996).

388 Hardee, M. E. *et al.* Resistance of glioblastoma-initiating cells to radiation mediated by the tumor microenvironment can be abolished by inhibiting transforming growth factor-beta. *Cancer Research* **72**, 4119-4129, doi:10.1158/0008-5472.Can-12-0546 (2012).

389 Hambardzumyan, D. & Bergers, G. Glioblastoma: Defining Tumor Niches. *Trends Cancer* **1**, 252-265, doi:10.1016/j.trecan.2015.10.009 (2015).

390 Covello, K. L. *et al.* HIF-2alpha regulates Oct-4: effects of hypoxia on stem cell function, embryonic development, and tumor growth. *Genes & development* **20**, 557-570, doi:10.1101/gad.1399906 (2006).

391 Moreno-Manzano, V. *et al.* FM19G11, a new hypoxia-inducible factor (HIF) modulator, affects stem cell differentiation status. *J Biol Chem* **285**, 1333-1342, doi:10.1074/jbc.M109.008326 (2010).

392 Seidel, S. *et al.* A hypoxic niche regulates glioblastoma stem cells through hypoxia inducible factor 2 alpha. *Brain : a journal of neurology* **133**, 983-995, doi:10.1093/brain/awq042 (2010).

393 Cheng, L. *et al.* Elevated invasive potential of glioblastoma stem cells. *Biochem Biophys Res Commun* **406**, 643-648, doi:10.1016/j.bbrc.2011.02.123 (2011).

394 Scheller, J., Chalaris, A., Garbers, C. & Rose-John, S. ADAM17: a molecular switch to control inflammation and tissue regeneration. *Trends in immunology* **32**, 380-387, doi:10.1016/j.it.2011.05.005 (2011).

395 Chen, X. *et al.* ADAM17 promotes U87 glioblastoma stem cell migration and invasion. *Brain research* **1538**, 151-158, doi:10.1016/j.brainres.2013.02.025 (2013).

396 Ortensi, B., Setti, M., Osti, D. & Pelicci, G. Cancer stem cell contribution to glioblastoma invasiveness. *Stem cell research & therapy* **4**, 18, doi:10.1186/scrt166 (2013).

397 Carro, M. S. *et al.* The transcriptional network for mesenchymal transformation of brain tumours. *Nature* **463**, 318-325, doi:10.1038/nature08712 (2010).

398 Goffart, N. *et al.* Adult mouse subventricular zones stimulate glioblastoma stem cells specific invasion through CXCL12/CXCR4 signaling. *Neuro Oncol* **17**, 81-94, doi:10.1093/neuonc/nou144 (2015).

399 Sherry, M. M., Reeves, A., Wu, J. K. & Cochran, B. H. STAT3 is required for proliferation and maintenance of multipotency in glioblastoma stem cells. *Stem cells (Dayton, Ohio)* **27**, 2383-2392, doi:10.1002/stem.185 (2009).

400 Velpula, K. K. *et al.* Glioma stem cell invasion through regulation of the interconnected ERK, integrin alpha6 and N-cadherin signaling pathway. *Cellular signalling* **24**, 2076-2084, doi:10.1016/j.cellsig.2012.07.002 (2012).

401 Brown, P. D. *et al.* Adult patients with supratentorial pilocytic astrocytoma: long-term follow-up of prospective multicenter clinical trial NCCTG-867251 (Alliance). *Neurooncol Pract* **2**, 199-204, doi:10.1093/nop/npv031 (2015).

402 Pedron, S., Becka, E. & Harley, B. A. Regulation of glioma cell phenotype in 3D matrices by hyaluronic acid. *Biomaterials* **34**, 7408-7417, doi:10.1016/j.biomaterials.2013.06.024 (2013).

403 Sarkar, S., Nuttall, R. K., Liu, S., Edwards, D. R. & Yong, V. W. Tenascin-C stimulates glioma cell invasion through matrix metalloproteinase-12. *Cancer Research* **66**, 11771-11780, doi:10.1158/0008-5472.Can-05-0470 (2006).

404 Pedron, S., Becka, E. & Harley, B. A. Spatially gradated hydrogel platform as a 3D engineered tumor microenvironment. *Advanced materials (Deerfield Beach, Fla.)* **27**, 1567-1572, doi:10.1002/adma.201404896 (2015).

405 Rao, S. S. *et al.* Glioblastoma behaviors in three-dimensional collagen-hyaluronan composite hydrogels. *ACS applied materials & interfaces* **5**, 9276-9284, doi:10.1021/am402097j (2013).

406 Florczyk, S. J. *et al.* Porous chitosan-hyaluronic acid scaffolds as a mimic of glioblastoma microenvironment ECM. *Biomaterials* **34**, 10143-10150, doi:10.1016/j.biomaterials.2013.09.034 (2013).

407 Hughes, C. S., Postovit, L. M. & Lajoie, G. A. Matrigel: a complex protein mixture required for optimal growth of cell culture. *Proteomics* **10**, 1886-1890, doi:10.1002/pmic.200900758 (2010).

408 Sigma. *Laminin from Engelbreth-Holm-Swarm murine sarcoma basement membrane*, <https://www.sigmaaldrich.com/catalog/product/sigma/l2020?lang=en&region=GB> (2020).

409 Storch, K. *et al.* Three-dimensional cell growth confers radioresistance by chromatin density modification. *Cancer Research* **70**, 3925-3934, doi:10.1158/0008-5472.Can-09-3848 (2010).

410 Smith, I. *et al.* Neuronal-glial populations form functional networks in a biocompatible 3D scaffold. *Neuroscience letters* **609**, 198-202, doi:10.1016/j.neulet.2015.10.044 (2015).

411 Hayman, M. W., Smith, K. H., Cameron, N. R. & Przyborski, S. A. Enhanced neurite outgrowth by human neurons grown on solid three-dimensional scaffolds. *Biochem Biophys Res Commun* **314**, 483-488, doi:10.1016/j.bbrc.2003.12.135 (2004).

412 Hill, D. S. *et al.* A Novel Fully Humanized 3D Skin Equivalent to Model Early Melanoma Invasion. *Molecular Cancer Therapuetics* **14**, 2665-2673, doi:10.1158/1535-7163.Mct-15-0394 (2015).

413 Koehler, B. C. *et al.* Beyond cell death - antiapoptotic Bcl-2 proteins regulate migration and invasion of colorectal cancer cells in vitro. *PLoS One* **8**, e76446, doi:10.1371/journal.pone.0076446 (2013).

414 Porcelli, L. *et al.* CAFs and TGF-beta Signaling Activation by Mast Cells Contribute to Resistance to Gemcitabine/Nabpaclitaxel in Pancreatic Cancer. *Cancers* **11**, doi:10.3390/cancers11030330 (2019).

415 Amith, S. R., Wilkinson, J. M. & Fliegel, L. Assessing Na(+)/H(+) exchange and cell effector functionality in metastatic breast cancer. *Biochimie open* **2**, 16-23, doi:10.1016/j.biopen.2016.01.001 (2016).

416 Caiazza, F. *et al.* Targeting ADAM-17 with an inhibitory monoclonal antibody has antitumour effects in triple-negative breast cancer cells. *British Journal of Cancer* **112**, 1895-1903, doi:10.1038/bjc.2015.163 (2015).

417 Ombrato, L. *et al.* Metastatic-niche labelling reveals parenchymal cells with stem features. *Nature* **572**, 603-608, doi:10.1038/s41586-019-1487-6 (2019).

418 Galavotti, S. *et al.* The autophagy-associated factors DRAM1 and p62 regulate cell migration and invasion in glioblastoma stem cells. *Oncogene* **32**, 699-712, doi:10.1038/onc.2012.111 (2013).

419 Shannon, S. *et al.* Dexamethasone-Mediated Activation of Fibronectin Matrix Assembly Reduces Dispersal of Primary Human Glioblastoma Cells. *PLoS One* **10**, e0135951, doi:10.1371/journal.pone.0135951 (2015).

420 Laks, D. R. *et al.* Neurosphere formation is an independent predictor of clinical outcome in malignant glioma. *Stem cells (Dayton, Ohio)* **27**, 980-987, doi:10.1002/stem.15 (2009).

421 Lee, J. *et al.* Tumor stem cells derived from glioblastomas cultured in bFGF and EGF more closely mirror the phenotype and genotype of primary tumors than do serum-cultured cell lines. *Cancer Cell* **9**, 391-403, doi:10.1016/j.ccr.2006.03.030 (2006).

422 Stricker, S. H. *et al.* Widespread resetting of DNA methylation in glioblastoma-initiating cells suppresses malignant cellular behavior in a lineage-dependent manner. *Genes & development* **27**, 654-669, doi:10.1101/gad.212662.112 (2013).

423 Galli, R. *et al.* Isolation and Characterization of Tumorigenic, Stem-like Neural Precursors from Human Glioblastoma. *Cancer Research* **64**, 7011, doi:10.1158/0008-5472.CAN-04-1364 (2004).

424 Iacobuzio-Donahue, C. A., Litchfield, K. & Swanton, C. Intratumor heterogeneity reflects clinical disease course. *Nature Cancer* **1**, 3-6, doi:10.1038/s43018-019-0002-1 (2020).

425 Shergalis, A., Bankhead, A., 3rd, Luesakul, U., Muangsin, N. & Neamati, N. Current Challenges and Opportunities in Treating Glioblastoma. *Pharmacological reviews* **70**, 412-445, doi:10.1124/pr.117.014944 (2018).

426 Eramo, A. *et al.* Chemotherapy resistance of glioblastoma stem cells. *Cell Death & Differentiation* **13**, 1238-1241, doi:10.1038/sj.cdd.4401872 (2006).

427 Stupp, R. *et al.* Effect of tumor-treating fields plus maintenance temozolomide vs maintenance temozolomide alone on survival in patients with glioblastoma: a randomized clinical trial. *JAMA* **318**, 2306-2316 (2017).

428 De Witt Hamer, P. C., Jonker, A., Leenstra, S., Ruijter, J. M. & Van Noorden, C. J. Quantification of viability in organotypic multicellular spheroids of human malignant glioma using lactate dehydrogenase activity: a rapid and reliable automated assay. *The journal of histochemistry and cytochemistry : official journal of the Histochemistry Society* **53**, 23-34, doi:10.1177/002215540505300104 (2005).

429 Lan, X. *et al.* Fate mapping of human glioblastoma reveals an invariant stem cell hierarchy. *Nature* **549**, 227-232, doi:10.1038/nature23666 (2017).

430 Criego, A. B. *et al.* Brain glucose concentrations in healthy humans subjected to recurrent hypoglycemia. *Journal of neuroscience research* **82**, 525-530, doi:10.1002/jnr.20654 (2005).

431 Walker, K., Boyd, N. H., Anderson, J. C., Willey, C. D. & Hjelmeland, A. B. Kinomic profiling of glioblastoma cells reveals PLCG1 as a target in restricted glucose. *Biomarker research* **6**, 22, doi:10.1186/s40364-018-0136-9 (2018).

432 Flavahan, W. A. *et al.* Brain tumor initiating cells adapt to restricted nutrition through preferential glucose uptake. *Nature neuroscience* **16**, 1373-1382, doi:10.1038/nn.3510 (2013).

433 Chung, J. K. *et al.* Comparison of [18F]fluorodeoxyglucose uptake with glucose transporter-1 expression and proliferation rate in human glioma and non-small-cell lung cancer. *Nuclear medicine communications* **25**, 11-17, doi:10.1097/00006231-200401000-00003 (2004).

434 Petrova, V., Annicchiarico-Petruzzelli, M., Melino, G. & Amelio, I. The hypoxic tumour microenvironment. *Oncogenesis* **7**, 10, doi:10.1038/s41389-017-0011-9 (2018).

435 Suslov, O. N., Kukekov, V. G., Ignatova, T. N. & Steindler, D. A. Neural stem cell heterogeneity demonstrated by molecular phenotyping of clonal neurospheres. *Proceedings of the National Academy of Sciences of the United States of America* **99**, 14506-14511, doi:10.1073/pnas.212525299 (2002).

436 Ruoslahti, E. Brain extracellular matrix. *Glycobiology* **6**, 489-492, doi:10.1093/glycob/6.5.489 (1996).

437 Grundy, T. J. *et al.* Differential response of patient-derived primary glioblastoma cells to environmental stiffness. *Scientific reports* **6**, 23353, doi:10.1038/srep23353 (2016).

438 Griep, L. M. *et al.* BBB on chip: microfluidic platform to mechanically and biochemically modulate blood-brain barrier function. *Biomedical microdevices* **15**, 145-150, doi:10.1007/s10544-012-9699-7 (2013).

439 Cho, C. F. *et al.* Blood-brain-barrier spheroids as an in vitro screening platform for brain-penetrating agents. *Nature communications* **8**, 15623, doi:10.1038/ncomms15623 (2017).

440 Miranda-Azpiazu, P., Panagiotou, S., Jose, G. & Saha, S. A novel dynamic multicellular co-culture system for studying individual blood-brain barrier cell types in brain diseases and cytotoxicity testing. *Scientific reports* **8**, 8784-8784, doi:10.1038/s41598-018-26480-8 (2018).

441 Heinrich, M. A. *et al.* 3D-Bioprinted Mini-Brain: A Glioblastoma Model to Study Cellular Interactions and Therapeutics. *Advanced materials (Deerfield Beach, Fla.)* **31**, e1806590, doi:10.1002/adma.201806590 (2019).

442 Xiao, Y. *et al.* Ex vivo Dynamics of Human Glioblastoma Cells in a Microvasculature-on-a-Chip System Correlates with Tumor Heterogeneity and Subtypes. *Advanced Science* **6**, 1801531, doi:10.1002/advs.201801531 (2019).

443 Arvanitis, C. D., Ferraro, G. B. & Jain, R. K. The blood–brain barrier and blood–tumour barrier in brain tumours and metastases. *Nature Reviews Cancer* **20**, 26-41, doi:10.1038/s41568-019-0205-x (2020).

444 Brown, N. F., Carter, T. J., Ottaviani, D. & Mulholland, P. Harnessing the immune system in glioblastoma. *British Journal of Cancer* **119**, 1171-1181, doi:10.1038/s41416-018-0258-8 (2018).

445 Matias, D. *et al.* Microglia/Astrocytes-Glioblastoma Crosstalk: Crucial Molecular Mechanisms and Microenvironmental Factors. *Frontiers in cellular neuroscience* **12**, 235, doi:10.3389/fncel.2018.00235 (2018).

446 Venkataramani, V. *et al.* Glutamatergic synaptic input to glioma cells drives brain tumour progression. *Nature* **573**, 532-538, doi:10.1038/s41586-019-1564-x (2019).

447 Venkatesh, H. S. *et al.* Electrical and synaptic integration of glioma into neural circuits. *Nature* **573**, 539-545, doi:10.1038/s41586-019-1563-y (2019).

448 Folkins, C. *et al.* Glioma tumor stem-like cells promote tumor angiogenesis and vasculogenesis via vascular endothelial growth factor and stromal-derived factor 1. *Cancer Research* **69**, 7243-7251, doi:10.1158/0008-5472.Can-09-0167 (2009).

449 Nelson, L. *et al.* A living biobank of ovarian cancer ex vivo models reveals profound mitotic heterogeneity. *Nature communications* **11**, 822, doi:10.1038/s41467-020-14551-2 (2020).

450 Broutier, L. *et al.* Human primary liver cancer-derived organoid cultures for disease modeling and drug screening. *Nature medicine* **23**, 1424-1435, doi:10.1038/nm.4438 (2017).

451 Qazi, M. A. *et al.* Intratumoral heterogeneity: pathways to treatment resistance and relapse in human glioblastoma. *Annals of oncology : official journal of the European Society for Medical Oncology* **28**, 1448-1456, doi:10.1093/annonc/mdx169 (2017).

452 Chang, E. *et al.* Synergistic inhibition of glioma cell proliferation by Withaferin A and tumor treating fields. *Journal of neuro-oncology* **134**, 259-268, doi:10.1007/s11060-017-2534-5 (2017).

453 Chang, E. *et al.* Tumor treating fields increases membrane permeability in glioblastoma cells. *Cell death discovery* **4**, 113-113, doi:10.1038/s41420-018-0130-x (2018).

454 Pavesi, A. *et al.* Engineering a 3D microfluidic culture platform for tumor-treating field application. *Scientific reports* **6**, 26584-26584, doi:10.1038/srep26584 (2016).

455 Sanai, N., Polley, M. Y., McDermott, M. W., Parsa, A. T. & Berger, M. S. An extent of resection threshold for newly diagnosed glioblastomas. *Journal of Neurosurgery* **115**, 3-8, doi:10.3171/2011.2.jns10998 (2011).

456 Jackson, C. M., Choi, J. & Lim, M. Mechanisms of immunotherapy resistance: lessons from glioblastoma. *Nature Immunology* **20**, 1100-1109, doi:10.1038/s41590-019-0433-y (2019).

457 Wen, P. Y. & Kesari, S. Malignant Gliomas in Adults. *New England Journal of Medicine* **359**, 492-507, doi:10.1056/NEJMra0708126 (2008).

458 Drumm, M. R. *et al.* Extensive brainstem infiltration, not mass effect, is a common feature of end-stage cerebral glioblastomas. *Neuro Oncol* **22**, 470-479, doi:10.1093/neuonc/noz216 (2020).

459 BMJ. *Correlation and regression*, <https://www.bmj.com/about-bmj/resources-readers/publications/statistics-square-one/11-correlation-and-regression> (2019).

460 Reya, T., Morrison, S. J., Clarke, M. F. & Weissman, I. L. Stem cells, cancer, and cancer stem cells. *Nature* **414**, 105-111, doi:10.1038/35102167 (2001).

461 Bulstrode, H. *et al.* Elevated FOXG1 and SOX2 in glioblastoma enforces neural stem cell identity through transcriptional control of cell cycle and epigenetic regulators. *Genes & development* **31**, 757-773, doi:10.1101/gad.293027.116 (2017).

462 Venugopal, J. & Blanco, G. On the Many Actions of Ouabain: Pro-Cystogenic Effects in Autosomal Dominant Polycystic Kidney Disease. *Molecules* **22**, 729, doi:10.3390/molecules22050729 (2017).

463 Pessetto, Z. Y. *et al.* Drug repurposing identifies a synergistic combination therapy with imatinib mesylate for gastrointestinal stromal tumor. *Molecular Cancer Therapuetics* **13**, 2276-2287, doi:10.1158/1535-7163.Mct-14-0043 (2014).

464 Jun, D. W. *et al.* Ouabain, a cardiac glycoside, inhibits the Fanconi anemia/BRCA pathway activated by DNA interstrand cross-linking agents. *PLoS One* **8**, e75905, doi:10.1371/journal.pone.0075905 (2013).

465 Du, J. *et al.* A CRISPR/Cas9-Based Screening for Non-Homologous End Joining Inhibitors Reveals Ouabain and Penfluridol as Radiosensitizers. *Molecular Cancer Therapuetics* **17**, 419-431, doi:10.1158/1535-7163.Mct-17-0090 (2018).

466 Galia, A. *et al.* PARP-1 protein expression in glioblastoma multiforme. *European journal of histochemistry : EJH* **56**, e9, doi:10.4081/ejh.2012.e9 (2012).

467 Carruthers, R. *Response to ionising radiation of glioblastoma stem-like cells (PhD thesis).* University of Glasgow, (2015).

468 da Silva, B. *et al.* Chemically induced neurite-like outgrowth reveals a multicellular network function in patient-derived glioblastoma cells. *J Cell Sci* **132**, doi:10.1242/jcs.228452 (2019).

469 Li, L. & Bhatia, R. Stem cell quiescence. *Clinical Cancer Research* **17**, 4936-4941, doi:10.1158/1078-0432.Ccr-10-1499 (2011).

470 Turinetto, V. & Giachino, C. Multiple facets of histone variant H2AX: a DNA double-strand-break marker with several biological functions. *Nucleic acids research* **43**, 2489-2498, doi:10.1093/nar/gkv061 (2015).

471 Bassing, C. H. & Alt, F. W. H2AX may function as an anchor to hold broken chromosomal DNA ends in close proximity. *Cell cycle (Georgetown, Tex.)* **3**, 149-153, doi:10.4161/cc.3.2.689 (2004).

472 Celeste, A. *et al.* Histone H2AX phosphorylation is dispensable for the initial recognition of DNA breaks. *Nature cell biology* **5**, 675-679, doi:10.1038/ncb1004 (2003).

473 Ward, J. F. Radiation-induced strand breakage in DNA. *Basic life sciences* **5b**, 471-472, doi:10.1007/978-1-4684-2898-8_7 (1975).

474 Radford, I. R. The level of induced DNA double-strand breakage correlates with cell killing after X-irradiation. *International journal of radiation biology and related studies in physics, chemistry, and medicine* **48**, 45-54, doi:10.1080/09553008514551051 (1985).

475 Frosina, G. *et al.* ATR kinase inhibitors NVP-BEZ235 and AZD6738 effectively penetrate the brain after systemic administration. *Radiation oncology (London, England)* **13**, 76, doi:10.1186/s13014-018-1020-3 (2018).

476 Min, A. *et al.* AZD6738, A Novel Oral Inhibitor of ATR, Induces Synthetic Lethality with ATM Deficiency in Gastric Cancer Cells. *Molecular Cancer Therapuetics* **16**, 566-577, doi:10.1158/1535-7163.Mct-16-0378 (2017).

477 Zha, S. *et al.* Ataxia telangiectasia-mutated protein and DNA-dependent protein kinase have complementary V(D)J recombination functions. *Proceedings of the National Academy of Sciences of the United States of America* **108**, 2028-2033, doi:10.1073/pnas.1019293108 (2011).

478 Gapud, E. J. *et al.* Ataxia telangiectasia mutated (Atm) and DNA-PKcs kinases have overlapping activities during chromosomal signal joint formation. *Proceedings of the National Academy of Sciences of the United States of America* **108**, 2022-2027, doi:10.1073/pnas.1013295108 (2011).

479 Callen, E. *et al.* Essential role for DNA-PKcs in DNA double-strand break repair and apoptosis in ATM-deficient lymphocytes. *Molecular Cell* **34**, 285-297, doi:10.1016/j.molcel.2009.04.025 (2009).

480 Chen, B. P. *et al.* Ataxia telangiectasia mutated (ATM) is essential for DNA-PKcs phosphorylations at the Thr-2609 cluster upon DNA double strand break. *J Biol Chem* **282**, 6582-6587, doi:10.1074/jbc.M611605200 (2007).

481 Davis, A. J., Chen, B. P. & Chen, D. J. DNA-PK: a dynamic enzyme in a versatile DSB repair pathway. *DNA Repair (Amst)* **17**, 21-29, doi:10.1016/j.dnarep.2014.02.020 (2014).

482 Meek, K., Dang, V. & Lees-Miller, S. P. DNA-PK: the means to justify the ends? *Advances in immunology* **99**, 33-58, doi:10.1016/s0065-2776(08)00602-0 (2008).

483 Jiang, W. *et al.* Differential phosphorylation of DNA-PKcs regulates the interplay between end-processing and end-ligation during nonhomologous end-joining. *Molecular Cell* **58**, 172-185, doi:10.1016/j.molcel.2015.02.024 (2015).

484 Wei, P. C. *et al.* Long Neural Genes Harbor Recurrent DNA Break Clusters in Neural Stem/Progenitor Cells. *Cell* **164**, 644-655, doi:10.1016/j.cell.2015.12.039 (2016).

485 Blundred, R., Myers, K., Helleday, T., Goldman, A. S. & Bryant, H. E. Human RECQL5 overcomes thymidine-induced replication stress. *DNA Repair (Amst)* **9**, 964-975, doi:10.1016/j.dnarep.2010.06.009 (2010).

486 Stringer, B. W. *et al.* A reference collection of patient-derived cell line and xenograft models of proneural, classical and mesenchymal glioblastoma. *Scientific reports* **9**, 4902, doi:10.1038/s41598-019-41277-z (2019).

487 Olmez, I., Shen, W., McDonald, H. & Ozpolat, B. Dedifferentiation of patient-derived glioblastoma multiforme cell lines results in a cancer stem cell-like state with mitogen-independent growth. *Journal of cellular and molecular medicine* **19**, 1262-1272, doi:10.1111/jcmm.12479 (2015).

488 Lawrence, T. S. Ouabain sensitizes tumor cells but not normal cells to radiation. *International journal of radiation oncology, biology, physics* **15**, 953-958, doi:10.1016/0360-3016(88)90132-0 (1988).

489 Kulikov, A., Eva, A., Kirch, U., Boldyrev, A. & Scheiner-Bobis, G. Ouabain activates signaling pathways associated with cell death in human neuroblastoma. *Biochimica et Biophysica Acta (BBA) - Biomembranes* **1768**, 1691-1702, doi:https://doi.org/10.1016/j.bbamem.2007.04.012 (2007).

490 McConkey, D. J., Lin, Y., Nutt, L. K., Ozel, H. Z. & Newman, R. A. Cardiac glycosides stimulate Ca2+increases and apoptosis in androgen-independent, metastatic human prostate adenocarcinoma cells. *Cancer Research* **60**, 3807-3812 (2000).

491 Saunders, R. & Scheiner-Bobis, G. Ouabain stimulates endothelin release and expression in human endothelial cells without inhibiting the sodium pump. *European journal of biochemistry* **271**, 1054-1062, doi:10.1111/j.1432-1033.2004.04012.x (2004).

492 Abramowitz, J. *et al.* Ouabain- and Marinobufagenin-Induced Proliferation of Human Umbilical Vein Smooth Muscle Cells and a Rat Vascular Smooth Muscle Cell Line, A7r5. *Circulation* **108**, 3048-3053, doi:10.1161/01.CIR.0000101919.00548.86 (2003).

493 Kometiani, P., Liu, L. & Askari, A. Digitalis-induced signaling by Na+/K+-ATPase in human breast cancer cells. *Molecular Pharmacology* **67**, 929-936, doi:10.1124/mol.104.007302 (2005).

494 Yang, X. S. *et al.* Ouabain suppresses the growth and migration abilities of glioma U87MG cells through inhibiting the Akt/mTOR signaling pathway and downregulating the expression of HIF1alpha. *Molecular medicine reports* **17**, 5595-5600, doi:10.3892/mmr.2018.8587 (2018).

495 Moeller, B. J. & Dewhirst, M. W. HIF-1 and tumour radiosensitivity. *British Journal of Cancer* **95**, 1-5, doi:10.1038/sj.bjc.6603201 (2006).

496 Marampon, F. *et al.* Hypoxia sustains glioblastoma radioresistance through ERKs/DNA-PKcs/HIF-1alpha functional interplay. *International journal of oncology* **44**, 2121-2131, doi:10.3892/ijo.2014.2358 (2014).

497 Eccles, L. J., Bell, A. C. & Powell, S. N. Inhibition of non-homologous end joining in Fanconi Anemia cells results in rescue of survival after interstrand crosslinks but sensitization to replication associated double-strand breaks. *DNA Repair (Amst)* **64**, 1-9, doi:10.1016/j.dnarep.2018.02.003 (2018).

498 Xie, Z. & Cai, T. Na+-K+--ATPase-mediated signal transduction: from protein interaction to cellular function. *Molecular interventions* **3**, 157-168, doi:10.1124/mi.3.3.157 (2003).

499 Chou, T. C. Drug combination studies and their synergy quantification using the Chou-Talalay method. *Cancer Research* **70**, 440-446, doi:10.1158/0008-5472.CAN-09-1947 (2010).

500 Di Veroli, G. Y. *et al.* Combenefit: an interactive platform for the analysis and visualization of drug combinations. *Bioinformatics* **32**, 2866-2868, doi:10.1093/bioinformatics/btw230 (2016).

501 Neftel, C. *et al.* An Integrative Model of Cellular States, Plasticity, and Genetics for Glioblastoma. *Cell* **178**, 835-849.e821, doi:10.1016/j.cell.2019.06.024 (2019).

502 Rasmussen, R. D. *et al.* BRCA1-regulated RRM2 expression protects glioblastoma cells from endogenous replication stress and promotes tumorigenicity. *Nature communications* **7**, 13398-13398, doi:10.1038/ncomms13398 (2016).

503 Bartkova, J. *et al.* Replication stress and oxidative damage contribute to aberrant constitutive activation of DNA damage signalling in human gliomas. *Oncogene* **29**, 5095-5102, doi:10.1038/onc.2010.249 (2010).

504 Metselaar, D. S. *et al.* Celastrol-induced degradation of FANCD2 sensitizes pediatric high-grade gliomas to the DNA-crosslinking agent carboplatin. *EBioMedicine* **50**, 81-92, doi:10.1016/j.ebiom.2019.10.062 (2019).

505 Balbous, A. *et al.* A radiosensitizing effect of RAD51 inhibition in glioblastoma stem-like cells. *Bmc Cancer* **16**, doi:10.1186/s12885-016-2647-9 (2016).

506 Taniguchi, T. *et al.* Disruption of the Fanconi anemia-BRCA pathway in cisplatin-sensitive ovarian tumors. *Nature medicine* **9**, 568-574, doi:10.1038/nm852 (2003).

507 Chirnomas, D. *et al.* Chemosensitization to cisplatin by inhibitors of the Fanconi anemia/BRCA pathway. *Molecular Cancer Therapuetics* **5**, 952-961, doi:10.1158/1535-7163.Mct-05-0493 (2006).

508 Collis, S. J., Barber, L. J., Ward, J. D., Martin, J. S. & Boulton, S. J. C. elegans FANCD2 responds to replication stress and functions in interstrand cross-link repair. *DNA Repair (Amst)* **5**, 1398-1406, doi:10.1016/j.dnarep.2006.06.010 (2006).

509 Zimmermann, M. *et al.* CRISPR screens identify genomic ribonucleotides as a source of PARP-trapping lesions. *Nature* **559**, 285-289, doi:10.1038/s41586-018-0291-z (2018).

510 Wang, C. *et al.* Genome-wide CRISPR screens reveal synthetic lethality of RNASEH2 deficiency and ATR inhibition. *Oncogene* **38**, 2451-2463, doi:10.1038/s41388-018-0606-4 (2019).

511 Hustedt, N. *et al.* A consensus set of genetic vulnerabilities to ATR inhibition. *Open Biology* **9**, 190156, doi:10.1098/rsob.190156 (2019).

512 Olivieri, M. *et al.* A genetic map of the response to DNA damage in human cells. *bioRxiv*, 845446, doi:10.1101/845446 (2019).

513 Chen, C. C., Kennedy, R. D., Sidi, S., Look, A. T. & D'Andrea, A. CHK1 inhibition as a strategy for targeting Fanconi Anemia (FA) DNA repair pathway deficient tumors. *Molecular Cancer* **8**, 24, doi:10.1186/1476-4598-8-24 (2009).

514 Andreassen, P. R., D'Andrea, A. D. & Taniguchi, T. ATR couples FANCD2 monoubiquitination to the DNA-damage response. *Genes & Development* **18**, 1958-1963, doi:10.1101/gad.1196104 (2004).

515 Knies, K. *et al.* Biallelic mutations in the ubiquitin ligase RFWD3 cause Fanconi anemia. *J Clin Invest* **127**, 3013-3027, doi:10.1172/jci92069 (2017).

516 Elia, A. E. *et al.* RFWD3-Dependent Ubiquitination of RPA Regulates Repair at Stalled Replication Forks. *Molecular Cell* **60**, 280-293, doi:10.1016/j.molcel.2015.09.011 (2015).

517 Feeney, L. *et al.* RPA-Mediated Recruitment of the E3 Ligase RFWD3 Is Vital for Interstrand Crosslink Repair and Human Health. *Molecular Cell* **66**, 610-621.e614, doi:10.1016/j.molcel.2017.04.021 (2017).

518 Inano, S. *et al.* RFWD3-Mediated Ubiquitination Promotes Timely Removal of Both RPA and RAD51 from DNA Damage Sites to Facilitate Homologous Recombination. *Molecular Cell* **66**, 622-634.e628, doi:10.1016/j.molcel.2017.04.022 (2017).

519 Kennedy, R. D. *et al.* Fanconi anemia pathway-deficient tumor cells are hypersensitive to inhibition of ataxia telangiectasia mutated. *J Clin Invest* **117**, 1440-1449, doi:10.1172/jci31245 (2007).

520 Sanai, N. Phase 0 Clinical Trial Strategies for the Neurosurgical Oncologist. *Neurosurgery* **85**, E967-e974, doi:10.1093/neuros/nyz218 (2019).

521 Etame, A. B. *et al.* Focused ultrasound disruption of the blood-brain barrier: a new frontier for therapeutic delivery in molecular neurooncology. *Neurosurgical Focus* **32**, E3-E3, doi:10.3171/2011.10.FOCUS11252 (2012).

522 Xie, F. *et al.* Effects of transcranial ultrasound and intravenous microbubbles on blood brain barrier permeability in a large animal model. *Ultrasound in Medicine & Biology* **34**, 2028-2034, doi:10.1016/j.ultrasmedbio.2008.05.004 (2008).

523 Chang, E. *et al.* Tumor treating fields increases membrane permeability in glioblastoma cells. *Cell Death & Discovery* **4**, 113, doi:10.1038/s41420-018-0130-x (2018).

524 Kessler, A. F. *et al.* Blood Brain Barrier (BBB) Integrity Is Affected By Tumor Treating Fields (TTFields) in Vitro and In Vivo. *International Journal of Radiation Oncology, Biology, Physics* **105**, S162-S163, doi:10.1016/j.ijrobp.2019.06.182 (2019).

525 Lukas, R. V. *et al.* Newly Diagnosed Glioblastoma: A Review on Clinical Management. *Oncology (Williston Park, N.Y.)* **33**, 91-100 (2019).

526 Hidalgo, M. *et al.* A pilot clinical study of treatment guided by personalized tumorgrafts in patients with advanced cancer. *Molecular Cancer Therapuetics* **10**, 1311-1316, doi:10.1158/1535-7163.Mct-11-0233 (2011).

527 Rubio-Viqueira, B. *et al.* An in vivo platform for translational drug development in pancreatic cancer. *Clinical Cancer Research* **12**, 4652-4661, doi:10.1158/1078-0432.Ccr-06-0113 (2006).

528 Garralda, E. *et al.* Integrated next-generation sequencing and avatar mouse models for personalized cancer treatment. *Clinical Cancer Research* **20**, 2476-2484, doi:10.1158/1078-0432.Ccr-13-3047 (2014).

529 Kato, S. & Kurzrock, R. An avatar for precision cancer therapy. *Nature Biotechnology* **36**, 1053-1055, doi:10.1038/nbt.4293 (2018).

530 MisvikBiology. *Misvik Biology*, <https://www.misvik.com> (2019).

531 Turnbull, C. *et al.* The 100 000 Genomes Project: bringing whole genome sequencing to the NHS. *BMJ* **361**, k1687, doi:10.1136/bmj.k1687 (2018).